frontiers | Research Topics

Coastal ecotones under anthropogenic influences: Conservation, restoration and realignment

Edited by
Xuechu Chen, Guanqiong Ye, Li Zhang, Yanpeng Cai, Serena Moseman-Valtierra, Xiuzhen Li and Qiang He

Published in
Frontiers in Marine Science

ISSN 1664-8714
ISBN 978-2-8325-3713-8
DOI 10.3389/978-2-8325-3713-8

About Frontiers

Frontiers is more than just an open access publisher of scholarly articles: it is a pioneering approach to the world of academia, radically improving the way scholarly research is managed. The grand vision of Frontiers is a world where all people have an equal opportunity to seek, share and generate knowledge. Frontiers provides immediate and permanent online open access to all its publications, but this alone is not enough to realize our grand goals.

Frontiers journal series

The Frontiers journal series is a multi-tier and interdisciplinary set of open-access, online journals, promising a paradigm shift from the current review, selection and dissemination processes in academic publishing. All Frontiers journals are driven by researchers for researchers; therefore, they constitute a service to the scholarly community. At the same time, the *Frontiers journal series* operates on a revolutionary invention, the tiered publishing system, initially addressing specific communities of scholars, and gradually climbing up to broader public understanding, thus serving the interests of the lay society, too.

Dedication to quality

Each Frontiers article is a landmark of the highest quality, thanks to genuinely collaborative interactions between authors and review editors, who include some of the world's best academicians. Research must be certified by peers before entering a stream of knowledge that may eventually reach the public - and shape society; therefore, Frontiers only applies the most rigorous and unbiased reviews. Frontiers revolutionizes research publishing by freely delivering the most outstanding research, evaluated with no bias from both the academic and social point of view. By applying the most advanced information technologies, Frontiers is catapulting scholarly publishing into a new generation.

What are Frontiers Research Topics?

Frontiers Research Topics are very popular trademarks of the *Frontiers journals series*: they are collections of at least ten articles, all centered on a particular subject. With their unique mix of varied contributions from Original Research to Review Articles, Frontiers Research Topics unify the most influential researchers, the latest key findings and historical advances in a hot research area.

Find out more on how to host your own Frontiers Research Topic or contribute to one as an author by contacting the Frontiers editorial office: frontiersin.org/about/contact

Coastal ecotones under anthropogenic influences: Conservation, restoration and realignment

Topic editors

Xuechu Chen — East China Normal University, China
Guanqiong Ye — Zhejiang University, China
Li Zhang — Florida Gulf Coast University, United States
Yanpeng Cai — Guangdong University of Technology, China
Serena Moseman-Valtierra — University of Rhode Island, United States
Xiuzhen Li — East China Normal University, China
Qiang He — Fudan University, China

Citation

Chen, X., Ye, G., Zhang, L., Cai, Y., Moseman-Valtierra, S., Li, X., He, Q., eds. (2023). *Coastal ecotones under anthropogenic influences: Conservation, restoration and realignment*. Lausanne: Frontiers Media SA. doi: 10.3389/978-2-8325-3713-8

Table of contents

frontiers | Frontiers in Marine Science

TYPE Review
PUBLISHED 22 August 2022
DOI 10.3389/fmars.2022.972426

OPEN ACCESS

EDITED BY
Yanpeng Cai,
Guangdong University of Technology, China

REVIEWED BY
Jun Xiao,
Institute of Earth Environment, (CAS), China
Chemseddine Fehdi,
University of Tébessa, Algeria
Hui Qian,
Chang'an University, China

*CORRESPONDENCE
Zongjun Gao
gaozongjun@126.com

SPECIALTY SECTION
This article was submitted to Coastal Ocean Processes, a section of the journal Frontiers in Marine Science

RECEIVED 18 June 2022
ACCEPTED 03 August 2022
PUBLISHED 22 August 2022

CITATION
Dong H and Gao Z (2022) Theoretical progress of groundwater chemical evolution based on Tóthian theory: A review.
Front. Mar. Sci. 9:972426.
doi: 10.3389/fmars.2022.972426

Theoretical progress of groundwater chemical evolution based on Tóthian theory: A review

Hongzhi Dong and Zongjun Gao*

College of Earth Science and Engineering, Shandong University of Science and Technology, Qingdao, China

Tóthian theory refers to the gravity driven groundwater flow system (GFS) theory represented by Tóth, which mainly expounds the driving and distribution law of groundwater. The establishment and development of this theory not only deepened people's understanding of the driving and distribution law of groundwater, but also greatly promoted the study of groundwater chemical evolution (GCE). Modern GCE research is mostly based on Tóthian theory, characterized by combining with advanced scientific and technological means. Based on the clue of time, this paper is divided into two parts. The first part mainly summarizes the establishment and development of Tóthian theory, including the exploration of groundwater driving force and distribution form by hydrogeologists before Tóthian theory, and the enrichment, development and application of Tóthian theory by geologists after its establishment. The second part mainly combs the main theories and application progress of GCE mechanism research, including the main theories and findings of GCE research before the emergence of Tóthian theory, as well as the research progresses of GCE after the emergence of Tóthian theory. With the flow of groundwater in GFS, groundwater undergoes continuous chemical evolution, which eventually leads to the transformation of hydrochemical types and the gradual increase of total dissolved solids (TDS). The distribution of GFS and GCE complement each other. The distribution of GFS directly determines the model of GCE, and the results of GCE also play a certain role in the distribution of GFS. GCE mainly includes dissolution, precipitation, cation exchange and adsorption, which is affected by the physical and chemical conditions of permeable media, organic matter content and microorganisms. GCE has the characteristics of universality, sustainability and diversity. With the increasing global population and the progresses of science and technology, the impact of human life, industrial and agricultural production on groundwater is deepening. The aggravation of pollution directly changes the chemical compositions of groundwater, resulting in changes of the law of GCE.

KEYWORDS

Tóthian theory, groundwater chemical evolution, groundwater flow system, gravity driven, human factor

Introduction

Groundwater, a complex solution containing more than 80 elements, is an important geological force, which is widely involved in geological processes such as karst, sedimentation, diagenesis, metamorphism and mineralization (Zhang et al., 2018). Driven by gravity, density difference and heat, groundwater continuously reacts with the surrounding environment to complete the transportation and distribution of materials and energy, and its chemical properties continue to evolve (Tóth, 2009; Jiang et al., 2011; Zhang et al., 2015; Luan et al., 2017; Zhang et al., 2018; Meng, 2021; Zhao et al., 2021). According to Tóthian theory, the distribution pattern of gravity driven GFS is mainly controlled by the terrain. Regional GFS has multi-level nested systems, i.e., local-GFS, intermediate-GFS and regional-GFS. It is recognized that regional-GFS is the reason for the diversity of geological processes (Tóth, 1999; Jiang et al., 2010; Judit and Tóth, 2015; Jia et al., 2020). The discovery of Tóthian theory makes people master the general law of GFS. The combination of Tóthian theory and groundwater evolution research greatly promotes the study of GCE, which makes it possible to reveal the general law of GCE.

The long-term circulation makes the main components of groundwater controlled by the stratum. Under natural conditions, the main anions are bicarbonate (HCO_3^-), sulfate (SO_4^{2-}), chloride ion (Cl^-) and carbonate (CO_3^{2-}), and the main cations are calcium (Ca^{2+} n), magnesium (Mg^{2+}), sodium (Na^+) and potassium (K^+) (Liang et al., 2012; Ren et al., 2014; Zhou et al., 2014; Zhang et al., 2018; Gao et al., 2020; Jia et al., 2020). Combined with the theory of GFS, the TDS of groundwater generally increases from the recharge area (RA) to the discharge area (DA), and the hydrochemical types often show horizontal zoning, gradually transforming from $HCO_3^- - Ca^{2+} \cdot Mg^{2+}$ to $SO_4^{2-} - Mg^{2+} \cdot Ca^{2+}$, and eventually evolve to Cl^-–Na^+ (Hao et al., 2020; Wang et al., 2021a; Zhao et al., 2021). In some areas with special geological environment, the chemical evolution of groundwater deviates from the general law. For example, due to the different geological backgrounds of each region, the phenomenon of element process in groundwater in some areas leads to various endemic diseases, such as Sri Lanka, India, the United States and China (Gao et al., 2014; Kaur et al., 2019; Imbulana et al., 2020).

With the gradual expansion of the impact of human activities on nature, human activities continue to change the surrounding environment of groundwater, leading to obvious man-made interference characteristics in the chemical evolution of groundwater, resulting in obvious changes in the chemical components of groundwater. Such as nitrate (NO_3^-) is added to the main ions in groundwater, the content of heavy metals in groundwater in some areas exceeds the background values, arsenic plumbum pollution is spread worldwide, and the change of chemical compositions of groundwater poses a threat to human health to a certain extent (Gao et al., 2014a; Nan et al., 2008; Sinha and Prasad, 2020; Paolalsiam and Mohan, 2021; Wang et al., 2021b; Xiao et al., 2021; Gao et al., 2022). In addition, with the development of industry and the growth of population, the natural recharge of groundwater is insufficient to meet people's increasing demand for groundwater, the natural balance of groundwater is broken, and overexploitation leads to a series of problems such as land subsidence, ground fissures, land collapse, seawater intrusion and other problems (Zhang and Zhang, 2019).

Although the research on the chemical evolution of groundwater combined with Tóthian theory has achieved rich results which were widely recognized, the distribution law and chemical evolution law of groundwater have changed significantly under the influence of human activities. In the context of today's industrial revolution, combined with Tóthian theory and human activities, mining the new laws of groundwater distribution and GCE under the influence of human activities can deepen our understanding of the diversity of geological processes, explain the chemical change process of groundwater more comprehensively and objectively, and better reveal the interaction relationship between groundwater and environment.

This paper fully integrates the relevant literatures, aiming at tracing the development and reform of the theory, focusing on combing the typical literature that can reflect the process of theoretical development, and analyzing the development of GCE theory and the main ways of GCE.

Establishment and development of Tóthian theory

Tóthian theory is the theory of gravity driven GFS firstly proposed by József Tóth, a Canadian hydrogeologist. Once published, it has been widely concerned. After the improvement and development of many hydrogeologists, it plays a leading role in hydrogeology. The theory was initially called "Groundwater multi-level nesting theory" (Tóth, 1963), and later evolved into "Gravity driven groundwater flow system theory" (Tóth, 2009). Finally, it was summarized as Tóthian theory in his article "The evolutionary concepts and practical utilization of the Tóthian Theory of regional groundwater flow", published in 2016 (Tóth, 2016). This section mainly reviews the theoretical establishment and development of Tóthian theory.

Establishment of Tóthian theory

The GFS theory proposed by Tóthian comes from a large number of previous scientific researches. The main classical

groundwater researches before Tóthian theory are shown in Table 1. In 1738, Daniel Bernoulli discovered the "Bernoulli theorem", which had been widely used in hydraulic research. It was defined as that the total head of groundwater is the sum of its position head, pressure head and velocity head, and groundwater always flows from the position with high total head to the place with low total head (Maranzoni, 2020). In 1856, French hydraulic scientist Darcy found that the seepage velocity is directly proportional to the power of hydraulic gradient based on the concept of head, which is called Darcy's Law (Darcy, 1857). In 1885, Chamberlin pointed out that the topographic elevation difference provided a driving force for groundwater flow (Chamberlin, 1885). King put forward the concept of gravity driven groundwater in 1899 (Figure 1A) (Cederstrom, 1946; Gao et al., 2014b), and Fourmarier proposed the concept of multistage GFS in 1939 (Figure 1b) (Zhang et al., 2015). Meinzer, Meinzer and Wenzel respectively discovered the three-dimensional properties of groundwater overflow and hydraulic gradient in 1936 and 1940 (Meinzer, 1936; Meinzer and Wenzel, 1940). Hubbert (1940) found that the driving force of groundwater was the negative value of the first derivative of fluid potential through Darcy's law, and drew an approximate flow model of homogeneous permeable medium between gas-water interface potential source and valley potential sink - inter River block network flow diagram (Figure 1C) (Hubbert, 1940). In 1962, Tóth found the defects of Hubbert flow model in the actual hydrogeological work. Combined with the general relationship between piezometric tube surface and terrain in the same well depth in the same rock unit, he applied Laplace equation to solve the drainage problems of simple basin (Tóth, 1962). After continuous correction and improvement, he finally put forward the theory of "Nested multistage flow system" in 1963 (Figure 1D) (Tóth, 1963). Tóth believed that under the control of specific physical, geographical and geological conditions, the groundwater in the basin presented a multi-level flow mode (composed of local-GFS, intermediate-GFS and regional -GFS). In each GFS, from the supply source to the discharge sink, the flow changes from downward movement to horizontal movement, and then upward movement (Tóth, 1962; Tóth, 1963; Zhang et al., 2018).

Development of Tóthian theory

Since 1961, Tóth has been committed to the research of GFS and continuously promoted Tóthian theory. The improvement of GFS and its environmental effects are shown in Figure 2. In 2009, Tóth systematically combed his scientific researches of nearly half a century and published the book "Graphic Systems of Ground Water Flow" (Tóth, 2009). During this period, Tóth's achievements in gravity driven GFS could be briefly summarized as follows: (1) the main driving force of groundwater is gravity. The gravity penetration theory is proposed to expand the application scope of GFS theory from homogeneous small basins to heterogeneous large basins (Tóth, 1978; Tóth, 1979; Tóth, 1980; Tóth, 1995); (2) Reveal the role of GFS in material transport, hydrochemical evolution and thermal evolution (Tóth, 1966a; Tóth, 1984; Tóth, 1996); (3) It is considered that groundwater is an ubiquitous geological agent and the main reason for geological diversity (Tóth, 1971; Tóth, 1999; Tóth, 2016); (4) It promotes the application of GFS theory in practical work (Tóth, 1966b; Tóth, 1977; Tóth and Corbet, 1986).

TABLE 1 Main classical theories on groundwater before Tóthian theory.

Year	Author (Country)	Mine theory (References)
1738	Bernouli (Switzerland)	**Bernoulli's theorem**: The hydraulic head of groundwater is the sum of its position head, pressure head and velocity head and groundwater always flow from the position where the hydraulic head is high to the place where the hydraulic head is low (Maranzoni, 2020).
1856	Darcy (France)	**Darcy's Law**: The seepage velocity is directly proportional to the power of hydraulic gradient (Darcy, 1857).
1885	Chamberlin (America)	The topographic elevation difference provides the driving force of groundwater flow.
1899	King (America)	Concept of gravity driven groundwater flow (Cederstrom, 1946; Gao et al., 2014b).
1936&1940	Meinzer (America)	Water in rocks tends to move from positions of high to low pressure, both along and across the strata; Proposed that the hydraulic gradient has three-dimensional properties (Meinzer, 1936; Meinzer and Wenzel, 1940).
1939	Fourmarier (France)	Proposed the concept of multistage GFS (Zhang et al., 2015).
1940	Hubbert (Canada)	Mapped the flow net of massif between two rivers; Proposed the concept of fluid potential and the driving force of groundwater is the negative value of the first derivative of fluid potential (Hubbert, 1940).
1961	Farvolden (Canada)	General relationship between piezometric surface with topography in wells of same depth within the same rock unit (Tóth, 1962).
1963	Tóth (Canada)	Groundwater flow pattern: The piezometric surface approximately the topography and several GFSs may be superimposed on one another (Tóth, 1962; Tóth, 1963).

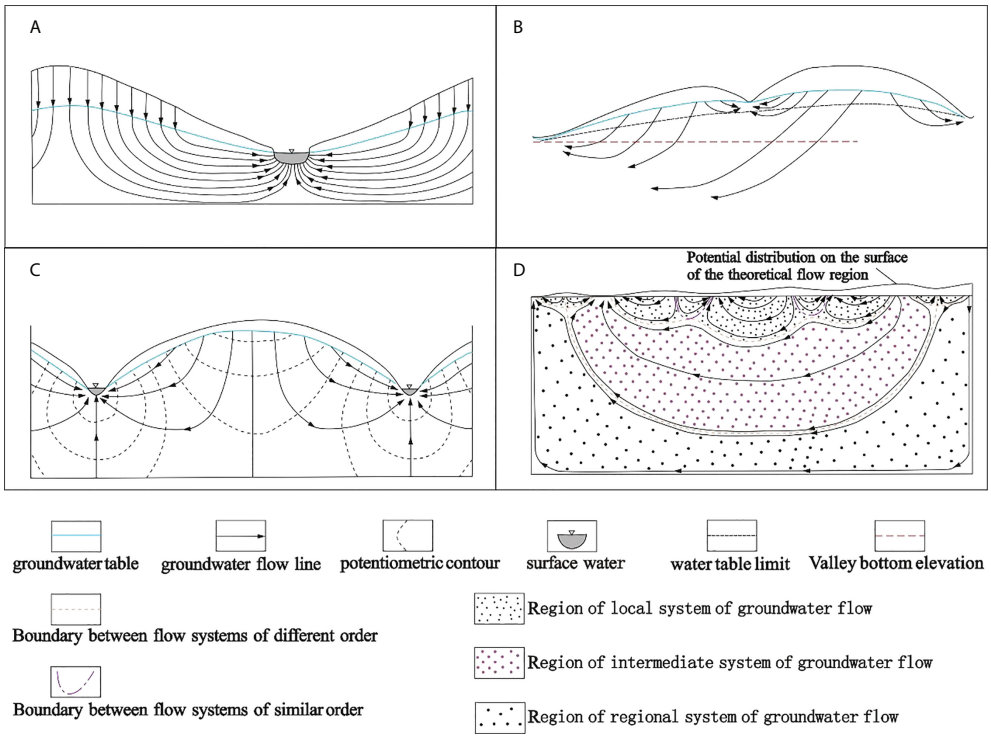

FIGURE 1
The evolution diagram of Tóthian Theory **(A)** The cross-section drawn of the gravity-driven groundwater flow by King in 1899; **(B)** A pattern of complex flow in unconfined aquifer by Fourmarier in 1939; **(C)** The groundwater flow net diagram of rivers block by Hubbert in 1940; **(D)** The use of upper head boundary for linear function and sine function superimposed conditions to conduct simulated groundwater flow field by Toth in 1963.

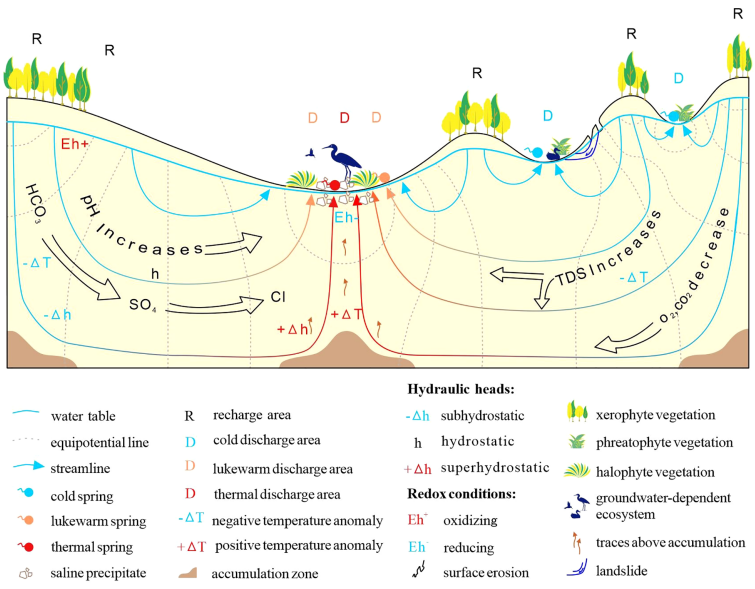

FIGURE 2
Natural conditions and phenomena due to environmental agency of flowing groundwater in drainage basin (modified after Tóth, 1999 and Tóth, 2016).

In addition to Tóth himself, other hydrogeological scholars have made continuous exploration based on Tóthian theory, which played an important role in the enrichment, development and promotion of the theory. Among them, the representative figures are Freeze and Witherspoon, Maclay, Jay, Schwartz, Engelen, Allen, Zijl, etc. Freeze and Witherspoon (1966;1967) extended the application scope of Tóthian theory from special cases to general cases through numerical methods, and explored the influence of water level and permeability coefficient on groundwater flow mode (Freeze and Witherspoon, 1966; Freeze and Witherspoon, 1967). Maclay and Winter (1967) combined Tóthian theory with the study of GCE. They found that the relative concentration of major ions in groundwater changed regularly from RA to DA. They believed that the combination of Tóthian theory and hydrochemical research could make people better understand the relationship between water quality and groundwater movement (Maclay and Winter, 1967). Lehr was one of early hydrogeological experts to carry out the indoor observation experiment of GFS. He used plexiglass to build a transparent box filled with sand and resin materials, simulated sandstone to build a hydraulic model, and clearly observed two main phenomena in the movement of groundwater: First, groundwater always moves from high head to low head and the second is the characteristics of layered movement of groundwater (Lehr, 1968). Schwartz and Domenico (1973) put forward the conceptual model of solute transport in GFS in combination with Tóthian theory, and summarized the law of groundwater evolution involved in the processes of groundwater flow (Schwartz and Domenico, 1973). Engelen and Jones (1986) participated in the compilation of the book "Developments in the Analysis of Ground Water Flow Systems" published by the International Association of Hydrological Sciences (Engelen and Jones, 1986). Later, Engelen and Kloosterman (1996) presided over the compilation of the book "Introduction to flow systems". The publication of these two books not only affirms Tóthian theory, but also extends Tóthian theory to a wider world to a great extent (Engelen and Kloosterman, 1996). In 1993, Allen et al. explored the movement law of groundwater in convergent aquifer, and the main conclusions obtained are basically the same as Tóthian theory, which further confirms the applicability of Tóthian theory (Allen T. Hjelmfelt and Pi, 1993). Zijl (1999) explored the temporal and spatial problems of GFS theory and found that Tóthian theory was also very useful in analyzing the time and space of GFS and their relationship (Zijl, 1999). Jiang et al. (2010) found that due to the attenuation of hydraulic conductivity and porosity depth, the renewal and aging of groundwater in the basin exist at the same time (Jiang et al., 2010). Tóth (2016) combed the development of groundwater flow evolution theory and believed that the current GFS had broken the traditional concept of aquifer, and most of the current GFS were non-confined cross stratum flow systems (Tóth, 2016). Zhang et al. (2020a) found that the change of salinity in groundwater DA would change the position of stagnation point in GFS, thus changing the migration law of groundwater flow (Zhang et al., 2020a). With the maturity of GFS theory, people actively apply Tóthian theory to practical hydrogeological work. For example, people in countries such as Canada, the United States, China and Japan have widely used GFS theory in hydrogeological survey and mapping, water source and sewage discharge site selection, ecosystem protection and so on; and fruitful theoretical and practical results were achieved (Cloutier et al., 2006; Palmer et al., 2006; Han et al., 2009; Tóth, 2009; Lei et al., 2012; Zhang et al., 2015; Ono et al., 2019). By means of isotopes, it was found that there was not only a recharge relationship between surface water and groundwater, but also a GFS at the bottom of the ocean (Krall et al., 2017; Xu et al., 2018b; Danish et al., 2020). This discovery further promoted the application of GFS to a broader world.

In China, Tóthian theory has also been widely concerned and applied. Chen introduced Tóthian theory into China (Chen, 1987). Wang briefly reviewed the development of Tóthian theory in the Book "Fundamentals of Hydrogeology" and fully affirmed the significance of Tóthian theory in the history of hydrogeology (Wang, 1995). Later, the book "Fundamentals of Hydrogeology" compiled by Zhang et al. fully drew lessons from Tóthian theory (Zhang et al., 2018). The book of Zhang et al. also includes the multi-level GFS observed by Liang through the GFS demonstrator (Liang et al., 2010). Based on Tóthian theory, Jiang et al. (2009; 2011; 2012b) explored the relationship between permeability coefficient and depth, the distribution law of stagnation points in GFS, the spatial division characteristics of groundwater age, etc. It was found that the permeability coefficient in regional GFS decreased exponentially with the increasing depth, which would affect the distribution of stagnation points (Jiang et al., 2009; Jiang et al., 2011; Jiang et al., 2012b). Gao et al. (2013; 2014b; 2014c) successfully observed the multistage distribution of GFS, the refraction of groundwater in aquifers with different permeabilities and the driving of heat to groundwater through simple sand trough experiment (Gao, 2013; Gao et al., 2014b; Gao et al., 2014c). In 2015, Zhang et al. translated and published Tóth's book "Gravitational Systems of Groundwater Flow", which greatly improved the systematic dissemination of Tóthian theory in China (Zhang et al., 2015). Zhao et al. (2008) and Zhang et al. (2017) respectively investigated the GFS in Ordos Basin and they found that the regional - GFS was consistent with the GFS of Tóthian theory, which provides an excellent example for the research of Tóthian theory and is of great value to the research and practical application of Tóthian theory (Zhao et al., 2008; Zhang et al., 2017). Wang et al. (2017) proposed three-dimensional groundwater circulation units and combined these units into a three-dimensional GFS to obtain the fine structure characteristics of groundwater circulation (Wang et al., 2017).

Tóthian theory breaks through the concept of aquifer and makes people realize that there is no absolute water resisting body (layer) in nature. In the huge structural unit (groundwater aquifer system or hydrogeological unit), driven by the potential energy given by the terrain of the RA and the energy difference between it and the discharge point (place), the continuously

moving groundwater flow runs in all directions of releasing energy, with low resistance and smooth flow speed. The gradient of potential energy reduction is large and so is the energy release, and vice versa (Gao et al., 2014b; Tóth, 1970; Tóth, 1978; Winter et al., 1998; Li and Hao, 1999; Tóth, 1999; Tóth, 2009; Liang et al., 2010; Jiang et al., 2011; Wang et al., 2011; Jiang et al., 2012a; Liang et al., 2013). If we combine the concept of GFS with hydrochemical methods, we can better understand the relationship between groundwater quality and movement, and better study the mechanism of GCE.

Chemical evolution of groundwater

Theoretical progress of groundwater chemical evolution

The theoretical study of GCE can be divided into two stages according to the establishment of Tóthian theory. The first stage is the study of GCE independent from Tóthian theory before 1963; The second stage is the study of GCE combined with Tóthian theory after 1963.

Before the emergence of Tóthian theory, the research on the chemical evolution of groundwater was generally limited to the aquifer, but a series of remarkable achievements were still made. For example, as early as the 1860s, geochemists established the basic principle of thermodynamic equilibrium that could be used to distinguish the types of natural water bodies (Glynn and Plummer, 2005). Early scientists believed that groundwater was partially balanced, and pH and redox conditions could reflect the ionic composition, mineral reaction and water stability of water (Korzhinskii, 1936; Krumbein and Garrels, 1952). There are many chemical classification methods for groundwater. In 1934, Schukarev took six main components in water as the basis of classification and proposed the classification method of natural water chemical analysis data, which is the most widely used classification method at present (Zhang and Zhang, 2019). In order to more conveniently represent the chemical types and characteristics of groundwater, Piper three-line diagram (1944) and Durov diagram (1948) appeared one after another. These two hydrochemical diagrams are still widely used in today's hydrochemical research. Chadha (1999) proposed a rectangular chart that could be directly classified by Excel based on the above two hydrochemical charts (Chadha, 1999). The replacement order of cations is basically determined. Magnesium is (Mg^{2+}) preferentially replaced in water containing calcium (Ca^{2+}) and Mg^{2+} The order of relative replaceability of cations in clay is as follows: Li^{+}>Na^{+}>H^{+}>K^{+}>Mg^{2+}>Ca^{2+} (Kelly, 1934; Ross, 1943). Cederstrom (1946) established a groundwater chemical model with the concept of aquifer (Cederstrom, 1946). It was found that the mineralization of groundwater in different aquifers decreased with the increase of depth. At the same time, combined with the sampling and analysis data, the groundwater near the coastal plain was divided into four zones from west to east: descending zone, hard water zone, soft water zone and high chlorine zone (Cederstrom, 1946). Back et al. (1960) proposed the concept of hydrochemical facies based on aquifer system to describe the main ions in groundwater. It was found that in shallow sediments of the North Atlantic coastal plain, the distribution ofHCO_3^- was wider thanSO_4^{2-} and Cl^-, whereas $NaCl$ was dominant in deeper sediments (Back, 1960; Back and Hanshaw, 1971b). In the 1950s, the study of groundwater isotopes began to show clues. Munnich and Vogel (1959) used the ^{14}C method to determine the age of groundwater (Munnich and Vogel, 1959). Craig (1961) established the global atmospheric precipitation linear equation $\delta D=8\delta^{18}O+10$ to trace the source of groundwater (Craig, 1961). During this period, great progress were made in the theoretical research of GCE and many of them are still used today. However, the research on GCE is still limited, and the exploration of GCE law in different stages is insufficient.

The emergence of Tóthian theory has greatly promoted the development of GCE. For example, Maclay and Winter (1967) found that the evolution sequence of main hydrochemical types of groundwater from RA to runoff area to DA: $HCO_3^- \rightarrow HCO_3^- + SO_4^{2-} \rightarrow SO_4^{2-} \rightarrow SO_4^{2-} + Cl^- \rightarrow Cl^- + SO_4^{2-} \rightarrow Cl^-$ (Maclay and Winter, 1967). Based on Tóthian Theory, Schwartz and Domenico (1973) proposed a conceptual model of solute transport in GFS, which could be defined as: the substance enters the GFS in the RA, then completes the transportation and distribution, and finally discharges in the DA; The chemical and biological effects continuously modify the dissolved substance throughout the process (as shown in Figure 3) (Schwartz and Domenico, 1973). Thorstenson put forward the concept of redox and its application in geochemistry; Then the sequence of redox reactions in GFS began to be studied (Thorstenson, 1984). Wang (1995) clearly distinguished the two concepts of aquifer system and GFS in his research, within which an ideal model diagram was proposed based on the hydrochemical evolution of GFS (as shown in Figure 4) (Wang, 1995). Due to the rapid development of computer technology, hydrogeochemical simulation based on GFS originated in the 1960s developed continuously, which played an important role in revealing the chemical evolution of groundwater. For example, the granite model proposed by Garrels and Mackenzi (1967) laid the foundation for hydrogeochemical simulation (Garrels and Mackenzie, 1967). In 1971, Back and Hanshaw (1971a) pointed out that the application of the basic principle of irreversible thermodynamics in GFS provided a theoretical basis for the construction of GCE and head distribution prediction model (Back and Hanshaw, 1971a). With the improvement of calculation level, PHREEQC began to be widely used in mass balance calculation based on hydrogen and oxygen in 1990

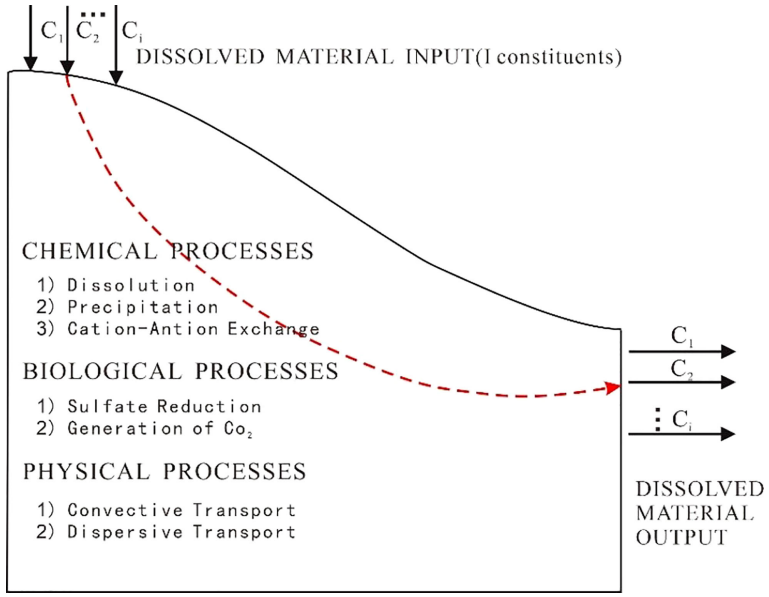

FIGURE 3
Conceptualization of mass transfer in regional groundwater flow (from Schwartz 1973).

(Wolery et al., 1990). The technology of computer greatly promoted the research of GCE theory, and provided a new research tool for this theoretical research. In particular, the emergence of hydrochemical simulation promoted the hydrochemical research from summarizing the current situations and laws to predicting gradually.

Main processes of groundwater chemical evolution based on Tóthian theory

In the local GFS which was widely distributed in the shallow part of the surface, the groundwater actively participating in the modern water cycle is discharged to the surface through short-

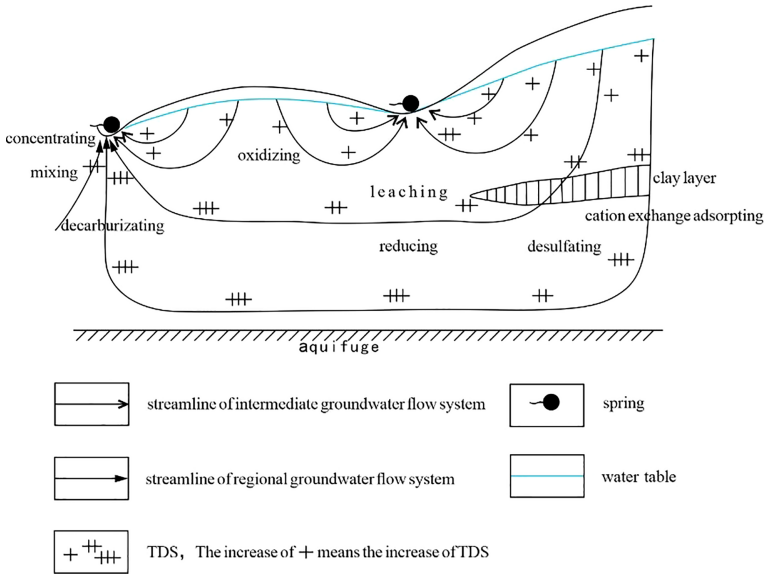

FIGURE 4
An ideal model for hydrochemical evolution of groundwater flow system (modified after Wang, 1995).

distance, shallow burial and short-time runoff, and its hydrochemical type remains unchanged in bicarbonate type, mostly fresh water with low TDS. However, the groundwater in the regional GFS needs to go through runoff with long distance, deep burial and long time, and the hydrochemical type of groundwater gradually evolves. For example, the transformation from HCO_3^- type to SO_4^{2-} type and then to Cl^- type mainly goes through certain evolution paths (as shown in Figure 5) (Li, 1991; Liang et al., 1991; Tóth, 1999; Chen et al., 2010; Liu et al., 2010; Jiang, 2013).

The chemical types of groundwater change with time, and vary from place to place. It is generally considered that groundwater experiences such actions as ion alternating adsorption, precipitation and dissolution of salt substances, microorganisms such as desulfurization bacteria and nitrifying bacteria participate in the action, and groundwater undergoes redox reaction, etc. (Gao et al., 2019; Chen et al., 2020a; Gao et al., 2020; Xia et al., 2020). The main evolution form of cations in groundwater are shown in Figure 6. In the RA, atmospheric precipitation enters the GFS through the aeration zone. In this process, leaching first occurs. Ca^{2+}, Mg^{2+}, Na^+ in soil or rock are dissolved into groundwater. Due to the low content of CO_2 in the RA and high content of TDS in atmospheric precipitation in the RA, the dissolution of Ca^{2+}, Mg^{2+} in this period is greater than Na^+. In the runoff area, with the migration of groundwater, TDS continues to increase and the content of CO_2 decreases, along with the decrease of the solubility of Ca^{2+} and Mg^{2+}, and the solubility of Na^+ changes little. At the same time, Ca^{2+}. and Mg^{2+} in groundwater exchange and adsorb with Na^+ in surrounding geological bodies, so that the content of Ca^{2+} and Mg^{2+} in groundwater in the runoff area can either be greater or smaller than Na^+. The TDS of groundwater in the DA continues to increase, the water pressure decreases during the discharge process, Ca^{2+} and Mg^{2+} precipitate, and Na^+ continues to dissolve. Finally, the Na^+ content in groundwar is greater than Ca^{2+} and Mg^{2+} (Ren et al., 2014; Wang, 1995; Zhang et al., 2015).

The evolution form of anions in GFS can be shown in Figure 7. In the local GFS, the groundwater actively participating in the modern water cycle is discharged to the surface through short-distance, shallow burial and short-time runoff, and its hydrochemical type remains unchanged in HCO_3^- type, characterized by low TDS of most fresh water. However, the groundwater in the regional GFS needs to go through long-distance, deep burial and long-time runoff, and the hydrochemical type of groundwater gradually evolves from HCO_3^- type to SO_4^{2-} type and then to Cl^- type (Wang, 1995; Ren et al., 2014; Zhang et al., 2018). When the RA is dominated by limestone and dolomite, the main chemical reactions are (Zhang et al., 2018):

$$① \quad CaCO_3 + H_2O + CO_2 \rightarrow 2HCO_3^- + Ca^{2+} \quad ;$$

$$② \quad MgCO_3 + H_2O + CO_2 \rightarrow 2HCO_3^- + Mg^{2+} \quad ;$$

When the RA is dominated by albite and calciclase, the main chemical reactions are:

$$③ \quad Na_2Al_2Si_6O_6 + 2CO_2 + 3H_2O \rightarrow 2HCO_3^- + 2Na^+ + H_4Al_2Si_2O_4 + 4SiO_4 \quad ;$$

$$④ \quad CaO \cdot Al_2O_3 \cdot 2SiO_2 + 2CO_2 + 3H_2O \rightarrow 2HCO_3^- + Ca^{2+} + H_4Al_2Si_2O_9 \quad ;$$

Main chemical reactions in RA:

$$⑤ \quad CaSO_4 \cdot 2H_2O \rightarrow Ca^{2+} + SO_4^{2-} + 2H_2O \quad ;$$

$$⑥ \quad FeS_2 + 7O_2 + 2H_2O \rightarrow 2FeSO_4 + 4H^+ + 2SO_4^{2-} \quad \text{(oxidation environment)}$$

Main chemical reactions in the DA:

$$⑦ \quad SO_4^{2-} + 2C + 2H_2O \rightarrow H_2S + 2HCO_3^- \quad \text{(reducing environment)}$$

New theories and methods of groundwater chemical evolution

In the current situation of increasingly serious water pollution caused by the development of industry and

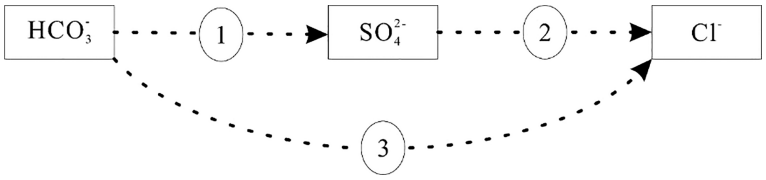

FIGURE 5
Three paths of groundwater chemical evolution.

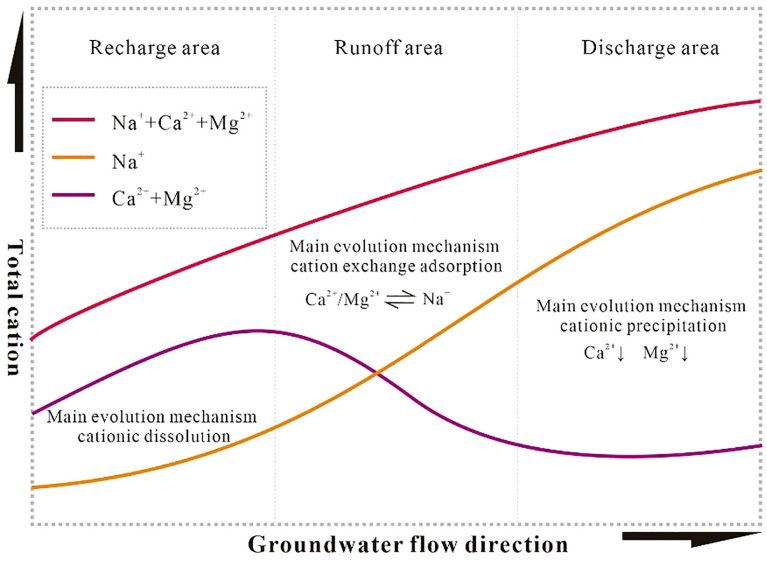

FIGURE 6
Schematic diagram of cation evolution in groundwater flow system.

agriculture, the traditional groundwater theories are facing enormous challenges. Therefore, new theories and wider research range related to groundwater arise. Due to the rapid development of computer level, the innovation of new testing methods like isotopic methods, the hydrogeochemical analysis has become more and more convenient and effective.

New theories of groundwater chemical evolution

(1) The reverse cation exchange mechanism has been gradually revealed. Monsoon climate (Kumar et al., 2009), environmental pollution (Reddy et al., 2012; Guma et al., 2021), water acidification (Zaidi et al., 2015), seawater intrusion (Chen et al., 2020b; Roy and Zahid, 2021) and other problems may become the trigger mechanism of the reverse cation exchange process. Through leaching experiment, David and Dimitrios (2002) found that when the soil leaching time reached 15-100h, reverse cation exchange occurred (David and Dimitrios, 2002). Reverse cation exchange can reduce the content of Ca^{2+} and increase the content of Na^{+} in groundwater (Askri, 2015), which can be expressed as: $Ca^{2+}(Mg^{2+})$−water+$2Na^{+}$−clay=$2Na^{+}$−water+$Ca^{2+}(Mg^{2+})$−clay (Chen et al., 2020b).

(2) The content of NO_3^- in groundwater increased significantly, and the traditional GCE theory encountered new challenges. Since the mid-20th century, nitrogen fertilizer has been widely used in agricultural production, resulting in the continuous increase of NO_3^-/Cl^- content in groundwater in agricultural areas (Abascal et al., 2021) and affecting hydrochemical types (Xu et al., 2018a). In some areas, nitric acid water has appeared (Zhou and Zhu, 2014). The entry of NO_3^- into groundwater triggered a series of chemical reactions (Mahaqi et al., 2021), which changed the original chemical evolution of groundwater to a great extent (Zaryab et al., 2022; Zhang et al., 2022). For example, the nitrate could be eliminated from nitrate-polluted groundwater by this chemical reaction: 5 CH_2O + 4 NO_3^- = $2N_2$ + $4HCO_3^-$ + CO_2+$3H_2O$ (Mahaqi et al., 2021). There is a strong correlation between NO_3^- and Cl^-, and denitrification occurs when the ratio of NO_3^-/Cl^- decreases (Rezaei et al., 2017; Su et al., 2020). NO_3^- content was negatively correlated with pH and Mn^{2+}, and positively correlated with ORP (Oxidation-Reduction Potential) (Cong et al., 2021; Gómez et al., 2002). Nitrogen cycle will affect the migration and transformation of arsenic (As) and iron (Fe) (Gao et al., 2021b; Smith et al., 2017)

(3) The atmosphere is providing more Cl^- for groundwater, resulting in significant changes in the hydrochemical type. Cl^- in groundwater mainly comes from precipitation and salt dissolution (Zhang et al., 2018). With the growth of runoff path, Cl^- in groundwater gradually occupies a dominant position (He et al., 2011). As mentioned above, most of the groundwater in the vadose zone is HCO_3^- type r and Cl^- type in

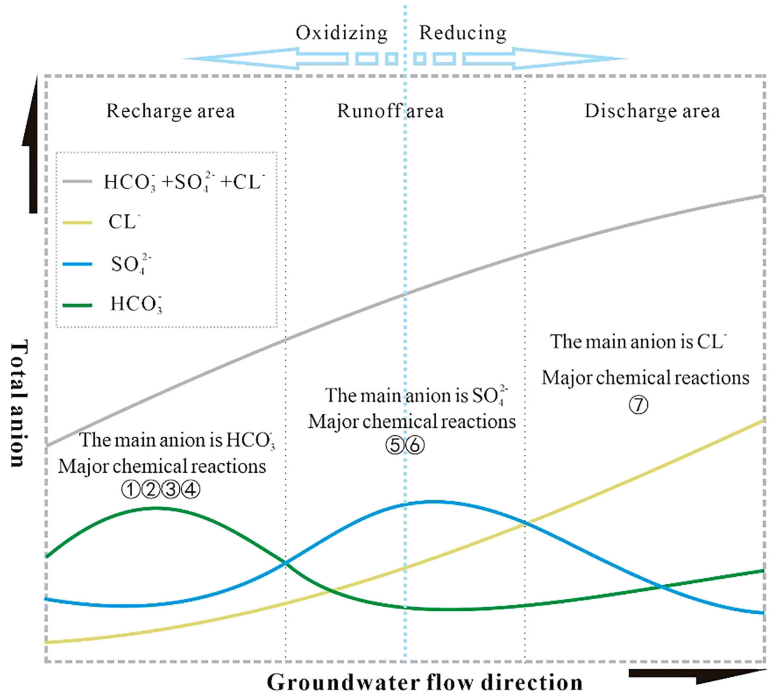

FIGURE 7
Schematic diagram of anion evolution in groundwater flow system.

the DA. However, with the intensification of industrial pollution, the concentration of Cl^- in the atmosphere increases due to the massive emission or discharge of chlorinated compounds, and the Cl^- supplied to the groundwater through rainfall continues to increase, which makes the groundwater in the vadose zone in some areas only present a Cl^- type. For example, it's found that Cl^- of the groundwater in vadose zones in some valleys may come from the atmosphere rather than geological bodies (Gardner et al., 2020). In some coastal areas, the initial type of groundwater may also show Cl^- type due to the influence of seawater aerosol (Gao et al., 2017).

(4) The research on the migration and transformation mechanism of heavy metals in groundwater has attracted more and more attention. With the rapid development of urbanization and industrialization, there are many forms of heavy metal pollution worldwide. The migration and transformation mechanism of heavy metals in groundwater have attracted extensive attention (Adimalla, 2019). For example, in recent years, scientists have found that the increase of Cl^- concentration is conducive to the migration of Mn^{2+} , and seawater intrusion can promote the release of Mn^{2+} from rocks to groundwater and enrich Mn^{2+} in groundwater (Russak et al., 2016; Gao et al., 2021a). Fe and Mn^{2+} ions can form complexes with other anions in groundwater to increase the dissolution of As (Zhang et al., 2020b). Natural colloids are conducive to the diffusion of heavy metal ions (Cai et al., 2016), and low pH conditions are more conducive to the dissolution of heavy metals (Jacques et al., 2008).

New methods of groundwater chemical evolution

(1) More isotopes and isotope models are involved in the study of hydrochemical evolution.

In addition to the traditional ^{14}C, ^{3}H and ^{18}O isotopes widely used in groundwater traceability analysis (Craig, 1961; Zhang et al., 2006), isotopes such as ^{32}Si, ^{37}Ar, ^{85}Kr, ^{87}Sr, ^{226}Ra and ^{222}Rn are gaining more and more popularity in terms of groundwater source and age analysis (Knies et al., 2000; Bauer et al., 2001; Krall et al., 2017; Danish et al., 2020; Seltzer et al., 2021), which makes the research on GCE more diversified. Isotope mixing model and Bayesian mixing model are also widely used in the identification of pollutants and the calculation of pollutant contribution rate (Zhang et al., 2022).

(2) Groundwater simulation is gradually moving towards artificial intelligence based on big data.

The traditional hydrogeochemical software such as MINTEQA2, WATEQ, Netpath, EQ3/6 and PHREEQC/QE are constantly upgraded (Zhang and Zhang, 2019), and the functions of groundwater flow numerical simulation software such as GMS, MODFLOW and FEFLOW are more and more perfect (Li et al., 2021; Liu et al., 2022a). Neural network learning, deep learning and machine learning based on big data have been widely applied to solve the problem of high-dimensional uncertain GCE (Mo, 2019; El Bilali et al., 2021). For example, Liu et al. (2022) explored the low-temperature hydrogeological process of frozen soil environment through three-dimensional numerical simulation (Liu et al., 2022b). Meanwhile, it is a significant trend that big data models were employed to study the groundwater pollution. Podgorski and Berg created a global prediction map of groundwater arsenic exceeding 10 mg/L using a random forest machine-learning model based on geospatial environmental parameters and more than 50,000 aggregated data points of measured groundwater arsenic concentration (Podgorski and Berg, 2020). Keesari et al. studied big data and environmental sustainability based integrated framework for isotope hydrology applications in India (Keesari et al., 2021). Correa et al. proposed and Embedded Edge-processing IoT-based Water Quality Monitoring system for the sake of proper decision-making (Correa et al., 2022). Wang et al. applied more than 4600 water samples for the artificial neural network to predict genesis, occurrence and distribution of high iodine groundwater in China (Wang et al., 2022). Using the similar method to Wang et al. (2022), Cao et al. predicted geogenic groundwater fluoride contamination throughout China (Cao et al., 2022). Xiong et al. (2022) applied machine learning to optimize the groundwater pollution monitoring network (Xiong et al., 2022). It is also noted that geological big data sharing service has received great attention from the governments. For example, the British Geological Survey, supported by the British government, is the first country to build the geological database and they are at the forefront of sharing data worldwide through a comprehensive system in this decade (Normile, 2019; Wen et al., 2021). In China, the Chinese Geological Survey also shows the sharing attitude by developing and opening a geological database called "GeoCloud", within which a wealth of groundwater data was accessible (Lei et al., 2021). By sharing the groundwater database between different regions, hydrologists can use different types of databases from similar geological background for reference and achieve comparative results of GFS and GCE (Normile, 2019).

In short summary, implementation of big-data methodology in terms of isotope hydrology, water pollution and environmental sustainability has drawn more and more attention. The connected and sharing geological database throughout China or other regions in the world makes it more convenient to carry out big-data based groundwater research.

Conclusion

From Darcy's Law (1856) to GFS theory (1963), then to Tóthian theory (2016), scientists have been exploring the flow law of water for more than 160 years and will continue to do so. In the more than 50 years since the establishment of GFS force theory to finally become Tóthian theory, its connotation has been gradually enriched through the continuous development, enrichment and practice of many hydrogeologists. Tóthian theory mainly covers the distribution and driving mechanism of GFS, the transmission and distribution of matter and energy by GFS, the interaction between groundwater and environment, and the environment associated phenomena brought by groundwater. Tóthian theory is a milestone in the history of hydrogeology, which breaks the concept of aquifer and promotes the development of hydrogeology from small-scale homogeneous basin to large-scale heterogeneous basin. As a universal geological agent, the environmental effect of groundwater is gradually accepted by people. With the progresses of science and technology, the research scopes of GFS have been extended from the original saturated zone to the non-saturated zone, realizing the leap from two-dimensional space to three-dimensional space, and describing the structural characteristics of GFS more finely.

The research on the mechanism of GCE based on GFS theory and Tóthian theory have promoted each other and grown together in the past 50 years. People have mastered some general laws of GCE, such as: (1) the replacement order of cations in the process of cation exchange adsorption, (2) the main water rock reactions and the main hydrochemical types in the RA, runoff area and DA under different geological backgrounds, (3) horizontal zoning of GCE. (4) in GFS, groundwater TDS generally increases from RA to DA, (5) sources of groundwater in GFSs in different regions, (6) location and sequence of redox reaction. With the expansion of the research scopes of GFS to the unsaturated zone, soil microorganisms and CO_2 have become a research hotspot in the study of GCE. The maturity of traditional isotopic methods and the addition of new isotopes have greatly improved the reliability of the research conclusion of hydrochemical evolution. The maturity of hydrochemical evolution software and the application of neural network learning and deep learning have solved the high-dimensional uncertainty problem.

With the deepening of theoretical research, more and more scientists are aware of the interaction between the distribution of GFS and GCE. The theoretical problems of GFS and the research of GCE are interdependent and inseparable. In order to better deal with the problems of GFS distribution change, GCE environment change and groundwater pollution caused by the further intensification of human transformation of nature in the 21st century, it is also a difficult problem for hydrogeologists to comprehensively use the scientific research results of Tóthian

theory and GCE mechanism to promote the harmonious coexistence between man and nature.

Author contributions

HD, original draft preparation, software, and visualization. ZG, review. All authors contributed to the article and approved the submitted version.

Funding

This review was supported by the Natural Science Foundation of Shandong Province (ZR2020MD109); National Natural Science Foundation of China (40772145, 41641022).

Conflict of interest

The authors declare that the research was conducted in the absence of any commercial or financial relationships that could be construed as a potential conflict of interest.

Publisher's note

References

Abascal, E., Gómez-Coma, L., Ortiz, I., and Ortiz, A. (2021). Global diagnosis of nitrate pollution in groundwater and review of removal technologies. *Sci. Total Environ.* 810, 152233. doi: 10.1016/j.scitotenv.2021.152233

Adimalla, N. (2019). Heavy metals contamination in urban surface soils of medak province, India, and its risk assessment and spatial distribution. *Environ. Geochem. Health*42 (1), 59–75. doi: 10.1007/s10653-019-00270-1

Allen T. Hjelmfelt, J., and Pi, Z. (1993). Movement of ground water in converging aquifer. *J. Irrig. Drain. Eng.*119 (2), 312–322. doi: 10.1061/(ASCE)0733-9437(1993)119:2(312)

Askri, B. (2015). Hydrochemical processes regulating groundwater quality in the coastal plain of al musanaah, sultanate of oman. *J. Afr. Earth Sci.*106, 87–98. doi: 10.1016/j.jafrearsci.2015.03.009

Back, W. (1960). Hydrochemical Facies and Ground-Water Flow Patterns in Northern Atlantic Coastal Plain: ABSTRACT. *AAPG Bulletin*, 44(7), 1244–1245.

Back, W., and Hanshaw, B. B. (1971a). Geochemical interpretations of groundwater flow systems. *J. Am. Water Resour. Assoc.*7 (5), 1008–1016. doi: 10.1111/j.1752-1688.1971.tb05021.x

Back, W., and Hanshaw, B. B. (1971b). *Rates of Physical and Chemical Processes in a Carbonate Aquifer* Washington:American Chemical Society. doi: 10.1021/ba-1971-0106.ch003

Bauer, S., Fulda, C., and Schäfer, W. (2001). A multi-tracer study in a shallow aquifer using age dating tracers 3H, 85Kr, CFC-113 and SF6 — indication for retarded transport of CFC-113. *J. Hydrol.*248 (1), 14–34. doi: 10.1016/S0022-1694(01)00381-X

Cai, L., Peng, S., Wu, D., and Tong, M. (2016). Effect of different-sized colloids on the transport and deposition of titanium dioxide nanoparticles in quartz sand. *Environ. pollut.*208 (JAN.PT.B), 637–644. doi: 10.1016/j.envpol.2015.10.040

Cao, H. L., Xie, X. J., Wang, Y. X., and Liu, H. X. (2022). Predicting geogenic groundwater fluoride contamination throughout China. *J. Environ. Sci.*115, 140–148. doi: 10.1016/j.jes.2021.07.005

Cederstrom, D. J. (1946). Genesis of ground waters in the coastal plain of Virginia. *Econ. Geol.*41 (3), 218–245. doi: 10.2113/gsecongeo.41.3.218

Chadha, D. K. (1999). A proposed new diagram for geochemical classification of natural waters and interpretation of chemical data. *Hydrogeol. J.*7 (5), 431–439. doi: 10.1007/s100400050216

Chamberlin, T. C. (1885). *U.S. Geol. Survey Annual Report*. 5, 131–175, U.S. Geological Survey, Washington.

Chen, M. (1987). *Study on groundwater resources and groundwater system* (Changchun: Editorial Committee of Journal of Changchun Institute of Geology).

Chen, Q., Hao, D. H., Gao, Z. J., Shi, M. J., Wang, M., Feng, J .G., et al. (2020a). The enrichment process of groundwater fluorine in sea water intrusion area of gaomi city, china. *Ground Water*58 (6), 882–891. doi: 10.1111/gwat.12990

Chen, Q., Jia, C. P., and Wei, J. C. (2020b). Geochemical process of groundwater fluoride evolution along global coastal plains: Evidence from the comparison in seawater intrusion area and soil salinization area. *Chem. Geol.*552, 119779. doi: 10.1016/j.chemgeo.2020.119779

Chen, Z., Wang, Y., Liu, J., and Wei, W. (2010). Evolution characteristics of groundwater in typical areas of northern China in recent 50 years. *Quat. Sci.*30 (01), 115–126. doi: 10.3969/j.issn.1001-7410.2010.01.11

Cloutier, V., Lefebvre, R., Savard, M. M., Bourque, É., and Therrien, R. (2006). Hydrogeochemistry and groundwater origin of the basses-laurentides sedimentary rock aquifer system, st. lawrence lowlands, québec, canada. *Hydrogeol. J.*14 (4). doi: 10.1007/s10040-005-0002-3

Cong, X., Zhang, S. S., Xu, Z. H., Xu, L. R., and Pan, W. Y. (2021). Spatio-temporal variation and driving factors of "three nitrogen"in shallow groundwater in typical over-exploited areas in north china. *Earth Environ.*49 (06), 603–614. doi: 10.14050/j.cnki.1672-9250.2021.49.051

Correa, C., Dujovne, D., and Bolano, F. (2022). *Design and implementation of an Embedded Edge-processing Water Quality Monitoring System for underground waters*. IEEE Embedded Systems Letters, 1.

Craig, H. (1961). Isotopic variations in meteoric waters. *Science*133, 1702–1703. doi: 10.1126/science.133.3465.1702

Danish, M., Tripathy, G. R., and Rahaman, W. (2020). Submarine groundwater discharge to a tropical coastal lagoon (Chilika lagoon, india): An estimation using Sr isotopes. *Mar. Chem.*224 (C). doi: 10.1016/j.marchem.2020.103816

Darcy, H. (1857). *Recherches expérimentales relatives au mouvement de l'eau dans les tuyaux* (Paris, France: Mallet-Bachelier).

David, R., and Dimitrios, P. (2002). Diffusion and cation exchange during the reclamation of saline-structured soils. *Geoderma*107 (3), 271–279. doi: 10.1016/S0016-7061(01)00152-5

El Bilali, A., Taleb, A., and Brouziyne, Y. (2021). Comparing four machine learning model performances in forecasting the alluvial aquifer level in a semi-arid region. *J. Afr. Earth Sci.*181, 104244. doi: 10.1016/j.jafrearsci.2021.104244

Engelen, G. B., and Jones, G. P. (1986). *Developments in the analysis of groundwater flow systems* (IAHS).

Engelen, G. B., and Kloosterman, F. H. (1996). *Introduction to flow systems* (Springer Netherlands).

Freeze, R. A., and Witherspoon, P. A. (1966). Theoretical analysis of regional groundwater flow: 1. analytical and numerical solutions to the mathematical model. *Water Resour. Res.*2 (4).doi: 10.1029/WR002i004p00641

Freeze, R. A., and Witherspoon, P. A. (1967). Theoretical analysis of regional groundwater flow: 2. effect of water-table configuration and subsurface permeability variation. *Water Resour. Res.* 3 (2). doi: 10.1029/wr003i002p00623

Gao, Z. (2013). Experimental demonstration and significance of groundwater flow system differentiation. *J. Shandong Univ. Sci. Technol.*32 (02), 17–24. doi: 10.16452/j.cnki.sdkjzk.2013.02.020

Gao, Y., Chen, J., Qian, H., Wang, H., Ren, W., and Qu, W. (2022). Hydrogeochemical characteristics and processes of groundwater in an over

2260year irrigation district: a comparison between irrigated and nonirrigated areas. *J. Hydrol.*606, 127437. doi: 10.1016/j.jhydrol.2022.127437

Gao, Z., Zhang, F., An, Y., Feng, J., Wang, M., Han, K., et al. (2014a). The Formation and model of highly-concentrated fluorite groundwater and in-situ fluoride dispelling assumption in Gaomi City of Shandong Province. *Earth Science Frontiers (China University of Geosciences (Beijing); Peking University)* 21 (4), 50–58. doi: 10.13745/j.esf.2014.04.005

Gao, Z., Wang, S., Li, J., Zhu, X., and Zheng, Q. (2014b). Study on difference of groundwater movement in seepage flow field based on experiment sand tank. *J. OF China Hydrol.* 34 (01), 14–19+13. doi: 10.3969/j.issn.1000-0852.2014.01.003

Gao, Z., Wang, S., Xu, C., Dong, H., and Zheng, Q. (2014c). A study of the discharge controlling the differentiation of groundwater flow systems. *Hydrogeol. & Eng. Geol.* 41 (04), 6–10. doi: 10.16030/j.cnki.issn.1000-3665.2014.04.005

Gao, Z., Xu, H., Zhang, P., Ji, D., Xia, L., Wang, X., et al. (2020). Variations in bacterial community structures during geothermal water recharge-induced bioclogging. *J. Environ. Sci. Health Part a-Tox./Hazard. Subst. Environ. Eng.* 55 (5), 629–637. doi: 10.1080/10934529.2020.1724744

Gao, Z., Wang, Z., Wang, S., Fu, T., and Liu, W. (2021a). Characteristics of heavy metals and health risk assessment of groundwater in tianjin coastal area. *Mar. Environ. Sci.* 40 (03), 384–391. doi: 10.13634/j.cnki.mes.2021.03.008

Gao, C., Feng, C., Liu, W., Ji, A., Yoshihiro, K., and Iwao, K. (2014). Patterns of arsenic cycle and groundwater arsenic contamination on the earth's surface. *Acta Geosci. Sin.*35 (06), 741–750. doi: 10.3975/cagsb.2014.06.10

Gao, Y., Qian, H., Ren, W., Wang, H., Liu, F., and Yang, F. (2020). Hydrogeochemical characterization and quality assessment of groundwater based on integrated-weight water quality index in a concentrated urban area. *J. Cleaner Production*260, 121006. doi: 10.1016/j.jclepro.2020.121006

Gao, Z., Sun, Z., Yang, Y., Mou, L., and CUI, Y. (2019). Occurrence characteristics and hydrochemical characteristics of geothermal water in shandong province. *Sci. Technol. Eng.* 19 (20), 85–90. doi: 10.3969/j.issn.1671-1815.2019.20.012

Gao, Z., Weng, H., and Guo, H. (2021b). Unraveling influences of nitrogen cycling on arsenic enrichment in groundwater from the hetao basin using geochemical and multi-isotopic approaches. *J. Hydrol.*595, 125981. doi: 10.1016/j.jhydrol.2021.125981

Gao, Z., Zhang, H., Sun, M., Xu, H., and Yao, D. (2017). The chemical characteristics and causes of shallow groundwater in the Rizhao coastal area of Shandong province are discussed. *Ground Water*39 (04), 1–4. doi: 10.3969/j.issn.1004-1184.2017.04.001

Gardner, P. M., Nelson, N. C., Heilweil, V. M., Solder, J. E., and Solomon, D. K. (2020). Rethinking a groundwater flow system using a multiple-tracer geochemical approach: A case study in moab-Spanish valley, Utah. *J. Hydrol.*590, 125512. doi: 10.1016/j.jhydrol.2020.125512

Garrels, R. M., and Mackenzie, F. T. (1967). Origin of the chemical compositions of some springs and lakes. *Equilib. Concepts Natural Water Systems.* doi: 10.1021/ba-1967-0067.ch010

Glynn, P. D., and Plummer, L. N. (2005). Geochemistry and the understanding of ground-water systems. *Hydrogeol. J.*13 (1), 263–287. doi: 10.1007/s10040-004-0429-y

Gómez, M. A., Hontoria, E., and González-López, J. (2002). Effect of dissolved oxygen concentration on nitrate removal from groundwater using a denitrifying submerged filter. *J. Hazard. Mater.*90, 267–278. doi: 10.1016/S0304-3894(01)00353-3

Guma, B. E., Muwanga, A., and Owor, M. (2021). Hydrogeochemical evolution and contamination of groundwater in the albertine graben, Uganda. *Environ. Earth Sci.*80 (8). doi: 10.1007/s12665-021-09587-6

Han, D., Liang, X., Jin, M., Currell, M., Han, Y., Song, X., et al. (2009). Hydrogeochemical indicators of groundwater flow systems in the yangwu river alluvial fan, xinzhou basin, shanxi, china. *Environ. Manage.*44 (2). doi: 10.1007/s00267-009-9301-0

Hao, Y., Wang, P., Zhang, M., Zhang, J., and Li, D. (2020). Hydrochemical characteristic and its driving force of groundwater in the covered karst in pearl river basin ecology and environmental sciences 29, 02, 337–344. doi: 10.16258/j.cnki.1674-5906.2020.02.015

He, J., Zhang, J., Ding, Z., and Ma, J. (2011). Evolution of groundwater geochemistry in the minqin basin: taking chloride as an indicator of groundwater recharge. *Resour. Sci.*33 (3), 416–421. doi: 10.1007/s12182-011-0123-3

Hubbert, M. K. (1940). The theory of ground-water motion. *J. Geol.* 48 (8, Part 1), 785–944. doi: 10.1097/00010694-194105000-00015

Imbulana, S., Oguma, K., and Takizawa, S. (2020). Evaluation of groundwater quality and reverse osmosis water treatment plants in the endemic areas of chronic kidney disease of unknown etiology (ckdu) in sri lanka. *Sci. Total Environ.*745 (3), 140716. doi: 10.1016/j.scitotenv.2020.140716

Jacques, D., SimuNek, J., Mallants, D., and Genuchten, M. (2008). Modelling coupled water flow, solute transport and geochemical reactions affecting heavy metal migration in a podzol soil. *Geoderma*145 (3-4), 449–461. doi: 10.1016/j.geoderma.2008.01.009

Jia, H., Ken, H., and Qian, H. (2020). Use of multiple isotopic and chemical tracers to identify sources of nitrate in shallow groundwaters along the northern slope of the qinling mountains, china. *Appl. Geochem.*113, 104512. doi: 10.1016/j.apgeochem.2019.104512

Jiang, X. (2013). *A review of regional groundwater flow theory* (Beijing: Geological Publishing House).

Jiang, X., Wan, L., Ge, S., Cao, G., Hou, G., Hu, F., et al. (2012a). A quantitative study on accumulation of age mass around stagnation points in nested flow systems. *Water Resour. Res.* 48 (12), W12502. doi: 10.1029/2012WR012509

Jiang, X., Wan, L., Cardenas, M. B., Ge, S., and Wang, X. (2010). Simultaneous rejuvenation and aging of groundwater in basins due to depth-decaying hydraulic conductivity and porosity. *Geophys. Res. Lett.*37 (5). doi: 10.1029/2010GL042387

Jiang, X., Wan, L., and Ge, S. (2011). An analytical study on stagnant points in nested flow systems in basins with depth-decaying hydraulic conductivity. *Water Resour. Res.*47 (1), 128–139. doi: 10.1029/2010WR009346

Jiang, X., Wan, L., Wang, X., Ge, S., and Liu, J. (2009). Effect of exponential decay in hydraulic conductivity with depth on regional groundwater flow. *Geophys. Res. Lett.*36 (24). doi: 10.1029/2009GL041251

Jiang, X., Wan, L., Wang, X., and Li, H. (2012b). Distribution of groundwater age in drainage basins. *Hydrogeol. & Eng. geol.*39 (04), 1–6. doi: 10.16030/j.cnki.issn.1000-3665.2012.04.014

Jia, H., Qian, H., Zheng, L., Feng, W., Wang, H., and Gao, Y. (2020). Alterations to groundwater chemistry due to modern water transfer for irrigation over decades. *Sci. Total Environ.*717, 137170. doi: 10.1016/j.scitotenv.2020.137170

Judit, M.-S., and Tóth, A. (2015). Basin-scale conceptual groundwater flow model for an unconfined and confined thick carbonate region. *Hydrogeol. J.*23 (7), 1–22. doi: 10.1007/s10040-015-1274-x

Kaur, G., Sharma, S., and Garg, U. K. (2019). Assessment of ground water contamination by inorganic impurities in ferozepur district of punjab state, India. *Asian J. Chem.*31 (3), 515–521. doi: 10.14233/ajchem.2019.21601

Keesari, T., Goyal, M. K., Gupta, B., Kumar, N., Roy, A., Sinha, U. K., et al. (2021). Big data and environmental sustainability based integrated framework for isotope hydrology applications in India. *Environ. Technol. Innovation*24, 101889. doi: 10.1016/j.eti.2021.101889

Kelly, W. P. (1934). Base exchange in relation to composition of clay with special reference to effect of sea water. *Bull. Amer. Assoc. Petrol. Geol.*18 (3), 358–367. doi: 10.2110/pec.55.04.0454

Knies, D. L., Grabowski, K. S., Hubler, G. K. Jr., , D., Deturck, T. M., Mignerey, A. C., et al. (2000). Determination of 32Si by AMS at the US naval research laboratory. *Nucl. Instrum. Methods Phys. Res.*172 (1), 321–327. doi: 10.1016/S0168-583X(00)00378-5

Korzhinskii, D. (1936). Mobility and inertia of components in metasomatism (in Russian). *Izv. AN USSR Ser. Geol*1 (1), 35–60.

Krall, L., Trezzi, G., Garcia-Orellana, J., Rodellas, V., Morth, C. M., Andersson, P., et al. (2019). Submarine groundwater discharge at forsmark, gulf of bothnia, provided by Ra isotopes. *Mar. Chem.* 196, 162–172. doi: 10.1016/j.marchem.2017.09.003

Krumbein, W. C., and Garrels, R. M. (1952). Origin and classification of chemical sediments in terms of pH and oxidation–reduction potentials. *J. Geol*60, 1–30. doi: 10.1086/625929

Kumar, M., Kumari, K., Singh, U. K., and Ramanathan, A. L. (2009). Hydrogeochemical processes in the groundwater environment of muktsar, punjab: conventional graphical and multivariate statistical approach. *Environ. Geol.*57 (4), 873–884. doi: 10.1007/s00254-008-1367-0

Lehr, J. H. (1968). Ground water movement. *Am. Water Works Assoc.*60, 281–285. doi: 10.1002/j.1551-8833.1968.tb03545.x

Lei, C. Y., Liu, Z. X., Wang, B., Fan, M., Xie, H. Y., and Yin, X. K. (2021). Research on geological big data sharing service under the background of "Internet plus. *Natural Resource Econ. China*11, 22–27. doi: 10.19676/j.cnki.1672-6995.000626

Lei, J., Zhang, L., Deng, Y., and Huang, Z. (2012). Research on utilization and protection of groundwater resources in Yangtze river basin. *Yangtze River*43 (03), 48–51. doi: 10.16232/j.cnki.1001-4179.2012.03.004

Li, W. (1991). Origin of deep fresh groundwater and shallow saline groundwater in the minming basin gansu province. *Geol Rev.*37 (06), 546–554. doi: 10.16509/j.georeview.1991.06.007

Liang, X., Liu, Y., Jin, M., Lu, X., and Zhang, R. (2010). Direct observation of complex tothian groundwater flow systems in the laboratory. *Hydrol. Processes.* doi: 10.1002/hyp.7758

Liang, X., Quan, D., Jin, M., Liu, Y., and Zhang, R. (2013). Numerical simulation of groundwater flow patterns using flux as upper boundary. *Hydrol. Processes*27 (24), 3475–3483. doi: 10.1002/hyp.9477

Liang, X., Sun, L., Zhao, F., and Li, Z. (1991). The study of groundwater quality problem based on the groundwater flow system theory. *Earth Sci. -J. China Univ. Geosci.*16 (01), 43–50.

Liang, X., Zhang, R., Niu, H., Jin, M., and SUN, R. (2012). Development of the theory and research method of groundwater flow system. *Geol Sci. Technol. Inf.*031 (005), 143–151.

Li, W., and Hao, A. (1999). Formation and evolution model of groundwater in inland arid basins in northwest china and its significance. *Hydrogeol. Eng. Geol.*26 (04), 30–34. doi: 10.16030/j.cnki.issn.1000-3665.1999.04.009

Liu, L., Chen, J., Niu, H., Li, L., and Yin, L. (2022a). Numerical simulation of three-dimensional soil-groundwater coupled chromium contamination based on FEFLOW. *Hydrogeol. Eng. Geol.* 49 (01), 164–174. doi: 10.16030/j.cnki.issn.1000-3665.202102008

Liu, W., Fortier, R., Molson, J., and Lemieux, J. (2022b). Three-dimensional numerical modeling of cryo-hydrogeological processes in a river-talik system in a continuous permafrost environment. *Water Resour. Res.*58 (3). doi: 10.1029/2021WR031630

Liu, Y., Liang, X., Quan, D., and Jin, M. (2010). Experiments of groundwater flow patterns under changes of infiltration intensity. *Earth Sci. Front.*17 (06), 111–116.

Li, Y., Zhang, Q., Li, J., and Wang, Y. (2021). Overview of research on visual modflow and gms. *Yellow River*43 (04), 89–93+130. doi: 10.3969/j.issn.1000-1379.2021.04.016

Luan, F., Zhou, J., Jia, R., Lu, C., and Bai, M. (2017). Hydrochemical characteristicsand formation mechanism of groundwater in plain areas of barkol-YiwuBasin, xinjiang. *Envionmental Chem.* 36 (02), 380–389. doi: 10.7524/j.issn.0254-6108.2017.02.2016062001

Maclay, R. W., and Winter, T. C. (1967). Geochemistry and ground-water movement in northwestern minnesotaa. *Ground Water*5 (1), 11–19. doi: 10.1111/j.1745-6584.1967.tb01233.x

Mahaqi, A., Mehiqi, M., Moheghy, M. A., Moheghi, M. M., and Hussainzadeh, J. (2021). Nitrate pollution in Kabul water supplies, afghanistan; sources and chemical reactions: a review. *Int. J. Environ. Sci. Technol.* doi: 10.1007/s13762-021-03551-4

Maranzoni, A. (2020). Galilean-Invariant expression for bernoulli's equation. *J. Hydraulic Eng.*146 (2), 04019061.1–04019061.8. doi: 10.1061/(ASCE)HY.1943-7900.0001680

Meinzer, O. E. (1936). Movement of ground-water. *Eos Trans. Am. Geophys. Union*17. doi: 10.1029/TR017i002p00478

Meinzer, O. E., and Wenzel, L. K. (1940). Present status of our knowledge regarding the hydraulics of ground water. *Eos Trans. Am. Geophys. Union*35 (2), 915–941. doi: 10.1029/TR021i002p00648-2

Meng, Q. (2021). Hydrochemical characteristics and controlling factors of the shallow groundwater in the midstream and downstream areas of shiyang river basin. *J. Arid Land Resources Environ.*35 (03), 80–87. doi: 10.13448/j.cnki.jalre.2021.072

Mo, S. (2019). *Towards efficient high-dimensional uncertainty quantification and inverse analysis in groundwater modeling using deep learning* (Nanjing University).

Munnich, K. O., and Vogel, J. C. (1959). *The recent increase in the c*sup 14/ content of the atmosphere, the biosphere and the ocean. report on the measurements of the C*SUP 14/Laboratory* (Heidelberg: Zweites Physikalisches Institut der Universitat).

Nan, J., Wang, H., and Lian, X. (2008). Progr ess on technology for pb contamination of groundwater remediation. *Environ. Sci. Technol.*31 (02), 56–60. doi: 10.19672/j.cnki.1003-6504.2008.02.015

Normile, D. (2019). Earth scientist plan a'Geological google'. *Science*363 (6430), 917. doi: 10.1126/science.363.6430.917

Ono, M., Machida, I., Ikawa, R., Kamitani, T., Oyama, K., Muuranaka, Y., Ito, A., and Marui, A. (2019). *Regional groundwater flow system in a stratovolcano adjacent to a coastal area: a case study of mt. Fuji and suruga bay*, Japan: Springer Berlin Heidelberg, 27(2), 717–730.

Palmer, P. C., Gannett, M. W., and Hinkle, S. R. (2006). Isotopic characterization of three groundwater recharge sources and inferences for selected aquifers in the upper klamath basin of Oregon and California, USA. *J. Hydrol.*336 (1). doi: 10.1016/j.jhydrol.2006.12.008

Paolalsiam, V. S., and Mohan, K. R. (2021). Hydrochemical characteristics and nitrate health risk assessment of groundwater through seasonal variations from an intensive agricultural region of upper Krishna river basin, telangana, India. *Ecotoxicol. Environ. Saf.* 213. doi: 10.1016/j.ecoenv.2021.112073

Podgorski, J., and Berg, M. (2020). Global threat of arsenic in groundwater. *Science*368, 845–850. doi: 10.1126/science.aba1510

Reddy, A. G. S., Saibaba, B., and Sudarshan, G. (2012). Hydrogeochemical characterization of contaminated groundwater in patancheru industrial area, southern India. *Environ. Monit. Assess.*184 (6), 3557–3576. doi: 10.1007/s10661-011-2208-2

Ren, J., Wu, Q., and Gao, Z. (2014). *Fundamentals of hydrogeochemistry (1st edition)* (Beijing, China: Geological publishing house).

Rezaei, M., Nikbakht, M., and Shakeri, A. (2017). Geochemistry and sources of fluoride and nitrate contamination of groundwater in lar area, south Iran. *Environ. Sci. pollut. R*24 (18), 15471–15487. doi: 10.1007/s11356-017-9108-0

Ross, C. S. (1943). Clays and soils in relation to geologic processes. *Jour. Wash. Acad. Sci.*33, 225–235. doi: 10.2307/24531882

Russak, A., Sivan, O., and Yechieli, Y. (2016). Trace elements (Li, B, Mn and Ba) as sensitive indicators for salinization and freshening events in coastal aquifers. *Chem. Geol.* 441, 35–46.

Roy, S. K., and Zahid, A. (2021). Assessment of river water–groundwater–seawater interactions in the coastal delta of Bangladesh based on hydrochemistry and salinity distribution. *SN Appl. Sci.*3 (4), 411. doi: 10.1007/s42452-021-04389-8

Schwartz, F. W., and Domenico, P. A. (1973). Simulation of hydrochemical patterns in regional groundwater flow. *Water Resour. Res.*9 (3), 707–720. doi: 10.1029/WR009i003p00707

Seltzer, A. M., Krantz, J. A., Ng, J., Danskin, W. R., Bekaert, D. V., and Barry, P. H. (2021). The triple argon isotope composition of groundwater on ten-thousand-year timescales. *Chem. Geol.* 583, 120458. doi: 10.1016/j.chemgeo.2021.120458

Sinha, D., and Prasad, P. (2020). Health effects inflicted by chronic low-level arsenic contamination in groundwater: A global public health challenge. *J. Appl. Toxicol.*40 (1). doi: 10.1002/jat.3823

Smith, R. L., Kent, D. B., Repert, D. A., and Böhlke, J. K. (2017). Anoxic nitrate reduction coupled with iron oxidation and attenuation of dissolved arsenic and phosphate in a sand and gravel aquifer. *Geochim. Cosmochim. Acta*196, 102–120. doi: 10.1016/j.gca.2016.09.025

Su, C., Zhang, F., Cui, X., Cheng, Z., and Zheng, Z. (2020). Source characterization of nitrate in groundwater using hydrogeochemical and multivariate statistical analysis in the muling-xingkai plain, northeast China. *Environ. Monit. Assess.*192 (7), 456. doi: 10.1007/s10661-020-08347-6

Thorstenson, D. C. (1984). The concept of electron activity and its relation to redox potentials in aqueous geochemical systems. *Open-File Rep.* doi: 10.3133/ofr8472

Tóth, J. (1962). A theory of groundwater motion in small drainage basins in central Alberta, Canada. *J. Geophys. Res.*67 (11), 4375–4388. doi: 10.1029/JZ067i011p04375

Tóth, J. (1963). *A theoretical analysis of groundwater flow in small drainage basins* Vol. 68 (John Wiley & Sons, Ltd).

Tóth, J. (1966a). *Groundwater Geology, Movement, Chemistry and Resources Near Olds.* Alberta, Canada:Research Council of Alberta, RCA/AGS Bulletin 17, p 148.

Tóth, J. (1966b). Mapping and interpretation of field phenomena for groundwater reconnaissance in a prairie environment, Albert, Canada. *Int. Assoc. Sci. Hydrology. Bull.*11 (2), 20–68. doi: 10.1080/02626666609493458

Tóth, J. (1970). A conceptual model of the groundwater regime and the hydrogeologic environment. *J. Hydrol.*10 (2), 164–176. doi: 10.1016/0022-1694(70)90186-1

Tóth, J. (1971). Groundwater discharge: a common generator of diverse geologic and morphologic phenomena. international association of scientific hydrology. *Bulletin*16, 7–24. doi: 10.1080/02626667109493029

Tóth, J. (1977). The hydrogeological reconnaissance maps of Alberta. *Alberta Res. council Bull.*35, 1–11.

Tóth, J. (1978). Gravity-induced cross-formational flow of formation fluids, red earth region, Alberta, Canada: Analysis, patterns, and evolution. *Water Resour. Res.*14 (5). doi: 10.1029/WR014i005p00805

Tóth, J. (1979). *Patterns of dynamic pressure increment of formation-fluid flow in large drainage basins, exemplified by the red earth region, Alberta* (Canada: China Social Sciences Pub. House).

Tóth, J. (1980). *Cross-formational gravity-flow of groundwater: a mechanism of the transport and accumulation of petroleum (the generalized hydraulic theory of petroleum migration). problems of petroleum migration.* Washington:American Association of Petroleum Geologists.

Tóth, J. (1984). The role of regional gravity flow in the chemical and thermal evolution of ground water. *Proceedings of the First Canadian/american Conference on Hydrogeology.* Alterta, Canada, 22–26 June 1984.

Tóth, J. (1995). Hydraulic continuity in large sedimentary basins. *Hydrogeol. J.*3 (4), 4–16. doi: 10.1007/s100400050250

Tóth, J. (1996). Thoughts of a hydrogeologist on vertical migration and near-surface geochemical exploration for petroleum. *AAPG Memoir*66 (20), 279–283. doi: 10.1306/M66606C20

Tóth, J. (1999). Groundwater as a geologic agent: An overview of the causes, processes, and manifestations. *Hydrogeol. J.*7 (1), 1–14. doi: 10.1007/s100400050176

Tóth, J. (2009). *Gravitational systems of groundwater flow : Theory, evaluation and utilization* (Cambridge, U.K.: Cambridge University Press). doi: 10.1017/CBO9780511576546

Tóth, J. (2016). The evolutionary concepts and practical utilization of the tóthian theory of regional groundwater flow. *Int. J. Earth Environ. Sci.*1, 111. doi: 10.15344/2456-351X/2016/111

Tóth, J., and Corbet, T. (1986). Post-Paleocene evolution of regional groundwater flow-systems and their relation to petroleum accumulations, Taber area, southern Alberta, Canada. *Bull. Can. Petrol. Geol.*75 (2), 331–335. doi: 10.35767/gscpgbull.34.3.339

Wang, D. (1995). *Fundamentals of hydrogeology (Fourth edition)* (Beijing: Geological Publishing House).

Wang, X. S., Wan, L., Jiang, X. W., Li, H., Zhou, Y., and Wang, J. (2017). Identifying three-dimensional nested groundwater flow systems in a tóthian basin. *Adv. Water Resour.* 108 (oct.), 139–156. doi: 10.1016/j.advwatres.2017.07.016

Wang, W., Li, W., Cai, Y., An, Y., Shao, X., Wu, X., and Yin, D. (2021a). A study of the hydrogeochemical evolution of groundwater in the middle reaches of the heihe river basin. *Earth Sci. Front.* 28 (04), 184–193. doi: 10.13745/j.esf.sf.2021.5.28

Wang, Z., Wang, S., Fu, T., Gao, Z., and Xu, X. (2021b). Characteristics and health risk assessment of heavy metals in groundwater of qinhuangdao coastal zone. *Environ. Chem.*40 (04), 1157–1166. doi: 10.7524/j.issn.0254-6108.2020091405

Wang, X. S., Jiang, X. W., Wan, L., Ge, S., and Li, H. (2011). A new analytical solution of topograghy-driven flow in drainage basin with depth-dependent anisotropy of permeability. *Water Resour. Res.*47 (9). doi: 10.1029/2011WR010507

Wang, Y. X., Li, J. X., and Xie, X. J. (2022). Genesis and occurrence of high iodine groundwater. *Earth Sci. Front.*29 (3), 001–010. doi: 10.13745/j.esf.sf.2022.1.47

Wen, D., Huang, H., Shi, Y. K., Yang, S. R., Yang, J., Wang, Y., et al. (2021). Big data management and sharing for earth sciences: An paradigm from British geological survey. *Geol J. China Universities*27 (1), 45–57. doi: 10.16108/j.issn1006-7493.2020098

Winter, T. C., Harvey, J. W., Franke, O. L., and Alley, W. M. (1998). *Ground water and surface water: A single resource. U.S. Geological Survey Circular 1139*. Colorado Geological Survey.

Wolery, T. J., Jackson, K. J., Bourcier, W. L., Bruton, C. J., and Delany, J. M. (1990). Current status of the EQ3/6 software package for geochemical modeling. *Chem. Modeling Aqueous Syst. II*. doi: 10.1021/bk-1990-0416.ch008

Xia, L., Gao, Z., Xu, H., and Feng, G. (2020). Variations in bacterial community during bioclogging in managed aquifer recharge (MAR): A laboratory study. *Int. Biodeterior. Biodegradation*147. doi: 10.1016/j.ibiod.2019.104843

Xiao, J., Wang, L., Chai, N., Liu, T., and Rinklebe, J. (2021). Groundwater hydrochemistry, source identification and pollution assessment in intensive industrial areas, eastern chinese loess plateau. *Environ. pollut.*278, 116930. doi: 10.1016/j.envpol.2021.116930

Xiong, Y., Luo, J., Liu, X., Liu, X., and Xin, X. (2022). Machine learning-based optimal design of groundwater pollution monitoring network. *Environ. Res.* 211, 113022. doi: 10.1016/j.envres.2022.113022

Xu, N., Gong, J., and Yang, G. (2018b). Using environmental isotopes along with major hydro-geochemical compositions to assess deep groundwater formation and evolution in eastern coastal China. *J. contam. hydrol.* 208. doi: 10.1016/j.jconhyd.2017.11.003

Xu, J., He, J., Peng, C., and Zeng, Y. (2018a). Characteristics and genesis of no_3 type water in shallow groundwater in liujiang basin. *Environ. Sci.*39 (9), 4142–4149. doi: 10.13227/j.hjkx.201712082

Zaidi, F. K., Nazzal, Y., Jafri, M. K., Naeem, M., and Ahmed, I. (2015). Reverse ion exchange as a major process controlling the groundwater chemistry in an arid environment: a case study from northwestern Saudi Arabia. *Environ. Monit. Assess.*187 (10), 607. doi: 10.1007/s10661-015-4828-4

Zaryab, A., Nassery, H. R., Knoeller, K., Alijani, F., and Minet, E. (2022). Determining nitrate pollution sources in the Kabul plain aquifer (Afghanistan) using stable isotopes and Bayesian stable isotope mixing model. *Sci. Total Environ.*823, 153749. doi: 10.1016/j.scitotenv.2022.153749

Zhang, J., Cao, M., Jin, M., Huang, X., Zhang, Z., and Kang, F. (2022). Identifying the source and transformation of riverine nitrates in a karst watershed, north China: Comprehensive use of major ions, multiple isotopes and a Bayesian model. *J. Contam. Hydrol.*246, 103957. doi: 10.1016/j.jconhyd.2022.103957

Zhang, J., Hou, R., Yin, L., Ma, H., and Huang, J. (2017). Formation and influencing factors of regional groundwater flow systems. *Hydrogeol. & Eng. Geol.*44 (04), 8–14. doi: 10.16030/j.cnki.issn.1000-3665.2017.04.02

Zhang, X., Jiao, J. J., Li, H., Luo, X., and Kuang, X. (2020a). Effects of downward intrusion of saline water on nested groundwater flow systems. *Water Resour. Res.*56 (10). doi: 10.1029/2020WR028377

Zhang, R., Liang, X., Jin, M., and Tóth, József (2015). *Gravitational systems of groundwater flow theory, evaluation, utilization* (Beijing: Geological Publishing House).

Zhang, R., Liang, X., Jin, M., Wan, L., and Yu, Q. (2018). *General hydrogeology. Seventh Edition* (Beijing China: Geological Publishing House).

Zhang, Y., Wu, Y., Wen, X., and Su, J. (2006). Application of environmental isotopes in water cycle. *Adv. In Water Sci.*17 (05), 738–747. doi: 10.14042/j.cnki.32.1309.2006.05.025

Zhang, Z., Xiao, C., Adeyeye, O., Yang, W., and Liang, X. (2020b). Source and mobilization mechanism of iron, manganese and arsenic in groundwater of shuangliao city, northeast china. *Water*12 (2), 534. doi: 10.3390/w12020534

Zhang, B., and Zhang, C. (2019). Progress on hydrogeochemical method applied in groundwater study. *Yellow River*41 (10), 135–142. doi: 10.3969/j.issn.1000-1379.2019.10.023

Zhao, Z., Wang, D., Tao, Z., and Li, Y. (2008). Multi- layer circulation model of groundwater flow systems on the ordos plateau, China: evidence from water head measurements at different depths of a deep borehole by the packer system. *Geol Bull. China* 27 (08), 1131–1137. doi: 10.1016/S1872-5791(08)60056-1

Zhao, N., Yan, X., Li, Q., Fu, S., and Chu, X. (2021). Hydrochemical characteristics and formation mechanism of shallow groundwater in around-lake area of poyang lake. *Yangtze River*52 (01), 44–48. doi: 10.16232/j.cnki.1001-4179.2021.01.008

Zhou, X., HU, F., and He, J. (2014). *Introduction to groundwater science (2nd edition)* (Beijing, China: Geological publishing house).

Zhou, X., and Zhu, C. (2014). The nitrate content characteristics of shallow groundwater in jinjiang city, fujian province, and their hydrochemical indication significance. *Acta Geosci. Sin.*35 (2), 177–182. doi: 10.3975/cagsb.2014.02.08

Zijl, W. (1999). Scale aspects of groundwater flow and transport systems. *Hydrogeol. J.*7 (1), 139–150. doi: 10.1007/s100400050185

frontiers | Frontiers in Marine Science

TYPE Original Research
PUBLISHED 14 October 2022
DOI 10.3389/fmars.2022.1015781

OPEN ACCESS

EDITED BY
Qiang He,
Fudan University, China

REVIEWED BY
Shuling Yu,
Tianjin Polytechnic University, China
Fangyan Cheng,
Fudan University, China

*CORRESPONDENCE
Honghua Shi
shihonghua@fio.org.cn
Xianqing Lv
xqinglv@ouc.edu.cn

SPECIALTY SECTION
This article was submitted to Coastal Ocean Processes, a section of the journal Frontiers in Marine Science

RECEIVED 10 August 2022
ACCEPTED 22 September 2022
PUBLISHED 14 October 2022

CITATION
Lu J, Zhang Y, Shi H and Lv X (2022) Coastal vulnerability modelling and social vulnerability assessment under anthropogenic impacts. *Front. Mar. Sci.* 9:1015781. doi: 10.3389/fmars.2022.1015781

Coastal vulnerability modelling and social vulnerability assessment under anthropogenic impacts

Jingfang Lu[1], Yibo Zhang[1], Honghua Shi[2,3]* and Xianqing Lv[1]*

[1]Frontier Science Center for Deep Ocean Multispheres and Earth System (FDOMES) and Physical Oceanography Laboratory, Ocean University of China, Qingdao, China, [2]First Institute of Oceanography, Ministry of Natural Resources, Qingdao, China, [3]Pilot National Laboratory for Marine Science and Technology (Qingdao), Qingdao, China

Coastal regions are highly vulnerable to the impacts of human activities, land cover change, sea level rise (SLR), and climate extremes. In this study, we attempt to address this issue by simulating the spatial interactions among natural hazards, ever-increasing human activities, and social vulnerability in the south coast of the Bohai Sea, China. It is found that the activities occurring on land, especially within coastal environments, such as agricultural pond and ports, and those in the ocean (tide and residual current) both impose disaster risks on the marine environment. In 2020, 25.2% of the total study area is highly vulnerable, which is 21% larger than that in 1997. The socially vulnerable areas are mainly distributed in the southeast coast of the Laizhou Bay. These areas should be strengthened to reduce and prevent the storm surge and flood disasters. Ultimately, we emphasize the urgent needs to implement effective policy measures for reducing tomorrow's risks from natural hazards.

KEYWORDS

coastal vulnerability index, reclamation, hazards, hydrodynamic environment, coastline change

1 Introduction

The south coast of the Bohai Sea (SCBHS) is an important region of mariculture and salt pan in China (Shi et al., 2022). In recent years, due to their special locations and unique natural resources, the artificial landscape areas in the coastal regions have been expending, and consequently, their landscape patterns have been remarkably changed (Zhu et al., 2018). Other than the land-based sources, the marine construction boom driven by the expansions of coastal cities, increasing population and economic

development including the constructions built in the marine environment with a wide range of purposes (ports and dams of aquaculture) also contributes to the changes in coastline and hydrodynamics, and causes natural disasters (SLR, storm surge and typhoons) (Arkema et al., 2013; Jiang et al., 2021; Huang et al., 2022). The natural disasters in the SCBHS mostly result from storm surges. The catastrophic storms in the Bohai Sea usually occur in summer and autumn, on an average frequency of once every 4 years, and smaller storms happen on the average frequency of 1-2 times a year, yet which have caused inestimable losses (Feng et al., 2018; Jiang et al., 2022). In particular, the coastal regions of the Bohai Bay and Laizhou Bay have undergone several severe storm disasters. The mean rate of SLR in the Bohai Sea was 3.8 $mmyr^{-1}$ between 1993 and 2015 (Peng and Han, 2013). Therefore, it is essential to analyze the coastal vulnerability to human activities.

The quantification of coastal vulnerability index (CVI) has been extensively studied and well developed in the past several years. Koroglu investigated effects of the specific hydro-geomorphological condition ranges in the CVI model parameter (Koroglu et al., 2019). Sajjad coupled the human and natural systems to highlight the necessity of reclamation in coastal conservation (Sajjad et al., 2018). However, reclamation changes the coastline and subsequently alters the hydrodynamics. Therefore, it becomes a key driving force of increasing the CVI caused by the changes of tidal residual currents, yet is neglected in previously produced scenarios (Jin et al., 2016). So far, very few models map the relative vulnerability of a coastal area to erosion and inundation from the perspective of land-sea coordination with the urban development characteristics of the region taken into consideration. It is our goal to fill this gap with a coastal vulnerability model.

Among the various impacts of SLR, city waterlogging and storms are the most devastating ones that can cause significant losses of lives and properties in the coastal regions (Koks et al., 2015). The original CVI model does not include the unique socio-economic and demographic characteristics, such as gender, age, income, access to education and health services of the region. In addition, the traditional approaches generally examine the impacts of a single natural hazard, while overlooking the relationships/interactions between multiple hazards and human activities. The concept of social vulnerability index (SoVI) proposed by Sodhi is defined as "the propensity across different population segments to be affected by natural hazards and other shocks" (Sodhi, 2016). It can help to identify the critical locations where disaster risks should be prioritized in the regional policy.

Herein, we conducted a comprehensive survey on reclamation, landscape type, hydrodynamic condition, urbanization, coastline change, and protection-development status of the SCBHS. The nature hazard susceptibility of the region was examined using a CVI model that included the changes in coastline and hydrodynamics caused by reclamation. The urban sprawl and reclamation activities were detected by remote sensing. The SoVI of the region was assessed with a composite index tailored for the case-study area. Finally, the spatial interaction between the CVI and SoVI was studied. Based on the results, we attempt to provide a guidance for the regulation of human activities which can facilitate the coastal management in the nearshore waters and promote the sustainable development of the area.

2 Materials and methods

2.1 Study area

The study area is a semi-enclosed area located from 37°N to 38.5°N and from 117.5°E to 121°E with 615 km long coastline from the south of the Binzhou Port to the Longkou Qimu Corner. The area is surrounded by land in the west and south, including the sea area from the Yellow River estuary to the Laizhou Bay and the corresponding coastal area (Figure 1). Coastal area is defined as a 20 km wide area along the coastline based on the definition of coastal zone in the Wetland Convention (Nature, International Union for Conservation of, and Natural Resources and Ramsar Convention Bureau, 1984). The study area runs across five cities including Binzhou City, Dongying City, Weifang City, Qingdao City and Yantai City in Shandong Province, China with a total regional GDP of 2327.7 billion RMB and a total population of 31.4 million (Shandong Statistical Yearbook, 2021).

2.2 Coastal vulnerability index

The CVI model proposed by Gornitz (1990) can assess the coastal vulnerability to SLR, particularly due to erosion and/or inundation. The model ranks the exposure index of each point of the coastline at a specified interval, but does not directly value any ecosystem service, such as coastal zone and coastal wetland (Gornitz et al., 1997; Hammar and Thieler, 2001). It is known that the characteristics of a given coastline result from the interactions among geomorphology, SLR, wave height, tidal range, and storm frequencies. The relative magnitudes of these variables change from place to place, which induces nonuniform responses of the coastline to SLR. Therefore, we attempt to establish a coastal vulnerability model under anthropogenic impacts, aiming to cover the deficiencies of the conventional model.

The CVI under the human activity framework involves the coastal assessment that quantifies the coastal vulnerability using remote sensing and satellite altimeter observation data. The conceptual framework is shown in Figure 2A. The traditional human activities on land, such as agricultural production and urban development, alter the natural landscapes and increase artificial landscapes (Yang et al., 2021). The ocean-based human activities, such as reclamation and mariculture, directly affect marine habitats. By incorporating the human activity responses into the CVI model, the parameters are determined as detailed in

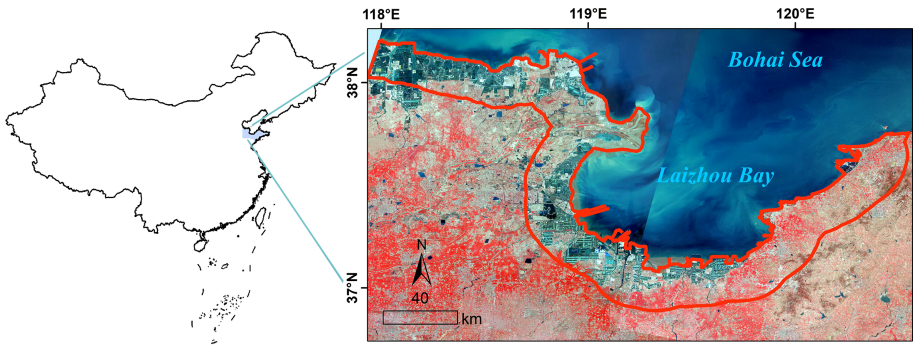

FIGURE 1
Location and topography of study area.

Figure 2B. The CVI is then calculated using a spatial representation of the bio-geophysical variables including geomorphology, SLR, coastal slope, regional elevation, coastline change, significant wave height and tidal range. The obtained CVIs are ranked from very low exposure (rank=1) to very high exposure (rank=7) based on the combination of the user- and model- defined criteria by the method of Gornitz (Gornitz et al., 1997; Hammar and Thieler, 2001). The score ranges and ranking are summarized in Table 1 (Koroglu et al., 2019; Wang et al., 2021). The calculation using a spatial representation of the bio-geophysical variables was referred to the InVEST User's Guide (https://naturalcapitalproject.stanford.edu/). The adjustments of major parameters are shown in Figure 2B.

2.2.1 Geomorphology

Geomorphology refers to the geomorphological features resistant to erosion. Rocky cliffs play a vital role in reducing the impacts of coastal hazards. They are less prone to erosion than beaches and deltas. Different coastline geomorphologies are ranked by the method of Hammar and Thieler, 2001. Since we will further assess the coastline in the study area by remote sensing (See 2.3.1), two more coastline geomorphologies, dams of aquaculture and salt, are included in this index based on the remote sensing images.

2.2.2 Coastal slope and regional elevation

Coastal slope and regional elevation are the indexes evaluating the relative risks of inundation. For the gently sloping coasts, any rise in sea level would inundate a large extent of land. The coastal slope and elevation data of the study area are downloaded from http://www.gscloud.cn.

2.2.3 Coastline change

Reclamation activities for industrial and agricultural developments expand the land area and change the coastline

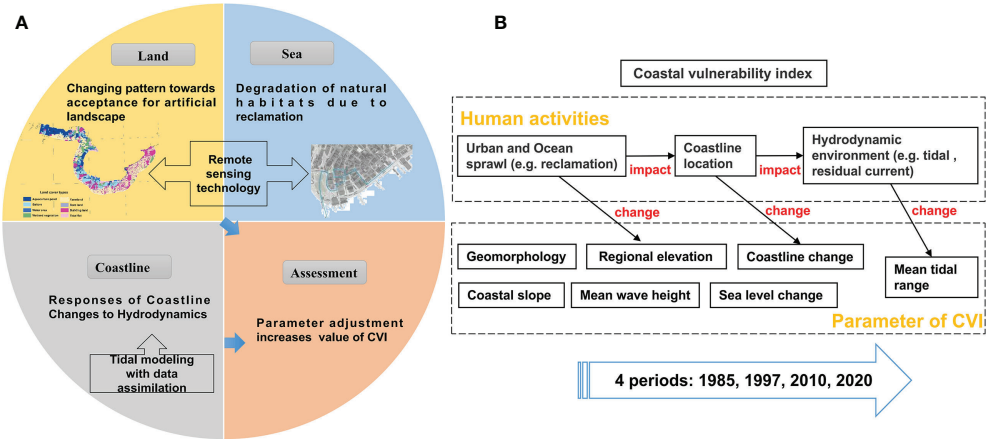

FIGURE 2
CVI under the human activity framework **(A)**; Parameter adjustment of the CVI model **(B)**.

TABLE 1 Evaluation system of CVI.

Indexes/score	Ranking of CVI				
	Very Low/0.2	Low/0.4	Moderate/0.6	High/0.8	Very High/1
I_1: Geomorphology	①	②	③	④	⑤
I_2: regional elevation (m)	>30	21-30	11-20	6-10	0-5
I_3: coastal slope (%)	>12	8-12	4-8	2-4	0-2
I_4: Coastline change(m/yr)	0	0-5	5-10	10-20	>20
I_5: Sea level change(mm/yr)	<0	0-1.0	1.1-2.0	2.1-4.0	>4.0
I_6: Mean wave height(m)	<1.1	1.1-2.0	2.0-2.25	2.25-2.6	>2.6
I_7: Mean tidal range(m)	>6.0	4.1-6.0	2.0-4.0	1.0-1.9	<1.0

①, Rock, high cliff, and seawall; ②, Medium cliffs, rugged coasts, bulkheads, and small seawall (dam of aquaculture and salt); ③, Low cliffs, glacier drifting, alluvial plains, revetments, and stone walls; ④, Estuary wetland and lagoon; and ⑤, Barrier beach, beach, tidal flat, farmland, and delta.

position. In the CVI model, coastline change is also an index for assessing the potential impacts of natural hazards (Koroglu et al., 2019). The change rate of coastline position is calculated using the ArcMap extension module and Digital Shoreline Analysis System (DSAS). DSAS generates a landward baseline from which orthogonal transects are cast at 3-km intervals. The intercepts between the transects and coastline are recorded to calculate the annual change rates (Thieler et al., 2009). A total of 205 change rates, each corresponding to a DSAS transect, are obtained.

2.2.4 Mean wave height

The data of wind and wave was obtained by reanalysis of the six-year (2005-2010) WAVEWATCH III model HINDCAST from NOAA (Gornitz, 1990; Sajjad et al., 2018).

2.2.5 Tidal range

To estimate the spatial variation range of tide in the SCBHS, multi-mission satellite observations from the TOPEX/Poseidon were assimilated into a 2-D tidal model by the adjoint method (Lu and Zhang, 2006). The assimilation process can be summarized as follows.

1) Land-sea grid construction

The land-sea grid is constructed by the following steps:

Step 1. A 2-dimensional (2D) hydrodynamic model with the medium resolution square meshes (2'×2' grid, approximately 30 m) fitting the coastline is constructed using the Arakawa C grid.

Step 2. By comparing the current geographic distribution data of land-sea from the National Earth System Science Data Center (http://www.geodata.cn/data) and those of different years, the shrinkage or expansion of coastline is processed.

Step 3. The ETOPO1 bathymetric data are matched to the grids and the values of the rest nodes are interpolated.

Step 4. The coastline in each grid versus water depth are matched, and the grids are divided based on the dryness and wetness to obtain the control field of sea-land distribution.

2) Tidal modeling with adjoint method

The distributions of the M_2 tidal constituent in the SCBHS in 1985, 1997, 2010 and 2020 are simulated by combining the T/P observation data. The numerical schemes for the forward model and the adjoint model are given in the Appendix A1 and A2. The coastline changes caused by reclamation and the corresponding hydrodynamic changes (tide level and velocity) are also included in the tidal model.

3) Model configuration

The 2-D tidal model covers the area of SCBHS from 37°N to 38.5°N and from 117.5°E to 121°E with the spatial resolution of 1/12°×1/12°. The gridded topography is adopted from ETOPO1. The maximum water depth of the study area is 85 m. The topography is gridded with the Arakawa C grid, where the water level is put at the grid center and the two velocity components are defined to be perpendicular to the edges of the grid.

The closed boundary conditions for our model are zero flow normal to the coast. That is, $\vec{\mathbf{u}} \cdot \vec{\mathbf{n}} = \mathbf{0}$ for the grid points at closed boundary, where $\vec{\mathbf{n}}$ is the outward unit vector and $\vec{\mathbf{u}} = (\mathbf{u},\mathbf{v})$ is the velocity vector. The Beijing standard time (referred to the meridian of 120°E) is adopted throughout this study.

Along the open boundaries, the water elevation of the M_2 tide at the *jth* time step is given as $\zeta^j_{m_l,n_l} = a_{0,l} + [a_l \cos(\omega j\Delta t) + b_l \sin(\omega j\Delta t)]$, where (m_l,n_l) stands for the grid points at the open boundaries, ω is the frequency of the M_2 constituent, and a_l, b_l are the Fourier coefficients. The open boundary conditions of water elevation are obtained by assimilating the T/P data using the adjoint method, and are fixed in all experiments (He et al., 2004).

4) Model validation

The reliability of the assimilation was evaluated by testing the harmonic constants using amplitude difference, phase difference and vector difference as the evaluation criteria. The vector difference can be expressed as:

$$\Delta = \left[(H_a\cos\ g_a - H_d\cos\ g_d)^2 + (H_a\sin\ g_a - H_d\ \sin\ g_d)^2\right]^{1/2} \quad (1)$$

The evaluation results are listed in Table 2.The simulation results are validated with the observation data of the 59 tide gauge stations. The mean absolute errors (MAEs) between the simulated and measured amplitudes, phases and vectors are less than 3.1 cm, 5.3°, and 4.4 cm, respectively. The root mean square errors (RMSEs) between the simulated and measured amplitudes, phases and vectors are smaller than 3.6 cm, 7.1°, and 5.1 cm, respectively. The MAEs and RMSEs of the three parameters meet the requirements, and thus the model is valid (Cheng et al., 2007; Pan et al., 2021).

2.2.6 SLR

A polygonal vector that can describe a unified range of sea level change is needed to characterize SLR. In this work, it is assumed that the eustatic sea-level in China is similar to the global SLR projected by IPCC in the 5th assessment report (IPCC, 2013).

2.2.7 Calculation of CVI

The CVI of the *i*-th section in the coastal wetland ecosystem is then calculated with Eq. (2).

$$CVI = \sqrt{I_1 + I_2 + I_3 + I_4 + I_5 + I_6 + I_7} \quad (2)$$

where "I" is the exposure rank of each variable.

2.2.8 Spatial visualization of CVI

The obtained CVIs are visualized by the GIS analysis method and equal interval breakpoint method with the vulnerability ranks of very low (0-1.39), low (1.40-2.79), medium (2.80-4.19), high (4.20-5.59) and very high (5.60-7.0). The amplified risks of natural hazards can lead to life-threatening storm surge and flooding and destruction of ports, villages, roads and other coastal infrastructures, which alarms the low-lying of SCBHS. To accommodate spatial heterogeneity, the visualization is extended 20 km inland from the edge of the coastline.

2.3 Human activity intensity

HAI refers to the degree of disturbance of an area affected by human activities (Wen, 1998; Xu et al., 2015). At present, the quantification of HAI based on the comprehensive indexes and land-use change has become the most widely used method with its advantages of simplicity and universal (Feng et al., 2017; Liu et al., 2018). In this study, HAI is calculated with the areas and influence coefficients of different types of land within a specific region to evaluate the disturbance of human activities to the nature (Chi et al., 2017; Chi et al., 2018a).

2.3.1 Remote sensing data processing

Landsat products of 1985, 1997, 2010, and 2020 (cloud cover: 0-5.46, resolution: 30 m×30 m) were obtained from the Geospatial Data Cloud site (http://www.gscloud.cn). Based on the remote sensing images, the landscapes in the study area are classified as natural landscape or artificial landscape. Wetland vegetation, tidal flats, bare lands, and water areas are natural landscapes. Farmland, aquaculture pond, saltern, and building land are considered as artificial landscapes (Sun et al., 2016; Chi et al., 2018a). The information of the remote sensing images (Table A1) and specific interpretation signs of different land cover types (Table A2) can be found in the Supplementary Material.

The verification method of remote sensing data: accurate control of landscape types is through corresponding Google Earth map with a resolution< 1 m, a total of 2145 validation sites (one site is set every 4 km) are selected, the contrast between our land cover types and the Google Earth map is conducted using an error matrix, the overall accuracy is 92.1%, which achieves a good performance (Chi et al., 2018b).

2.3.2 Spatial visualization of HAI

To characterize the spatial heterogeneity of HAI in the study area, the impact intensity of different types of landscape are estimated. The maximum impact intensity is applied to the center of the landscape. Each type of landscape is assigned with a

TABLE 2 The comparison of the calculated and measured.

	AD (cm)		PD (°)		VD (cm)	
	MAE	RMSE	MAE	RMSE	MAE	RMSE
1985	2.9	3.2	4.4	7.1	4.0	4.8
1997	3.1	3.4	5.3	7.7	3.9	4.5
2010	3.0	3.0	4.5	5.8	4.0	4.4
2020	3.1	3.6	4.5	5.0	4.4	5.1

AD, amplitude difference; PD, phase difference; VD, vector difference; MAE, mean absolute error; and RMSE, root mean square error.

human impact value, 1 for building area, 0.4 for saltern and aquaculture pond, and 1 for farmland (Chi et al., 2018b).

The spline function can interpolate points onto a grid surface by the 2D minimum curvature spline method to form a smooth surface passing exactly through the input points (Shi et al., 2020). Herein, the evaluation indexes are spatially interpolated. HAI is ranked from low vulnerability (0-0.33), medium vulnerability (0.34-0.66) to high (>0.67) vulnerability and visualized by the equal interval breakpoint method and the GIS analysis method.

2.4 Social vulnerability index

SoVI emphasizes the different burdens of disaster losses within and between places (Chen et al., 2014). It has been well recognized, and can be adapted to other different contexts (Boruff and Cutter, 2007; Holand and Lujala, 2013). The most frequently used SoVI methods are based on composite indicators (Boruff and Cutter, 2007). This paper aims to provide the empirical analysis of the spatial distribution of SoVI and its underlying social, economic, and political causes in SCBHS region at the local scale.

2.4.1 SoVI identification

The rapid economic development and population growth have caused more natural hazards in the SCBHS (Feng et al., 2018). With the focus on assessing the social vulnerability and responses of coastal cities to natural hazards, we identified 7 secondary indexes from the most recent *Statistical Bulletin of Shandong Province* and placed them into three first level indexes, e.g., population, informatization level, and social security (Table 3). The population index is composed of two variables. Young children (under 14 years old) and older adults (over 60 years old) are commonly regarded as the most vulnerable members of the population. The urban areas with higher population densities are more challenging in evacuation after a disaster. The informatization level index is composed of two variables, e.g., the number of mobile telephone subscribers and the number of broadband internet subscribers, that reflect the accessibility to disaster information for timely rescue. The lack of access to these services indicates a lower capability of hazard warning. The social security index is composed of three secondary indexes. The lack of access to basic social security services, such as health institutions and hospitals, may compromise the health and safety of the local population (Siagian et al., 2013; Mesta et al., 2022).

Given the unique local characteristics of the study area, we only chose the 7 variables from those leveraged by Mesta et al. (2022) for further analysis. The study area has undergone rapid urbanization and substantial economic growth since the Chinese economic reform. The nine-year compulsory education has been implemented since 2006, which provides basic safety education and training for all minors. Therefore, the economy and education indexes are excluded, but the indexes of health institutions and hospital beds proposed by Holand and Lujala (2013) are included in our study.

TABLE 3 Evaluation system of SoVI.

First level indexes	Second level indexes
Population	I_8: Percentage of population under age 14 and over age 60
	I_9: Population density f(cap/km^2)
Informatization level	I_{10}: Average number of mobile telephone subscribers per person
	I_{11}: Average number of internet broad band subscribers per person
Social security	I_{12}: Average number of participated in social insurance per person
	I_{13}: Number of health institutions per square kilometers
	I_{14}: Number of hospitals beds per square kilometers

The indicators may be positive or negative, depending on their properties. The greater the positive indicators, the higher the SoVI. The negative indicators are the opposite. I_8 and I_9 are positive. I_{10}, I_{11}, I_{12}, I_{13} and I_{14} can be negative.

Previous studies suggest that social vulnerability remains in a stable state over time. Zhou et al. (2019) reported that only 18% of counties in China underwent significant increases/decreases in social vulnerability in the past 30 years. However, the potential changes in social vulnerability can occur gradually due to the influences of population changes, such as aging and family planning policy, or take place almost instantaneously owing to typhoon and flood disasters that cause casualties, losses of constructions, and decreases in crop land. These changes are ongoing, which makes it more difficult to measure and quantify social vulnerability. Therefore, this paper excludes the effects of potential changes in indexes.

2.4.2 Calculation of SoVI

Each index value (I_m) is normalized into the score range of 0-1.0, where the minimum index value (min_m) is 0 and the maximum index value (max_m) is 1. Max_m and Min_m are the maximum value and minimum value, respectively, of indicator I within each administrative unit. The normalized value (NV_m) is calculated with the equations below.

$$NV_m = \max_m - I_m / \max_m - \min_m \text{ (is the positive indicator)} \quad (3)$$

$$NV_m = I_m - \min_m / \max_m - \min_m \text{ (is the negative indicator)} \quad (4)$$

The score of each index is defined as the arithmetic mean of the corresponding NV_m values. The overall SoVI is obtained as the weighted average of each of the first level indexes, i.e.:

$$SoVI = \left(\frac{I_8 + I_9}{2} + \frac{I_{10} + I_{11}}{2} + \frac{I_{12} + I_{13} + I_{14}}{3}\right)/3 \quad (5)$$

2.4.3 Spatial visualization of SoVI

The obtained SoVIs were then ranked from low vulnerability (rank=0) to high vulnerability (rank=1) and visualized by the equal interval breakpoint method and the GIS analysis method.

3 Results

3.1 Coastal vulnerability index

3.1.1 Evaluation results of sub-indexes

3.1.1.1 Changes in reclamation and change rate

Figure 3A shows the three development stages of reclamation in the SCBHS which have resulted in 1139.5 km^2 increase in the cumulative reclamation area. During the study period, reclamation activities mainly occurred on the north coast of the Yellow River estuary (36.5%) and the south coast of the Laizhou Bay (28.0%). The activities caused the mean net coastline movement of 184.8 m/yr (median, 73 m/yr). Most coastline movements were distributed on the north coast of the Yellow River and the south coast of the Laizhou Bay, with the mean net values of 344.8 m/yr and 263.2 m/yr, respectively. 81.3% of the SCBHS coastline mapped in 2020 is within 0-140.4 m from their positions in 1985, and more than 52.3% of coastline expands more than 1 km to the sea (Figures 3B–D). In particular, the reclamation in 1985-1997 is much more aggressive than those in other periods, and the reclaimed lands are mainly used for agriculture and mariculture.

3.1.1.2 Changes in hydrodynamics

In the past 35 years, the coastline in SCBHS has already undergone significant spatial-temporal changes. Marine constructions, such as ports and wharves, rapidly bulge along the coast and extend toward the ocean. In addition, a ginormous amount of sediment from the loess region has formed a mega-delta in the Yellow River Estuary (Figures 4A–D).

Figure 4 shows the co-tidal charts in 1985, 1997, 2001, and 2020. The M_2 tidal constituent was stable in 1985, and only slight movements were observed on the amphidromic points, but its amplitude increased in 1997, 2010 and 2020 as the coastline changed (Figures 4A–D). It is worth noting that, compared with that in 1985, the amplitude of the M_2 tidal constituent in the north of the Yellow River Estuary increased by 14-20 cm in 2020, equivalent to the 14-20 cm rise of seabed (Figures 4E–G).

3.1.2 Spatial-temporal changes in CVI

From 1997 to 2020, the high-intensity urban construction, reclamation and the corresponding hydrodynamic changes led to the rapid natural habitat loss and significantly increased the coastal vulnerability. In particular, the very high vulnerability area increased by 3.6-folds in 2010 (Figure 5D). The CVI on the coast is 1.1 (very low vulnerability) in 1997, 3.4 (medium vulnerability) in 2010, and 4.1 (medium vulnerability) in 2020 (Figures 5A–C). In terms of spatial distribution, most locations in the central of less elevated wetland plains, especially the western area of the SCBHS, show very low or low vulnerabilities. In contrast, the vulnerabilities of many artificial

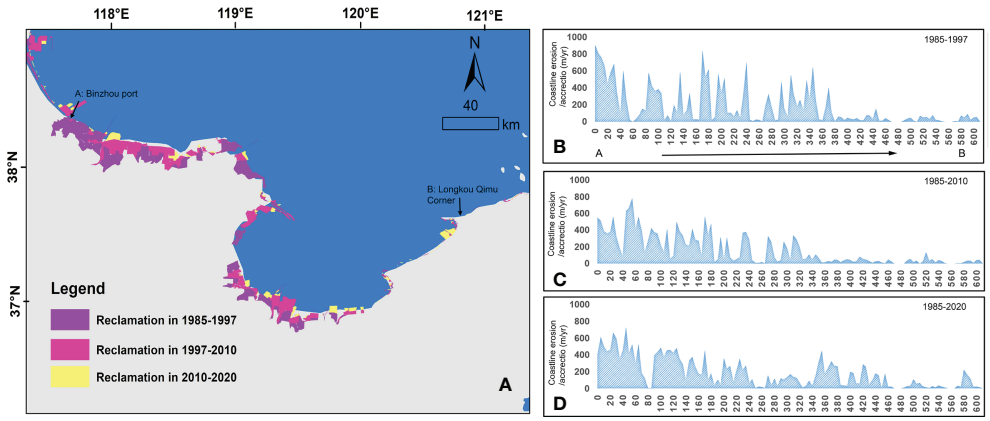

FIGURE 3
Spatial distribution of reclamation activities **(A)** and coastline change rates determined by DSAS from 1985 to 1997 **(B)**, 2010 **(C)** and 2022 **(D)**.

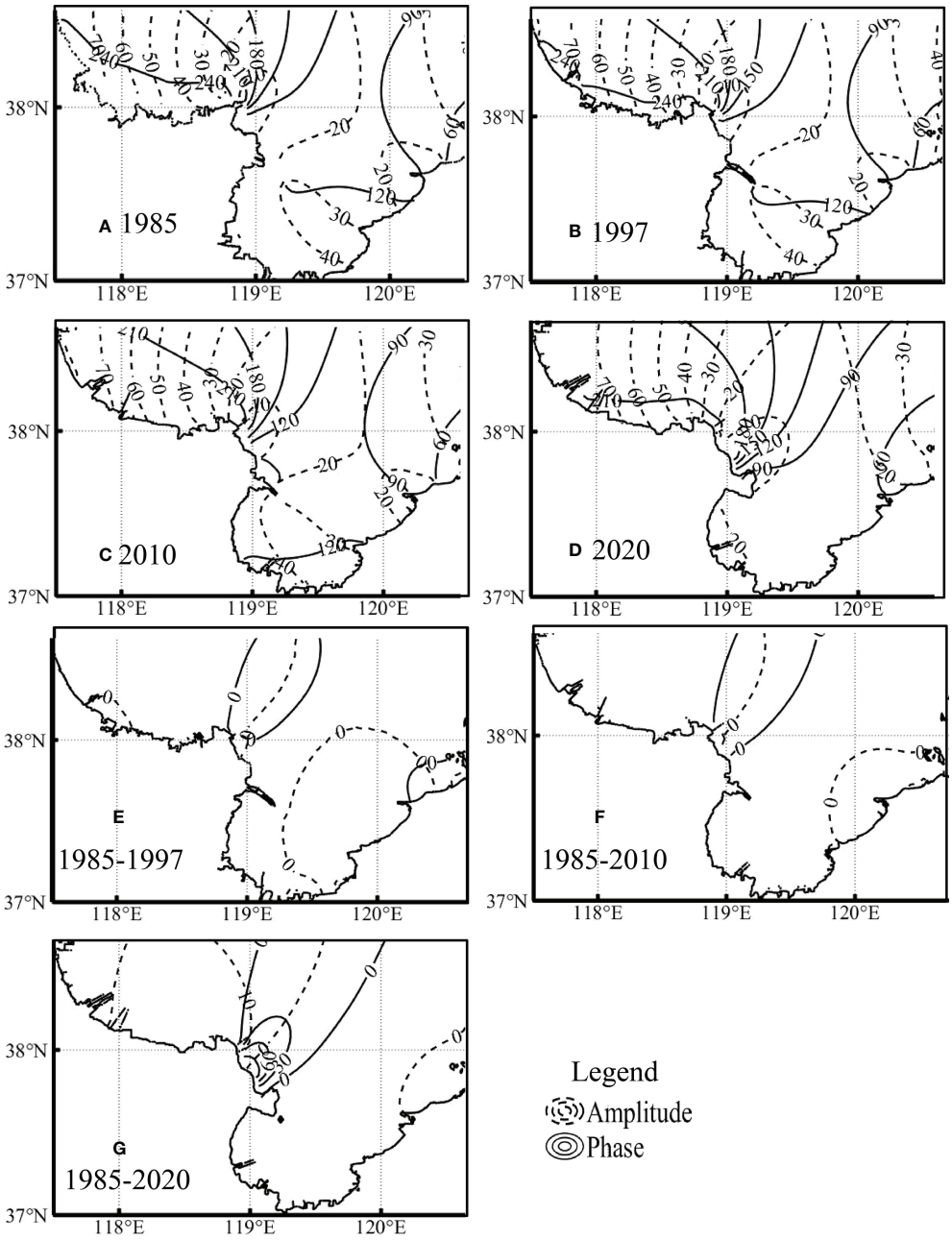

FIGURE 4
Amplitudes and phases of M_2 tidal constituents in 1985 **(A)**, 1997 **(B)**, 2010 **(C)** and 2020 **(D)**. Solid black lines represent the phase (°), and dotted black lines denote the amplitude (cm). **(E–G)** show the changes in M2 tidal constituents during these three periods. Solid black lines represent the phase (°) and dotted black lines denote the amplitude (cm).

landscapes, mostly in the southeastern areas of the SCBHS, are high or very high.

The spatial distribution of CVI in 2020 reveals that 35.8% of the study area with the total area of 3082 km^2 is moderately vulnerable, and the highly vulnerable areas with the CVI values of 4.1-6.0 account for 11.4% of the total area. These highly vulnerable areas are mainly distributed along the eastern coastline of the Laizhou Bay.

3.2 Spatial-temporal changes in HAI

3.2.1 Natural landscape degradation

Figures 6, 7 summarize the spatial and temporal distributions and area changes of artificial landscape in the SCBHS during 1985-2020. The artificial landscape area including saltern, aquaculture ponds and building land increased from 504 km^2

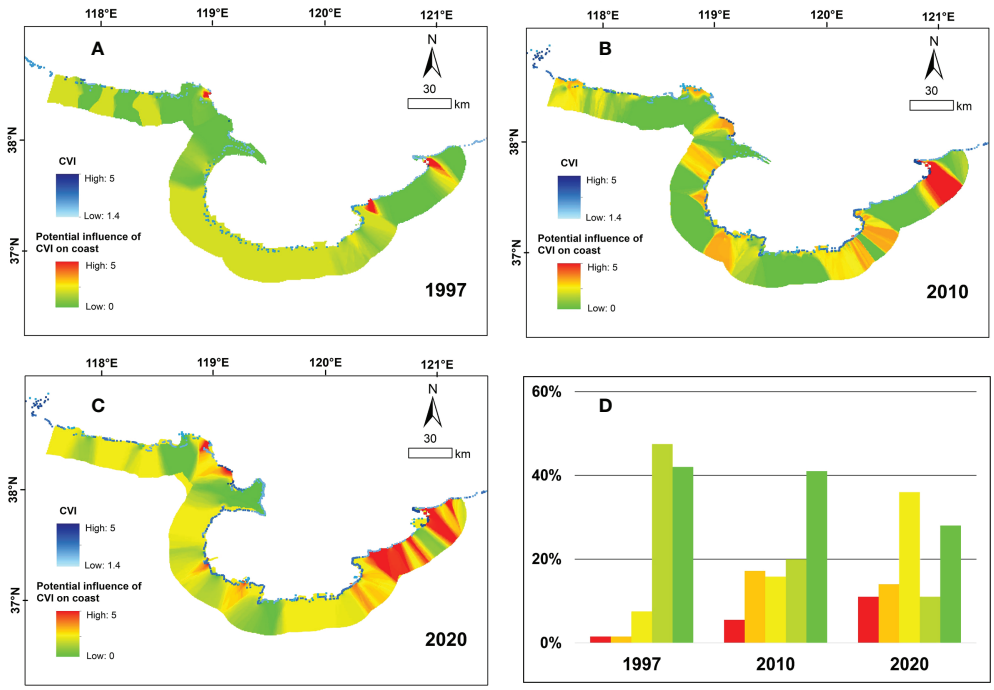

FIGURE 5
Temporal-spatial distribution of CVI in 1997 **(A)**, 2010 **(B)**, and 2020 **(C)**, and the area proportions of different ranks of CVI visualized by the equal interval breakpoint method with red, orange, yellow, light green, and green representing very high vulnerability, high vulnerability, medium vulnerability, low vulnerability and very low vulnerability **(D)**.

(6% of the total area) to 2647 km^2 (31% of the total area) in the 35 years. The changing trends of the areas of different types of artificial landscapes are different. The total building land area showed an obvious increasing trend, especially an increase of 17% from 1997 to 2010, due to the rapid urbanization. The areas of aquaculture pond and salt pan consistently increased by 5% and 11%, respectively, from 1985 to 2020. On the contrary, the areas of farmland, wetland land and tidal flat consistently decreased by 16%, 6% and 11%, respectively.

3.2.2 Spatial-temporal changes of HAI

The spatial distributions of HAI in SCBHS during different periods of time are obtained by the spatial analysis in GIS. It is found that the HAI of SCBHS in 2020 is highly intense with the average value of 0.74, and its spatial change is dramatic. From 1985 to 2020, the total area of moderate and high vulnerabilities increased from 935 km^2 (11% of the total area) to 1532 km^2 (18% of the total area) and the high HAI areas were mainly distributed in the western and central regions (Figure 8). The HAI of urban expansion is 0.92 in Yantai City, 0.70 in Weifang City, 0.85 in Qingdao City, 0.58 in Dongying City, and 0.46 in Binzhou City. From 1985 to 1997, building land experienced the highest annual growth rate of 7.6% during the three periods, showing a very high HAI. The comparison of the spatial distribution maps of CVI and HAI suggests that the increases in artificial landscape area cause the rise of HAI to 0.78, and 77% of artificial landscape area show high or very high CVIs.

3.3 SoVI

The SoVIs of the 5 cities involved in the study area are then calculated with the socio-economic data. (Figures 9) shows the distribution of SoVI and those of the 7 second level indexes over the five cities. The overall SoVI of the study area in 2020 is 0.49, suggesting that the area is moderately vulnerable. The SoVI of Weifang City is the highest with the value of 0.84 and that of Dongying City is the lowest (0.32). Yantai City is ranked the second highest with the SoVI of 0.51, followed closely by Binzhou City (0.41) and Qingdao City (0.40). The score of each secondary index is calculated with the normalization Eq. (5). Weifang City is scored the highest in health institution and the number of telephone subscribers, which explains its high vulnerability. The index sores of Dongying City are low in population under age 14 and over age 60, hospitals beds, and number of mobile telephone subscribers, suggesting its low vulnerability, which is consistent with its low SoVI. The relatively high SoVI of Yantai City can be attributed to its high scores in the indexes of population density and number of telephone subscribers.

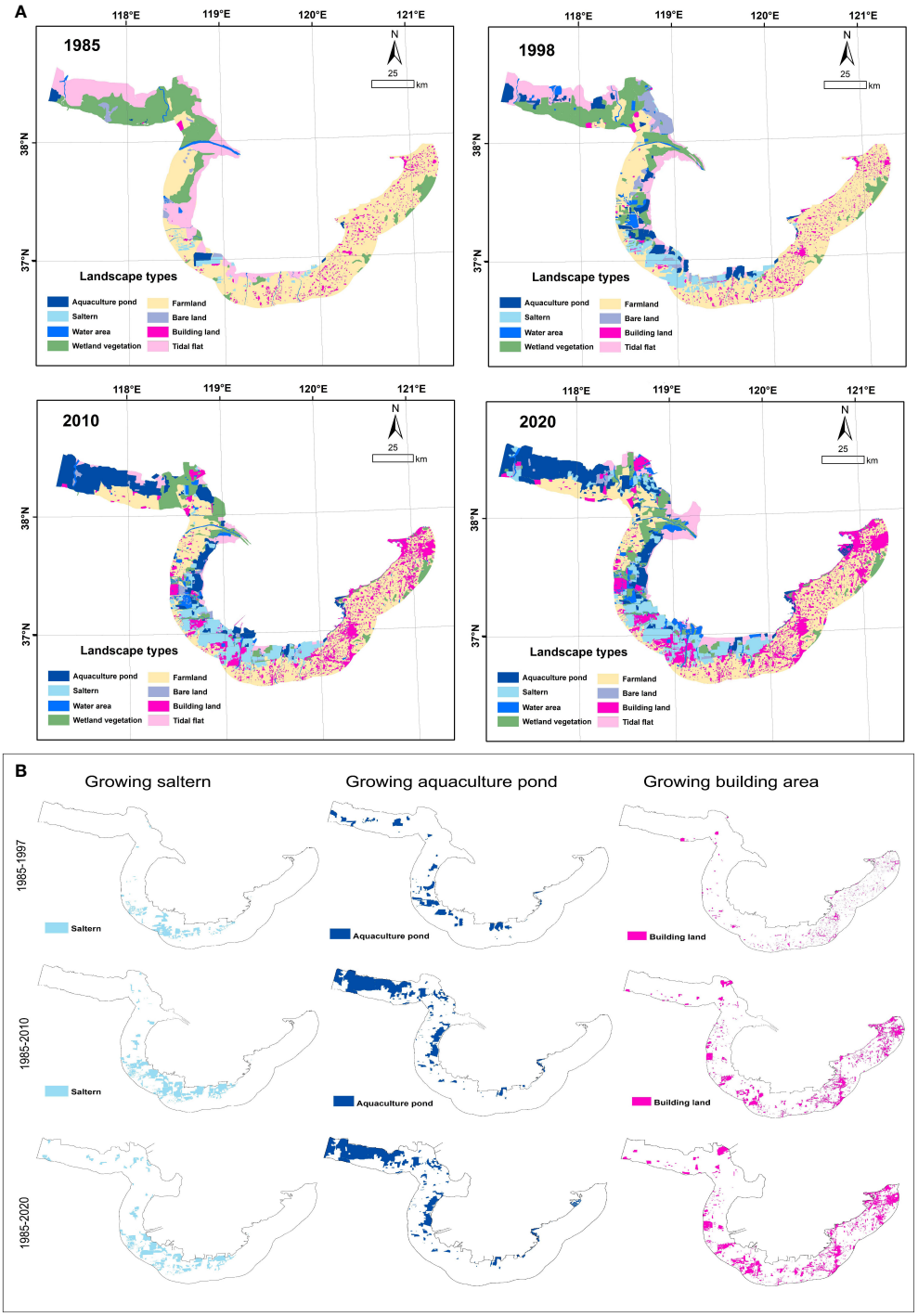

FIGURE 6
Landscape types and their distributions in 1985, 1997, 2010 and 2020 **(A)**; Temporal and spatial distributions of the increases in the areas of saltern, aquaculture pond and building land **(B)**.

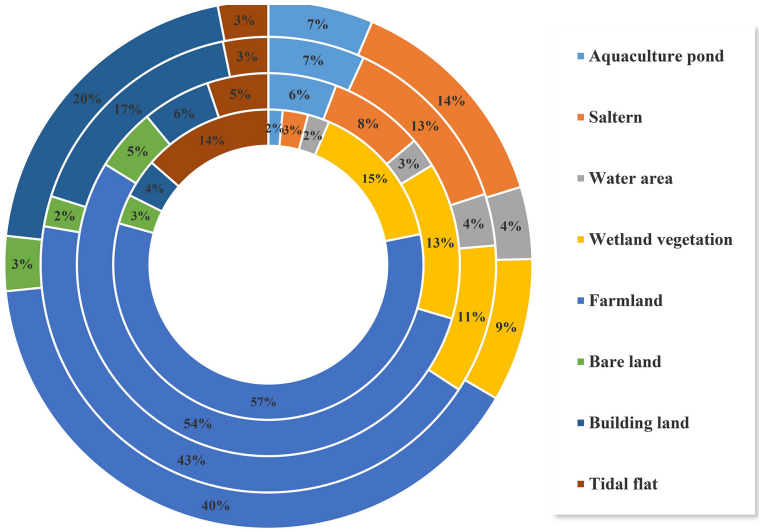

FIGURE 7
Area distributions by land use type in 1985 (most inside circle), 1997 (second most inside circle), 2010 (second most outside circle), and 2020 (most outside circle).

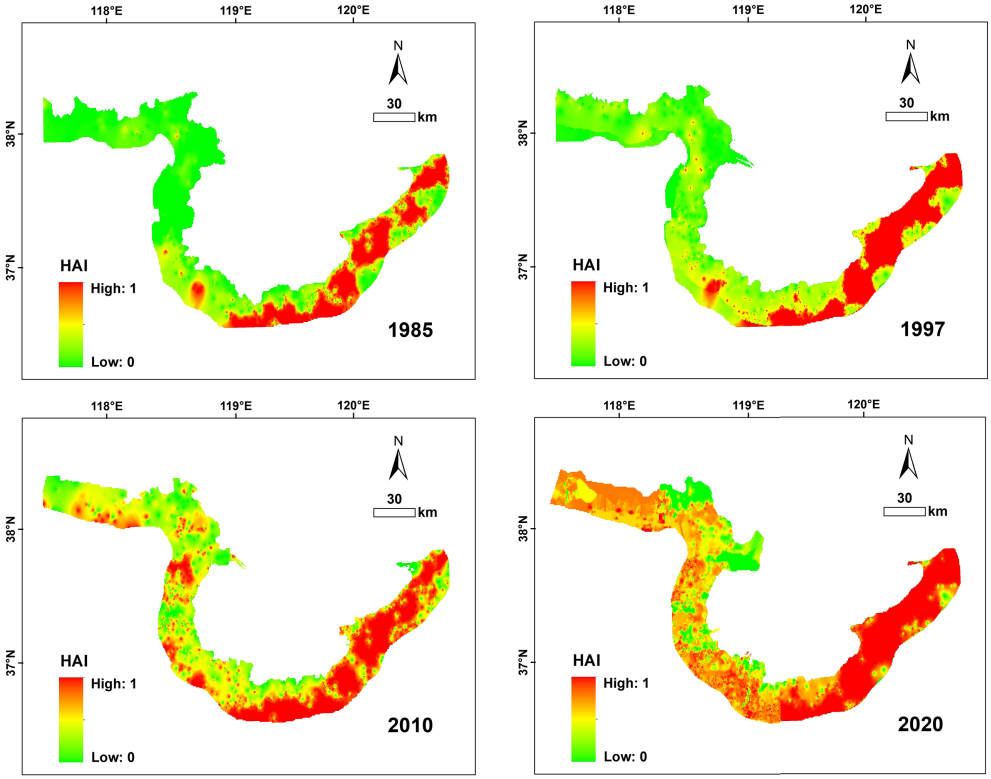

FIGURE 8
Temporal-spatial evolution of HAI from 1985 to 2020.

3.4 Overall assessment

The CVI and SoVI of the entire study area in 2020 are 4.1 and 0.49, respectively, with distinct spatial heterogeneity, which both are classified as moderate vulnerability. The overall HAI is determined to be 0.74, suggesting that the area is highly vulnerable. In terms of the specific regions, the CVI of Yantai City is the highest and the SoVI of Weifang City is the highest. Both cities show very high HAIs. Figure 5, Figure 8 and Figure 9 summarize the spatial-temporal changes in the CVI, HAI and SoVI of SCBHS. In the spatial scale, the CVI values along most parts of the coastline are low, except for the western coastline of the Laizhou Bay that is the most vulnerable to the impact of natural hazard. Yantai City shows the highest score of SoVI, which is highly vulnerable to coastal flooding.

4 Discussion

4.1 CVI model validation

The natural hazard susceptibility of SCBHS is characterized by a comparative spatial assessment of the regional response to coastal hazards using a modified CVI model that integrates the changes in reclamation activities, coastline and hydrodynamics between 1985 and 2020. The modeling reveals that the M_2 amplitude constituent in the northern coast of Yellow River Estuary increased by 20 cm-40 cm, consistent with the results of previous studies (Pelling et al., 2013). The increases in M_2 amplitude constituent mostly occur around the coastline, and thus are directly related to mean tidal range (I_7). In addition, the CVI assessment results of the studied area are compared with the coastal natural hazard index under current sea level scenario published by Sajjad et al. (2018) over the same period. Sajjad et al. predicated that the eastern coast region of the Laizhou Bay would meet the high-risk criteria by 2020. Their simulated CVI values in the SCBHS are also similar to our modeling results, except that their predicated values of the northern coast of Yellow River Estuary are generally greater possibly due to insufficient evaluation of the numerical tidal model.

4.2 Interactions among HAI, CVI and SoVI

The recent severe storm surges and occurrence of extensive floods that cause numerous casualties and significant economic losses in the SCBHS have reignited the need to understand the risks resulting from the intersection of vulnerable populations and marine hazards (Wang et al., 2018). It has been evidenced that the populations with higher social vulnerabilities, such as low-income and less support from social security and communication technology (insurance, mobile phone and internet), disproportionally suffer from the impacts of natural hazards. Therefore, our study includes these indexes to portray the

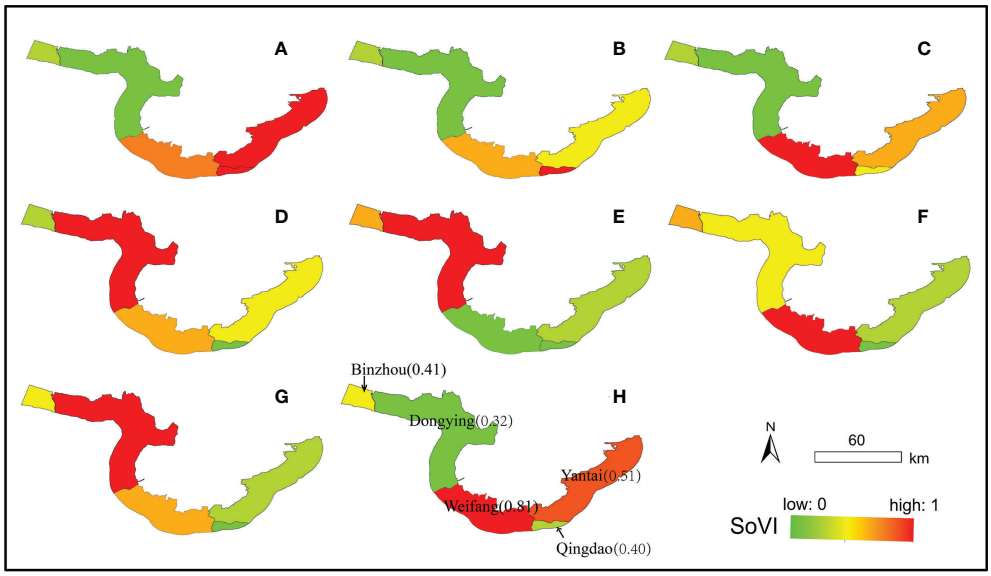

FIGURE 9
Social vulnerability score per index in 2020: **(A)** I_8: percentage of people under age 14 and over age 60; **(B)** I_9: population density; **(C)** I_{10}: average number of mobile telephone subscribers per people; **(D)** I_{11}: average number of internet broad band subscribers per people; **(E)** I_{12}: average number of participated in social insurance per people; **(F)** I_{13}: number of health institutions per square kilometers; **(G)** I_{14}: number of hospitals beds per square kilometers; and **(H)** SoVI.

dynamic representation of risks from natural hazards that affect local social vulnerability.

The CVI modeling indicates that the CVI of SCBHS has been increasing from 1985 to 2020, and the increasing trend is related to the HAI in the area. With the acceleration of human activities, such as industrialization and urbanization, large areas of natural wetlands are occupied by aquaculture pond, saltern, and building land in the south coast of the Laizhou Bay, which destructs natural habitats and results in the higher CVIs. Natural habitats, such as marshes, coastal dunes, and so on, play a vital role in resisting the impacts of coastal hazards that erode shorelines and harm coastal communities. Low revetments and seawalls are classified as highly vulnerable as they have limited abilities in preventing inundation and may fail during extreme events (Gornitz, 1990).

The second influencing factor to be considered is storm surge in the area. Studies have confirmed the significant inter-decadal variations of storm in the Bohai Sea, and the extreme storm surge events have been intensifying since 2010 (Feng et al., 2018). The visualization of the spatial distributions of HAI and SoVI facilitates the identification of the critical areas where disaster risks tend to increase drastically, and potential hazard events are likely to occur in the future. It is found in our study that the building land area in the north coast of Yantai City has dramatically expanded, and its exposure to storm surge risk has been increasing, which challenges the habitat stability of the surrounding areas.

The coastal region is a complex area with land-ocean interactions. Changes in coastline and artificial reclamation, as well as coastal landscape, can intensify marine hazards. The relationships of coastal land, offshore areas, and the ocean should be considered in the coastal vulnerability assessment, and it is necessary to study the human activities, natural processes, and social-economic aspects as one system. Attentions should be particularly paid to the coastal development regulation in disaster risk management and control. Understanding and identifying the populations vulnerable to natural hazard risks can improve future mitigation measures and reduce potential impacts of natural disasters.

4.3 Implications for coastal management

By providing a relative ranking of coastal areas in terms of CVI, the outcome of this study can be used by the coastal managers to define and prioritize risk management and adaptation measures. First, banning destructive economic activities and coastal development can improve the restoration of coastal natural habitats in the SCBHS. Second, man-made engineering structures, such as sea dikes, breakwaters, and spur dams, should be constructed along the western coast of the Laizhou Bay. For the CVI assessment model, dams are undoubtedly stronger for the resistance to marine hazards than rocks and high cliffs. Third, the coastal projects should be regulated to cause minimum changes in tidal regime and thus lower flood risk. Importantly, the most stringent management and control measures should be implemented on reclamation projects in the future.

By providing a relative ranking of coastal areas in terms of the SoVI, the outcome of this study can be used by the coastal managers to understand the underlying social, economic, and political context, and consequently address the factors that increase risk and vulnerability of the area. Based on the regional assessment, special attentions should be paid to the most vulnerable study units including Yantai City and Weifang City, as well as the identification of the driven indexes of the social vulnerability. By gradually bridging the gap between rural and urban areas in income, social and medical service levels, overall societal vulnerability is likely to be reduced (Chen et al., 2014).

5 Conclusion

Our study has made the following contributions: 1) An InVEST coastal vulnerability model including the influences of human activities is put forward; 2) the changes in coastline and hydrodynamics caused by reclamations are integrated into the model. 3) The spatial interactions between natural hazards and social vulnerability in the south coast of Bohai Sea are revealed.

The comprehensive evaluation of the vulnerability of SCBHS suggests that: 1) Coastal reclamation changes the coastline position and alters marine hydrodynamics, which influences the CVI; 2) The rapid coastal urbanization increases the artificial landscape area and causes high HAIs, which results in irreversible natural-hazard risks and thus increases the CVI; 3) The spatial distributions of HAI and SoVI obtained in this study can help to identify the critical locations where natural hazards related disasters likely occur and potentially cause great losses in the future.

Data availability statement

The original contributions presented in the study are included in the article/Supplementary Material. Further inquiries can be directed to the corresponding authors.

Author contributions

JL: Conceptualization, Data curation, Formal analysis, Investigation, Methodology, Software, Validation, Visualization, Writing - original draft, Writing - review & editing. YZ: Data curation, Formal analysis, Methodology, Supervision, Visualization. HS: Conceptualization, Funding acquisition, Methodology, Project administration, Resources. XL: Formal analysis, Methodology, Writing - review & editing, Project

administration, Resources. All authors contributed to the article and approved the submitted version.

Funding

This study is supported by the National Natural Science Foundation of China (No.U1806214 & No.51779048) and the National Key Research and Development Program of China (No. 2018YFD0900806).

Conflict of interest

The authors declare that the research was conducted in the absence of any commercial or financial relationships that could be construed as a potential conflict of interest.

Publisher's note

Supplementary material

The Supplementary Material for this article can be found online at: https://www.frontiersin.org/articles/10.3389/fmars.2022.1015781/full#supplementary-material

References

Arkema, K. K., Guannel, G., Verutes, G., Wood, S. A., and Silver, J. M. (2013). Coastal habitats shield people and property from sea-level rise and storms. *Nat. Climate Change* 3, 913–918. doi: 10.1038/nclimate1944

Boruff, B. J., and Cutter, S. L. (2007). The environmental vulnerability of Caribbean island nations. *Geograph. Review.* 97 (1), 24–45. doi: 10.1111/j.1931-0846.2007.tb00278.x

Chen, W., Cutter, S. L., Emrich, C. T., and Shi, P. (2014). Measuring social vulnerability to natural hazards in the Yangtze River Delta region, China. *Int. J. Disaster Risk Sci.* 4, 169–81. doi: 10.1007/s13753-013-0018-6

Cheng, Y., Lv, X. Q., Liu, Y. G., and Xu, Q. (2007). Application of adjoint assimilation technique in simulating tides and tidal currents of the bohai Sea, the yellow Sea and the East China Sea. *High Technol. Newslett.* 13 (1), 7. (in Chinese with English abstract)

Chi, Y., Shi, H. H., Sun, J. K., Li, J., Yang, F., and Fu, Z. Y. (2017). The temporal and spatial characteristics and main influencing factors of vegetation net primary productivity of the yellow river delta in recent 30 years. *Acta Ecol. Sin.* 38 (08), 82–96. doi: 10.5846/stxb201705301000

Chi, Y., Shi, H., Zheng, W., Sun, J., and Fu, Z. (2018a). Spatiotemporal characteristics and ecological effects of the human interference index of the yellow river delta in the last 30 years. *Ecol. Indicators.* 89, 880–892. doi: 10.1016/j.ecolind.2017.12.025

Chi, Y., Zheng, W., SHI, H. H., Sun, J. K., and Fu, Z. Y. (2018b). Spatial heterogeneity of estuarine wetland ecosystem health influenced by complex natural and anthropogenic factors. *Sci. Tot. Environ.* 634, 1445–1462. doi: 10.1016/j.scitotenv.2018.04.085

Feng, J., Li, D., Li, Y., Liu, Q., and Wang, A. (2018). Storm surge variation along the coast of the Bohai Sea. *Sci. Rep.* 8, 11309. doi: 10.1038/s41598-018-29712-z

Feng, Z., Zhang, J., Hou, W., and Zai, L. (2017). Dynamic changes of hemeroby degree based on the land cover classifcation: A case study in Beijing. *Chin. J. Ecol.* 36 (2), 508–516.

Gornitz, V. (1990). Vulnerability of the east coast, U.S.A. to future sea level rise. *J. Coast. Res.* 9, 201–237. doi: 10.2307/44868636

Gornitz, V. M., Beaty, T. W., and Daniels, R. C. (1997). *A coastal hazards database for the U.S. West coast. ORNL/CDIAC-81, NDP-043C* (Oak Ridge, Tennessee: Oak Ridge National Laboratory).

Hammar, K., and Thieler, E. R. (2001). "Coastal vulnerability to Sea-level rise," in *A preliminary database for the U.S. Atlantic, pacific, and gulf of Mexico coasts. U.S* (Denver, CO: Geological Survey, Digital Data Series DDS-68, 1 CD-ROM).

He, Y., Lu, X., Qiu, Z., and Zhao, J. (2004). Shallow water tidal constituents in the bohai Sea and the yellow Sea from a numerical adjoint model with TOPEX/POSEIDON altimeter data. *Cont. Shelf Res.* 24, 1521–1529. doi: 10.1016/j.csr.2004.05.008

Holand, I. S., and Lujala, P. (2013). Replicating and adapting an index of social vulnerability to a new context: A comparison study for Norway. *Prof. Geographer.* 65 (2), 312–328. doi: 10.1080/00330124.2012.681509

Huang, M., Xia, C., Li, Y., Zeng, C., and Zhang, B. (2022). Coupling responses of landscape pattern to human activity and their drivers in the hinterland of three gorges reservoir area. *Global Ecol. Conserv.* 33, e01992. doi: 10.1016/j.gecco.2021.e01992

IPCC (2013). "Climate change 2013: The physical science basis," in *Contribution of working group I to the fifth assessment report of the intergovernmental panel on climate change*. Eds. T. F.Stocker, D. Qin, G.-K. Plattner, M. Tignor, S. K. Allen, J. Boschung, A. Nauels, Y. Xia, V. Bex and P. M. Midgley (Cambridge, United Kingdom and New York, NY, USA: Cambridge University Press).

Jiang, T., Wu, G., Niu, P. L., Cui, Z. G., Bian, X. D., Xie, Y. X., et al. (2022). Short-term changes in algal blooms and phytoplankton community after the passage of super typhoon lekima in a temperate and inner sea (Bohai Sea) in China. *Ecotoxicol Environ. Saf.* 232, 113223. doi: 10.1016/j.ecoenv.2022.113223

Jiang, S., Xu, N., Li, Z., and Huang, C. (2021). Satellite derived coastal reclamation expansion in China since the 21st century. *Global Ecol. Conserv.* 30, e01797. doi: 10.1016/j.gecco.2021.e01797

Jin, Y., Yang, W., Sun, T., Yang, Z., and Li, M. (2016). Effects of seashore reclamation activities on the health of wetland ecosystems: A case study in the yellow river delta, China. *Ocean Coast. Manage.* 123, 44–52. doi: 10.1016/j.ocecoaman.2016.01.013

Koks, E. E., Jongman, B., Husby, T. G., and Botzen, W. J. W. (2015). Combining hazard, exposure and social vulnerability to provide lessons for food risk management. *Environ. Sci. Policy* 47, 42–52. doi: 10.1016/j.envsci.2014.10.013

Koroglu, A., Ranasinghe, R., Jiménez, J., and Ali, D. (2019). Comparison of coastal vulnerability index applications for Barcelona province. *Ocean Coast. Manag.* 178, 104799. doi: 10.1016/j.ocecoaman.2019.05.001

Liu, S., Liu, L., Wu, X., Hou, X., Zhao, S., and Liu, G. (2018). Quantitative evaluation of human activity intensity on the regional ecological impact studie. *Acta Ecol. Sin.* 38 (19), 6797–6809. doi: 10.5846/stxb201711172048

Lu, X. Q., and Zhang, J. C. (2006). Numerical study on spatially varying bottom friction coefficient of a 2D tidal model with adjoint method. *Cont. Shelf Res.* 26, 1905–1923. doi: 10.1016/j.csr.2006.06.007

Mesta, C., Cremen, G., and Galasso, C. (2022). Urban growth modelling and social vulnerability assessment for a hazardous Kathmandu valley. *Sci. Rep.* 12, 6152. doi: 10.1038/s41598-022-09347-x

Nature, International Union for Conservation of, and Natural Resources and Ramsar Convention Bureau (1984). Convention on Wetlands of International Importance especially as Waterfowl Habitat. *Proceedings of the second conference of the contracting parties*, Groningen, Netherlands, 1984, 7–12.

Pan, H. D., Wang, Y. Z., and Lv, X. Q. (2021). The study of the trends of tidal amplitudes of major constituents in the south China Sea. *Hai yang Xuebao* 43 (6), 26–34. doi: 10.12284/hyxb2021096

Pelling, H. E., Uehara, K., and Green, J. A. M. (2013). The impact of rapid coastline changes and sea level rise on the tides in the bohai Sea, China. *J. Geophys. Res.: Oceans.* 118, 3462–3472. doi: 10.1002/jgrc.20258

Peng, F., and Han, Z. L. (2013). Characteristics of climate change in coastal cities around the bohai Sea and their responses to urban development. *Mar. Dev. Manage.* 11, 30–34. doi: 10.3969/j.issn.1005-9857.2013.11.008

Sajjad, M., Li, Y. F., Tang, Z. H., Cao, L., and Liu, X. P. (2018). Assessing hazard vulnerability, habitat conservation and restoration for the enhancement of china's coastal resilience. *Earths Future.* 6 (3), 326–338. doi: 10.1002/2017EF000676

Shandong Statistical Yearbook (2021) *Shandong Provincial bureau of statistics*. Available at: http://tjj.shandong.gov.cn.

Shi, H. H., Lu, J. F., Zheng, W., Sun, J., Li, J., Guo, Z., et al. (2020). Evaluation system of coastal wetland ecological vulnerability under the synergetic influence of land and sea: A case study in the yellow river delta, China. *Mar. pollut. Bulletin.* 161, 111735. doi: 10.1016/j.marpolbul.2020.111735

Shi, H. H., Yu, D. L., Yin, L. T., Sui, Y. D., Liu, Y. Z., Qiao, S. Q., et al. (2022). Source-sink process of microplastics in watershed-estuary-offshore system. *J. Cleaner Prod.* 338, 130612. doi: 10.1016/j.jclepro.2022.130612

Siagian, T. H., Purhadi, P., Suhartono, S., and Ritonga, H. (2013). Social vulnerability to natural hazards in Indonesia: driving factors and policy implications. *Natural Hazards.* 70, 1603–1617. doi: 10.1007/s11069-013-0888-3

Sodhi, M. S. (2016). Natural disasters, the economy and population vulnerability as a vicious cycle with exogenous hazards. *J. Operations Manag.* 45, 101–113. doi: 10.1016/j.jom.2016.05.010

Sun, T., Lin, W., Chen, G., Guo, P., and Zeng, Y. (2016). Wetland ecosystem health assessment through integrating remote sensing and inventory data with an assessment model for the hangzhou bay, China. *Sci. Total Env.* 566–567, 627–640. doi: 10.1016/j.scitotenv.2016.05.028

Thieler, E. R., Himmelstoss, E. A., Zichichi, J. L., and Ergul, A. (2009) *The digital shoreline analysis system (DSAS) version 4.0-an ArcGIS extension for calculating shoreline change.* Available at: http://woodshole.er.usgs.gov/projectpages/DSAS/version4/index.html.

Wang, C., Cai, L., Wu, Y., and Ouyang, Y. (2021). Numerical simulation of the impact of an integrated renovation project on the maowei Sea hydrodynamic environment. *Sci. Rep.* 11, 17059. doi: 10.1038/s41598-021-96441-1

Wang, Y., Mao, X., and Jiang, W. (2018). Long-term hazard analysis of destructive storm surges using the ADCIRC- SWAN model: A case study of bohai Sea, China. *Int. J. Appl. Earth Observation Geoinformat.* 73, 52–62. doi: 10.1016/j.jag.2018.03.013

Wen, Y. (1998). *Preliminary discussion on quantitative evaluation method of human activity intensity. Science and Society*. (Beijing: University of Posts and Telecommunications Press), 56–61.

Xu, Y., Sun, X., and Tang, Q. (2015). Human activity intensity of land surface: concept, method and application in China. *J. Geogr. Sci.* 70 (7), 1068–1079. doi: 10.1007/s11442-016-1331-y

Yang, F., Li, J., Wang, J., Huang, J., and Zhao, L. (2021). Spatiotemporal characteristics of human activity on coastal landscape of laizhou bay. *Wetlands Ecol. Manage.* 29, 789–808. doi: 10.1007/s11273-021-09810-y

Zhou, Y., Varquez, A. C. G., and Kanda, M. (2019). High-resolution global urban growth projection based on multiple applications of the SLEUTH urban growth model. *Sci. Data.* 6, 34–34. doi: 10.1038/s41597-019-0048-z

Zhu, G., Xie, Z., Xie, H., Li, T., Gu, X., and Xu, X. (2018). Land-sea integration of environmental regulation of land use/land cover change-a case study of bohai bay, China. *Ocean Coast. Manag.* 151, 109–117. doi: 10.1016/j.ocecoaman.2017.10.015

frontiers | Frontiers in Marine Science

TYPE Original Research
PUBLISHED 25 October 2022
DOI 10.3389/fmars.2022.982263

OPEN ACCESS

EDITED BY
Jose A. Jimenez,
Universitat Politecnica de Catalunya,
Spain

REVIEWED BY
Ariel Blanco,
University of the Philippines Diliman,
Philippines
Daniele Brigolin,
Università Iuav di Venezia,
Italy

*CORRESPONDENCE
Guanqiong Ye
gqy@zju.edu.cn

SPECIALTY SECTION
This article was submitted to
Coastal Ocean Processes,
a section of the journal
Frontiers in Marine Science

RECEIVED 30 June 2022
ACCEPTED 26 September 2022
PUBLISHED 25 October 2022

CITATION
Han Y, Zhang Y, Zhang H, Feng C, Hua T, Yang Y, Yun P, Zeng J, Peng L, Zeng J and Ye G (2022) Spatiotemporal resilience assessment and comparison in China's bay area. *Front. Mar. Sci.* 9:982263. doi: 10.3389/fmars.2022.982263

Spatiotemporal resilience assessment and comparison in China's bay area

Yu Han[1], Yaowen Zhang[2], Han Zhang[2], Cuicui Feng[2], Tianran Hua[2], Yiqun Yang[2], Peng Yun[1], Jian Zeng[1], Li Peng[3], Jiangning Zeng[4] and Guanqiong Ye[2]*

[1]Zhejiang Institute of Marine Planning and Design, Zhejiang Institute of Hydraulics & Estuary, Zhejiang, China, [2]Ocean College, Zhejiang University, Zhejiang, China, [3]School of Internet of Things Engineering, Jiangnan University, Jiangsu, China, [4]Second Institute of Oceanography, Ministry of Natural Resources (MNR), Zhejiang, China

The bay area is a crucial land–sea junction zone containing essential urban clusters while receiving extremely complex internal and external disturbances that challenge more on its resilience management. However, a sound management tool based on the bay area's resilience is widely lacking due to the difficulty of unifying resilience indicators and quantifying resilience relationships between regions. This paper tries to establish a comprehensive resilience index for coastal bays from four major resilience-related dimensions, namely, physical structure, social development, ecological environment, and hazards, and applies it into the three major developed bay areas in China. A coupling coordination degree model was used to further reveal the resilience development and its internal coordination by temporal and spatial differences. The results show that the index could clearly reveal the resilience changes from the year 2000 to 2020 of the three bays with the common key drivers of socioeconomic development. It also explains the resilience changes among three bay areas through analyzing synergistic and conflict relationships between the four sub-resilience systems.

KEYWORDS

bay area, resilience, sustainable development, spatial and temporal assessment, ecological economic equilibrium

1 Introduction

Resilience is the ability of a system to adapt, overcome external disturbances, maintain its own stability, and restore its own function through a series of processes such as "resistance, absorption, repair, enhancement, and learning" (Adger et al., 2005). Resource depletion and potential environmental damage have triggered considerable concern about introducing resilience theory into regional management framework to

achieve sustainable development (Brand, 2009; Yang et al., 2018). The resilience concept is permeating policymaking, for example, the National Science & Technology Council (NSTC) of the US published the "Opportunities and Actions for Ocean Science and Technology 2022–2028," which encouraged the development of key elements for building resilient coastal communities, such as knowledge, technology, and capital (NSTC, 2022). Moreover, China has included the concept of urban resilience in the 14th Five-Year Plan and outline of long-term goals for 2035. However, even if increasing academic research and debates have discussed resilience management from multiple perspectives, there still a lack of comprehensive general discussions on evaluation strategies in this new and growing field (Li et al., 2020; Liu et al., 2022). A critical but largely inadequate need for resilience management is scientific information (Brown and Williams, 2015). Thus, government occupies the primary position in promoting resilience development systemically through public policies. For practical policy guidance, understanding the overall character of the systemic resilience based on quantifying interactions of impact factors within the system would facilitate better results (Nathwani et al., 2019). Since resilient development of the coastal zone requires consideration of the nexus between the land and sea, it is difficult to process in coastal areas.

The degree of resilience in land–sea intersection areas remains poorly understood, as the difficulty on unraveling interaction relationships between coastal community development and marine ecosystem changes. Nevertheless, coastal cities, especially in bay areas, are, in many cases, global economic centers (e.g., manufacturing, technology, trade, and finance) where the massive population aggregation and speeding up of industrialization make them vulnerable in facing complex disturbances from both the land and sea areas (Gao et al., 2022). For example, Bohai Bay, Yangtze river Delta, and Pearl River Delta of Chinese important bay areas and other international bay areas, e.g., the Tokyo Bay, San Francisco Bay, and New York Bay, are in a dilemma between economic growth and ecological degradation. In particular, the coastal urban ecosystem is vulnerable to disturbance (Nathwani et al., 2019). Thus, improving the resilience of the bay area has become a critical way to pursue sustainable development and tackle multi-risks (Sellberg et al., 2018; Jozaei et al., 2020; Wang et al., 2021). Among the existing literatures about urban resilience, conceptual studies have received more attention than analytical studies. Resilience is an important attribute to describe the dynamics of urban social–ecological system (SES), which has been studied in many fields from different perspectives (Adger et al., 2005; Folke et al., 2010). The Land–Ocean Interactions in the Coastal Zone (LOICZ) project constructed the framework of resilience and transformation on urban coasts (Ramesh et al., 2015), while contemporary studies have not devoted enough concern to the resilience assessment of the bay area ecosystem (Adger et al., 2005; Nathwani et al., 2019; Büyüközkan et al., 2022). An integrated vision of resilience evaluation suggests quantifying the dynamics and interactive relationships among various factors within the system to identify holistic properties of resilient systems. Otherwise, as is the case with most studies, qualitative or quantitative evaluation of the integrated resilience generally does not capture the breadth and depth of resilient evolution (Gari et al., 2015; Angeler and Allen, 2016; Liang and Li, 2020). Moreover, one issue that stands out in these studies is that they mostly focus on one risk, one disaster, or one region, which makes results lack comparability and universality (Diaz-Sarachaga and Jato-Espino, 2020; Kasmalkar et al., 2020; Li et al., 2021). In consequence, it is necessary to develop a comprehensive and informative resilience assessment framework tailored to the characteristics of the bay area and help formulate strategies in these areas to respond positively to crisis that might occur in the future.

The understanding of how changing patterns of resilience in the bay area is related to the broader dimensions of socioeconomic and environmental development is thus far largely unresolved. Here, we addressed these knowledge gaps by estimating the temporal and spatial variation in resilience of typical bay areas of China and then relating these resilience changes to human stressors and socioeconomic status. By subdividing the structure, impact, and process of resilience in the bay area system, the study innovatively constructed a resilience framework including the internal resilience structure and the external resilience of the bay area, and a total of 15 indicators were selected. Subsequently, we took the Bohai Bay, Hangzhou Bay, and Pearl River Delta as research objects, applied the framework to measure the resilience dynamic in the region, and analyzed differences in the development of resilience levels between regions by means of spatial and temporal variability analysis. Furthermore, coupling coordination degree model (CCDM) is often used to analyze the relationship between economic and ecological open systems with coupled characteristics (Jia et al., 2008, Zhang and Mo, 2014, Luo et al., 2021). Thus, the coupling coordination degree model (CCDM), correlation analysis, and significance test were used to illustrate the variation of resilience in the bay area through analyzing synergistic and conflict relationships between internal-resilience-related attributes. In a continuous changing world, this work can be used to explore enabling conditions for resilience building and guide effective policy and actions for promoting sustainable development of the bay area.

2 Methods

2.1 Study areas

We chose the three major bays as study areas, namely, Bohai Bay, Hangzhou Bay, and the Pearl River Delta from the north coast to the south coast of China, which ensured regional

representativeness. They have been experiencing rapid economic development in the recent 30 years, accounting for 15.6% of the 2020 gross national product (GNP), and thus represented a high level and intensity of economic activities and dense urban development. As the epitome of many coastal cities in China, they have been already struggling with coastal ecosystem degradation, inadequate urban infrastructure and services, and so on, which may in turn restrict the resilient development of bays (Gao et al., 2013). Therefore, bays are especially sensitive to threats due to high population density and resource consumption but are capable of coping with resilient threats as an important engine for ocean economic development. The dual characteristics of high economic development level and high marine ecological stress in Chinese coastal areas are the motivation to study the resilience of Chinese bays. The locations and socioeconomic information are shown in Figure 1. Among them, Bohai Bay covers Qinhuangdao, Tangshan, Tianjin, Cangzhou, and Binzhou; Hangzhou Bay covers Shanghai, Jiaxing, Hangzhou, and Ningbo; and the Pearl River Delta covers Shenzhen, Dongguan, Guangzhou, Zhongshan, and Zhuhai.

2.2 Index construction

Frameworks play an important role in analyzing social–ecological systems (Joerin et al., 2014), which provide shared concepts and variables that enable comparison across multiple cases. Some studies have proposed the conceptual framework of urban resilience (Galderisi, 2014; Ribeiro and Gonalves, 2019; Zhang et al., 2020), most of which reflect the ability of urban systems to resist, recover, adapt, or transform in the face of a series of disturbances. The adaptive cycle, a central mechanism of resilience theory, characterizes the dynamics of social–ecological systems (Yan and Tang, 2020). As a complex adaptive system in the bay area, current studies have focused strongly on a single subsystem and the single threats affecting that subsystem (Kuenzer et al., 2020). Therefore, to better make a

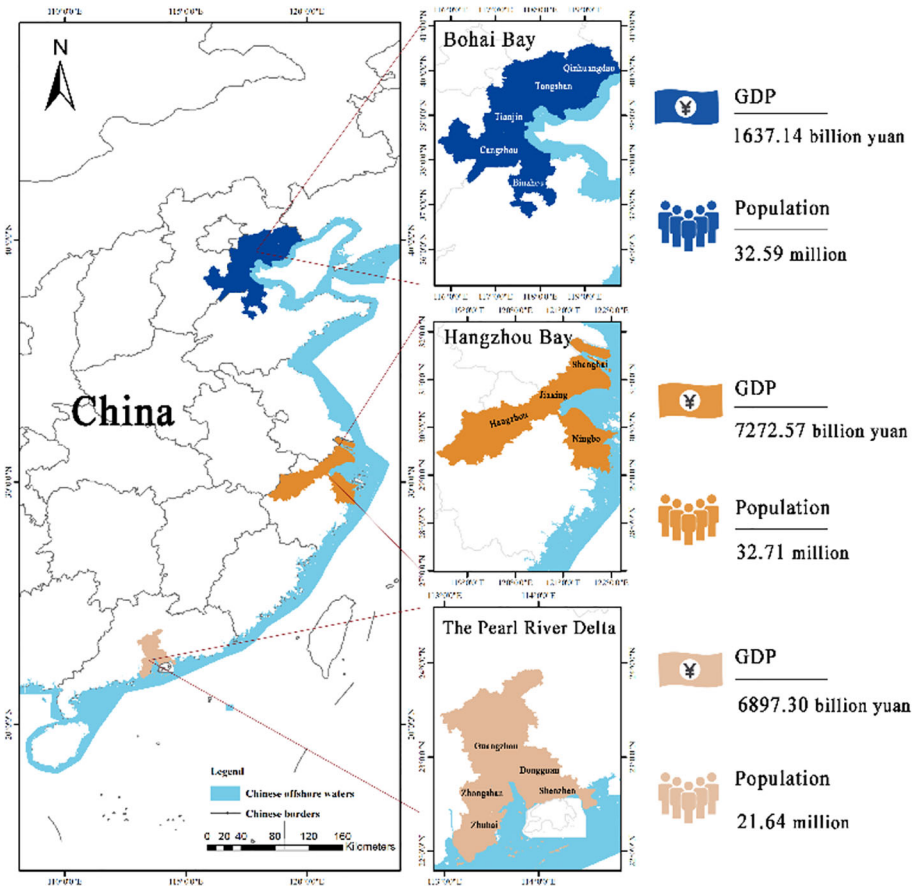

FIGURE 1
Location of Bohai Bay, Hangzhou Bay, and the Pearl River Delta in China. GDP and population are counted in 2020.

reasonable and valid assessment of the resilience of the bay, we instantiated the complex framework of multiple subsystems (Figure 2) to reveal the changes in resilience resulting from the spatial and temporal variability of the three major bay area in China. The interactions between the internal attributes of coastal zone resilience were further explored. In light of the conceptual framework, specific indicators were selected based on previous studies (Zheng et al., 2018; da Silva et al., 2019; Oke et al., 2020), field survey, and adaptive resilience theory (Lak et al., 2020; Wardekker et al., 2020) (Table 1). Fifteen indicators in the index were extracted from the bay areas' status of urban economy and social and coastal ecological environment. Thus, the evaluation index system of bay areas' resilience was composed of four sub-resilience systems: physical space resilience, social development resilience, ecology resilience, and disasters resilience.

2.3 Mathematical processing

2.3.1 Assessment of bay area resilience

Due to the inconsistency of the units of the indicators in the resilience assessment framework, it is necessary to first standardize the original indicator data across multiple regions using the range method according to the effect direction of indicators on bay areas' resilience.

$$\begin{cases} N_{ij} = \frac{N_{ij} - min\{N_{ij}\}}{max\{N_{ij}\} - min\{N_{ij}\}} \ if & + \\ N_{ij} = \frac{\max\{N_{ij}\} - N_{ij}}{max\{N_{ij}\} - min\{N_{ij}\}} \ if & - \end{cases} \quad (1)$$

where N_{ij} refers to the specific value of the j indicator in the i_{th} year.

The entropy method is an objective weighting method widely used in evaluating environmental time series data (Delgado and Romero, 2016) that is calculated according to the degree of variation in the data series. The advantage of the entropy method in multidimensional comprehensive evaluation is that it is more objective, avoiding the influence of human factors in subjective evaluation (Zhang et al., 2011). Compared with the analytic hierarchy process (AHP), principal component analysis (PCA), and other subjective weighting methods, this method is more objective and convenient (Lin et al., 2022). Therefore, it was applied to give weight to the bay area resilience index system. In this study, the weights of indicators determined by entropy method were calculated by Equations (2–4):

$$\rho_{ij} = \frac{N_{ij}}{\sum_{i=1}^{n} N_{ij}} \quad (2)$$

$$e_j = -k \sum_{i=1}^{n} \rho_{ij} \cdot \ln(\rho_{ij}) \quad (3)$$

$$w_j = \frac{1 - e_j}{\sum_{j=1}^{m} (1 - e_j)} \quad (4)$$

where N_{ij} indicates the normalized data of Equation (1), and e_j and w_j are the entropy value and the calculated weight of each indicator, respectively. In Equation (3), $k = \frac{1}{\ln n}$, which is used to make sure that the logarithm has meaning.

Ultimately, the quantifying results of resilience through standardized values and weights of indicators are:

$$R_{ij} = \sum_{j=1}^{m} N_{ij} \cdot w_j \quad (5)$$

2.3.2 Correlation analysis

In order to better explore the interactions between the internal attributes of coastal zone resilience, this paper adopts the method of calculating Pearson's coefficient to determine the degree of correlation between two factors. This paper also used the one-way ANOVA method for significance testing of indicators in different bays.

Overall correlation coefficients ρ for the two factors X, Y are as follows:

$$\rho_{X,Y} = \frac{cov(X, Y)}{\sigma_X \sigma_Y} = \frac{E[(X - \mu_X)(Y - \mu_Y)]}{\sigma_X \sigma_Y} \quad (6)$$

Pearson correlation coefficient r:

$$r = \frac{\sum_{i=1}^{n} (X_i - \bar{X})(Y_i - \bar{Y})}{\sqrt{\sum_{i=1}^{n} (X_i - \bar{X})^2} \sqrt{\sum_{i=1}^{n} \sum_{i=1}^{n} (Y_i - \bar{Y})^2}} \quad (7)$$

where r can also be estimated by (X_i, Y_i)

$$r = \frac{1}{n-1} \sum_{i=1}^{n} \left(\frac{(X_i - \bar{X})}{\sigma_X} \right) \left(\frac{(Y_i - \bar{Y})}{\sigma_Y} \right) \quad (8)$$

2.3.3 The coupling coordination degree model

The coupling coordination degree model (CCDM) were employed to analyze the coupling coordination relationship among the four sub-resilience systems in the three bay areas of China. According to the ecological coupling evaluation model (Li et al., 2019), the formulas were given as follows.

$$D = (C \times T)^{1/2} \quad (9)$$

where D represents the coupling coordination degree, $D \in [0,1]$; C denotes the coupling degree, $C \in [0,1]$; and T represents the integrated evaluation index of the four sub-resilience (physics, social economy, ecology, and disaster). The closer the D value is to 1, the better is the coordination relationship, anssd the closer the D value is to 0, the worse is the coordination relationship. In the study, the criteria for classifying the coupling coordination level are determined according to the distribution function (Liao, 1996).

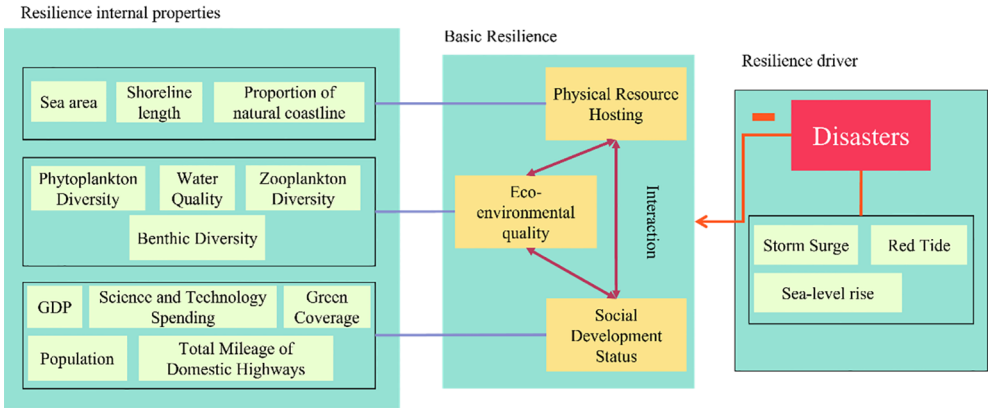

FIGURE 2
The conceptual framework of resilience assessment. The resilience system consists of four sub-resilience systems, namely, physical space, social development, ecology, and disasters, and the sub-resilience system of disasters may act negative impacts on the overall coastal resilience while the other three sub-resilience systems form the basic resilience with multiple internal properties of the coastal bay areas.

$$C = \sqrt[4]{\frac{R \times S \times E \times D}{[(R+S+E+D)/4]^4}} \tag{10}$$

where R, S, E, and D denote the calculation result of the physics, social economy, ecology, and disaster sub-resilience, respectively.

$$T = \alpha R + \beta S + \gamma E + \delta D \tag{11}$$

where α, β, γ, and δ represent their contribution. In the study, it is assumed that $\alpha=\beta=\gamma=\delta=1/4$, considering that the core of bay area's resilience is coordination.

2.4 Data sources

The index data of social development status was obtained from the National Bureau of Statistics, the China City Statistical Yearbook, and the statistical yearbooks/bulletins of various provinces and cities. Environmental data came from the Bulletin on the State of China's Marine Ecological Environment and the Environmental Protection Bulletin of various provinces and cities. Disaster data came from China Marine Disaster Bulletin, China Sea Level Bulletin, and Marine Disaster Bulletin of various provinces and cities. Physical space

TABLE 1 Indicators for assessing the resilience of the bay area.

Theme	Sub-resilience system	Indicators	Symbols	Unit	Direction
Bay area resilience	Physical Space Resources	Sea area	R_1	km^2	+
		Shoreline length	R_2	km	+
		Proportion of natural coastline	R_3	%	+
	Social Development	Population	S_1	Million people	+
		GDP	S_2	CNY billion	+
		Science and Technology Expenditure	S_3	CNY million	+
		Total Mileage of Highways	S_4	km	+
		Green Coverage	S_5	ha	+
	Ecology	Water quality	E_1	%	+
		Phytoplankton Diversity	E_2		+
		Zooplankton Diversity	E_3		+
		Benthic Diversity	E_4		+
	Disasters	Number of Storm Surge	D_1	Count	–
		Number of Algal Bloom	D_2	Count	–
		Sea-level rise	D_3	millimeter	–

The direction of the "+" indicates that the larger the indicator value is, the better the performance of resilience will be, while the "–" indicates that the larger the index value is, the worse the performance of resilience will be.

resource data came from the literature (Zhang et al., 2016; Sun et al., 2017; Li, 2020; Peng et al., 2020). Although very little data were missing, a nearest neighbor interpolation method was used to fit the data when needed to ensure the data continuity. More information about the data sources could be found in Table 2.

3 Results

3.1 The spatiotemporal evolution of bays' resilience and sub-resilience over 21 years

As shown in Figure 3, the resilience in Bohai Bay (BHB), Hangzhou Bay (HZB), and the Pearl River Delta (PRD) presented positive improvement overall with slight fluctuation over 21 years, mainly due to the positive growth of the social development sub-resilience. The highest growth rate of resilience was in HZB where resilience level raised from 0.32 in 2000 to 0.72 in 2020, an increase of approximately 127.61%, followed by the PRD with value of +110.35% and BHB with value of +46.16%. This indicated that the development level of resilience in BHB lagged behind that in other two bays. Among them, troughs occurred in 2005, 2005, and 2010 for the PRD, HZB, and PRD, respectively. The time nodes coincided with the frequent emergence of marine disaster in China, which largely affected resilience growth (Figure 4). It was worth noting that ecological resilience in all the study areas fluctuated greatly and remained at a low level during the observation years.

Regarding physical space resources resilience, the resilient level in BHB was relatively stable and increased slightly, and the resilience level dropped first then grew and ultimately dropped in HZB, and the resilient level dropped first then grew and ultimately grew in PRD. The resilient level of physical space resources developed in a differentiated manner among different regions, which resulted from local disparities in socioeconomic status, policies, technology, and so on. The resilient level of social development showed a rapid upward trend in the three bay areas.

3.2 Interaction relationship of properties within resilience

Figure 5 demonstrates how all factors affecting the resilience level interacted. The result shows that the resilient change in BHB was significantly positively correlated with those of in HZB ($R=0.56$, $p<0.01$), followed by those of in PRD ($R=0.36$, $p<0.01$). For BHB, we found that the disasters sub-resilience trend was significantly positively correlated with the social development sub-resilience trend ($R=0.12$, $p<0.0001$) and was significantly negative correlated with the ecology sub-resilience trend ($R=-0.19$, $p<0.0001$), followed by those of the physical resources sub-resilience ($R=-0.16$, $p<0.0001$). For HZB, the social development sub-resilience trend was significantly positively correlated with sub-resilience of physical resource ($R=0.33$, $p<0.01$) and ecology trends ($R=0.087$, $p<0.0001$) and was significantly negative correlated with the disaster sub-resilience trend ($R=-0.14$, $p<0.01$). For PRD, the sub-resilience trend of physical resource was significantly positive correlated with that of social development ($R=0.7$, $p<0.001$) and was significantly negative correlated with that of the ecology trend ($R=-0.52$, $p<0.05$). Physical space resources have a very obvious positive correlation with social development, which were the two

TABLE 2 Data sources of the indicators for assessing the resilience of the bay area.

Indicators	Data source
R_1	Zhang et al., 2016; Sun et al., 2017; Peng et al., 2020; Li, 2020
R_2	
R_3	
S_1	Statistical Yearbook of Guangdong/Zhejiang/Hebei/Shandong (2001-2021), Statistical Bulletins of Tianjin/Shanghai (2000–2020)
S_2	The China City Statistical Yearbook (2001–2021)
S_3	The China City Statistical Yearbook (2001–2021)
S_4	Statistical Yearbook of Guangdong/Zhejiang/Hebei/Shandong (2001–2021), Statistical Bulletins of Tianjin/Shanghai (2000–2020)
S_5	The China City Statistical Yearbook (2001–2021)
E_1	Bulletin on the State of China's Marine Ecological Environment (2006–2020), Marine Environmental Quality Bulletin of Guangdong (2001–2005)
E_2	
E_3	
E_4	
D_1	China Marine Disaster Bulletin (2006–2020)
D_2	
D_3	China sea level Bulletin (2000–2020)

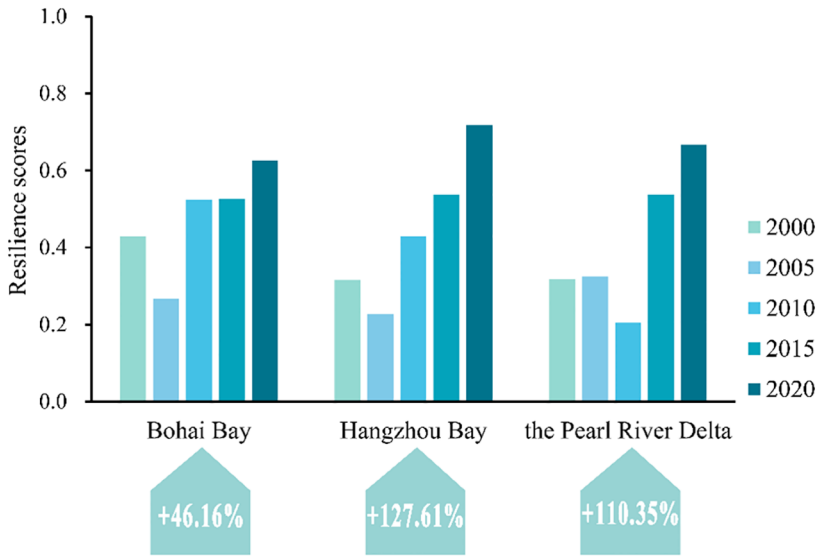

FIGURE 3
Changes in the three bays' resilience scores by regions from 2000 to 2020. The percentage below it shows that the change rate in the resilience scores from 2000 to 2020 HZB and PRD have higher increasing rates of the resilience score than BHB.

sub-resilience systems with the strongest correlation found in this study.

3.3 Coupling and coordinated development between sub-resilience

The spatiotemporal evolution of the coupling coordination level is shown in Figure 6. The coupling coordinated level of the three bay areas increased slightly in the long term, and the overall growth gradient was between grades 1 and 2. Up to 2019, the coupling coordination level of the three bay areas was still imbalanced, which regional social, ecological, and environmental coordination developments in Chinese bay areas affecting integrated resilience growth. In the past 20 years, the spatiotemporal evolution characteristics of the coupling coordinated level in the three bay areas are different. The coupling coordinated level of BHB fluctuated greatly, and the degree of coordinated development reached the highest around 2009, showing a trend of fluctuation improvement. The coupling coordinated levels of HZB and PRD have shown a stable upward trend since 2001. The worst level of coupling coordination was observed in BHB compared with other regions. In summary, the coupling coordination level within resilience

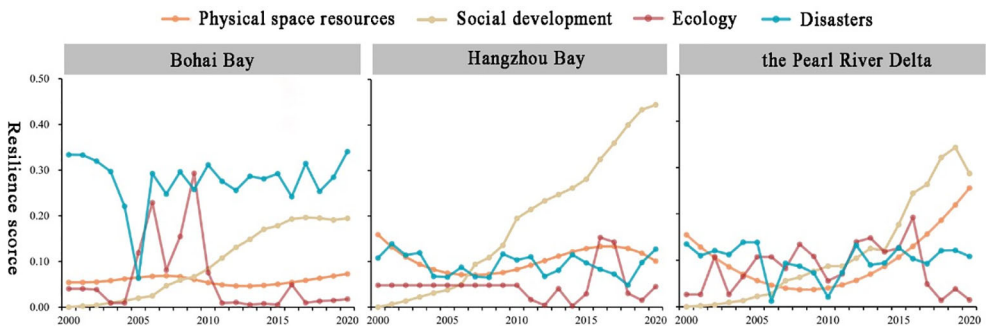

FIGURE 4
Line chart of resilience value for bays from 2000 to 2020. Different color indicates the four sub-resilience systems within the resilient system of bays. The ecological sub-resilience system has maintained a low level in the three bay areas, while the social development sub-resilience system has maintained an upward trend.

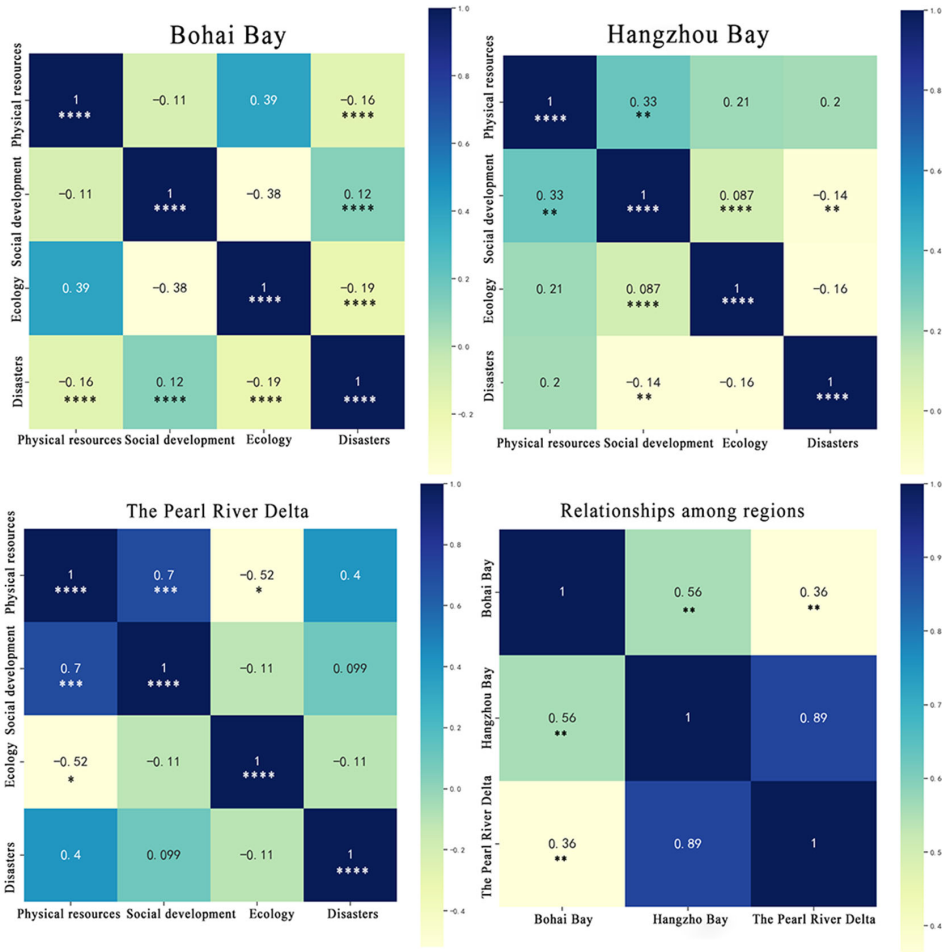

FIGURE 5
The interactive relationships between sub-resilience systems in and among three bay areas. t significance test below the value (*p<0.05, **p<0.01, ***p<0.001, and ****p<0.0001). The correlations among the four sub-resilience systems show significant spatial heterogeneity in Chinese bay areas.

for the bay areas was not optimistic, and the coordinated development of the four sub-resilience among regions was biased.

4 Discussions

4.1 Resilience assessment for coastal bays

It is an essential effort in the field of sustainable development to explore quantifying the resilience of the bay area and analyzing the synergistic and conflict relationships among sub-resilience systems. In this study, an assessment framework of resilience in the bay area was constructed, including four sub-resilience systems: physical space resilience, social development resilience, ecology resilience, and disasters resilience, and a total of 15 indicators were selected. Our results show that the indicator system in the study can be used to clarify the evolution of resilience in the bay area. As we all know, constructing the indicator system and quantifying the comprehensive score have been a mature method used in scientific research (Davies and Tonts, 2010; Meerow et al., 2016; Zhang, 2016). The resilience assessment in coastal areas mainly achieves the purpose of quantification by constructing the evaluation indicators system, selecting the corresponding mathematical method, and establishing the operation model. At present, the construction of resilience assessment indicator system mainly considers the comprehensive performance of resilience in coastal social–ecological systems under multiple disturbances of human and nature (Joerin et al., 2014; Lam et al., 2015). The indicator system generally covers multiple dimensions such as ecology, society, economy, infrastructure, and policy, which has been applied in the resilience assessment

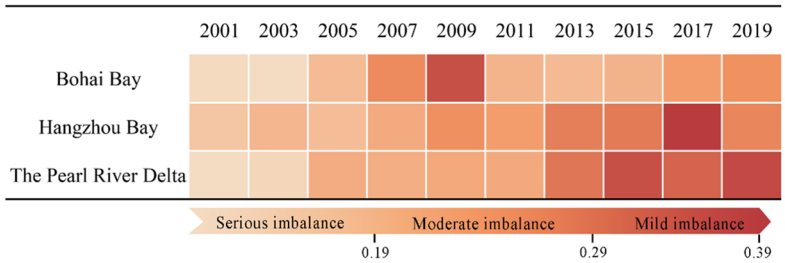

FIGURE 6
Coupling coordinated level of the three bay areas during 2001–2019. The coupling coordination level in the three bay areas is overall imbalance, but they show a trend of fluctuation improvement. The coordinated development of PRD and HZB in south China is better than that of BHB in north China.

of coastal areas such as Shenzhen (Liang and Li, 2020) in China and Saudi Arabia (Alshehri et al., 2015).

In our study, we first standardized the original data of each indicator, then used entropy method to determine the weight of each indicator, and finally carried out Pearson correlation test and calculate coupling coordination level. The concept of entropy first appeared in thermodynamics, developed by Rudolph Clausius in 1865, as a way of describing the disorder of a system. In the information theory, entropy is a measure of the uncertainty associated with a random variable (Zhang et al., 2011). Therefore, in the entropy method, the greater the change range, the higher the index weight, which makes the system score more different. In other similar studies, PCA and AHP are also important methods for assigning index weights. At the same time, some scholars use DPSIR, ENA, and other methods to analyze the direct and indirect environmental interactions among economic components, which provides a framework for the investigation of the function, resilience, and dynamics of an ecosystem (Xu et al., 2018; Nathwani et al., 2019). Compared with subjective weight determination methods such as AHP, the entropy method is more objective and accurate and can better explain the obtained results (Prachee et al., 2005; Lee and Philip, 2013). This method can modify the obtained weight and has high adaptability. Nevertheless, the method determines the weight of the indicator according to the variation degree of the indicator, ignoring its importance degree (Tomson and Danny, 2021). Therefore, when the indicator value changes suddenly or not much, the weights given by it may be far from the reality. To sum up, the entropy weight method can provide basis for multidimensional comprehensive evaluation and avoid the influence of human factors in subjective evaluation; we finally adopt this method (Zhou et al., 2021; Huang and Ling, 2018).

The selection of indicators directly affects the final results. In this paper, a total of 15 indicators are selected and clustered into four sub-resilience systems to represent the physical space resources, social development, ecology, and disasters in the bay area. In view of the special geographical conditions of the bay area, we comprehensively consider the coupling of land and sea, focus on the changes in the coastal zone, and take into account the conditions of land and sea. Although there are few studies on the resilience in bay areas at present, based on similar studies, we believe that the percent of attainment days meeting excellent air quality standard, renewable resource recycling rate (Liang et al., 2020), urbanization rate, total economic losses due to marine disasters (Nathwani et al., 2019), dumping amounts of dredged materials in unit sea area (Gao et al., 2022), and other indicators can be further defined. Due to the limit of data, we failed to collect these data. If relevant data can be obtained and analyzed, the research results will be more convincing.

4.2 Spatial heterogeneity and internal interconnections of coastal resilience

The ecological sub-resilience at a low level revealed great vulnerability for marine ecosystem to answer the threats of environmental risks and disasters, which may be attributed to serious environmental problems under sustained high economic growth and prosperity. Nevertheless, social development sub-resilience currently became the key driver in bay areas to promote overall resilience even though the overall ecological resilience was low. There was not enough evidence to show that social development sub-resilience would have a significant negative impact on ecological sub-resilience system. Our results showed that there were significant differences in the sub-resilience systems of the three bay areas. There are two main reasons for spatial heterogeneity: physical geographical conditions and different patterns of development in the three bay areas. Different from HZB and PRD, BHB is not conducive to the diffusion of pollutants objectively because there is no river with large runoff into the sea and the ocean current activity is not active, resulting in the water exchange time being longer. It may lead to the easier correlation between marine disasters

(especially algal bloom) and human activities. From the time scale, the regional development patterns can be summarized as four stages of prepare, absorb, recover, and adapt (Linkov et al., 2014; Liang and Li, 2020). Different development patterns in the three bay areas also make their resilience have different characteristics. Comparing the results of resilience trends in the study with previous studies, BHB and HZB are more likely to be in the recover stage, while PRD may have evolved into the adapt stage. Therefore, PRD has stronger resilience than BHB and HZB. Greater resilience is also the next evolution trend of BHB and HZB.

At present, there have been several studies on the resilience of HZB and PRD (Xiao et al., 2019a; Bi et al., 2020; Liang and Li, 2020), but the research on the relationship among sub-resilience in the bay areas is widely lacking. During our study period, the social economy in the PRD developed rapidly, but due to the negative effects caused by the pressure of socioeconomic system, pressure on marine ecological of the area has not been reversed in recent 20 years. Most cities are in the stage that socioeconomic development and marine ecological damage coexist (Gao et al., 2022). Although abundant financial resources supported marine ecological restoration projects, the improvement of ecological environment often lagged behind the restoration effect of physical space. Ignoring the role of the ocean and the impact of global climate change will lead to significant deviation in the sustainability assessment of coastal cities or regions (Li et al., 2021). For HZB, the regional ecosystem health status continued to degrade at city scale in 2001–2013, and this decline spread to the surrounding areas from Shanghai and Jiaxing (Xiao et al., 2019a; Xiao et al., 2019b). Only from 2001 to 2013, the resilience in HZB did not show an improvement trend, but after 2013, HZB began to improve significantly. To a large extent, the increasing governance capacity given by the social development to environmental issues promoted improvements in regional marine physical resources and ecology sub-resilience, and serious marine disasters produced the negative impact on social development sub-resilience. Studies on BHB found that islands are most sensitive to stressors from inland activities and coastline development (Shen et al., 2016), but there is lack of overall analysis for this bay area. Although disasters sub-resilience had a certain destructive effect on the sub-resilience of physical space resources and ecology, it had a certain promoting effect on the sub-resilience of social development through facilitating the construction of urban infrastructure. Urban resilience levels in the Beijing–Tianjin–Hebei region (BTH) have shown an upward trend with slight fluctuation between 1998 and 2019, and the differences between cities have gradually decreased (Liu et al., 2022), which also confirmed with the results of our research.

Meanwhile, few studies involve quantitative analysis of the interaction relationship within resilience. From the comprehensive performance of coupling coordinated level, the coordinated development of PRD and HZB (in southern China) was better than that of BHB (in northern China), which was also consistent with the existing research conclusion (Fan et al., 2019). Although the disaster sub-resilience level was high, serious environmental pollution and low level of economic development led to the low level of coordinated development. In HZB and PRD, where ocean economy was developing rapidly, the sub-resilience of ecology and physical space resources was slightly improved, benefiting from the implementation of marine ecological protection strategy. This made their internal resilience more coordinated than that of BHB. However, it is not optimistic that economic development and urbanization process are exerting strong pressures on the ecological security system, which makes it in a passive and restrained position in Chinese coastal cities (Nathwani et al., 2019; Gao et al., 2022). In addition, coastal cities have efficiency disaster response, which could decrease the negative impact in case marine disasters occur. The conclusions of these studies are mutually confirmed with the results of this paper, which further enhances the credibility of our study. In summary, owing to the complex influence of multiple sub-resilience factors, the study could provide some implications and help urban managers to develop an integrated vision to better understand resilience.

5 Conclusions

This paper proposed a sound resilience index system for the bay areas by considering both the internal resilience structure and the external disturbances and has been validated through the practical assessment in three major bay areas in China from 2000 to 2020. The resilience indicator system effectively evaluated the temporal and spatial variation of resilience level in the bay areas. It also revealed the resilience level changes among three bay areas and the interaction relationships between the four sub-resilience systems. Base on the results, the resilience level in BHB, HZB, and PRD presented positive improvement overall with slight fluctuation during the study period, and the social development was the key driver factor. In the three bay areas, the interaction relationship between sub-resilience systems obviously showed regional heterogeneity, which could be explained by regional development patterns. Moreover, what was not so optimistic was that the coupling coordination level in the three bay areas remained imbalanced for long term even though it has increased slightly. Furthermore, we innovatively connected the resilience changes to human stressors and socioeconomic status, which was of great significance to explore enabling conditions for resilience building and guide effective policy and actions for promoting sustainable development in the bay area.

It should be noted that coastal resilience as a core ability for maintaining coastal health and sustainability is of great importance but is very challenging understand and manage. Our study is an early trial to quantify the resilience, the connections with coastal ecosystem health are still unclear, and the proposed

index system is still lacking of some key indicators due to the unavailability, e.g., marine food web information and coastal hydrological attributes. More research efforts including theoretical and practical investigations should be invested both for research institutes and coastal government to explore, uncover, and regulate the coastal resilience for promoting coastal sustainability.

Data availability statement

The raw data supporting the conclusions of this article will be made available by the authors, without undue reservation.

Author contributions

Conceptualization: GY, YH, and YZ. Methodology: GY, YZ, HZ, TH, CF, and YY. Validation: GY, YH, LP, and JZ (Jian Zeng). Data curation and analyses: HZ, YZ, YH, and JZ (Jiangning Zeng). Writing: all authors. All authors contributed to the article and approved the submitted version.

Funding

This work was supported by National Natural Science Foundation of China (No. 42176216), the Science Technology Department of Zhejiang of China (No. 2022C15008), the Key Laboratory of Marine Ecosystem Dynamics, Ministry of Nature Resources (No. MD202001), and Fujian Provincial Key Laboratory of Marine Ecological Conservation and Restoration (No. 2021003).

Conflict of interest

The authors declare that the research was conducted in the absence of any commercial or financial relationships that could be construed as a potential conflict of interest.

Publisher's note

All claims expressed in this article are solely those of the authors and do not necessarily represent those of their affiliated organizations, or those of the publisher, the editors and the reviewers. Any product that may be evaluated in this article, or claim that may be made by its manufacturer, is not guaranteed or endorsed by the publisher.

Supplementary material

The Supplementary Material for this article can be found online at: https://www.frontiersin.org/articles/10.3389/fmars.2022.982263/full#supplementary-material

References

Adger, W. N., Hughes, T. P., Folke, C., Carpenter, S. R., and Rockstrom, J. (2005). Social-ecological resilience to coastal disasters. *Science* 309 (5737), 1036–1039. doi: 10.1126/science.1112122

Alshehri, S. A., Rezgui, Y., and Li, H. (2015). Disaster community resilience assessment method: A consensus- based Delphi and AHP approach. *Natural Hazards.* 78 (1), 395–416. doi: 10.1007/s11069-015-1719-5

Angeler, D. G., and Allen, C. R. (2016). Quantifying resilience. *J. Appl. Ecol.* 53, 617–624. doi: 10.1111/1365-2664.12649

Bi, M. L., Xie, G. D., and Yao, C. Y. (2020). Ecological security assessment based on the renewable ecological footprint in the guangdong -Hong Kong -Macao greater bay area, China. *Ecol. Indic.* 116, 106432. doi: 10.1016/j.ecolind.2020.106432

Brand, F. (2009). Critical natural capital revisited: Ecological resilience and sustainable development. *Ecol. Econ.* 68 (3), 605–612. doi: 10.1016/j.ecolecon.2008.09.013

Brown, E. D., and Williams, B. K. (2015). Resilience and resource management. *Environ. Manag.* 56, 1416–1427. doi: 10.1007/s00267-015-0582-1

Büyüközkan, G., Ilcak, O., and Feyziolu, O. A. (2022). Review of urban resilience literature. *Sustain. Cities. Soc.* 77, 103579. doi: 10.1016/j.scs.2021.103579

da Silva, C. A., dos Santos, E. A., Maier, S. M., and da Rosa, F. S. (2019). Urban resilience and sustainable development policies: An analysis of smart cities in the state of S˜aoPaulo. *REGE* 27, 61–78. doi: 10.1108/REGE-12-2018-0117

Davies, A., and Tonts, M. (2010). Economic diversity and regional socioeconomic performance: An empirical analysis of the Western Australian grain belt. *Geograp. Res.* 48 (3), 223–234. doi: 10.1111/j.1745-5871.2009.00627.x

Delgado, A., and Romero, I. (2016). Environmental conflict analysis using an integrated grey clustering and entropy-weight method: A case study of a mining project in Peru. *Environ. Model. Software.* 77, 108–121. doi: 10.1016/j.envsoft.2015.12.011

Diaz-Sarachaga, J. M., and Jato-Espino, D. (2020). Analysis of vulnerability assessment frameworks and methodologies in urban areas. *Nat. Hazards.* 100, 437–457. doi: 10.1007/s11069-019-03805-y

Fan, Y. P., Fang, C. L., and Zhang, Q. (2019). Coupling coordinated development between social economy and ecological environment in Chinese provincial capital cities-assessment and policy implications. *J. Cleaner. Prod.* 229, 289–298. doi: 10.1016/j.jclepro.2019.05.027

Folke, C., Carpenter, S. R., Walker, B., Scheffer, M., Chapin, T., and Rockström, J. (2010). Resilience thinking: integrating resilience, adaptability and transformability. *Ecol. Soc.* 15 (4), 20. doi: 10.5751/ES-03610-150420

Galderisi, A. (2014). Urban resilience: A framework for empowering cities in face of heterogeneous risk factors. *ITU. A|Z.* 11 (1), 36–58.

Gao, X., Li, P., and Chen, C.-T. A. (2013). Assessment of sediment quality in two important areas of mariculture in the bohai Sea and the northern yellow Sea based on acid-volatile sulfide and simultaneously extracted metal results. *Mar. pollut. Bull.* 72 (1), 281–288. doi: 10.1016/j.marpolbul.2013.02.007

Gao, L. H., Ning, J., Bao, W. L. T. Y., Yan, A., and Yin, Q. R. (2022). A study on the marine ecological security assessment of guangdong-Hong Kong-Macao great bay area. *Mar. pollut. Bull.* 113416, 176. doi: 10.1016/j.marpolbul.2022.113416

Gari, S. R., Newton, A., and Icely, J. D. (2015). A review of the application and evolution of the DPSIR framework with an emphasis on coastal social-ecological systems. *Ocean. Coast. Manage.* 103, 63–77. doi: 10.1016/j.ocecoaman.2014.11.013

Huang, W. J., and Ling, M. Z. System resilience assessment method of urban lifeline system for GIS. *Comput. Environ. Urban. Syst.* 71, 67–80. doi: 10.1016/j.compenvurbsys.2018.04.003

Jia, S.J., Liu, Y.C., and Xing, M.J. (2008) On coordination development of agricultural ecological-environment and economy in different regions based on coupling degree model. *Research of Agricultural Modernization*. 5, 573–5. doi: 10.1016/S1002-0721(08)60105-2 (In Chinese).

Joerin, J., Shaw, R., Takeuchi, Y., and Krishnamurthy, R.. (2014). The adoption of a climate disaster resilience index in chennai, India. *Disasters* 38 (3), 540–561. doi: 10.1111/disa.12058

Jozaei, J., Mitchell, M., and Clement, S. (2020). Using a resilience thinking approach to improve coastal governance responses to complexity and uncertainty: a Tasmanian case study. *Australia. J. Environ. Manag.* 253, 109662. doi: 10.1016/j.jenvman.2019.109662

Kasmalkar, I. G., Serafin, K. A., Miao, Y., Bick, I. A., Ortolano, L., Ouyang, D., et al. (2020). When floods hit the road: Resilience to flood-related traffic disruption in the San Francisco bay area and beyond. *Sci. Adv.* 6, eaba2423. doi: 10.1126/sciadv.aba2423

Kuenzer, C., Heimhuber, V., Day, J., Varis, O., Bucx, T., Renaud, F., et al. (2020). Profiling resilience and adaptation in mega deltas a comparative assessment of the Mekong, yellow, Yangtze, and Rhine deltas. *Ocean. Coast. Manag.* 198, 105362. doi: 10.1016/j.ocecoaman.2020.105362

Lak, A., Hasankhan, F., and Garakani, S. A. (2020). Principles in practice: Toward a conceptual framework for resilient urban design. *J. Environ. Plann. Manage.* 0, 1–33. doi: 10.1080/09640568.2020.1714561

Lam, N. S. N., Qiang, Y., Arenas, H., Brito, P., and Liu, K.B. (2015). Mapping and assessing coastal resilience in the Caribbean region. *Cartogr. Geogr. Inf. Sci.* 42 (4), 315–322. doi: 10.1080/15230406.2015.1040999

Lee, P. H., and Philip, L. H. (2013). An r package for analyzing and modeling ranking data. *BMC Med. Res. Methodol.* 13 (1), 65. doi: 10.1186/1471-2288-13-65

Li, N. (2020). Long-term remote sensing dynamic monitoring and ecological assessment of coastal wetland in hangzhou bay. *China. Nanjing. Nanjing. Forest. University. Master. Degree*. doi: 10.27242/d.cnki.gnjlu.2020.000002

Liang, J., and Li, Y. F. (2020). Resilience and sustainable development goals based social- ecological indicators and assessment of coastal urban areas: A case study of dapeng new district, shenzhen, China. *Watershed. Ecol. Environ.* 2), 6–15. doi: 10.1016/j.wsee.2020.06.001

Liao, C. B. (1996). Quantitative evaluation and classification system of the coordinated development of environment and economy: taking the urban agglomeration in the pearl river delta as an example. *Guangzhou. Environ. Sci.* 1), 12–16.

Li, G., Kou, C., Wang, Y., and Yang, H. (2020). System dynamics modelling for improving urban resilience in Beijing, China. *Resour. Conserv. Recycling.* 161, 104954. doi: 10.1016/j.resconrec.2020.104954

Li, X., Long, X., and Qi, X. (2019). Dynamic evolution and analysis of coupling development of economy society and environment in Yangtze river economic belt. *Resour. Environ. Yangtze. Basin.* 28 (3), 505–516.

Linkov, I., Bridges, T., Creutzig, F., Decker, J., Fox-Lent, C., Kroger, W., et al. (2014). Changing the resilience paradigm. *Nat. Climate Change* 4 (6), 407–409. doi: 10.1038/nclimate2227

Lin, Y., Zhang, H. W., Ye, G. Q., Jiang, J. G., and Jiang, Q. T. (2022). Marine eco-civilization performance evaluation in oujiang estuary, Zhejiang province, China. *Environ. Dev. Sustainabil.*, 1–22. doi: 10.1007/s10668-021-02047-y

Liu, L., Lei, Y., Zhuang, M., and Ding, S. (2022). The impact of climate change on urban resilience in the Beijing-Tianjin-Hebei region. *Sci. Total. Environ.* 827, 154157. doi: 10.1016/j.scitotenv.2022.154157

Li, Q., Wu, J., Su, Y., Zhang, C., Wu, X., Wen, X., et al. (2021). Estimating ecological sustainability in the guangdong-Hong Kong-Macao greater bay area, China retrospective analysis and prospective trajectories. *J. Environ. Manage.* 303, 114167. doi: 10.1016/j.jenvman.2021.114167

Lou, Y., Yin, G., Xin, Y., Xie, S., Li, G., Liu, S., Wang, X, et al. Recessive transition mechanism of arable land use based on the perspective of coupling coordination of input–output: a case study of 31 provinces in China. *Land* (2021),10, 1–27. doi: 10.3390/land10010041

Meerow, S., Newell, J. P., and Stults, M. (2016). Defining urban resilience: A review. *Landscape Urban. Plann.* 147, 38–49. doi: 10.1016/j.landurbplan.2015.11.011

Nathwani, J., Lu, X., Wu, C., Fu, G., and Qin, X. (2019). Quantifying security and resilience of Chinese coastal urban ecosystems. *Sci. Total. Environ.* 672, 51–60. doi: 10.1016/j.scitotenv.2019.03.322

NSTC (2022) *Opportunities and actions for ocean science and technology 2022-2028* (US, Washington). Available at: https://trumpwhitehouse.archives.gov/wpcontent/uploads/2018/11/Science-and-Technology-for-Americas-Oceans-A-Decadal-Vision.pdf (Accessed June 7, 2022).

Oke, A. E., Aghimien, D. O., Akinradewo, O. I., and Aigbavboa, C. O. (2020). Improving resilience of cities through smart city drivers. *Australasian Journal of Construction Economics and Building* 20, 45–64. doi: 10.5130/AJCEB.v20i2.6647

Peng, X. J., Lin, X. R., Fang, J., Wang, T., and Jiang, X. S. (2020). Analysis on coastline and coastal wetland changes in the hangzhou bay in recently 30 years. *J. Ocean. Technol.* 39, 9–16.

Prakash, P., Yellaboina, S., Ranjan, A., and Hasnain, S.E.. (2005). Computational prediction and experimental verification of novel IdeR binding sites in the upstream sequences of mycobacterium tuberculosis open reading frames. *Bioinformatics* 21 (10), 2161–2166. doi: 10.1093/bioinformatics/bti375

Ramesh, R., Chen, Z., Cummins, V., Day, J., D'Elia, C., Dennison, B., et al. (2015). Land–ocean interactions in the coastal zone: Past, present & future. *Anthropocene* 12, 85–98. doi: 10.1016/j.ancene.2016.01.005

Ribeiro, P., and Gonalves, L. (2019). Urban resilience: a conceptual framework. *Sustain. Cities. Soc.* 50, 101625. doi: 10.1016/j.scs.2019.101625

Sellberg, M. M., Ryan, P., Borgström, S. T., Norström, A. V., and Peterson, G. D. (2018). From resilience thinking to resilience planning: lessons from practice. *J. Environ. Manage.* 217, 906–918. doi: 10.1016/j.jenvman.2018.04.012

Shen, C. C., Shi, H. H., Zheng, W., and Ding, D. W. (2016). Spatial heterogeneity of ecosystem health and its sensitivity to pressure in the waters of nearshore archipelago. *Ecol. Indic.* 61, 822–832. doi: 10.1016/j.ecolind.2015.10.035

Sun, B. S., Zuo, S. H., Xie, H. L., Li, H. Y., and Yang, Z. W. (2017). Analysis of impact effects and changes of the coastline in the bohai bay during the past 40 years. *J. East. China Normal. Univ. (Natural. Science).* 04, 012.

Tomson, O., and Danny, C. I. (2021). Olympic Rankings based on objective weighting scheme. *J. Appl. Stat* 48 (3), 573–582. doi: 10.1080/02664763.2020.1736525

Wang, J., Shen, T., and Gou, A. (2021). Coastal resilience assessment of the San Francisco bay in USA and its enlightenment. *Trans. Oceanol. Limnol.* 43 (5), 149–158. 020.

Wardekker, A., Wilk, B., Brown, V., Uittenbroek, C., Mees, H., Driessen, P., et al. (2020). *A diagnostic tool for supporting policymaking on urban resilience* Vol. 101 (Cities London, England).

Xiao, R., Liu, Y., Fei, X. F., Yu, W. X., Zhang, Z. H., and Meng, Q. X. (2019a). Ecosystem health assessment: A comprehensive and detailed analysis of the case study in coastal metropolitan region, eastern China. *Ecol. Indic.* 98, 363–376. doi: 10.1016/j.ecolind.2018.11.010

Xiao, R., Yu, X. Y., Shi, R. X., Zhang, Z. H., Yu, W. X., Li, Y. S., et al. (2019b). Ecosystem health monitoring in the shanghai-hangzhou bay metropolitan area: A hidden Markov modeling approach. *Environ. Int.* 133, 105170. doi: 10.1016/j.envint.2019.105170

Xu, W., Cai, Y. P., Rong, Q. Q., Yang, Z. F., Li, C. H., and Wang, X. (2018). Agricultural non-point source pollution management in a reservoir watershed based on ecological network analysis of soil nitrogen cycling. *Environ. Sci. pollut. Res.* 25 (9), 9071–9084. doi: 10.1007/s11356-017-1092-x

Yang, D., Gao, X., Xu, L., and Guo, Q. (2018). Constraint-adaptation challenges and resilience transitions of the industry–environmental system in a resource-dependent city. *Resour. Conserv. Recycling.* 134, 196–205. doi: 10.1016/j.resconrec.2018.03.016

Yan, S., and Tang, J. (2020). Progress on the theory and practice of resilient city. *J. Hum. Settlements. West. China.* 35 (2), 111–118.

Zhang, K. . Regime shifts and resilience in china's coastal ecosystems. *Ambio* 45 (1), 89–98. doi: 10.1007/s13280-015-0692-2

Zhang, M.D., and Mo, D.Y. (2014) Coupling coordination degree of urban land use benefit and urbanization. *Resour. Sci.* 1, 8–16 (In Chinese).

Zhang, H., Gu, C. L., Gu, L. W., and Zhang, Y. (2011). The evaluation of tourism destination competitiveness by TOPSIS & information entropy - a case in the Yangtze river delta of China. *Tourism. Manage.* 32 (2), 443–451. doi: 10.1016/j.tourman.2010.02.007

Zhang, X. H., Huang, H. M., Wang, P., Chen, M. R., Wang, J. H., and Sun, Q. Y. (2016). Change analysis of coastline and Sea reclamation in pearl river estuary from 1973 to 2015. *Trans. Oceanol. Limnol.* 05, 002. doi: 10.13984/j.cnki.cn37-1141.2016.05.002

Zhang, M., Yang, Y., Li, H., and Dijk, M. V. (2020). Measuring urban resilience to climate change in three Chinese cities. *Sustainability* 12 (22), 9735. doi: 10.3390/su12229735

Zheng, Y., Xie, X.-L., Lin, C.-Z., Wang, M., and He, X.-J. (2018). Development as adaptation: Framing and measuring urban resilience in Beijing. *Adv. Climate Change Res.* 9, 234–242. doi: 10.1016/j.accre.2018.12.002

Zhou, Q., Zhu, M. K., Qiao, Y. R., Zhang, X. L., and Chen, J. (2021). Achieving resilience through smart cities? Evidence from China. *Habitat International*, 111, 102348. doi: 10.1016/j.habitatint.2021.102348

frontiers | Frontiers in Marine Science

TYPE Original Research
PUBLISHED 18 November 2022
DOI 10.3389/fmars.2022.1019619

OPEN ACCESS

EDITED BY
Zeng Zhou,
Hohai University, China

REVIEWED BY
Robin Kundis Craig,
University of Southern California, United States
Qin Zhu,
Southern Marine Science and Engineering Guangdong Laboratory (Guangzhou), China

*CORRESPONDENCE
Xiuzhen Li
xzli@sklec.ecnu.edu.cn

SPECIALTY SECTION
This article was submitted to Coastal Ocean Processes, a section of the journal Frontiers in Marine Science

RECEIVED 15 August 2022
ACCEPTED 03 November 2022
PUBLISHED 18 November 2022

CITATION
Lin S, Li X, Wu R, Ma Y, Zhao W and Wang J (2022) Identifying priority areas for tidal wetland restoration by integrating ecosystem services supply and demand mismatches. *Front. Mar. Sci.* 9:1019619. doi: 10.3389/fmars.2022.1019619

Identifying priority areas for tidal wetland restoration by integrating ecosystem services supply and demand mismatches

Shiwei Lin[1,2,3], Xiuzhen Li[2,3]*, Ruidong Wu[4,5], Yuxi Ma[2,3], Wenzhen Zhao[2,3] and Jiangjing Wang[2,3]

[1]College of Plant Protection, Yangzhou University, Yangzhou, China, [2]State Key Laboratory of Estuarine and Coastal Research, Institute of Eco-Chongming, East China Normal University, Shanghai, China, [3]Yangtze Delta Estuarine Wetland Ecosystem Observation and Research Station, Ministry of Education and Shanghai Science and Technology Committee, Shanghai, China, [4]Conservation Biogeography Research Group, Institute of International Rivers and Eco-Security, Yunnan University, Kunming, Yunnan, China, [5]Yunnan Key Laboratory of International Rivers and Transboundary Eco-security, Yunnan University, Kunming, Yunnan, China

Governments and non-governmental organizations have widely recognized tidal wetland restoration as a sustainable instrument to lessen the threat of climate change, which is reflected by the expansion of the spatial scale of coastal restoration projects. However, approaches to large-scale spatial planning of tidal wetland restoration remain sparse. Previous studies on site selection for restoration planning have focused on the potential supply of ecosystem services (ES) or restoration feasibility with less emphasis on the mitigation of the status of regional ES supply and demand mismatches. We developed a five-step workflow based on systematic conservation planning to identify priority areas for tidal wetland restoration and applied it to the coastal reclaimed areas of Shanghai, China. With this workflow, we analyzed the changes in spatial distribution and the potential ecosystem services supply and restoration costs of priority areas between the two different scenarios of ES demand ignored and ES demand considered. Results showed that the potential restorable areas only accounted for 31.4% (425.2 km^2) of the original reclaimed area because of other land use demands (e.g., permanent basic farmland conservation). We extracted 50% of the potential restorable areas as priority areas based on Aichi Target 15. Compared with the ES demand-ignored scenario, the ES demand scenario resulted in a substantial increase in the priority areas of Baoshan District (~177%) and Pudong New Area (~15%) and a small decrease in Chongming District (~4%). No significant change in the potential ES supply for all priority areas was observed between the two scenarios. However, the total restoration cost of the ES demand scenario is 10% higher than that of the ES demand-ignored scenario. Our study highlights the importance of considering the status of regional ES supply and demand (mis)matches in large-scale spatial planning for tidal wetland restoration.

KEYWORDS

tidal wetland, priority areas, ecological restoration, systematic conservation planning, reclaimed area, Shanghai, ecosystem service, supply and demand

1 Introduction

Coastal lowlands are frequently exposed to climate change-related risks (e.g., storm flooding), which evokes the need to explore new solutions for maintaining human well-being (Temmerman et al., 2013; Pittman et al., 2022). Healthy tidal wetlands can provide various valuable ecosystem services (ES) in a sustainable manner (e.g., coastal protection service; Liquete et al., 2013a; Temmerman and Kirwan, 2015; Zhu et al., 2020). Thus, restoring degraded tidal wetlands to strengthen the resilience of coastal zones has been well recognized by scientists in recent decades (Temmerman and Kirwan, 2015; Perillo et al., 2019). The spatial extent of coastal restoration projects has also gradually expanded recently (Gilby et al., 2021). Given that not all degraded tidal wetlands can be restored because of limited resources (e.g., the target area for restoration plans is often fixed; WWF, 2020), restoration actions must be prioritized in space (Wiens and Hobbs, 2015). To date, approaches for identifying priority areas for tidal wetland restoration at large spatial scales are still lacking (Adame et al., 2014; Liu et al., 2016; Gilby et al., 2021).

Target-based planning focuses on two types of conservation resource allocation problems: *meeting the targets with the least cost (the minimum-set approach)* and *maximizing the number of targets met with a given resource (maximum coverage approach)* (Moilanen, 2007). Systematic conservation planning (SCP), a typical target-based planning method, is widely considered the most influential paradigm for designing a protected area network (Kukkala and Moilanen, 2013). This method is composed of six stages: (1) collecting biodiversity data for the planning area, (2) setting conservation targets for the planning area, (3) assessing the conservation effectiveness of existing protected areas, (4) identifying additional protected areas, (5) implementing conservation actions, and (6) maintaining and monitoring protected areas (Margules and Pressey, 2000). Using the site selection algorithms (e.g., simulated annealing of MARXAN) of SCP to identify priority areas has more advantages than using scoring methods or expert opinions (McBride et al., 2010), such as reducing socio-economic investment and improving the connectivity of priority areas. Therefore, the SCP has been increasingly used to identify restoration priority areas for different ecosystems since 2006 (Crossman and Bryan, 2006; Qu et al., 2019; Costa et al., 2021; Gilby et al., 2021).

Studies applying SCP to the spatial planning of coastal ecosystem restoration have been conducted (e.g., Adame et al., 2014; Gilby et al., 2021), but they deserve improvement in at least two aspects. First, few studies have incorporated social and economic costs into the spatial planning of coastal restoration actions (Pittman et al., 2022; Su et al., 2022). For example, Adame et al. (2014) used a uniform indicator to represent the cost of hydrological restoration and afforestation. However, in practice, the cost of restoring the same ecosystem often varies considerably from site to site (Bayraktarov et al., 2016). Furthermore, Strassburg et al. (2020) confirmed that the cost-effectiveness of priority areas can be significantly improved by introducing a reduction in restoration costs as a key criterion for optimization. Therefore, mapping the spatial variation of costs and incorporating it into spatial optimization are two essential steps for identifying priority restoration areas, especially considering that economic feasibility is often the decisive factor in determining whether a restoration action can be implemented on the ground (Primack, 2010; Brancalion et al., 2019).

Second, previous studies used the biophysical supply of ES to represent restoration benefits (Strassburg et al., 2019; Strassburg et al., 2020) while ignoring that the supply of ES is not a good surrogate for the demand in many situations (Burkhard et al., 2012; Zhao et al., 2018; Cui et al., 2019). ES supply represents what is potentially available from ecosystem processes and functions, while ES demand represents the amount of ES consumed or expected to be obtained by human society (Villamagna et al., 2013; Peng et al., 2017). For example, the supply of carbon sequestration service is often quantified with the net primary productivity of natural ecosystems, while the demand for carbon sequestration service is expressed with the carbon dioxide emitted by socioeconomic systems (Shi et al., 2020). Currently, one of the important targets of ecological restoration is to improve human well-being (Gann et al., 2019; Peng et al., 2020). The maintenance of human well-being usually depends on the degree of coordination between ES supply and demand (Burkhard et al., 2012; Liquete et al., 2013b). Thus, the regional context of the degree of coordination between ES supply and demand serves as another important basis for guiding restoration action (Shi et al., 2020; Wang et al., 2021a). However, only a few studies have addressed the mitigation of regional ES supply and demand mismatches as an essential target of restoration planning (Costa et al., 2021; Goyette et al., 2021). A recent study by Costa et al. (2021) proved that ES demand should be integrated into forest landscape restoration to enhance local human well-being. However, Costa et al. (2021) did not examine the changes in restoration costs when improving the representativeness of ES demand in the priority area network. To the best of our knowledge, approaches for optimizing the allocation of restoration resources that simultaneously combine the status of regional ES supply–demand (mis)matches and restoration costs remain rare (Goyette et al., 2021).

China is one of the world's largest resource countries in coastal wetlands (Perillo et al., 2019), but the country lost 58% of its coastal wetlands from 1950 to 2014 (Sun et al., 2015). Since 2000, China has gradually increased its investment in conserving coastal wetlands to reverse this situation (Sun et al., 2015; Liu et al., 2016; Wang et al., 2021b). China's central government issued the "*Master Plan for the Protection and Restoration of Important National Ecosystems* (MPPRINE) (2021–2035)" in

early June 2020 to promote ecological security and sustainability (Guan et al., 2021). In this plan, coastal ecological conservation and restoration are listed as one of the nine major national projects (Guan et al., 2021). MPPRINE has proposed general goals for restoration projects of different shore sections along the Chinese coast, such as improving the habitat quality of rare and endangered wildlife in the Yangtze River Estuary (Guan et al., 2021). MPPRINE does not provide site-selection methods to guide the deployment of ecological restoration projects. Soon after, China's central government approved a national standard of *Regulation Compiling Implementation Plan of Ecological Conservation and Restoration Project of Territorial Space* (TD/T 1068–2022) to strengthen the top-level design of protection and restoration of multiple ecosystems in territorial space (http://gi.mnr.gov.cn/202207/t20220711_2742011.html). However, this document does not provide detailed information on the basis of site selection of coastal restoration projects (e.g., indicators for representing the restoration feasibility of hydrological connectivity). Therefore, the development of a systematic workflow and defensible indicators to guide the implementation of tidal wetland restoration planning is urgently needed (Liu et al., 2016).

In this study, we developed a framework for identifying priority areas for tidal wetland restoration and considered the reclaimed area of Shanghai coast as a case study. Our framework includes five steps: (1) removal of unsuitable restoration areas for delineating the planning area, (2) analysis of the status of regional ES supply and demand (mis)matches, (3) estimation of the potential ES supply to represent restoration benefits of the planning area, (4) construction of a concept model for quantifying restoration costs, and (5) identification of restoration priority areas based on the optimization algorithm of SCP. With this framework, we tested whether the introduction of regional ES supply and demand (mis)matches would significantly shift the spatial distribution of priority restoration areas and increase restoration costs. The results of this study would have important implications for optimizing spatial planning for coastal ecosystem restoration.

2 Materials and methods

2.1 Study area

The loss of tidal wetlands in Shanghai has been largely caused by coastal reclamation over the past 60 years (Wei et al., 2010; Lin et al., 2021). The remaining tidal wetlands cover a total area of 614 km², most of which are concentrated on Chongming Island and Jiuduansha Shoal (Cai et al., 2014; Figure 1). Annual average temperature, amount of precipitation, evaporation, and sunlight hours of Shanghai are 17.7°C, 1597.1 mm, 1027.9 mm, and 1668.6 h, respectively (SMSB and SONBS, 2017). The average and maximum tidal range are 2.67 and 4.62 m along Shanghai Coast, respectively (Zhang, 2015). The surface water salinity (> 1‰) in the north east of Chongming Island and the north bank of Hangzhou Bay is higher than that (< 0.45‰) along the coast of Baoshan District and part of southern Chongming Island (Zhang, 2015). The sediment types of Shanghai's tidal wetlands are mainly sandy silt and silty sand (Wei et al., 2010). Common vegetation types of Shanghai's tidal wetlands are *Phragmites australis*, *Cyperaceae* Juss., and *Spartina alterniflora* (Cai et al., 2014).

In this study, we focused on the reclamation area of Shanghai between the 1950s and 2020, including the northern part of Chongming Island, which belongs to the Jiangsu Province (Figure 1). Five administrative districts can be found along the Shanghai coast: Jinshan District, Fengxian District, Pudong New Area, Baoshan District, and Chongming District (Figure 1; SMSB and SONBS, 2017). Chongming District consists of three islands: Changxing Island, Hengsha Island, and Chongming Island (Figure 1). In the *Shanghai Master Plan* (2017–2035), the Shanghai Municipal People's Government proposed the target of keeping the total amount of wetland resources unchanged (SUPLRAB, 2018). However, previous studies have shown that Shanghai's tidal wetlands cannot be recovered to their historical maximum area through natural sedimentation, especially under the impacts of sediment declination, sea level rise, and coastal erosion (Ge et al., 2016; Luan et al., 2021). To promote the implementation of the *Shanghai Master Plan* (2017–2035), it is necessary to implement tidal wetland restoration in the reclaimed areas (SUPLRAB, 2018).

2.2 Overview of the framework

Based on the first four stages of the SCP paradigm (Margules and Pressey, 2000), we developed a five-step workflow to identify priority areas for tidal wetland restoration (Figure 2). The first step was to extract potential restorable areas from the reclaimed tidal wetlands. Multiple raster layers used for spatial prioritization were then produced through steps 2–4. In step 2, the status of regional ES supply and demand (mis)matches was assessed using the benefit transfer method and by analyzing the status of socioeconomic development. We calculated the ratio of ES demand to supply for each township. If this ratio is greater than one, then the ES in the township is in short supply. The potential benefits of the restored wetlands were estimated by combining the recovery rate, degree of land degradation, and ES value. Restoration costs were quantified by combining socio-economic costs and ecological feasibility. Finally, we input these layers into the SCP software and identified the priority areas for restoration under the two scenarios. In our workflow, steps 1–3 refer to stage 1 of the SCP, and steps 4–5 refer to stages 2 and 4 of the SCP.

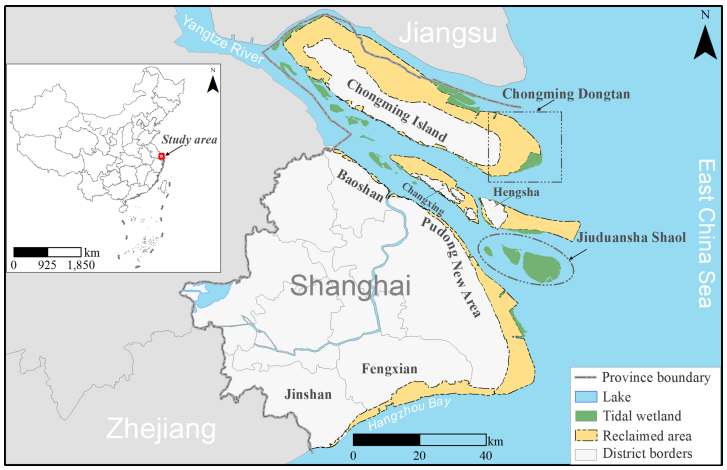

FIGURE 1
Map of the reclaimed area along Shanghai Coast between the 1950s and 2020. Inset shows the location of the study area in China (Left).

2.2.1 Extraction of the potential restorable areas

Ecological protection and restoration often face strong competition with other land-use demands such as coastal urbanization, food production, and low-carbon energy development (e.g., solar farms; Seddon, 2022). Therefore, we first eliminated reclaimed tidal wetlands that could not be restored for non-ecological reasons. Reclaimed areas from the 1950s to 2020 are regarded as degraded areas for tidal wetlands (Lin et al., 2021), which were digitized from the *Shanghai Urban Geology* (Wei et al., 2010) and Google Earth images. With reference to a previous study (Strassburg et al., 2019), we first excluded impervious surfaces (e.g., built-up land and roads) from the reclaimed area. Subsequently, several land use types used for social and economic development were erased from the map of reclaimed areas, including permanent basic farmland, urban drinking water sources, and advanced manufacturing bases. These land-use types are commonly known as "masks" in conservation planning (Groves, 2003). Among them, permanent basic farmland is determined in accordance with land use planning and is permanently protected and not allowed to be occupied for other uses, which has been implemented as a national policy for food security in China (Chen et al., 2017). Impervious surfaces were obtained from GlobeLand30 (V2020) (available at http://www.globallandcover.com/). The

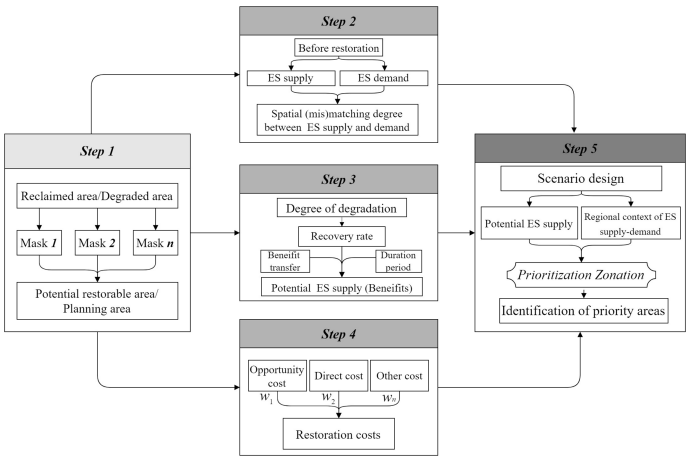

FIGURE 2
Workflow for identifying priority areas for tidal wetland restoration. w_n represents the weight of the restoration cost *n* used for assessing the total restoration costs.

remaining "masks" were digitized based on the *Atlas of the Shanghai Master Plan* (2017–2035) (available at https://www.shanghai.gov.cn/nw42806/index.html).

2.2.2 Quantifying the spatial mismatch of ES supply and demand

We mapped ES supply and demand at the town scale according to Shi et al. (2020) to ensure a comparison of the results of different studies at the same spatial resolution. The economic value per unit area of ES was used to express the ES supply capacity of each town, which was calculated using the following equation:

$$TESV = \sum_{i=1}^{n} w_i \times ESV_i \quad (1)$$

where $TESV$ represents the ES value per unit of each town in 2007$/ha/yr (same hereafter), w_i is the area proportion of ecosystem i in the whole town, and ESV_i is the ES value per unit area of ecosystem i. The composition data of the different ecosystems in each town were extracted from Globeland30 (V2020). We used the vector files of Shanghai's dike in 2020 to divide "wetland" in Globeland30 (V2020) into two ecosystem types, namely, inland and tidal wetland. The ES values per unit area of different ecosystems were retrieved from a global database provided by Costanza et al. (2014). This database is one of the few that includes marine and terrestrial ES value data.

As recommended by previous studies (Peng et al., 2017; Zhao et al., 2018; Shou et al., 2020), we mapped ES demand by combining indicators representing land use intensity and socio-economic development:

$$DI_i = BAP_i \times \lg(PD_i) \times \lg(GDP_i) \quad (2)$$

where DI_i is the ES demand index of town i, BAP_i is the area proportion of built-up land in the town i, PD_i is population density of town i in individuals/ha, and GDP_i is the value per unit area of gross domestic product (commonly as GDP) of town i in CNY/ha. Population density and GDP data were derived from the 2017 statistical yearbook of each district.

We used the ES demand–supply ratio index (DSR_i hereinafter) to quantify the proximity between ES supply and demand. DSR can be calculated using the following equation:

$$DSR_i = \frac{D_i + 1}{S_i + 1} \quad (3)$$

where S_i and D_i are the ES supply and demand index of town i, respectively, using the min-max normalization method. The ES supply and demand of the town are more imbalanced when the DSR_i value is higher.

2.2.3 Assessing benefits for tidal wetland restoration

In this study, we assumed that the potential ES supply of fully restored wetlands is consistent with global averages. The functional restoration of degraded tidal wetlands often takes a long time, ranging from 20 to 30 years (Bayraktarov et al., 2016). A global meta-analysis showed that the average annual recovery rate of degraded tidal wetlands is approximately 4% per year (Jones et al., 2018). The recovery rate of ecosystem properties is closely related to the degree of degradation before restoration (Ghazoul and Chazdon, 2017). Thus, we adjusted the recovery rate of different land cover types in potentially restorable areas according to their degree of degradation. Thus, the potential ES supply of tidal wetland restoration at the end of a pre-specified time can be calculated using the following equation:

$$RBLC_i = 0.04 \times c_i \times T \times TWESV \quad (4)$$

where $RBLC_i$ represents the value per unit area of the potential ES supply of land cover type i at the end of year T, when it is used for restoration. In this study, we set T to 10 years according to the post-2020 outcome goals. c_i is the coefficient used to adjust the recovery rate of land cover type i, which indicates the difference in the average degree of degradation for all land cover types in the reclaimed area. We used the ES value of each land cover type to represent the degree of degradation according to the concept of land degradation (IPBES, 2018). Thus, c_i can be calculated using the following equation:

$$c_i = \frac{ESV_i}{\overline{ESV}} \quad (5)$$

where ESV_i is the ES value per unit area of land cover type i and $\overline{ESV}$ is the average ES value per unit area for all land cover types in the potential restorable area.

2.2.4 Quantification of restoration costs

Restoration costs include opportunity costs, direct costs, contingency costs, transaction costs, external costs, and time lags (Wang et al., 2021a). Previous studies have used various indicators to represent monetary restoration costs, such as anthropogenic pressure (Qu et al., 2019; Goyette et al., 2021) and ecological restoration feasibility (Orsi and Geneletti, 2010). Considering that the available data on costs are often limited (Wang et al., 2022), we built a conceptual model for estimating restoration costs, which can be expressed by the following equation:

$$RC = w_1 \times NOC + w_2 \times NDC \quad (6)$$

where RC is the restoration cost. NOC and NDC are the standardized indicators (based on the min-max normalization method) for opportunity cost and direct cost, respectively. w_1 and w_2 are the weights of NOC and NDC , respectively. In this study, both values were set to 0.5 in this study. Opportunity costs were represented by the housing prices of different districts in 2016, which were derived from Shanghai's statistical yearbook (SMSB and SONBS, 2017).

The direct costs of restoration include investment in hydrological restoration, revegetation, sediment replenishment, raw material, and others (Wang et al., 2021a). Therefore, we assumed that direct costs were related to ecological feasibility. In this study, we propose the following equation to measure the direct costs:

$$DC = \sqrt[n]{\prod_{i=1}^{n} RF_i} \quad (7)$$

where DC is the indicator for direct cost, and RF_i is the normalized indicator for restoration feasibility i with the min-max normalization method. Based on previous studies and the availability of data (Widis et al., 2015; Liu et al., 2021), five key factors were adopted to assess restoration feasibility (Table 1). The methods and data sources for these indicators are listed in Table 1. The spatial extent of the tidal range and SSC data was restricted to offshore water. Therefore, we first divided the study area into multiple drainage basins using the hydrology tools of ArcGIS 10.2.1. The GEBCO_2021 Grid (with a spatial resolution of 15″; available at https://www.gebco.net/) was used to depict the drainage basins. Then, the average tidal range and SSC of the drainage basins intersected with coastal water were extracted from their original layers (Table 2) with the spatial analyst tools of ArcGIS 10.2.1. Finally, we assigned the values of the drainage basins intersecting with coastal water to those intersecting with or near the reclaimed area according to Tobler's first law of geography (Tobler, 1970).

2.2.5 Identifying priority areas for tidal wetland restoration

Zonation can produce a priority scoring map by repeatedly calculating the importance values of all pixels across the planning region and excluding the pixels that have the lowest value until all pixels are excluded (Moilanen, 2007). Accordingly, the impacts of newly added features on the spatial distribution of priority ranking can be flexibly assessed. The additive benefit function (ABF) of Zonation was selected to address the spatial prioritization problem (Moilanen, 2007). The grid size of the three layers was resampled to 100 m × 100 m to ensure consistency with the units of the ES value.

In this study, two scenarios were designed to determine the impact of regional ES supply and demand (mis)matches on the distribution of priority areas. The first was "ES demand-ignored" scenario. In particular, the potential ES supply and restoration cost layers were inputted into Zonation 4.0. An edge removal function was used to improve the connectivity of the priority area network. The second scenario was the "ES demand" scenario. In particular, all three layers (potential ES supply, restoration costs, and ES demand-supply ratio) were inputted into the Zonation software and run under the same settings as in the first scenario. Referring to the methods of Costa et al. (2021), we extracted priority areas for tidal wetland restoration according to Aichi Biodiversity Target 15, which proposed the restoration of at least 15% of degraded ecosystems (IPBES, 2018). The potentially restorable areas may be much smaller than the original reclaimed areas. Thus, the threshold used for extracting priority areas should be modified according to potential restorable area ratio (Threshold = 0.15/potential restorable area ratio).

2.3 Statistical analysis

Kendall correlations were used to analyze the spatial association among the potential supply of ES, restoration costs, and the ES demand–supply ratio to explain the spatial characteristics of priority areas in different scenarios. The degree of spatial overlap of the priority areas generated from the two scenarios was evaluated. We then quantified the difference in priority areas for the different districts between the two scenarios. Changes in potential ES supply and restoration costs between the two scenarios were also calculated to analyze the impacts of incorporating the regional context of ES supply and demand into restoration planning.

TABLE 1 Indicators for assessing the ecological restoration feasibility in reclaimed area.

Indicator types	Methods	Data sources
Tidal range	Inverse distance weighted interpolation	Bao and Zhu, 2017.
Suspended sediment concentration (SSC)	Quantitative remote sensing retrieval based on Landsat8 OLI images (Pan and Guo, 2020).	Landsat8 images were downloaded from USGS web (available at: https://earthexplorer.usgs.gov/)
Distance from river	Euclidean distance	1:250,000 basic geographic information data of Shanghai provided by the National Earth System Science Data Center
Distance from road	Euclidean distance	1:250,000 basic geographic information data of Shanghai provided by the National Earth System Science Data Center
Distance from settlements	Euclidean distance	1:250,000 basic geographic information data of Shanghai provided by the National Earth System Science Data Center

3 Results

3.1 Spatial distribution of the potential restorable areas

From the 1950s to 2020, 1353 km² of tidal wetlands and coastal water along the Shanghai coast were reclaimed, among which 68.6% of the original reclaimed area was unsuitable for tidal wetland restoration because it had been converted into built-up land or other types for socio-economic development. The remaining 31.4% (425.2 km²) of the reclaimed area was considered suitable for ecological restoration (Figure 3), referred to as the potential restorable area hereinafter. Approximately 93.3% of the potential restorable areas were distributed in Pudong New Area and Chongming District (Figures 3A, B). Only 1.5% of the potential restorable areas were distributed in the Baoshan and Jinshan districts (Figures 3A, B). In terms of the proportion of different land cover types, cropland accounted for the largest proportion (72.3%) of the potential restorable areas, followed by water (15.2%), and inland wetlands (9.3%) (Figure 3C). Based on the method described in Section 2.2.5, we set the threshold for extracting priority areas to 50%.

3.2 Spatial relationships among restoration benefits, costs, and ES demand–supply ratio

The results showed that the ES demand–supply ratio in most potential restorable areas of Chongming District was lower than that of the other four districts (Figure 4A). Potential restorable areas with high ES demand–supply ratios were mainly distributed along the northeast coast of the Pudong New Area (Figure 4A). The estimation results showed that most potentially restorable areas had low ES values (Figure 4B). Only a few patches could provide high ES values after 10 years, such as the patches along the coast of the Jinshan District (Figure 4B). Restoration costs in Chongming District were significantly lower than those in the other districts (Figure 4C). The results of the Kendall correlation showed that the ES demand–supply ratio was significantly negatively correlated with the restoration costs (Figure 5, $p < 0.05$). The potential ES supply was insignificantly correlated with the ES demand–supply ratio and restoration costs (Figure 5, $p > 0.05$).

3.3 Spatial distribution of priority areas in different scenarios

The spatial distribution of the two priority ranking maps for the tidal wetlands varied greatly (Figure 6). The priority ranking of the northwest coast of Chongming Island in the ES demand scenario was lower than in the ES demand-ignored scenario (Figure 6C). In contrast, the priority ranking of many potential restorable areas in the central Pudong New Area was raised in the ES demand scenario compared with that in the ES demand-ignored scenario (Figure 6C). Among the five administrative districts, Fengxian and Chongming districts demonstrated declining performance in priority ranking, the two had average declines of 0.01 and 0.05, respectively (Figure 6C). The potential

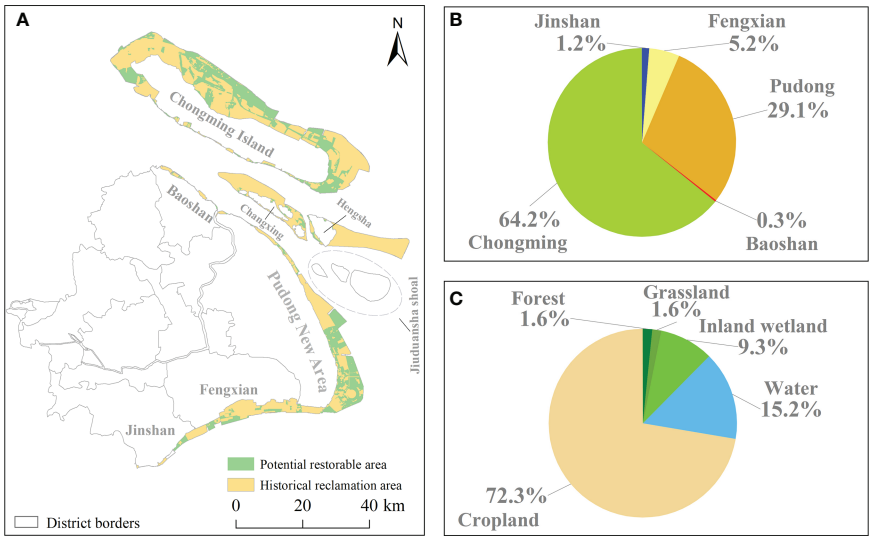

FIGURE 3
Spatial distribution of the potential restorable areas **(A)**. The two pie charts were used to present the proportion of potential restorable areas contained in different districts **(B)** and the land cover composition of potential restorable areas **(C)**, respectively.

TABLE 2 Priority areas of each district under different scenarios (unit: ha).

Districts	ES demand-ignored	ES demand	Ratio
Jinshan	429 (2.2%)	438 (2.3%)	2.0%
Fengxian	607 (3.2%)	607 (3.2%)	0
Pudong New Area	3,516 (18.3%)	4,051 (21.0%)	15.2%
Baoshan	13 (0.07%)	36 (0.2%)	176.9%
Chongming	14,690 (76.3%)	14,121 (73.3%)	-3.9%

restorable areas of Baoshan District had the largest increase in priority ranking, on average (Figure 6C).

The total priority areas that we extracted accounted for approximately 45% of the potential restorable area instead of 50% (Table 2). This is because Zonation software requires all raster data to have the same number of rows and columns. However, the spatial resolution and format of the original data were different, which caused information loss during the data preparation. The overlapping area between the two scenarios accounted for 85% of the total priority areas. The priority areas of Chongming District in the ES demand scenario decreased by 3.9% compared with that in the ES demand-ignored scenario (Figure 7A and Table 2). For example, compared with the ES demand-ignored scenario, a larger number of potential restorable areas on eastern Chongming Island did not exist in the priority area network (Figure 7A). Conversely, many potential restorable patches along the coast of Baoshan District and the northern Pudong New Area were identified as priority areas for tidal wetland restoration only when combining the status of regional ES supply and demand (mis)matches (Figures 7B, C). For example, we found that restoration priority areas in Baoshan District increased by 1.8 times compared with the ES demand-ignored scenario (Table 2).

3.4 Comparison of restoration benefits and costs between the two scenarios

Compared to the ES demand-ignored scenario, the total potential ES supply and restoration costs increased by 0.34% and 10%, respectively (Figure 8). Of the five administrative districts, only Chongming District showed a decrease in potential ES supply (2.3%) but an increase in restoration costs (3.0%) when accounting for the ES demand–supply ratio index (Figure 8). The change trend of the potential ES supply and restoration costs in the remaining four districts was consistent with that of the priority areas between the two scenarios. For example, the potential ES supply and restoration costs of Baoshan District increased by 57.6% and 161.1%, respectively, under the ES demand scenario (Figure 8).

4 Discussion

4.1 Availability of the potential restorable areas

Less than one-third of the original reclamation areas were potentially available for tidal wetland restoration along the

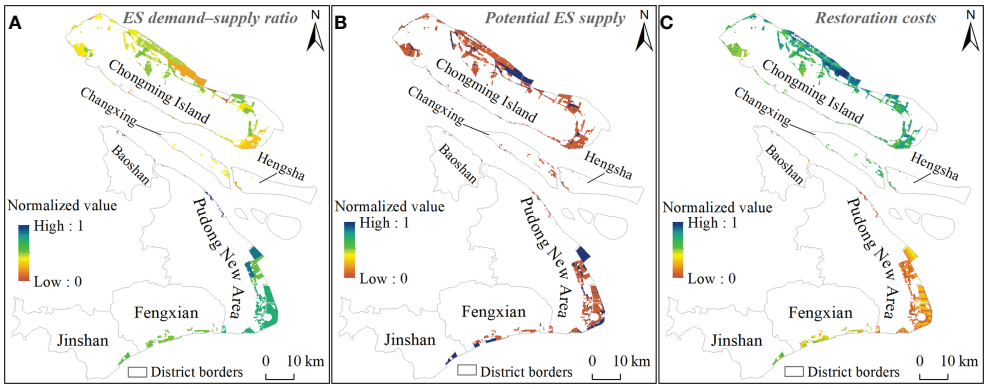

FIGURE 4
Spatial characteristics of ES demand–supply ratio **(A)**, potential ES supply **(B)**, and restoration costs **(C)**. In **(C)**, higher grid values correspond to lower restoration costs in reality.

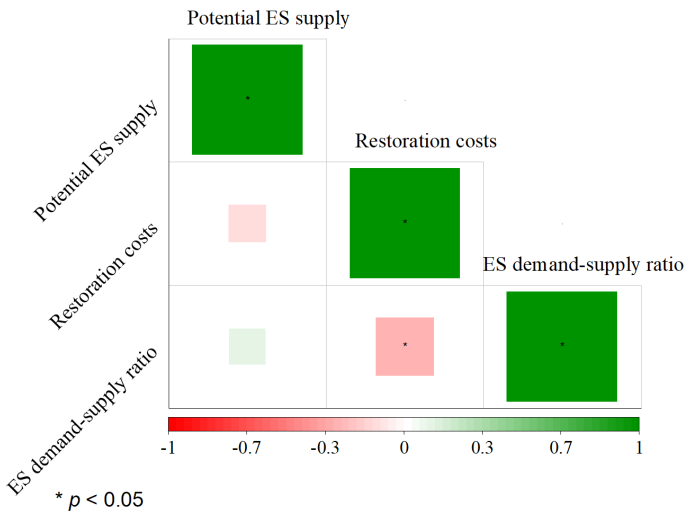

FIGURE 5
Correlation among the potential ES supply, restoration costs and ES demand–supply ratio. The size of the square represents the absolute value of the correlation coefficient. * means p < 0.05.

Shanghai coast. This result demonstrates that previous studies may have overestimated the amount of land resources available for restoration because of the low availability of spatial data on the needs and interests of all relevant stakeholders (e.g., Qu et al., 2019; Strassburg et al., 2020). Excluding these specific land-use types from reclaimed areas is an essential step in the process of restoration planning. Many tidal wetlands are transformed to provide valuable services that cannot be offered by natural ecosystems, such as transport services provided by Shanghai Pudong International Airport and freshwater supply services provided by Qingcaosha Reservoir of Changxing Island (Chen et al., 2007). Similar projects are also being conducted abroad, such as the Eko Atlantic City project in Africa (Martín-Antón et al., 2016). Therefore, incorporating detailed information on competing land use demands into decision making by building a mechanism such as participatory land use planning is necessary to promote the benefits of ecological restoration (Gann et al., 2019).

4.2 Significance of incorporating ES demand–supply ratio index into restoration planning

In this study, trade-offs among the ES demand–supply ratio, potential ES supply, and restoration cost were mitigated using

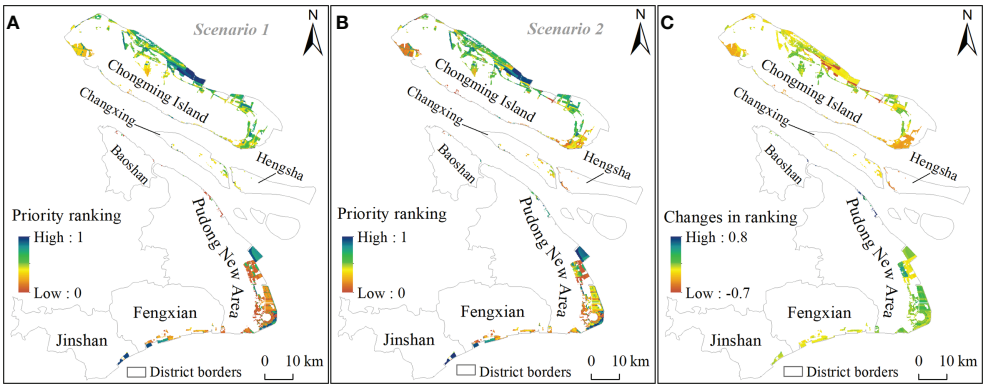

FIGURE 6
Spatial distribution of restoration priority ranking of potential restorable areas under ES demand-ignored **(A)** and ES demand scenario **(B)**. **(C)** shows changes in the priority ranking between the two scenarios.

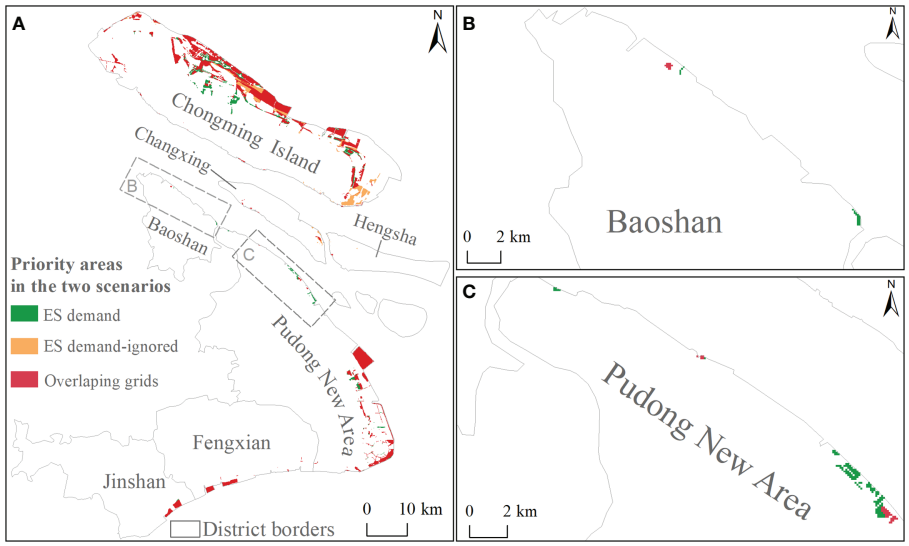

FIGURE 7
Spatial distribution of priority areas for tidal wetland restoration under different scenarios **(A)**. **(B)** and **(C)** show the spatial distribution of priority areas along the coast of Baoshan District and the northern Pudong New Area, respectively.

the ABF of Zonation. The ranking rule of the ABF is characterized by considering the overall high value for all the abovementioned features in a given planning unit instead of one feature that has the highest value. For this reason, we could explain why only considering the potential supply of ES and restoration costs would result in priority areas being concentrated in Chongming District (Figure 4A). Specifically, recent studies have shown that ES supply was lower than human demand in Baoshan District and the central Pudong New Area due to anthropogenic impacts (e.g., huge demand for land resources on industrial, residential, and commercial development; Chen et al., 2019; Jiang et al., 2020; Shi et al., 2020). The restoration costs in the two districts were much higher than those in Chongming District, which can be attributed to the high opportunity costs represented by local high housing prices (SMSB and SONBS, 2017). Given that the spatial distribution of potential ES supply was relatively homogeneous (Figure 4B), potential ES supply was not correlated with either the ES demand–supply ratio or restoration costs in this study. Thus, considering only the potential supply of ES and restoration costs would result in priority areas concentrated in districts with low economic development but relatively healthy ecosystems (e.g., Chongming District) (Figure 4A). Therefore, regional disparities in human well-being cannot be reduced by implementing ecological restoration projects.

The overlapping areas accounted for 85% of the priority areas in the two scenarios. However, the status of regional ES supply and demand (mis)matches cannot be neglected in restoration planning. Such a high proportion might have been caused by the high threshold for extracting priority areas in this study. In practice, the target of restoring 15% of degraded land is

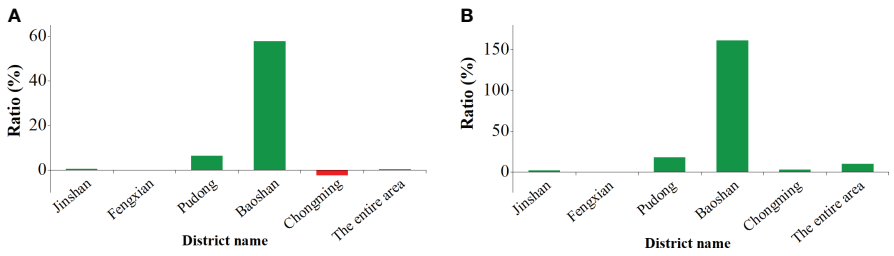

FIGURE 8
Comparison of potential ES supply **(A)** and restoration costs **(B)** between the two scenarios.

unlikely to be approved by the local government because of the scarcity of land resources in Shanghai (Chen et al., 2007). Discrepancies in the ranking score of many patches between the two scenarios were significant (Figure 6C), which means that patches with high ES demand–supply ratios but low restoration benefits or high restoration costs will be excluded from the priority area network as the threshold declines. For example, Wang et al. (2018) found that land subsidence exacerbates the threat of storm flooding to administrative districts with high housing prices (e.g., Baoshan District and northern Pudong New Area), which implies that coastal protection needs to be strengthened in these places. Restoring reclaimed tidal wetlands can attenuate wave energy, provide additional water storage, and improve the resilience of densely populated areas to flood risks (Temmerman and Kirwan, 2015). Coincidentally, parts of the local restorable areas only under the ES demand scenario could be included in the priority area network (Figures 7B, C). Future studies can design a scientific target for tidal wetland restoration based on the concept of 'no net loss' (He, 2019). For example, the total restoration area can be determined using the changes in the tidal wetland area over a certain period as a reference.

We used a conservative multiplier to calculate the benefits of restoration projects, which may have resulted in a low benefit-to-cost ratio in the first 10 years. However, a global meta-analysis found that the net benefits of restoration projects will ultimately outweigh the costs of that within a timeframe of approximately 70 years (Stewart-Sinclair et al., 2021). The case of the Yingwuzhou wetland restoration (located on the coast of Jinshan District) shows that the project investment can be recovered within 18 years according to the cost–benefit calculation of ES (Wu et al., 2020). Recent evidence also suggests that people are more inclined to pay for ES, which directly benefits them (Liu, 2020). Thus, tidal wetland restoration is worth implementing when ES is in high demand, even if restoration costs are high.

4.3 Applications for restoration planning

Regional ecosystem health deteriorates as the mismatch between ES demand and supply increases (Villamagna et al., 2013; Pan et al., 2021). Thus, restoration actions should be prioritized in areas with serious deficits in ES supply and demand to truly improve local human-being (Peng et al., 2020). In other words, if the information on regional supply and demand mismatches is ignored for spatial prioritization, it may lead to an increase in the overall potential ES supply only, but without the improvement in human well-being. Using our framework for implementing restoration projects can avoid this situation by addressing the trade-offs among the need to improve human well-being, the potential ES supply obtained from tidal wetland restoration, and restoration costs. In particular, our framework can guide the specific implementation of large-scale restoration projects such as China's "MPPRINE (2021–2035)". Many studies have quantified the spatial relationship between ES supply and demand to support environmental management in the Shanghai or Yangtze River Delta (e.g., Chen et al., 2019; Shi et al., 2020). However, they do not propose explicit spatial strategies to guide the deployment of restoration projects. For example, Shi et al. (2020) only recommended that priority areas for restoration should be placed in the central and suburbs of Shanghai City based on the analysis of ES flow. Priority areas identified by our framework not only provide essential ES to nearby people but are also highly cost-effective when they are implemented on the ground.

Our workflow has potential as a useful tool for informing restoration planning of other coastal ecosystems (e.g., mangroves and seagrass) by scientists and policymakers. First, most of the data and indicators used in this study also serve as an ecological and economic basis for the site selection of mangrove planting (e.g., tidal range; Worthington and Spalding, 2018). Second, the flexibility of our workflow allows the adjustment of indicators to adapt to different regional contexts. For instance, housing prices can be replaced by income from farming or aquaculture to represent the opportunity costs in tropical areas.

4.4 Refining the framework

Our framework has several limitations that should be addressed in the future. First, spatial (mis)matches of ES supply and demand were not assessed in a one-to-one manner because of the lack of unified methods for mapping ES demand (Zhao et al., 2018). Spatial mapping of ES demand is particularly scarce in coastal ES studies (Solé and Ariza, 2019). Second, the restoration cost equation can be further refined when the cost information on restoration engineering is available. For instance, external costs were ignored in this study because of the difficulty in defining the scope of the impact of external costs (Wang et al., 2021a). Finally, we used the global average recovery rate as the unique parameter of the reference system to estimate the potential ES supply, while ignoring the spatial heterogeneity of the environmental context. Future studies can build a reference ecosystem using the integrated database method, that is, a method derived from big data analysis (Pang et al., 2020).

5 Conclusions

In this study, a five-step framework was established to rank the spatial priorities of tidal wetland restoration. Compared with previous studies, we integrated the status of regional ES supply and demand (mis)matches into spatial prioritization to effectively improve human well-being through ecological restoration. We found that ignoring the comprehensive needs of socio-economic

development (e.g., using reclaimed land to develop cutting-edge technology) can lead to the overestimation of potential restorable areas. The results showed that many potential restorable areas (e.g., the coast of Baoshan District and northern Pudong New Area) with a high demand for improving human well-being will be excluded from the priority area network unless the ES demand–supply ratio index is incorporated into spatial prioritization. Increasing the proportion of priority areas in districts with high ES demand–supply ratios increased the total restoration costs (up to 10%) and potential ES supply (approximately 0.3%) at the same time. This result was caused by the low spatial association between the status of regional ES supply and the demand matching degree before restoration and the potential ES supply thereafter. Overall, we advocate that information on the status of regional ES supply and demand (mis)matches should be incorporated into spatial planning to ensure the availability of restoration benefits to those who truly need them.

Data availability statement

The raw data supporting the conclusions of this article will be made available by the authors, without undue reservation.

Author contributions

SL designed the study, analyzed the data, and wrote the manuscript. SL and XL revised the manuscript. RW reviewed the manuscript and provided valuable feedback. YM, JW, and WZ contributed significantly to the data collection and manuscript preparation. All authors contributed to the article and approved the submitted version.

Funding

This work was supported by the National Natural Science Foundation of China (42141016) and Scientific Research Foundation for Advanced Talents, Yangzhou University (137012618).

Conflict of interest

The authors declare that the research was conducted in the absence of any commercial or financial relationships that could be construed as a potential conflict of interest.

Publisher's note

All claims expressed in this article are solely those of the authors and do not necessarily represent those of their affiliated organizations, or those of the publisher, the editors and the reviewers. Any product that may be evaluated in this article, or claim that may be made by its manufacturer, is not guaranteed or endorsed by the publisher.

References

Adame, M. F., Hermoso, V., Perhans, K., Lovelock, C. E., and Herrera-Silveira, J. A. (2014). Selecting cost-effective areas for restoration of ecosystem services. *Conserv. Biol.* 29, 493–502. doi: 10.1111/cobi.12391

Bao, D. Y., and Zhu, J. R. (2017). The effects of river regimes changes in the Changjiang Estuary on hydrodynamics and salinity intrusion in the past 60 years II. hydrodynamics. *Acta Oceanologica Sin.* 39, 1–15. doi: 10.3969/j.issn.0253-4193.2017.02.001

Bayraktarov, E., Saunders, M. I., Abdullah, S., Mills, M., Beher, J., Possingham, H. P., et al. (2016). The cost and feasibility of marine coastal restoration. *Ecol. Appl.* 26, 1055–1074. doi: 10.1890/15-1077

Brancalion, P. H. S., Meli, P., Tymus, J. R. C., Lenti, F. E. B., Benini, R. M., Silva, A. P. M., et al. (2019). What makes ecosystem restoration expensive? a systematic cost assessment of projects in Brazil. *Biol. Conserv.* 240, 108274. doi: 10.1016/j.biocon.2019.108274

Burkhard, B., Kroll, F., Nedkov, S., and Müller, F. (2012). Mapping ecosystem service supply, demand and budgets. *Ecol. Ind.* 21, 17–29. doi: 10.1016/j.ecolind.2011.06.019

Cai, Y. M., Zhou, Y. X., and Tian, B. (2014). *Shanghai wetlands.* (Shanghai: Shanghai Scientific & Technical Publishers).

Chen, J. Y., Cheng, H. Q., and Dai, Z. J. (2007). Compatibility of utilization and protection of tidal flat and wetland: a case study in Shanghai area. *Eng. Sci.* 9, 11–17.

Chen, J. Y., Jiang, B., Bai, Y., Xu, X. B., and Alatalo, J. M. (2019). Quantifying ecosystem services supply and demand shortfalls and mismatches for management optimization. *Sci. Total Environ.* 650, 1426–1439. doi: 10.1016/j.scitotenv.2018.09.126

Chen, C. Q., Jiang, P. H., Cai, L. Y., Shan, J. X., Zhang, Y. Q., Wang, L. Y., et al. (2017). Delineation of a permanent basic farmland protection area around a city centre: case study of Changzhou city, China. *Land Use Policy.* 60, 73–89. doi: 10.1016/j.landusepol.2016.10.014

Costa, T., Mazzochini, G. G., Oliveira-Filho, A. T., Ganade, G., Carvalho, A. R., and Manhães, A. P. (2021). Priority areas for restoring ecosystem services to enhance human well-being in a dry forest. *Restor. Ecol.* 29, e13426. doi: 10.1111/rec.13426

Costanza, R., de Groot, R., Sutton, P., van der Poleg, S., Anderson, S. J., Kubiszewski, I., et al. (2014). Changes in the global value of ecosystem services. *Glob. Environ. Change.* 26, 152–158. doi: 10.1016/j.gloenvcha.2014.04.002

Crossman, N. D., and Bryan, B. A. (2006). Systematic landscape restoration using integer programming. *Biol. Conserv.* 128, 369–383. doi: 10.1016/j.biocon.2005.10.004

Cui, F. Q., Tang, H. P., Zhang, Q., Wang, B. J., and Dai, L. W. (2019). Integrating ecosystem services supply and demand into optimized management at different scales: a case study in Hulunbuir, China. *Ecosyst. Serv.* 39, 100984. doi: 10.1016/j.ecoser.2019.100984

Gann, G. D., McDonald, T., Walder, B., Aronson, J., Nelson, C. R., Jonson, J., et al. (2019). International principles and standards for the practice of ecological restoration. second edition. *Restor. Ecol.* 27, S1–S46. doi: 10.1111/rec.13035

Ge, Z. M., Wang, H., Cao, H. B., Zhao, B., Zhou, X., Peltola, H., et al. (2016). Responses of eastern Chinese coastal salt marshes to sea-level rise combined with vegetative and sedimentary processes. *Sci. Rep.* 6, 28466. doi: 10.1038/srep28466

Ghazoul, J., and Chazdon, R. (2017). Degradation and recovery in changing forest landscapes: a multiscale conceptual framework. *Annu. Rev. Environ. Resour.* 42, 161–188. doi: 10.1146/annurev-environ-102016-060736

Gilby, B. L., Olds, A. D., Brown, C. J., Connolly, R. M., Henderson, C. J., Maxwell, P. S., et al. (2021). Applying systematic conservation planning to improve the allocation of restoration actions at multiple spatial scales. *Restor. Ecol.* 29, e13403. doi: 10.1111/rec.13403

Goyette, J. O., Cimon-Morin, J., Mendes, P., Thériault, M., Pellerin, S., and Poulin, M. (2021). Planning wetland protection and restoration for the safeguard of ecosystem service flows to beneficiaries. *Landsc. Ecol.* 36, 2691–2706. doi: 10.1007/s10980-021-01267-x

Groves, C. R. (2003). *Drafting a conservation blueprint: a practitioner's guide to planning for biodiversity.* (Washington DC: Island Press).

Guan, F. J., Liu, L. H., Liu, J. W., Fu, Y., Wang, L. Y., Wang, F., et al. (2021). Systematically promoting the construction of natural ecological protection and governance capacity: experts comments on master plan for major projects of national important ecosystem protection and restoration, (2021-2035). *J. Nat. Resour.* 36, 290–299. doi: 10.31497/zrzyxb.20210202

He, Q. (2019). Conservation: 'no net loss' of wetland quantity and quality. *Curr. Biol.* 29, R1070–R1093. doi: 10.1016/j.cub.2019.08.027

IPBES (2018). *The IPBES assessment report on land degradation and restoration.* (Bonn: Secretariat of the Intergovernmental Science-Policy Platform on Biodiversity and Ecosystem Services).

Jiang, B., Bai, Y., Chen, J. Y., Alatalo, J. M., Xu, X. B., Liu, G., et al. (2020). Land management to reconcile ecosystem services supply and demand mismatches-a case study in Shanghai municipality, China. *Land Degrad. Dev.* 31, 2684–2699. doi: 10.1002/ldr.3614

Jones, H. P., Jones, P. C., Barbier, E. B., Blackburn, R. C., Rey Benayas, J. M., Holl, K. D., et al. (2018). Restoration and repair of earth's damaged ecosystems. *Proc. Biol. Sci.* 185, 20172577. doi: 10.1098/rspb.2017.2577

Kukkala, A., and Moilanen, A. (2013). Core concepts of spatial prioritisation in systematic conservation planning. *Biol. Rev.* 88, 443–464. doi: 10.1111/brv.12008

Lin, S. W., Li, X. Z., Yang, B., Ma, Y. X., Jiang, C., Xue, L. M., et al. (2021). Systematic assessments of tidal wetlands loss and degradation in Shanghai, China: from the perspectives of area, composition and quality. *Glob. Ecol. Conserv.* 25, e01450. doi: 10.1016/j.gecco.2020.e01450

Liquete, C., Piroddi, C., Drakou, E. G., Gurney, L., Katsanevakis, S., Charef, A., et al. (2013a). Current status and future prospects for the assessment of marine and coastal ecosystem services: a systematic review. *PloS One.* 8, e67737. doi: 10.1371/journal.pone.0067737

Liquete, C., Zulian, G., Delgado, I., Stips, A., and Maes, J. (2013b). Assessment of coastal protection as an ecosystem service in Europe. *Ecol. Indic.* 30, 205–217. doi: 10.1016/j.ecolind.2013.02.013

Liu, Y. X. (2020). The willingness to pay for ecosystem services on the Tibetan plateau of China. *Geogr. Sustain.* 1, 141–151. doi: 10.1016/j.geosus.2020.06.001

Liu, Z. Z., Cui, B. S., and He, Q. (2016). Shifting paradigms in coastal restoration: six decades' lessons from China. *Sci. Total Environ.* 566, 205-214. doi: 10.1016/j.scitotenv.2016.05.049

Liu, Z. Z., Fagherazzi, S., and Cui, B. S. (2021). Success of coastal wetlands restoration is driven by sediment availability. *Commun. Earth Environ.* 2, 44. doi: 10.1038/s43247-021-00117-7

Luan, H. L., Ding, P. X., Yang, S. L., and Wang, Z. B. (2021). Accretion-erosion conversion in the subaqueous Yangtze delta in response to fluvial sediment decline. *Geomorphology.* 382, 107680. doi: 10.1016/j.geomorph.2021.107680

Margules, C. R., and Pressey, R. L. (2000). Systematic conservation planning. *Nature.* 405, 243–253. doi: 10.1038/35012251

Martín-Antón, M., Negro, V., del Campo, J. M., López-Gutiérrez, J. S., and Esteban, D. (2016). Review of coastal land reclamation situation in the world. *J. Coast. Res.* 75, 667–671. doi: 10.2112/si75-133.1

McBride, M. F., Wilson, K. A., Burger, J., Fang, Y. C., Lulow, M., Olson, D., et al. (2010). Mathematical problem definition for ecological restoration planning. *Ecol. Model.* 211, 2243–2250. doi: 10.1016/j.ecolmodel.2010.04.012

Moilanen, A. (2007). Landscape zonation, benefit functions and target-based planning: unifying reserve selection strategies. *Biol. Conserv.* 134, 571–579. doi: 10.1016/j.biocon.2006.09.008

Orsi, F., and Geneletti, D. (2010). Identifying priority areas for forest landscape restoration in Chiapas (Mexico): an operational approach combining ecological and socioeconomic criteria. *Landsc. Urban Plan.* 94, 20–30. doi: 10.1016/j.landurbplan.2009.07.014

Pang, B., Cui, B. S., Cai, Y. Z., Xie, T., Wang, Q., and Ning, Z. H. (2020). Studies on selection method of reference condition for ecological restoration of coastal wetlands in China. *Environ. Ecol.* 2 (1-9), 25.

Pan, L. Y., and Guo, B. Y. (2020). Remote sensing research of suspended sediment concentration in Zhoushan archipelago sea area based on Landsat8 data. *Ocean Dev. Manage.* 37, 82–90. doi: 10.20016/j.cnki.hykfygl.2020.09.014

Pan, Z. Z., He, J. H., Liu, D. F., Wang, J. W., and Guo, X. N. (2021). Ecosystem health assessment based on ecological integrity and ecosystem services demand in the middle reaches of the Yangtze river economic belt, China. *Sci. Total Environ.* 774, 144837. doi: 10.1016/j.scitotenv.2020.144837

Peng, J., Li, B., Dong, J. Q., Liu, Y. X., Lü, D. N., Du, Y. Y., et al. (2020). Basic logic of territorial ecological restoration. *China Land Sci.* 34, 18–26. doi: 10.11994/zgtdkx.20200427.124442

Peng, J., Yang, Y., Xie, P., and Liu, Y. X. (2017). Zoning for the construction of green space ecological networks in Guangdong province based on the supply and demand of ecosystem services. *Acta Ecol. Sin.* 37, 4562–4572. doi: 10.5846/stxb201601020007

Perillo, G. M. E., Wolanski, E., Cahoon, D. R., and Hopkinson, C. H. (2019). *Coastal wetlands: an integrated ecosystem approach (2th).* (Netherlands: Elsevier).

Pittman, S. J., Stamoulis, K. A., Antonopoulou, M., Das, H. S., Shahid, M., Delevaux, J. M. S., et al. (2022). Rapid site selection to prioritize coastal seascapes for nature-based solutions with multiple benefits. *Front. Mar. Sci.* 9, 832480. doi: 10.3389/fmars.2022.832480

Primack, R. B. (2010). *Essentials of conservation biology (5th).* (Sunderland: Sinauer Associates).

Qu, Y., Sun, G. Q., Luo, C. Y., Zeng, X. Y., Zhang, H. Q., Murray, N. J., et al. (2019). Identifying restoration priorities for wetlands based on historical distributions of biodiversity features and restoration suitability. *J. Environ. Manage.* 231, 1222–1231. doi: 10.1016/j.jenvman.2018.10.057

Seddon, N. (2022). Harnessing the potential of nature-based solutions for mitigating and adapting to climate change. *Science.* 376, 1410–1416. doi: 10.1126/science.abn9668

Shanghai Municipal Statistics Bureau (SMSB) and Survey office of the National Bureau of Statistics in Shanghai (SONBS) (2017). *Shanghai statistical yearbook 2016.* (Beijing: China Statistics Press).

Shanghai Urban Planning and Land Resource Administration Bureau (SUPLRAB) (2018). *Shanghai master plan (2017-2035): string for the excellent global city.* (Shanghai: Shanghai Urban Planning and Land Resource Administration Bureau).

Shi, Y. S., Shi, D. H., Zhou, L. L., and Fang, R. B. (2020). Identification of ecosystem services supply and demand areas and simulation of ecosystem service flows in Shanghai. *Ecol. Indic.* 115, 106418. doi: 10.1016/j.ecolind.2020.106418

Shou, F. Y., Li, Z. F., Huang, L., Huang, S. R., and Yan, L. J. (2020). Spatial differentiation and ecological patterns of urban agglomeration based on evaluations of supply and demand of ecosystem services: a case study on the Yangtze river delta. *Acta Ecol. Sin.* 40, 2813–2826. doi: 10.5846/stxb201904120734

Solé, L., and Ariza, E. (2019). A wider view of assessments of ecosystem services in coastal areas: the perspective of social-ecological complexity. *Ecol. Soc.* 24, 24. doi: 10.5751/ES-10883-240224

Stewart-Sinclair, P. J., Klein, C. J., Bateman, I., and Lovelock, C. E. (2021). Spatial cost-benefit analysis of blue restoration and factors driving net benefits globally. *Conserv. Biol.* 35, 1850–1860. doi: 10.1111/cobi.13742

Strassburg, B. B. N., Beyer, H. L., Crouzeilles, R., Iribarrem, A., Barros, F., de Siqueira, M. F., et al. (2019). Strategic approaches to restoring ecosystems can triple conservation gains and halve costs. *Nat. Ecol. Evol.* 3, 62–70. doi: 10.1038/s41559-018-0743-8

Strassburg, B. B. N., Iribarrem, A., Beyer, H. L., Cordeiro, C. L., Crouzeilles, C. L., Jakovac, C. C., et al. (2020). Global priority areas for ecosystem restoration. *Nature.* 586, 724–729. doi: 10.1038/s41586-020-2784-9

Sun, Z. G., Sun, W. G., Tong, C., Zeng, C. S., Yu, X., and Mou, X. J. (2015). China's coastal wetlands: conservation history, implementation efforts, existing issues and strategies for future improvement. *Environ. Int.* 79, 25–41. doi: 10.1016/j.envint.2015.02.017

Su, J., Yin, B. C., Chen, L. Z., and Gasparatos, A. (2022). Priority areas for mixed-species mangrove restoration: the suitable species in the right sites. *Environ. Res. Lett.* 17, 065001. doi: 10.1088/1748-9326/ac6b48

Temmerman, S., and Kirwan, M. L. (2015). Building land with a rising sea: cost-efficient nature-based solutions can help to sustain coastal societies. *Science.* 349, 588–589. doi: 10.1126/science.aac8312

Temmerman, S., Meire, P., Bouma, T. J., Herman, P. M. J., Ysebaert, T., and De Vriend, H. J. (2013). Ecosystem-based coastal defence in the face of global change. *Nature.* 504, 79–83. doi: 10.1038/nature12859

Tobler, W. R. (1970). A computer movie simulating urban growth in the Detroit region. *Econ. Geogr.* 46 (Supp1), 234–240. doi: 10.2307/143141

Villamagna, A. M., Angermeier, P. L., and Bennett, E. M. (2013). Capacity, pressure, demand, and flow: a conceptual framework for analyzing ecosystem service provision and delivery. *Ecol. Complex.* 15, 114–121. doi: 10.1016/j.ecocom.2013.07.004

Wang, J. J., Li, X. Z., Lin., S. W., and Ma, Y. X. (2022). Economic evaluation and systematic review of salt marsh restoration projects at a global scale. *Front. Ecol. Evol.* 10, 865516. doi: 10.3389/fevo.2022.865516

Wang, C. X., Liu, Y. X., Yu, C. Y., and Liu, X. Q. (2021a). Research progress on the arrangement of territorial ecological restoration. *Prog. Geogr.* 40, 1925–1941. doi: 10.18306/dlkxjz.2021.11.011

Wang, X. X., Xiao, X. M., Xu, X., Zou, Z. H., Chen, B. Q., Qin, Y. W., et al. (2021b). Rebound in China's coastal wetlands following conservation and restoration. *Nat. Sustain.* 4, 1076–1083. doi: 10.1038/s41893-021-00793-5

Wang, J., Yi, S., Li, M. Y., Wang, L., and Song, C. C. (2018). Effects of sea level rise, land subsidence, bathymetric change and typhoon tracks on storm flooding in the coastal areas of Shanghai. *Sci. Total Environ.* 62, 228–234. doi: 10.1016/j.scitotenv.2017.11.224

Wei, Z. X., Di, G. Y., Yan, X. X., Fang, Z., Yang, J. G., He, Z. F., et al. (2010). *Shanghai urban geology.* (Beijing: Geological Publishing House).

Widis, D. C., BenDor, T. K., and Deegan, M. (2015). Prioritizing wetland restoration sites: a review and application to a large-scale coastal restoration program. *Ecol. Restor.* 33, 358–377. doi: 10.3368/er.33.4.358

Wiens, J. A., and Hobbs, R. J. (2015). Integrating conservation and restoration in a changing world. *Biosci.* 65, 302–312. doi: 10.1093/biosci/biu235

Worthington, T., and Spalding, M. (2018). *Mangrove restoration potential: a global map highlighting a critical opportunity.* (Cambridge: University of Cambridge).

Wu, W., Li, C. X., and Chen, X. C. (2020). Evaluation of the effectiveness of a coastal ecological restoration project based on ecosystem services: a case study on Yingwuzhou wetland, China. *J. East China Normal Univ. (Nat Sci.).* 211, 98–108. doi: 10.3969/j.issn.1000-5641.201941027

WWF (2020) *The Bezos Earth Fund & WWF: investment in community and climate.* Available at: https://www.worldwildlife.org/pages/the-bezos-earth-fund-wwfinvestment-in-community-and-climate.

Zhang, J. (2015). *Ecological continuum from the Changjiang (Yangtze river) watersheds to the East China Sea continental margin.* (Switzerland: Springer International Publishing).

Zhao, W. W., Liu, Y., Feng, Q., Wang, Y. P., and Yang, S. Q. (2018). Ecosystem services for coupled human and environment systems. *Prog. Geogr.* 37, 139–151. doi: 10.18306/dlkxjz.2018.01.015

Zhu, Z. C., Vuik, V., Visser, P. J., Soens, T., van Wesenbeeck, B., van de Koppel, J., et al. (2020). Historic storms and the hidden value of coastal wetlands for nature-based flood defence. *Nat. Sustain.* 3, 853–862. doi: 10.1038/s41893-020-0556-z

frontiers | Frontiers in Marine Science

TYPE Original Research
PUBLISHED 15 December 2022
DOI 10.3389/fmars.2022.1054402

OPEN ACCESS

EDITED BY
Serena Moseman-Valtierra,
University of Rhode Island,
United States

REVIEWED BY
Sikai Wang,
Chinese Academy of Fishery Sciences,
China
Guanglong Qiu,
Guangxi Academy of Sciences, China

*CORRESPONDENCE
Jianbin Shi
jbshi@bnu.edu.cn
He-Bo Peng
hebo.peng@outlook.com

†These authors have contributed equally to this work

SPECIALTY SECTION
This article was submitted to Coastal Ocean Processes, a section of the journal Frontiers in Marine Science

RECEIVED 26 September 2022
ACCEPTED 30 November 2022
PUBLISHED 15 December 2022

CITATION
Peng H-B, Shi J, Gan X, Zhang J, Ma C, Piersma T and Melville DS (2022) Efficient removal of *Spartina alterniflora* with low negative environmental impacts using imazapyr. *Front. Mar. Sci.* 9:1054402. doi: 10.3389/fmars.2022.1054402

Efficient removal of *Spartina alterniflora* with low negative environmental impacts using imazapyr

He-Bo Peng[1,3,4*†], Jianbin Shi[2*†], Xiaojing Gan[5], Jing Zhang[6], Chao Ma[6], Theunis Piersma[1,3,4] and David S. Melville[7]

[1]CEAAF Center for East Asian-Australasian Flyway Studies, Beijing Forestry University, Beijing, China, [2]School of Environment, Beijing Normal University, Beijing, China, [3]Groningen Institute for Evolutionary Life Sciences (GELIFES), University of Groningen, Groningen, Netherlands, [4]Department of Coastal Systems, NIOZ Royal Netherlands Institute for Sea Research, Texel, Netherlands, [5]Paulson Institute, Beijing, China, [6]College of Biological Science and Technology, Beijing Forestry University, Beijing, China, [7]Global Flyway Network, Nelson, New Zealand

Invasion by smooth cordgrass (*Spartina alterniflora* Loisel) has greatly impacted the intertidal ecosystems of China. Worldwide, chemical control is the most widely used method to control *Spartina* species, but it has not been widely implemented along the Chinese coast due to concerns about the potential impacts of herbicide residues on the environment and organisms. Macrobenthos, both natural and cultured on intertidal mudflats, is an important seafood resource, so human food safety is a particular concern. Here we tested the effectiveness of imazapyr (an imidazolinone herbicide inhibiting the synthesis of branched-chain amino acids) in controlling *S. alterniflora* from August 2020 to June 2021 on the Jiangsu Coast, an area severely impacted by *S. alterniflora*. We used two different concentrations of the herbicide and monitored the density of *S. alterniflora* seedlings and flower spikelets, the effects of herbicide use on macrobenthos, and residues in organisms and the environment at different times post-application. Ten months after application, imazapyr had killed all plants and within 30 days it inhibited the two reproductive processes of germination and flowering; there were no significant differences between the two concentrations used. Imazapyr residues were detected in the environment for up to 14 days post-application, but at very low concentrations and exponentially decreased with time. No residues were found in any macrobenthos. Imazapyr use did not result in a reduction of macrobenthos density. We conclude that the herbicide imazapyr effectively removes *S. alterniflora* with little collateral damage to other organisms and the environment. However, in view of the relatively small scale of our trials and the great extent of *S. alterniflora* in many sites in China, we recommend that larger scale field trails be conducted to assess any potential adverse effects when imazapyr is used at a landscape level.

KEYWORDS

***Spartina alterniflora*, imazapyr, macrobenthos, Jiangsu coast, intertidal mudflats, biological invasion**

1 Introduction

Human activities, both deliberate and accidental, have brought a long list of species from their places of origin to the far corners of the world. Some of them have become invasive, displacing local species and dominating communities (Seebens et al., 2015; Early et al., 2016). Cordgrasses (*Spartina* spp.) are perennial C4 grasses that are important ecosystem engineers in their native ecosystems, modifying, maintaining and/or creating habitats (Strong and Ayres, 2013). Because of their capacity to dissipate wave action, thus protecting dikes, reducing erosion and trapping sediments, various *Spartina* taxa have been introduced to coastal areas worldwide, frequently resulting in serious ecological problems (Li et al., 2009; Strong and Ayres, 2013; Meng et al., 2020). The world's largest invasion of *S. alterniflora* is in China (Strong and Ayres, 2013), where it is now found in all coastal provinces; in 2019 it covered 67,532 hectares and is still increasing (Gu et al., 2021). The most severely impacted region is the coast of Jiangsu Province and Shanghai (Gu et al., 2021). In China *S. alterniflora* has resulted in serious negative impacts on local biodiversity, fisheries, aquaculture and ecosystem functioning (Chen et al., 2004; Chen et al., 2009; Ju et al., 2017; Zhang et al., 2019a; Jackson et al., 2021). As a result, effective treatments to control or remove *S. alterniflora* have been sought (Ju et al., 2017).

Worldwide, coastal managers have tried various methods to control or remove *Spartina* including physical removal, biological treatment and treatment with herbicides. These methods vary in terms of effectiveness, cost and potential adverse effects (Roberts and Pullin, 2008; Table 1). Physical removal includes burning, hand pulling, smothering by covering with plastic, mowing, waterlogging, and tilling, but always with limited success (Roberts and Pullin, 2008; Xie et al., 2019). Physical methods are costly and destroy the physical structure of underlying sediments and, when impoundments are constructed, result in the loss of intertidal habitat (Yuan et al., 2011; Xie et al., 2019). Biological control, e.g., using the plant hopper *Prokelisia marginata* (Grevstad et al., 2003), has yet to be demonstrated as an effective method of biological control of *S. alterniflora* and potentially may exacerbate problems by selecting for resistant genotypes (Garcia-Rossi et al., 2003). Herbicides are the most widely used method worldwide for controlling *Spartina* species (Roberts and Pullin 2006) because they are highly efficient, low cost, fast-acting, with small impacts on the physical characteristics of the habitat, and potentially with limited impacts on other organisms.

Among the numerous herbicides used to control *Spartina*, glyphosate, imazapyr, fluazifop-p, haloxyfop, clethodim, and glufosinate have been used with success (Patten, 2002; Roberts and Pullin 2008; Knott et al., 2013; Liang et al., 2020), imazapyr and haloxyfop are the most widely used (Roberts and Pullin 2006; Liang et al., 2020; Mo et al., 2021). Each of these herbicides has advantages and disadvantages (reviewed in Table 1). In China, haloxyfop has been used to control *Spartina* for more than 10 years, especially in Shanghai, which is one of the coastal areas most heavily invaded by *Spartina* (Liang et al., 2020). Imazapyr is among the most tested and used herbicides worldwide for *Spartina* control (Patten, 2002; Roberts and Pullin 2008), however it has been used only once in China, but not in the most heavily invaded area, and no assessment of potential impacts on macrozoobenthos were made (Mo et al., 2021).

Macrobenthic animals play core roles in coastal wetland food webs both as primary and secondary consumers and as food for higher trophic level consumers such as fish and birds (Herman et al., 1999; Rakhimberdiev et al., 2018; Zhang et al., 2019b). Macrobenthos also influence the physicochemical processes in sediments through bioturbation (van der Zee et al., 2012; Adámek and Maršálek, 2013; Donadi et al., 2013; Donadi et al., 2014). Because of their generally limited mobility and sensitivity to environmental changes, macrobenthic species can serve as environmental indicator organisms (Bianchelli et al., 2018). Along China's coasts, macrobenthos (especially bivalves) are important economic products; most intertidal flats along the Chinese coast are occupied by mollusc aquaculture, and cultured species dominate the macrobenthic communities (Peng et al., 2021) affecting the survival of other organisms in the ecosystem (Piersma et al., 2016). Since macrobenthos is important as seafood for humans (Li et al., 2011), smooth cordgrass in China usually has been subject to physical control rather than the use of herbicides (Ju et al., 2017) due to concerns about possible contamination. However, the extent of *Spartina* invasion in China is now such that herbicides are the only effective method of control in most areas, but there is a need to ensure they have no adverse ecological effects.

Imazapyr is an imidazolinone herbicide with excellent herbicidal activity against a broad range of plants, including terrestrial annual and perennial grasses and broadleaved herbs, woody species, and riparian and emergent aquatic species (USEPA, 2006). Its mechanism of action is to inhibit the synthesis of branched-chain amino acids (WSSA, 2014). Imazapyr possesses a low sorption capacity, high water solubility, and high persistence in soils (WSSA, 2014), and has been proved to present no risk to or toxic effects on local aquatic organisms, birds and insects (Fisher, 2003; USEPA, 2006). This study was designed to test the effectiveness of, and assess the impact on macrobenthos of, imazapyr used to control smooth cordgrass. To explore the effectiveness of imazapyr for the removal of smooth cordgrass, and to study the effects of herbicide residues in the environment and macrobenthos, we used controlled field experiments and monitored the residues of herbicides in macrobenthos, sediment and water.

TABLE1 The efficiency, advantages and disadvantages of various methods of controlling or removing *Spartina* species.

Methods	Efficiency	Advantages	Disadvantages
1.Physical removal (Roberts and Pullin, 2008; Xie et al., 2019)			
Burning	Low	Lowest cost	1.Short exposure time of the intertidal area 2.Wet vegetation in the intertidal zone 3.Regrows quickly
Hand pulling	Low	Environment- and habitat-friendly	1.Deep rhizomes 2.High cost
Plastic covers	Medium	Effective in combination with mowing for low vegetation	1.Tide will frequently damage the plastic covers 2.Potential plastic pollution
Mowing	Low	Removes the above-ground part quickly	1.Does not remove rhizomes 2.Re-grows very quickly 3.Compaction of substrate
Waterlogging	High	Completely removed if undertaken properly	1.Need to build dykes 2.Change the intertidal area into ponds 3.Very difficult to revert to intertidal 4.Very high cost
Tilling	Medium	Completely removed by deep tilling	1.Very high cost 2.Deeply disturbed sediments 3.Destroys the whole habitat 4.Rhizomes may regenerate
2.Biological treatment (Grevstad et al., 2003; Hinz et al., 2019)			
Insects or plant diseases	Medium	May be environment- and habitat- friendly when organisms are properly screened	1.Potential new biological invasion 2.Time costly in preparation and testing 3.High cost 4.May select for resistant genotypes
3.Chemical herbicides (Patten, 2002; USEPA, 2006; Durkin, 2014; Liang et al., 2020; Zhao et al., 2020)			
Glyphosate	50%-90%	1.Fast acting 2.A half-life of 33 hrs	1.Low efficiency 2.Herbicide residues
Imazapyr	> 90%	1.High efficiency 2.Low usage amount 3.A half-life of 3-5 days, rapid photolysis in water 4.Formulation can be mixed with salt water	1.Herbicide residues 2.Broad-spectrum herbicide
Fluazifop-p	> 90%	1.Low usage amount 2.Specific to monocotyledons 3.a half-life of a few days	1.Stable in water, hard to decompose 2.Herbicide residues
Haloxyfop	> 90%	1.High efficiency. 2.Fast acting 3.A half-life of a few hours in seawater 4.Low usage amount 5.Specific to monocotyledons	1.Herbicide residues
Clethodim	68%	1.Low usage amount 2.A half-life of 1-3 days 3.Specific to monocotyledons	1.Low efficiency 2.Herbicide residues
Glufosinate	> 90%	1.Medium acting rate 2.Low usage amount	1.A half-life of 25 days 2.Herbicide residues

2 Methods and materials

2.1 Study area

This study was conducted at Dongtai Estuary (Figure 1), within the 'experimental zone' of the Yancheng National Rare Birds Nature Reserve (YNRBNR), located on the coast of Jiangsu Province, China (N 32.95°, E 120.92°) (Ma et al., 2009). On the border between the northern subtropical zone and the southern warm temperate zone, it has four distinct seasons with cold winters and hot summers, and light but abundant precipitation (average precipitation is 1000 mm, Huang et al., 2015). YNRBNR is a key staging site for hundreds of thousands of waterbirds along the East Asian-Australasian Flyway (EAAF), and was listed as a World Heritage Site in 2019 (UNESCO, 2019).

Spartina alterniflora was first planted in Jiangsu in 1982 (Chung, 2006), since when it has rapidly invaded open mudflats (Gu et al., 2021), resulting in the loss of habitat for migrating birds (Ju et al., 2017). The experiments took place in the

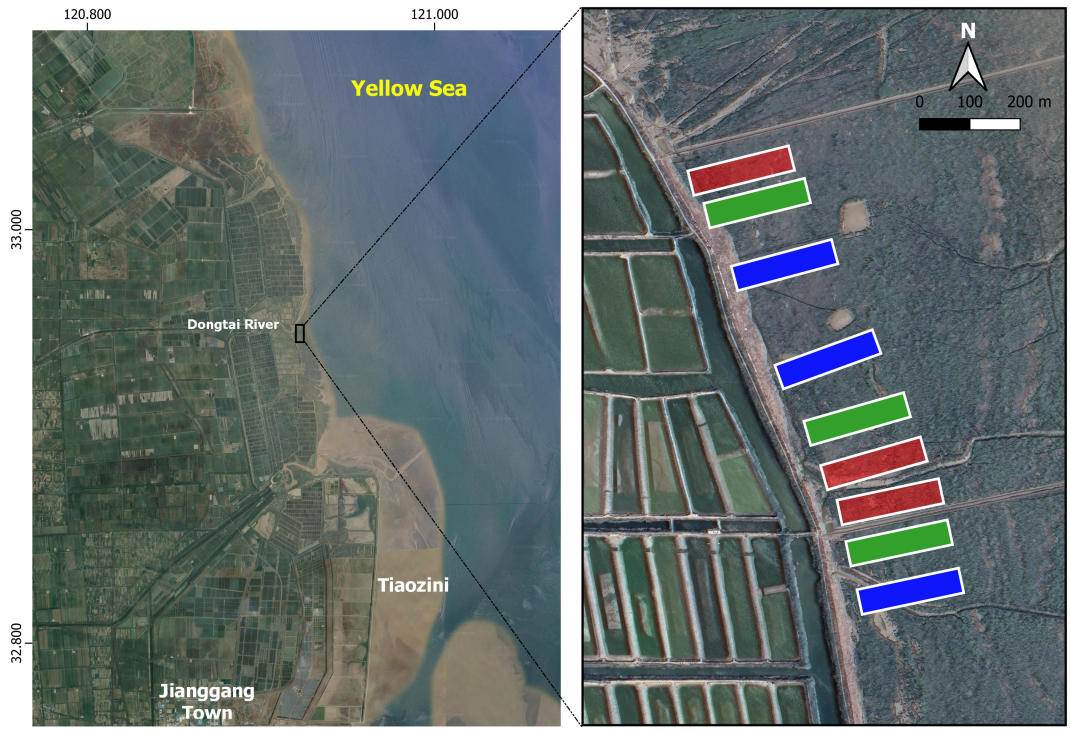

FIGURE 1
Study area in Jiangsu Province, China. Red plots are those treated with a high concentration of imazapyr, green plots are those treated with a low concentration of imazapyr, and blue plots show the untreated control plots.

southern area of YNRBNR, where *S. alterniflora* has taken over all of the shoreline and extends up to 1.5 km or more offshore.

2.2 Plot setting and experiment treatment

Nine plots adjacent to the seawall were selected, each being 50 m × 200 m in size (1 ha in area). The tides submerged the plots for one (neap tide) to four (spring tide) hours during the high tide almost every day in August, but in September the plots did not submerge during the neap tide.

The plots received three treatments of imazapyr herbicide (Polaris, Nufarm Americas Inc.) (Table 2): high concentration group (10%), low concentration group (5%), and the control group which was not sprayed, with three replicates for each treatment (Figure 1). The minimum distance between sprayed plots was 20 m, and the minimum distance between the control and sprayed groups was 50 m to minimize the potential effect of spray drift on the control group. We used the same dose of Polaris (7L/ha) in both the high and low concentration plots, which was recommended by the herbicide manufacturer and previous researchers in the United States (Patten, 2002), the difference in concentration being due to the amount of water mixed; the application rate was twice as much using the low concentration mix (Table 2). We did this to test whether the application of more spray volume may lead to increased runoff (loss) of Polaris to the ground/water, which may have an impact on uptake by *S. alterniflora*.

The spraying of imazapyr was conducted on 13 August 2020 (Table 3); a sunny day with a neap tide, and wind speed < 4 m/s;

TABLE 2 The concentrations and composition of the imazapyr mixture.

Treatments	Herbicide application	Imazapyr Polaris® [a]	Freshwater	Red Swift® adjuvant [b]	Active ingredientconcentration
High concentration	20 L/ha	7 L	12.8 L	0.2 L	10%
Low concentration	40 L/ha	7 L	32.6 L	0.4 L	5%
Control group	\	\	\	\	\

[a]Imazapyr Polaris® produced by Nufarm Americas Inc., the active ingredient of imazapyr is 28.7%.
[b]Red Swift® is produced by Shenzhen Yu Yuan Technology Co. Ltd.

TABLE 3 The overall view of the sampling.

Stages	Sampling date	Sampling items		
		Environment (water/soil)	*Spartina alterniflora*	Macrozoobenthos
Day 0	2020-08-11	NS	Collected	NS
Day 0	2020-08-12	NS	NS	Collected
Processing	2020-08-13	**Spray treatment**		
Day 1	2020-08-14	Collected	NS	NS
Day 7	2020-08-20	Collected	NS	NS
Day 14	2020-08-27	Collected	NS	NS
Day 15	2020-08-28	NS	NS	Collected
Day 21	2020-09-03	Collected	NS	NS
Day 30	2020-09-12	Collected	NS	Collected
Day 31	2020-09-13	NS	Collected	NS
Day 61	2020-10-13	NS	Collected	NS
Day 300	2021-06-09	NS	Collected	Collected

NS, not sampled.

water only submerged the lower parts of the stems of plants in our plots for 1 hour over a single tide which occurred 10 hours after spraying, thus ensuring that neither tide nor rain washed off the imazapyr shortly after spraying. Agricultural drones (DJI Agras T20) were used for spraying. To ensure effective spraying and prevent wastage, we set fixed computerized GPS tracks, flying at a height of 2.5 - 4 m above ground level (~1.5m above *S. alterniflora*) with a spraying range (the width of the area sprayed by each drone track) of 3.6 m.

2.3 Monitoring methods

The monitoring was conducted from 11 August 2020 to 9 June 2021. *S. alterniflora* and macrobenthos were measured both before and after spraying. Imazapyr residues were measured 5 times within 31 days after spraying (Table 2).

2.3.1 Plant

In each plot, 5 subplots (1m x 1m each) selected randomly at a distance of 20 m from adjacent subplots were sampled. We cut off all plants above the ground in each subplot and checked whether they were dead or alive, and counted the number of living *S. alterniflora* stems. No other plant species were found in our study plots. We randomly selected ten *S. alterniflora* plants in each subplot and measured the height (measured from the base of the plant (above ground) to the tip of the stems), leaf length and leaf width (of the longest leaf of the selected plant), stem diameter (at the thickest part of the selected plant), and the length of the flower spikelet.

S. alterniflora propagates sexually *via* seeds and also asexually by tillers and rhizomes (Patten, 2002). To understand the effect of imazapyr on the reproduction of *S. alterniflora*, we monitored seedlings and spikelets to assess the effects of imazapyr on reproduction. We identified all *S. alterniflora* plants which were <5 cm tall as 'seedlings' (although these could include new growth from tillers and rhizomes), taller shoots were noted as 'stems'. Spikelet length was only measured after the plant was eared. Plant monitoring was carried out 2 days before treatment, and 31, 61, and 300 days after treatment (Table 3).

2.3.2 Macrozoobenthos

In each plot, three sampling sites were randomly selected with a distance of at least 50m from each other, and a sediment core (surface area 0.019 m^2) was taken to a depth of 20 cm and washed over a 0.5 mm sieve (Peng et al., 2021). The sieved macrozoobenthos were stored frozen (-18°C) prior to analysis. In the laboratory, macrozoobenthos were identified to species level using a dissecting microscope and counted (Peng et al., 2021). Macrozoobenthos monitoring was carried out 2 days before treatment, and 15, 31, 300 days after treatment (Table 2).

2.3.3 Residues of imazapyr

Samples for testing imazapyr residues were collected from 6 treated plots (3 high and 3 low concentration plots) and one untreated plot. In each plot, four sampling sites were selected with three being in vegetated areas and one in bare ground (with a size > 4m^2). At each vegetated sample site, three benthic species (the gastropods *Cerithideopsis largillierti* and *Assiminea latericea*, and the crab *Helice latimera*) were collected by hand from the surface. Because these three species live on cordgrass or on the soil surface, they are more likely to be exposed to herbicides; furthermore, all three species feed on *S. alterniflora*, which makes them more likely to accumulate herbicides. At least 30g wet weight flesh for each species was collected at each sampling site, to enable sufficient flesh to be sampled for analysis. In areas of bare ground only one species,

Cerithideopsis largillierti, was found. Approximately 10 g of soil was collected using a small shovel from the surface and at a depth of 5 cm, respectively and stored in sealed ziplock bags for measuring herbicide residues. Additionally, two 50ml water samples were collected from channels or shallows in the plots and saved in 50-ml centrifuge tube. All benthos, soil, and water samples were stored in a freezer (-18°C) within 12 hours of collection. Residue sampling was carried out on 1, 7, 14, 21, 30 days after treatment (Table 3).

2.4 Determination of the imazapyr residues in sediments and benthic organisms

2.4.1 Pretreatment of samples

For sediment samples, 1g of sediment was weighed and transferred into a 5.0-ml brown centrifuge tube, and then 2.0 ml of ammonium acetate solution (2.0 mM) was added and vortexed for 5 min, after which the mixture was treated with ultrasonic power of 100W for 15 min on an ice bath. Then, the samples were centrifuged at 10000 g for 10 min to collect the supernatant, followed by filtration through 0.45 μm hydrophilic filter. For benthic organisms, 1g of flesh pooled from several animals was put into a 10-ml tube, followed by the addition of 2.0 ml ammonium acetate solution (2.0 mM). Then, the samples were fully homogenized using a hand-held tissue homogenizer, after which 1.0 ml of the homogenate was transferred into a 4.0-ml centrifuge tube, and 2.0 ml of trichloroacetic acid (12.0%, w/w) was added to precipitate proteins in the solution. After vortex treatment for 5 minutes, the mixture was subjected to ultrasonic treatment for 15 minutes on an ice bath, followed by centrifugation (10000 g) for 10 minutes at 4°C. Finally, the supernatant was collected for determination after filtration through 0.45 μm hydrophilic filter.

2.4.2 UPLC-ESI-MSn determination of imazapyr

UPLC-ESI-MSn analyses were carried out using an Agilent 1260 Infinity II LC system coupled with a QTRAP® 5500 system (AB, USA). Analytical separation was carried out at 30°C on a ZORBAX RRHD SB-C18 column (2.1 mm id × 50 mm, 1.8 μm). Isocratic gradient elution was performed with a mixture of 94% ammonium acetate solution and 6% acetonitrile. The flow rate was kept at 0.3 mL/min, and 3.0 μL of each sample solution was injected in each run. Multiple reaction monitoring (MRM) was used for detecting transitions in a positive ionization mode. The operating parameters were set as follows: electrospray source; spray voltage, 4000 V; source temperature, 350°C; nebulizing gas, 15 psi; heating gas, 55 psi; curtain gas, 12 psi; gas flow rate 11L/min. The quantitative ion-pair was selected as 262.1/117.1, and external calibration curves of imazapyr were established with ten concentrations ranging from 0.0144 to 144 ng/mL. The calibration curve was linear over the entire concentration range and the Pearson's correlation coefficient (r) was more than 0.99. The limit of detection (LOD) and limit of quantification (LOQ) of the imazapyr ranged from 0.0014 to 0.042 ng/mL. Analyst 1.6.1 software (Applied Biosystems, MDS Sciex, Canada) was used to run the above analysis.

2.5 Data analysis

Tukey's HSD test was used to compare the difference among the groups at different times, including the density of plant, plant height, leaf length, leaf width, stem diameter, the density of seedlings and spikelet, and length of spikelet. Tukey's HSD test was used to compare the difference in the density and number of species of macrobenthos among the groups at different times. To compare the residues of imazapyr in the surface soil, deep soil, water and macrobenthos among groups in different stages, Tukey's HSD test was used separately. For the density of macrozoobenthos in June 2021, because the snail *A. latericea* falls to the ground when *S. alterniflora* dies, we compared the density of *A. latericea* in three treated groups by paired t-test; we further compared the density of all macrozoobenthos excluding *A. latericea* to remove the effect of their falling down with the dead plants. $p < 0.05$ indicates a significant difference. All statistical analyses were made using RStudio 1.4 for Windows.

3 Results

3.1 Plants

Only *S. alterniflora* was recorded in the nine plots we monitored; no other plants were found. Before treatment, the overall density of *S. alterniflora* stems across the plots was 113 ± 27 m^{-2} (n = 45), and there were no differences among the plots ($p>0.05$ in all cases. Figure 2A). Plant densities measured 31 days and 61 days after treatment did not change significantly for each of the three groups (Figure 2A, all $p > 0.05$). After 300 days post-treatment (the second growing season of our study), stem density of the untreated group increased significantly to 180 ± 19 stems m^{-2} (n = 15), but all plants in the high and low concentration treatment groups were dead (Figure 2A). Before treatment, the height of *S. alterniflora* was 140.4 ± 31.0 cm (n=448), with no differences among the three groups ($p>0.05$ in all cases. Figure 2D). After treatment, the heights of *S. alterniflora* measured on Day 31 and Day 61 did not change in either the high ($p=0.55$) or low concentration group ($p=0.18$), and all plants in these two groups were dead after 300 days (Figure 2D). In contrast, the plant height increased significantly in the untreated control group during the first two months after treatment ($p<0.001$), but decreased to the lowest level measured 300 days after treatment, the second growing season of our study as the stems died naturally over winter (Figure 2D).

10.3389/fmars.2022.1054402

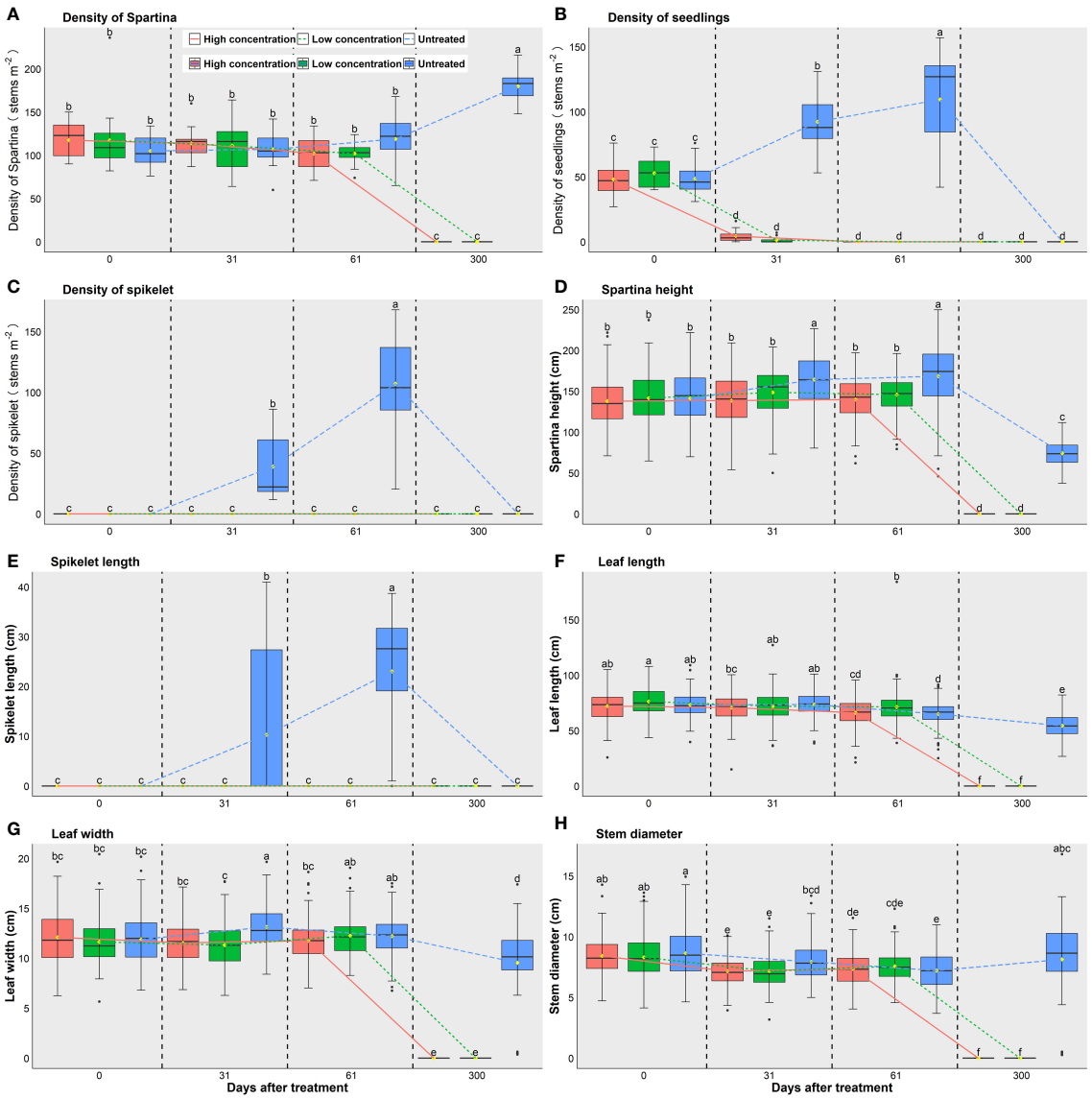

FIGURE 2
Plant densities and features of *S. alterniflora* in different treatment groups at different times. **(A)** Density of *S. alterniflora*. **(B)** Density of seedlings. **(C)** Density of flower spikelet. **(D)** Height of *S. alterniflora*. **(E)** Length of flower spikelet. **(F)** Length of leaves. **(G)** Width of leaves. **(H)** Diameter of stem. The different lowercase letters indicate significant differences between groups ($p < 0.05$). Red symbols and lines show plots treated with a high concentration of imazapyr, green symbols and lines show low concentration plots, blue symbols and lines show untreated control plots.

The average length of leaves was 74.0 ± 12.7 cm (n=448) before treatment, with no differences among groups ($p<0.05$ in all cases. Figure 2F). After treatment, the leaf length in both high and low concentration plots decreased slightly by Day 31, but significantly by Day 61, and no leaf was found on Day 300 when all plants were dead (Figure 2F). In contrast, the leaf length in the untreated plots did not change much after 31 days, but had decreased greatly after 300 days ($p<0.001$. Figure 2F) as the stems died naturally overwinter. The width of leaves was on average 11.9 ± 2.4 mm (n=448) before treatment and there was no difference between groups ($p<0.05$ in all cases. Figure 2G). In high concentration plots, the leaf width did not change by Day 31 and Day 61 ($p=0.20$), and no leaves were left by Day 300 when all plants were dead. In low concentration plots, the leaf width did not change by Day 31, but increased by Day 61 with an overall increasing trend during this period ($p=0.02$, Figure 2G). In untreated plots, the leaf width increased as measured on Day 31, and then decreased to the lowest level as measured on Day 300 in the next year ($p<0.001$). The stem diameter was 7.9 ± 1.5 mm (n=146) before treatment and no differences were

10.3389/fmars.2022.1054402

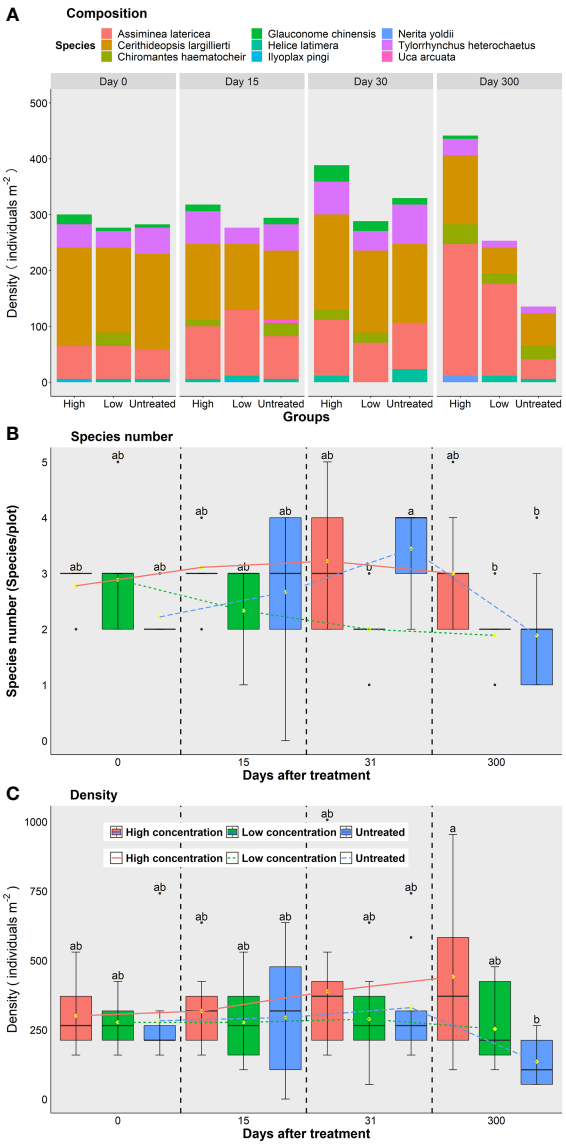

FIGURE 3
Species number and density of macrobenthos under different treatments at different times. **(A)** Overview of the composition of macrobenthos, different colors show the different species, the length of bar indicates the density of each species. **(B)** Species number and **(C)** density of macrobenthos in different treatments at different times, the different lowercase letters indicate significant differences between groups ($p < 0.05$). Red symbols and lines show high concentration plots, green symbols and lines show low concentration plots, blue symbols and lines show untreated control plots.

detected between groups ($p>0.05$ in all cases. Figure 2H). The stem diameters in both high and low concentration plots decreased within 61 days after spraying ($p<0.001$). In untreated plots, the stem diameter also decreased within 61 days after spraying ($p<0.001$), but it increased to a similar level after 300 days to that measured at Day 0 (Figure 2H).

The density of seedlings of *S. alterniflora* was 50 ± 12 stems m^{-2} (n=45) before treatment, and not significantly different among the three groups ($p>0.05$ in all cases). After treatment, the densities of seedlings decreased to a very low level on Day 31 and even to zero on Day 61 in both high ($p<0.001$) and low concentration plots ($p<0.001$) (Figure 2B). In contrast, the seedling density in untreated plots increased significantly on Day 31 and Day 61 ($p<0.001$), but was recorded as 'zero' on Day 300 in the following June because all stems were taller than 5 cm. Because the experiment started before flowering, no spikelet was recorded in all three groups before the treatment. After treatment, no spikelet was found in either the high or the low concentration plots during the whole experiment. However, the density and length of the spikelet in untreated plots increased significantly after 31 days and 61 days ($p<0.001$. Figures 2C, E), and was zero 300 days later in the following June before the next flowering season.

3.2 Macrobenthos

Nine benthic species were found from 2020 to 2021 in the study plots (Figure 3A). The most abundant species were the gastropods *Cerithideopsis largillierti* (average density 131 individuals m^{-2}), followed by *Assiminea latericea* (96 individuals m^{-2}), the nereid polychaete *Tylorrhynchus heterochaetus* (39 individuals m^{-2}), the crab *Chiromantes haematocheir* (14 individuals m^{-2}), the bivalve *Glauconome chinensis* (10 individuals m^{-2}), the crab *Ilyoplax pingi* (1 individual m^{-2}), the gastropod *Nerita yoldii* (1 individual m^{-2}), and the crab *Uca arcuata* (1 individual m^{-2}). Before treatment, the mean number of species of macrobenthos was 2.6 ± 0.7 species/plot (n = 27); there were no differences between high concentration, low concentration and untreated plots ($p > 0.05$, Figure 3B).

After treatment, the species number of macrobenthos remained relatively stable in the high ($p>0.05$) and low concentration ($p>0.05$) plots across all study stages Figure 3B. The species number of macrobenthos in the untreated plots did not change significantly after 31 and 61 days ($p>0.05$), but it had decreased to 1.9 ± 1.1 species/plot (n = 9) when measured on Day 300 in June 2021 Figure 3B. The average density of macrobenthos across all 9 plots was 287 ± 126 individuals m^{-2} (n=27) before treatment, and there were no differences among the three groups ($p>0.05$). After treatment, the densities of macrobenthos in all three groups were similar when measured on Day 31 ($p>0.05$) and Day 61 ($p>0.05$), but the density in the high concentration group was significantly higher than those in the untreated plots when measured on Day 300 ($p<0.05$, Figure 3C). This is because the density difference of *A. latericea* among groups, where densities of *A. latericea* in untreated plots were significantly lower than treated plots (all $p < 0.05$). When excluding *A. latericea*, the densities of macrozoobenthos among the three treatments showed no differences on Day 300 (all $p > 0.05$).

3.3 Imazapyr residues

Samples from four kinds of environmental materials (i.e., surface soil, deep soil, water and macrobenthos) were tested for imazapyr residues. No imazapyr residues were detected in any macrobenthos sample collected from the treated and untreated plots (Figure 4). Imazapyr residues were detected in the surface and deep (5cm) soil samples from both the high concentration and low concentration plots, however the concentration of residues decreased exponentially with time until Day 21 after which no residue was detected in any soil sample (Figure 4).

The concentration of the residues was higher in the surface soil than in the deep soil as measured at the same time for both high concentration and low concentration plots, but the residues remained in the soil longer in the high concentration plots than in the low concentration plots (Figure 4). No residue was detected in the soil beyond Day 14 in the low concentration plots, but beyond Day 21 in the high concentration plots, although at very low concentrations (0.08± 0.21 μg/kg for surface soil and 0.06 ± 0.14 μg/kg for deep soil). For the untreated plots, the residue was found in one out of three surface samples at an average concentration of 0.11 ± 0.18 μg/kg (n = 3) on Day 1 only, and not detected after Day 7 (Figure 4A).

No imazapyr residue was detected in the water samples from the high concentration plots on Day 1, but was detected from one out of three samples at an average concentration of 19.01 ± 32.93 μg/Kg (n = 3) on Day 7, and no imazapyr residue was found on or beyond Day 14. For the low concentration plots, imazapyr residues were found in two out of three samples at 268.37 ± 464.29 μg/kg (n=3) on Day 1, but was not recorded in the following sampling. The residues were detected in the water samples from the untreated plots at 560.57 μg/kg (n = 1) on Day 1, but thereafter was not detected (Figure 4C).

4 Discussion

4.1 The efficiency of imazapyr herbicide in killing *Spartina alterniflora*

All *S. alterniflora* was dead within 10 months of spraying in both high and low concentration plots. In addition, both asexual and sexual reproduction were effectively prevented in the treatment groups, and no new plants were produced in the following summer. The high control efficiency was consistent with other reported results (Roberts and Pullin, 2008; Mo et al., 2021), confirming that imazapyr can effectively inhibit the tillering and flowering of *S. alterniflora*, as well as the growth of plants, and eventually kill all the plants.

This study showed that there was no significant change in the density of living *S. alterniflora* (average height of 1.5 m) as measured within 61 days after spraying. In contrast, more than 95% of 'seedlings' (<5 cm in our study) were dead by 30 days post-spraying, and all were dead after 61 days. In a study in Fujian Province, southern China, half of the *S. alterniflora* was

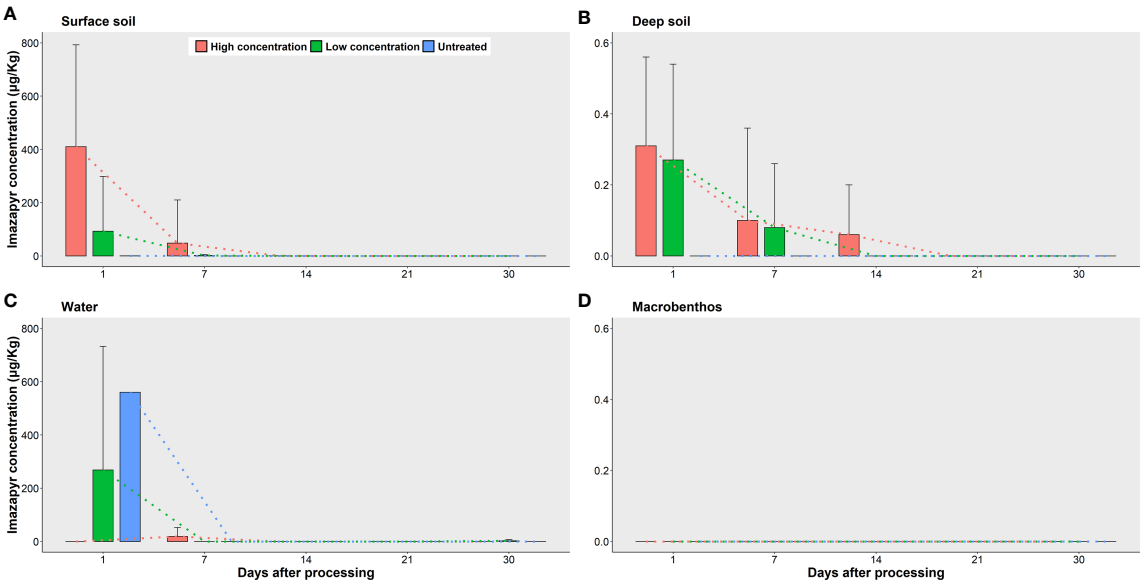

FIGURE 4
Changes of the concentration of Imazapyr acid residues in different environmental substances of different treated groups at different times. **(A)** Surface soil. **(B)** Deep soil (5cm). **(C)** Water. **(D)** Macrobenthos. Red symbols and lines show high concentration plots, green symbols and lines show low concentration plots, blue symbols and lines show untreated plots.

dead 30 days after spraying, and more than 90% of the plants were dead by 60 days (Mo et al., 2021), even though the concentration (5.7%) of active ingredient (imazapyr) was lower than the high concentration treatment in our study (10%). Although *S. alterniflora* on the Jiangsu Coast took longer to die completely than elsewhere (Patten, 2002; Mo et al., 2021), the final efficiency using imazapyr was nearly 100% in our sampling subsamples, and more than 95% in the entire treated plots (Figure 5). Imazapyr effectively inhibits both sexual and asexual reproduction of *S. alterniflora*, so the plants are unable to complete generation turnover, and also can kill the mature, tall plant, so it is possible to use imazapyr to completely remove all the invasive *S. alterniflora*.

When using similar or higher doses of imazapyr, it took longer to kill *S. alterniflora* in Jiangsu than in Fujian. This may be related to the fact that the stems of *S. alterniflora* along the Jiangsu coast are 3 times higher than those in Fujian; furthermore, we sprayed at a time when the plants were nearing flowering (August), whereas in Fujian, Mo et al. (2021) sprayed during the active growing period (May), and it is recognized that a higher-concentration of herbicide and longer-acting time is required to kill mature plants (DNR, 2012).

We found no differences in any of the metrics of *S. alterniflora* that we monitored between the high and low concentration treatment groups across the study period, and there were also no significant differences in macrobenthos density and imazapyr residues. This suggests that mixing different amounts of water does not affect the absorption of imazapyr by *S. alterniflora* and the environmental impacts of imazapyr. As a result, we recommend using the high concentration of imazapyr (10%) to remove *S. alterniflora*, because this reduces the amount of drone flying time needed to apply it, which will therefor reduce costs.

4.2 Residues of imazapyr in the environment

The highest herbicide residues were detected in water samples from channels and shallows. Surprisingly, these herbicide residues were found in the untreated plot on Day 1 after spraying. However, on Day 7, no imazapyr residues were found in the water of the low concentration and untreated plots, while only a very low amount was detected in the high concentration plots where none was detected on Day 1. No residues were detected two weeks later, or subsequently. All plots were subject to tidal inundation for 1-4 h every day in August, which will have washed imazapyr from the plants while the high tidal range ~5m (Kang et al., 2015) will have resulted in strong tidal flushing. Since the half-life of imazapyr in water averages 3-5 days (USEPA, 2006), it is likely that any imazapyr flowing elsewhere decomposed quickly. It is possible that the detection of imazapyr residue in water samples of the untreated plots on Day 1 resulted from spray-drift, but we think that this is unlikely as spraying was done on a calm day and there was no evidence of *S. alterniflora* mortality in the control plots.

We found imazapyr residues in the sediments (both surface soil and deep (5cm) soil) of the treatment plots, with higher residues in the high concentration plots than in the low concentration plots; none was found in the control plots. The concentration of residues decreased exponentially with time until only a very low level was detected in high concentration plots and none in low concentration plots in the second week, and no residues were detected in the third week or thereafter. In view of the fact that imazapyr is stable to hydrolysis, aerobic and anaerobic soil degradation (USEPA, 2006), this suggests that residues were washed from the sediment by tidal movement. Thus, imazapyr residues did not accumulate in the sediments of the intertidal area. For these reasons, we also recommend that spraying should be done during the neap tides such that the tide only submerges the plants and tidalflats for a short period, thereby ensuring that plants have enough time to absorb the herbicide, while also allowing tidal flushing of herbicide residues.

The imazapyr residues found in the deep soil may be due to the effects of tidal water. The plots were covered by tides one (neap tide) to four (spring tide) hours per day in August, and the water might carry the residues from the surface layer to the deeper layers. It is also possible that the residues flowed into the deeper soils with the water during our sampling.

4.3 Effects of imazapyr use on macrozoobenthos

Organisms other than the target plants have been the most important indicators to assess the safety of herbicides (Rani et al., 2021). A previous study using herbicides to control *S. alterniflora* along the Chinese coast suggested that the use of haloxyfop-r-methyl or glyphosate herbicide may lead to a short-term decline in crab density (Qiao et al., 2019), but the authors did not investigate whether this may have resulted from direct effects or indirect effects such as the death of *S. alterniflora* affecting habitat structure and/or food resources. Whilst this could be taken as suggesting that herbicides may affect the biomass of benthic fauna and thus potentially the yield of the human seafood, the U.S. Environmental Protection Agency determined that for imazapyr 'there are no risks of concern to terrestrial birds, mammals, and bees, or to aquatic invertebrates and fish' (USEPA, 2006), and Sheng et al. (2014) using haloxyfop, and Zhao et al. (2020) using haloxyfop, detected no adverse effects on macrozoobenthos and meiofauna respectively. We did not detect imazapyr residues in any macrobenthos samples throughout the study period, whether snails or crabs, the most abundant species in the study area. These two groups of benthic animals are active in plants and on the surface soil, feeding on plant debris and the plants themselves (Wang et al., 2014), and thus may be more vulnerable to exposure to herbicides than macrobenthos in the

10.3389/fmars.2022.1054402

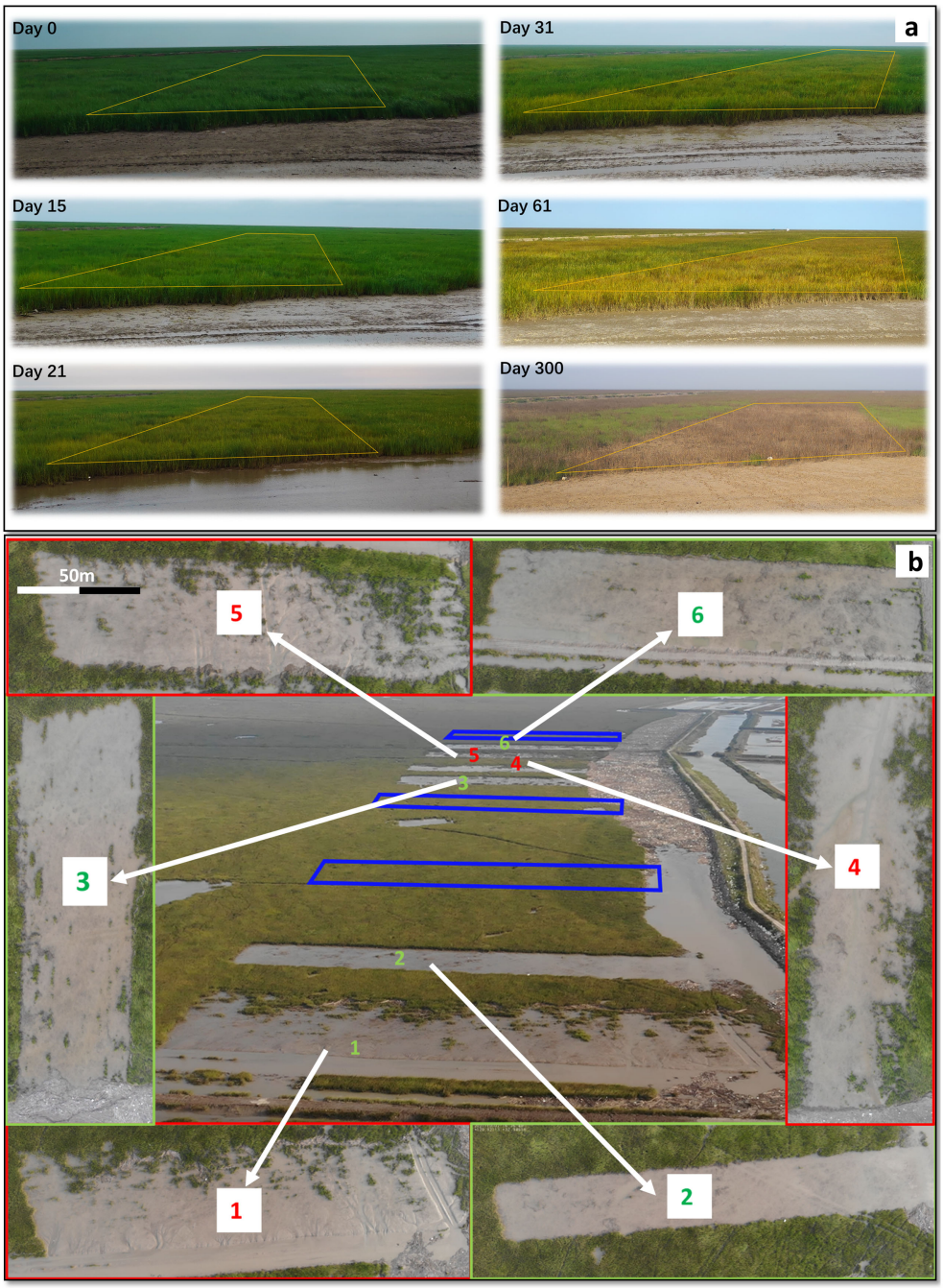

FIGURE 5
The effectiveness of imazapyr herbicide on *S. alterniflora*. **(A)** The changes of *S. alterniflora* in one treated plot (plot 2 in b) from day 0 to day 300 after treatment. **(B)** The overview of treatment effectiveness, photos were taken after treatment for 14 months, a typhoon had cleared away the dead vegetation. Red letters and plots show high concentrations plots, green letters and plots show low concentrations, and blue plots show the untreated plots.

mudflats, however our results suggest that imazapyr did not accumulate in macrobenthos.

There were no differences in macrobenthos density when *S. alterniflora* density was similar during the first 61 days following spraying among the three treatments, but by June 2021 (300 days post-spraying) *A. latericea* was significantly more abundant in the treatment plots where all plants had died. Because *A. latericea* prefers to attach itself to the stems and leaves of *S. alterniflora* (Wang et al., 2014), it may be that *A. latericea* scattered to the ground surface after the dead *S. alterniflora* collapsed. We sampled the macrobenthos mainly from the surface to 20 cm deep sediment, and did not survey the macrobenthos on the plants, which may have caused the density of *A. latericea* to be significantly higher in treated plots than in untreated plots on Day 300.

The densities of macrozoobenthos 300 days post-spraying did not differ significantly among the three treated groups when *A. latericea* was excluded the from the analysis. This supports the contention that the herbicide itself may not affect the survival of macrobenthos directly, because it does not accumulate in macrobenthos.

Previous toxicological studies have proven that imazapyr has little toxicity effect on mammals, birds, fish and aquatic invertebrates and it is considered to be non-toxic to them when it is used as instructed (USEPA, 2006). Additionally, the short half-life of imazapyr in water (3-5 days) (USEPA, 2006) and strong tidal flushing along much of China's Yellow Sea coast, indicate that the toxicity risk of imazapyr to benthic animals in the intertidal area is very low. In view of the importance of China's intertidal areas for seafood production future studies should further assess imazapyr levels in commercially important species to ensure their safety for consumption – currently the USA has a safety level for imazapyr of >1.0 ppm for fish and > 0.1 ppm for shellfish (Department of Health and Human Services, 2022) and Germany has a limit of 0.1 ppm (De Witte et al., 2022).

5 Conclusion

The present study demonstrates that the herbicide imazapyr results in a high mortality of *S. alterniflora* with low ecological risk if applied strictly in accordance with the product instructions, however further study may still be needed in the future to confirm its safety with respect to commercial seafood. The application of imazapyr thus seems a rather benign option for the control of *S. alterniflora* in China and the use of plant protection drones provides a practical method for future large-scale operations. However, as imazapyr is a broad-spectrum herbicide, it needs to be used with caution in coastal wetlands where native salt marsh plants and mangroves also occur. Indeed, as *S. alterniflora* now occupies more than 60,000 ha in China, the amount of herbicides required for eradication will be very high. We recommend that larger scale field tests be conducted to examine the environmental impacts of the wider application of imazapyr.

Data availability statement

The original contributions presented in the study are included in the article/supplementary material. Further inquiries can be directed to the corresponding authors.

Author contributions

H-BP, JS, and XG designed and performed the experiments. H-BP drafted the manuscript. H-BP took samples. JZ and CM measured the imazapyr residues. H-BP performed the statistical analysis of the original data. JS, TP and DM revised the manuscript. All authors contributed to the article and approved the submitted version.

Funding

This project was supported by the Paulson Institute and Heren Charitable Foundation.

Acknowledgments

We thank Shou-Dong Zhang, Wanjuan Ke, Yan Gao for their help in the sampling and measurement. We thank Shou-Dong Zhang for the help in processing macrobenthic samples. We thank Jinjin Du for his help in coordinating the fieldwork.

Conflict of interest

The authors declare that the research was conducted in the absence of any commercial or financial relationships that could be construed as a potential conflict of interest.

Publisher's note

References

Adámek, Z., and Maršálek, B. (2013). Bioturbation of sediments by benthic macroinvertebrates and fish and its implication for pond ecosystems: a review. *Aquacult. Int.* 21, 1–17. doi: 10.1007/s10499-012-9527-3

Bianchelli, S., Buschi, E., Danovaro, R., and Pusceddu, A. (2018). Nematode biodiversity and benthic trophic state are simple tools for the assessment of the environmental quality in coastal marine ecosystems. *Ecol. Indic.* 95, 270–287. doi: 10.1016/j.ecolind.2018.07.032

Chen, Z., Guo, L., Jin, B., Wu, J., and Zheng, G. (2009). Effect of the exotic plant spartina alterniflora on macrobenthos communities in salt marshes of the Yangtze river estuary, China. *Estuar Coast. Shelf S.* 82, 265–272. doi: 10.1016/j.ecss.2009.01.014

Chen, Z., Li, B., Zhong, Y., and Chen, J. (2004). Local competitive effects of introduced spartina alterniflora on scirpus mariqueter at dongtan of chongming island, the Yangtze river estuary and their potential ecological consequences. *Hydrobiologia* 528, 99–106. doi: 10.1007/s10750-004-1888-9

Chung, C. H. (2006). Forty years of ecological engineering with *Spartina* plantations in China. *Ecol. Eng.* 27, 49–57. doi: 10.1016/j.ecoleng.2005.09.012

Food and Drug Administration (FDA) (2011). *Fish and fishery products hazards and controls guidance*, 4th Edn. (Washington, DC: Department of Health and Human Services, Food and Drug Administration, Center for Food Safety and Applied Nutrition).

De Witte, B., Coleman, B., Bekaert, K., Boitsov, S., Botelho, M. J., Castro-Jiménez, J., et al. (2022). Threshold values on environmental chemical contaminants in seafood in the European economic area. *Food Control* 138, 108978. doi: 10.1016/j.foodcont.2022.108978

DNR (2012) *Imazapyr chemical fact sheet*. Available at: https://dnr.wisconsin.gov/sites/default/files/topic/Lakes/ImazapyrFactsheet.pdf.

Donadi, S., van der Zee, E. M., van der Heide, T., Weerman, E. J., Piersma, T., van de Koppel., J., et al. (2014). The bivalve loop: Intra- specific facilitation in burrowing cockles through habitat modification. *J. Exp. Mar. Biol. Ecol.* 461, 44–52. doi: 10.1016/j.jembe.2014.07.019

Donadi, S., Westra, J., Weerman, E. J., van der Heide, T., van der Zee, E. M., van de Koppel, J., et al. (2013). Non-trophic interactions control benthic producers on intertidal flats. *Ecosystems* 16, 1325–1335. doi: 10.1007/s10021-013-9686-8

Durkin, P. R. (2013). *Scoping/Screening level risk assessment on fluazifop-p-butyl* (Syracuse Environmental Research Associates Inc., New York, NY, USA), 293. Available online: https://www.fs.fed.us/foresthealth/pesticide/pdfs/Fluazifop-P-butyl.pdf (accessed on 7 July 2019).

Early, R., Bradley, B. A., Dukes, J. S., Lawler, J. J., Olden, J. D., Blumenthal, D. M., et al. (2016). Global threats from invasive alien species in the twenty-first century and national response capacities. *Nat. Commun.* 7, 12485. doi: 10.1038/ncomms12485

Fisher, J.P., Mavros, B., Walker, D., Heller, M., Suedel, B., Gillespie, B., and Slocomb, J. (2003). Ecological risk assessment of the proposed use of the herbicide imazapyr to control invasive cordgrass (Spartina spp.) in estuarine habitat of Washington State. (Prepared for the Washington State Department of Agriculture by ENTRIX, INC., Olympia, Washington), pp 163.

Garcia-Rossi, D., Rank, N., and Strong, D. R. (2003). Potential for self-defeating biological control? variation in herbivore vulnerability among invasive *Spartina* genotypes. *Ecol. Appl.* 13, 1640–1649. doi: 10.1890/01-5301

Grevstad, F. S., Strong, D. R., Garcia-Rossi, D., Switzer, R. W., and Wecker, M. S. (2003). Biological control of spartina alterniflora in willapa bay, Washington using the planthopper prokelisia marginata: agent specificity and early results. *Biol. Control* 27, 32–42. doi: 10.1016/S1049-9644(02)00181-0

Gu, J., Jin, R., Chen, G., Ye, Z., Li, Q., Wang, H., et al. (2021). Areal extent, species composition, and spatial distribution of coastal saltmarshes in China. *IEEE J-STARS.* 14, 7085–7094. doi: 10.1109/JSTARS.2021.3093673

Herman, P. M. J., Middelburg, J. J., Van de Koppel, J., and Heip, C. H. R. (1999). Ecology of estuarine macrobenthos. *Adv. Ecol. Res.* 29, 195–240. doi: 10.1016/S0065-2504(08)60194-4

Hinz, H. L., Winston, R. L., and Schwarzländer, M. (2019). How safe is weed biological control? a global review of direct nontarget attack. *Q. Rev. Biol.* 94, 1–27. doi: 10.1086/702340

Huang, L., Zhang, Y., Shi, Y., Liu, Y., Wang, L., and Yan, N. (2015). Comparison of phosphorus fractions and phosphatase activities in coastal wetland soils along vegetation zones of yancheng national nature reserve, China. *Estuar Coast. Shelf S.* 157, 93–98. doi: 10.1016/j.ecss.2014.09.027

Jackson, M. V., Fuller, R. A., Gan, X., Li, J., Mao, D., Melville, D. S., et al. (2021). Dual threat of tidal flat loss and invasive spartina alterniflora endanger important shorebird habitat in coastal mainland China. *J. Environ. Manage.* 278, 111549. doi: 10.1016/j.jenvman.2020.111549

Ju, R., Li, H., Shang, L., Qiu, S., Li, J., Nie, M., et al. (2017). "Saltmarsh cordgrass spartina alterniflora loisel," in *Biological invasions and its management in China* (Singapore: Springer), 187–198. doi: 10.1007/978-981-10-3427-5_14

Kang, Y. Y., Ding, X. R., and Zhang, C. K. (2015). Maximum tidal range analysis of radial sand ridges in the southern yellow Sea. *Indian J. Geo-Marine Sci.* 44, 971–976.

Knott, C. A., Webster, E. P., and Nabukalu, P. (2013). Control of smooth cordgrass (Spartina alterniflora) seedlings with four herbicides. *J. Aquat. Plant Manage.* 51, 132–135.

Liang, Q., Yan, Z., and Li, X. (2020). Influence of the herbicide haloxyfop-r-methyl on bacterial diversity in rhizosphere soil of spartina alterniflora. *Ecotox. Environ. Safe.* 194, 110366. doi: 10.1016/j.ecoenv.2020.110366

Li, B., Liao, C.-H., Zhang, X.-D., Chen, H.-L., Wang, Q., Chen, Z.-Y., et al. (2009). *Spartina alterniflora* invasions in the Yangtze river estuary, China: an overview of current status and ecosystem effects. *Ecol. Eng.* 35, 511–520. doi: 10.1016/j.ecoleng.2008.05.013

Li, X., Li, J., Wang, Y., Fu, L., Fu, Y., Li, B., et al. (2011). Aquaculture industry in China: current state, challenges, and outlook. *Rev. Fisheries Sci.* 19, 187–200. doi: 10.1080/10641262.2011.573597

Ma, Z., Li, B., Li, W., Han, N., Chen, J., and Watkinson, A. R. (2009). Conflicts between biodiversity conservation and development in a biosphere reserve. *J. Appl. Ecol.* 46, 527–535. doi: 10.1111/j.1365-2664.2008.01528.x

Meng, W., Feagin, R. A., Innocenti, R. A., Hu, B., He, M., and Li, H. (2020). Invasion and ecological effects of exotic smooth cordgrass spartina alterniflora in China. *Ecol. Eng.* 143, 105670. doi: 10.1016/j.ecoleng.2019.105670

Mo, X., Dong, P., Xie, L., Xiu, Y., Wang, Y., Wu, B., et al. (2021). Effects of imazapyr on spartina alterniflora and soil bacterial communities in a mangrove wetland. *Water* 13, 3277. doi: 10.3390/w13223277

Patten, K. (2002). Smooth cordgrass (Spartina alterniflora) control with imazapyr. *Weed Technol.* 16, 826–832. doi: 10.1614/0890-037X(2002)016[0826:SCSACW]2.0.CO;2

Peng, H.-B., Chan, Y.-C., Compton, T. J., Cheng, X. F., Melville, D. S., Zhang, S. D., et al. (2021). Mollusc aquaculture homogenizes intertidal soft-sediment communities along the 18,400 km long coastline of China. *Diver. Distr.* 27, 1553–1567. doi: 10.1111/ddi.13302

Piersma, T., Lok, T., Chen, Y., Hassell, C. J., Yang, H.-Y., Boyle, A., et al. (2016). Simultaneous declines in summer survival of three shorebird species signals a flyway at risk. *J. Appl. Ecol.* 53, 479–490. doi: 10.1111/1365-2664.12582

Qiao, P., Wang, A., Xie, B., Wang, L., Han, G., Mei, B., et al. (2019). Effects of herbicides on invasive spartina alterniflora in the yellow river delta. *Acta Ecologica Sin.* 39, 5627–5634.

Rakhimberdiev, E., Duijns, S., Karagicheva, J., Camphuysen, C. J., Dekinga, A., Dekker, R., et al. (2018). Fuelling conditions at staging sites can mitigate Arctic warming effects in a migratory bird. *Nat. Commun.* 9, 1–10. doi: 10.1038/s41467-018-06673-5

Rani, L., Thapa, K., Kanojia, N., Sharma, N., Singh, S., Grewal, A. S., et al. (2021). An extensive review on the consequences of chemical pesticides on human health and environment. *J. Clean. Prod.* 283, 124657. doi: 10.1016/j.jclepro.2020.124657

Roberts, P. D., and Pullin, A. S. (2008). The effectiveness of management interventions for the control of spartina species: A systematic review and meta-analysis. *Aquat. Conserv.* 18, 592–618. doi: 10.1002/aqc.889

Seebens, H., Essl, F., Dawson, W., Fuentes, N., Moser, D., Pergl, J., et al. (2015). Global trade will accelerate plant invasions in emerging economies under climate change. *Glob. Change Biol.* 21, 4128–4140. doi: 10.1111/gcb.13021

Sheng, Q., Huang, M., Tang, C., Niu, D., Ma, Q., and Wu, J. (2014). Effects of different eradication measures for controlling spartina alterniflora on plants and macrobenthic invertebrates. *Acta Hydrobiologica Sin.* 38, 279–290.

Strong, D. R., and Ayres, D. R. (2013). Ecological and evolutionary misadventures of spartina. *Annu. Rev. Ecol. Evol. S.* 44, 389–410. doi: 10.1146/annurev-ecolsys-110512-135803

UNESCO (2019) *Migratory bird sanctuaries along the coast of yellow Sea-bohai gulf of China (Phase I)*. Available at: https://whc.unesco.org/en/list/1606/.

USEPA (2006). *Reregistration eligibility decision (RED) for imazapyr* (Washington, DC, USA: United States Environmental Protection Agency).

van der Zee, E. M., van der Heide, T., Donadi, S., Eklöf, J. S., Eriksson, B. K., Olff, H., et al. (2012). Spatially extended habitat modification by intertidal reef- building bivalves has implications for consumer-resource interactions. *Ecosystems* 15, 664–673. doi: 10.1007/s10021-012-9538-y

Wang, S. K., Chu, T. J., Huang, D. Q., Li, B., and Wu, J. H. (2014). Incorporation of exotic spartina alterniflora into diet of deposit-feeding snails in the Yangtze river estuary salt marsh: stable isotope and fatty acid analyses. *Ecosystems* 17, 567–577. doi: 10.1007/s10021-013-9743-3

WSSA (2014). "Imazapyr," in *Herbicide handbook, 10th ed.* Ed. D. L. Shaner (Lawrence, KS, USA: Weed Science Society of America), 258–259.

Xie, B., Han, G., Qiao, P., Mei, B., Wang, Q., Zhou, Y., et al. (2019). Effects of mechanical and chemical control on invasive spartina alterniflora in the yellow river delta, China. *PeerJ* 7, e7655. doi: 10.7717/peerj.7655

Yuan, L., Zhang, L., Xiao, D., and Huang, H. (2011). The application of cutting plus waterlogging to control spartina alterniflora on saltmarshes in the Yangtze estuary, China. *Estuar. Coast. Shelf S.* 92, 103–110. doi: 10.1016/j.ecss.2010.12.019

Zhang, S.-D., Ma, Z., Choi, C.-Y., Peng, H.-B., Melville, D. S., Zhao, T. T., et al. (2019b). Morphological and digestive adjustments buffer performance: How staging shorebirds cope with severe food declines. *Ecol. Evol.* 9, 3868–3878. doi: 10.1002/ece3.5013

Zhang, Y., Pennings, S. C., Li, B., and Wu, J. (2019a). Biotic homogenization of wetland nematode communities by exotic spartina alterniflora in China. *Ecology* 100, e02596. doi: 10.1002/ecy.2596

Zhao, Z. Y., Xu, Y., Yuan, L., Li, W., Zhu, X. J., and Zhang, L. Q. (2020). Emergency control of spartina alterniflora re-invasion with a chemical method in chongming dongtan, China. *Water Sci. Eng.* 13, 24–33. doi: 10.1016/j.wse.2020.03.001

frontiers | Frontiers in Marine Science

TYPE Original Research
PUBLISHED 04 January 2023
DOI 10.3389/fmars.2022.1059353

OPEN ACCESS

EDITED BY
Guanqiong Ye,
Zhejiang University, China

REVIEWED BY
Huang Honghui,
South China Sea Fisheries Research Institute (CAFS), China
Youhui Huang,
East China University of Science and Technology, China

*CORRESPONDENCE
Zhiquan Liu
liuzhiquan1024@163.com

†These authors have contributed equally to this work

SPECIALTY SECTION
This article was submitted to Coastal Ocean Processes, a section of the journal Frontiers in Marine Science

RECEIVED 01 October 2022
ACCEPTED 12 December 2022
PUBLISHED 04 January 2023

CITATION
Zhang Y, Wan H, Zhao Y, Ding J, Zhu Z, Zhang H and Liu Z (2023) Macrobenthic functional group analysis of ecological health of the intertidal artificial oyster reefs in the Yangtze Estuary, China.
Front. Mar. Sci. 9:1059353.
doi: 10.3389/fmars.2022.1059353

Macrobenthic functional group analysis of ecological health of the intertidal artificial oyster reefs in the Yangtze Estuary, China

Yinan Zhang[1,2†], Hang Wan[3†], Yunlong Zhao[4], Jiafeng Ding[1,2], Zhenchang Zhu[5], Hangjun Zhang[1,2] and Zhiquan Liu[1,2*]

[1]School of Life and Environmental Sciences, Hangzhou Normal University, Hangzhou, China, [2]School of Engineering, Hangzhou Normal University, Hangzhou, China, [3]Southern Marine Science and Engineering Guangdong Laboratory (Guangzhou), Guangzhou, China, [4]State Key Laboratory of Estuarine and Coastal Research, School of Life Science, East China Normal University, Shanghai, China, [5]School of Ecology, Environment and Resources, Guangdong University of Technology, Guangzhou, China

The functional groups and the ecological health of a constructed oyster reef were investigated during April 2016 to October 2017 in the Yangtze estuary. The data of the long-term monitoring program (14 years) confirmed the feasibility of creating an artificial oyster reef in Yangtze estuary. One or two functional groups were absent from moderate salinity conditions (5.17% - 8.73%), while macrobenthos functional group species richness, abundance, and biomass were greatest under high salinity conditions. The feeding evenness index (j_{FD}) showed that 14 years after construction, the ecosystem health of the artificial oyster reefs were good or high, and was better under high salinity conditions. Ecological health was lower under moderate levels of salinity, possibly due to the absence of some functional groups. Redundancy analysis indicated ecosystem health was associated with changes in salinity and substrate factors. Our study confirmed artificial oyster reef construction is feasible and has a positive effect on estuarine ecosystem health.

KEYWORDS

functional group, macrobenthos, Yangtze estuary, oyster reef, ecological restoration

1 Introduction

Estuaries are highly productive, yet threatened ecological systems that deliver a range of ecosystem services and benefits to human society. However, the health of many estuaries is under threat from high levels of anthropogenic activities and pollution associated with the dense human populations that occur in these regions (Adger et al., 2005).

For example, sediment and organic material deposited by rivers in estuaries include nutrients, heavy metals, microplastics, and other contaminants (Chen et al., 2012; Han et al., 2017; Xu et al., 2018) that have led to biodiversity loss and reduced ecological resilience in estuarine environments (Lotze et al., 2006; Liu et al., 2018a).

The recognition of the essential role of estuaries for humans and other organisms has led to the initiation of ecological restoration programs (Lotze et al., 2006), where rehabilitation or construction oyster reefs represent an effective estuarine restoration technique. The biological structure formed by a large number of oysters is called an oyster reef, which is an important coastal habitat, because they provide many ecological services and bring multiple ecological benefits (Grabowski et al., 2022), such as water purification through water filtration and the removal of phytoplankton and heavy metals, and habitat provisioning through creation of three-dimensional habitats for macrobenthos and fish (Breitburg et al., 2000; Coen and Luckenbach, 2000; Grabowski and Peterson, 2007; Thomsen et al., 2007; La Peyre et al., 2014; Liu et al., 2018b). Thus, construction of oyster reefs has been increasingly used for shoreline protection and ecological restoration (La Peyre et al., 2014; Chakraborty, 2016; Walles et al., 2016).

The Yangtze Estuary is the largest in Asia and is one of the most globally important ecotones (Chen et al., 2012) that provides vital ecological services, including breeding grounds for aquatic organisms and stopover and overwintering sites for millions of migratory birds (Xu and Zhao, 2005). However, it is affected by rising sea-level and anthropogenic pressures that have culminated over centuries of overexploitation, reclamation, and pollution (He et al., 2011; Kirwan and Megonigal, 2013; Liu et al., 2016b; Yu et al., 2018); consequently, eutrophication and reduction in biodiversity have led to a deterioration in the ecological health of the Yangtze Estuary (Chai et al., 2006; Chen et al., 2012; Huang et al., 2021; Huang et al., 2022). In response, an oyster reef restoration project was initiated in the region (Quan et al., 2009), based on previous studies that showed the construction of artificial oyster reefs in the Yangtze River estuary was feasible and effective in the restoration of the ecosystem (Quan et al., 2009; Quan et al., 2012; Lv et al., 2016a; Liu et al., 2018b).

It is likely that artificial and restored oyster reefs may be affected by human activities and pollution, such as over-fishing of the nursery beds and oil contamination, therefore, monitoring of such restoration schemes is crucial for their success. Macrobenthos represents a vital component of oyster reefs, and are ideal indicators for use in ecosystem health monitoring schemes due to their limited mobility, ease of collection, and high sensitivity (Borja et al., 2000; Borja et al., 2003; Gamito and Furtado, 2009; Liu et al., 2019); however, studies of oyster reefs have tended to focus on taxonomic macrobenthos community structure, abundance, biomass, diversity, and ecosystem health (Quan et al., 2009; Quan et al., 2012; Lv et al., 2016a; Liu et al., 2018b) that may be more appropriate in the evaluation of biodiversity rather than ecosystem health (Cummins et al., 2005; Peng et al., 2013). Macrobenthos functional groups represent taxa that have similar ecological characteristics, so assessment of their responses to environmental change is more meaningful than that of individuals or taxonomic families, because it provides a more accurate indication of ecosystem-level responses to ecological perturbations (Yang et al., 2017).

Ecological restoration may trigger the emergence of novel functional groups and turnover of existing functional groups (Lv et al., 2018). Previous studies of the Yangtze Estuary oyster reef have quantified biological resources, including macrobenthos and nektons, macrobenthic taxonomic diversity and ecological health (Quan et al., 2007; Quan et al., 2009; Quan et al., 2012; Lv et al., 2016a; Liu et al., 2018b); however, assessment of macrobenthos functional groups remains lacking. Here, we identified macrobenthos functional groups to assess the ecological status of the artificial oyster reef in the Yangtze estuary. Specifically, the objectives were to (1) assess the composition and abundance of macrobenthos functional groups; (2) measure long-term variation in macrobenthos functional group composition; (3) test the relationship between macrobenthos functional groups and environmental variables; and, (4) use macrobenthos functional groups to assess ecosystem health.

2 Materials and methods

2.1 Study site

The Yangtze estuary (29°30′N–32°00′N, 121°00′E–124°00′E) artificial intertidal oyster reef (c. 260 ha) was constructed in 2004 in the north passage of the southern Yangtze River channel (Figures 1A, B), and comprises two dikes (south and north) with 19 groins (S1-S9 in the south dike and N1-N10 in the north dike). The north dike (total length: 48 km) is located along the southern margin of Hengsha Island, and the south dike (total length: 49.2 km) is located along the northern edge of Jiuduansha National Nature Reserve. The artificial reef is vaulted in cross-section (Figure 1C).

2.2 Sampling

Macrobenthos were sampled in April and September 2016, and in August and October 2017 from three paired sites (N = 6) at the two dikes along an increasing salinity gradient, where salinity at sites S2 and N2 was 0.43 ± 0.03 and 0.43 ± 0.04, respectively, S5 and N6 was 6.55 ± 1.38 and 7.86 ± 0.87, respectively, and S8 and N9 was 16.43 ± 0.34 and 15.50 ± 1.09, respectively. At low spring tide from three site (high, mid, and low tidal zones), four quantitative samples of macrobenthos

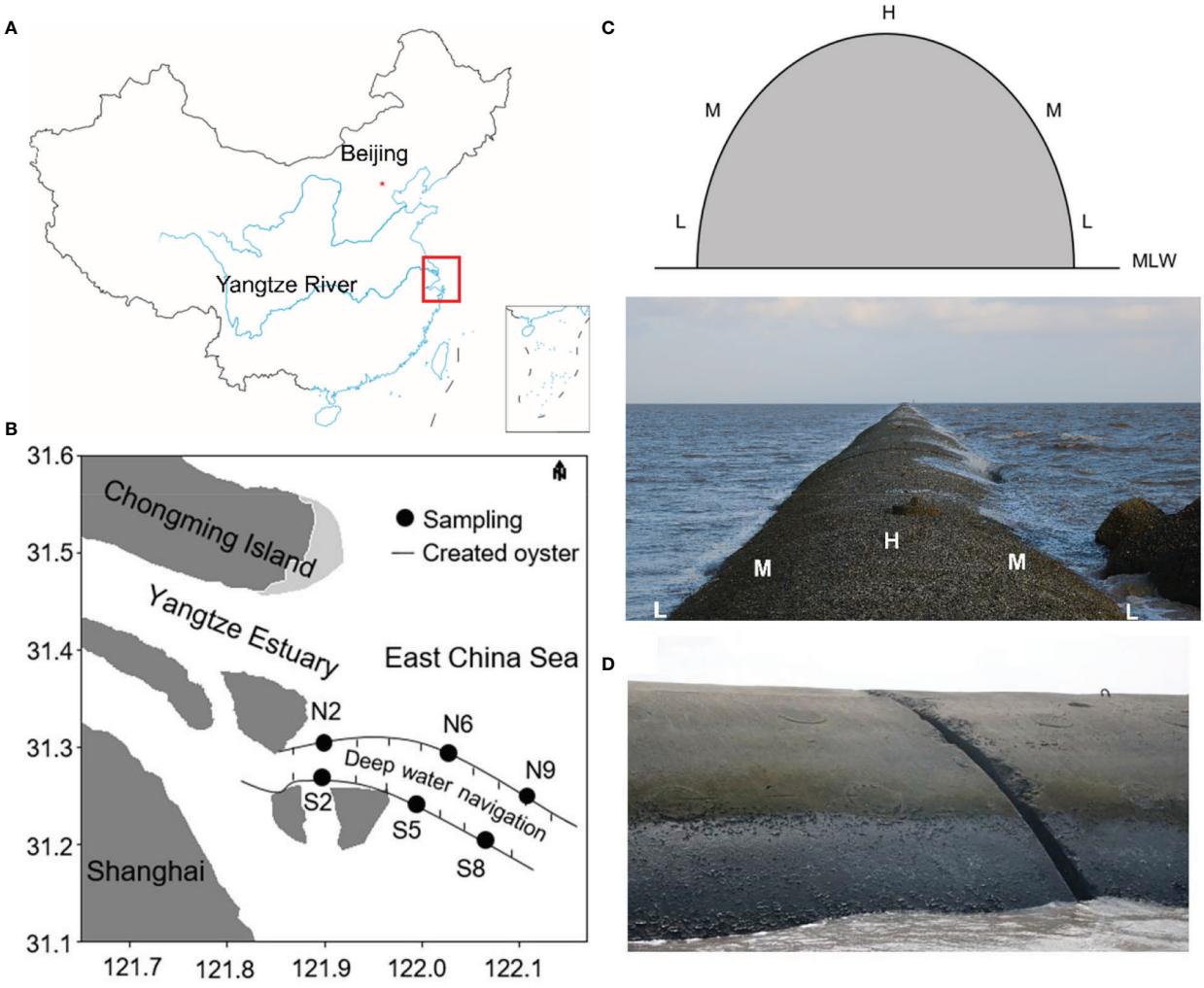

FIGURE 1
Study site locations. **(A)** Yangtze River estuary, China; **(B)** Sampling sites on the artificial intertidal oyster reef; **(C)** Schematic drawing of the sampling transect and cross-section of the artificial reef; **(D)** No organisms were recorded from the low-salinity sites (S2 and N2).

(25 × 25 cm) were collected from each site (Quan et al., 2009), where the high tidal zone was located on the crest of the reef, the mid zone was on the flank, and the low zone was at the reef base. In addition, as many qualitative samples as possible were collected from an area of 25.0 m^2 from the sampling center. Samples were immediately sieved (1.0-mm mesh) and the collected macrobenthos were preserved in 75% alcohol prior to subsequent identification at the laboratory to the lowest possible taxonomic level; individuals were counted and weighed to the nearest 0.01g wet weight. No organisms were recorded from both quantitative and qualitative investigations from the low salinity sites (S2 and N2) (Figure 1D).

Water temperature (WT), salinity (SAL), pH, and dissolved oxygen (DO) at the sampling sites were measured using a HQ 40D multi-parameter water quality meter (Hach, Loveland, Colorado, USA). The abundance of oyster (OA) and barnacles (BA) were defined as the substrate variables of the oyster reef.

2.3 Long-term variation in functional groups

Including the 2016 and 2017 data collected, changes over a 14-year period in the macrobenthic functional groups were integrated in an analysis of dynamics from 2004 to 2017. Historical data points (2004–2014) were obtained from the literature, namely for September 2004, August 2005, August and November 2007, April and July 2008, May and September 2009, April and November 2011, July and October 2012, August and October 2013, August and October 2014 (Quan et al., 2009; Quan et al., 2012; Lv et al., 2016a).

2.4 Macrobenthos functional groups and trophic levels

We defined five macrobenthos functional groups according to feeding strategy (Zhu and Lu, 2003; Peng et al., 2013; Yang et al., 2017) that comprised planktivore (Pl) herbivore (He); predator (Pr); omnivore (O); and, detritivore (D). From these, we defined four trophic levels (Figure 2), where the first level comprised primary producers (we did not survey this group), the second level comprised primary consumers (Pl, He, and D), the third level comprised omnivore secondary consumers of levels I and II, while the fourth level comprised predatory (Pr) secondary consumers of levels II and III.

2.5 Statistical analysis

We used CLUSTER (hierarchical clustering) and NMDS (two-dimensional nonmetric multidimensional scaling) in PRIMER v5.0 to test the degree of similarity of the macrobenthic functional groups (Clarke and Gorley, 2001). Macrobenthos functional group data were fourth-root transformed to calculate the community similarity according to the Bray-Curtis similarity index, and similarity analysis (ANOSIM 2-way) was used to test for tidal zone and site differences in the abundance of macrobenthos functional groups.

Detrended correspondence analysis determined linear redundancy analysis (RDA) was more appropriate than a unimodal analysis (maximum gradient length of the axes<3) to describe the effects of environmental variables on macrobenthos functional group abundance. With the exception of pH, environmental data were log10 (x+1) transformed prior to analysis.

A feeding evenness index (j_{FD}) was used to assess the ecological health status of the macrobenthos trophic levels, following the methodology reported by (Gamito and Furtado, 2009):

$$j_{FD} = H'_{FD}/Log_2 n \quad (1)$$

where H' is the Shannon–Wiener index and n is the number of trophic groups. Ecosystem health was determined as low (j_{FD} =<0.20), poor (j_{FD} = 0.20-0.40), moderate (j_{FD} = 0.40-0.60), good (j_{FD} = 0.60-0.80), and high (j_{FD} = >0.80) (Gamito et al., 2012).

Two-way ANOVA, with *post-hoc* Turkey test, was used to test the effects of site and tidal zone on macrobenthos species richness and abundance, and biomass of macrobenthos functional group at P< 0.05. When assumptions of homogeneity of variances were not met, data were fourth-root transformed; if variances remained non-homogenous, we applied the Scheirer-Ray-Hare extension of the Kruskal-Wallis test. Associations between environmental variables and macrobenthos were tested using correlation analysis at P< 0.05. Analyses were performed using SPSS statistics 19.0 and presented data are means ± SEM.

3 Results

3.1 Temporal variation in functional group structure

The species composition of the macrobenthos functional groups varied between 2004 and 2017, where total number of species increased immediately after reef creation, before it declined in 2008, and then peaked in 2011 (36 species); species richness remained stable from 2012 to 2017 (Figure 3). The number of

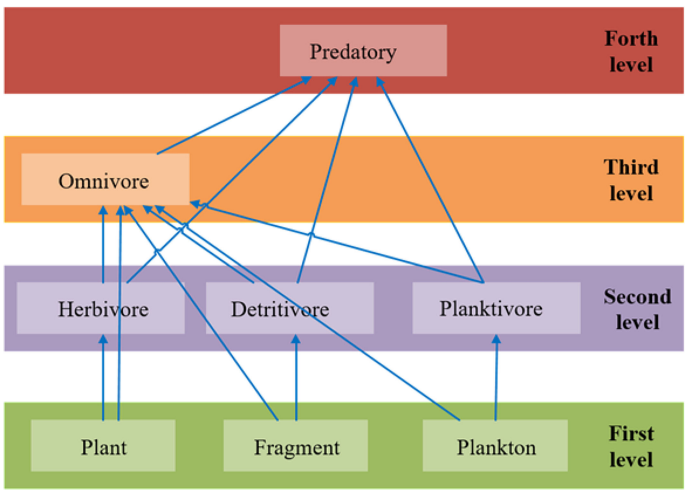

FIGURE 2
Trophic levels and food web of the microbenthic community, redrawn from Li et al. (2007).

functional groups increased with restoration time, from three in 2004 (O, He, and Pl) to five from 2009 onwards (Figure 3).

3.2 Study site and tidal zone variations in macrobenthos community

We identified three and four macrobenthos functional groups at the moderate salinity sites N6 and S5, respectively (Figure 4 and Table 1), and five groups at both high salinity sites (S8 and N9) during 2016-2017. O and He groups comprised higher numbers of species at the high salinity sites (S8 and N9) than at the moderate-salinity (S5 and N6) sites ($P< 0.05$, Table 2). There were more species in the O group in the low intertidal zone, but fewer in the mid zone; species richness varied among the three tidal zones ($P< 0.05$, Table 2).

3.3 Functional group abundance and biomass

Abundance of C, O, and He and biomass of C were higher in high-salinity (N9 and S8) sites than in the moderate salinity sites (N5 and S6) ($P<0.05$, Tables 3–6), and there was no effect of tidal zone on abundance and biomass of the five functional groups (Tables 5, 6).

3.4 Functional group community structure

Cluster analysis revealed similarities and differences in macrobenthos functional groups among sites and tidal zones, where there were three clusters comprising S8-L, S8-M, N9-L, S5-M, S8-H, N9-H, and N9-M; S5-H; and, N6-H, N6-M, and N6-L (Figure 5A). The nMDS analysis results were consistent with the cluster analysis, with a stress value = 0.08 indicating the results were reliable (Figure 5B). There were site differences in macrobenthos functional groups (ANOSIM 2 Global $R = 0.719$; $P = 0.029$); however, there were no tidal zone differences (Global $R = 0.167$; $P = 0.34$).

3.5 Ecological health

We found that j_{FD} values for the macrobenthos functional groups were<0.8 in the moderate salinity sites (S5 and N6), indicating ecological health was good, and >0.8 in the high salinity sites (S8 and N9), indicating high quality ecological health (Figure 6).

3.6 Relationship between macrobenthic functional group abundance and environmental variables

Monte Carlo tests for the first and all Redundancy analysis (RDA) canonical axes were significant ($P = 0.004$), indicating these parameters may be important in explaining the composition of the macrobenthos functional groups. The first axis explained 62.4% of total variation in the functional group data and all canonical axes accounted for 72.3% of the variance in the functional group abundance-environment relationship. Functional groups were correlated with environmental variables: groups O, Pl, D, and He were positively correlated with barnacle

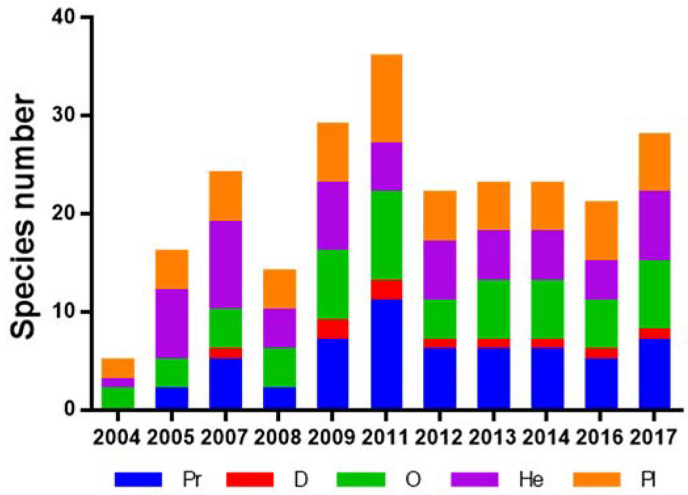

FIGURE 3
Long-term variation in macrobenthos functional group species richness. Pr, predator; D, detritivore; O, omnivore; He, herbivore; and Pl, planktivore.

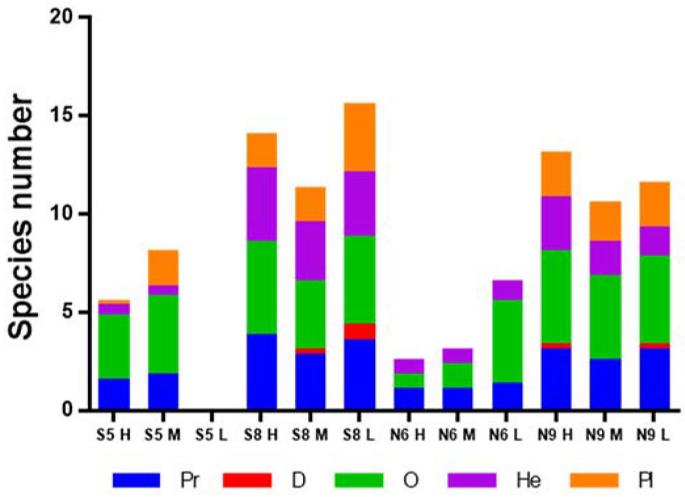

FIGURE 4
Average functional group species richness. Pr, predator; D, detritivore; O, omnivore; He, herbivore; and Pl, planktivore.

TABLE 1 Macrobenthos collected from the artificial intertidal oyster reef.

	Sites	Tidal zone	Functionalgroup	Reference
Coelenterata				
Haliplanella sp.	S5S8N6N9	HML	O	(Cai, 2015)
Sipuncula				
Phascolosoma esculenta	S8N9	HML	D	(Cai, 2015)
Annelida				
Perinereis aibuhitensis	S5S8N6N9	HML	O	(Zheng and Fan, 1986)
Neanthes japonica	S5S8N6N9	HML	O	(Ye, 2010)
Dentinephtys glabra	S8N6N9	HML	Pr	
Perinnereis nuntia	S8	L	O	
Hydroides ezoensis	S8N9	H	PI	
Mollusca				
Nerita yoldi	S5S8N6N9	HML	O	
Littorina brevicula	S8N9	HML	He	(Bao et al., 2008)
Littorinopsis intermedia	S8N6N9	HML	Ph	
Pyrene bella	S8N6N9	HML	He	
Purpura clavigera	S8N9	HML	Pr	
Rapana bezoar	S8N9	HML	Pr	
Potamocorbula amurensis	S5N9	HML	PI	(Lv et al., 2013)
Musculus senhousia	S8N9	HML	PI	(Liu et al., 2016a)
Modiolus flavidus	S8N9	HL	PI	(Li et al., 2014)
Vignadula atrata	S8N9	HML	Pl	

(Continued)

TABLE 1 Continued

	Sites	Tidal zone	Functionalgroup	Reference
Barbatia bistrigata	S8N9	HML	Pl	
Unkonwn species (GASTROPODA)	N6	L	He	
Arthropoda				
Corophium acherusicum	S5N6	L	He	(Chen, 2001)
Metopograpsus quadridentatus	S5S8N6N9	HML	He	(Zhang et al., 2017)
Macromedaeus distinguendus	S5S8N9	HML	Pr	
Eriocheir leptognathus	S5S8	HM	Pr	
Scylla serrata	N9	M	Pr	(Yuan et al., 2002)
Pinnotheres sinensis	N6	H	O	
Alpheus japonicus	S8	H	Pr	(Zhang et al., 2017)
Gnorimosphaeroma rayi	S5S8N6N9	HML	Pr	
Cleantioides annaandalei	S8	HML	He	
Eohaustorius cheliferus	S5S8N6N9	HML	O	(Zhu and Lu, 2003)
Chordata				
Liciogobius guttatus	S5S8N9	ML	Pl	(Li et al., 2014)
Echinodermata				
Amphiura vadicola	S8	L	D	(Li et al., 2013)

No organisms were recorded from the low-salinity sites (S2 and N2) Pr, predator; D, detritivore; O, omnivore; He, herbivore; Pl, planktivore. H, high; M, middle; and L, Low tidal zone.

abundance, oyster abundance, salinity, and temperature, and negatively correlated with pH, whereas group C was negatively correlated with dissolved oxygen (Figure 7).

Discussion

Restored and artificial oyster reefs play a vital role in improving the ecological health status of estuarine environments, because they improve water quality and provide a three-dimensional structure that may be colonized by macrobenthos and fish (Breitburg et al., 2000; Thomsen et al., 2007). In the first year (2004) since its creation, the artificial oyster reef in the Yangtze estuary was found to have become host to three functional groups (comprising five species) of macrobenthos; the species richness of the functional groups rapidly increased with time, with the exception of 2008, before it peaked in 2011 and remained stable from 2012. This increase in functional group species richness occurred after oyster abundance had stabilized (2011) (Liu et al., 2018b) and prior to the increase in macrobenthos taxonomic diversity that occurred from 2012 to 2016-2017 (Liu et al., 2018b). These results support previous studies that have indicated the oyster reefs in the Yangtze Estuary be develop into self-sustaining systems (Walles et al., 2016; Liu et al., 2018b).

Water salinity is a key factor that affects the distribution of macrobenthos in estuarine habitats (Holland et al., 1987; Liu

TABLE 2 Study site and tidal zone effects on macrobenthic functional group species richness during 2016-2017.

Functional group	Sites			Tidal zone		
	df	*F* or *H*	*P*	df	*F* or *H*	*P*
C	3	5.870	0.12	2	0.168	0.92
D	3	0.609	0.89	2	0.429	0.81
O	3	10.329	<0.001	2	4.212	0.023
Ph	3	16.546	<0.001	2	0.873	0.427
Pl	3	6.045	0.11	2	0.472	0.79

10.3389/fmars.2022.1059353

TABLE 3 Abundance of macrobenthos functional groups in the constructed intertidal oyster reef in Yangtze River Estuary during 2016-2017.

	S5			S8			N6			N9		
	H	M	L	H	M	L	H	M	L	H	M	L
Pr	346.0 ± 140.2	249.0 ± 116.2	—	501.0 ± 165.2	263.0 ± 103.2	348.0 ± 89.9	40.0 ± 26.8	164.5 ± 126.8	168.0 ± 73.8	652.0 ± 146.3	491.0 ± 126.9	247.0 ± 70
D	0.0 ± 0.0	0.0 ± 0.0	—	0.0 ± 0.0	1.0 ± 1.0	3.0 ± 1.0	0.0 ± 0.0	0.0 ± 0.0	0.0 ± 0.0	1.0 ± 1.0	0.0 ± 0.0	3.0 ± 3.0
O	83.0 ± 36.5	180.0 ± 66.4	—	342.0 ± 15.8	171.0 ± 57.3	180.0 ± 21.3	7.0 ± 5.7	209.0 ± 70.8	368.0 ± 73.2	355.0 ± 56.4	258.0 ± 88.9	329.0 ± 50.8
He	3.0 ± 3.0	12.0 ± 7.1	—	166.0 ± 29.5	53.0 ± 24.6	282.0 ± 59.8	11.0 ± 7.5	13.0 ± 5.5	19.0 ± 10.4	75.0 ± 32.3	57.0 ± 26.0	74.0 ± 33.1
Pl	1.0 ± 1.0	15.0 ± 5.0	—	122.0 ± 6.2	89.0 ± 36.1	132.0 ± 14.0	0.0 ± 0.0	0.0 ± 0.0	0.0 ± 0.0	61.0 ± 36.1	42.0 ± 24.7	76.0 ± 44.2

H, high tidal zones; M, mid tidal zones; L, low tidal zones.

TABLE 4 Biomass of macrobenthic functional groups in the constructed intertidal oyster reef in Yangtze River Estuary during 2016-2017.

	S5			S8			N6			N9		
	H	M	L	H	M	L	H	M	L	H	M	L
Pr	2.1 ± 1.1	3.8 ± 1.2	—	28.7 ± 15.6	22.6 ± 15.3	89.3 ± 45.2	25.3 ± 20.5	17.4 ± 13.4	1.5 ± 1.5	8.2 ± 4.0	6.1 ± 3.4	8 ± 5.7
D	0.0 ± 0.0	0.0 ± 0.0	—	0.0 ± 0.0	0.0 ± 0.0	0.1 ± 0.0	0.0 ± 0.0	0.0 ± 0.0	0.0 ± 0.0	0.0 ± 0.0	0.0 ± 0.0	0.0 ± 0.0
O	9.1 ± 5.2	23.5 ± 13.1	—	38.3 ± 15.3	42.5 ± 18.9	19.3 ± 5.4	11.9 ± 5.6	53.3 ± 29.6	54.2 ± 33.6	115.9 ± 16.2	75.5 ± 6.4	72.5 ± 5.0
He	0.2 ± 0.2	1.3 ± 1.0	—	8.6 ± 4.5	8.2 ± 3.9	16.1 ± 9.5	13.6 ± 7.9	7.4 ± 4.0	0.3 ± 0.3	2.1 ± 1.0	0.9 ± 0.3	2.1 ± 1.0
Pl	0.1 ± 0.1	1.9 ± 0.7	—	6.1 ± 3.2	8.9 ± 3.3	21.8 ± 6.2	11.3 ± 8.0	8.9 ± 5.3	0.0 ± 0.0	1.1 ± 0.8	0.8 ± 0.5	1.1 ± 0.7

H, high tidal zones; M, mid tidal zones; L, low tidal zones.

et al., 2018a), where species richness, abundance, and biomass increase with increase in salinity (Yuan et al., 2002). In this study, the increase in salinity (from S5 and N6 to S8 and N9) resulted in an increase in species richness, abundance, and biomass of macrobenthic functional group ($P< 0.05$; Figure 7), indicating salinity affects the distribution of macrobenthos functional groups in the artificial Yangtze Estuary oyster reefs. Adaptation to salinity varies among species (Yuan et al., 2002); for example, *Phascolosoma esculenta*, which was only collected from the high salinity sites (S8 and N9), belongs to the D functional group, and has a survival salinity of 5-30 ‰, with a salinity range for embryo development of 17.10-30.15 ‰ (Jin et al., 2011). We found that functional group D, whose main species comprise polychaetes and Sipuncula that are sensitive to fluctuations in environmental conditions (Dauvin and Ruellet, 2007; Cai, 2015), was absent from the moderate salinity study sites (S5 and N6). There are marked seasonal changes in natural environmental variables, such as salinity and dissolved oxygen,

TABLE 5 Effect of study site and tidal zone on macrobenthos functional group abundance in the constructed intertidal oyster reef in Yangtze River Estuary during 2016-2017.

	Sites			Tidal zone		
	df	*F* or *H*	*P*	df	*F* or *H*	*P*
Pr	3	4.814	0.007	2	1.388	0.264
D	3	0.582	0.9	2	0.449	0.8
O	3	3.817	0.019	2	1.554	0.227
He	3	12.491	<0.001	2	1.278	0.292
Pl	3	7.221	0.07	2	0.0989	0.95

TABLE 6 Effect of study site and tidal zone on macrobenthos functional group biomass in the constructed intertidal oyster reef in Yangtze River Estuary during 2016-2017.

	Sites			Tidal zone		
	df	*F* or *H*	*P*	df	*F* or *H*	*P*
Pr	3	2.998	0.045	2	0.016	0.984
D	3	0.42	0.94	2	0.044	0.98
O	3	4.304	0.23	2	0.124	0.94
He	3	2.565	0.46	2	0.068	0.97
Pl	3	2.567	0.46	2	0.157	0.92

and tidal conditions in the area where study sites S5 and N6 were located: it is possible that mud trapped at the bottom of the oyster reef is removed by tidal action, resulting in a lack of food source required by functional group D.

Salinity not only influences estuarine macrobenthos distribution patterns, but also affects growth and survival of oysters (Hulathduwa and Brown, 2006; Liu et al., 2018b). Effects of salinity on oyster size and abundance vary with region, therefore oyster substrate of the artificial reefs is likely to similarly vary with region, and may lead to diverse distribution patterns of macrobenthos functional groups. Our RDA confirmed that salinity, barnacle abundance, and oyster abundance (substrate parameters) were the main factors that influenced the distribution of macrobenthos functional groups in the Yangtze River estuary artificial oyster reefs (Figure 7). Although there were differences in growth and abundance of oysters between regions and at different tidal zones within a region, there was no difference in macrobenthos functional group species richness, abundance or biomass, with the exception of species richness of group D among the tidal zones. These results indicate that while there are differences in substrate habitat with salinity and among tidal zones within a salinity range, the distribution pattern of macrobenthos functional groups varies with salinity, but not with different tidal zone, such that tidal zone and associated effects on substrate elicit little effect on the artificial oyster reef macrobenthic functional groups in the Yangtze Estuary. This finding is inconsistent with those of other local natural habitats, such as Jiuduansha and Quanzhou Bay (Zhu and Lu, 2003; Zhuo et al., 2014), possibly because the habitat of artificially constructed oyster reef lacks diversity. We suggest enrichment and diversification of artificial oyster reef habitats may improve the recruitment of functional group types to increase biodiversity and ecosystem stability.

In general, healthy environments contain most types of feeding guild, whereas degraded environments tend to be dominated by a few trophic groups, with others absent (Gamito and Furtado, 2009; Peng et al., 2013). In this study, we found one or two groups were absent from the moderate

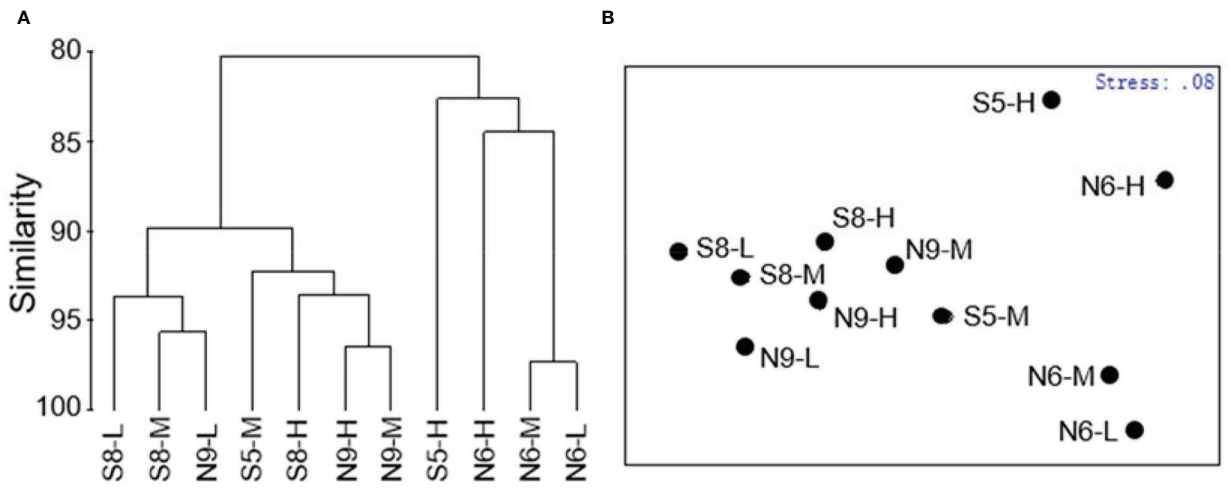

FIGURE 5
(A) Cluster and **(B)** non-metric multidimensional scaling (NMDS) ordinations of the macrobenthos functional groups.

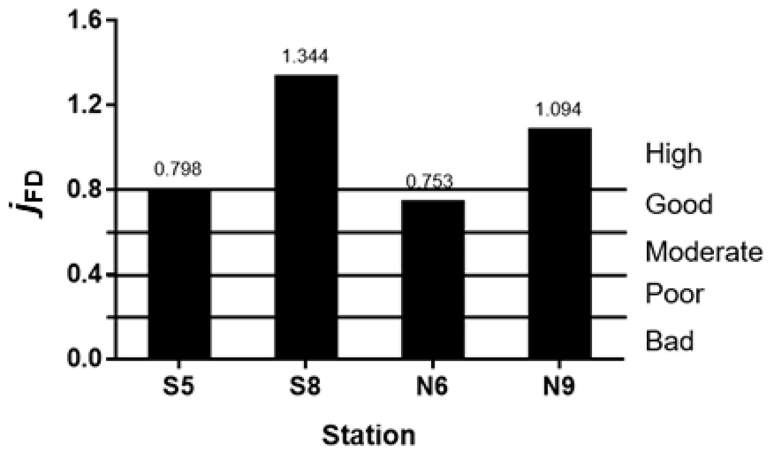

FIGURE 6
Ecological health status.

salinity study sites (S5 and N6), where they included functional groups that play an important role in estuarine food web nutrient cycling and energy flow. For example, Pl is the main source of nutrition for predators and omnivores, and plays an important role in controlling the growth of plankton, such as cyanobacteria (Figure 2). The absence of this functional group from the moderate salinity study sites indicates compromised ecological health, as supported by our results for j_{FD}, and previous results for AMBI, M-AMBI, and ABC curve (Liu et al., 2018b). Our ANOSIM 2 analysis showed site differences in ecological health, where it was better in the high salinity study sites. These results indicate that 14 years after construction, the habitat status of the artificial oyster reefs in the Yangtze Estuary was good or high, and was better under high salinity conditions (S8 and N9) than under moderate salinity (S5 and N6). Long-term artificial oyster reef monitoring confirms the feasibility of artificial oyster reef construction in the Yangtze estuary, and can be applied to estuarine areas or tidal flats within the same salinity

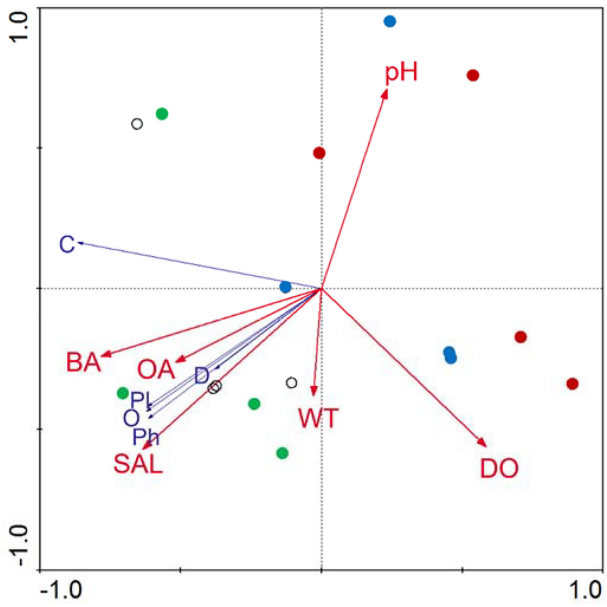

FIGURE 7
Redundancy analysis ordination of the macrobenthos functional groups and environmental variables (S5, S8, N6, and N9). DO, dissolved oxygen; WT, water temperature; SAL, water salinity; BA, barnacle abundance; and OA, oyster abundance.

range, such as east shoal of Nanhui, which are mainly affected by reclamation (Liu et al., 2018a). Coupled with the complex habitat of natural intertidal zone, it is inevitably more conducive to the ecological restoration of artificial oyster reef in these areas.

We found that macrobenthos functional group structure was more heterogeneous under high salinity conditions (S8 and N9) than under moderate levels of salinity (S5 and N6). Substrate parameters and environmental variables, such as dissolved oxygen, pH, temperature, and salinity, were similar between S5 and N6, and S8 and N9. However, functional group species richness, abundance, and biomass, and j_{FD} of the southern dike (S5 and S8) was higher than in the north dike (N6 and N9), possibly due to site conditions. The southern region of the oyster reef in the Yangtze Estuary is proximate to the ecologically protected Jiuduansha Nature Reserve (Zhang et al., 2018) that may affect the structure and ecological environment of macrobenthos (Lv et al., 2016b). In contrast, the lack of such protection measures in the north dike may render the oyster and macrobenthos in this area susceptible to human activities, such as overfishing. Therefore, we suggest the establishment of a nature reserve to protect this important oyster reef habitat in the Yangtze estuary.

In summary, artificial oyster reef was feasibility and has positive effect on the ecological health in the Yangtze estuary. Further, the ecological health was worse in medium salinity than high salinity, may due to the absence of functional groups. The release of species of absent functional group can be taken in the medium salinity region. The artificial oyster reef may be disturbed by human activities, thus a nature reserve should be established to protect this important habitat in the Yangtze estuary.

Data availability statement

The raw data supporting the conclusions of this article will be made available by the authors, without undue reservation.

Author contributions

YNZ: Conceptualization, Methodology, Resources, Formal analysis, Investigation, Data curation, Visualization, Writing - original draft, Writing - review and editing. HW: Conceptualization, Methodology, Resources, Visualization, Data curation, Writing - review and editing. YLZ: Conceptualization, Methodology, Resources, Visualization, Funding acquisition, Writing - review and editing. JD: Writing - original draft, Writing - review and editing. ZZ: Investigation, Data curation, Writing - review and editing. HZ: Conceptualization, Methodology, Writing - review and editing. ZL: Conceptualization, Methodology, Resources, Visualization, Supervision, Writing - review and editing, Project administration, Funding acquisition. All authors contributed to the article and approved the submitted version.

Funding

This study was sponsored by the Natural Science Foundation of Zhejiang Province of China (LQ22C030003), the special fund of State Environmental Protection Key Laboratory of Environmental Health Impact Assessment of Emerging Contaminants (SEPKL-EHIAEC-202201), the National Natural Science Foundation of China (42207323, 52009023) and the Scientific Reuter Foundation for Scholars of Hangzhou Normal University (2021QDL063).

Acknowledgments

We thank Elixigen for English language editing. We thank the editor and reviewers for their constructive and insightful feedback that improved the manuscript.

Conflict of interest

The authors declare that the research was conducted in the absence of any commercial or financial relationships that could be construed as a potential conflict of interest.

Publisher's note

References

Adger, W. N., Hughes, T. P., Folke, C., Carpenter, S. R., and Rockström, J. (2005). Social-ecological resilience to coastal disasters. *Science* 309, 1036–1039. doi: 10.1126/science.1112122

Bao, Y., Hu, Z., Li, H., Ge, B., and Cheng, H. (2008). Seasonal variation and functional groups of macrobenthic communities at diked and natural tidal flat China. *Acta Entomol. Sin.* 51, 1099–1128. doi: : 10.17520/biods.2015264

Borja, A., Franco, J., and Pérez, V. (2000). A marine biotic index to establish the ecological quality of soft-bottom benthos within European estuarine and coastal environments. *Mar. Pollut. Bull.* 40, 1100–1114. doi: 10.1016/S0025-326X(00)00061-8

Borja, A., Muxika, I., and Franco, J. (2003). The application of a marine biotic index to different impact sources affecting soft-bottom benthic communities along European coasts. *Mar. Pollut. Bull.* 46, 835–845. doi: 10.1016/S0025-326X(03)00090-0

Breitburg, D. L., Coen, L. D., Luckenbach, M. W., Mann, R., Posey, M., and Wesson, J. A. (2000). Oyster reef restoration: Convergence of harvest and conservation strategies. *J. Shellfish. Res.* 19, 371–377. doi: 10.1093/plankt/22.6.1213

Cai, L. (2015). *Zoobenthic ecology in shenzhen bay* (Xiamen: Xiamen University Press).

Chai, C., Yu, Z., Song, X., and Cao, X. (2006). The status and characteristics of eutrophication in the Yangtze river (Changjiang) estuary and the adjacent East China Sea China. *Hydrobiologia* 563, 313–328. doi: 10.1007/s10750-006-0021-7

Chakraborty, P. (2016). Oyster reef restoration in controlling coastal pollution around India: A viewpoint. *Mar. Pollut. Bull.* 115, 190–193. doi: 10.1016/j.marpolbul.2016.11.059

Chen, J. (2001). Primary study on chrouosome of corophium sinense. *J. Fujian. Fisher.* 1, 011. doi: 10.14012/j.cnki.fjsc.2001.01.011

Chen, Y., Liu, R., Sun, C., Zhang, P., Feng, C., and Shen, Z. (2012). Spatial and temporal variations in nitrogen and phosphorous nutrients in the Yangtze river estuary. *Mar. Pollut. Bull.* 64, 2083–2089. doi: 10.1016/j.marpolbul.2012.07.020

Clarke, K., and Gorley, R. N. (2001). *PRIMER (Plymouth routines in multivariate ecological research) v5: User manual/tutorial* (Plymouth: Primer-E Ltd), 1–91.

Coen, L. D., and Luckenbach, M. W. (2000). Developing success criteria and goals for evaluating oyster reef restoration: Ecological function or resource exploitation? *Ecol. Eng.* 15, 323–343. doi: 10.1016/S0925-8574(00)00084-7

Cummins, K. W., Merritt, R. W., and Andrade, P. C. (2005). The use of invertebrate functional groups to characterize ecosystem attributes in selected streams and rivers in south Brazil. *Stud. Neotrop. Fauna. Environ.* 40, 69–89. doi: 10.1080/01650520400025720

Dauvin, J., and Ruellet, T. (2007). Polychaete/amphipod ratio revisited. *Mar. Pollut. Bull.* 55, 215–224. doi: 10.1016/j.marpolbul.2006.08.045

Gamito, S., and Furtado, R. (2009). Feeding diversity in macroinvertebrate communities: A contribution to estimate the ecological status in shallow waters. *Ecol. Indic.* 9, 1009–1019. doi: 10.1016/j.ecolind.2008.11.012

Gamito, S., Patrício, J., Neto, J. M., Teixeira, H., and Marques, J. C. (2012). Feeding diversity index as complementary information in the assessment of ecological quality status. *Ecol. Indic.* 19, 73–78. doi: 10.1016/j.ecolind.2011.08.003

Grabowski, J. H., Baillie, C. J., Baukus, A., Carlyle, R., Fodrie, F. J., Gittman, R. K., et al. (2022). Fish and invertebrate use of restored vs. natural oyster reefs in a shallow temperate latitude estuary. *Ecosphere* 13, e4035. doi: 10.13140/RG.2.2.24829.51681

Grabowski, J. H., and Peterson, C. H. (2007). Restoring oyster reefs to recover ecosystem services. *Ecosyst. engineers.: Plants to. protists.* 4, 281–298. doi: 10.1016/S1875-306X(07)80017-7

Han, D., Cheng, J., Hu, X., Jiang, Z., Mo, L., Xu, H., et al. (2017). Spatial distribution risk assessment and source identification of heavy metals in sediments of the Yangtze river estuary China. *Mar. Pollut. Bull.* 115, 141–148. doi: 10.1016/j.marpolbul.2016.11.062

He, W. P., Li, Y. X., Liu, M., Radhakrishnan, K., Li, Z. J., Murphy, B., et al. (2011). Reproductive biology of coilia mystus (Linnaeus) from the Yangtze estuary China: Responses to overexploitation. *J. Appl. Ichthyol.* 27, 1197–1202. doi: 10.1111/j.1439-0426.2011.01767.x

Holland, A., Shaughnessy, A. T., and Hiegel, M. H. (1987). Long-term variation in mesohaline Chesapeake bay macrobenthos: Spatial and temporal patterns. *Estuaries* 10, 227–245. doi: 10.2307/1351851

Huang, Y., Huang, Y., Du, X., Li, Y., Tian, J., Chen, Q., et al. (2022). Assessment of macrobenthic community function and ecological quality after reclamation in the changjiang (Yangtze) river estuary wetland. *Acta Oceanolog. Sin.* 41, 96. doi: 10.1007/s13131-022-2046-9

Huang, Y., Li, Y., Chen, Q., Huang, Y., Tian, J., Cai, M., et al. (2021). Effects of reclamation methods and habitats on macrobenthic communities and ecological health in estuarine coastal wetlands. *Mar. Pollut. Bull.* 168, 112420. doi: 10.1016/j.marpolbul.2021.112420

Hulathduwa, Y. D., and Brown, K. M. (2006). Relative importance of hydrocarbon pollutants salinity and tidal height in colonization of oyster reefs. *Mar. Environ. Res.* 62, 301–314. doi: 10.1016/j.marenvres.2006.04.069

Jin, C.-H., Zhu, J.-Q., Xu, S.-J., and Wang, W. (2011). Study on the embryonic and larval development of phascolosoma esculenta. *Oceanolog. Limnolog. Sin.* 1, 014. doi: 10.1007/s13131-011-0129-0

Kirwan, M. L., and Megonigal, J. P. (2013). Tidal wetland stability in the face of human impacts and sea-level rise. *Nature* 504, 53. doi: 10.1038/nature12856

La Peyre, M., Furlong, J., Brown, L. A., Piazza, B. P., and Brown, K. (2014). Oyster reef restoration in the northern gulf of Mexico: Extent methods and outcomes. *Ocean. Coast. Manage.* 89, 20–28. doi: 10.1016/j.ocecoaman.2013.12.002

Li, H., Bao, Y., Hu, Z., and Ge, B. (2007). Seasonal dynamics of macrobenthic functional groups and trophic levels in the bridge construction zone at the south bank of hangzhou bay China. *J. Zool.* 6, 1011–1023. doi: 10.1016/S1005-8885(07)60162-9

Li, X., Cai, L., Zhuo, Y., Guo, T., Rao, Y., Yan, L., et al. (2014). Functional groups of macrofauna in xunpu intertidal zone quanzhou bay. *Mar. Sci. Bull.* 33, 497–504. doi: 10.1007/s11434-013-0074-8

Li, S., Liu, Y., Li, F., Zhang, Y., Xu, Z., Lü, Z., et al. (2013). Macrobenthic functional groups in laizhou bay East China. *Chin. J. Ecol.* 32, 380–388. doi: 10.13292/j.1000-4890.2013.0143

Liu, Z., Chen, M., Li, Y., Huang, Y., Fan, B., Lv, W., et al. (2018a). Different effects of reclamation methods on macrobenthos community structure in the Yangtze estuary China. *Mar. Pollut. Bull.* 127, 429–436. doi: 10.1016/j.marpolbul.2017.12.038

Liu, Z., Fan, B., Huang, Y., Yu, P., Li, Y., Chen, M., et al. (2019). Assessing the ecological health of the chongming dongtan nature reserve China using different benthic biotic indices. *Mar. Pollut. Bull.* 146, 76–84. doi: 10.1016/j.marpolbul.2019.06.006

Liu, K., Lin, H., He, X., Huang, Y., Lin, J., Mu, J., et al. (2016a). Functional feeding groups of macrozoobenthos and their relationships to environmental factors in xiamen coastal waters. *Haiyang. Xuebao.* 38, 95–105. doi: : 10.3969/j.issn.0253-4193.2016.12.010

Liu, Z., Lv, W., Huang, Y., Fan, B., Li, Y., and Zhao, Y. (2016b). Effects of cadmium on lipid metabolism in female estuarine crab chiromantes dehaani. *Comp. Biochem. Physiol. Part C.: Toxicol. Pharmacol.* 188, 9–16. doi: 10.1016/j.cbpc.2016.06.002

Liu, Z., Yu, P., Chen, M., Cai, M., Fan, B., Lv, W., et al. (2018b). Macrobenthic community characteristics and ecological health of a constructed intertidal oyster reef in the Yangtze estuary China. *Mar. Pollut. Bull.* 135, 95–104. doi: 10.1016/j.marpolbul.2018.07.019

Lotze, H. K., Lenihan, H. S., Bourque, B. J., Bradbury, R. H., Cooke, R. G., Kay, M. C., et al. (2006). Depletion degradation and recovery potential of estuaries and coastal seas. *Science* 312, 1806–1809. doi: 10.1126/science.1128035

Lv, W., Huang, Y., Liu, Z., Yang, Y., Fan, B., and Zhao, Y. (2016a). Application of macrobenthic diversity to estimate ecological health of artificial oyster reef in Yangtze estuary China. *Mar. Pollut. Bull.* 103, 137–143. doi: 10.1016/j.marpolbul.2015.12.029

Lv, W., Liu, Z., Yang, Y., Huang, Y., Fan, B., Jiang, Q., et al. (2016b). Loss and self-restoration of macrobenthic diversity in reclamation habitats of estuarine islands in Yangtze estuary China. *Mar. Pollut. Bull.* 103, 128–136. doi: 10.1016/j.marpolbul.2015.12.030

Lv, W., Ma, C., Yu, J., Tian, W., Yuan, X., and zhao, Y. (2013). Macrobenthic functional groups at the reclamation and natural tidal flats of hengsha East shoal the estuary of changjiang river. *Acta Ecolog. Sin.* 33, 6825–6833. doi: 10.5846/stxb201207100969

Lv, W., Zhou, W., and Zhao, Y. (2018). Macrobenthos functional groups as indicators of ecological restoration in reclaimed intertidal wetlands of china's Yangtze estuary. *Regional. Stud. Mar. Sci.* 22, 93–100. doi: 10.1016/j.rsma.2018.06.003

Peng, S., Zhou, R., Qin, X., Shi, H., and Ding, D. (2013). Application of macrobenthos functional groups to estimate the ecosystem health in a semi-enclosed bay. *Mar. Pollut. Bull.* 74, 302–310. doi: 10.1016/j.marpolbul.2013.06.037

Quan, W., Humphries, A. T., Shen, X., and Chen, Y. (2012). Oyster and associated benthic macrofaunal development on a created intertidal oyster (Crassostrea ariakensis) reef in the Yangtze river estuary China. *J. Shellfish. Res.* 31, 599–610. doi: 10.2983/035.031.0302

Quan, W.-M., Zhang, J.-P., Ping, X.-Y., Shi, L.-Y., Li, P.-J., and Chen, Y.-Q. (2007). Purification function and ecological services value of crassostrea sp. in Yangtze river estuary. *Ying. yong. sheng. tai. xue. bao. = J. Appl. Ecol.* 18, 871–876.

Quan, W.-m., Zhu, J.-x., Ni, Y., Shi, L.-y., and Chen, Y.-q. (2009). Faunal utilization of constructed intertidal oyster (Crassostrea rivularis) reef in the Yangtze river estuary China. *Ecol. Eng.* 35, 1466–1475. doi: 10.1016/j.ecoleng.2009.06.001

Thomsen, M. S., Silliman, B. R., and McGlathery, K. J. (2007). Spatial variation in recruitment of native and invasive sessile species onto oyster reefs in a temperate soft-bottom lagoon. *Estuar. Coast. Shelf. Sci.* 72, 89–101. doi: 10.1016/j.ecss.2006.10.004

Walles, B., Troost, K., van den Ende, D., Nieuwhof, S., Smaal, A. C., and Ysebaert, T. (2016). From artificial structures to self-sustaining oyster reefs. *J. Sea. Res.* 108, 1–9. doi: 10.1016/j.seares.2015.11.007

Xu, Z. (2015). *Preliminary study of functional groups and ecological study of macrofauna in jiaozhou bay* (Ocean University of China).

Xu, P., Peng, G., Su, L., Gao, Y., Gao, L., and Li, D. (2018). Microplastic risk assessment in surface waters: A case study in the changjiang estuary China. *Mar. Pollut. Bull.* 133, 647–654. doi: 10.1016/j.marpolbul.2018.06.020

Xu, H., and Zhao, Y. (2005). *Scientific survey on chongming dongtan migratory birds nature reserve of shanghai* (Beijing: China Forestry Publishing House), 2–24.

Yang, W., Li, X., Sun, T., Pei, J., and Li, M. (2017). Macrobenthos functional groups as indicators of ecological restoration in the northern part of china's yellow river delta wetlands. *Ecol. Indic.* 82, 381–391. doi: 10.1016/j.ecolind.2017.06.057

Ye, J.-s. (2010). Biological characteristics of neanthes japonica and their application in shrimp aquaculture. *J. Anhui. Agric. Sci.* 15, 069. doi: 10.13989/j.cnki.0517-6611.2010.15.164

Yuan, X., Lu, J., and Liu, H. (2002). Distribution pattern and variation in the functional groups of zoobenthos in the changjiang estuary. *Acta Ecolog. Sin.* 22, 2054–2062. doi: 10.5846/stxb201607011353

Yu, P., Liu, Z., Wu, D., Chen, M., Lv, W., and Zhao, Y. (2018). Accumulation of polystyrene microplastics in juvenile eriocheir sinensis and oxidative stress effects in the liver. *Aquat. Toxicol.* 200, 28–36. doi: 10.1016/j.aquatox.2018.04.015

Zhang, S., He, X., Wang, J., Lin, H., Huang, Y., Lin, J., et al. (2017). Characteristics of the benthic crustacean community structures and functional groups around the luoyang estuary in fujian. *Acta Ecolog. Sin.* 37, 5961–5972.

Zhang, T., Tian, B., Bo, S., Yuan, L., Zhao, Y., and Yuan, X. (2018). Mapping the conservation priority of migratory shorebird habitat on a dynamic deltaic coast. *Estuar. Coast. Shelf. Sci.* 212, 219–232. doi: 10.1016/j.ecss.2018.07.010

Zheng, G., and Fan, B. (1986). Ecological studees on perinereis aibuhitensis grube in ma yi isjand of zhoushan archipelago. *J. Zhejiang. Ocean. Univ.* 1, 009.

Zhu, X., and Lu, J. (2003). Functional groups of zoobenthos in the intertidal zone of jiuduansha the Yangtze river estuary. *Zool. Res.* 24, 355–361.

Zhuo, Y., Cai, L., Tao, G., Sujing, F., Xinwei, C., and Chen, W. (2014). Temporal and spatial variation of macrobenthic communities in the intertidal zone of xunpu quanzhou bay. *Acta Ecolog. Sin.* 34, 1244–1252. doi: 10.5846/stxb201210191456

frontiers | Frontiers in Marine Science

TYPE Original Research
PUBLISHED 16 January 2023
DOI 10.3389/fmars.2022.1086775

OPEN ACCESS

EDITED BY
Qiang He,
Fudan University, China

REVIEWED BY
Junlin Ren,
Fudan University, China
Ivan Sekovski,
Priority Actions Programme/Regional Activity Centre (PAP/RAC), Croatia

*CORRESPONDENCE
Ling Cao
caoling@sjtu.edu.cn

SPECIALTY SECTION
This article was submitted to Coastal Ocean Processes, a section of the journal Frontiers in Marine Science

RECEIVED 01 November 2022
ACCEPTED 20 December 2022
PUBLISHED 16 January 2023

CITATION
Cheng S, Zeng X, Wang Z, Zeng C and Cao L (2023) Spatiotemporal variations of tidal flat landscape patterns and driving forces in the Yangtze River Delta, China.
Front. Mar. Sci. 9:1086775.
doi: 10.3389/fmars.2022.1086775

Spatiotemporal variations of tidal flat landscape patterns and driving forces in the Yangtze River Delta, China

Shuo Cheng, Xu Zeng, Zihan Wang, Cong Zeng and Ling Cao*

School of Oceanography, Shanghai Jiao Tong University, Shanghai, China

As a crucial coastal wetland habitat in the transition zone between land and sea, global tidal flats have severely declined by 16% over the last two decades under the dual threats of intense human activities and climate change. The Yangtze River Delta of China, the largest estuary in the western Pacific Ocean, has abundant mudflat resources and a dense human population. It also has some of the most prominent conflicts between economic development and ecological conservation. The current lack of understanding of landscape patterns and influencing factors of the Yangtze River Delta mudflats has severely hampered the region's ecological conservation and restoration efforts. Based on Landsat time-series images, this study generated a 30-m spatial resolution map of mudflats in the Yangtze River Delta, which shrank by 47% during 1990–2020, with a higher density of mudflat loss in Yancheng and Nantong cities of the Jiangsu province and Hangzhou, Shaoxing, and Ningbo cities of the Zhejiang province. Landscape indices, such as the patch density of tidal flats, have gradually changed since 2000, with most of them showing significant changes in 2010. Mudflats in Lianyungang, northwestern Yancheng, Nanhui, Jiaxing, and Hangzhou showed sharp negative changes in landscape characteristics. Natural and anthropogenic factors had synergistic effects on the above changes in mudflat landscape patterns in the Yangtze River Delta. Mudflat landscape features were mainly influenced by population growth, economic development, reclamation, sediment discharge, and air temperature. Based on the evolving characteristics of mudflat landscape patterns, we recommend improving mudflat landscape management and planning by strengthening mudflat policies, laws, and regulations, developing countermeasures against threats from major stressors, and enhancing the effectiveness of nature reserves for mudflat protection.

KEYWORDS

intertidal zone, mudflats, Yangtze River Delta, landscape dynamics, protected areas

1 Introduction

Coastal wetlands, including coastal vegetation areas and tidal flats, are transition zones between marine and terrestrial ecosystems (Wang et al., 2020; Song et al., 2021). Tidal flats are an essential part of highly productive coastal zones, which contain abundant mineral, biological, and marine resources (Hill et al., 2021). They provide essential biodiversity maintenance services, serving as energy supply stations for water birds and spawning and nursery grounds for fish and invertebrates (Murray et al., 2014; Ghosh et al., 2016; Jackson et al., 2021). Meanwhile, tidal flats also play an essential role in storm protection, shoreline stabilization, nutrient cycling, as well as carbon storage and sequestration (Barbier et al., 2011; Spalding et al., 2014; Jin et al., 2017; Li et al., 2020b; Lin et al., 2020). However, tidal flats are one of the most vulnerable ecosystems along the coast, under intense pressure from human interference and natural disturbances (Rodriguez et al., 2017; Murray et al., 2022). A worldwide crisis of tidal flat degradation has taken place, with tidal flats falling by 16% globally over the past 20 years (Murray et al., 2019; Lin et al., 2020). Understanding the spatial and temporal changes in tidal landscapes and their drivers is critical for tidal flat conservation (Zahran et al., 2006; Ma et al., 2014; Larson, 2015).

With their dynamic processes, tidal flats are relatively independent ecosystems, but they also depend on surrounding landscapes for the exchange of materials and energy (Mitsch, 1994). Patterns of tidal landscapes refer to the quantity, attributes, geospatial distribution, type conversion, and connectivity of tidal resources, and are related to the resistance to disturbance, resilience, stability, and biodiversity of tidal ecosystems (Zhang et al., 2017; Yang et al., 2021; Zhang et al., 2021). The landscape pattern of tidal flats is constantly changing and evolving. As the expression of dynamic changes in tidal flats, landscape pattern evolution is a comprehensive spatial representation, indicating not only the changing extent of tidal flats and changes in landscape types but also changes in their evolutionary rates and ecological functions (Kahara et al., 2009; Bai et al., 2013). The landscape pattern evolution of tidal flats reflects a combination of different ecological progress and human activities acting upon the tidal flats (Cao, 2008; Huang et al., 2012). Thus, landscape pattern analysis can help understand the rules and mechanisms needed for the conservation of tidal flats.

On the southeastern coast of China, the Yangtze River Delta (YRD) is an ecologically important area with extensive tidal flats (Han and Ma, 2021; Zhang et al., 2022). The YRD is also one of China's most developed regions, subjected to rapid urbanization and stressed by human activities (Du et al., 2016; Sun et al., 2016). The YRD is, therefore, essential for the sustainable development of regional ecology and economics. Tidal flats in the YRD are crucial for biodiversity conservation, acting as critical habitats for birds migrating between East Asia and Australia (Jackson et al., 2021). However, due to a combination of natural environmental succession and human activities, the tidal flats in the YRD have experienced a noticeable degradation (Wang et al., 2021b). Given the YRD's strategic position in China, tracking landscape dynamics and identifying the corresponding drivers of tidal flat changes are of great importance for the conservation of tidal flats and the sustainability of coastal development.

Changes in tidal flats and their driving factors have received increasing attention in recent years (Chen et al., 2016; Li et al., 2020b; Wang et al., 2021b). Globally, the distribution and trajectory of tidal flats have been mapped using satellite images and machine-learning technology (Murray et al., 2019). The drivers of tidal flats dynamics mainly include anthropogenic disturbance through coastal development projects (e.g., road construction), which leads to tidal flat degradation and reduction of biodiversity (Reimer et al., 2015). Within China, reclamation of coastal wetlands for urban construction and agriculture in the Yellow River Delta has been shown to have destructive effects on coastal ecosystems (Murray et al., 2014). Over the past three decades, the driving forces of tidal flat evolution have included factors such as river sand transport and afforestation (Wang et al., 2021b). Studies focusing on the YRD examined the trend of tidal flats in the Yangtze estuary and their extent and classification, and also assessed the potential impacts of various estuarine projects such as land reclamation and sedimentation on mudflats (Chen et al., 2016; Zhang et al., 2019; Li et al., 2020b). It concluded that land reclamation and coastal development were the major drivers of tidal flat loss in the YRD (Wang et al., 2020). However, few studies have examined the landscape pattern dynamics of the YRD tidal flats, implying a lack of information on variations of the tidal flats' landscape patterns and their causal responses to driving factors. By analyzing the landscape patterns of the tidal flats and their drivers over time, we can gain insight into the environment of the YRD and how to develop guidelines for protecting and assessing tidal flats.

In this study, we combined the latest remote sensing and ecological datasets, integrating remote sensing (RS), geographic information system (GIS), landscape dynamic analysis, landscape pattern metrics, and mathematical statistics, in an attempt to (1) determine the distribution of tidal flats between 1990 and 2020 by remote sensing cloud computing; (2) investigate the evolutionary processes of landscape patterns of the YRD tidal flats and quantitatively identify the drivers. Our research aims to improve our understanding of the landscape patterns of tidal flats and explore possible pathways for improved conservation measures that will ultimately help achieve sustainable development in the YRD region.

2 Materials and methods

2.1 Study area

This study determined the geographic location of coastal tidal flats based on existing definitions of tidal flats (Murray et al., 2019; Zhang et al., 2019; Wang et al., 2020). In accordance with the concept of intertidal zones as stated in the *Comprehensive Survey of China's Coastal Zones and Tideland Resources*, and considering the topography and coastal type of the YRD, we delineated a remote sensing monitoring area for the coastal tidal flats as the zone extending 10 km from land to sea, from using the Open Street Map (OSM) as a benchmark (29°N–35°N, 119°E–23°E) (Figure 1). Hangzhou Bay is the natural line of distinction between the northern and southern coastal wetlands of China (Sun et al., 2016; Zhang et al., 2019). Therefore, the boundary of this study extended from Hangzhou Bay of Zhejiang Province to Lianyungang in Jiangsu Province, where tidal flats are abundant, and most coast types are silty. This study area is the most rapidly urbanizing region in China, accompanied by rapid population growth and economic development (Haas and Ban, 2014). An estimated 225 million people reside in the YRD region, contributing about one-quarter of China's GDP (Wei, 2020). Industrialization in the YRD has progressed rapidly over the past two decades, and the development of the maritime industry in particular has made the region the largest and fastest location for port construction in China (Zhao et al., 2021; Lu et al., 2022). Thus, the study area represents a focal area of global change and human activities.

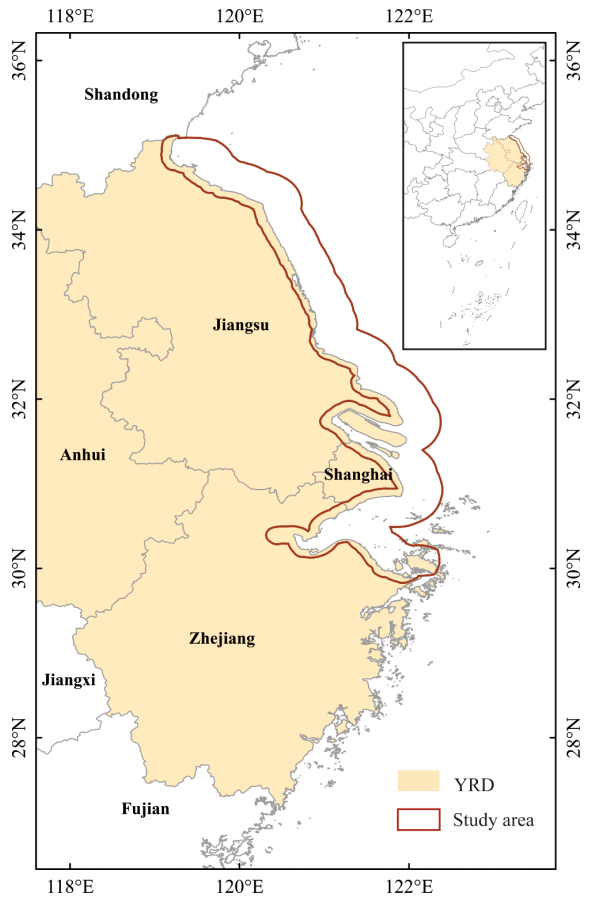

FIGURE 1
Geographical location map of the study area. YRD: Yangtze River Delta, including Shanghai, Jiangsu, Zhejiang, and Anhui provinces.

2.2 Tidal flat mapping

This study used remote sensing images generated by the Google Earth Engine (GEE) (https://earthengine.google.com) cloud computing platform to map the YRD tidal flats. For remote sensing mapping of the tidal flats in the target years (1990, 2000, 2010, and 2020), we selected time-series images for each target year and the year before and after it. Landsat TM/ETM+/OLI images were first retrieved and then pre-processed for cloud removal, shadow masking, and mosaicking through the GEE algorithm. The cloud removal was performed using the mask function (FMask), and the recognition results were recorded in the QA band (Foga et al., 2017). Along with spectral information from remote sensing images, NDVI, EVI, LSWI, mNDWI, and ETOPO1 topographic bathymetry data were selected as signature variables in this study, while supervised classification was performed using the Random Forest algorithm on the GEE platform (Pal, 2005).

Based on the historical images from Google Earth Pro, random samples for supervised classification were derived by visual interpretation. We classified the study area following a review of the Guidelines for the *Classification of Land Use for Land Use Spatial Survey, Planning, and Use Control* as well as the available studies (Fan et al., 2013; Murray et al., 2019; Zhang et al., 2019; Wang et al., 2020). In total, there were five categories identified in this study: tidal flats (**TF**), seawater (**SW**), coastal vegetation zones (**CV**), farmland and forestry land (**FL**), and construction land (**CL**). For the final map of coastal tidal flats, the supervised classification results were post-processed according to spatial topological relationships. We first filtered the classification results using plural filtering and then smoothed out the irregular edges by boundary cleaning. Due to spectral overlap, there was a mixed classification of tidal flats and other feature types. Consequently, patches that were incorrectly categorized as not conforming to the spatial distribution of tidal flats were removed (e.g., patches located within the artificial shoreline). We applied overall accuracy (OA) and Kappa coefficient (K) in the confusion matrix for classification accuracy assessment in GEE (Lewis and Brown, 2001). OA refers to the ratio between the number of correctly classified pixels and the total number of pixels. K reflects the confusion matrix

balance, which is generally used in consistency tests and contributes to overall classification accuracy (Cohen, 1960).

2.3 Kernel density analysis

To investigate the overall spatial pattern of tidal flat landscapes in the YRD, kernel density analysis was used to represent the evolution of tidal flat landscapes over time. Based on kernel density estimation (KDE), the kernel density analysis assumes that geographical events can occur anywhere in space with varying probabilities (Seaman and Powell, 1996). Points with dense clusters have a higher probability of events than those with sparse clusters (Bonnier et al., 2019). Tidal flats have been experiencing constant variation in their spatial pattern in the YRD for many decades. In addition to changing in size, distribution characteristics of tidal flats landscape may also have changed. The formula for Kernel density calculation is as follows:

$$f_n(x) = \frac{1}{nh}\sum_{i=1}^{n} K\left(\frac{X - X_i}{h}\right) \quad (1)$$

where $f_n(x)$ is the estimated value of kernel density for tidal flat evolution, n is the observation numbers, k is the kernel function, X–X_i is the distance from the estimated point to the sample position, and h is the smoothing parameter. In this study, spatial distribution information on changes of the tidal flat area between 1990 and 2020 was first obtained by overlaying tidal flat maps. Next, kernel density in ArcGIS was used to estimate the nuclear density of the tidal flat change for each point, using patch area as a weighting metric. In addition, the KDE result was graded according to Jenks' (natural breaks) method to determine the three classes of loss and gain for tidal flats (Jiang et al., 2018; Yuan et al., 2019).

2.4 Landscape transfer matrix

A transfer matrix describes the changes in different landscape types within a certain period, which reveals the rules of landscape pattern evolution (Foody, 2002). In this study, the transfer matrix was applied to clarify the quantity of shifts between tidal flats and other landscape types at each phase. The formula for the transfer matrix is:

$$p_{ij}\begin{bmatrix} p_{11} & p_{12} & \cdots & p_{1n} \\ p_{21} & p_{22} & \cdots & p_{2n} \\ \vdots & \vdots & \vdots & \vdots \\ p_{n1} & p_{n2} & \cdots & p_{nn} \end{bmatrix} \quad (2)$$

Where P_{ij} is the area of each land use type, i and j represent the types of landscapes before and after the transfer, respectively, and n is the total number of landscape types before and after the transformation. We used the transfer matrix to reveal the outflow and inflow of the YRD tidal flat area.

2.5 Landscape index calculation

Landscape index changes have been commonly used to analyze the dynamic evolution of landscape patterns (Chen et al., 2022). A landscape index is the result of highly concentrated information about landscape patterns. In addition, a landscape pattern index has important ecological significance since it specifies the characteristics of ecosystem landscape elements. Different sizes, shapes, types, numbers, and spatial configurations of landscape elements reflect the quality of landscape functions and ecological processes throughout the region. Tidal flats in the study area were studied using landscape indices selected from the classes at the YRD to quantify the variation process and characterize the functions of the tidal flat system. The following seven landscape pattern indices were selected for this study: largest patch index (**LPI**), patch density (**PD**), mean patch area distribution (**MPS**), mean shape index (**SHAPE_MN**), area-weighted mean patch fractal dimension (**FRAC_AM**), patch cohesion index (**COHESION**), and splitting index (**SPLIT**) (Table S1). The LPI values indicate the abundance of tidal flats across the entire landscape. PD values represent the density of tidal flat patches and reflect the heterogeneity of the landscape within a unit area. MPS reflects the average condition of the tidal flats patch. The SHAPE_MN is an indication of the complexity of the tidal flat landscape. Because they express the influence of human activities on a landscape pattern, the FRAC_AM values of natural landscapes with less interference are higher than the values for disturbed landscapes (Li et al., 2020a). COHESION refers to the connectivity between tidal flats within a YRD, while SPLIT represents the degree of separation.

2.6 Driving factor analysis

Both anthropogenic and natural factors can drive tidal flat variations. Tidal flats are often considered potential areas for urban development. Therefore, urban development activities like reclamation significantly affect tidal flats (Jackson et al., 2021). There has been a substantial economic benefit to the region from aquaculture, which also occupies tidal flats (Ma et al., 2014). Factors such as population and GDP are also closely associated with the development of tidal flats (Murray et al., 2014; Wang et al., 2021b). Likewise, natural factors play an important role in influencing tidal flat landscapes. Tidal flats are formed and changed primarily by sediment carried by incoming rivers, so sediment plays a crucial role in their evolution (Bi et al., 2014; Chen et al., 2016). There is also evidence that sea-level rise has a significant effect on tidal flats (Zhao et al., 2020). Temperature and precipitation also have an impact on the landscape patterns

of tidal flats (Wang et al., 2021b). A total of eight potential factors were selected to analyze the evolution of YRD's tidal flat landscape: population (**POP**), gross domestic product (**GDP**), urban area (**UA**), aquaculture area (**ACA**), sediment discharge (**Sediment**), sea-level rate (**SL**), annual precipitation (**Prcp**), and annual average air temperature (**Tavg**) (Table S2).

To investigate the motives for tidal flat evolution, landscape pattern characteristics of the flats were associated with potential driving factors using correlation analysis. Correlation coefficients were used to investigate the extent and direction of each influencing factor that drove tidal flat dynamics (Humphreys et al., 2019). Further analysis of the driving factors influencing tidal flat landscape patterns was conducted using principal component analysis (PCA). In principal component analysis (PCA), multiple indices are merged into one composite index, or several comprehensive indices are constructed to reduce the dimensionality of a large dataset. To concentrate on potential drivers of tidal flat dynamics, redundant variables (closely related variables) can be eliminated in PCA. For this study, principal components were selected based on the eigenvalue being greater than one and the cumulative contribution rate exceeding 85% (Fang et al., 2017).

3 Results

Following classification and post-processing, maps of YRD coastal tidal flats were produced at 30 m resolution for four different time periods: 1990, 2000, 2010, and 2020 (Figure 2). We evaluated tidal flat mapping results in the YRD using the OA and K. The study showed that the average OA was 94.40%, and the average K was 0.93. In 1990, 2000, 2010, and 2020, the OA was 96.75%, 96.21%, 92.35% and 92.27%, with K of 0.96, 0.95, 0.90, and 0.90, respectively.

3.1 Characteristics of spatial pattern dynamics

Area changes of the YRD tidal flats are illustrated in Figure 3. The YRD's tidal flats have decreased significantly over the past three decades, from 4231 km^2 in 1990 to 2236 km^2 in 2020, a 47% reduction (Figure 3A). During the period 1990 to 2000, the area of tidal flats decreased by 24%. This was the most dramatic decline during the study period, with an average annual decrease of 100 km^2. Since then, the Chinese government has enacted more management measures and nature reserves to protect coastal wetlands. Therefore, tidal flat loss in the YRD slowed down over the next decade, decreasing by 439 km^2. In the period 2010 to 2020, the YRD lost 20% of its tidal flats. Based on the KDE results, tidal flats change zones were classified into three levels (class I, class II, and class III). The two classes with high tidal flat loss in the YRD, classes II and III, occurred mainly in Yancheng and Nantong of Jiangsu, but also in Hangzhou, Shaoxing, and Ningbo in Zhejiang, along with sporadic distribution in Shanghai (Figure 3B). The map of the kernel density distribution of tidal flat gains shows that classes II and III with high density occurred mainly in the radial sand ridges of Yancheng in Jiangsu and of Jiuduansha and Nanhui in Shanghai, with scattered occurrence in Zhejiang (Figure 3C). There was a more significant loss of tidal flats in the YRD than a gain. The regions with a high kernel density of tidal flat loss had a greater geographic spread than regions with low kernel density.

Inflows and turnovers of tidal flats from 1990 to 2020 were examined using the landscape transfer matrix (Figure 4). Tidal flat influx increased and then decreased from 1990 to 2020. Over the first three periods (1990, 2000, and 2010), seawater replenishment of tidal flats accounted for 94.54%, 97.83%, and 95.52%, respectively, of the total inflow to tidal flats. Seawater was the major outflow from tidal flats. As an overall result of conversions

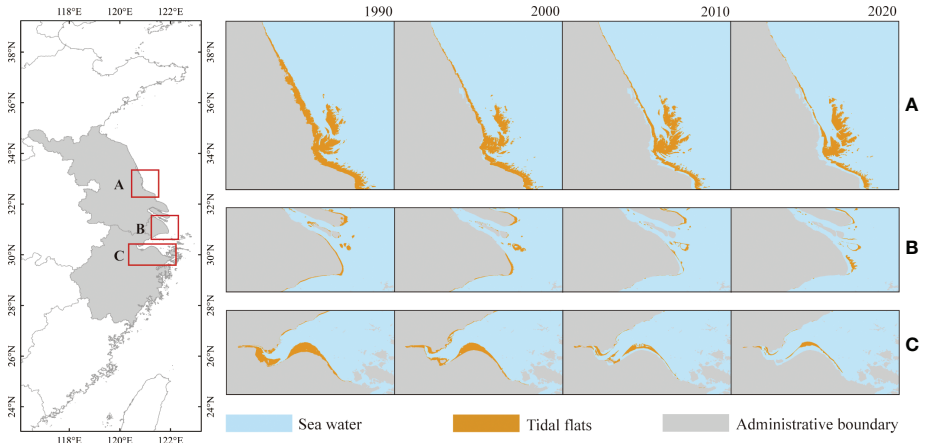

FIGURE 2
Tidal flat maps for the Yangtze River Delta in the years 1990, 2000, 2010, and 2020. **(A)** Detection of tidal flats in Jiangsu (32 °15′N~34 °15′N, 120 °15′E~121 v45′E). **(B)** Detection of tidal flats in Shanghai (29 °55′N~30 °50′N, 120°30′E~122 °00′E). **(C)** Detection of tidal flats in Zhejiang (30 °40′N~31 °40′N, 121°15′E~122 °15′E).

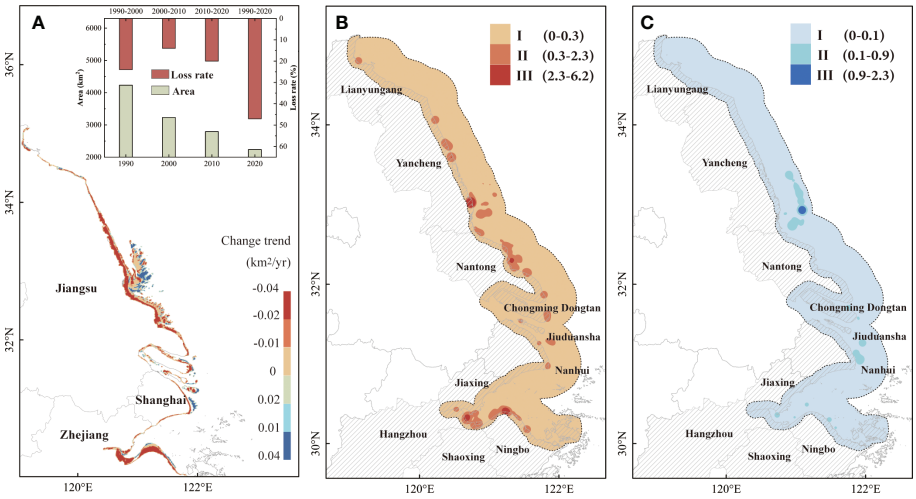

FIGURE 3
Distribution of tidal flat dynamics in the study area. **(A)** Tidal flat area changes. **(B)** Kernel density analysis of tidal flat losses from 1990 to 2000. **(C)** Kernel density analysis of tidal flat gains from 1990 to 2000.

between seawater areas and tidal flats, the tidal flat area increased by 91 km^2 between 1990 and 2020. Tidal flats were largely outflowing during the study period due to urban construction, which was the main cause of the decrease in tidal flat area. There was a notable conversion of tidal flats to construction land in 1990 and 2000, with 593 km^2 and 693 km^2 of tidal flats being converted to construction land, respectively. After 2010, comprehensive environmental regulations and laws were enacted, and reclamation projects were tightened (Chen et al., 2016; Zhao et al., 2020; Wang et al., 2021b). The National Marine Function Zoning Plan (2011-2020) published in 2012 strengthened reclamation management and rationalized the reclamation scale (Liu et al., 2018). Therefore, the conversion from tidal flats to construction land moderated slightly after 2010. The conversion between tidal flats and construction land accounted for 66% of the area decrease of tidal flats throughout the study period. The conversion of tidal flats to coastal vegetation zones, farmland, and forests did not show significant changes from 1990 to 2020. The loss of tidal flat area has partly been attributed to the conversion of tidal flats to coastal vegetation zones (16.62%) and the conversion of tidal flats to farmlands and forests (9.51%).

3.2 Characteristics of landscape morphology changes

The landscape metrics at the class level for the YRD tidal flats have changed over the last three decades (Figure 5). Tidal

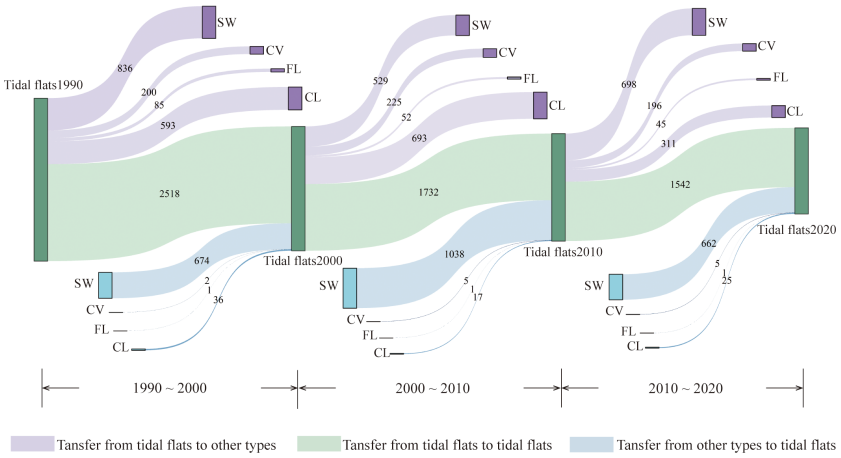

FIGURE 4
Sankey diagram of tidal flat conversion in the Yangtze River Delta (km^2) (SW, seawater; CV, coastal vegetation zones; FL, farmland and forestry land; CL, construction land).

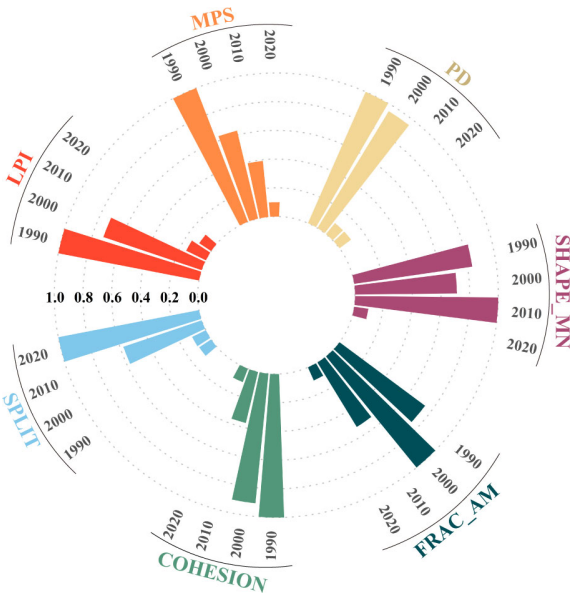

FIGURE 5
Landscape characteristics (normalized) of tidal flats from 1990 to 2020 (LPI, largest patch index; PD, patch density; MPS, mean patch area distribution; SHAPE_MN, mean shape index; FRAC_AM, area-weighted mean patch fractal dimension; COHESION, patch cohesion index; SPLIT, splitting index).

flat dominance was indicated by the LPI values for the entire landscape, whereas the LPI values for the YRD tidal flats have decreased over the past thirty years. In particular, the LPI value decreased dramatically (from 0.72 to 0.1) after 2000. The MPS value declined steadily between 1990 and 2020, reflecting the average interannual degradation conditions for the YRD tidal flats. According to the falling PD values of the YRD, tidal flats of the unit area decreased by 0.86 following the year 2000. The decrease in MPS and PD values indicated a fragmentation of the tidal flat patches. There was a slight fluctuation in the SHAPE_MN value between 1990 and 2010, then it decreased during the last decade. The fluctuation in SHAPE_MN suggested that the shape of the tidal flats was constantly changing. As reflected by FRAC_AM indexes that increased and then dramatically decreased, the tidal flats were unstable and susceptible to human activity. The SPLIT value rose 0.89 during the period 2000–2020, denoting that the spatial dispersion of the tidal flats intensified. COHESION decreased by 0.81 simultaneously, showing that the physical connectivity of tidal flat patches in the YRD decreased.

Based on the landscape index for 2020 (Figure 6), it was clear that the distribution characteristics differed spatially. Tidal flats with high LPI and MPS values can be found mainly in southeast Yancheng and northwest Nantong of Jiangsu, clustered here with high patch densities. The mean patch areas were also high among the tidal flats of Shaoxing and Ningbo in Zhejiang. However, the tidal flats in Lianyungang and northwest Yancheng were even more fragmented, with low LPI, MPS, and PD values. Ningbo's eastern region has the highest SHANPE_MN value, showing a relatively complex shape for tidal flats. Tidal flats in Lianyungang and northwest Yancheng showed low COHESION and FRAC_AM values and high SPLIT values, indicating poor spatial connectivity and a high degree of disturbance and dispersal. The southeast Yancheng and the northwest Nantong had a few scattered patches of tidal flats with good physical connectivity, which were high in COHESION values and low in SPLIT values. In Zhejiang province, Jiaxing, and Hangzhou cities had low LPI values, low COHESION values, and high SPLIT values. These results indicated low dominance of tidal flats, as well as a scattered distribution and poor connectivity. Shanghai's tidal flats ranked most frequently in the middle of the landscape index results. Notably, the SPLIT values of the Shanghai tidal flats were high, and LPI and COHESION values were low, particularly in Nanhui, where the tidal flats were widely dispersed and lacked dominance and connectivity.

3.3 Driving factor analysis

Both human and natural factors influenced the YRD's tidal flat landscape (Figure S1). The population of the study area has grown by 37.6% since 1990. The urban area in 2020 has already exceeded ten times that of 1990. As of 2020, the region's GDP was over 20 trillion yuan. With high growth in aquaculture, the aquaculture area in 2000 became 2,034 km^2. There has been a decrease in the annual sediment discharge recorded at the Datong station. The annual precipitation value fluctuated during the study period, with the lowest value in 2010. An upward trend in mean yearly temperature was observable in the study area. The rate of sea level rise in the Yangtze River Delta was as low as 1.4 mm/year in 1990 and peaked at 3.3 mm/year in 2020, with an upward trend.

Relevant analysis was conducted to investigate the correlation between anthropogenic and natural factors affecting tidal flat landscape changes (Figure 7A). The correlations between features of the tidal flat landscape and four human factors ranged from –0.99 to 0.99, whereas the correlations with natural factors ranged from –0.16 to 1. Significant correlations were found between population and four landscape features and between GDP and one landscape characteristic. The UA was significantly relevant to three landscape indices ($p< 0.05$). For natural factors, sediment discharge affected three landscape characteristics positively, with annual precipitation related to one feature and average yearly temperature related to five features ($p< 0.05$). Sediment discharge and mean annual temperature were each significantly related to one tidal flat landscape feature ($p< 0.01$). Based on the PCA analysis, a contribution of 81.12% was attributed to the first principal component, followed by a

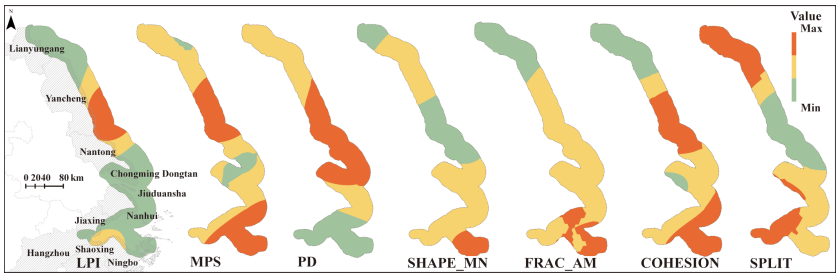

FIGURE 6
Distribution of landscape pattern indexes of tidal flats in 2020 (LPI, largest patch index; PD, patch density; MPS, mean patch area distribution; SHAPE_MN, mean shape index; FRAC_AM, area-weighted mean patch fractal dimension; COHESION, patch cohesion index; SPLIT, splitting index).

contribution of 11.03% (Figure 7B). The driving factors with high load values of the first principal component were, in order, POP, GDP, UA, Tavg, and Sediment.

4 Discussion

The time-series distribution maps of the YRD tidal flats were generated by the random forest algorithm on the GEE platform for four decadal periods from 1990 to 2020. Integrating methods such as KDE, land transfer matrix, landscape index, and correlation analysis were used to examine the evolution of landscape patterns and response factors in the study area. In the YRD, tidal flat area decreased during the study period, along with decreased landscape dominance, intensification of fragmentation, decrease in connectivity, and a more dispersed distribution. Both artificial and natural factors influence the landscape features of tidal flats. Quantifying the changes in the landscape and the factors driving those changes in the YRD tidal flats could provide a reference for further tidal flat conservation and management.

4.1 Reliability and uncertainty of tidal flat mapping

We mapped the tidal flats of the YRD using Landsat images and the GEE platform with a spatial resolution of 30 m. For all four decadal periods between 1990 and 2020, the overall accuracy of the tidal flats maps was greater than 90% and the Kappa coefficients were all greater than 0.9, indicating relatively stable classification accuracy throughout the study period. Further validation was provided by comparing our tidal flat map with published maps with the same spatial resolution. There was a strong correlation between our map of the tidal flats and Murray's research, with R^2 of 0.83 and a slope of 1.22 (Figure S2) (Murray et al., 2019). Regarding the spatial distribution of the two tidal flat maps in 2010, our map corresponded well with Murray's, which was larger in extent and also included parts of supratidal flats. Overall, the tidal flat mapping conducted in this study was accurate and reliable. There are, however, some inaccuracies inherent in the classification of satellite images. Landsat images provide only partial information on the full tidal range, and satellites are usually unable to observe extreme low and high

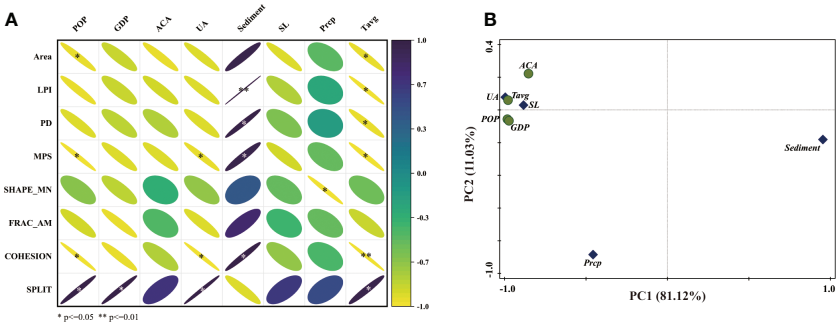

FIGURE 7
Relevant analysis results. **(A)** Correlation coefficient thermodynamic diagram of landscape characteristics of tidal flats and driving factors (* p<=0.05, ** p<=0.01). **(B)** PCA analysis of driving factors on mudflat landscape patterns.

tides (Dhanjal-Adams et al., 2016; Sagar et al., 2017). Remote sensing data with a low spatial resolution may also contribute to lower classification accuracy (Dang et al., 2021). Although the image fusion technique used in our study can improve classification accuracy, the medium resolution (30 m) Landsat images used may exacerbate the mixing of classes with similar spectral characteristics.

4.2 Evolution trends of tidal flats in the YRD

The YRD coast is primarily a silty coast with vast tidal flats. The tidal flats in the YRD decreased continuously during the study period from 1990 to 2020 (Wang et al., 2020). The dramatic reduction in tidal flats in the YRD occurred mainly in two time periods, 1990–2000 and 2010–2020. Geographically, the losses of tidal flats in the YRD were concentrated in Yancheng and Nantong of Jiangsu, as well as in Hangzhou, Shaoxing, and Ningbo of Zhejiang. The high-density areas of tidal flat gains occurred primarily at Radiation Sand Ridge in Yancheng of Jiangsu and in Jiuduansha and Nanhui of Shanghai. It is crucial to manage and protect tidal flats that suffer from frequent dynamics with high kernel density. There was a significant interconversion of seawater and tidal flats due to deposition and erosion (Murray et al., 2015). Throughout the study area, the main reason for the reduction in tide flats was the conversion of tidal flats to construction land. There was also a conversion between coastal vegetated zones and tidal flats. Particularly, the invasion of cordgrass (*Spartina alterniflora*) has had a significant impact on the coastal zone, resulting in changes to tidal flat landscapes (Mao et al., 2019; Jackson et al., 2021). In recent years, *Spartina alterniflora* has invaded and encroached rapidly on tidal flats in Shanghai and Jiangsu (Huang and Zhang, 2007; Zhu et al., 2022). With the implementation of the *Spartina alterniflora* management projects, its threat to mudflats has gradually moderated (Liu et al., 2020). With regard to the morphological characteristics of the tidal flats' landscape, the landscape index changed gradually between 2000 and 2020, with most of the indexes showing significant changes in 2010. According to the results of landscape index analysis, tidal flats in Lianyungang, northwest Yancheng, Nanhui, Jiaxing, and Hangzhou require attention in terms of management and protection.

4.3 Potential driving forces of tidal flat dynamics in the YRD

Characteristics of the tidal flat ecosystem can be directly affected by human activities within a relatively short period. Over the past three decades, the population and economy of the study area have grown rapidly, thereby increasing human–land conflicts. A series of large reclamation projects have been carried out in the YRD since the 1980s, resulting in the loss of vast coastal tidal flats (Ma et al., 2014; Wang et al., 2014; Chen et al., 2016). Through reclamation, the tidal flats were converted into construction land for ports, terminals, transportation, and industry (Zhao et al., 2020). Consequently, the urban area in the YRD expanded significantly between 1990 and 2020. Although offshore aquaculture brings economic benefits to the YRD, it has also resulted in continued encroachment on tidal flats along the coast (Ma et al., 2014). As humans continually transform the land for socioeconomic objectives, substantial ecological impacts occur (Sun et al., 2015). Urban expansion in the YRD may contribute significantly to climate change due to the heat island effect (Yang et al., 2017). Aquaculture may negatively affect regional water quality since it contributes to the eutrophication of water bodies (Li et al., 2021; Wang et al., 2021a). Based on the correlation and PCA analysis, four human factors (i.e., population, GDP, urban area, aquaculture area) were strongly correlated with the characteristics changes of the tidal flat landscape. In response to urbanization, the YRD tidal flats have been shrinking. Urbanization-induced reclamation is the primary cause of the shrinkage. Furthermore, tidal flats have been encroached upon irregularly by human activities, which has adversely affected their original spatial distribution. There has been significant disruption of tidal flats in the YRD due to human activities, resulting in a fragmented, dispersed, and less integrated landscape.

Natural factors have also influenced the development of the YRD's tidal flats. In terms of climatic factors, temperature and precipitation were important variables affecting the YRD tidal flat ecosystem. A warming temperature without increased precipitation will intensify wetland evaporation, reducing the tidal flat area (Harley et al., 2006). Temperatures in the study area increased gradually from 1990 to 2020, while rainfall fluctuated within a small range. There was a significant correlation between tidal flat area and mean annual temperature in the YRD, but no significant correlation with mean annual rainfall. As a region sensitive to global change, the YRD has also experienced sea-level rise due to global warming (Cazenave and Cozannet, 2014; Moftakhari et al., 2017). The coastal seawall defense capacity of the YRD has been reduced by sea-level rise, and coastal erosion has increased, causing tidal flat loss (Gong et al., 2012; Wang et al., 2012; Kuang et al., 2014). Coastal tidal flat development is driven by sediment transportation and accumulation by rivers and tides. Sediment deposition and the hydrodynamic environment contribute to tidal flat dynamics due to "loss and gain" (Dyer et al., 2000; Xing et al., 2012). With increasing evaporation and water engineering projects, sedimentation in the YRD has weakened, leading to a slowdown in coastal tidal flat development (Zhao et al., 2017; Li et al., 2020b). There was a significant correlation between sediment discharge and characteristics of tidal flats in the YRD from 1990 to 2020, indicating that higher sediment discharges

lead to a larger area of tidal flats. Tidal flat morphology and other natural factors, however, had a weak relationship. During the continuous urbanization process, human activities have greatly affected the landscape of the tidal flats (Jiang et al., 2015).

4.4 Recommendations for improving the conservation of the YRD tidal flats

Policies, laws, and regulations provide the basis for the management of tidal flats. Since the 1990s, China has taken a series of measures to manage coastal wetlands, which have played a role in protecting coastal tidal flats (Table S3). The dynamic changes analysis of the tidal flats showed that the reduction of the tidal flats has moderated after 2000. Nonetheless, rapid economic development and the growing reliance of human activities on tidal flats have negatively affected the remaining tidal flats (Jiang et al., 2015; Wei et al., 2015). The YRD tidal flats are still experiencing declines in quantity and landscape quality. Tidal flats are not covered by any national laws or administrative regulations in China. Only local rules are in place. Local government regulations for managing tidal flats are more concerned with resource management than environmental protection. Tidal flats have also been considered a wasteland and the principal source of resource extraction (Zhao et al., 2020). The general public has not yet fully understood the ecological function and value of tidal flats. A strict, science-based, and effective policy, legislative, and regulatory framework will be required for tidal flat protection (Sun et al., 2015). Existing legislation that governs coastal tidal flat management should be improved, and new policies, laws, and regulations should be adopted. Furthermore, local governments should ensure that their policies, laws, and regulations for tidal flat management take into account the ecological environment and need for the protection of tidal flats.

Both natural and human factors have influenced tidal flat landscape evolution. Tidal flat dynamics in the YRD were closely correlated with sediments, temperature, sea level, and human activities. The protection and management of tidal flats can be improved by exploring effective measures to address the main threats. Tidal flats form primarily from sediment carried by rivers into the sea. Due to various evaporation and water engineering projects, sedimentation in the study area decreased, resulting in the loss of tidal flats (Zhao et al., 2017; Li et al., 2020b). Providing artificial silt and sand nourishment can enhance the protection of tidal flats (Deltacommissie, 2008). Sea-level rise has been triggered by rising temperatures, resulting in threats to the integrity and stability of tidal flats (Morris et al., 2002). The YRD should implement a long-term monitoring system and set up an early warning system to prevent damage to tidal flats (Leorri et al., 2013). There are also nature-based solutions for coastal management that can be used to adapt to SLR (Schuerch et al., 2018). Restoration of degraded coastal wetlands is a nature-based solution that can help strengthen coastal protection caused by SLR and associated extreme events (Kim, 2010; Narayan et al., 2016). Besides restoring existing habitats, it is also possible to use hybrid designs, such as natural habitats combined with built infrastructure, providing coastal protection against SLR (Sutton-Grier et al., 2015; Moller, 2019). Human activities such as high intensity development and frequent reclamation have significantly contributed to the loss of tidal flats (Mai and Bartholomä, 2000). The reclamation of tidal flats should be reduced in the future, with a goal of maintaining them within their natural proliferation rate (Hodoki and Murakami, 2006). Moreover, a "red line" could be defined for tidal flats, and reclamation prohibited in the "red line" area to effectively limit the negative impact of human activities on the landscape (Sun et al., 2015).

The establishment of nature reserves may contribute to the conservation of tidal flats (Hill et al., 2021). Nine nature reserves exist in the study area (Figure 8). There were areas within nature reserves with frequent tidal flat dynamics (Zone I) based on KDE results. Landscape index analysis showed a reduction in the tidal flats' integrity, connectivity, and stability between 1990 and 2020. Geographically, it was evident that the landscape index had changed negatively in some regions (Zone II) not covered by nature reserves. Although natural reserves exist, the degradation of their tidal flats cannot be prevented, which may be because natural factors have caused tidal flats to move outside current reserves, or the reserves were unable to effectively manage them (Carranza et al., 2014; Murray et al., 2019). Reserves in the study area are managed by different departments at a local level, leading to conflicting management goals (Dhanjal-Adams et al., 2016; Zeng et al., 2022). It might be possible to consolidate overlapping reserves and manage them under one department. In Jiangsu and Shanghai, the tidal flats would benefit from combining the jurisdictions of their reserves and coordinating the management. In addition, expanding existing reserves could enhance the connectivity and integrity of the landscape within the various

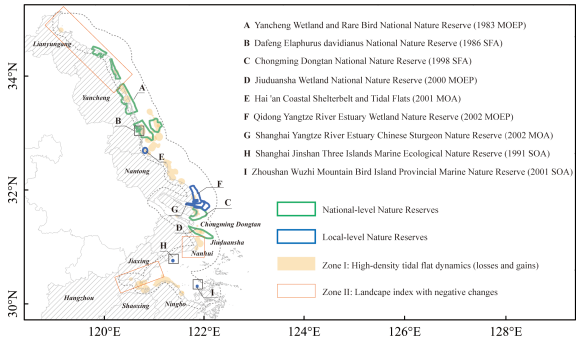

FIGURE 8
Distribution of nature reserves within the study area (Department of Nature Reserves at the local level: MOEP, Ministry of Environmental Protection; SOA, State Oceanic Administration; MOA, Ministry of Agriculture; SFA, State Forestry Administration).

functional zones (Watson et al., 2014). As Yancheng National Reserve extends north-south, it could encompass wetland areas meeting international standards, such as the Ganyu, Dongtai, and Rudong tidal flats (Paulson Institute, 2016). Due to the lack of nature reserves covering tidal flats in Nanhui, Jiaxing, and Hangzhou, new protected areas need to be established to mitigate adverse effects. Finally, nature reserves do not forbid human activities, so their establishment may slow the loss of tidal flats but will not stop it. Consequently, adequate buffer zones should be maintained between human activities and tidal flat protection areas to alleviate anthropogenic impacts.

5 Conclusion

It has been observed that tidal flats in the YRD have been degraded from 1990 to 2020, as evidenced by shrinking size, increased fragmentation and disturbance, as well as reduced dominance and connectivity across the tidal flat landscape. Yancheng and Nantong of Jiangsu, Hangzhou, Shaoxing, Ningbo of Zhejiang, and Jiuduansha and Nanhui of Shanghai were found to have high densities of tidal flat dynamics. It is worth mentioning that Lianyungang, northwestern Yancheng, Nanhui, Jiaxing, and Hangzhou have experienced a considerable negative change in their tidal flat landscape. In the YRD tidal flats, variations in landscape characteristics have been driven by various factors such as population, economy, reclamation, climate change, sea-level rise, and sedimentation. Future actions should include three aspects of tidal flat management and protection: strengthening policies, laws, and regulations related to tidal flat protection, preparing measures to counteract threats to tidal flat landscapes, and improving the efficiency of nature reserves to reduce tidal flat degradation.

Data availability statement

The original contributions presented in the study are included in the article/Supplementary Material. Further inquiries can be directed to the corresponding author.

Author contributions

SC: Conceptualization, Data processing, Writing-original draft. LC: Conceptualization and Supervision. XZ, ZW, CZ, and LC revised and improved the manuscript. All authors contributed to the article and approved the submitted version.

Acknowledgments

We would like to thank the Ministry of Science and Technology of China (2022YFC3102400), National Natural Science Foundation of China (42142018, 42206082), Shanghai Pilot Program for Basic Research-Shanghai Jiao Tong University (21TQ1400220), the Key Laboratory of Marine Ecological Monitoring and Restoration Technologies (MEMRT202112), the Oceanic Interdisciplinary Program of Shanghai Jiao Tong University (SL2021PT101), and Shanghai Frontiers Science Center of Polar Science (SCOPS) for financial support. Any opinions, findings, and conclusions or recommendations expressed in this material are those of the authors and do not necessarily reflect the views of the funders. We thank the editor and reviewers, whose comments would help to improve this manuscript.

Conflict of interest

The authors declare that the research was conducted in the absence of any commercial or financial relationships that could be construed as a potential conflict of interest.

Publisher's note

Author disclaimer

Any opinions, findings, conclusions or recommendations expressed in this material are those of the authors and do not necessarily reflect the views of the funders.

Supplementary material

The Supplementary Material for this article can be found online at: https://www.frontiersin.org/articles/10.3389/fmars.2022.1086775/full#supplementary-material

References

Bai, J. H., Lu, Q. Q., Wang, J. J., Zhao, Q. Q., Ouyang, H., Deng, W., et al. (2013). Landscape pattern evolution processes of alpine wetlands and their driving factors in the zoige plateau of China. *J. Mountain Sci.* 10 (1), 54–67. doi: 10.1007/s11629-013-2572-1

Barbier, E. B., Hacker, S. D., Kennedy, C., Koch, E. W., Stier, A. C., and Silliman, B. R. (2011). The value of estuarine and coastal ecosystem services. *Ecol. Monogr.* 81 (2), 169–193. doi: 10.1890/10-1510.1

Bi, N. S., Wang, H. J., and Yang, Z. S. (2014). Recent changes in the erosion-accretion patterns of the active huanghe (Yellow river) delta lobe caused by human activities. *Continental Shelf Res.* 90, 70–78. doi: 10.1016/j.csr.2014.02.014

Bonnier, A., Finne, M., and Weiberg, E. (2019). Examining land-use through GIS-based kernel density estimation: A re-evaluation of legacy data from the berbati-limnes survey. *J. Field Archaeology* 44 (2), 70–83. doi: 10.1080/00934690.2019.1570481

Cao, X. X. (2008). Dynamics of wetland landscape pattern in Kaifeng City from 1987 to 2002. *Chin. Geographical Sci.* 18 (2), 146–154. doi: 10.1007/s11769-008-0146-x

Carranza, T., Balmford, A., Kapos, V., and Manica, A. (2014). Protected area effectiveness in reducing conversion in a rapidly vanishing ecosystem: The Brazilian cerrado. *Conserv. Lett.* 7 (3), 216–223. doi: 10.1111/conl.12049

Cazenave, A., and Cozannet, G. L. (2014). Sea Level rise and its coastal impacts. *Earths Future* 2 (2), 15–34. doi: 10.1002/2013ef000188

Chen, K. X., Cong, P. F., Qu, L. M., Liang, S. X., and Sun, Z. C. (2022). Annual variation of the landscape pattern in the liao river delta wetland from 1976 to 2020. *Ocean Coast. Manage.* 224. doi: 10.1016/j.ocecoaman.2022.106175

Chen, Y., Dong, J. W., Xiao, X. M., Zhang, M., Tian, B., Zhou, Y. X., et al. (2016). Land claim and loss of tidal flats in the Yangtze estuary. *Sci. Rep.* 6. doi: 10.1038/srep24018

Cohen, J. (1960). A coefficient of agreement for nominal scales. *Educ. Psychol. Measurement* 20 (1), 37–46. doi: 10.1177/001316446002000104

Dang, A. T. N., Kumar, L., Reid, M., and Nguyen, H. (2021). Remote sensing approach for monitoring coastal wetland in the Mekong delta, Vietnam: Change trends and their driving forces. *Remote Sens.* 13 (17), 3359. doi: 10.3390/rs13173359

Deltacommissie (2008) *Working together with water: A living land builds for its future*. Available at: http://resolver.tudelft.nl/uuid:af79991f-31e7-47a4-a6ef-bfd54ca59c57 (Accessed October 29, 2021).

Dhanjal-Adams, K. L., Hanson, J. O., Murray, N. J., Phinn, S. R., Wingate, V. R., Mustin, K., et al. (2016). The distribution and protection of intertidal habitats in Australia. *Emu-Austral Ornithology* 116 (2), 208–214. doi: 10.1071/mu15046

Du, H. Y., Wang, D. D., Wang, Y. Y., Zhao, X. L., Qin, F., Jiang, H., et al. (2016). Influences of land cover types, meteorological conditions, anthropogenic heat and urban area on surface urban heat island in the Yangtze river delta urban agglomeration. *Sci. Total Environ.* 571, 461–470. doi: 10.1016/j.scitotenv.2016.07.012

Dyer, K. R., Christie, M. C., Feates, N., Fennessy, M. J., Pejrup, M., and van der Lee, W. (2000). An investigation into processes influencing the morphodynamics of an intertidal mudflat, the dollard estuary, the Netherlands: I. hydrodynamics and suspended sediment. *Estuar. Coast. Shelf Sci.* 50 (5), 607–625. doi: 10.1006/ecss.1999.0596

Fang, S. B., Jia, R. F., Tu, W. R., and Sun, Z. L. (2017).). assessing factors driving the change of irrigation water-use efficiency in China based on geographical features. *Water* 9 (10), 759. doi: 10.3390/w9100759

Fan, D. D., Wang, Y., and Liu, M. (2013). Classifications, sedimentary features and facies associations of tidal flats. *J. Palaeogeogr.* 2 (1), 66–80. doi: 10.3724/SP.J.1261.2013.00018

Foga, S., Scaramuzza, P. L., Guo, S., Zhu, Z., Dilley, R. D., Beckmann, T., et al. (2017). Cloud detection algorithm comparison and validation for operational landsat data products. *Remote Sens. Environ.* 194, 379–390. doi: 10.1016/j.rse.2017.03.026

Foody, G. M. (2002). Status of land cover classification accuracy assessment. *Remote Sens. Environ.* 80 (1), 185–201. doi: 10.1016/S0034-4257(01)00295-4

Ghosh, S., Mishra, D. R., and Gitelson, A. A. (2016). Long-term monitoring of biophysical characteristics of tidal wetlands in the northern gulf of Mexico - a methodological approach using MODIS. *Remote Sens. Environ.* 173, 39–58. doi: 10.1016/j.rse.2015.11.015

Gong, Z., Zhang, C. K., Wan, L. M., and Zuo, J. C. (2012). Tidal level response to Sea-level rise in the Yangtze estuary. *China Ocean Eng.* 26 (1), 109–122. doi: 10.1007/s13344-012-0008-2

Haas, J., and Ban, Y. F. (2014). Urban growth and environmental impacts in jing-Jin-Ji, the Yangtze, river delta and the pearl river delta. *Int. J. Appl. Earth Observation Geoinformation* 30, 42–55. doi: 10.1016/j.jag.2013.12.012

Han, Z. C., and Ma, H. L. (2021). Adaptability assessment and analysis of temporal and spatial differences of water-Energy-Food system in Yangtze river delta in China. *Sustainability* 13 (24). doi: 10.3390/su132413543

Harley, C. D., Randall Hughes, A., Hultgren, K. M., Miner, B. G., Sorte, C. J., Thornber, C. S., et al. (2006). The impacts of climate change in coastal marine systems. *Ecol. Lett.* 9 (2), 228–241. doi: 10.1111/j.1461-0248.2005.00871.x

Hill, N. K., Woodworth, B. K., Phinn, S. R., Murray, N. J., and Fuller, R. A. (2021). Global protected-area coverage and human pressure on tidal flats. *Conserv. Biol.* 35 (3), 933–943. doi: 10.1111/cobi.13638

Hodoki, Y., and Murakami, T. (2006). Effects of tidal flat reclamation on sediment quality and hypoxia in Isahaya bay. *Aquat. Conservation-Marine Freshw. Ecosyst.* 16 (6), 555–567. doi: 10.1002/aqc.723

Huang, L. B., Bai, J. H., Yan, D. H., Chen, B., Xiao, R., and Gao, H. F. (2012). Changes of wetland landscape patterns in dadu river catchment from 1985 to 2000, China. *Front. Earth Sci.* 6 (3), 237–249. doi: 10.1007/s11707-012-0312-4

Huang, H., and Zhang, L. (2007).). a study of the population dynamics of spartina alterniflora at jiuduansha shoals, Shanghai, China. *Ecol. Eng.* 29 (2), 164–172. doi: 10.1016/j.ecoleng.2006.06.005

Humphreys, R. K., Puth, M. T., Neuhauser, M., and Ruxton, G. D. (2019). Underestimation of pearson's product moment correlation statistic. *Oecologia* 189 (1), 1–7. doi: 10.1007/s00442-018-4233-0

Jackson, M. V., Fuller, R. A., Gan, X., Li, J., Mao, D., Melville, D. S., et al. (2021). Dual threat of tidal flat loss and invasive spartina alterniflora endanger important shorebird habitat in coastal mainland China. *J. Environ. Manage.* 278, 111549. doi: 10.1016/j.jenvman.2020.111549

Jiang, Y. L., Liang, Z. Z., Gao, H., Guo, Y., Zhong, Z. M., Yang, C., et al. (2018). An improved constraint-based Bayesian network learning method using Gaussian kernel probability density estimator. *Expert Syst. Appl.* 113, 544–554. doi: 10.1016/j.eswa.2018.06.058

Jiang, T. T., Pan, J. F., Pu, X. M., Wang, B., and Pan, J. J. (2015). Current status of coastal wetlands in China: Degradation, restoration, and future management. *Estuar. Coast. Shelf Sci.* 164, 265–275. doi: 10.1016/j.ecss.2015.07.046

Jin, H. R., Huang, C. Q., Lang, M. W., Yeo, I. Y., and Stehman, S. V. (2017). Monitoring of wetland inundation dynamics in the Delmarva peninsula using landsat time-series imagery from 1985 to 2011. *Remote Sens. Environ.* 190, 26–41. doi: 10.1016/j.rse.2016.12.001

Kahara, S. N., Mockler, R. M., Higgins, K. F., Chipps, S. R., and Johnson, R. R. (2009). Spatiotemporal patterns of wetland occurrence in the prairie pothole region of Eastern south Dakota. *Wetlands* 29 (2), 678–689. doi: 10.1672/07-09.1

Kim, S. G. (2010). The evolution of coastal wetland policy in developed countries and Korea. *Ocean Coast. Manage.* 53 (9), 562–569. doi: 10.1016/j.ocecoaman.2010.06.017

Kuang, C. P., Chen, W., Gu, J., Zhu, D. Z., He, L. L., and Huang, H. C. (2014). Numerical assessment of the impacts of potential future Sea-level rise on hydrodynamics of the Yangtze river estuary, China. *J. Coast. Res.* 30 (3), 586–597. doi: 10.2112/Jcoastres-D-13-00149.1

Larson, C. (2015). Hostile shores. *Science* 350 (6257), 150–152. doi: 10.1126/science.350.6257.150

Leorri, E., Cearreta, A., García-Artola, A., Irabien, M. J., and Blake, W. H. (2013). Relative sea-level rise in the Basque coast (N spain): Different environmental consequences on the coastal area. *Ocean Coast. Manage.* 77, 3–13. doi: 10.1016/j.ocecoaman.2012.02.007

Lewis, H. G., and Brown, M. (2001). A generalized confusion matrix for assessing area estimates from remotely sensed data. *Int. J. Remote Sens.* 22 (16), 3223–3235. doi: 10.1080/01431160152558332

Li, H. K., Chen, S. H., Liao, K., Lu, Q., and Zhou, W. G. (2021). Microalgae biotechnology as a promising pathway to ecofriendly aquaculture: A state-of-the-art review. *J. Chem. Technol. Biotechnol.* 96 (4), 837–852. doi: 10.1002/jctb.6624

Lin, W. J., Wu, J., and Lin, H. J. (2020). Contribution of unvegetated tidal flats to coastal carbon flux. *Global Change Biol.* 26 (6), 3443–3454. doi: 10.1111/gcb.15107

Liu, Y. F., Ma, J., Wang, X. X., Zhong, Q. Y., Zong, J. M., Wu, W. B., et al. (2020). Joint effect of spartina alterniflora invasion and reclamation on the spatial and temporal dynamics of tidal flats in Yangtze river estuary. *Remote Sens.* 12 (11). doi: 10.3390/rs12111725

Liu, L., Xu, W., Yue, Q., Teng, X., and Hu, H. (2018). Problems and countermeasures of coastline protection and utilization in China. *Ocean Coast. Manage.* 153, 124–130. doi: 10.1016/j.ocecoaman.2017.12.016

Li, X., Zhang, X., Qiu, C. Y., Duan, Y. Q., Liu, S. A., Chen, D., et al. (2020b). Rapid loss of tidal flats in the Yangtze river delta since 1974. *Int. J. Environ. Res. Public Health* 17 (5). doi: 10.3390/ijerph17051636

Li, J. H., Zhou, K. C., Dong, H. M., and Xie, B. G. (2020a). Cultivated land change, driving forces and its impact on landscape pattern changes in the dongting lake basin. *Int. J. Environ. Res. Public Health* 17 (21). doi: 10.3390/ijerph17217988

Lu, T., Lin, C., Wang, Y. P., Wu, H., Zhou, M. X., Chen, Y., et al. (2022). Mapping the most heavily reclaimed shorelines of the Yangtze river delta urban agglomerations. *Front. Earth Sci.* 10. doi: 10.3389/feart.2022.981606

Mai, S., and Bartholomä, A. (2000). The missing mud flats of the wadden Sea: a reconstruction of sediments and accommodation space lost in the wake of land reclamation. *Proc. Mar. Sci.* 2, 257–272. doi: 10.1016/S1568-2692(00)80021-2

Ma, Z., Melville, D. S., Liu, J., Chen, Y., Yang, H., Ren, W., et al. (2014). Rethinking china's new great wall. *Science* 346 (6212), 912–914. doi: 10.1126/science.1257258

Mao, D. H., Liu, M. Y., Wang, Z. M., Li, L., Man, W. D., Jia, M. M., et al. (2019). Rapid invasion of spartina alterniflora in the coastal zone of mainland China: Spatiotemporal patterns and human prevention. *Sensors* 19 (10). doi: 10.3390/s19102308

Mitsch, W. J. (1994). *Global wetlands* (Amsterdam: Elsevier).

Moftakhari, H. R., Salvadori, G., AghaKouchak, A., Sanders, B. F., and Matthew, R. A. (2017). Compounding effects of sea level rise and fluvial flooding. *Proc. Natl. Acad. Sci. U. S. A.* 114 (37), 9785–9790. doi: 10.1073/pnas.1620325114

Moller, I. (2019). Applying uncertain science to nature-based coastal protection: Lessons from shallow wetland-dominated shores. *Front. Environ. Sci.* 7. doi: 10.3389/fenvs.2019.00049

Morris, J. T., Sundareshwar, P. V., Nietch, C. T., Kjerfve, B., and Cahoon, D. R. (2002). Responses of coastal wetlands to rising sea level. *Ecology* 83 (10), 2869–2877. doi: 10.2307/3072022

Murray, N. J., Clemens, R. S., Phinn, S. R., Possingham, H. P., and Fuller, R. A. (2014). Tracking the rapid loss of tidal wetlands in the yellow Sea. *Front. Ecol. Environ.* 12 (5), 267–272. doi: 10.1890/130260

Murray, N. J., Ma, Z. J., and Fuller, R. A. (2015). Tidal flats of the yellow Sea: A review of ecosystem status and anthropogenic threats. *Austral Ecol.* 40 (4), 472–481. doi: 10.1111/aec.12211

Murray, N. J., Phinn, S. R., DeWitt, M., Ferrari, R., Johnston, R., Lyons, M. B., et al. (2019). The global distribution and trajectory of tidal flats. *Nature* 565 (7738), 222–225. doi: 10.1038/s41586-018-0805-8

Murray, N. J., Worthington, T. A., Bunting, P., Duce, S., Hagger, V., Lovelock, C. E., et al. (2022). High-resolution mapping of losses and gains of earth's tidal wetlands. *Science* 376 (6594), 744–749. doi: 10.1126/science.abm9583

Narayan, S., Beck, M. W., Reguero, B. G., Losada, I. J., van Wesenbeeck, B., Pontee, N., et al. (2016). The effectiveness, costs and coastal protection benefits of natural and nature-based defences. *PloS One* 11 (5). doi: 10.1371/journal.pone.0154735

Pal, M. (2005). Random forest classifier for remote sensing classification. *Int. J. Remote Sens.* 26 (1), 217–222. doi: 10.1080/01431160412331269698

Paulson Institute (2016) *Blueprint of coastal wetland conservation and management in China*. Available at: https://paulsoninstitute.org.cn/ (Accessed April 09, 2020).

Reimer, J. D., Yang, S. Y., White, K. N., Asami, R., Fujita, K., Hongo, C., et al. (2015). Effects of causeway construction on environment and biota of subtropical tidal flats in Okinawa, Japan. *Mar. Pollut. Bull.* 94 (1-2), 153–167. doi: 10.1016/j.marpolbul.2015.02.037

Rodriguez, J. F., Saco, P. M., Sandi, S., Saintilan, N., and Riccardi, G. (2017). Potential increase in coastal wetland vulnerability to sea-level rise suggested by considering hydrodynamic attenuation effects. *Nat. Commun.* 8 (1), 1–12. doi: 10.1038/ncomms16094

Sagar, S., Roberts, D., Bala, B., and Lymburner, L. (2017). Extracting the intertidal extent and topography of the Australian coastline from a 28 year time series of landsat observations. *Remote Sens. Environ.* 195, 153–169. doi: 10.1016/j.rse.2017.04.009

Schuerch, M., Spencer, T., Temmerman, S., Kirwan, M. L., Wolff, C., Lincke, D., et al. (2018). Future response of global coastal wetlands to sea-level rise. *Nature* 561 (7722), 231. doi: 10.1038/s41586-018-0476-5

Seaman, D. E., and Powell, R. A. (1996). An evaluation of the accuracy of kernel density estimators for home range analysis. *Ecology* 77 (7), 2075–2085. doi: 10.2307/2265701

Song, K., Choi, Y. E., Han, H. J., and Chon, J. (2021). Adaptation and transformation planning for resilient social-ecological system in coastal wetland using spatial-temporal simulation. *Sci. Total Environ.* 789. doi: 10.1016/j.scitotenv.2021.148007

Spalding, M. D., McIvor, A. L., Beck, M. W., Koch, E. W., Moller, I., Reed, D. J., et al. (2014). Coastal ecosystems: A critical element of risk reduction. *Conserv. Lett.* 7 (3), 293–301. doi: 10.1111/conl.12074

Sun, T. T., Lin, W. P., Chen, G. S., Guo, P. P., and Zeng, Y. (2016). Wetland ecosystem health assessment through integrating remote sensing and inventory data with an assessment model for the hangzhou bay, China. *Sci. Total Environ.* (566), 627–640. doi: 10.1016/j.scitotenv.2016.05.028

Sun, Z., Sun, W., Tong, C., Zeng, C., Yu, X., and Mou, X. (2015). China's coastal wetlands: conservation history, implementation efforts, existing issues and strategies for future improvement. *Environ. Int.* 79, 25–41. doi: 10.1016/j.envint.2015.02.017

Sutton-Grier, A. E., Wowk, K., and Bamford, H. (2015). Future of our coasts: The potential for natural and hybrid infrastructure to enhance the resilience of our coastal communities, economies and ecosystems. *Environ. Sci. Policy* 51, 137–148. doi: 10.1016/j.envsci.2015.04.006

Wang, J., Gao, W., Xu, S. Y., and Yu, L. Z. (2012). Evaluation of the combined risk of sea level rise, land subsidence, and storm surges on the coastal areas of Shanghai, China. *Climatic Change* 115 (3), 537–558. doi: 10.1007/s10584-012-0468-7

Wang, W., Liu, H. I., Li, Y. Q., and Su, J. L. (2014). Development and management of land reclamation in China. *Ocean Coast. Manage.* 102, 415–425. doi: 10.1016/j.ocecoaman.2014.03.009

Wang, R. J., Wang, Q. B., Dong, L. S., and Zhang, J. F. (2021a). Cleaner agricultural production in drinking-water source areas for the control of non-point source pollution in China. *J. Environ. Manage.* 285. doi: 10.1016/j.jenvman.2021.112096

Wang, X. X., Xiao, X. M., Xu, X., Zou, Z. H., Chen, B. Q., Qin, Y. W., et al. (2021b). Rebound in China's coastal wetlands following conservation and restoration. *Nat. Sustainability* 4 (12), 1076–1083. doi: 10.1038/s41893-021-00793-5

Wang, X. X., Xiao, X. M., Zou, Z. H., Chen, B. Q., Ma, J., Dong, J. W., et al. (2020). Tracking annual changes of coastal tidal flats in China during 1986-2016 through analyses of landsat images with Google earth engine. *Remote Sens. Environ.* 238. doi: 10.1016/j.rse.2018.11.030

Watson, J. E. M., Dudley, N., Segan, D. B., and Hockings, M. (2014). The performance and potential of protected areas. *Nature* 515, 67–73. doi: 10.1038/nature13947

Wei, L. (2020) *The total GDP accounts for one-fourth of the country the Yangtze river delta depends on what*. Available at: https://baijiahao.baidu.com/s?id=1673940305900228629&wfr=spider&for=pc (Accessed December 27, 2021).

Wei, W., Tang, Z. H., Dai, Z. J., Lin, Y. F., Ge, Z. P., and Gao, J. J. (2015). Variations in tidal flats of the changjiang (Yangtze) estuary during 1950s-2010s: Future crisis and policy implication. *Ocean Coast. Manage.* 108, 89–96. doi: 10.1016/j.ocecoaman.2014.05.018

Xing, F., Wang, Y. P., and Wang, H. V. (2012). Tidal hydrodynamics and fine-grained sediment transport on the radial sand ridge system in the southern yellow Sea. *Mar. Geology* 291, 192–210. doi: 10.1016/j.margeo.2011.06.006

Yang, M., Gong, J. G., Zhao, Y., Wang, H., Zhao, C. P., Yang, Q., et al. (2021). Landscape pattern evolution processes of wetlands and their driving factors in the xiong'an new area of China. *Int. J. Environ. Res. Public Health* 18 (9). doi: 10.3390/ijerph18094403

Yang, X. C., Leung, L. R., Zhao, N. Z., Zhao, C., Qian, Y., Hu, K. J., et al. (2017). Contribution of urbanization to the increase of extreme heat events in an urban agglomeration in east China. *Geophysical Res. Lett.* 44 (13), 6940–6950. doi: 10.1002/2017gl074084

Yuan, K. X. J., Cheng, X. Q., Gui, Z. P., Li, F., and Wu, H. Y. (2019). A quad-tree-based fast and adaptive kernel density estimation algorithm for heat-map generation. *Int. J. Geographical Inf. Sci.* 33 (12), 2455–2476. doi: 10.1080/13658816.2018.1555831

Zahran, S., Brody, S. D., Grover, H., and Vedlitz, A. (2006). Climate change vulnerability and policy support. *Soc. Natural Resour.* 19 (9), 771–789. doi: 10.1080/08941920600835528

Zeng, X., Chen, M. Y., Zeng, C., Cheng, S., Wang, Z. H., Liu, S. R., et al. (2022). Assessing the management effectiveness of china's marine protected areas: Challenges and recommendations. *Ocean Coast. Manage.* 224. doi: 10.1016/j.ocecoaman.2022.106172

Zhang, W. D., Bussmann, R. W., Li, J., Liu, B., Xue, T. T., Yang, X. D., et al. (2022). Biodiversity hotspots and conservation efficiency of a large drainage basin: Distribution patterns of species richness and conservation gaps analysis in the Yangtze river basin, China. *Conserv. Sci. Pract.* 4 (4). doi: 10.1111/csp2.12653

Zhang, K. Y., Dong, X. Y., Liu, Z. G., Gao, W. X., Hu, Z. W., and Wu, G. F. (2019). Mapping tidal flats with landsat 8 images and Google earth engine: A case study of the china's Eastern coastal zone circa 2015. *Remote Sens.* 11 (8). doi: 10.3390/rs11080924

Zhang, F., Kung, H. T., and Johnson, V. C. (2017). Assessment of land-Cover/Land-Use change and landscape patterns in the two national nature reserves of ebinur lake watershed, xinjiang, China. *Sustainability* 9, (5) 724. doi: 10.3390/su9050724

Zhang, X. J., Wang, G. Q., Xue, B. L., Zhang, M. X., and Tan, Z. X. (2021). Dynamic landscapes and the driving forces in the yellow river delta wetland region in the past four decades. *Sci. Total Environ.* 787. doi: 10.1016/j.scitotenv.2021.147644

Zhao, Y. F., Liu, Q., Huang, R. Q., Pan, H. C., and Xu, M. (2020). Recent evolution of coastal tidal flats and the impacts of intensified human activities in the modern radial sand ridges, East China. *Int. J. Environ. Res. Public Health* 17 (9). doi: 10.3390/ijerph17093191

Zhao, X., Zhang, Q., He, G. Z., Zhang, L., and Lu, Y. L. (2021). Delineating pollution threat intensity from onshore industries to coastal wetlands in the bohai rim, the Yangtze river delta, and the pearl river delta, China. *J. Cleaner Production* 320. doi: 10.1016/j.jclepro.2021.128880

Zhao, Y., Zou, X., Liu, Q., Yao, Y., Li, Y., Wu, X., et al. (2017). Assessing natural and anthropogenic influences on water discharge and sediment load in the Yangtze river, China. *Sci. Total Environ.* 607-608, 920–932. doi: 10.1016/j.scitotenv.2017.07.002

Zhu, W. Q., Ren, G. B., Wang, J. P., Wang, J. B., Hu, Y. B., Lin, Z. Y., et al. (2022). Monitoring the invasive plant spartina alterniflora in jiangsu coastal wetland using MRCNN and long-time series landsat data. *Remote Sens.* 14 (11). doi: 10.3390/rs14112630

frontiers | Frontiers in Marine Science

TYPE Original Research
PUBLISHED 02 February 2023
DOI 10.3389/fmars.2023.1081827

OPEN ACCESS

EDITED BY
Dimitris Poursanidis,
Terrasolutions marine environment research, Greece

REVIEWED BY
Li Wen,
NSWNSW Department of Planning, Industry and Environment, Australia
Junhong Bai,
Beijing Normal University, China

*CORRESPONDENCE
Xuechu Chen
xcchen@des.ecnu.edu.cn

SPECIALTY SECTION
This article was submitted to Coastal Ocean Processes, a section of the journal Frontiers in Marine Science

RECEIVED 27 October 2022
ACCEPTED 12 January 2023
PUBLISHED 02 February 2023

CITATION
He K, Song A, Zhang Z, Ramdat N, Wang J, Wu W and Chen X (2023) Restored coastal wetlands with low degree of separation and high patch connectivity attract more birds.
Front. Mar. Sci. 10:1081827.
doi: 10.3389/fmars.2023.1081827

Restored coastal wetlands with low degree of separation and high patch connectivity attract more birds

Kun He[1,2], Annan Song[1], Ziyu Zhang[1], Naven Ramdat[3], Jiayi Wang[1], Wei Wu[1] and Xuechu Chen[3,4]*

[1]Ecological Technique and Engineering College, Shanghai Institute of Technology, Shanghai, China, [2]The Research Institution of Beautiful China and Ecological Civilization, Shanghai Institute of Technology, Shanghai, China, [3]State Key Laboratory of Estuarine and Coastal Research, School of Ecological and Environmental Sciences, East China Normal University, Shanghai, China, [4]Yangtze Delta Estuarine Wetland Ecosystem Observation and Research Station, Ministry of Education & Shanghai Science and Technology Committee, Shanghai, China

Coastal wetlands, the major component of coastal ecotones with indispensable ecosystem services, are threatened by anthropogenic disturbance, resulting in continuous loss of ecosystem functions. Coastal wetland restoration can be implemented to deter the ecosystem losses; however, it is unclear whether it could provide appropriate habitat for the birds using on coastal ecotones. Here, we utilize a newly restored wetland as an example to investigate the impacts of coastal restoration on bird diversity, and test the hypothesis - if a reasonable habitat pattern is created, more birds will be attracted, thereby helping decision-makers develop efficient and sustainable coastal restoration strategies. We used Fragstats for landscape pattern analysis, and derived the variability in different habitat patterns by independent sample T-test and Mann-Whitney U test. The results suggested that the restored wetland exhibited a positive effect on attracting birds, with a total of 70 species, 35 families, and 15 orders of birds being recorded over a three-year period after restoration. Passeriformes are the main species, and accounted for 52.8% of bird species. Additionally, waterbird species, i.e., Ciconiiformes and Anseriformes, accounted for 24.67% of the total number of species. The number of bird species in the wetlands increased annually, especially during the overwintering and the breeding period. Furthermore, the results of this study indicate that water-centered mosaic-type habitat consisting of a relatively low degree of separation and high patch connectivity was beneficial to attracting different types of birds. The number of bird species, density, bird biodiversity index, evenness index, and dominance index for mosaic-type habitats were all higher than those for even habitat pattern with independent patches and sharp boundaries. In particular, the mosaic-type habitat attracted migratory waterbirds such as *Anas zonorhyncha*, *Aix galericulata*, *Mareca penelope*, *Hydrophasianus chirurgus*, *Emberiza pallasi*, *Xenus cinereus*, and *Spatula querquedula*, which expanded the range of birds attracted by coastal restoration projects. This study illustrated that coastal wetland restoration combined with a creation of water-centered mosaic-type habitat attracted more birds and could provide a reference for the restoration of degraded ecosystems in coastal zones.

KEYWORDS

coastal wetlands, ecological restoration, bird diversity, habitat pattern, landscape separation

1 Introduction

As a buffer zone that connects and intersects terrestrial and marine systems, coastal wetlands are one of the most valuable ecosystems in the world due to their unique structure and biogeochemical cycle processes. Coastal wetlands are the major component of coastal ecotones and provide areas with high biodiversity and important habitats for plant and animal communities, especially birds (Amano et al., 2010). In recent years, due to the impact of natural and anthropogenic disturbances, such as sea level rise and coastal reclamation, coastal wetlands have been increasingly threatened (Jiang et al., 2015), resulting in the continuous destruction of wetland structures and the degradation of ecosystem functions (Wang et al., 2012; Yang et al., 2020). Therefore, coastal wetland restoration has become a hot topic in international ecological research, and many non-governmental and governmental organizations have elevated habitat restoration to be a primary method for wetland conservation (Renzi et al., 2019). Coastal wetland restoration is usually implemented to combat ecosystem losses with the goal of establishing self-sustaining coastal wetlands, that may be a set of specific objectives (e.g., presence of particular species, plant cover, biomass, etc.) or functional equivalency with natural habitats (Borja et al., 2010). However, many restored wetlands fail to completely achieve the restoration targets in a timely manner (Borja et al., 2010). Wetlands diversity through restoration can take decades which can limit the ecosystem services they provide, especially the restoration of biodiversity (Das, 2017). So we need to improve wetland restoration eficiency and implement restoration designs that support the rapid creation of natural, high functioning wetlands (Renzi et al., 2019).

Birds, active components of wetland ecosystems, are sensitive to environmental changes, and they are therefore frequently used as indicators in various ecological studies and are often considered a good surrogate of biodiversity in a particular area (Alexandrino et al., 2016). Wetland bird community composition and species numbers are important indicators for monitoring and evaluating the effectiveness of coastal restoration. Comparing changes in wetland bird populations enhances our knowledge of the ecological value of a restored coastal wetland system (Hughes et al., 2018). Restored wetlands and natural wetlands differ in their ability to perform basic functions (improving water quality, reducing food damage, and supporting food webs), but all provide habitats for plants and animals (Borja et al., 2010). Some endangered birds also choose to restore wetlands as alternatives to natural habitats (Chen et al., 2012). Some recent studies have argued that restored or artificial wetlands compensate for wetland losses and are valuable for waterbird conservation, and indicated that wetland creation may be the best alternative when restoration is not possible due to irreversible damage to former wetlands. Some studies have emphasized the importance of restored wetlands for waterbirds (Sripanomyom et al., 2011; Márquez-Ferrando et al., 2014) and suggested that restored wetlands promote bird diversity to a level similar to that in natural wetlands (Desrochers et al., 2008; Bantilan-Smith et al., 2009). The construction of artificially restored wetlands has increased the diversity of coastal habitats, attracting waterbirds to roost or escape environmental stresses (Piersma et al., 2017) and increasing species diversity. The use of coastal restoration projects for wetland restoration and habitat function enhancement has become an important method to protect coastal bird habitats (Cooke and Suski, 2008). The relationships between the distribution of most waterbirds and habitat characteristics, were in agreement with the birds' ecological requirements. For instance, the shorebirds are significantly concentrated in the mudflat wetlands (Clemens et al., 2014; Murray and Fuller, 2015). The wintering ducks and coots clearly preferred the water area next to the wastelands cover and avoided dry forest cover (Ma et al., 2010). In China, a study of restoration project in Dianchi Lake suggested that distinct habitat requirements of different waterbird groups, indicating different types of restoration and arrangements should be implemented. Although there are mounting evidences that habitats characteristics are the important driver for the waterbird assemblages, the mechanisms behind habitat patches and wetland bird diversity at landscape scales still need explore (Angelini et al., 2015). On the other hand, habitat patterns are the basis for maintaining bird diversity, as different habitat patterns have different effects on attracting birds (Ma et al., 2010). Studies have shown that birds have certain preferences for different habitats. Their distribution and habits will be affected by the factors such as waters, aquatic plants and beaches in wetlands (Guan et al., 2015). Different habitat patch structures show the current status and potential trends of the habitat quality in the coastal wetland, while there are differences in water birds for their needs and adaptability (Dias et al., 2013). Therefore, whether the distribution and diversity of bird communities will be affected by coastal restoration measures and wetland habitat patterns is also a key issue that should be further explored in coastal restoration projects.

Hangzhou Bay is an important stopover site for migratory waterbirds on the East Asia–Australasia Flyway (EAAF). Since 2016, coastal restoration projects have been launched on the north shore of Hangzhou Bay with the goal of recovering salt marshes and improving ecosystem services. After the implementation of coastal restoration projects, the ecosystem service value of the coastal zone was significantly enhanced, and the restored wetlands provided good habitat conditions and abundant food resources for various types of organisms (Chen et al., 2020). To assess whether coastal restoration projects have played an important role in attracting birds, our team has been observing and recording the dynamics of bird populations in these restored wetlands since 2018. By comparing the differences in wetland bird diversity under different habitat patterns, we sought to reveal the habitat selection tendency of birds, thereby providing practical experience and references for future coastal restorations.

2 Materials and methods

2.1 Study area

The Yingwuzhou wetland is located in Jinshan District in Shanghai, China (N30°42′26.73″, E121°20′04.15″), and covers a total area of 23.2 ha. It was originally a silty muddy tidal flat formed by sediment accumulation in the estuary. Under the combined effect of anthropogenic disturbance and natural erosion,

the ecosystem functions of the coastal wetland have degraded, with wildlife habitats being lost. In order to restore the coastal wetland ecosystem and salt marsh landscape, comprehensive coastal restoration projects have been carried out to build a diverse coastal wetland and recover the ecosystem functions in the coastal zone since 2016, that adopted technologies such as beach protection, wetland water purification, native plant planting, and tidal hydrodynamics regulation (Figure 1).

2.2 Habitat pattern construction

The purpose of the Yingwuzhou wetland restoration was to remediate the degraded coastal wetland with the help of the ecological engineering measures and to restore the structural, functional, and biological characteristics of the wetland. Therefore, it is necessary to comprehensively consider the diversified habitats of salt marsh plants, plankton, fish and birds in wetlands and reconstruct habitat patches, as well as landscape elements such as water, reeds, woodlands, grasslands, and roads, in coastal restoration projects. Considering the comprehensive relationship between wetland habitat and ecological function, we constructed two typical wetland habitat patterns in the core wetland (Figure 2).

Habitat pattern A is located in the northern site of the Yingwuzhou wetland and consists consisted of four core units: "Ecological pond I, surface flow wetland, ecological pond II, and salt marsh restoration area", forming a combined ecological restoration and purification system. This site restored water quality by combining the water system regulation with the purification function of wetland plants (mainly reeds). The ecological pond I was arranged with plants floating islands and submerged plants. The surface flow wetland was mainly planted with *Phragmites communis* and *Typha latifolia*. The ecological pond II was automatically controlled to provide tidal water flow for salt marsh restoration area. The salt marsh restoration area was composed of several shallow ponds and tidal ditches, and the area was mainly planted with *Phragmites communis* and *Scirpus mariqueter*. The roads in Habitat Pattern A divided the water area and reed community into scattered patches with relatively uniform spacing. These patches were independent of each other, with clear boundaries and regular edges, presenting an even habitat pattern.

Habitat Pattern B is located in the south of the wetland, and it is the main area designed for attracting wetland bird, which is formed of a series of habitat patches with the central water as the core. The edges of each patch were linked to generate a composite mosaic-type habitat. Engineering measures were taken to build deep pits, shallow ponds, shoals, plant islands and hills to form diversified wetland hydrological and habitat conditions at this site, and diversified patches such as woodlands, grasslands and reeds were arranged around the water to provide habitat for wetland animals of different trophic levels. A sandy beach and a pebble beach were constructed at the intersection of land and water. *Phragmites communis* and *Scirpus mariqueter* were planted. The two habitat patterns are connected by a small streamway that acted as the ecological corridor connecting them together (Table 1).

2.3 Bird survey

The survey period was from January 2018 to August 2021. The bird surveys were conducted in the middle of each month (the survey was not conducted from January 2020 to July 2020 due to the pandemic) and were performed along a fixed route through the core area of the wetland. At 08:00-10:00 on each survey day, three people moving at a normal walking speed (1.0-1.5 km/h), used binoculars (8*42 mm) and long-focal-length cameras to observe and take photos of the birds within the range of the wetland. The species, number, and area in which the birds were observed were recorded, and the activities of the birds and habitat conditions were noted. *Birds of China* (Liu and Chen, 2021) and *A Checklist on the Classification and Distribution of the Birds of China* (Zheng, 2017) were referenced for the identification of bird species.

2.4 Data analysis

2.4.1 Landscape pattern analysis

The remote sensing images of the study area were obtained by using Google Earth Pro. The images were registered and geometrically corrected in ArcMap 10.2 and then converted into a raster map (grid resolution 1 m*1 m) for export as soon as a vector map of the habitat patch was generated using manual interpretation. After

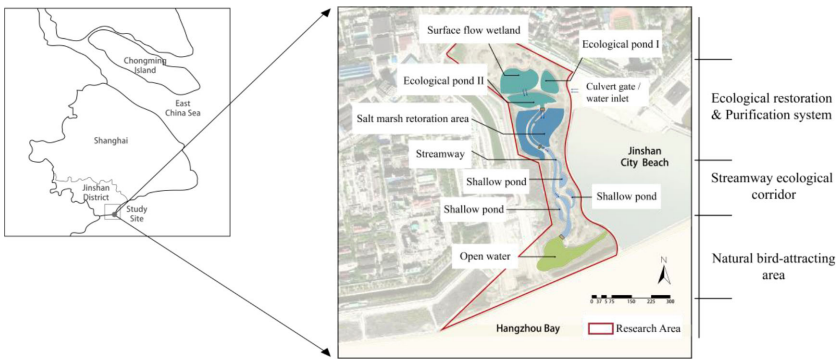

FIGURE 1
Location of the Study Area and Engineering Zoning.

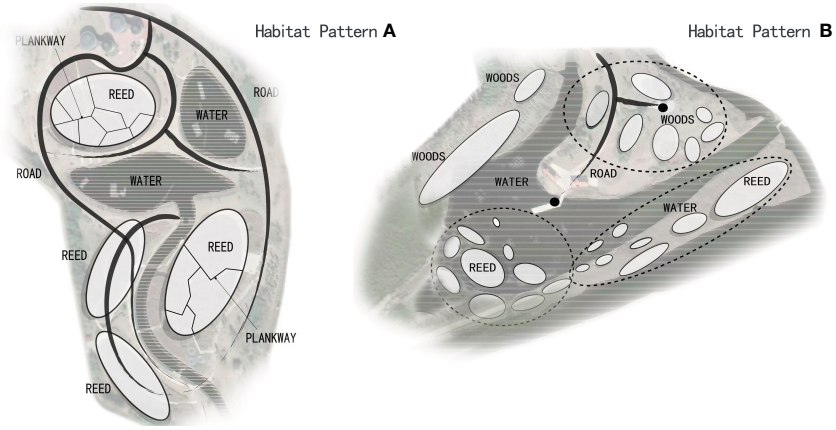

FIGURE 2
The diagram of Habitat Pattern A and Habitat Pattern B in the wetland.

interpretation, the landscape pattern index was analyzed in Fragstats 4.2. The landscape level was analyzed by selecting five indices: total landscape area (TA, hm^2), which represents the total area of the landscape; landscape sprawl index (CONTAG, %), which represents the aggregation degree or extension trend of different patch types in the landscape; landscape splitting index (SPLIT), which represents the degree of separation of the different patches in the landscape to evaluate the landscape shape and fragmentation in the study area; and Shannon's Diversity Index (SHDI) and Shannon evenness index (SHEI), which can reflect the heterogeneity of landscape. The meaning and calculation method of the 5 landscape pattern indicies are detailed in the Fragstats 4.2 instructions (Wu et al., 2021).

2.4.2 Bird data analysis

We used the Berger-Parker dominance index (D) to determine the degree of bird dominance. Specifically, $D \geq 0.05$ represents dominant species, $0.005 \leq D < 0.05$ represents common species, and $D < 0.005$ indicates rare and/or accidental species. We calculate the bird density of each habitat according to the number of birds in different habitat areas (hm^2). Besides, we estimated bird diversity using Shannon–Wiener diversity index (*H'*), Pielou evenness index (*J'*), Simpson dominance index (*D'*) and Gleason index (*G'*). These four indices reflect richness (*H'*), evenness (*J'*), dominance (*D'*) and within-habitat diversity (*G'*) dimension of bird diversity and thus provide complementary information.

TABLE 1 Location of the Study Area and Habitat Pattern Zoning.

Habitat Pattern	Habitat Pattern A				Habitat Pattern B
	Ecological pond I	Surface flow wetland	Ecological pond II	Salt marsh restoration area	
Total area (hm^2)	9.58				6.21
Water depth (m)	1.5-2.5	0.1	1.5-2.5	0.1	1.5-2.5
Reed area (hm^2)	0.52	0.81	0.52	0.81	0.52
Grasslands area (hm^2)	0.58	0.33	0.51	0.64	2.95
woodlands area (hm^2)	0.30	0.14	0	0.34	11.88
Water area (hm^2)	0.16	0	0.16	0	0.16
Floating island	3	0	3	0	3
Habitat characteristics	Each patch was relatively independent, and different patches had obvious boundaries. The waters and reeds were scattered and distributed in series through roads and water systems to form an even distribution pattern.				A large area of water was the core patch, and the surrounding woodlands, grasslands and other patches were mosaicked. The edges of different patches were nested and interlaced with each other.

The reeds were primarily wetland areas covered (full coverage or patchy coverage) by reed-based aquatic plants.

The data statistical analysis and mapping were completed by using SPSS 26.0, Excel and GraphPad Prism, and the normal distribution was tested by Shapiro-Wilk test. The species and number of birds in different habitats were tested by independent sample T-test under the condition of normal distribution, but the Mann-Whitney U test was used for the nonnormal distribution.

3 Results and discussion

3.1 Effect of coastal wetland restoration on bird attraction

A total of 70 species of birds belonging to 35 families and 15 orders (Table 2) were recorded in the study area within 3 years. Among them, there was 1 China's first-class key protected bird (*Emberiza aureola*) and 6 China's second-class key protected birds (*Aix galericulata*, *Paradoxornis heudei*, *Falco tinnunculus*, *Falco subbuteo*, *Pandion haliaetus*, and *Hydrophasianus chirurgus*); there was 1 (*Emberiza aureola*) critically endangered species (CR) on the International Union for Conservation of Nature (IUCN) Red List (IUCN, 2020) and 2 near-threatened species (NT) (*Paradoxornis heudei* and *Anas falcata*). Members of Passeriformes were the main species, accounting for approximately 52.8% of the wetland birds. This order was dominant because the coastal restoration project has created near-natural ecological zones in the Yingwuzhou wetland, consisting of ponds, salt marshes, grasslands and woodlands that provide various types of terrestrial habitat for birds to forage, rest and escape from predators. Among the non-Passeriformes species, the number of waterbird species was relatively high, including members of the Ciconiiformes (Jacanidae, Charadriidae, Scolopacidae, and Laridae), Anseriformes (only Anatidae), and Ciconiiformes (only Ardeidae), each with six species, accounting for 9.6% of the total number of species recorded. There were seven dominant species of wetland birds, i.e., *Remiz consobrinus*, D=0.135; *Gallinula chloropus*, D=0.084; *Acridotheres cristatellus*, D=0.080; *Tachybaptus ruficollis*, D=0.065; *Sturnus cineraceus*, D=0.065; *Passer montanus*, D=0.058; and *Hirundo rustica*, D=0.057. In addition, there were 15 common species and 51 rare and accidental species were observed in the restored wetland.

In 2018, 33 species of birds were observed in the wetland, consisting of 22 species of resident birds, seven species of wintering migratory birds, and four species of summering migratory birds. In 2019, 41 species of birds were observed in the wetland, consisting of 24 species of resident birds, 12 species of wintering migratory birds, three species of summering migratory birds, and two species of passing birds. Sixty-one species of birds were observed in the wetland from September 2020 to August 2021, consisting of 31 resident birds, 18 wintering migratory birds, 8 summering migratory birds, and 4 passing birds (Figure 3, left). The number of wetland bird species during the overwintering period and the breeding period exhibited an increasing trend annually (Figure 3, right). Since 2018, the cumulative number of wetland bird species has increased linearly (Figure 3, bottom). Compared with 2018, 13 new species were added in 2019. The newly added birds were mainly winter migratory birds (seven species), including *Mareca falcata*, *Aix galericulata*, and *Emberiza pallasi*. There were 20 new species of wetland birds recorded from September 2020 to August 2021, primarily resident birds and wintering migratory birds. There were nine species of resident birds, including *Ardeola bacchus* and *Phasianus colchicus*, and seven species of wintering migratory birds, including *Chroicocephalus ridibundus* and *Mareca penelope*. In addition, four species of summering migratory birds, including *Hydrophasianus chirurgus* and *Vanellus cinereus*, and four species of passing birds, including *Xenus cinereus*, were added.

TABLE 2 Composition of different bird taxa in the Yingwuzhou wetland.

Order	Family	Genus	Species	Percentage (%)
Columbiformes	1	2	2	2.74
Podicipediformes	1	1	1	1.37
Suliformes	1	1	1	1.37
Cuculiformes	1	1	1	1.37
Ciconiiformes	1	5	6	8.22
Gruiformes	1	3	3	4.11
Coraciiformes	1	1	1	1.37
Passeriformes	18	25	37	52.79
Anseriformes	1	1	6	8.22
Falconiformes	1	1	2	2.74
Charadriiformes	4	4	6	8.22
Galliformes	1	1	1	1.37
Accipitriformes	1	1	1	1.37
Bucerotiformes	1	1	1	1.37
Apodiformes	1	1	1	1.37

10.3389/fmars.2023.1081827

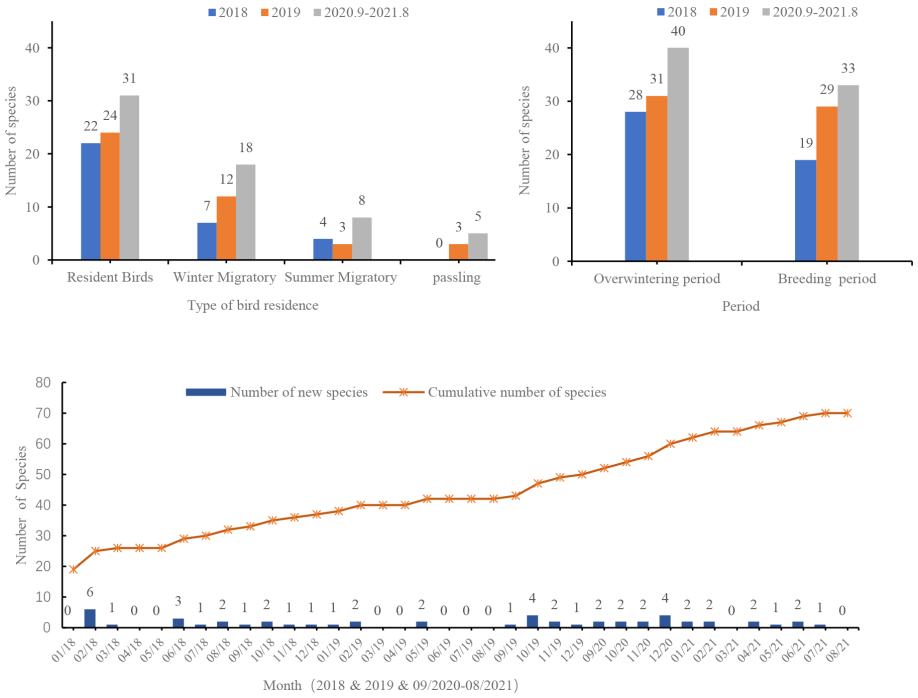

FIGURE 3
Changes in bird species number.

(Left: residential types; Right: bird species in the migration period; Bottom: monthly changes of bird number)

3.2 Effect of the wetland habitat structure on bird diversity

Increasing attractiveness to birds mainly depends on wetland restoration measures, habitat structure, and management mode (Jackson et al., 2019). The landscape characteristics of wetlands also influence bird ecological processes such as habitat dependencies, foraging, and distribution (Lee and Carroll, 2014). Over the 3 years, a total of 1,737 birds of 53 species were recorded in Habitat Pattern A, and a total of 1,510 birds of 55 species were recorded in Habitat Pattern B (Table 3). However, no significant differences were found in the number of birds between the two habitats (Z=-2.005, P=0.64) by using the Mann-Whitney U test, and the density of birds in Habitat Pattern A was far lower than that in Habitat Pattern B.

In addition, the diversity of bird species under the different habitat patterns was different, and the evenness index and dominance index of Habitat Pattern B over the years were all greater than those of Habitat Pattern A. The Gleason Diversity Index and Shannon-Wiener Diversity Index were significantly higher in Habitat B than in Habitat A (Figure 4). The above results indicated that the bird species diversity of Habitat Pattern B was relatively high.

Figure 5 shows that the number of resident bird species in Habitat Pattern A was slightly higher than that in Habitat Pattern B, primarily because the area of Habitat Pattern A was larger and the reeds and sparse forests provided more habitats for resident birds such as

TABLE 3 The records of bird diversity during the research.

Time	Habitat Pattern	Bird richness index			Bird diversity index		
		Species	Individuals	Density	*H′*	*J*	*D′*
01/2018-12/2018	Habitat A	26	623	66.6	2.547	0.782	0.873
	Habitat B	22	356	57.8	2.647	0.856	0.912
01/2019-12/2019	Habitat A	26	410	43.9	2.583	0.793	0.896
	Habitat B	31	456	74.0	2.746	0.800	0.900
09/2020-08/2021	Habitat A	45	677	72.4	2.924	0.768	0.923
	Habitat B	45	653	106.0	3.019	0.793	0.929
Total	Habitat A	52	1737	182.3	2.911	0.733	0.916
	Habitat B	55	1510	245.1	3.055	0.762	0.933

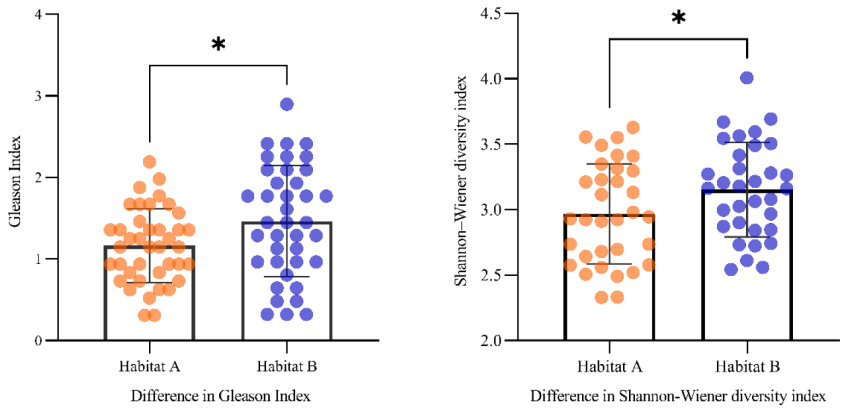

FIGURE 4
Variability of different diversity indices in different habitat patterns (*P < 0.05).

Passeriformes. The number of migratory bird species in Habitat Pattern B was higher than that in Habitat Pattern A, and the total number of bird species in Habitat Pattern B was higher than that in Habitat Pattern A regardless of the period (overwintering period or breeding period). As shown in Table 4, there were 37 bird species in both habitats and 15 bird species endemic to Habitat Pattern A, primarily Passeriformes (nine species). There were 18 species endemic to Habitat Pattern B, primarily Anseriformes and Charadriiformes, which mainly inhabit open waters.

Table 5 shows that the area in Habitat Pattern B was only two-thirds of that in Habitat Pattern A, but Habitat Pattern B had a higher CONTAG value and a lower degree of landscape SPLIT than Habitat Pattern A, indicating that the water-centered mosaic-type habitat patches in this area had good connectivity and low separation. Habitat Pattern B has a complex habitat structure and diversified patches, such as large areas of water, woodlands, grasslands, reeds and other patches were nested and interlaced to form a large wetland composite habitat, which is conducive to attracting different types of birds. On the other hand, high connectivity between habitat patches is important for the safe dispersal of individuals, providing them with optimal foraging and mating conditions. The SHDI index and SHEI index of Habitat Pattern A were higher than those of Habitat Pattern B, indicating that Habitat Pattern A had abundant land use, with numerous patches and an even distribution of different patch types in the wetland, a high degree of habitat fragmentation and a lack of dominant patches.

4 Discussion

4.1 Coastal restoration projects provide good habitat for birds and effectively increase the abundance of wetland birds

In recent years, coastal restoration projects have been conducted worldwide to restore degraded ecosystems and improve the ecological service functions of coastal zones (Chen et al., 2012). The results of bird observations at the Yingwuzhou wetland suggested that the number of bird species has increased after restoration. Approximately 70 species of birds in 35 families were observed over 3 years, including some key protected species. The dominant birds were Passeriformes (over 50%), which inhabited reeds and woodlands. This order was dominant because the coastal restoration project created near-nature ecotones in the Yingwuzhou wetland, composed of ponds, salt marshes, grasslands, and woodlands, providing various types of terrestrial habitats for Passeriformes in which to forage, rest, and escape from predators (Hughes et al., 2018).

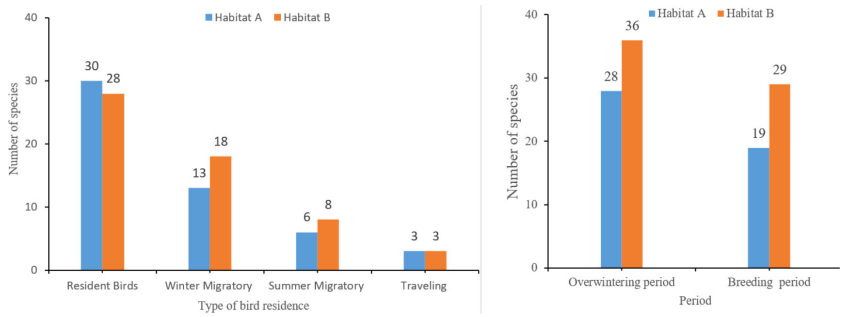

FIGURE 5
Changes in bird residential types and bird species during the migration season in different habitats.

TABLE 4 The records of bird species numbers in different habitat pattern.

Habitat Pattern	Number of species				
	Total	Resident Birds	Winter Migratory	Summer Migratory	Passing Birds
Species only observed in Habitat A	15	7	3	2	3
Species only observed in Habitat B	18	3	8	4	3
Species observed in both habitats	37	24	10	4	0

The results of field investigation suggested that the number of wetland bird species increased yearly after restoration. The proportion of resident bird species was close to 50% of the wetland bird species, significantly different from that of the surrounding coastal mudflat wetlands, where the species are primarily migratory waterbirds such as Anatidae, Charadriiformes, and Ardeidae (Chen et al., 2012). The restored wetland habitats were more suitable for resident birds, because they consisted of a large area of water, reeds, woodlands, and grasses, with much higher heterogeneity than the nearby tidal flat wetlands or artificial wetlands (fishponds and rice fields) (Giosa et al., 2018). For instance, *Gallinula chloropus* and *Tachybaptus ruficollis* were observedbreeding and brooding on the floating islands, and *Paradoxornis heudei*, which exclusively inhabited reed patches.

Since 2019, more migratory birds have entered the wetland from surrounding waters and mudflats to overwinter or breed, such as *Fulica atra*, *Anas zonorhyncha* and *Egretta garzetta*, et al. The newly added bird species were mainly members of the Charadriiformes and Anatidae, indicating that in addition to providing a suitable habitat for resident birds, the wetland is becoming more attractive to migratory birds. The main reason is that Yingwuzhou wetland created a certain water area with high connectivity and complex shapes, and has diversified tidal flat features composed of open water, pebble beach and vegetation through regulating water level through tidal flow, which provide a suitable habitat for migratory birds such as *Anas zonorhyncha*, *Bubulcus coromandus*, and *Fulica atra*.

The number of birds observed during the overwintering period and the breeding period increased annually, indicating that the wetland gradually attracted more migratory birds. There were more waterbird species observed during the overwintering period than during the breeding period. In particular, from October to November, a large number of wintering waterbirds moved into the wetland, while from December to January of the following year, Anatidae entered the wetland from adjacent waters, resulting in a significant increase in wintering waterbirds, including X*enus cinereus*, *Chroicocephalus ridibundus*, *Mareca penelope*, *Anas crecca*, and *Spatula querquedula*. Bird species richness in different period which may be related to breeding demand, food availability and suitable foraging areas. Birds tend to be highly mobile in winter, moving to the suitable wetlands in response to factors such as cold weather and changes in water levels and in food resources (Zhang et al., 2022).

4.2 Habitats with a low degree of separation and high patch connectivity have a more positive impact on bird diversity

The location of the coastal wetlands affected the variation in bird populations, and the interaction between habitat patches also increased uncertainty regarding habitat selection by birds (Kleijn et al., 2014). Studies have shown that the quality of wetland habitats and the areas of core patches exert a positive impact on bird diversity, and that wetlands with high bird diversity generally have larger woodlands and open waters (Chapman and Reich, 2006) which were the main characteristics of Habitat Pattern B and might had a more positive impact on attracting birds. In addition, the degree of habitat patch separation has an important impact on bird diversity and has a negative effect on species evenness (Chen et al., 2012). There were heterogeneous small patches in Habitat Pattern B. For instance, the woodlands and reeds were scattered around a large area of water, and the floating islands covered the central water area. Therefore, the patches have a mosaic-type layout, and the habitat structure in this area is more complex, which could provide stepping-stones and reduce interspecific competition for birds within the patches. Furthermore, the tidal flat patches in Habitat Pattern B were affected by the movement of outside water and characteristics of patch patterns (uneven distribution and complex edge shape), which are conducive to the restoration of hydrological fluctuations and support for bird feeding and habitation. This condition should be the reason why Pattern B could attract *Anas zonorhyncha, Mareca penelope, Hydrophasianus chirurgus, Xenus cinereus, Spatula querquedula* and other migratory waterbirds from the nearby waters. The patch types in Habitat Pattern A were mainly waters and reeds, were clearly separated and evenly distributed, which low heterogeneity might impede the distribution of birds to a certain extent and reduce the number of bird species. In addition, the vegetation in Habitat Pattern A is dominated by large areas of grasslands and reeds, with relatively little woodland, so the vegetation biomass is relatively low, and the interior areas of the habitat are more exposed to the disturbance, which affects the bird diversity. Therefore, the total number of bird species observed in Habitat Pattern A, as well as the endemic species, density, and bird diversity index, were lower. Compared with Habitat Pattern A,

TABLE 5 Analysis of wetland habitat landscape patterns.

Habitat pattern	TA (hm^2)	CONTAG (%)	SPLIT	SHDI	SHEI
Habitat Pattern A	9.35	47.60	21.77	1.58	0.88
Habitat Pattern B	6.16	56.39	7.13	1.37	0.57

Habitat Pattern B has more woodland patches scattered in groups in addition to water and reeds, which can be used as ecological stepping-stones to avoid the exposure of birds. The rich vegetation layers and stable community structure increase the spatial heterogeneity and improve the vegetation biomass in this area, providing birds with complex survival opportunities for foraging, nesting, and avoiding natural enemies (McCain, 2009).

Birds' preference for wetlands is influenced by a complex of characteristics such as water chemistry, aquatic vegetation, and physical features (Patra et al., 2011). The study showed that the inorganic nitrogen, reactive phosphate and suspended solids in the water of the Yingwuzhou wetland were reduced after purification from Habitat Pattern A into Habitat Pattern B (Chen et al., 2020) which might also lead birds to choose Habitat Pattern B with better water quality as their habitat. However, the effectiveness of wetland water quality characteristics on bird diversity has yet to be confirmed by in-depth studies based on actual data. In addition, the disturbance could have a relatively large impact on wetland bird diversity. In most areas of Habitat Pattern B, visitors are not allowed to enter daily to minimize the anthropogenic disturbance to the greatest extent. Under normal circumstances, visitor's activities in Habitat Pattern A would be relatively frequent and the disturbance would be greater. However, as the construction of the wetland had just been completed, and due to the epidemic in recent years, there had been few visitors. Therefore, we did not pay special attention to the effect of disturbance on the habitat selection of birds in this study. However, the increase of visitors and the surrounding construction in the future will inevitably have an impact on the diversity of wetland birds. How to reduce the disturbance to help wetland waterbirds conservation is the focus of wetland management.

4.3 Lessons from the Yingwuzhou wetland for coastal ecological restoration projects

Coastal wetlands provide key ecosystems for many species with important ecological and economic functions, including food web support, nutrient cycling, and stable habitat (Minello et al., 2003). However, only approximately 10% of biodiversity studies manipulate the diversity of ecological restoration projects with the aid of purposeful design (Hughes et al., 2018). The main purpose of coastal wetland restoration is rarely to protect important biological species, and most biodiversity assessments only focus on the rationality of ecological restoration interventions (Fitzgerald et al., 2021). Moreover, bird diversity research in ecological restoration projects is less than research on microorganisms, fish, etc. (Mahoney et al., 2021).

The studies showed that bird communities are related to the landscape heterogeneity of wetlands, and the richness & abundance of bird species are closely related to the use of patches in wetland landscapes. On the scale of wetland habitat, the structure and characteristics will also directly or indirectly affect the utilization of wetlands by bird, thereby affecting the structure of bird communities. Compared with the Eastern Chongming Tidal Flat and the Hangzhou Bay National Wetland Park around Shanghai (Lv et al., 2011; Cao et al., 2018), the scope of the Yingwuzhou wetland is relatively smaller and the range of the wetland habitat is relatively narrower, so the results of bird species and individual number are lower than those of the above wetlands. However, the bird diversity index of the Yingwuzhou wetland is relatively higher, and the biological maintenance value per unit area of wetland is higher than that of other surrounding coastal wetlands (Wu et al., 2021), indicating that the ecological restoration project of the Yingwuzhou wetland has improved the bird diversity in this region. The results of this study indicated that the two typical habitat patterns in the Yingwuzhou wetland both had high bird diversity. In particular, water-centered mosaic-type habitats consisting of a relatively low degree of separation and high patch connectivity had more positive impacts on bird diversity. The heterogeneity of mosaic-type habitat could provide high habitat structural diversity, thereby offering more places for birds to feed, hide, roost, and nest and producing more positive effects on the number, and evenness of wetland bird species. The results provide important information for understanding relationship between bird diversity and habitat patterns in a smaller landscape scale, and we can gain experience from the bird diversity studies of the Yingwuzhou wetland, and further provide "guidance" for the implementation of similar coastal ecological restoration projects.

The bird observation in the Yingwuzhou wetland lasted for 3 years. However, the lack of long-term experiments and comparative analysis in a larger environmental range may led to an underestimate of the intensity of the biodiversity effect. Therefore, it is very important to carry out long-term bird diversity observations with restoration projects and analyze the impact of wetland habitat patterns on bird diversity on a larger terrestrial-marine spatial scale, the results of which will help improve the understanding of the effectiveness of coastal wetland biodiversity restoration. In addition, wetland vegetation biomass, water quality, and other factors would affect bird diversity, which we also need to focus on in further research.

5 Conclusions

The coastal ecological restoration project in the Yingwuzhou wetland explicitly incorporated the habitat requirements of various birds by creating a mosaic of inter-connected habitat patches. The comprehensive restoration of wetland ecosystem provides a appropriate habitat for birds. The restored wetland has exhibited a positive effect on attracting birds, with 70 species of birds recorded over a three-year period. Passeriformes are the main species, accounting for 52.8% of wetland bird species, while waterbird species accounted for 24.67% of bird species. The number of bird species in the wetlands increased annually, especially during the overwintering and the breeding period. The water-centered mosaic-type habitat was located in the south of the wetland with a relatively low degree of separation and high patch connectivity, which are beneficial to attracting different types of birds. The number of bird species, density, bird biodiversity index, evenness index, and dominance index were all higher than those of the even habitat pattern with independent patches. The practice provided important information for understanding the relationship between bird diversity and restored wetland habitat patterns.

Data availability statement

The raw data supporting the conclusions of this article will be made available by the authors, without undue reservation.

Ethics statement

Ethical review and approval were not required for the animal study because no specific permits were needed for the described field studies. All experiments were conducted in accordance with the regulations of the local and central governments.

Author contributions

KH and XC conceived and designed the experiments. AS and ZZ participated in the research and wrote the paper. NR analyzed the data and revised the paper. KH and XC acquired the funding. JW and WW participated in the research. All authors contributed to the article and approved the submitted version.

Funding

This work was supported by the Project of National Key R&D Program of China (2017YFC0506002), Shanghai Key Lab for Urban Ecological Processes and Eco-Restoration (SHUES2022A08), the Scientific Research Plan Project of Science and Technology Commission of Shanghai Municipality (22dz1202600), Ministry of Education/Shanghai Field Scientific Observation, and the Research Station of Yangtze Delta Estuarine Ecosystem Open Project (K202007).

Acknowledgments

We sincerely thank Dr. Yuhao Zhao for his guidance on this research. We thank the Shanghai Key Lab for Urban Ecological Processes and Eco-Restoration for its support, which is a co-organizer of this paper. The authors would like to express their sincere thanks to the personnel of these teams for their kind assistance.

Conflict of interest

The authors declare that the research was conducted in the absence of any commercial or financial relationships that could be construed as a potential conflict of interest.

Publisher's note

All claims expressed in this article are solely those of the authors and do not necessarily represent those of their affiliated organizations, or those of the publisher, the editors and the reviewers. Any product that may be evaluated in this article, or claim that may be made by its manufacturer, is not guaranteed or endorsed by the publisher.

Supplementary material

The Supplementary Material for this article can be found online at: https://www.frontiersin.org/articles/10.3389/fmars.2023.1081827/full#supplementary-material

References

Alexandrino, E. R., Buechley, E. R., Piratelli, A. J., Barros, K. M., Andrade, M. R., Şekercioğlu, Ç.H., et al. (2016). Bird sensitivity to disturbance as an indicator of forest patch conditions: an issue in environmental assessments. *Ecol. Indicators.* 66, 369–381. doi: 10.1016/j.ecolind.2016.02.006

Amano, T., Székely, T., Koyama, K., Amano, H., and Sutherland, W. J. (2010). A framework for monitoring the status of populations: An example from wader populations in the East Asian-Australasian flyway. *Biol. Conserv.* 143, 2238–2247. doi: 10.1016/j.biocon.2010.06.010

Angelini, C., Heide, T., Griffin, J. N., Morton, J. P., Derksen-Hooijberg, M., Lamers, L. P. M., et al. (2015). Foundation species' overlap enhances biodiversity and multifunctionality from the patch to landscape scale in southeastern united states salt marshes. *Proc. R. Soc. London B Biol. Sci.* 282, 2050421. doi: 10.1098/rspb.2015.0421

Bantilan-Smith, M., Bruland, G. L., MacKenzie, R. A., Henry, A. R., and Ryder, C. R. (2009). A comparison of the vegetation and soils of natural, restored, and created coastal lowland wetlands in Hawaii. *Wetlands.* 29 (3), 1023–1035. doi: 10.1672/08-127.1

Borja, Á., Dauer, D. M., Elliott, M., and Simenstad, C. A. (2010). Medium-and long-term recovery of estuarine and coastal ecosystems: patterns, rates and restoration effectiveness. *Estuaries Coasts.* 33, 1249–1260. doi: 10.1007/s12237-010-9347-5

Cao, M., Jiang, S. Y., Chen, T. Y., Chen, W. P., Tang., , , C. D., Jing, X. W., et al. (2018). Characteristics of the avian communities in the natural wetland and artificially restored wetland in Chongming Dongtan-Shanghai. *Journal of Nanjing Forestry University (Natural Sciences Edition).* 42(6), 113–120. doi: 10.3969/j.issn.1000-2006.201708029

Chapman, K. A., and Reich, P. B. (2006). Land use and habitat gradients determine bird community diversity and abundance in suburban, rural and reserve landscapes of Minnesota, USA. *Biol. Conserv.* 135 (4), 527–541. doi: 10.1016/j.biocon.2006.10.050

Chen, X. C., Huang, Y. Y., Yang, H. L., Pan, L. P., Danielle, C. P., Xu, P., et al. (2020). Restoring wetlands outside of the seawalls and to provide clean water habitat. *Sci. Total Environ.* 721, 1–8. doi: 10.1016/j.scitotenv.2020.137788

Chen, W. Y., Zhang, L. Q., and Yuan, L. (2012). Habitat assessment on wetland restoration project for avian habitats at nanhui dongtan, shanghai. *Mar. Environ. Sci.* 31 (4), 561–566. doi: 1007-6336(2012) 04-0561-06

Clemens, R. S., Herrod, A., and Weston, M. A. (2014). Lines in the mud: Revisiting the boundaries of important shorebird areas. *J. Nat. Conserv.* 22, 59–67. doi: 10.1016/j.jnc.2013.09.001

Cooke, S. J., and Suski, C. D. (2008). Ecological restoration and physiology: an overdue integration. *Bioscience.* 58 (10), 957–968. doi: 10.1641/B581009

Das, S. (2017). Ecological restoration and livelihood: contribution of planted mangroves as nursery and habitat for artisanal and commercial fishery. *World Dev.* 94, 492–502. doi: 10.1016/j.worlddev.2017.02.010

Desrochers, D. W., Keagy, J. C., and Cristol, D. A. (2008). Created versus natural wetlands: Avian communities in Virginia salt marshes. *Écoscience.* 15 (1), 36–43. doi: 10.2980/1195-6860(2008)15[36:cvnwac]2.0.co;2

Dias, M. P., Lecoq, M., Moniz, F., and Rabaca, J. E. (2013). Can human-made saltpans represent an alternative habitat for shorebirds? Implications for a predictable loss of estuarine sediment flats. *Environ. Manage.* 53, 163–171. doi: 10.1007/s00267-013-0195-5

Fitzgerald, M., Gonzalez, K., Funk, J. L., Whitcraft, C. R., and Allen, B. J. (2021). Recovering ecosystem functions in a restored salt marsh by leveraging positive effects of biodiversity. *Ecosphere.* 12 (8), 1–15. doi: 10.1002/ecs2.3664

Giosa, E., Mammides, C., and Zotos, S. (2018). The importance of artificial wetlands for birds: A case study from Cyprus. *PLoS ONE.* 13(5), e0197286–e0197303. doi: 10.1371/journal.pone.0197286

Guan, L., Lei, J. L., Zuo, A. J., Zhang, H., Lei, G. C., and Wen, L. (2015). Optimizing the timing of water level recession for conservation of wintering geese in dongting lake, China. *Ecol. Eng.* 88, 90–98. doi: 10.1016/j.ecoleng.2015.12.009

Hughes, A. R., Grabowski, J. H., Leslie, H. M., Scyphers, S., and Williams, S. L. (2018). Inclusion of biodiversity in habitat restoration policy to facilitate ecosystem recovery. *Conserv. Lett.* 11, 1–8. doi: 10.1111/conl.12419

IUCN (2020) *The IUCN red list of threatened species. version 2020-2*. Available at: https://www.iucnredlist.org/.

Jackson, M. V., Carrasco, L. R., Choi, C. Y., Li, J., Ma, Z. J., Melville, D. S., et al. (2019). Multiple habitat use by declining migratory birds necessitates joined-up conservation. *Ecol. evolution.* 9 (5), 2505–2515. doi: 10.1002/ece3.4895

Jiang, T. T., Pan, J. F., Pu, X. M., Wang, B., and Pan, J. J. (2015). Current status of coastal wetlands in China: Degradation, restoration, and future management. *Estuarine Coast. Shelf Sci.* 164 (5), 265–275. doi: 10.1016/j.ecss.2015.07.046

Kleijn, D., Cherkaoui, I., Goedhart, P. W., van der Hout, J., and Lammertsma, D. (2014). Waterbirds increase more rapidly in ramsar-designated wetlands than in unprotected wetlands. *J. Appl. Ecol.* 51 (2), 289–298. doi: 10.1111/1365-2664.12193

Lee, M. B., and Carroll, J. P. (2014). Relative importance of local and landscape variables on site occupancy by avian species in a pine forest, urban, and agriculture matrix. *For. Ecol. Management.* 320, 161–170. doi: 10.1016/j.foreco.2014.03.017

Liu, Y., and Chen, S. H. (2021). *The CNG field guide to the birds of China* (Hunan: Hunan Science and Technology Press).

Lv, Y., Ying, S. Y., Howes, J., and Zhu, B. R. (2011). Survey of waterbird resource in cixi hangzhou bay wetland center in zhejiang province. *Chin. J. Wildlife.* 32 (6), 312–315. doi: 10.19711/j.cnki.issn2310-1490.2011.06.006

Ma, Z. J., Cai, Y. T., Li, B., and Chen, J. K. (2010). Managing wetland habitats for waterbirds: An international perspective. *Wetlands.* 30, 15–27. doi: 10.1007/s13157-009-0001-6

Mahoney, R. D., Beal, J. L., Lewis, D. M., and Cook, G. S. (2021). Quantifying the response of an estuarine nekton community to coastal wetland habitat restoration. *Sustainability.* 13 (23), 1–18. doi: 10.3390/su132313299

Márquez-Ferrando, R., Figuerola, J., Hooijmeijer, J. C. E. W., and Piersma, T. (2014). Recently created man-made habitats in doñana provide alternative wintering space for the threatened continental European black-tailed godwit population. *Biol. Conserv.* 171, 127–135. doi: 10.1016/j.biocon.2014.01.022

McCain, C. M. (2009). Global analysis of bird elevation diversity. *Global Ecol. Biogeogr.* 18, 346–360. doi: 10.1111/j.1466-8238.2008.00443.x

Minello, T. J., Able, K. W., Weinstein, M. P., and Hays, C. G. (2003). Salt marshes as nurseries for nekton: Testing hypotheses on density, growth and survival through meta-analysis. *Mar. Ecol. Prog. Series.* 246, 39–59. doi: 10.3354/meps246039

Murray, N. J., and Fuller, R. A. (2015). Protecting stopover habitat for migratory shorebirds in East Asia. *J. Ornithol.* 156, 217–225. doi: 10.1007/s10336-015-1225-2

Patra, A., Santra, K. B., and Manna, C. K. (2011). Limnological studies related to physico-chemical characteristics of water of santragachi and joypur jheel, W.B., India. *Our Nat.* 8 (1), 185–203. doi: 10.3126/on.v8i1.4328

Piersma, T., Chan, Y.-C., Mu, T., Hassell, C. J., David, S., Peng, H.-B., et al. (2017). Loss of habitat leads to loss of birds: Reflections on the jiangsu, China, coastal development plans. *Wader Study* 124, 93–98. doi: 10.18194/ws.00077

Renzi, J. J., He, Q., and Silliman, B. R. (2019). Harnessing positive species interactions to enhance coastal wetland restoration. *Front. Ecol. Evolution.* 131. doi: 10.3389/fevo.2019.00131

Sripanomyom, S., Round, P. D., Savini, T., Trisurat, Y., and Gale, G. A. (2011). Traditional salt-pans hold major concentrations of overwintering shorebirds in southeast Asia. *Biol. Conserv.* 144 (1), 526–537. doi: 10.1016/j.biocon.2010.10.008

Wang, M. J., Qi, S. Z., and Zhang, X. X. (2012). Wetland loss and degradation in the yellow river delta, Shandong province of China. *Environ. Earth Sci.* 67 (1), 185–188. doi: 10.1007/s12665-011-1491-0

Wu, W., Li, C. X., and Chen, X. C. (2021). Study on change sand characteristics of urban coastal landscape pattern driven by coastal zone rehabilitation–a case study of yingwuzhou wetland. *J. Northwest Normal Univ. (Natural Science).* 57 (4), 24–30. doi: 10.16783/j.cnki.nwnuz.2021.04.004

Yang, H. L., Tang, J. W., Zhang, C. S., Dai, Y. H., Zhou, C., Xu, P., et al. (2020). Enhanced carbon uptake and reduced methane emissions in a newly restored wetland. *J. Geophys Research: Biogeosciences.* 125 (01), 1–36. doi: 10.1029/2019JG005222

Zhang, Y., Shi, H., Liu, L. T., Shen, W., and Zhao, Z. X. (2022). Wintering waterbirds diversity and their impact factors in coastal lake wetlands of the Yangtze River in Jiangsu Province. *J. Lake Sci.* 34(6), 2005–2015. doi: 10.18307/2022.0616

Zheng, G. M. (2017). *A checklist on the classification and distribution of the birds of China* (Beijing: Science Press).

frontiers | Frontiers in Marine Science

TYPE Original Research
PUBLISHED 09 March 2023
DOI 10.3389/fmars.2023.1115896

OPEN ACCESS

EDITED BY
Guanqiong Ye,
Zhejiang University, China

REVIEWED BY
Huang Honghui,
South China Sea Fisheries Research Institute (CAFS), China
Periyadan K. Krishnakumar,
King Fahd University of Petroleum and Minerals, Saudi Arabia

*CORRESPONDENCE
Dehai Song
songdh@ouc.edu.cn

SPECIALTY SECTION
This article was submitted to Coastal Ocean Processes, a section of the journal Frontiers in Marine Science

RECEIVED 04 December 2022
ACCEPTED 20 February 2023
PUBLISHED 09 March 2023

CITATION
Wu W, Hu J and Song D (2023) Assessment of marine ecosystem health and its key influencing factors in Laizhou Bay, China.
Front. Mar. Sci. 10:1115896.
doi: 10.3389/fmars.2023.1115896

Assessment of marine ecosystem health and its key influencing factors in Laizhou Bay, China

Wen Wu[1,2], Jinming Hu[1] and Dehai Song[3,4]*

[1]College of Oceanic and Atmospheric Sciences, Ocean University of China, Qingdao, China, [2]Institute of Marine Development, Ocean University of China, Qingdao, China, [3]Frontier Science Center for Deep Ocean Multispheres and Earth System (FDOMES) and Physical Oceanography Laboratory, Ocean University of China, Qingdao, China, [4]Laoshan Laboratory, Qingdao, China

Introduction: Major bays worldwide have been disturbed by human pressures to varying degrees in recent years, resulting in many ecological and environmental issues. Maintaining the health of the bay ecosystem has national and international significances, as it enhances the environmental regulation function and resource development value of the region. This study aims to examine the evolution trend and regulatory mechanism of ecosystem health in Laizhou Bay (LZB), China.

Methods: A comprehensive DPSIR-based indicator framework is established, comprising 40 representative indicators of the natural environment status, ecological service function, and social values of the LZB ecosystem. The subjective and objective integrated weighting method is applied to determine the indicator weight. The Ecosystem Health Index is then calculated to assess the LZB ecosystem health from 1980 to 2019 and key influencing factors are identified through the scenario analysis.

Results: The results show that the health status of the LZB ecosystem has fluctuated and then increased overall over the past 40 years, with a fairly healthy state in the 1980s, an unhealthy state in 2005, and then a rebound to a subhealthy state. The key factors affecting the LZB ecosystem health are mostly pressure items, with land-based pollution, particularly agricultural non-point source pollution, having a more significant impact than reclamations.

Discussion: Reasonable recommendations are finally put forward on improving the ecosystem health in the study area, including refining the legislation and integrated mechanism related to regional management, building a coordinated land-sea governance system and exploring new technologies for integrated marine management. This study fills the knowledge gap of ecosystem health assessment for the entire LZB in such a long-time scale, and the research outcomes are expected to provide scientific references and guidance for decision-making and social-economic sustainable development in LZB and other bays.

KEYWORDS

marine ecosystem health assessment, DPSIR-based indicator framework, evolution trend, key influencing factors, Laizhou Bay

1 Introduction

Bays are a vital resource for human survival and a crucial support for the sustainable development of marine economy and society. In recent years, with the increased utilization of resources and the rapid growth of marine economy, the major bays in the world have been subject to various human pressures (Lyu et al., 2022; Yu et al., 2022). This leads to the saturation of environmental carrying capacity and a serious decline in the health of the bay ecosystem. Now it has been widely recognized that maintaining the health of the bay ecosystem is conducive to enhancing the environmental regulation function and resource development value of the region (Borja et al., 2016; Padua et al., 2023).

Marine ecosystems are composed of abundant biological communities in seawater and marine environment, with functions of energy flow, material circulation and information transmission. As the largest ecosystem in the biosphere, they play an important role in regulating the global climate and maintaining the water cycle and carbon cycle in the biosphere (Editorial Committee of Biological Volume in General Editorial Committee of China Agricultural Encyclopedia, 1991). The term "marine ecosystem health" was initiated in 1990s by Leppard and Munawar (1992). A healthy marine ecosystem is considered to be "a living organism" with sustainable productivity and metabolic vitality, internal structure maintenance ability, self-control and maintenance, threat-response and resilience capability, etc. (Epstein, 1999; First Institute of Oceanography, State Oceanic Administration, 2007; Shi et al., 2010). In addition to these characteristics, the marine ecosystem's function of providing sustainable services for human society is also emphasized (Wiegand et al., 2010; Costanza, 2012; Halpern et al., 2012; Borja et al., 2016). Human activities have a profound impact on the health of the marine ecosystem, which can produce direct or cumulative effects and lead to the deterioration of the marine ecosystem (Epstein et al., 1994; Rombouts et al., 2013; Lyu et al., 2022; Yu et al., 2022).

Various methods have been applied to assess the marine ecosystem health, such as the Ocean Health Index (OHI), the bio-evaluation method, the indicator framework method and others. For example, based on 10 representative indicators and the utilization of assessment area, OHI has been used to effectively quantify the degree of variation in marine ecosystem health (Halpern et al., 2012). It provides a new idea and method for China's research and management practice in this field (e.g., Xu, 2012; Zheng and You, 2013; Wu and Chen, 2019). The core aspect of bio-evaluation method is to select specific species that can reflect the ecosystem health within a certain range. The health of the ecosystem in the study area can be determined through the physiological state of the selected species directly or by calculating relevant biological indices or mapping based on it indirectly (Quan and Zhu, 2011). The bio-evaluation methods mainly include the indicator species method (e.g., Kennedy and Jacoby, 1999; Wells et al., 2004; Mallory et al., 2006; Vassallo et al., 2006; Whitfield and Harrison, 2008; Zhao et al., 2015; Aguirre-Rubí et al., 2018), the biological index method (e.g. Borja et al., 2003; Cai, 2003; Sun, 2013; Baek et al., 2014; Zhao et al., 2015; Zhang and Zhao, 2018), the graphic analysis method (e.g., Gray, 1981; Warwick, 1986; Zhang, 2005; Tang et al., 2006), etc.

The indicator framework method is based on the selection of appropriate evaluation indicators, the clarification of indicator weights, and the determination of appropriate evaluation criteria (Quan and Zhu, 2011). The indicator framework can systematically illustrate the evolution process of the ecosystem as well as fully reflect its complexity of structure and function, which is helpful for assessing the health status of the regional ecosystem in a comprehensive matter. The Pressure-State-Response (PSR) model, jointly developed by the Organization for Economic Co-operation and Development (OECD) and the United Nations Environment Programme (UNEP), is one of the most widely used conceptual framework and report tools (OECD, 1993; Hammond, 1995; UNEP, 2006). The PSR model answers the following three questions: what happened, why it happened and how humans should respond. Pressure indicators (P) describe human activities that can affect the marine ecosystem, representing the pressures caused by human activities on the environment. State indicators (S) reflect the ecosystem's response on human activities, representing the status of environmental qualities and natural resources. Response indicators (R) refer to social actions to environmental and ecological problems (OECD, 1993; OECD, 2003; UNEP, 2006).

The PSR model has been modified to form the Driver-Pressure-State-Impact-Response (DPSIR) model (see Section 3.2) by the UNEP and the European Environment Agency (EEA) (EEA, 2005; Ramos et al., 2007), which has been applied to the studies of evaluating the sustainable development of marine economy, marine ecological security, sustainable utilization of resources and marine ecosystem health, etc. (e.g., Xu and Ma, 2017; Chen and Chen, 2021; Ma and Sun, 2021). The PSR/DPSIR models provide the basis for many other frameworks and pathways for the indicator development and are used worldwide (Wu et al., 2017). Furthermore, the PSR model considers both ecological and social connotations of marine ecosystems; while the DPSIR model formulates the coupling relationship between human activities and ecosystems in a more intuitive and effective way. Thus, in this study, the DPSIR model is accepted as the fundamental direction for the indicator establishment and ecosystem health assessment.

Laizhou Bay (LZB) is one of the three major bays in the Bohai Sea and the largest bay in Shandong Province, China (Wang et al., 2021). Since the 1980s, the rapid development of marine economy in LZB has been driven by its geographical location advantages, resources and environment endowment (Li et al., 2014). Now LZB has become a high-quality development strategic location for Shandong Province to promote the construction of a strong marine province. However, due to its dense population distribution and diverse human activities, there are many environmental and ecological problems, and the ecosystem health of this region is not optimistic. Therefore, it is of great importance to identify the evolution trend of its ecological environment and the key factors that affect the health of the LZB ecosystem.

So far, a few studies have been conducted on the ecosystem health assessment of LZB and its internal waters and adjacent sea areas, as summarized in Table 1. It can be seen that the study periods of existing studies are relatively short, which could not sufficiently illustrate the dynamic changes of LZB ecosystem health. In addition, the majority of

current studies have adopted the Analytic Hierarchy Process (AHP) as the weighting method which is relatively subjective and have ignored the use of objective methods such as the Entropy method. Few studies have considered the impact of human activities on the ecosystem and the social values of marine ecosystem. Currently, there is a lack of long-time-scale research on the assessment of ecosystem health covering both the watershed and sea area of LZB. Therefore, this paper aims to fill this knowledge gap by investigating the ecosystem health assessment and environmental management strategies of LZB.

This paper is arranged as follows: in Section 2, the study area will be briefly introduced and main anthropogenic pressures and their impacts on LZB will be analyzed; a comprehensive and supportive indicator framework incorporating natural environment, ecological service function and social values will be presented in Section 3; a weighting procedure combining subjective and objective methods will be conducted to determine the index weight, and data and assessment method will also be described in this section; Section 4 will provide results and discussion on the LZB ecosystem health assessment through the calculation of Ecosystem Health Index (EHI); key factors of anthropogenic influence will be identified and the impacts of single and composite factors on the LZB ecosystem health be explored through the scenario analysis subsequently; countermeasures and suggestions on how to improve the LZB ecosystem health will be given in Section 5; and Section 6 offers conclusions of this study.

2 Study area

The study area consists of both sea and land areas, as shown in Figure 1. The sea study area covers the entire LZB (36°25′~37°45′N, 118°17′~120°45′E), including the Yellow River estuary in the west of the bay, which is a typical semi-enclosed bay with a coast length of 319.06 km and bay area of 6966.93 km^2 (Li et al., 2007; Zhao et al., 2016). The basin of rivers discharged into LZB covers a total of 51 counties (districts and county-level cities) belonging to 14 prefecture-level cities in Shandong Province, which are taken as the land study area.

The water-depth in LZB is less than 10 m on average, with a maximum of about 18 m. The bay is dominated by semidiurnal tides, with an average tidal range is 0.92~1.43 m. There are over 10 rivers discharged into the bay such as the Yellow River, the Xiaoqing River, the Weihe River and so on. The Xiaoqing River, with a length of 240 km, is the second longest river (secondary to the Yellow River) draining into LZB. Since the 1970s, the industrialization progress along the Xiaoqing River has altered the river functions from flood, irrigation and shipping to sewage discharge. The annual runoff of Xiaoqing River is much smaller than that of the Yellow River; however, it carries a large amount of pollutants (e.g., nutrients, organic pollutants, and heavy metals) into the sea. That is one of the main reasons for the substantial degeneration of water quality in LZB (Ma et al., 2004; Shandong Academy for Environmental Planning, 2018).

According to the statistics, in 2019, the population and gross domestic product (GDP) in the study area accounted for 35.9% and 34.4% of Shandong Province respectively. The population growth and economic development already generated severe ecological and environmental issues in LZB, including pollution, eutrophication, habitat destruction, decline of marine ecological services and potential marine hazard risk, which lead to increased pressures on the health of the bay ecosystem. This would in turn impose rigid constraints on the sustainable development of economy, society, resources and environment in coastal zones surrounding LZB.

TABLE 1 Summary of existing studies on ecosystem health assessment in Laizhou Bay.

Study area and period	Assessment method			Consideration of social values and ecosystem service function (Yes/No)	Reference
	Indicator selection method	Weighting method	Assessment results		
West of Laizhou Bay, May 2002	Structure-Function Index	Analytic Hierarchy Process (AHP)	Comprehensive Index Method	No	Yang et al. (2003)
Laizhou Bay, May and August 2004 and 2006	In accordance with the *Guidance for the Assessment of Coastal Marine Ecosystem Health*			No	Xie (2009)
Laizhou Bay and its adjacent sea areas, August 2009, May and Semptember 2010, May and August 2011	Biological index method	—	—	No	Zhang (2013)
Laizhou Bay, May, August, Octorber, December 2011	Bio-evaluation method (indicator species method, biological index method, graphic analysis method)	—	Cluster analysis	No	Zhang et al. (2013)
Laizhou Bay, 2009	—	AHP	Comprehensive Index Method	Yes	Li et al. (2015)
Yellow River Estuary, October 1991 and 2013	PSR model	AHP	Comprehensive Index Method	Yes	Niu et al. (2017)
Laizhou Bay, 2014-2016	Structure-Function Index	AHP	Comprehensive Index Method	No	Song et al. (2017)

FIGURE 1
The map of the study area.

3 Data and methods

3.1 Data sources

Due to the instability of Shandong Province's administrative divisions and the difficulty of collecting statistical material prior to China's Opening Policy in the late 1970s, as well as the human pressures on LZB since 1990, this paper chooses 1980~2019 as the research scale. Nine years (i.e., 1980, 1985, 1990, 1995, 2000, 2005, 2010, 2015 and 2019) are selected for analysis with a time interval of five years, except for the last interval which is four years due to the impact of COVID-19 on statistical work.

Relevant data and information are all obtained from secondary data sources, including bulletins (e.g., China River Sediment Bulletin, Bulletin of China Marine Ecological Environment Status, Bulletin of China Offshore Environmental Quality, Bulletin of China Marine Disaster, Bulletin of Ecological Environment Status of Shandong Province, Bulletin of Marine Environmental Quality of Shandong Province, Bulletin of Marine Environment Status of North China Sea Region, Bulletin of Marine Disaster of North China Sea Region), yearbooks (e.g., China Statistical Yearbook On Environment, China Country Statistical Yearbook, Shandong Statistical Yearbook, statistical yearbooks of related cities), monitoring stations, literatures (e.g., Gao and Zhang, 1996; Wang, 2000; Zhao and Kong, 2000; Ma et al., 2002; Hao et al., 2005; Jiang et al., 2005; Li et al., 2006; Zhang et al., 2006; Zhao et al., 2010; Lin et al., 2013; Ma et al., 2015; Zhou et al., 2015; Jiang et al., 2018; Song et al., 2018; Wei et al., 2018; Xin et al., 2019; Huang et al., 2021), monographs (e.g., Shandong Association for Science and Technology, 1991; Tian et al., 1996; Zhang et al., 2003; He et al., 2009; Liu et al., 2010; Xu et al., 2013; Project Team of "Research on Monitoring and Controlling Technology of Economic Activities Around Bohai Sea Based on Environmental Carrying Capacity", 2016; Yu et al., 2016; Zhang and Hu, 2019; Ye et al., 2021), dissertations (e.g., Zhang, 2013; Yang, 2018), reports (e.g., Technical Report on the Study of Spatial and Temporal Distribution Characteristics and Variation Trend of Pollution in Shandong Coastal Sea Areas), official websites (e.g., Ministry of Natural Resources of the People's Republic of China, Ministry of Ecology and Environment of the People's Republic of China, Tidal Table on the China Maritime Service webpage; Department of Ecology and Environment of Shandong Province) and other kinds of statistical data (e.g., Shandong Cencus Data 1990). The analogy and interpolation methods are used to supplement the data missing at the initial and middle time periods for each indicator, respectively.

3.2 Establishment of the indicator framework

In order to explore the internal logic of land-sea coupling in LZB, a DPSIR conceptual model is adopted for the establishment of the indicator framework, taking into account previous research outcomes related to the assessment of marine ecosystem health and specific features of the study area. Figure 2 illustrates the closed feedback loop structure of the DPSIR model, which provides a clear logic and comprehensive explanations of the internal causal relationship between socio-economic development and ecosystem evolution.

To assess the health of the LZB marine ecosystem, an indicator framework is developed based on economic and social value related factors of the land area, and environmental characteristics and ecosystem service function related factors of the sea area. Principles such as policy consistency, representativeness, simplicity, understandability, data accessibility, information precision, data-computing readiness and communication convenience, have been considered while selecting indicators (Wu et al., 2017).

The indicator framework is divided into target layer, criterion layer and indicator layer (Table 2). The target layer is Laizhou Bay Ecosystem Health Index. According to the classification criteria of DPSIR model, the criterion layer contains five dimensions: driving force (D); pressure (P); state (S); impact (I); and response (R). The indicator layer covers 40 indicators affecting the ecosystem health of LZB.

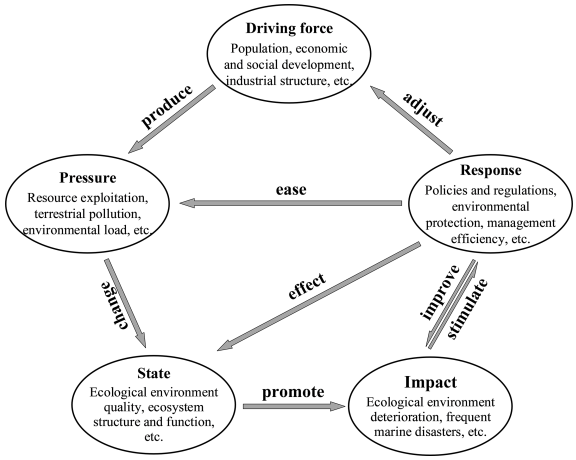

FIGURE 2
The DPSIR conceptual model for the ecosystem health assessment indicator framework in Laizhou Bay.

TABLE 2 The indicator framework for the ecosystem health assessment in Laizhou Bay.

Target layer	Criterion layer	Description of criterion layer	Indicator layer	Unit
Laizhou Bay Ecosystem Health Index	Driving force (D)	Potential cause of changes in the bay ecosystem health (Fundamentally induced ecological and environmental pressures *via* driving the population growth, socio-economic development and industrial structure layout)	Total population (D1)	10^4 capita
			GDP per capita (D2)	RMB100mn/ 10^4 capita
			Value-added of primary industry (D3)	RMB100mn
			Value-added of secondary industry (D4)	RMB100mn
			Value-added of tertiary industry (D5)	RMB100mn
			Proportion of primary industry (D6)	%
			Proportion of secondary industry (D7)	%
			Proportion of tertiary industry (D8)	%
	Pressure (P)	Disturbance and stress of human activities and natural processes on the bay ecosystem (Influenced by the driving force dimension; revealing the direct causes of damage to the bay ecosystem; reflecting the intensity of human demands for resources from the bay ecosystem; further changing the state dimension)	Marine catch (P1)	t
			Discharge of total nitrogen (TN) from mariculture (P2)	t
			Discharge of TN from livestock and poultry breeding (P3)	t
			Amount of agricultural chemical fertilizer entering the sea (P4)	t
			Amount of pesticides entering the sea (P5)	t
			Industrial wastewater discharge (P6)	10^4 t
			Domestic sewage discharge (P7)	10^4 t
			Annual runoff of the Yellow River (P8)	10^8 m^3/a
			Annual sediment discharge of the Yellow River (P9)	10^8 t/a
			Dissolved inorganic nitrogen (DIN) flux of the Yellow River (P10)	10^4 t/a
			Annual runoff of the Xiaoqing River (P11)	10^8 m^3/a
			Chemical Oxygen Demand (COD) flux of the Xiaoqing River (P12)	t/a
			Reclamation area (P13)	km^2
	State (S)	Reflecting the actual situation of habitat quality and ecosystem structure and function in the bay (The changes of hydrodynamics, water quality and biological community caused by the pressure dimension which promote the occurrence of influence)	Natural wetland area (S1)	km^2
			Maximum tidal range (S2)	cm
			Phytoplankton biodiversity (S3)[a]	—
			Salinity (S4)	‰
			Water temperature (S5)	°C
			Dissolved oxygen (DO) (S6)	mg/L
			COD (S7)	mg/L
			pH (S8)	—
			Chlorophyll *a* (S9)	μg/L
			DIN (S10)	mg/L
			Active phosphate (PO_4-P) (S11)	mg/L

(Continued)

TABLE 2 Continued

Target layer	Criterion layer	Description of criterion layer	Indicator layer	Unit
	Impact (I)	The feedback effect of the state of the bay on human health, social economy and ecosystem (Inducing the occurrence of the response dimension)	Occurrence area of red tide in coastal waters (I1)	km^2
			Maximum offshore distance of sea ice outer line (I2)	n mile
			Proportion of sea area below Class I sea water quality standard (I3)	%
			Ratio of nitrogen and phosphorus (N/P) (I4)	—
	Response (R)	Protection and management measures to deal with the destruction of ecological balance (Conversely relieving the pressure, acting on the state and improving the impact)	Centralized treatment rate of sewage treatment plant (R1)	%
			Perfection of relevant policies, laws and regulations (R2)[b]	—
			Retention rate of natural coastline (R3)	%
			Proportion of marine nature/special reserves (marine parks) (R4)	%

[a]Phytoplankton biodiversity (S3) is expressed by the Shannon Wener Diversity Index (H' Index) (Zhao et al., 2015); [b]The score of R2 within each time interval is calculated based on the given values in light of the ranks of legal effect of relevant policies and regulations (i.e., the value for laws is given as 7; administrative regulations as 6; local administrative regulations as 5; departmental rules and regulations as 4; local government and department rules and regulations as 3; departmental normative documents as 2; and local normative and work documents as 1).

3.3 Indicator standardization and weighting

After building the indicator framework, the positive processing and standardization should be conducted for the indicators. According to Ye (2003), there are four types of indicators classified during the positive processing based on the indicator attribute: (1) maximum-style indicator, also called benefit-style indicator, denoting that the larger the value the better; (2) minimum-style indicator, also called cost-style indicator, denoting that the smaller the value the better; (3) intermediate-style indicator, denoting that the closer the value is to a specific value the better; and (4) interval-style indicator, denoting that it is better if the value falls within an optimal range. The deviation standardization is achieved through the dimensionless processing for the indicators.

The comprehensive weighting method, combining with the subjective AHP (Saaty, 1977) and objective Entropy Weight Method (EWM) (Dong, 2019), is used to determine the indicator weight, in order to understand the contribution rate of different indicators to the health evolution of LZB ecosystem. This method effectively eliminates subjectivity and uncertainty of assessment and improves the rationality of indicator weighting. An expert indicator ranking procedure was conducted following the AHP method, expecting to highlight indicator priorities. A total of 21 experts, selected based on their knowledge and experience of marine management, ecosystem health assessment and the study area, were invited to conduct the indicator ranking process.

Through reasonably integrating subjective and objective weights, the comprehensive weight W_j of each indicator is calculated according to Liu et al., (2015):

$$W_j = W_j^1(1 - e_j) + W_j^2 e_j \quad (j = 1,\ 2,\ \ldots,\ m) \tag{1}$$

where e_j is the information entropy of the jth indicator; and m denotes the indicator (m=40).

3.4 Assessment method and criteria

The Ecosystem Health Index (EHI) is calculated by the weighted summation of standardized indicator data, with a higher value indicating a higher health degree (Lu et al., 2013):

$$EHI = \sum_{j=1}^{m}\sum_{i=1}^{n}(\tilde{z}_{ij} W_j)(i = 1, 2, \ldots, n; j = 1, 2, \ldots, m) \tag{2}$$

where $\tilde{z}_{ij}$ is standardized indicator data; W_j is the comprehensive weight the jth indicator; n and m denotes the number of time interval and indicator, respectively (n=9 ; and m=40).

As given in Table 3, the assessment criteria are divided into five levels, namely, morbid, unhealthy, subhealthy, fairly healthy and healthy (e.g., Lu et al., 2013; Wu and Chen, 2019).

4 Results and discussion

4.1 Assessment of LZB ecosystem health

According to Section 3.3, the results of positive processing and deviation standardization of indicators are presented in Tables A1, A2, respectively; the results of indicator weighting are presented in Table A3 (Supplementary Material). Figure 3 illustrates the proportion of integrated indicator weight value of criterion layer and comparison of integrated weight values of each indicator. It can be seen that the pressure dimension has the highest proportion of weight, followed by the state, driving force, response and impact dimensions. Of the top 10 indicators, six belong to the pressure dimension, indicating that multiple pressure sources from land and bay environment are the primary factors affecting the LZB ecosystem health.

According to Section 3.4, the EHI value are calculated and the health degree of each year can be obtained accordingly, so as to determine the evolution trend of LZB ecosystem health in the past 40 years. Table 4 shows that the highest EHI value (0.6359) was observed in 1985, indicating a fairly healthy state; the lowest value (0.3813) was observed in 2005, indicating an unhealthy state, which is consistent with the results of Xie (2009). Additionally, the EHI value in 1980 was the second highest, and the rest of the years were in a subhealthy status, which is also in agreement with previous studies (Song et al., 2017).

The evolution trend of EHI value from 1980 to 2019 is shown in Figure 4A. It can be seen that the overall health status of LZB ecosystem has demonstrated a phased feature with a trend of first fluctuating and then continuously rising. China initiated the Openings Policy since the 1980s, when economic development just started. The LZB ecological environment can be treated as a baseline without pollution, thus its ecosystem health was good in the 1980s. However, in the 1990s, the environmental status of the bay was not optimistic due to multivariate and composite pressures along the coast (e.g. reclamation, land-based pollution, marine aquaculture, and overfishing), resulting in the continuous deterioration of LZB ecosystem health. After reaching the lowest value in 2005, the EHI recovered to a certain extent, indicating that the comprehensive environmental improvement of LZB was well implemented at this stage (Li et al., 2020).

4.2 DPSIR analysis

As the health status of LZB ecosystem is jointly determined by the variation trend of indicators at each criterion layer, this section will discuss the evolution trends of sub-index in criterion layers and their motivations (Figure 5).

(1) Driving force

With the rapid and high-quality development of marine economy in LZB in recent 40 years (Li et al., 2014), the driving force index presents a fluctuating and rising trend as a whole. According to Figure 3, indicators such as total population (D1) and GDP per capita (D2) play a leading role in the driving force layer. This indicates the population growth and socio-economic development in the land areas surrounding LZB are likely to cause ecological and environmental pressures and impact the ecosystem health, as described in Section 2.

(2) Pressure

Following the positive processing of indicators, a higher pressure index represents a lower pressure. The pressure index has been dominant from 1980 to 2005. During this period, it had a slight downward trend between 1980 and 1990, followed by a sharp decrease until reaching the minimum value in 2005 and a subsequent slow rebound. Indicators such as discharge of TN from livestock and poultry breeding (P3), marine catch (P1), DIN flux of the Yellow River (P10), COD flux of the Xiaoqing River (P12) and annual runoff of the Xiaoqing River (P11) all reached relatively low or lowest values in 2005 (Table A2). This suggests that non-point source pollution from agricultural, animal husbandry and fishery production activities in the land areas surrounding LZB were likely major contributors to the bay's ecosystem health, particularly in 2005.

On one hand, the implementation of a summer fishing moratorium in the Bohai Sea since 1995 has increased the amount of fishery resources in the Bohai Sea, resulting in a peak marine catch in LZB in 2005. However, the strong fishing volume has not been able to prevent the decline of fishery resources, leading to a decrease in marine catch in LZB after 2005 (Hu et al., 2020). On the other hand, the Yellow River and Xiaoqing River basins, which are densely populated and contain numerous chemical industry zones, are two of the main pollution sources in LZB (Zhang et al., 2022). Industrial wastewater and domestic sewage, carrying large amounts of nutrients into the sea (Section 2; Shandong Academy for Environmental Planning, 2018; Li et al., 2020), have great impact on the distribution and structure of nutrients in the seawater (Strokal et al., 2017). For example, as reported by the Bulletin of Marine Environmental Quality of Shandong Province, 87% of the 23 sections in the Xiaoqing River basin, had a Class IV water quality (Sea Water Quality Standard of China) or worse in 2019. Excessive use of nitrogen fertilizer in agricultural production has also contributed to the pollutant flux into the sea. For example, the fertilizer consumption in Shandong Province increased by over three times between the 1980s and the 1990s (Xiong and Weng, 2015). These factors have caused water eutrophication, altered the nutrient structure and biodiversity of the sea area, and ultimately led to the deterioration of ecosystem health in LZB (Wang et al., 2021; Zhang et al., 2022).

(3) State

The state index of LZB ecosystem has exhibited a fluctuating evolution trend, with higher values in the 1980s and 2010s and the lowest value in 2005. The DIN concentration (S10) reached the highest value in 2005 (Figure 4B), which is in agreement with the findings of Zhang et al. (2022). This can be attributed to the increased nutrient flux from rivers and the reduction of sea area due to reclamations before 2005 (Ding et al., 2018; Xu et al., 2021). Zhang et al. (2022) also found the riverine inputs are the primary contributor to the increase of DIN

TABLE 3 Classification of EHI levels in Laizhou Bay.

Health level	EHI range	Health degree
5	[0.0, 0.2)	Morbid
4	[0.2, 0.4)	Unhealthy
3	[0.4, 0.6)	Subhealthy
2	[0.6, 0.8)	Fairly healthy
1	[0.8, 1.0]	Healthy

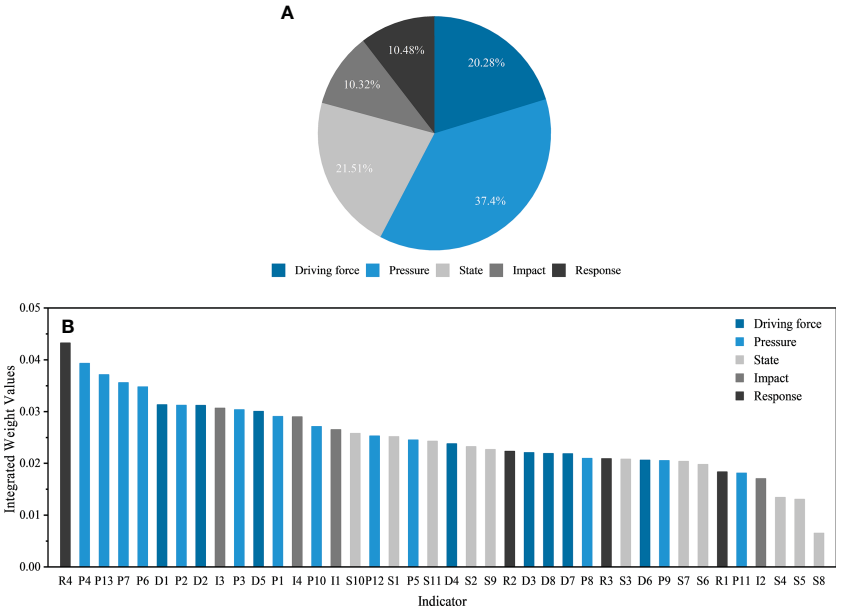

FIGURE 3
The indicator framework of ecosystem health assessment in Laizhou Bay: **(A)** the proportion of integrated indicator weight value of criterion layer; and **(B)** comparison of integrated weight values of each indicator.

concentration. Subsequently, the implementation of pollution control and environmental protection surrounding LZB have led to a decrease in nutrient concentration (Feng et al., 1999; Zhang et al., 2022).

(4) Impact

The impact index of LZB ecosystem has a certain degree of uncertainty and contingency, yet its overall downward trend with fluctuation has resulted in an increasing negative impact on the ecosystem health. After 2010, the impact index rebounded mainly due to the cold current weather. As reported by the Bulletin of China Marine Disaster, in 2010, the most severe sea ice disaster occurred in LZB in the past 40 years.

(5) Response

Overall, the response index of LZB ecosystem has presented an upward trend with fluctuation and the growth rate during 2005~2010 has been particularly rapid. This is mainly due to the indicator "proportion of marine nature/special reserves (marine parks)" (R4), which has the highest weight in the indicator framework and is the key factor affecting the ecosystem health (Section 4.3). The establishment of the first national marine reserve in LZB, the Dongying Yellow River Estuary Ecological National Marine Special Reserve, in November 2008 has contributed to the rise of the response index. This indicates an increased awareness of marine protection and improved abilities to prevent and respond to marine pollution, marine disasters and other events, ultimately demonstrating the stable and sound development of LZB ecosystem.

4.3 Identification of key factors on EHI

For the past 40 years, the key factors affecting the health of LZB ecosystem can be distinguished according to the weight value of each indicator (Section 4.1.2). As shown in Figure 3, the integrated indicator

TABLE 4 Ecosystem Health Index (EHI) and health degree of the ecosystem health in Laizhou Bay.

Year	Driving force (D)	Pressure (P)	State (S)	Impact (I)	Response (R)	EHI	Health degree
1980	0.0893	0.2921	0.1291	0.0830	0.0199	0.6134	Fairly healthy
1985	0.0911	0.2905	0.1298	0.0935	0.0310	0.6359	Fairly healthy
1990	0.0771	0.2888	0.0954	0.0620	0.0258	0.5491	Subhealthy
1995	0.0837	0.2186	0.1090	0.0832	0.0283	0.5228	Subhealthy
2000	0.0930	0.1713	0.0851	0.0647	0.0235	0.4376	Subhealthy
2005	0.0803	0.1227	0.0792	0.0632	0.0360	0.3813	Unhealthy
2010	0.0895	0.1244	0.1234	0.0325	0.0886	0.4585	Subhealthy
2015	0.1157	0.1260	0.1216	0.0537	0.0881	0.5053	Subhealthy
2019	0.1391	0.1410	0.1362	0.0557	0.0880	0.5599	Subhealthy

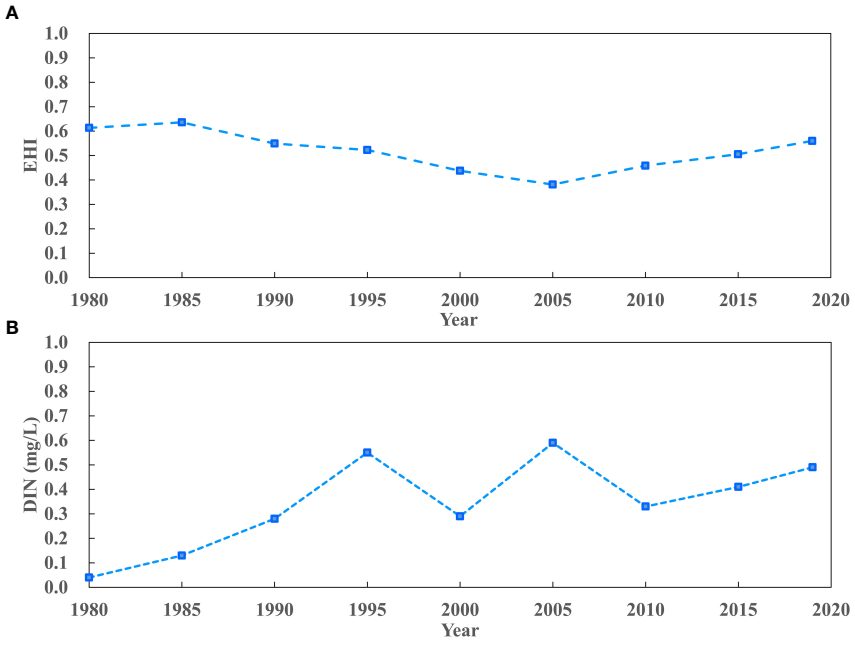

FIGURE 4
(A) The evolution trend of EHI value and **(B)** the DIN concentration in Laizhou Bay from 1980 to 2019.

weight of both pressure and state layers has exceeded 50%, with the weight of pressure layer exceeding one-third of the total weight. This indicates that the key influencing factors are mostly indicators in the two criterion layers. Among all 40 indicators, R4 in the response layer has the highest weight, which may be attributed to the small information entropy of indicator data.

In the pressure layer, indicators with high weight include amount of agricultural chemical fertilizer entering the sea (P4), reclamation area (P13), domestic sewage discharge (P7) and industrial wastewater discharge (P6), etc. This suggests that the ecological and socio-economic damage caused by land-based sewage discharge and reclamation has severely restricted the healthy development of LZB ecosystem. For example, land-based sewage discharge is the main source of pollution in the Bohai Sea, accounting for approximately 90% of the total pollution (Zhang et al., 2007). Therefore, this section adopts the limit thought method to conduct a scenario analysis. It is assumed to remove one single key factors such as reclamation and different types of land-based sewage discharge (e.g., agricultural and productions, residents' daily life) as well as the combined effect of these two kinds of anthropogenic pressures. Thus, the variation degree and trend of EHI value can be observed, in order to explore the direction of efforts to improve the LZB ecosystem health in the future.

The scenario simulation results (Figure 6) illustrate that the EHI value of removing the combined effect of reclamation and land-based sewage discharge is the highest. Different from the trend of original index, its highest value appeared in 2019 which was fairly healthy, and the removal of combined key factors has a more significant impact over time. The lowest values of seven broken lines in Figure 6 all appeared in 2005, while all simulated scenarios were in a subhealthy status in that year except for the original index. As illustrated in Table 5, the health status of LZB ecosystem after removing the composite effect was improved in 2015 and 2019 which was fairly healthy, indicating that

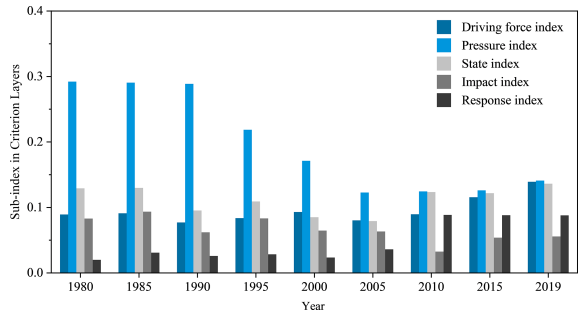

FIGURE 5
The evolution trends of sub-index in criterion layers for the ecosystem health assessment in Laizhou Bay.

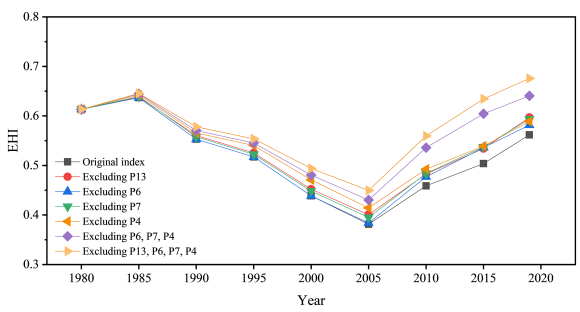

FIGURE 6
Scenario analysis of ecosystem health in Laizhou Bay.

reducing the intensity of human pressures can effectively alleviate the LZB ecosystem health. In terms of the effects of removing single key factor, the highest EHI values appeared while removing "amount of agricultural chemical fertilizer entering the sea" (P4) from 1985 to 2015 and "reclamation area" (P13) in 2019, respectively.

Reclamation in the Bohai Sea has been halted since 2017, yet the impacts of reclaimed areas on the hydrodynamic, water environment and ecosystem factors of the bay are irreversible, such as changes in landforms, reduced environmental and tidal capacities, occupation of biological habitats and accelerated coastal erosion (Choi et al., 2010; Park et al., 2014). For example, from 1968 to 2015, the natural wetland and intertidal area of LZB was reduced by 17.2% and 56.1%, respectively; from 2003 to 2013, the LZB water area was reduced by 7.38% and the average tidal volume by 5.75% due to the reclamation (Xu et al., 2021). Thus, the sea area should be restored by returning farmland and dikes to the sea and dismantling abandoned aquaculture ponds, etc.; the hydrodynamic environment of LZB should be improved by dredging key waterways and bay crest, etc.

Meanwhile, the main agricultural production areas in northern Shandong are distributed along the LZB coast (Project Team of "Research on Monitoring and Controlling Technology of Economic Activities Around Bohai Sea Based on Environmental Carrying Capacity", 2016). As stated above, agricultural chemical fertilizers infiltrate into the surface or underground through surface runoff and leaching and eventually enter the bay, affecting its ecological environment. Since 2015, the Ministry of Agriculture (now as the Ministry of Agriculture and Rural Areas) of the People's Republic of China has made great efforts to promote rational and scientific fertilization and achieved optimistic results to some extent. Additionally, the LZB region has a solid industrial foundation (see Section 5.2 in detail). However, industrial production is accompanied by pollutant discharge, particularly the compact industrial layout and concentrated wastewater discharge around the Xiaoqing River basin, which pollutes the LZB ecological environment (Section 2; Wang et al., 2021). With the continuous improvement of urbanization level in the LZB area, the domestic sewage discharge has been gradually increasing in recent years (Zhang et al., 2022). Therefore, measures should be taken to explore scientific methods to reduce discharges of land-based pollutants. A long-term mechanism for economic and ecological assessment of environmental damage caused by land-based pollution should be established. These measures are beneficial in reducing the amount of land-based pollutants entering the sea and improving the LZB ecosystem health.

5 Recommendations for improving LZB ecosystem health

Although the healthy status of LZB ecosystem has become increasingly obvious in recent years, the disturbance and stress suffered by the bay still exist and the health level (EHI) is still lower than the historical situation. Therefore, based on the above assessment results and the situation of study area, this section will put forward specific countermeasures and suggestions for improving the LZB ecosystem health. The following recommendations are expected to achieve the sustainable development of regional economy and ecological environment in a coordinated way.

5.1 Refining regional management of LZB ecosystem health

(1) Perfecting the legislation related to regional management

It is evident from the evolution trend of R2 (Section 4.1) that the legal system construction based on the LZB ecosystem health presents certain phased characteristics, which is closely related to its health status. The introduction of policies and regulations has been beneficial in improving the efficiency of ecological pollution control, while the intensification of environmental pollution has also, to some extent, driven the construction of a legal system. In China, relevant laws concerning land and sea ecological protection and governance have been established. However, there is still a lack of a basic law that comprehensively guides integrated marine management from the perspective of land and sea coordination. Furthermore, the majority of existing relevant provisions are scattered in policies and regulations with lower legal effect (e.g., administrative regulations, and departmental rules) (Section 3.2) which can hinder departmental collaboration and resource allocation, thus affecting the effectiveness of marine management. Taking into account the strong regional characteristics of the generation of environmental pressure, the features of aquatic ecology and the rigid demand for resource utilization, relying solely on laws and regulations within the national management scope for ecological governance is insufficient. The *Law on Special Measures for Seto Naikai Environmental Protection* of Japan is a good example of how to address this issue. Therefore, China can draw lessons from the experience of other countries to refine relevant law making of regional management. For example, special laws for specific regions (e.g., the Bohai Sea, Laizhou Bay or the Xiaoqing River) can be formulated, establishing strategic objectives, responsibility subjects, and regulatory requirements for governance of regional ecosystem. The strictest mechanism and most rigorous rule of law should be adhered to in order to maintain the LZB ecosystem health.

(2) Improving the integrated mechanism of regional management

The management of sea and land areas in LZB is generally based on the division of administrative ownership (Section 2). This can lead to fragmentation and unclear rights and responsibilities among multiple local administrative departments, making it difficult to achieve the high-level coordinated decision-making management. Thus, this paper suggests the establishment of an integrated and coordinated organization to guide the management, strengthen the overall planning, coordination and communication among administrative departments, and improve the regional management integration mechanism of LZB.

Extreme weather events, such as heavy rainfall, can have significant cumulative impacts on the ecological environment of coastal waters, as evidenced by the influx of large amounts of fresh water and nutrients (Walker et al., 2021). Human activities can further exacerbate the risks posed by these extreme weather events, necessitating the exploration of an integrated mechanism for managing the cumulative impacts of

TABLE 5 Summary of ecosystem health level corresponding to EHI obtained by removing the key factors of pressure layer in Laizhou Bay.

Year	Original index	Excluding P13	Excluding P6	Excluding P7	Excluding P4	Excluding P6, P7, P4	Excluding P13, P6, P7, P4
1980	F	F	F	F	F	F	F
1985	F	F	F	F	F	F	F
1990	S	S	S	S	S	S	S
1995	S	S	S	S	S	S	S
2000	S	S	S	S	S	S	S
2005	U	**S**	**S**	**S**	**S**	**S**	**S**
2010	S	S	S	S	S	S	S
2015	S	S	S	S	S	**F**	**F**
2019	S	S	S	S	S	**F**	**F**

"F" denotes "Fairly healthy", "S" denotes "Subhealthy" and "U" denotes "Unhealthy", respectively.

human activities and extreme weather processes on the environment and ecosystem in the LZB area, supported by long-term observation.

5.2 Building a coordinated land-sea governance system

To strengthen the linkage between land and sea areas in LZB, it is essential to consider the socio-economic and ecological functions of these two spatial domains as an organic entirety. The specific layout ways can be summarized as follows.

(1) Source-based Pollution Control

Based on the results of assessment (Section 4.1) and key factor identification (Section 4.3), the regulation and control of pollution sources should be prioritized. For example, a comprehensive consideration of LZB resources and environmental carrying capacity should be taken into account when establishing an environmental permit constraint mechanism; rewards and punishments should be provided accordingly. The utilization efficiency and management (e.g., utilization type, proportion, method and intensity) of fertilizer and pesticide should be strengthened and improved. Cleaner production technology should be promoted; production evaluation standards and audit should be improved. Additionally, the pollutant diffusion pathway should be changed. All sewage outlets into the sea should be investigated, recorded and renovated (Wang et al., 2021); wastewater treatment plants and pipe networks should be built, modified or expanded; and the sewage treatment process should be improved if necessary. The quality of cultivated land and farming methods should be improved; intensive and large-scale livestock and poultry breeding models should be established. Ponds and wetlands should be rehabilitated and the aquaculture scale be controlled. These measures should assist in controlling the total amount of pollutants and enhancing the management efficiency of joint prevention and control of land and sea pollution.

(2) Industrial structure adjustment and layout optimization

From the indicator weight results (Section 4.1), it can be seen that the structures of three types of industries in the LZB area do not directly affect its ecosystem health. However, influenced by factors such as natural environment, social background, industrial foundation and national policy guidance, the adjustment of industrial structure and layout will regulate the resource allocation, thus indirectly promoting the evolution trend of the LZB ecosystem health. As shown in Figure 7, in the past 40 years, the industrial structure of the LZB area has gradually changed from "secondary-primary-tertiary" to "secondary-tertiary-primary" and finally presented a preliminary "tertiary-secondary-primary" pattern.

As the predominant industry for a long period in the LZB area, the cumulative effect of environmental pollution caused by the industrial production cannot be ignored (Section 4.1). Consequently, the LZB area should optimize the structure of secondary industry and accelerate the process of new industrialization according to the principles of market demand guidance, scientific and technological conditions, regional coordinated development, pillar industry orientation, comprehensive benefits and sustainable development, etc. The tertiary industry should be the strategic focus of deepening the adjustment of industrial structure and modern competitive service industries should be vigorously developed (e.g., biotechnology, environmental monitoring, transportation, port logistics and eco-tourism). The transformation and upgrading of traditional marine industries should be promoted (e.g., marine chemical industry, marine mineral resources exploitation and marine fishery); new growth aspects for the development of marine innovative and service-oriented high-tech industries should be created (e.g., marine engineering equipment, marine biomedicine, seawater desalination and comprehensive utilization, and marine new energy).

(3) Promoting protection and restoration of the bay habitat

The highest weight of the R4 indicator (Section 4) implies that the protection and restoration of habitats is essential for the recovery of the LZB ecosystem health. To this end, a range of countermeasures can be implemented to protect and restore fragile and sensitive bay habitats, such as establishing marine reserves, strictly adhering to ecological protection red lines, strengthening the supervision of important ecological functional areas, implementing the siltation promotion and shoal reinforcement projects, and enhancing the coastal environment renovation. These measures would be beneficial for the

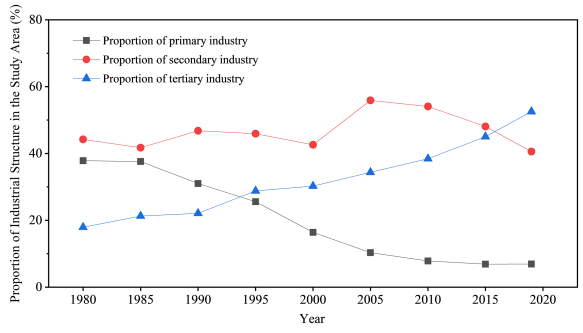

FIGURE 7
Industrial structure variations in the Laizhou Bay Area from 1980 to 2019.

sustainable development of marine resources and the construction of marine ecological civilization.

(4) Strengthening the capacity of marine spatial governance

According to the analysis in Section 4.3, reclamation is one of the key factors affecting the LZB ecosystem health. Therefore, the dynamic management of coastline use should be strengthened, the exploitation and utilization of coastal and island spatial resources should be strictly controlled, and the retention rate of natural coastline should be improved. The sea area functions should be clarified to meet the requirements for marine spatial planning under the new round of territorial spatial planning system in China (Xinhua News Agency, 2019). Additionally, the three fundamental systems regulated by the *Law of the People's Republic of China on the Administration of the Use of Sea Areas* (i.e., management of sea area ownership, sea area use demonstration, paid use of sea area system) should be further refined to achieve the synchronous improvement of social function values and ecological benefits in LZB.

5.3 Exploring new technologies for integrated marine management

In view of the assessment results and analysis in Section 4, the comprehensive governance of LZB necessitates scientific and technological innovation to address numerous issues at hand.

(1) Strengthening environmental monitoring and supervision mechanism

The environmental monitoring and emergency response capacity-building systems and a dynamic monitoring mechanism for coastal ecological environment based on the land and sea coordination should be established in the LZB region. Additionally, the risk prevention and control system for major marine environmental risk sources and environmental sensitive factors should be improved; the capability of marine observation and ecological early warning should be strengthened. Moreover, the integrated law-enforcement system for LZB should be refined with clearer responsibilities at all administrative levels and all kinds of illegal marine development activities must be punished resolutely.

(2) Promoting marine science and technology innovation capability

Shandong Province is a leader in marine science and technology in China, with advantages in promoting marine scientific and technological innovation. For example, it has nearly 50% of China's marine science and technology talents, more than 50 marine scientific research and teaching institutions, and over 230 marine science and technology platforms above provincial level (China Shandong Network, 2020). However, the transformation mechanism of scientific and technological achievements specific for the entire sea area of LZB is relatively weak; the allocation of scientific research resources is inadequate; the strategic support for marine science and technology is still insufficient. These issues impede the construction of a scientific and technological innovation system, which is not conducive to the healthy development of the bay ecosystem. Thus, for the LZB area, an integrated innovation platform of "Industry-University-Research" for marine science and technology should be gradually built and the transformation of scientific and technological achievements be steadily promoted. Additionally, an information resources sharing mechanism should be established to avoid the data fragmentation and strengthen the data management. Furthermore, the construction of "Smart Ocean" should be carried out in depth, using advanced technical means such as artificial intelligence, big data and cloud computing to achieve the marine informatization.

6 Conclusions

The effective maintenance and management of ecosystem health and its balanced operation are essential for the sustainable development of human society and economy. This study established a DPSIR-based assessment indicator framework and quantitatively assessed the status and evolution trend of LZB ecosystem health from 1980 to 2019. The key factors affecting the health of LZB ecosystem were identified, and the influential effects of single and composite factors were simulated. Based on this, specific regulation strategies and management recommendations were put forward.

Over the past 40 years, the LZB ecosystem has been in a subhealthy status for a long period of time, with a healthy state demonstrated in the 1980s. Subsequently, due to the compound effect of multiple human pressures and imperfect management policies, the health status of the LZB ecosystem deteriorated and reached an unhealthy state in 2005. With the improvement of public awareness of environmental protection and the implementation of ecological renovation, its health status has rebounded, showing a subhealthy state.

The key factors affecting the health of the LZB ecosystem are mostly pressure indicators, including the amount of agricultural chemical fertilizer entering the sea, reclamation area, the discharge of domestic sewage and industrial wastewater, etc. The scenario analysis indicates that land-based pollutant discharge, particularly agricultural

non-point source pollution, has a more significant impact than the construction of reclamation projects. Consequently, eliminating the impacts of the above indicators will help to improve and restore the LZB ecosystem health.

This study is an initial attempt to develop a comprehensive indicator framework incorporating "physical-chemical-biological-social" coupling factors for the assessment of ecosystem health in LZB. The research outcomes provide theoretical basis and practical guidance for the reasonable management of LZB ecosystem, and may also serve as references for the ecosystem health assessment of other bays if necessary.

It should be noted that some indicators are difficult to quantify due to data availability and temporal continuity limitations. Thus, they are not included in the indicator framework (e.g., seawater intrusion area, marine oil spill area, fish biomass, sediment quality, the proportion of capital investment for marine environmental protection in GDP, public participation, etc.). Additionally, the LZB area is divided by many administrative regions, making it difficult to carry out unified statistics. The average values of selected 51 counties (districts and county-level cities) in 14 cities of Shandong Province (Section 2) are used as the data of land area indicators; however, the responsibility sharing of each region for the health evolution of LZB ecosystem has not been considered yet. These issues are expected to be addressed in future research.

Data availability statement

The original contributions presented in the study are included in the article/Supplementary Material. Further inquiries can be directed to the corresponding author.

Author contributions

WW: Conceptualization, Data curation, Formal analysis, Validation, Visualization, Writing -original draft, review & editing. JH: Investigation, Software, Data curation, Formal analysis, Writing -original draft. DS: Conceptualization, Visualization, Review, Funding acquisition. All authors contributed to the article and approved the submitted version.

Funding

This paper was financially supported by the National Natural Science Foundation of China (U1706215 and 41806132), the National Key Research and Development Program of China (2018YFC1407602), the Special Funds for Taishan Scholar Project (No. tsqn202211056), and the Fundamental Research Funds for the Central Universities of China (202042008).

Acknowledgments

The authors would like to thank Prof. Shengkang Liang and Prof. Keqiang Li from Ocean University of China for their constructive suggestions and data collection, as well as indicator ranking experts for their participation and support. Furthermore, the authors are grateful to the reviewers of this paper.

Conflict of interest

The authors declare that the research was conducted in the absence of any commercial or financial relationships that could be construed as a potential conflict of interest.

Publisher's note

Supplementary material

The Supplementary Material for this article can be found online at: https://www.frontiersin.org/articles/10.3389/fmars.2023.1115896/full#supplementary-material

References

Aguirre-Rubí, J., Luna-Acosta, A., Ortiz-Zarragoitia, M., Zaldibar, B., Izagirre, U., Ahrens, M. J., et al. (2018). Assessment of ecosystem health disturbance in mangrove-lined Caribbean coastal systems using the oyster Crassostrea rhizophorae as sentinel species. *Sci. Total Environ.* 618, 718–735. doi: 10.1016/j.scitotenv.2017.08.098

Baek, S. H., Son, M., Kim, D., Choi, H.-W., and Kim, Y.-O. (2014). Assessing the ecosystem health status of Korea Gwangyang and Jinhae bays based on a planktonic index of biotic integrity (P-IBI). *Ocean Sci. J.* 49 (3), 291–311. doi: 10.1007/s12601-014-0029-2

Borja, Á., Elliott, M., Andersen, J. H., Berg, T., Carstensen, J., Halpern, B. S., et al. (2016). Overview of integrative assessment of marine systems: The ecosystem approach in practice. *Front. Mar. Sci.* 3. doi: 10.3389/fmars.2016.00020

Borja, Á., Franco, J., and Muxika, I. (2003). Classification tools for marine ecological quality assessment: the usefulness of macrobenthic communities in an area affected by a submarine outfall. In *ICES CM 2003/Session J-02* Tallinn (Estonia), 24–28 September, 2003.

Cai, L. Z. (2003). Macrozoobenthos pollution index (MPI). *Acta Scientiae Circumstantiae* 23 (5), 625–629. doi: 10.13671/j.hjkxxb.2003.05.012. (in Chinese)

Chen, M. H., and Chen, F. (2021). Evaluation and analysis of ecosystem health of the coastal zone in Zhanjiang Bay based on the DPSIR model. *Environ. Dev.* 33 (2), 18–23 +30. doi: 10.16647/j.cnki.cn15-1369/X.2021.02.003. (in Chinese)

China Shandong Network (2020) *Nearly half of china's marine science and technology talents gather in Shandong.* Available at: http://news.sdchina.com/show/4551572.html (Accessed November 13 2022). (in Chinese)

Choi, B. H., Kim, K. O., Lee, H. S., and Yuk, J. H. (2010). Perturbation of regional ocean tides due to coastal dikes. *Continental Shelf Res.* 30 (6), 553–563. doi: 10.1016/j.csr.2009.09.009

Costanza, R. (2012). Ecosystem health and ecological engineering. *Ecol. Eng.* 45, 24–29. doi: 10.1016/j.ecoleng.2012.03.023

Ding, X. S., Shan, X. J., Chen, Y. L., Jin, X. S., Yuan, Z. H., and Yang, T. (2018). Study on the change rate of shoreline based on digital coastal analysis system (DSAS): taking the shoreline of the Yellow River Delta and Laizhou Bay as an example. *Mar. Sci. Bull.* 37 (5), 565–575. (in Chinese)

Dong, J. (2019). *Evaluation and empirical analysis of marine ecological civilization construction in China: Shandong Province as a case study* (Qingdao: Ocean University of China). (in Chinese)

Editorial Committee of Biological Volume in General Editorial Committee of China Agricultural Encyclopedia (1991). *China Agricultural Encyclopedia· Biology Volume* (Beijing: Agricultural Publishing House). (in Chinese)

Epstein, P. R. (1999). "Large marine ecosystem health and human health," in *The Gulf of Mexico large marine ecosystem: assessment, sustainability, and management*, vol. 417-438. (S.l: Blackwell Science).

Epstein, P. R., Ford, T. E., Puccia, C., and Possas, C. A. (1994). Marine ecosystem health-implications for public-health. *Ann. New York Acad. Sci.* 740:13–23. doi: 10.1111/j.1749-6632.1994.tb19850.x

European Environment Agency (EEA) (2005). *EEA core set of indicators-guide, EEA technical report no 1/2005* (Luxembourg: Office for Official Publications of the European Communities).

Feng, S. Z., Li, F. Q., and Li, S. J. (1999). *Introduction to marine science* (Beijing: Higher Education Press). (in Chinese)

First Institute of Oceanography in State Oceanic Administration (2007). *Specifications for oceanographic survey-part 9: Guidelines for marine ecological survey (GB/T 12763.9-2007)* (Beijing: General Administration of Quality Supervision, Inspection and Quarantine of the People's Republic of China). (in Chinese)

Gao, Y. X., and Zhang, G. Z. (1996). Current situation and prospect of poultry industry in Shandong Province. *China Poultry* 4, 31–33. (in Chinese)

Gray, J. S. (1981). Detecting pollution induced changes in communities using the log-normal distribution of individuals among species. *Mar. Pollut. Bull.* 12 (5), 173–176. doi: 10.1016/0025-326X(81)90230-7

Halpern, B. S., Longo, C., Hardy, D., McLeod, K. L., Samhouri, J. F., Katona, S. K., et al. (2012). An index to assess the health and benefits of the global ocean. *Nature* 488, 615–620. doi: 10.1038/nature11397

Hammond, A. (1995). *Environmental indicators: A systematic approach to measuring and reporting on environmental policy performancee in the context of sustainable development* Vol. 43 (Washington, DC: World Resources Institute).

Hao, Y. J., Wang, Z. L., Zhu, M. Y., Li, R. X., Sun, P. X., Xia, B., et al. (2005). Investigation and assessment of nutrients and phytoplankton diversity in the Laizhou Bay. *Adv. Mar. Sci.* 23 (2), 197–204. (in Chinese)

He, G. S., Wang, X. H., and Zhou, Y. P. (2009). *Research on environmental legislation of Bohai Sea based on regional economic development* (Beijing: China Ocean Press). (in Chinese)

Hu, Z. J., Shan, X. J., Yang, T., and Ding, Q. (2020). Preliminary evaluation of summer fishing moratorium in the Bohai Sea. *Prog. Fishery Sci.* 41 (5), 13–21. doi: 10.19663/j.issn2095-9869.20190623001

Huang, J. T., Zheng, W., Wan, N. X., Lu, J. F., and Li, J. (2021). Characteristics of changes occurring in the landscape patterns in the coastal wetlands of the Laizhou Bay in the last 30 years. *Mar. Sci.* 45 (2), 76–90. doi: 10.11759/hykx20191003001. (in Chinese)

Jiang, H., Cui, Y., Chen, B. J., Chen, J. F., and Song, Y. L. (2005). The variation trend of nutrient salts in the Bohai Sea. *Mar. Fisheries Res.* 26 (6), 61–67. (in Chinese)

Jiang, H. C., Wang, Y. J., Li, J. H., Tao, H. M., Bai, Y. Y., Su, B., et al. (2018). Annual variation and spatial distribution of nutrients in the Laizhou Bay. *Mar. Pollut. Bull.* 37 (4), 411–423. (in Chinese)

Kennedy, A. D., and Jacoby, C. A. (1999). Biological indicators of marine environmental health: Meiofauna–A neglected benthic component? *Environ. Monit. Assess.* 54, 47–68. doi: 10.1023/A:1005854731889

Leppard, G. G., and Munawar, M. (1992). The ultrastructural indicators of aquatic ecosystem health. *J. Aquat. Ecosystem Health* 1, 309–317. doi: 10.1007/BF00044172

Li, G. L., Chen, B. J., Cui, Y., Ma, S. S., and Tang, X. X. (2006). Ecological characteristics of phytoplankton in the Laizhou Bay. *J. Fishery Sci. China* 13 (2), 292–299. (in Chinese)

Li, C., Chen, L. G., and He, Z. S. (2020). Analysis of water quality change and causes of Xiaoqing River estuary in Laizhou Bay. *Environ. Dev.* 32 (11), 118–119+121. doi: 10.16647/j.cnki.cn15-1369/X.2020.11.054

Li, G. L., Cui, Y., Chen, B. J., Chen, J. F., Song, Y. L., and Guo, F. (2007). Status and evaluation on nutrients in Laizhou Bay in autumn. *Mar. Environ. Sci.* 26 (1), 45–48+57.

Li, Y. F., Song, X. X., Wu, Z. X., and Yu, Z. M. (2015). An integrated methodology for quantitative assessment on impact of human activities on marine ecosystems: A case study in Laizhou Bay, China. *Oceanologia Et Limnologia Sin.* 46 (1), 133–139. (in Chinese)

Li, H., Song, X. X., Yu, Z. M., Liang, Y. B., and Wu, Z. X. (2014). An integrative assessment of marine ecosystem health in coastal waters along the Shandong Peninsula. *Mar. Sci.* 38 (10), 40–45. (in Chinese)

Lin, L., Li, F. L., Chen, X. Q., Huang, J. W., Bu, Q. W., and Fu, S. D. (2013). Characteristics of channel evolution and runoff temporal and spatial distribution in Hsiao-Ching River. *Yellow River* 35 (12), 77–79+82. (in Chinese)

Liu, D. H., Gong, W., Xing, W. X., Li, X. X., Ma, X. J., and Yu, Y. (2015). Comprehensive method for determining the weights of vulnerability assessment indexes on islands and the coastal zone based on the AHP weight method and entropy weight method. *Mar. Environ. Sci.* 34 (3), 462–467. doi: 10.13634/j.cnki.mes.2015.03.024. (in Chinese)

Liu, P., Zhang, Z. H., and Wang, J. (2010). *State of the coastal report of dongying Municipality, Shandong Province, People's Republic of China* (Beijing: China Ocean Press). (in Chinese)

Lu, W. H., Zeng, R., and Xiang, X. Q. (2013). Study of the marine ecological health assessment for the coastal area. *Mar. Sci. Bull.* 32 (5), 580–585. (in Chinese)

Lyu, H., Song, D., Zhang, S., Wu, W., and Bao, X. (2022). Compound effect of land reclamation and land-based pollutant input on water quality in Qinzhou Bay, China. *Sci. Total Environ.* 154183. doi: 10.1016/j.scitotenv.2022.154183

Ma, X., and Sun, Y. H. (2021). Dynamic evaluation of tourism ecological security in the Yellow River basin based on DPSIR framework. *Ecol. Economy* 37 (12), 145–151 +162.

Ma, S. S., Xin, F. Y., Cui, Y., and Qiao, X. Y. (2004). Assessment of main pollution matter volume into the sea from Yellow River and Xiaoqing River. *Mar. Fisheries Res.* 25 (5), 47–51. (in Chinese)

Ma, Y. X., Zang, J. Y., Che, H., Zheng, L. L., Zhang, B. T., and Ran, X. B. (2015). Trend and distributions of nutrient elements in the Huanghe (Yellow) River. *Oceanologia Et Limnologia Sin.* 46 (1), 140–147. (in Chinese)

Ma, J. X., Zheng, Z. H., Li, Y. P., Xing, H. Y., and Liu, Y. H. (2002). The distribution characteristics of phytoplankton in Laizhou Bay. *Trans. Oceanology Limnology* 4, 63–67. doi: 10.13984/j.cnki.cn37-1141.2002.04.011

Mallory, M. L., Gilchrist, H. G., Braune, B. M., and Gaston, A. J. (2006). Marine birds as indicators of Arctic marine ecosystem health: Linking the northern ecosystem initiative to long-term studies. *Environ. Monit. Assess.* 113, 31–48. doi: 10.1007/s10661-005-9095-3

Niu, M. X., Wang, J., and Xu, B. D. (2017). Assessment of the ecosystem health of the Yellow River estuary based on the pressure-state-response model. *Acta Ecologica Sin.* 37 (3), 943–952. doi: 10.5846/stxb201508131702. (in Chinese)

Organization for Economic Co-operation and Development (OECD) (1993). *OECD core set of indicators for environmental performance reviews-a synthesis report by the group on the state of the environment* (Paris: OECD).

Organization for Economic Co-operation and Development (OECD) (2003). *OECD environmental indicators-development, measurement and use* (Nairobi: UNEP).

Padua, S., Kripa, V., Prema, D., Mohamed, K. S., Jeyabaskaran, R., Kaladharan, P., et al. (2023). Assessment of ecosystem health of a micro–level ramsar coastal zone in the Vembanad Lake, Kerala, India. *Environ. Monit Assess.* 195, 95. doi: 10.1007/s10661-022-10692-7

Park, Y. G., Kim, H. Y., Hwang, J. H., Kim, T., Park, S., Nam, J. H., et al. (2014). Dynamics of dike effects on tidal circulation around Saemangeum, Korea. *Ocean Coast. Manage.* 102, 572–582. doi: 10.1016/j.ocecoaman.2014.02.016

Project Team of "Research on Monitoring and Controlling Technology of Economic Activities Around Bohai Sea Based on Environmental Carrying Capacity" (2016). *Study on the overall control of pollution pressure and marine response around Bohai Sea* (Beijing: China Ocean Press). (in Chinese)

Quan, F., and Zhu, L. (2011). The methods of coastal ecosystem health assessment. *J. Hainan Normal Univ. (Natural Science)* 24 (2), 204–209. (in Chinese)

Ramos, T. B., Alves, I., Subtil, R., and de Melo, J. J. (2007). Environmental performance policy indicators for the public sector: The case of the defence sector. *J. Environ. Manage.* 82, 410–432. doi: 10.1016/j.jenvman.2005.12.020

Rombouts, I., Beaugrand, G., Artigas, L. F., and Dauvin, J. C. (2013). Evaluating marine ecosystem health: Case studies of indicators using direct observations and modelling methods. *Ecol. Indic.* 24, 353–365. doi: 10.1016/j.ecolind.2012.07.001

Saaty, T. L. (1977). A scaling method for priorities in hierarchical structures. *J. Math. Psychol.* 15 (3), 234–281. doi: 10.1016/0022-2496(77)90033-5

Shandong Academy for Environmental Planning (2018). *Research and practice on environmental protection strategy of Shandong Province during the "Twelfth five year plan"* (Beijing: China Environment Publishing Group). (in Chinese)

Shandong Association for Science & Technology (1991). *Study on the comprehensive treatment of Xiaoqing River* (Jinan: Shandong Science and Technology Press).

Shi, H., Zheng, W., Ding, D., and Yang, J. (2010). "Several views on the study of evaluation of marine ecosystem health in China," in *2010 International Conference on Challenges in Environmental Science & Computer Engineering* (Wuhan, China), 124-127. doi: 10.1109/CESCE.2010.252

Song, D. B., Gao, Z. Q., Zhang, H., Xu, F. X., Zheng, X. Y., Ai, J. Q., et al. (2017). GIS-based health assessment of the marine ecosystem in Laizhou Bay, China. *Mar. pollut. Bull.* 125, 242–249. doi: 10.1016/j.marpolbul.2017.08.027. (in Chinese)

Song, N. Q., Wang, N., Wu, N., and Lin, W. N. (2018). Temporal and spatial distribution of harmful algal blooms in the Bohai Sea during 1952~2016 based on GIS. *China Environ. Sci.* 38 (3), 1142–1148. doi: 10.19674/j.cnki.issn1000-6923.2018.0136

Strokal, M., Kroeze, C., Wang, M., and Lin, M. (2017). Reducing future river export of nutrients to coastal waters of China in optimistic scenarios. *Sci. Total Environ.* 579, 517–528. doi: 10.1016/j.scitotenv.2016.11.065

Sun, Y. K. (2013). *The study of jiaozhou bay ecological environment comprehensive evaluation method based on index of biotic integrity* (Qingdao: University of Chinese Academy of Sciences (Institute of Oceanology). (in Chinese)

Tang, Y. J., Yu, S. X., Ke, Z. J., He, G. W., Gan, E. C., He, Z. F., et al. (2006). An evaluation on the environment condition of Zhanjiang mangrove nature reserves by the ABC curve method. *J. Guangdong Educ. Institute* 26 (3), 70–74. (in Chinese)

Tian, J. Y., Mu, J. B., and Wang, A. D. (1996). *Study on water pollution and water quality management of Xiaoqing River basin in Shandong Province* (Dongying: China University of Petroleum Press). (in Chinese)

United Nations Environment Programme (UNEP) (2006). *Environmental indicators for north America* (Nairobi: UNEP).

Vassallo, P., Fabiano, M., Vezzulli, L., Sandulli, R., Marques, J. C., and Jørgensen, S. E. (2006). Assessing the health of coastal marine ecosystems: A holistic approach based on sediment micro and meio-benthic measures. *Ecol. Indic.* 6 (3), 525–542. doi: 10.1016/j.ecolind.2005.07.003

Walker, L. M., Montagna, P. A., Hu, X., and Wetz, M. S. (2021). Timescales and magnitude of water quality change in three Texas estuaries induced by passage of hurricane Harvey. *Estuaries Coasts* 44 (4), 960–971. doi: 10.1007/s12237-020-00846-6

Wang, J. (2000). Study on population dynamics of phytoplankton in Laizhou Bay. *Mar. Fisheries Res.* 21 (3), 33–38. (in Chinese)

Wang, Y., Mu, X. J., and Xu, C. F. (2021). Preliminary study on marine ecological environment and pollution prevention in Laizhou Bay. *Mar. Environ. Sci.* 40 (6), 823–837. doi: 10.13634/j.cnki.mes.2021.06.003. (in Chinese)

Warwick, R. M. (1986). A new method for detecting pollution effects on marine macrobenthic communities. *Mar. Biol.* 92, 557–562. doi: 10.1007/BF00392515

Wei, F., Han, G. X., Zhang, J. P., Li, Y. Z., and Zhao, J. M. (2018). Evolution of coastal wetlands under the influence of sea reclamation in bohai rim during 1985-2015. *Chin. J. Ecol.* 37 (5), 1527–1537. doi: 10.13292/j.1000-4890.201805.028. (in Chinese)

Wells, R. S., Rhinehart, H. L., Hansen, L. J., Sweeney, J. C., Townsend, F. I., Stone, R., et al. (2004). Bottlenose dolphins as marine ecosystem sentinels: Developing a health monitoring system. *EcoHealth* 1, 246–254. doi: 10.1007/s10393-004-0094-6

Whitfield, A. K., and Harrison, T. D. (2008). Fishes as indicators of estuarine health and estuarine importance. *Encyclopedia Ecol.* 2, 1593–1599. doi: 10.1016/B978-008045405-4.00104-X

Wiegand, J., Raffaelli, D., Smart, J. C. R., and White, P. C. L. (2010). Assessment of temporal trends in ecosystem health using a holistic indicator. *J. Environ. Manage.* 91, 1446–1455. doi: 10.1016/j.jenvman.2010.02.004

Wu, Z., and Chen, R. S. (2019). A comparative analysis of the ocean health index and the Pressure-State-Response evaluation methods for Shanghai's ocean ecosystem health. *J. East China Normal Univ. (Natural Science)* 4, 174–187. (in Chinese)

Wu, W., Yan, S., Feng, R., Song, D., and Chen, X. (2017). Development of an environmental performance indicator framework to evaluate management effectiveness for jiaozhou bay coastal wetland special marine protected area, Qingdao, China. *Ocean Coast. Manage.* 142, 71–89. doi: 10.1016/j.ocecoaman.2017.03.021

Xie, E. N. (2009). *Pre-warning system research for bay ecosystem health-the case of Laizhou Bay* (Qingdao: Ocean University of China) (in Chinese).

Xin, M., Wang, B. D., Xie, L. P., Sun, X., Wei, Q. S., Liang, S. K., et al. (2019). Long-term changes in nutrient regimes and their ecological effects in the Bohai Sea, China. *Mar. Pollut. Bull.* 146, 562–573. doi: 10.1016/j.marpolbul.2019.07.011

Xinhua News Agency (2019) *Opinions of the CPC central committee and the state council on establishing and supervising the implementation of the territorial spatial planning system*. Available at: http://www.gov.cn/zhengce/2019-05/23/content_5394187.htm (Accessed December 22 2020).

Xiong, H., and Weng, Z. L. (2015). The influence of factor input and institutional innovation on grain production of eastern, central and western regions––Based on comparative analysis of Shandong, Jiangxi and Sichuan Province. *Chin. Agric. Sci. Bull.* 31 (1), 258–264. (in Chinese)

Xu, Y. (2012). *The marine ecosystem Dalian Haiwang nine islands* (Dalian: Dalian Maritime University). (in Chinese)

Xu, Y., Gao, H., Wei, X., and Zhu, J. L. (2021). The effects of reclamation activity and Yellow River runoff on coastline and area of the Laizhou Bay, China. *J. Ocean Univ. China* 20 (3), 729–739. doi: 10.1007/s11802-021-4746-8. (in Chinese)

Xu, S., and Ma, Z. W. (2017). Sustainable development evaluation of marine economy based on the DPSIR model–a case study of the Bohai rim region. *Mar. Economy* 8 (3), 28–35. doi: 10.19426/j.cnki.cn12-1424/p.2017.04.004

Xu, X. M., Shi, J., and Ling, X. (2013). *Study of the current legal document management in Bohai* (Beijing: People's Publishing House).

Yang, F. (2018). *Human activity intensity and the ecological effects of coastal wetland in Laizhou Bay* (Qingdao: Qingdao Technological University). (in Chinese)

Yang, J. Q., Cui, W. L., Zhang, H. L., and Xu, Z. J. (2003). Marine ecosystem health structure and function index assessment in the West of Laizhou Bay. *Mar. Sci. Bull.* 22 (5), 58–63. (in Chinese)

Ye, Z. Y. (2003). On the choice of the methods of the positive and dimensionless indexes in multi-index comprehensive evaluation. *Zhejiang Stat* 4, 25–26. (in Chinese)

Ye, S. Y., Xie, L. J., and He, L. (2021). *Wetlands: The kidney of the earth, the boat of life* (Beijing: China Science Press). (in Chinese)

Yu, F. J., Dong, J. X., and Xu, F. X. (2016). *China Coastal Sea areas: Marine disasters* (Beijing: China Ocean Press). (in Chinese)

Yu, W. W., Zhang, D., Liao, J. J., Ma, L., Zhu, X. F., Zhang, W. T., et al. (2022). Linking ecosystem services to a coastal bay ecosystem health assessment: A comparative case study between Jiaozhou Bay and Daya Bay, China. *Ecol. Indic.* 135, 108530. doi: 10.1016/j.ecolind.2021.108530

Zhang, P. Y. (2005). *Studies on ecology of zoobenthos and environmental quality assessment in coastal waters of Bohai Bay* (Qingdao: Ocean University of China). (in Chinese)

Zhang, J. (2013). *Health assessment of benthic habitat based on the biotic index in Laizhou Bay and its adjacent waters* (Qingdao: Ocean University of China). (in Chinese)

Zhang, X. (2013). *Spatio-temporal variability of principal pollutants in Laizhou Bay in near 30 years and establishment of evaluation index system in water of Xiaoqing River Estuary* (Qingdao: Ocean University of China). (in Chinese)

Zhang, A. J., Gao, Z. H., and Liu, Y. T. (2007). "The main impact of land-based pollution on the offshore environment and management countermeasures," in *2007 national advanced seminar and exchange on water pollution control, treatment, ecological restoration technology and emergency treatment system construction for sudden water pollution accidents* (Shanghai: Chinese Society of Environmental Sciences), 108–112.

Zhang, C., and Hu, R. F. (2019). *Chinese farmers' pesticide use: Behavior characteristics, health impacts and driving factors* (Beijing: Beijing Institute of Technology Press). (in Chinese)

Zhang, Y., Li, S. W., Lü, Z. B., Ma, Y. Q., Liu, Y. J., Wei, Z. H., et al. (2013). Application of polychaete in ecological environment evaluation of Laizhou Bay. *Acta Ecologica Sin.* 33 (8), 2522–2530. doi: 10.5846/stxb201207311086. (in Chinese)

Zhang, Z. R., Li, B. Q., and Wang, F. D. (2003). *Study on the evaluation and countermeasures of Xiaoqing River comprehensive treatment* (Jinan: Shandong Science and Technology Press). (in Chinese)

Zhang, M., Lu, Q. Y., Wang, D. W., Ding, D. S., Cui, Z. G., and Shi, H. H. (2022). Spatiotemporal evolution of nutrients and the influencing factors in Laizhou Bay over the past 40 years. *Mar. Pollut. Bull.* 184, 114186. doi: 10.1016/j.marpolbul.2022.114186. (in Chinese)

Zhang, H. L., Yang, J. Q., and Cui, W. L. (2006). Status of salinity changes and the effect on marine environments and ecosystem in Laizhou Bay. *Mar. Environ. Sci.* 25 (S1), 11–14. (in Chinese)

Zhang, X. J., and Zhao, S. (2018). Relationship between phytoplankton community and environmental factors in western Laizhou Bay. *J. Dalian Ocean Univ.* 33 (4), 532–538. doi: 10.16535/j.cnki.dlhyxb.2018.04.019. (in Chinese)

Zhao, P., Jiang, W. S., Mao, X. Y., Gao, H. W., and Guo, X. Y. (2010). Salinity change and influencing factor in the Laizhou Bay from 2000 to 2005. *Oceanologia Et Limnologia Sin.* 41 (1), 12–23. (in Chinese)

Zhao, Z. Y., and Kong, L. H. (2000). Environmental status quo and protection countermeasures in Bohai marine areas. *Res. Environ. Sci.* 13 (2), 23–27. doi: 10.13198/j.res.2000.02.26.zhaozhy.008. (in Chinese)

Zhao, Y. T., Liu, X., Li, J. H., Tao, H. M., Sun, S., and Ma, Y. Q. (2016). Distribution and seasonal variation in nutrients in Laizhou Bay. *Mar. Environ. Sci.* 35 (1), 95–99. doi: 10.13634/j.cnki.mes.2016.01.015. (in Chinese)

Zhao, M., Yu, J., Chen, P. M., Feng, X., and Nie, Y. K. (2015). Research advances in assessment of bay ecosystem health. *J. Anhui Agric. Sci.* 43 (35), 8–11. doi: 10.13989/j.cnki.0517-6611.2015.35.004. (in Chinese)

Zheng, T., and You, X. Y. (2013). Assessment of marine ecosystem health of Tianjin offshore, China. *Oceanological Hydrobiological Stud.* 42 (4), 442–450. doi: 10.2478/s13545-013-0100-0. (in Chinese)

Zhou, F. X., Gao, X. L., Zhuang, W., Zhang, J. F., and Li, P. M. (2015). The impact of rivers on the chl a concentrations in coastal surface waters of the Laizhou Bay. *Mar. Environ. Sci.* 34 (2), 184–189. doi: 10.13634/j.cnki.mes.2015.02.005. (in Chinese)

frontiers | Frontiers in Marine Science

TYPE Original Research
PUBLISHED 14 April 2023
DOI 10.3389/fmars.2023.1106070

OPEN ACCESS

EDITED BY
Dominic Reeve,
Swansea University, United Kingdom

REVIEWED BY
Barbara Zanuttigh,
University of Bologna, Italy
Ana Genua-Olmedo,
Rey Juan Carlos University, Spain
Qin Chen,
Northeastern University, United States

*CORRESPONDENCE
Longhuan Zhu
lzhu7@mtu.edu
Xiuzhen Li
xzli@sklec.ecnu.edu.cn

SPECIALTY SECTION
This article was submitted to Coastal Ocean Processes, a section of the journal Frontiers in Marine Science

RECEIVED 23 November 2022
ACCEPTED 20 March 2023
PUBLISHED 14 April 2023

CITATION
Ma Y, Zhu L, Peng Z, Xue L, Zhao W, Li T, Lin S, Bouma TJ, Hofland B, Dong C and Li X (2023) Wave attenuation by flattened vegetation *(Scirpus mariqueter)*. *Front. Mar. Sci.* 10:1106070. doi: 10.3389/fmars.2023.1106070

Wave attenuation by flattened vegetation *(Scirpus mariqueter)*

Yuxi Ma[1], Longhuan Zhu[2*], Zhong Peng[1,3], Liming Xue[1], Wenzhen Zhao[1], Tianyou Li[1], Shiwei Lin[1], Tjeerd J. Bouma[4], Bas Hofland[5], Chuning Dong[6] and Xiuzhen Li[1*]

[1]State Key Laboratory of Estuarine and Coastal Research, East China Normal University, Shanghai, China, [2]Great Lakes Research Center, Michigan Technological University, Houghton, MI, United States, [3]Institute of Eco-Chongming, East China Normal University, Shanghai, China, [4]Department of Estuarine and Delta Systems, Netherlands Institute for Sea Research (NIOZ), Yerseke, Netherlands, [5]Faculty of Civil Engineering and Geosciences, Delft University of Technology, Delft, Netherlands, [6]State Key Laboratory of Hydrology-Water Resources and Hydraulic Engineering, Hohai University, Nanjing, China

With the capacity to reduce wave energy and trap sediment, *Scirpus mariqueter* has become an important native species of annual grass for ecology restoration at the Yangtze Estuary in eastern China. Due to seasonal variances of biophysical characteristics, *S. mariqueter* usually bends and breaks in winter, resulting in flattened stems that may reduce its wave attenuation capacity. To investigate the effects of vegetation flattening on wave attenuation, a set of flume experiments were conducted for flattened and standing vegetation under different wave conditions. The model vegetation was designed to represent the wilted *S. mariqueter* collected in winter with dynamic similarity. Results showed that the wave damping coefficient for flattened vegetation (β_F) was 33.6%-72.4% of that for standing vegetation (β_S) with the same vegetation length. Both β_F and β_S increased with wave height but decreased with water depth. A wave attenuation indicator (*WAI*) was defined to generate empirical formulas for β_S and β_F as well as their ratio β_F/β_S. The empirical formulas were then applied to modify the existing standing vegetation-based wave attenuation model for flattened vegetation and performed successfully. Understanding the wave attenuation characteristics of flattened vegetation is essential for the management of ecological restoration and coastal protection.

KEYWORDS

***Scirpus mariqueter*, wave attenuation, flattened vegetation, wave attenuation indicator, flume experiment, natural coastal protection, empirical model**

1 Introduction

Saltmarshes play a key role in coastal ecosystems by providing habitats to numerous species (e.g., birds, fish, etc.), cycling nutrients, trapping sediment, and sequestering carbon (Chmura et al., 2003; Sousa et al., 2010; Barbier et al., 2011; Chen et al., 2018). Saltmarshes can also serve as a buffer for storm surges and waves (Jadhav et al., 2013; Anderson and Smith, 2014; Möller et al., 2014; Maza et al., 2015; Christie et al., 2018; Garzon et al., 2019;

Maza et al., 2022).With these features, saltmarshes have been widely identified as one of the most important components in nature-based solutions for coastal protection, which are more ecological and sustainable than conventional hard engineering structures (Temmerman et al., 2013).

The most common saltmarshes along the shoreline of the Yangtze Estuary in China include *Scirpus mariqueter* (Figure 1B), *Phragmites australis* (Figure 1B), and *Spartina alterniflora* (Figure 1B). The change of the percentages of different plant species in saltmarshes would significantly influence their wave attenuation capacity and characteristics, due to different land cover types, positions, and transect lengths (Xue et al., 2021) as well as different geometrical and mechanical properties (Ysebaert et al., 2011). For example, when the coverage of *S. mariqueter* increased from 50% to 75% and *Spartina alterniflora* coverage decreased from 50% to 25%, the wave attenuation of *S. mariqueter* increased by 91% and and that of *S. alterniflora* decreased by 43% respectively (Zhao et al., 2023). Therefore, quantifying the wave attenuation capacity of *S. mariqueter* is essential to understand the function of saltmarshes for coastal protection and resilience.

Wave attenuation by vegetation is mainly dependent on its geometrical and mechanical properties (e.g.,stem stiffness, vegetation height, plant population density, meadow length, standing biomass, age etc.) and wave conditions (wave height, wavelength, and water depth)(Bouma et al., 2005; Anderson and Smith, 2014; Paul et al., 2016; van Veelen et al., 2020; Zhu et al., 2020b; Zhu et al., 2020c; Maza et al., 2021; Maza et al., 2022). Currents can also strengthen or waken the wave attenuation by vegetation (Hu et al., 2014; Maza et al., 2015; Losada et al., 2016). Although the plant density of *S. mariqueter* was much larger than that of *S. alterniflora* (2352 ± 355 and 334 ± 12 stems/m^2), with thinner and shorter stems, *S. mariqueter* marshes reduce less wave height than *S. alterniflora* (Ysebaert et al., 2011). The wave attenuation of *S. mariqueter* is more sensitive to water level change compared to *S. alterniflora*, especially under submergence conditions (Ysebaert et al., 2011; Garzon et al., 2019). Associated with seasonal variance, the stem diameter and plant density decrease dramatically in winter, resulting in smaller wave attenuation, e.g., the field observation in Ge et al. (2018) indicated that the wave height attenuation by 180 m-width *S. mariqueter* dropped by 30% from 80% in summer to 50% in winter.

In winter, *S. mariqueter* begins to wilt in November and stops growing. Under the continuous actions of hydrodynamic forces, wilted stems are easy to bend, break, and even swiped away (Ge et al., 2018). The vegetation with a broken stem displays a flattened posture (Figure 1B). As wilted vegetation cannot recover like in growing seasons, the vegetation flattening continues through the whole winter until the aboveground biomass totally disappears at the end of January. Compared to unbroken vegetation that has a

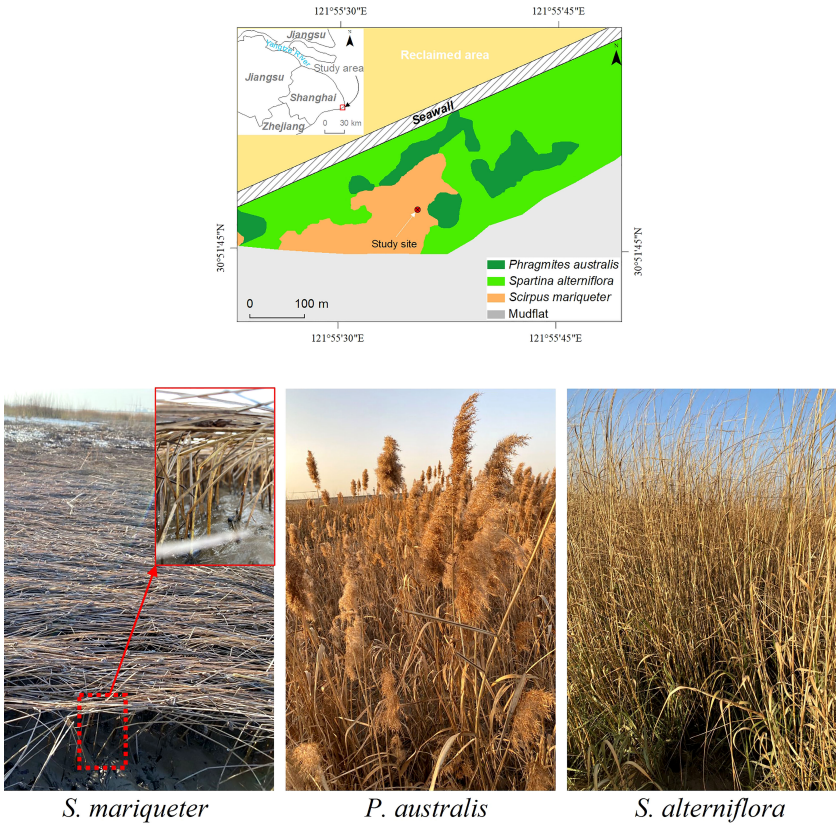

FIGURE 1
(A) Sampling site (Nanhui shore, Shanghai), **(B)** and photos of *S. mariqueter*, *P. australis* and *S. alterniflora* in January 2021. The *S. mariqueter* was flattened and the photo in red solid square showed broken stems in red dashed square.

standing posture, flattened vegetation with bending stems experiences a less drag (Vuik et al., 2018). Generally, the wave attenuation is due to the work of vegetation drag. The drag can be decomposed into form drag in the stem-normal direction and friction drag in the stem-tangential direction (Dean and Dalrymple, 1991; Luhar and Nepf, 2016; Zhu et al., 2020b). For rigid vegetation without motion, the form drag dominates for standing vegetation while the friction drag dominates for flattened vegetation (Vuik et al., 2018). Usually, friction is much smaller than form drag, such that the flattened vegetation showed a smaller wave attenuation compared with standing vegetation. Take *Scirpus maritimus* as an example, the wave attenuation by flattened vegetation is 66% of that by standing vegetation (Vuik et al., 2018). However, for flexible vegetation, both form drag and friction drag are important due to vegetation motion under wave force (Zhu et al., 2020b). Therefore, it is challenging to quantify the wave attenuation by flattened flexible vegetation, leading to a significant knowledge gap in restoring *S. mariqueter* for coastal protection, especially in winter storms.

The objective of this study is to quantify the wave attenuation by *S. mariqueter* with flattened flexible stems. The *S. mariqueter* was collected in Nanhui, Shanghai, China on Jan 4th 2021. Based on the measured geometrical and mechanical properties of *S. mariqueter*, representative model vegetation with dynamical similarity was used in the flume experiments to explore the difference between the wave attenuations by standing and flattened vegetation. The characteristics of standing and flattened vegetation in different wave conditions are analyzed. Based on the experimental data, an empirical formula to quantify the effects of vegetation flattening is developed and applied to existing wave attenuation models for flattened vegetation. Finally, the wave attenuation of standing vegetation, flattened vegetation, and the vertical part of the flattened vegetation is investigated through a case study under storm events.

2 Materials and methods

2.1 Sampling of *S. mariqueter*

The sampling site (30°51'N, 121°55'E) is located at the Nanhui Foreland salt marshes on the seaward side of a seawall (Figure 1A). The area behind the seawall was reclamation area which had been wetlands before 2001(Tian et al., 2016). This area has a mixed semidiurnal tide with a mean tide tidal range of 3.2 m and a maximum tidal range of over 4 m during spring tides (Zhu et al., 2014). The sampling site is submerged in water at high tide and exposed to air at low tide. With the spreading of the invasive species *S. alterniflora*, the native species *S. mariqueter* has shrunk to a small region (Figure 1A). To preserve biodiversity and improve the resilience of the coastal ecosystem, ecological measures are being conducted to restore *S. mariqueter* (Yuan et al., 2022). *S. mariqueter* is usually observed to start to flatten in December and last until January at the end of the growing season. We collected *S. mariqueter* samples on Jan 4th 2021 when most *S. mariqueter* are flattened. Almost all of the *S. mariqueter* stems were broken at 10 cm from the base, resulting in flattened stems above the breaking point (Figure 1B). Three 25 × 25 cm^2 quadrats of *S. mariqueter* were collected for measurements. The measured plant density (N) was 2148 ± 414 stems/m^2, calculated from the average number of shoots over the three quadrats. All of the stems were cut from the base and taken to the lab to measure the geometrical and mechanical properties.

The stem length (l) was measured from total 30 stems from the three quadrats with 10 stems for each quadrat. The measured stem length ranged from 21.4 to 44.3 cm with an average of 34.2 cm. The cross section of *S. mariqueter* was triangular and oriented in a random direction. The height of each side of the cross-section was measured using a caliper. As the cross-section is close to an equilateral triangle, the mean height at three sides is defined as the section height (h_s), such that the second moment of area is $I = \sqrt{3}h_s^4/54$. The measured section height ranged from 1.27 to 1.89 mm with an average of 1.56 mm. The elastic modulus (Young's modulus, E) was measured with 20 specimens from 20 stems by a three-point bending test (Vuik et al., 2018). The measured E ranged from 1.9 to 7.2 GPa with an average of 3.9 GPa. The measured values are summarized in Table 1 and also compared with the values in literature.

2.2 Flume experiments

As it is difficult to keep the flattening state and bioactivity of stems by moving *S. mariqueter* in the flume, we used dynamically

TABLE 1 The morphological and mechanical properties of *S. mariqueter* and the representative vegetation model.

study site and date	mass density ρ [g/cm^3]	plant density N [stems/m^2]	elastic modulus E [GPa]	flexural rigidity EI [N·mm^2]	stem length l [cm]	section height h_S [mm]	data source
Nanhui, China 2021-01-04	0.35 ± 0.05	2148 ± 414	3.9 ± 1.3 (1.9 - 7.2)	303 ± 158 (113 - 676)	34.2 ± 6.5 (21.4 - 44.3)	1.56 ± 0.2 (1.27 - 1.89	this study
Chongming Island, China 2017-12-29		1016 ± 919			13.47 ± 5.52 (5.25 - 16.8)	0.95 ± 0.32	Ge et al. (2018)
Chongming Island, China 2005-09-05		2352 ± 355			38 ± 4	2.2 ± 0.1	Ysebaert et al. (2011)
	0.64	1980	1.739	876	50	1.8 (outer diameter)	representative vegetation model

similar model vegetation to explore the effects of stem flattening on wave attenuation. The field measurements of the wave attenuation by *S. mariqueter* will be documented in another paper in preparation, where the plant properties and wave conditions were measured from May to November 2021 covering the whole growing season of *S. mariqueter*. The field measurements included plant properties and wave data from May to November 2021 across the growing season of *S. mariqueter*. To model the vegetation, hollow polypropylene (PP) tubes with circular cross-section were selected based on the dynamic similarity. The model was full scale. The outer diameter of the model stem was 1.8 mm, which was comparable to the measured section height (1.27-1.89 mm) and side lengths of *S. mariqueter*. The wall thickness of the model stem was 0.4 mm and the elastic modulus was 1.739 GPa, yielding a flexural rigidity (*EI*) of 876 N·mm^2, which was slightly larger than the maximum measured value of 676 N·mm^2 for *S. mariqueter*. The *EI* of the model vegetation is 30% larger than the measured maximum *EI* of *S. mariqueter*. The wave attenuation by the model vegetation is estimated to be larger than the real *S. mariqueter*. However, the effects of *EI* on wave attenuation become less sensitive when the vegetation is very flexible. For example in Zhu et al. (2021), the wave energy dissipation decreased by 6.7% when *EI* decreased by 76%. The mass density of the model stem was 0.92 g/cm^3. As the PP tubes were filled with air, the effective mass density of PP tube was 0.64 g/cm^3, which was larger than the measured value of 0.35 ± 0.05 g/cm^3, yielding a smaller buoyancy. However, according to the theory in Henderson (2019), the effects of buoyancy on stem motion were much smaller than stiffness and therefore ignorable. Although there are some other parameters governing the motion of stems (Zhu et al., 2021), these parameters are not as important as the stiffness and buoyancy for the wave conditions in this study and therefore not discussed in detail here. The designed vegetation length (l) was 50 cm (Figures 2A, C), slightly longer than the maximum measurement of 44.3 cm. To represent flattened vegetation, the model vegetation was folded at 10 cm above the base (Figures 2B, D), which was comparable to the folding point at 13.3 ± 2.6 cm observed in the field. To keep the same configuration, the vegetation was folded towards the direction of wave propagation after finishing the experiments for standing vegetation. Due to buoyancy, the horizontal part of the vegetation curves upward at 20° with the horizontal line (Figure 2D). The model vegetation was installed in

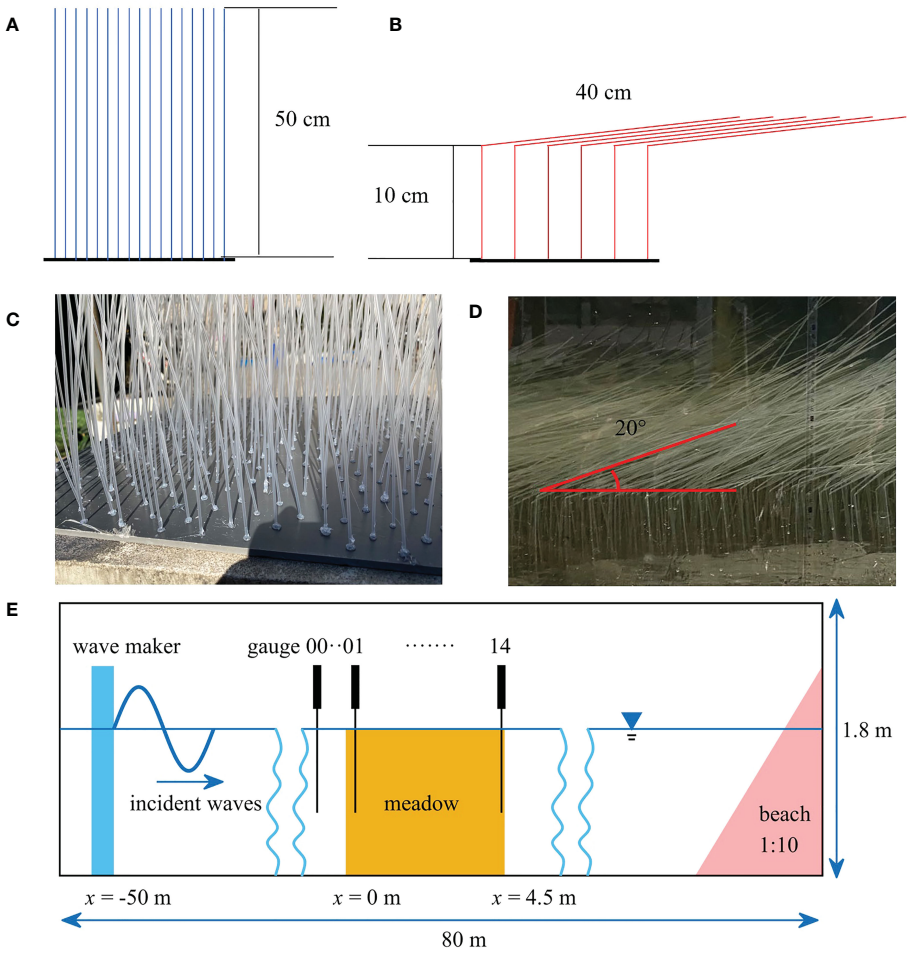

FIGURE 2
Sketches of **(A)** standing and **(B)** flattened vegetation. Photos of the **(C)** standing and **(D)** flatten model vegetation in the flume. **(E)** Experimental setup for measuring the wave attenuation by vegetation (dimensions are not scaled).

and evenly distributed on a 5 mm-thick acrylic plate, which was fixed at the bottom of the flume. There are 4455 stems over 9 acrylic plates, covering a 4.5 m-long area along the flume (Figure 2E). The plant density was therefore 1980 stems/m^2, similar to the measured plant density in this study and literature (e.g. Ysebaert et al., 2011; Ge et al., 2018).

The laboratory experiments were conducted in the 80 m-long, 1 m-wide, and 1.8 m-high wave flume at Hohai University in Nanjing, China. In common condition at Nanhui, the mean water depth was from 0.58 to 1.13 m, with wave height from 0.06 to 0.15 m and wave period from 0.8 s to 2.8 s (Liu et al., 2021). So the wave conditions in the present study can represent most wave periods and wave heights under common conditions. In the present study, the water depth (h) was from 0.5 m to 0.6 m, such that both standing and flattened vegetation were completely submerged. Due to the limitation of flume and wave paddle, the water depth cannot be over 0.7 m. The regular incident wave height (H_{I0}) was from 0.05 to 0.15 m. The wave period (T) was from 1.2 to 3 s, yielding wavelength (λ) of 2.05 to 6.4 m, where λ=2π/k with k the wave number. The wave number is determined from the dispersion relation $(2\pi/T)^2$=gk tanh kh with g the gravitational acceleration (Dean and Dalrymple, 1991). The meadow length was 4.5 m, covering 0.7 to 2.2 wavelength. The designed wave conditions are summarized in Table 2.

The wave height over the meadow was measured by 15 wave gauges. A reference gauge was placed 50 cm upstream in front of the leading edge. Other gauges were fixed across the meadow with 10-30 cm intervals depending on the wavelength. The sampling time was 5 min at a rate of 1 kHz, including 100-250 waves. The data were extracted after 3 mins, when the measured waves are at steady state. According to Dalrympleet al. (1984), the wave height decays as,

$$\frac{H(x)}{H_{I0}} = \frac{1}{1+\beta x} \quad (1)$$

where $H(x)$ is the local wave height at x m from the leading edge (Figure 2A), H_{I0} is the incident wave height at x = 0, and β is wave damping coefficient. The wave damping coefficient is fitted based on the measured wave heights along the meadow using the methods in Appendix A.

3 Results

3.1 Wave attenuation

β is more related to wave height which had a wide range in the experiment. The wave attenuation under different wave conditions can be more significantly shown with β. The measured wave damping coefficients for both standing vegetation (β_S) and flattened vegetation (β_F) are shown in Table 3. To investigate the characteristics of the wave attenuation capacity of vegetation in different wave conditions, β was presented as a function of H_{I0}, h, and λ as shown in Figure 3. Obviously, β_F is smaller than β_S for all the tested cases with β_F/β_S ranged from 33.6% to 72.4%, indicating that the wave attenuation of flattened vegetation is smaller than that of standing vegetation. Nevertheless, β_F varies with wave conditions in a similar pattern to β_S (Figure 3).

As shown in Figure 3A, both β_S and β_F increase with H_{I0}, indicating that both standing and flattened vegetation can damp more wave energy in larger waves. However, the wave attenuation reduces with increasing water depth (Figure 3B). As water depth rises, the wave orbital velocity decreases, yielding a smaller drag and therefore reducing wave attenuation. Associated with the water level rise, the wave energy also moves upward because the wave energy concentrates near the water surface and decays along water depth. Consequently, less wave energy is damped by the more deeply submerged flattened vegetation such that β_F drops more dramatically than β_S (Figure 3B). For instance in Figure 3B, β_S dropped 16.7% from 0.066 m^{-1} to 0.056 m^{-1} while β_F dropped 36.8% from 0.038 m^{-1} to 0.024 m^{-1} when the water depth increased by 20% from 0.5 m to 0.6 m. The wave damping coefficient does not show a significant change with λ in these experiments (Figure 3C).

3.2 Empirical formulas for wave damping coefficients

Numerous studies have been conducted to quantify the wave damping coefficient (β) of standing vegetation based on the formula in (Dalrymple et al., 1984), which is given by,

TABLE 2 Wave conditions for the flume experiments, where H_{I0} is incident wave height, h is water depth, T is wave period, λ is wavelength, k is wave number, and l is stem length.

Case	H_{I0} [m]	h [m]	T [s]	λ [m]	l/h	H/h	H/λ	kh
1	0.15	0.5	1.2	2.05	1	0.30	*0.073*	1.53
2	0.15	0.5	1.7	3.33	1	0.30	0.045	0.94
3	0.15	0.5	2.2	4.53	1	0.30	0.033	0.69
4	0.1	0.5	2.2	4.53	1	0.20	0.022	0.69
5	0.05	0.5	2.2	4.53	1	0.10	0.011	0.69
6	0.15	0.5	3	6.40	1	0.30	0.023	0.49
7	0.15	0.6	2.2	4.89	0.83	0.25	0.031	0.77

TABLE 3 Measurements for the damping coefficients of standing (β_S) and flattened (β_F) vegetation.

Case	H_{I0} [m]	h [m]	T [s]	λ [m]	ΔH_S [m]	ΔH_F [m]	β_S [m^{-1}]	β_F [m^{-1}]	β_F/β_S
1	0.15	0.5	1.2	2.05	0.032	0.022	0.060	0.038	0.63
2	0.15	0.5	1.7	3.33	0.032	0.025	0.060	0.043	0.72
3	0.15	0.5	2.2	4.53	0.034	0.022	0.066	0.038	0.57
4	0.10	0.5	2.2	4.53	0.018	0.012	0.050	0.029	0.59
5	0.05	0.5	2.2	4.53	0.008	0.003	0.042	0.014	0.34
6	0.15	0.5	3	6.40	0.033	0.023	0.063	0.041	0.65
7	0.15	0.6	2.2	4.89	0.030	0.015	0.056	0.024	0.42

In this table, H_{I0} is designed incident wave height, ΔH_S and ΔH_F are the reduced wave height over standing and flattened vegetation. h is water depth, T is wave period, k is wavenumber and l is vegetation length.

$$\beta = \frac{4}{9\pi} C_D b N H_{I0} k \frac{\sinh^3 kl_v + 3\sinh\ kl_v}{(\sinh\ 2kh + 2kh)\sinh\ kh} \quad (2)$$

The challenge is to calibrate the bulk drag coefficient C_D for a vegetation meadow. Conventionally, C_D is fitted as a function of Reynolds number (Re) or Keulegan–Carpenter number (KC) (e.g., Mendez and Losada (2004); Anderson and Smith (2014); Hu et al. (2014); Ozeren et al. (2014); van Veelen et al. (2020)). As Re and KC do not include vegetation rigidity (EI), these formulas are not applicable to other vegetation with different flexibilities. Alternatively, Luhar and Nepf (2016) proposed a technique that considers the effects of blade flexibility by using effective blade length (l_e), which is defined as the length of a rigid blade that dissipates the same wave energy as the flexible blade with the original length (l). The effective blade length is usually fitted as a function of the Cauchy number (Ca) and the ratio of the blade length to wave excursion (L) (Luhar and Nepf, 2016; Lei and Nepf, 2019). Zhu et al. (2023) demonstrated that the combination of C_D–Re relation and effective plant height (EPH) can provide high

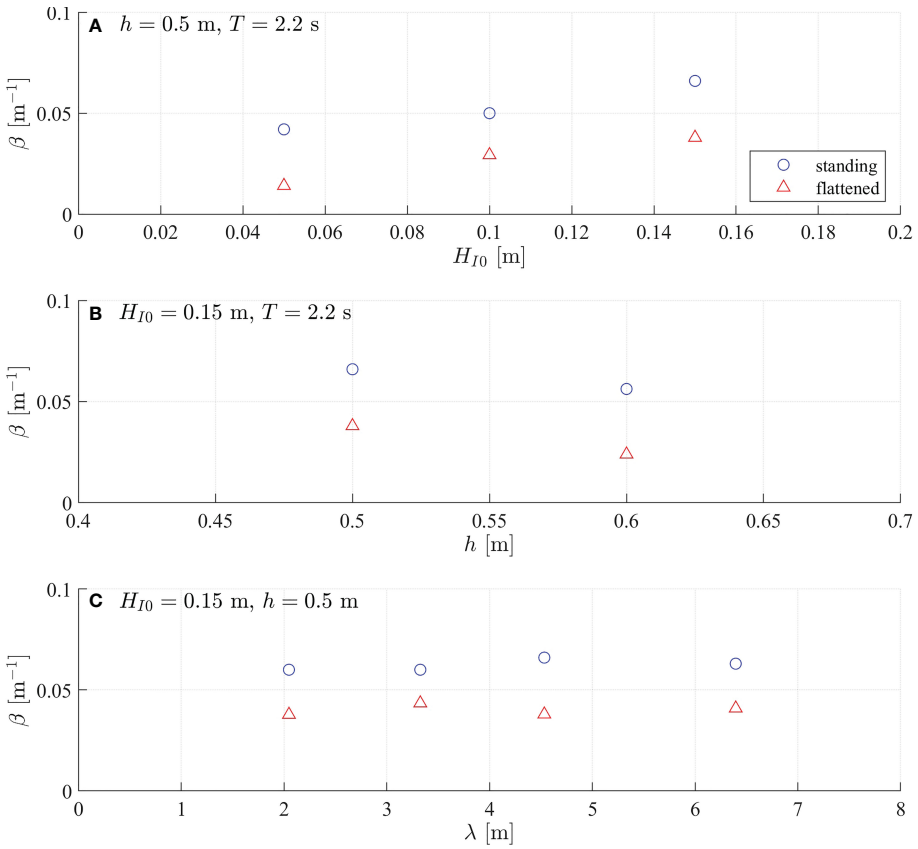

FIGURE 3
Measured wave damping coefficient (β,m^{-1}) as a function of **(A)** incident wave height (H_{I0},m), **(B)** water depth (h,m), and **(C)** wavelength (λ,m). The results for standing and flattened vegetation are denoted by blue circles and blue triangles, respectively.

accuracy in predicting wave attenuation in salt marshes. In the meantime, to avoid the uncertainties in using the formulas of bulk drag coefficient or effective blade length, Maza et al. (2022) developed a parameter, hydraulic standing biomass (*HSB*), to fit the wave damping coefficient, where *HSB* is defined as a function of the meadow mean height, standing biomass, and incident flow characteristics.

Unlike standing vegetation, flattened vegetation is composed of two parts: the vertical part and the horizontal part. The vertical part has no free end and the horizontal part is not clamped. Thus, the flattened vegetation cannot be simplified as a cantilever beam such that the *CaL*-based scaling law for effective blade length (Luhar and Nepf, 2016; Lei and Nepf, 2019) is not applicable to flattened vegetation because that *CaL*-based scaling law is derived from the static forcing balance between drag and blade stiffness by assuming the blade is a cantilever beam (Luhar and Nepf, 2016).

As it is challenging to define an effective blade length for flattened vegetation due to its complicated morphology, we developed a dimensionless wave attenuation indicator (*WAI*, -) to formulate β_S and β_F, inspired from Maza et al. (2019; 2021; 2022). The wave attenuation indicator is defined based on the characteristics of β_S and β_F with respect to H_{I0}, h, and λ and given by

$$WAI = \frac{H_{I0}}{h}\frac{l}{h}\frac{1}{tanh\ kh} \tag{3}$$

Note that the first two terms of the right hand side of equation (3) reflect wave attenuation in shallow water waves since the wave damping coefficient in shallow water waves is proportional to $H_{I0}l/h^2$ (Dalrymple et al., 1984; Zhu et al., 2021).Therefore, we add a term 1/tanh *kh* such that *WAI* can be used for a wider range of wave conditions. As *WAI* approaches 0, β should be 0. Thus, we use an exponential form β=$aWAI^b$ to generate empirical formulas for the wave damping coefficients for both standing and flattened vegetation. The sample size was 7.

The β_S has the following relation with *WAI*,

$$\beta_S = (0.078 \pm 0.008)WAI^{(0.32\pm0.10)} \tag{4}$$

with R^2 = 0.789 and the *p*-value of 0.008 (Figure 4A). The relation between β_F and *WAI* is

$$\beta_F = (0.07 \pm 0.02)WAI^{(0.8\pm0.3)} \tag{5}$$

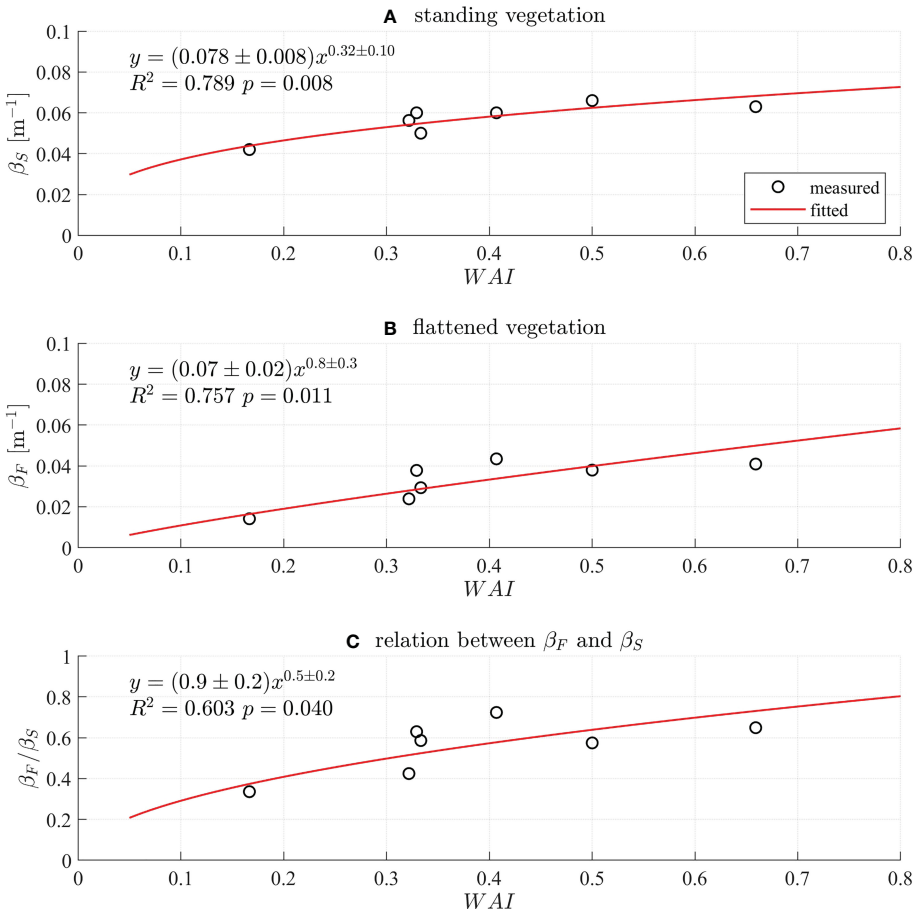

FIGURE 4
Empirical formulas for the wave damping coefficient of **(A)** standing vegetation (β_S, m^{-1}) and **(B)** flattened vegetation (β_F, m^{-1}) with respect to *WAI* defined in (3). **(C)** Relation between β_F and β_S as a function of *WAI*.

with $R^2 = 0.757$ and the p-value of 0.011 (Figure 4B). The ratio β_F/β_S also shows a relation with WAI and given by

$$\frac{\beta_F}{\beta_S} = (0.9 \pm 0.2)WAI^{(0.5\pm0.2)} \quad (6)$$

with $R^2 = 0.603$ and the p-value of 0.04 (Figure 4C). The empirical formulas (4) and (5) provide a simple way to predict the wave attenuation by standing and flattened vegetation. The results are believed to be applicable to the vegetation species that have similar dynamics of the model vegetation.

3.3 Wave attenuation model for flattened vegetation

Most previous research focused on modeling wave attenuation by standing vegetation (e.g. Dalrymple et al., 1984; Kobayashi et al., 1993; Mendez and Losada, 2004; Zhu et al., 2020b; Zhu et al., 2022). Although there are some wave attenuation models for flattened vegetation (Vuik et al., 2018), or the horizontal part of mangrove roots (Suzuki et al., 2019), they assumed rigid vegetation without swaying in waves, and therefore are not applicable for flattened flexible vegetation. Due to the complicated physic processes induced by the blade sheltering and interaction from horizontal stems (Figure 2D), it is difficult to develop a new sophisticated wave attenuation model, particularly for flattened flexible vegetation. A simple technique to predict the wave attenuation by flattened vegetation is modifying an existing wave attenuation model for standing flexible vegetation by using a factor such as equation (6). To assess this idea, we selected the newest analytical wave attenuation model developed by Zhu et al. (2022) for standing flexible vegetation, which considered drag, inertia force, and the effects of higher-order blade motions. The inputs of Zhu et al. (2022) model included hydrodynamic parameters (water depth, wave height, wave period), plant properties (stem mass density, stem length, stem rigidity, stem cross-section dimensions, stem Young's modulus, canopy density, and meadow length) and hydrodynamic coefficients. As the model vegetation is a flexible cylinder, the formulas for drag coefficient and added mass coefficient in Hu et al. (2021) were used is study. After obtaining the damping coefficient for standing vegetation (β_s), the damping coefficient for flattened vegetation is calculated from $\beta_F = \beta_S \times \frac{\beta_F}{\beta_S}$ with β_F/β_S given by equation (6).

The fitted β by equation (4) and (5) compared with measured β and showed good agreement with normalized root mean square error (NRMSE) of 0.07 and 0.2 for standing and flattened vegetation, respectively (Figure 5A), where the normalization is based on the average of measured β. Additionally, the calculated β is compared with measured β in Figure 5B. For standing vegetation, the calculated damping coefficient from the model in Zhu et al. (2022) showed a small NRMSE of 0.31 (Figure 5B), which is larger than that of fitted β with NRMSE = 0.07 (Figure 5A). The calculated β overestimated by 16% (calculated from the slope of the linear fitting in Figure 5B). For flattened vegetation, the calculated β has a NRMSE of 0.46 (Figure 5B), which is larger than fitted β with NRMSE= 0.20 (Figure 5A). The calculated β for flattened vegetation is overestimated by 10% (Figure 5B). It should be noted that if the calculated β for standing vegetation is not overestimated with a slope of 1, the slope for the corresponding β for flattened vegetation would be 1.1*1/1.16 = 0.95, indicating that the β for flattened vegetation may be underestimated by 5%. This is also acceptable for engineering application, indicating the success of modifying the existing standing vegetation-based wave attenuation model for flattened vegetation.

3.4 Case study under storm wave conditions

To explore the wave attenuation potential of flattened vegetation under extreme water depth and wave height during storms, a case study was performed based on the observed wave conditions in a storm at Nanhui shore, Shanghai. The wave conditions were measured from Sept. 10 to 17 in 2021. Two TWR-2050 (RBR cooperation, Canada) wave sensors were deployed at marsh edge (s1) and 35 m inside the vegetation (s2). The wave data at s1 was used in the present study. The storm closed to Shanghai with the shortest distance 116 km in East China Sea and

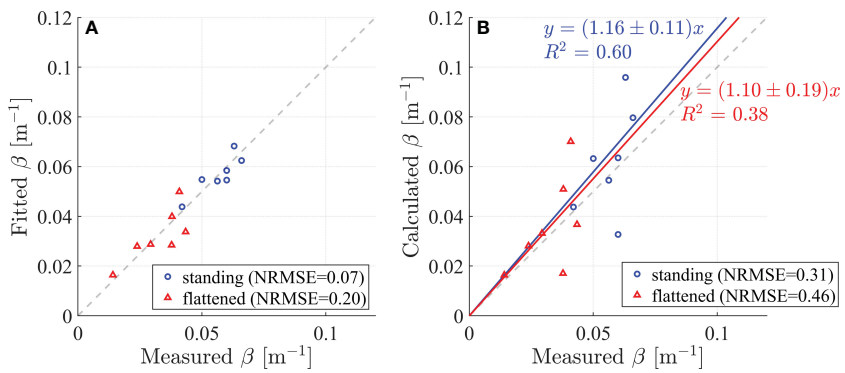

FIGURE 5
(A) Comparison between measured and fitted wave damping coefficients (β). **(B)** Comparison between measured and calculated β. The results for standing and flattened vegetation are denoted by blue circles and red triangles, respectively.

wind speed up to 42 m/s, classified as Severe Typhoon. The peak wave period (T_p) ranged from 3 to 9 s. The maximum depth was 1.43 m and the significant wave height was up to 0.68 m (Li et al., 2022). The sample size was 104. The wave conditions of the experiments can cover part of storm conditions. The linear relation between water depth and wave height is

$$H_S = (0.39 \pm 0.01)h \tag{7}$$

with $R^2 = 0.29$ (Figure 6A). The linear relation between wavelength and wave height is

$$\lambda = (34.65 \pm 0.69)H_S \tag{8}$$

with $R^2 = 0.75$ (Figure 6B). In this preliminary case study, the vegetation are assumed to have the same properties as the model vegetation in the experiments, namely, the vegetation length is l = 50 cm and the flattened vegetation folds at 10 cm above bottom, the vegetation diameter is b = 1.8 mm, and the plant density is N = 1980 stems/m^2. We assumed that we can use the modification factor for flattened vegetation in equation (6), that was derived for regular waves, for the irregular waves in the case study using $H = H_s$, and $T = T_p$. This seems to be a fair assumption as the significant wave height is the average of the highest $\frac{1}{3}$ of wave height in a short-term record that is linked to the mean wave transmission, and the modification β_F/β_S is a relative factor. The water depth is designed as 0.5 m to 1.5 m such that the vegetation is fully submerged. With a given water depth, the wave height and wavelength are calculated from equation 7 and 8, respectively. The wave damping coefficients for standing vegetation and flattened vegetation are calculated from the empirical formulas 4 and 5, respectively. The flattened vegetation is composed of two parts: the vertical unfolded part and the horizontal folded part. To further understand the wave attenuation by flattened vegetation, especially the contribution of the folded horizontal part, the wave damping coefficient by the vertical unfolded part (l_v = 10 cm) is also calculated by using the equation (2). Equation (2) is sensitive to the bulk drag coefficient C_D. We selected some representative formulas for cylinder-type vegetation from literature as shown in Table 4. The results were shown in Figure 6C.

Comparisons between the wave damping coefficient by fully standing vegetation (β_S), flattened vegetation (β_F), and the vertical

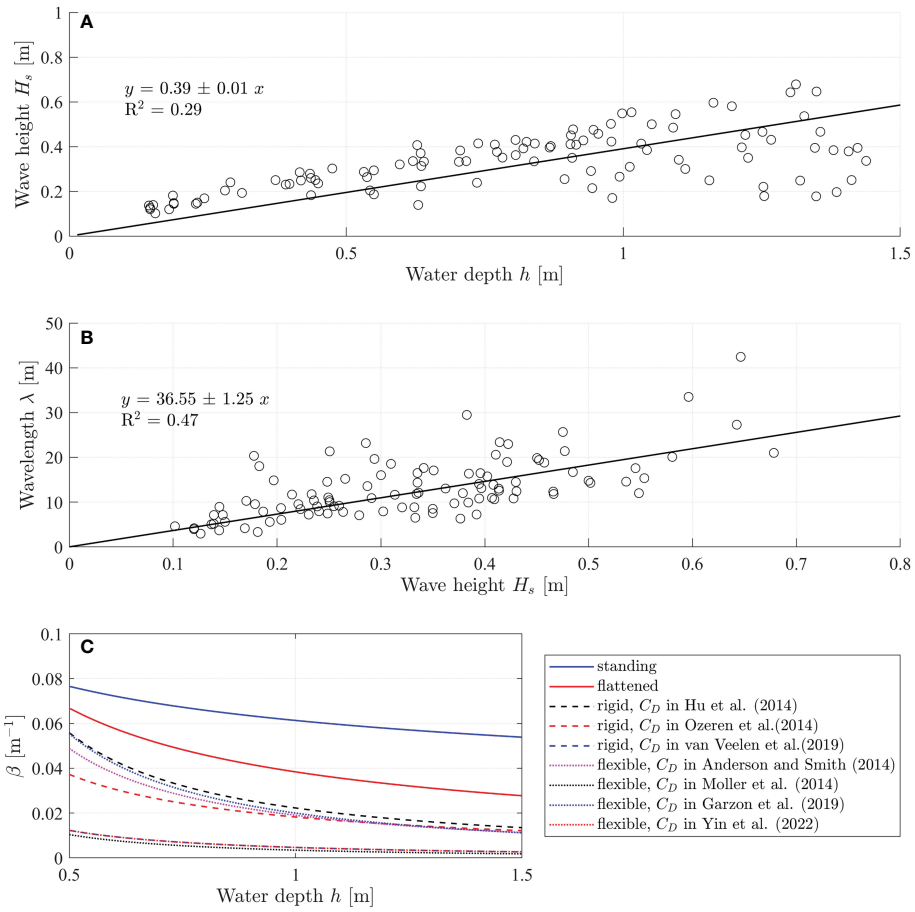

FIGURE 6
(A) Measured significant wave height (H_s) and water depth (h) during September 10 to 17 in 2021 at Nanhui shore (Li et al., 2022). **(B)** Relation between wave length and wave height. **(C)** Comparisons between the wave damping coefficient by fully standing vegetation (solid blue line), flattened vegetation (solid red line), and the 10 cm vertical unfolded part of the flattened vegetation (dashed and dotted lines). The (β) by standing vegetation and flattened vegetation were calculated based on the empirical formulas (4) and (5), respectively. The β by the 10 cm vertical unfolded part of the flattened vegetation was calculated by the formula (2) in Dalrymple et al. (1984) with the bulkdrag coefficient for rigid cylinder-type vegetation (dashed lines) and flexible cylinder-type vegetation (dotted lines).

TABLE 4 Formulas of the bulk drag coefficient (C_D) for the wave attenuation by standing cylinder-type vegetation.

reference	formula	scope	material	Young's modulus (MPa)	plant density (stems/m^2)	submerged ratio *(l/h)*
Anderson and Smith (2014)	$0.76 + (744.2/Re)^{1.27}$	533<Re<2296	XLPO	172.4	200, 400	0.78-1.36
Hu et al. (2014)	$1.04 + (730/Re)^{1.37}$	300<Re<4700	wooden rods	–	62-556	0.72-1.44
Ozeren et al. (2014)	$1.36 + (5.316/KC)^{2.07}$	5<Kc<40	rigid cylinder	–	623	0.886-1.24
Möller et al. (2014)	$6 + (305.5/Re)^{0.977}$	16.8<Re<1040	*Puccinellia maritima* *Elymus athericus*	111.6 ± 66.3 2696.3 ± 1963.8	49 ± 23	0.35
Garzon et al. (2019)	$0.205 + (1329/Re)^{1}$	500<1750	*S.alterniflora*	–	344 ± 80	0.43-0.96
van Veelen et al. (2020)	$(81/KC)^{0.36}$	53<KC<133	bamboo dowels	2917	1111	0.5-1
Yin et al. (2022)	$(150.5/KC)^{0.5952}$	50<KC<310	polyurethane	160	1012	0.5-0.71

Re is Reynolds number and KC is Keulegan-Carpenter number.

unfolded part of the flattened vegetation (β_V) under storm events are shown in Figure 6C. During the storm, the wave height and wavelength increase as the storm comes associated with increasing water depth (storm surge). With increasing water depth, all the wave damping coefficients β_S, β_F, and β_V decrease indicating that the wave attenuation capacity decreases as the storm strengthens. The wave attenuation by flattened vegetation drops quicker as water depth increases. As expected, $\beta_S > \beta_F > \beta_V$, indicating that standing vegetation provides the largest wave attenuation. As the vegetation breaks to be flattening, the wave attenuation decreases. However, the wave attenuation by flattened vegetation is larger than that by only the vertical part of the flattened vegetation, indicating that the horizontal part of the flattened vegetation also plays a significant role in wave attenuation and contributes to wave attenuation.

4 Discussion

Flattening of *S. mariqueter* is very common in winter due to its wilting and intensified storms and waves in winter. On one hand, the flattening stems construct a 'shelter' to prevent the resuspension of sediment and therefore enhance their ability to stabilize sediment. On the other hand, the flattening of *S. mariqueter* reduces its wave attenuation capacity remarkably and therefore increases the risk of sediment erosion and the vulnerability of sheltered species. The reduction of wave attenuation is more dramatic in high water levels such as high tides and storm surges since the wave attenuation indicator *WAI* is inversely proportional to h^2 in equation (3). The reduction of wave attenuation also makes more stems behind the leading stems exposed to large wave conditions, which will affect the establishment and restoration of *S. mariqueter* (Schwarz et al., 2011; Zhao et al., 2021) and its ecological services. To improve the coastal ecosystem services, especially with flattened *S. mariqueter*, it is important to take measures to compensate for the reduction of wave attenuation, e.g., installing wooden defense (Van Cuong et al., 2015; Dao et al., 2018), bamboo fences (Dao et al., 2021; Mai Van et al., 2021), floating vegetation offshore (Zhu et al., 2020a),or other nature-based coastal structures on the offshore site.

As the vegetation flattening has shown significant effects on wave attenuation, it is essential to quantify the effects of vegetation flattening on wave attenuation for the restoration of *S. mariqueter* and coastal protection and management. The developed empirical formulas (4-6) as well as the modification of the existing standing vegetation-based wave attenuation model for flattened vegetation (Section 3) presented good performance to predict wave attenuation for tested model conditions, which can be applied in the restoration of *S. mariqueter* and coastal management. The formulas are also easy to implement into large-scale models such as SWAN (Booij et al., 1999), XBeach (Roelvink et al., 2009) and TOMAWAC (http://www.opentelemac.org/) to analyze the influences of flattening-induced reduction of wave attenuation on sediment transport, shoreline changes, and regional ecosystem services. In practice, the flattened vegetation maybe considered as bottom roughness and using a wave friction factor to describe the effects of vegetation on wave decay. But the formulas are developed with limited data, which limited its application to other conditions with different wave and vegetation parameters. The transform between the wave damping coefficient and wave friction factor is shown in Appendix B.

As a first step to quantify the wave attenuation by flattened flexible vegetation, this study focused on the 'bulk' wave attenuation under different wave conditions. To explore the detailed mechanisms for wave attenuation, it is essential to understand the motion and drag of flattened flexible vegetation, which is more challenging due to the vegetation interaction and sheltering since

the flattened vegetation are overlapped (Figures 1B, 2D). Our next step is to investigate the drag of flattened flexible vegetation with different overlaps, which will be used to further analyze the effects of overlaps on vegetation sheltering and wave attenuation. In addition, the folding/breaking point determines the lengths of the erect part (dominated by normal drag) and flattened part (dominated by friction drag) and therefore influences the wave attenuation, which needs fully understanding. Due to technical limitations, we used circular cylinders to mimic *S. mariqueter*. Although dynamical similarities were considered, there may still be uncertainties. To solve the issues in flume experiments, future work will focus on field observations for real *S. mariqueter*. In the field, the percentage of flattened vegetation in a marsh decreases from seaward to landward, resulting mixing of flattened and standing vegetation, whose wave attenuation is also worth further studies.

5 Conclusion

In this study, the wave attenuation of flattened *S. mariqueter* was investigated using flume experiments with dynamically similar model vegetation. The results showed that the wave attenuation of flattened vegetation is smaller than that of standing vegetation. However, wave attenuation characteristics of flattened vegetation showed a similar pattern with standing vegetation: the wave damping coefficient (β) increased with wave height but decreased with water depth. Based on the wave attenuation characteristics, a wave attenuation indicator *WAI* was defined to generate empirical formulas for β_S and β_F as well as their ratio β_F/β_F. The empirical formulas were applied to modify the existing standing vegetation-based wave attenuation model for flattened vegetation and performed very well. A case study showed that the wave attenuation of both standing and flattened vegetation decreases when the storm approaches associated with increasing water depth by storm surge. The wave attenuation by flattened vegetation is larger than that by only the vertical part of the flattened vegetation, indicating that the horizontal folded stems also contribute significantly to the wave attenuation. Precisely quantifying the wave attenuation of flattened vegetation is essential for the restoration of *S. mariqueter* and coastal protection and management. Future work will focus on the field observation of wave attenuation by *S. mariqueter* under storm events.

Data availability statement

The original contributions presented in the study are included in the article/supplementary material. Further inquiries can be directed to the corresponding authors. The code is accessible through the link: https://github.com/lzhu7/waveAttenuationByFlexibleVegetation.

Author contributions

LZ, YM, and XL contributed to the conception and design of the study. CD supported flume experiments. YM conducted the flume experiments and data collection. YM, LX, WZ, TL, and SL collected field data. YM and LZ performed the data analysis and wrote the original draft of the manuscript. ZP, BH, TB, and XL provided scientific insights and edited the manuscript. LZ and XL directed and supervised the study. XL acquired funding. All authors contributed to the article and approved the submitted version.

Funding

This study was funded by the National Natural Science Foundation of China (42176164, 42141016). This paper is also supported by the project "Coping with deltas in transition" within the Programme of Strategic Scientific Alliances between China and The Netherlands (PSA). This study was also financed by the Chinese Ministry of Science and Technology (2016YFE0133700, 2022YFE0136700), Science and Technology Commission of Shanghai Municipality (22JC1400900), and Royal Netherlands Academy of Arts and Sciences (PSA-SA-E-02). The support was provided by China Scholarship Council (CSC) during the visit to NIOZ and TU Delft (No: 202106140131).

Acknowledgments

The authors would like to thank Yuxin Bi, Lin Su and Lv Gong for helping with field work. All the data are included in the paper.

Conflict of interest

The authors declare that the research was conducted in the absence of any commercial or financial relationships that could be construed as a potential conflict of interest.

Publisher's note

References

Anderson, M. E., and Smith, J. M. (2014). Wave attenuation by flexible, idealized salt marsh vegetation. *Coast. Eng.* 83, 82–92. doi: 10.1016/j.coastaleng.2013.10.004

Barbier, E. B., Hacker, S. D., Kennedy, C., Koch, E. W., Stier, A. C., and Silliman, B. R. (2011). The value of estuarine and coastal ecosystem services. *Ecol. Monogr.* 81, 169–193. doi: 10.1890/10-1510.1

Booij, N., Ris, R. C., and Holthuijsen, L. H. (1999). A third-generation wave model for coastal regions: 1. model description and validation. *J. Geophys. Res.: Oceans* 104, 7649–7666. doi: 10.1029/98JC02622

Bouma, T. J., Vries, M. B. D., Low, E., Kusters, L., Herman, P. M. J., Tánczos, I. C., et al. (2005). Flow hydrodynamics on a mudflat and in salt marsh vegetation: identifying general relationships for habitat characterisations. *Hydrobiologia* 540, 259–274. doi: 10.1007/s10750-004-7149-0

Chen, Y., Li, Y., Thompson, C., Wang, X., Cai, T., and Chang, Y. (2018). Differential sediment trapping abilities of mangrove and saltmarsh vegetation in a subtropical estuary. *Geomorphology* 318, 270–282. doi: 10.1016/j.geomorph.2018.06.018

Chmura, G. L., Anisfeld, S. C., Cahoon, D. R., and Lynch, J. C. (2003). Global carbon sequestration in tidal, saline wetland soils. *Global Biogeochem. Cycles* 17, 1111. doi: 10.1029/2002GB001917

Christie, E. K., Spencer, T., Owen, D., McIvor, A. L., Möller, I., and Viavattene, C. (2018). Regional coastal flood risk assessment for a tidally dominant, natural coastal setting: North Norfolk, southern north Sea. *Coast. Eng.* 134, 177–190. doi: 10.1016/j.coastaleng.2017.05.003

Dalrymple, R. A., Kirby, J. T., and Hwang, P. A. (1984). Wave diffraction due to areas of energy dissipation. *J. Waterway Port Coastal Ocean Eng.* 110, 67–79. doi: 10.1061/(ASCE)0733-950X(1984)110:1(67

Dao, H. T., Hofland, B., Suzuki, T., Stive, M. J. F., Mai, T., and Tuan, L. X. (2021). Numerical and small-scale physical modelling of wave transmission by wooden fences. *J. Coast. Hydraulic Structures* 1, 22. doi: 10.48438/jchs.2021.0004

Dao, T., Stive, M. J., Hofland, B., and Mai, T. (2018). Wave damping due to wooden fences along mangrove coasts. *J. Coast. Res.* 34, 1317–1327. doi: 10.2112/JCOASTRES-D-18-00015.1

Dean, R. G., and Dalrymple, R. A. (1991). *Water wave mechanics for engineers and scientists* (Singapore: World Scientific Publishing Company).

Garzon, J. L., Maza, M., Ferreira, C. M., Lara, J. L., and Losada, I. J. (2019). Wave attenuation by *Spartina* saltmarshes in the Chesapeake bay under storm surge conditions. *J. Geophys. Res.: Oceans* 124, 5220–5243. doi: 10.1029/2018JC014865

Ge, F., Bo, T., Zhou, Y.-X., He, Q., and Qian, W.-W. (2018). Analyzing the role of salt marshes on attenuating waves with Rb16-2050 mesearues in changjiang estuary. *Resour. Environ. Yangtze Basin* 27, 1784–1792. doi: 10. 11870 /cjlyzyyhj201808014

Henderson, S. M. (2019). Motion of buoyant, flexible aquatic vegetation under waves: simple theoretical models and parameterization of wave dissipation. *Coast. Eng.* 152, 103497. doi: 10.1016/j.coastaleng.2019.04.009

Hu, J., Mei, C. C., Chang, C.-W., and Liu, P. L. (2021). Effect of flexible coastal vegetation on waves in water of intermediate depth. *Coast. Eng.* 168, 103937. doi: 10.1016/j.coastaleng.2021.103937

Hu, Z., Suzuki, T., Zitman, T., Uittewaal, W., and Stive, M. (2014). Laboratory study on wave dissipation by vegetation in combined current–wave flow. *Coast. Eng.* 88, 131–142. doi: 10.1016/j.coastaleng.2014.02.009

Jadhav, R. S., Chen, Q., and Smith, J. M. (2013). Spectral distribution of wave energy dissipation by salt marsh vegetation. *Coast. Eng.* 77, 99–107. doi: 10.1016/j.coastaleng.2013.02.013

Kobayashi, N., Raichle, A. W., and Asano, T. (1993). Wave attenuation by vegetation. *J. Waterway Port Coastal Ocean Eng.* 119, 30–48. doi: 10.1061/(ASCE)0733-950X(1993)119:1(30)

Lei, J., and Nepf, H. (2019). Wave damping by flexible vegetation: Connecting individual blade dynamics to the meadow scale. *Coast. Eng.* 147, 138–148. doi: 10.1016/j.coastaleng.2019.01.008

Li, G.-r., Gong, G.-N., Zhang, S.-L., Gao, M.-H., Zhang, B.-L., Ma, Y.-X., et al. (2022). Observation of physical variables of coastal wetland and response of wetland system under the influence of typhoon process. *Haiyang Xuebao* 45, 1–10. doi: 10.12284/hyxb2022-00

Liu, B., Chen, Y., Cai, T., Li, Y., and Sun, L. (2021). Estimating waves and currents at the saltmarsh edge using acoustic doppler velocimeter data. *Front. Mar. Sci.* 987. doi: 10.3389/fmars.2021.708116

Losada, I. J., Maza, M., and Lara, J. L. (2016). A new formulation for vegetation-induced damping under combined waves and currents. *Coast. Eng.* 107, 1–13. doi: 10.1016/j.coastaleng.2015.09.011

Luhar, M., and Nepf, H. M. (2016). Wave-induced dynamics of flexible blades. *J. Fluids Structures* 61, 20–41. doi: 10.1016/j.jfluidstructs.2015.11.007

Madsen, O. S., Poon, Y.-K., and Graber, H. C. (1988). Spectral wave attenuation by bottom friction. *Theory*, 492–504. doi: 10.1061/9780872626874.035

Mai Van, C., Ngo, A., Mai, T., and Dao, H. T. (2021). Bamboo fences as a nature-based measure for coastal wetland protection in Vietnam. *Front. Mar. Sci.* 8. doi: 10.3389/fmars.2021.756597

Maza, M., Lara, J. L., and Losada, I. J. (2019). Experimental analysis of wave attenuation and drag forces in a realistic fringe rhizophora mangrove forest. *Adv. Water Resour.* 131, 103376. doi: 10.1016/j.advwatres.2019.07.006

Maza, M., Lara, J. L., and Losada, I. J. (2021). Predicting the evolution of coastal protection service with mangrove forest age. *Coast. Eng.* 168, 103922. doi: 10.1016/j.coastaleng.2021.103922

Maza, M., Lara, J. L., and Losada, I. J. (2022). A paradigm shift in the quantification of wave energy attenuation due to saltmarshes based on their standing biomass. *Sci. Rep.* 12, 1–13. doi: 10.1038/s41598-022-18143-6

Maza, M., Lara, J., Losada, I., Ondiviela, B., Trinogga, J., and Bouma, T. (2015). Large-Scale 3-d experiments of wave and current interaction with real vegetation. part 2: Experimental analysis. *Coast. Eng.* 106, 73–86. doi: 10.1016/j.coastaleng.2015.09.010

Mendez, F. J., and Losada, I. J. (2004). An empirical model to estimate the propagation of random breaking and nonbreaking waves over vegetation fields. *Coast. Eng.* 51, 103–118. doi: 10.1016/j.coastaleng.2003.11.003

Möller, I., Kudella, M., Rupprecht, F., Spencer, T., Paul, M., van Wesenbeeck, B. K., et al. (2014). Wave attenuation over coastal salt marshes under storm surge conditions. *Nat. Geosci.* 7, 727–731. doi: 10.1038/ngeo2251

Ozeren, Y., Wren, D. G., and Wu, W. (2014). Experimental investigation of wave attenuation through model and live vegetation. *J. Waterway Port Coastal Ocean Eng.* 140, 04014019. doi: 10.1061/(ASCE)WW.1943-5460.0000251

Paul, M., Rupprecht, F., Möller, I., Bouma, T. J., Spencer, T., Kudella, M., et al. (2016). Plant stiffness and biomass as drivers for drag forces under extreme wave loading: A flume study on mimics. *Coast. Eng.* 117, 70–78. doi: 10.1016/j.coastaleng.2016.07.004

Roelvink, D., Reniers, A., van Dongeren, A., van Thiel de Vries, J., McCall, R., and Lescinski, J. (2009). Modelling storm impacts on beaches, dunes and barrier islands. *Coast. Eng.* 56, 1133–1152. doi: 10.1016/j.coastaleng.2009.08.006

Schwarz, C., Ysebaert, T., Zhu, Z., Zhang, L., Bouma, T. J., and Herman, P. M. J. (2011). Abiotic factors governing the establishment and expansion of two salt marsh plants in the Yangtze estuary, China. *Wetlands* 31, 1011–1021. doi: 10.1007/s13157-011-0212-5

Sousa, A. I., Lillebø, A. I., Pardal, M. A., and Caçador, I. (2010). Productivity and nutrient cycling in salt marshes: Contribution to ecosystem health. *Estuarine Coast. Shelf Sci.* 87, 640–646. doi: 10.1016/j.ecss.2010.03.007

Suzuki, T., Hu, Z., Kumada, K., Phan, L. K., and Zijlema, M. (2019). Non-hydrostatic modeling of drag, inertia and porous effects in wave propagation over dense vegetation fields. *Coast. Eng.* 149, 49–64. doi: 10.1016/j.coastaleng.2019.03.011

Temmerman, S., Meire, P., Bouma, T. J., Herman, P. M. J., Ysebaert, T., and De Vriend, H. J. (2013). Ecosystem-based coastal defence in the face of global change. *Nature* 504, 79–83. doi: 10.1038/nature12859

Tian, B., Wu, W., Yang, Z., and Zhou, Y. (2016). Drivers, trends, and potential impacts of long-term coastal reclamation in china from 1985 to 2010. *Estuarine Coast. Shelf Sci.* 170, 83–90. doi: 10.1016/j.ecss.2016.01.006

Van Cuong, C., Brown, S., To, H. H., and Hockings, M. (2015). Using melaleuca fences as soft coastal engineering for mangrove restoration in kien giang, Vietnam. *Ecol. Eng.* 81, 256–265. doi: 10.1016/j.ecoleng.2015.04.031

van Veelen, T. J., Fairchild, T. P., Reeve, D. E., and Karunarathna, H. (2020). Experimental study on vegetation flexibility as control parameter for wave damping and velocity structure. *Coast. Eng.* 157, 103648. doi: 10.1016/j.coastaleng.2020.103648

Vuik, V., Suh Heo, H. Y., Zhu, Z., Borsje, B. W., and Jonkman, S. N. (2018). Stem breakage of salt marsh vegetation under wave forcing: A field and model study. *Estuarine Coast. Shelf Sci.* 200, 41–58. doi: 10.1016/j.ecss.2017.09.028

Xue, L., Li, X., Shi, B., Yang, B., Lin, S., Yuan, Y., et al. (2021). Pattern-regulated wave attenuation by salt marshes in the Yangtze estuary, China. *Ocean Coast. Manage.* 209, 105686. doi: 10.1016/j.ocecoaman.2021.105686

Yin, K., Xu, S., Gong, S., Chen, J., Wang, Y., and Li, M. (2022). Modeling wave attenuation by submerged flexible vegetation with xbeach phase-averaged model. *Ocean Eng.* 257, 111646. doi: 10.1016/j.oceaneng.2022.111646

Ysebaert, T., Yang, S.-L., Zhang, L., He, Q., Bouma, T. J., and Herman, P. M. J. (2011). Wave attenuation by two contrasting ecosystem engineering salt marsh macrophytes in the intertidal pioneer zone. *Wetlands* 31, 1043–1054. doi: 10.1007/s13157-011-0240-1

Yuan, L., Liu, D., Tian, B., Yuan, X., Bo, S., Ma, Q., et al. (2022). A solution for restoration of critical wetlands and waterbird habitats in coastal deltaic systems. *J. Environ. Manage.* 302. doi: 10.1016/j.jenvman.2021.113996

Zhao, Y., Peng, Z., He, Q., and Ma, Y. (2023). Wave attenuation over combined salt marsh vegetation. *Ocean Eng.* 267. doi: 10.1016/j.oceaneng.2022.113234

Zhao, Z., Zhang, L., Li, X., Yuan, L., and Bouma, T. J. (2021). The onset of secondary seed dispersal is controlled by germination-features: A neglected process in sudden saltmarsh establishment. *Limnol. Oceanogr.* 66, 3070–3084. doi: 10.1002/lno.11860

Zhu, L., Chen, Q., Ding, Y., Jafari, N., Wang, H., and Johnson, B. D. (2023). Towards a unified drag coefficient formula for quantifying wave energy reduction by salt marshes. *Coast. Eng.* 180, 104256. doi: 10.1016/j.coastaleng.2022.104256

Zhu, L., Huguenard, K., Fredriksson, D. W., and Lei, J. (2022). Wave attenuation by flexible vegetation (and suspended kelp) with blade motion: Analytical solutions. *Adv. Water Resour.* 162, 104148. doi: 10.1016/j.advwatres.2022.104148

Zhu, L., Huguenard, K., Zou, Q.-P., Fredriksson, D. W., and Xie, D. (2020a). Aquaculture farms as nature-based coastal protection: Random wave attenuation by suspended and submerged canopies. *Coast. Eng.* 160, 103737. doi: 10.1016/j.coastaleng.2020.103737

Zhu, L., Lei, J., Huguenard, K., and Fredriksson, D. W. (2021). Wave attenuation by suspended canopies with cultivated kelp (*Saccharina latissima*). *Coast. Eng.* 168, 103947. doi: 10.1016/j.coastaleng.2021.103947

Zhu, Z., Yang, Z., and Bouma, T. J. (2020c). Biomechanical properties of marsh vegetation in space and time: effects of salinity, inundation and seasonality. *Ann. Bot.* 125, 277–290. doi: 10.1093/aob/mcz063

Zhu, Q., Yang, S., and Ma, Y. (2014). Intra-tidal sedimentary processes associated with combined wave–current action on an exposed, erosional mudflat, southeastern Yangtze river delta, China. *Mar. Geol.* 347, 95–106. doi: 10.1016/j.margeo.2013.11.005

Zhu, L., Zou, Q.-P., Huguenard, K., and Fredriksson, D. W. (2020b). Mechanisms for the asymmetric motion of submerged aquatic vegetation in waves: a consistent-mass cable model. *J. Geophys. Res.: Oceans* 125, e2019JC015517. doi: 10.1029/2019JC015517

Appendix A. Methods to fit the wave damping coefficient β with wave reflection

According to Dalrymple et al. (1984), the wave height decays as,

$$\frac{H(x)}{H_{I0}} = \frac{1}{1+\beta x} = \frac{1}{1+k_D H_{I0} x} \tag{A1}$$

where $H(x)$ is the local wave height at x m from the leading edge (Figure 2A), H_{I0} is the incident wave height at $x = 0$. β was expressed as, β=$k_D H_{I0}$, where k_D is wave decay coefficient.

The wave reflection is less than 10% in this flume. Due to wave reflection, the wave height oscillated along the vegetation meadow (Figure A1). Assuming the reflected wave height decays at the same wave decay coefficient k_D as the incident wave, the local wave height over the vegetation is expressed as Zhu et al. (2021),

$$H(x) = \sqrt{\left(\frac{H_{I0}}{1+k_D H_{I0} x}\right)^2 + \left(\frac{H_{RL_v}}{1+k_D H_{RL_v}(L_v - x)}\right)^2 + 2\frac{H_{I0}}{1+k_D H_{I0} x}\frac{H_{RL_v}}{1+k_D H_{RL_v}(L_v - x)}\cos\,(2kx+\varepsilon)}, \tag{A2}$$

where H_{RL_v} is the reflective wave height by beach at the end of the flume, which induced fluctuation of wave height as shown in (Figure A1). Phase lag ϵ means phase lag of wave propagation. Thus, k_D, H_{RL_v} and ϵ can be fitted from equation (A2) with given H_{I0} and $H(x)$ along the meadow. In this study, the nonlinear regression model 'fitnlm' in MATLAB R2022a was used to fit these variables. To remove the effects of the bottom roughness and wall friction from the flume, the wave decay coefficient (k_{DW}) from the empty flume under the same wave condition was subtracted from the measured wave decay coefficient (k_{DWV}), such that the wave decay coefficient by only vegetation is

$$k_D = k_{DWV} - k_{DW} \tag{A3}$$

With fitted k_D, the wave damping coefficient β can be obtained from

$$\beta = k_D H_{I0} \tag{A4}$$

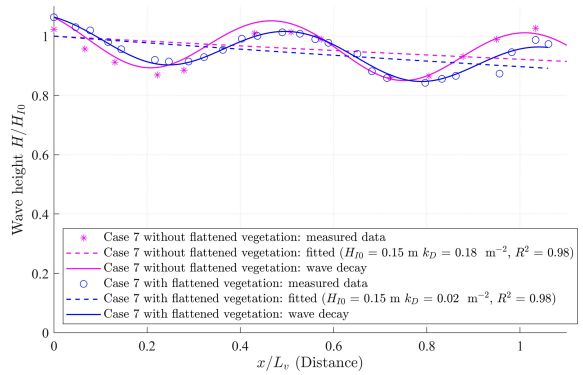

FIGURE A1
Measured (magenta asterisks for that without vegetation and blue circles for that with vegetation) and fitted (solid lines) wave heights (H) normalized by the incident wave height (H_{I0}) along the vegetation regions for Case 7. The calculated incident wave height decay with fitted H_{I0} and k_D is denoted by dashed lines. The magenta lines are for the case without vegetation while the blue lines are for the case with vegetation. The horizontal distance is normalized by the canopy length as x/L_v.

Appendix B. Wave friction factor (f_w) due to vegetation

Under storm and large water depth, the vegetation was deeply submerged and serves strengthening the bottom roughness. According to Madsen et al. (1988), the bottom stress (τ_b) due to vegetation can be expressed as

$$\tau_b = \frac{1}{2}\rho f_w u_b |u_b| \tag{B1}$$

where f_w is wave friction factor and u_b=0.5ω/sinh kh is the near-bottom maximum orbital velocity. Thus the wave height decay can be obtained from the energy equation

$$\frac{\partial Ec_g}{\partial x} = \frac{1}{T}\int_0^T \tau_b u_b dt \tag{B2}$$

Solving equation B2 yields

$$\frac{H}{H_{I0}} = \frac{1}{1+\beta x} \tag{B3}$$

with the wave damping coefficient (β) given by

$$\beta = \frac{4 f_w}{3\pi}\frac{k^2 H_{I0}}{sinh\;\; kh(2kh + sinh\;\; 2kh)} \tag{B4}$$

Note that the factor 4 in the first term on the right side of equation (B4) is 1 in equation (18) in (Dalrymple et al., 1984) and equation (9.41) in Dean and Dalrymple (1991) because they defined the bottom stress as $\tau_b = \frac{1}{8}\rho f_w u_b |u_b|$ (equation 9.15 in Dean and Dalrymple (1991), which is $\frac{1}{4}$ of our definition $\tau_b = \frac{1}{2}\rho f_w u_b |u_b|$ (B1). Therefore, with given wave damping coefficient (β), the wave friction factor can be obtained by solving equation (B4), which yields

$$f_w = \frac{3\pi}{4k^2}\,\text{sinh}\;\; kh(2kh + \text{sinh}\;\; 2kh)\frac{\beta}{H_{I0}} \tag{B5}$$

frontiers | Frontiers in Marine Science

TYPE Original Research
PUBLISHED 25 April 2023
DOI 10.3389/fmars.2023.1081353

OPEN ACCESS

EDITED BY
Zeng Zhou,
Hohai University, China

REVIEWED BY
Tian Xie,
Beijing Normal University, China
Zhenchang Zhu,
Guangdong University of Technology, China
Steven G. Sandi,
Deakin University, Australia

*CORRESPONDENCE
Xiuzhen Li
xzli@sklec.ecnu.edu.cn

SPECIALTY SECTION
This article was submitted to Coastal Ocean Processes, a section of the journal Frontiers in Marine Science

RECEIVED 27 October 2022
ACCEPTED 04 April 2023
PUBLISHED 25 April 2023

CITATION
Jiang C, Li X, Zhao W, Xue L and Su L (2023) Mud cracks promote colonization by pioneer saltmarsh plants. *Front. Mar. Sci.* 10:1081353. doi: 10.3389/fmars.2023.1081353

Mud cracks promote colonization by pioneer saltmarsh plants

Can Jiang[1,2,3], Xiuzhen Li[1,4]*, Wenzhen Zhao[1], Liming Xue[1] and Lin Su[1]

[1]State Key Laboratory of Estuarine and Coastal Research, Institute of Eco-Chongming, East China Normal University, Shanghai, China, [2]East China Sea Environmental Monitoring Center, State Oceanic Administration, Shanghai, China, [3]Key Laboratory of Marine Ecological Monitoring and Restoration Technologies, Ministry of Natural Resources, Shanghai, China, [4]Yangtze Delta Estuarine Wetland Ecosystem Observation and Research Station, Ministry of Education and Shanghai Science and Technology Committee, Shanghai, China

Saltmarshes are valued as key buffering ecosystems against global climate change and sea level rise. However, the knowledge deficit regarding links between colonization of saltmarsh fringes by plants and mud cracking in the lateral dimension considerably limits our understanding of marsh resilience. Here, the role of mud cracks in colonization by saltmarsh plants was investigated. A combination of field experiments, remote sensing, and experimental results revealed that: (1) potential mud cracking zones were formed at the seaward edge of saltmarshes under the influence of tide-induced wetting–drying cycles, where mud cracks were extensively distributed and colonized by new seedlings. (2) The seedling density in the mud cracks was higher than that in the patches, and seedlings in the mud cracks sprouted earlier than those in the patches. The results implied that mud cracking enhanced colonization by saltmarsh plants, rather than being a water stressor. (3) The two main ecological functions of mud cracks in saltmarsh colonization were acting as "seed traps" and "seedling growth promoters." (4) Mud cracking could be a key factor influencing saltmarsh resilience, especially by promoting the colonization and dispersal of saltmarsh plants. Rapid colonization of potential zones with mud cracks could occur as soon as seeds are available. Our results could facilitate the development of appropriate saltmarsh rehabilitation strategies.

KEYWORDS

mud cracks, colonization, tidal regime, saltmarsh, restoration

1 Introduction

Coastal wetlands such as saltmarshes are among the most valuable and productive ecosystems on the globe (Costanza et al., 1997), which perform key ecosystem functions such as wave attenuation (Bouma et al., 2010; Möller et al., 2014), shoreline stabilization (Temmerman et al., 2013; Bouma et al., 2014), carbon sequestration, nutrient retention (Li

et al., 2014), and biodiversity conservation (Costanza et al., 2014; Kelleway et al., 2017). Thus, saltmarshes are crucial ecosystems that naturally buffer the effects of global climate change and sea level rise (SLR) (Duarte et al., 2013; Zhu et al., 2020). However, several saltmarshes are extensively eroded at the edges (Deegan et al., 2012; Silliman et al., 2012; Leonardi et al., 2016), and vegetation recovery forms the Achilles' heel of saltmarsh resilience to SLR (Zhu et al., 2020). Consequently, effective and rapid efforts to restore vegetation at saltmarsh edges are essential.

The most notable characteristic of saltmarshes is the alternating wetting–drying periods with semimonthly inundation-exposure cycles, which leave the areas with high elevation and weak tides not submerged in seawater except during the spring tides. Consequently, extensive mud cracks have occurred on intertidal mudflats (Han, 2017). Elevation and tidal regime are two principle factors affecting mud cracking processes. Coastal wetlands in many areas are gradually expanding due to sediment-induced vertical accretion, such as in the Oosterschelde estuary in the Netherlands (Ma et al., 2014) and Yangtze River estuary (Yang et al., 2003; Ge et al., 2015a). As these are elevated features relative to the low-lying bare mudflats, saltmarshes are no longer subjected to inundation during each tide, but they become exposed to desiccation and evaporation, which are strongly associated with semilunar tidal cycles (Gardel et al., 2009). According to Fiot and Gratiot (2006), mud cracks appear if desiccation and evaporation processes last sufficiently at a given elevation (>2.6 m above hydrographic zero), and five consecutive days of emersion (CDOE) are sufficient for mud cracking to occur. Moreover, elevation-induced wetting-drying cycles vary considerably at the highest and seaward edges of a saltmarsh, which modifies the physical characteristics of mud surfaces in different ways. The study sites in Chongming Dongtan wetland still exhibit healed cracks that are a manifestation of previous wetting–drying cycles in the low-lying saltmarsh. Wetting cycles caused by tides do not shift cracks but heal them, thereby leaving scars on the mud surface (Figure 1B). Previous studies have only investigated the mud cracking process and factors influencing the process, such as moisture conditions, confining pressures (Morris et al., 1992; Mitchell, 1993), pore water pressure or suction (Fredlund and Rahardjo, 1993; Yesiller et al., 2000), and meteorological parameters (Gardel et al., 2009); however, ecological roles, such as the trapping of floating propagules during the formation of mud cracks, remain unknown.

Mud cracks, which are affected by wetting–drying cycles induced by tides, are widely distributed in coastal wetlands, especially at saltmarsh edges. Mud cracks have previously been considered water stress indicators that reflect desiccation, which is potentially harmful to plant growth (Clarke and Myerscough, 1993; McKee et al., 2004). However, the conclusion has raised concerns among researchers. Fiot and Gratiot (2006) demonstrated that colonization of mudflats by vegetation was caused by mud dewatering and consolidation, which were dependent on the local topography (Anthony et al., 2008), including tide submersion frequency and wetting–drying cycles on intertidal mudflats. Gardel et al. (2009) also suggested that mud cracks are a key factor influencing mangrove resilience. In addition, vegetation recovery in tidal mudflats adjacent to a saltmarsh edge is essential for revegetation in relation to SLR (Zhu et al., 2020). Extensive mud cracks at the highest and seaward edge affect microtopography, as well as plant colonization and growth. The zones at the saltmarsh edges are substantially influenced by wave-induced erosion dynamics on tidal flats (Leonardi and Fagherazzi, 2014; Bouma et al., 2016; Wang et al., 2017), resulting in cliff erosion or seedling dislodgement. Therefore, the interplay between mud surface microtopography and the colonization of saltmarsh edges by plant seedlings should be investigated (Xie et al., 2019). Current studies on mud cracks have only focused on mud bar colonization and associated processes (Fiot and Gratiot, 2006; Gardel et al., 2009; Proisy et al., 2009). The knowledge deficit regarding links between

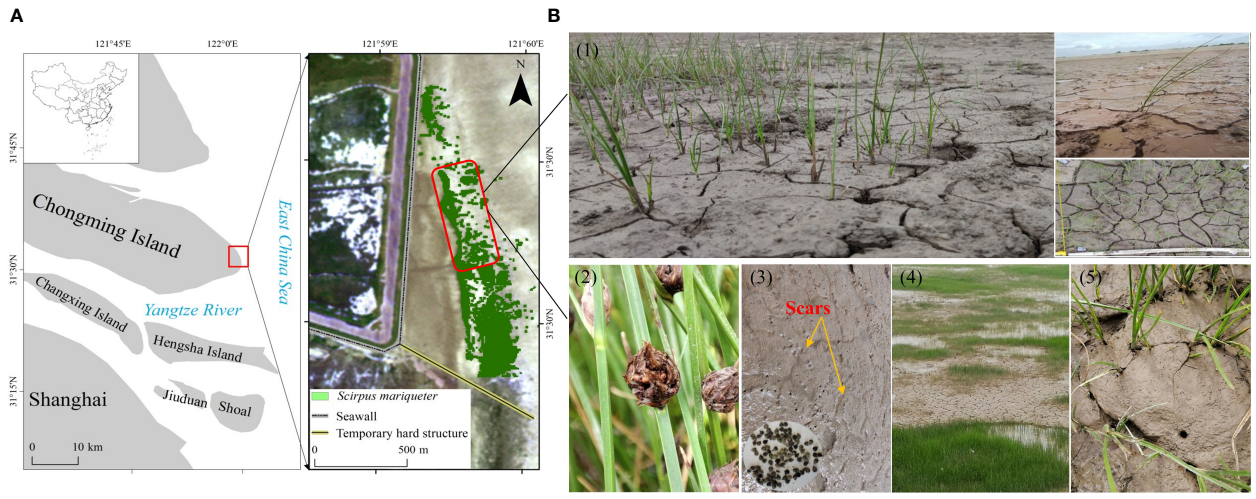

FIGURE 1
Study area and field site. **(A)** Location of the Chongming Dongtan wetland and distribution of *S. mariqueter*. **(B1)** Extensive formation of mud cracks on mud surfaces at the saltmarsh edge. **(B2)** Mature seeds and seed retention on mud surfaces and cracks in August 2021. **(B3)** Healed scars of mud cracks as an indicator of previous wetting–drying cycles on bare mudflats and *S. mariqueter* seeds trapped in mud cracks. **(B4, B5)** Seedlings in mud cracks and patches.

colonization of saltmarsh fringes by plants and mud cracking in the lateral dimension substantially limits our understanding of marsh resilience to SLR.

To comprehensively elucidate the spatial synchronization of desiccation and propagule availability, there is a need for additional insights into the temporal synchronization of mud crack formation and seed availability. Therefore, the aim of this study was to investigate the mud cracking process and its ecological function in the establishment of saltmarsh plants. Our results revealed that mud cracks in coastal wetlands were not a stressor for plant activity, although they were a vital factor in the dispersal and colonization of saltmarsh fringes by plants. Furthermore, our study contributed to the promotion of vegetation establishment in mud crack zones in future saltmarsh restoration activities.

2 Materials and methods

2.1 Study site and field experiments

The study site was located at the east headland of Chongming Island (31°25′–31°38′N, 121°50′–122°05′E; Figure 1A), which is a part of the Chongming Dongtan National Nature Reserve and the largest alluvial island (total area of 1,267 km^2) in the Yangtze Estuary, China (Zhao et al., 2019). The climate is subtropical monsoon, with an annual average temperature of 15.5 and being located on an intertidal mudflat, which is influenced by irregular semidiurnal tides and two maximum and minimum tides (15-day intervals) occurring monthly. The maximum and average tide heights range from 4.62 to 5.95 m and from 1.96 to 3.08 m, respectively (Ge et al., 2008; Li et al., 2014; Jiang et al., 2022). Under normal weather conditions, the mean current velocity in the saltmarsh is approximately 0.1 m s^{-1}, while that in the low-lying mudflats is 0.3 m s^{-1} (Yang et al., 2020).

Our field investigation began in August 2021. The study area was in a low-lying saltmarsh, where the dominant pioneer plant species, *Scirpus mariqueter*, has colonized under frequent wetting–drying cycles. Narrow areas of mud cracks were distributed along the seaward edge of the saltmarsh, and extensive mud cracks were observed in the inner saltmarsh, where tidal flat elevation was relatively high (Figure 1). The saltmarsh plants are dispersed in a northwest and seaward direction owing to suitable elevation and hydrodynamics (Jiang et al., 2022). Propagules can be easily washed away at sites exposed to waves due to strong hydrodynamics. However, numerous mature seeds and new seedlings were observed in the mud cracks (Figures 1B1, B3, B5). To compare the differences in seedling densities between mud cracks and patches, 10 sample squares (50 cm × 50 cm) were randomly selected, and parameters such as plant density and the number of mud cracks and patches were recorded.

2.2 Tidal regime and water levels

To determine the effects of the tidal regime on mud cracking and plant establishment, we obtained tidal data between April and August 2021. Tide information was obtained from Sheshan station and tide tables published by the National Marine Data and Information Service (http://www.nmdis.gov.cn).

In this study, low-cloud Sentinel-2 remote sensing images from January to August 2021 were selected. The binary system of Sentinel-2A and Sentinel-2B guarantees a revisit period of five days and a spatial resolution of up to 10 m in the visible near-infrared band. Therefore, the high spatiotemporal resolution overcomes the adverse effects of cloudiness in estuarine and coastal regions to a certain extent and considerably enhances data availability.

The images (level 2A) used in this study, which covered seven periods, were downloaded from the European Space Agency (http://scihub.copernicus.eu/dhus/#/home); that is, the images were subjected to geometric and atmospheric (bottom-of-atmosphere reflectance) corrections. After the initial cropping of images, the water levels at the moment the satellite transited the study area were extracted based on a visual interpretation of each period. Based on the tidal level data obtained from Sheshan station (approximately 20 km east of Chongming Dongtan), the water levels were assumed to be the contour lines, and their elevation was the tidal height at the corresponding time (Fan et al., 2018). Because the multi-period images covered different tidal conditions, the highest and lowest water levels were considered the highest and lowest tide levels, respectively. The area between the highest and lowest tide levels was the potential mud cracking zone affected by wetting–drying cycles from periodic tides.

2.3 Manipulative experiments

2.3.1 Seed collection and experimental setup

Manipulative experiments were conducted to elucidate the phenomenon that mud cracks at the seaward edge promote colonization by *S. mariqueter* (Figure 2). Mature *S. mariqueter* seeds were randomly collected, and the mud used for the experiment was dug up in the Chongming Dongtan wetland in August 2021 (Figure 1A). All seeds were air-dried in the laboratory until absolutely dry (Xiao et al., 2016). The mud was transported to the laboratory and transferred into high-density polyethylene containers (65 cm × 41 cm × 15.5 cm, Figure 2). The properties of mud samples collected from the study site are presented in Table 1. Nine repeated treatments were set up, and 4,300 seeds (seed density of approximately 1.6 seeds/cm^2) were evenly buried at a depth of 10 cm from the bottom of each container and covered with 3 cm of mud (Figure 2).

To avoid disturbance, all containers were placed at a fixed location until the experiment ended. The experiment was conducted for 1 month (August 2021) at an average daily temperature of 28°C. To simulate the effects of the tidal regime on mud crack formation and plant colonization, immersion–emersion cycles were conducted by draining seawater at 6:00 am and adding seawater at 18:00 pm for the first two days. Afterward, sediment moisture was used to maintain plant survival until day 15, and the procedure was repeated again.

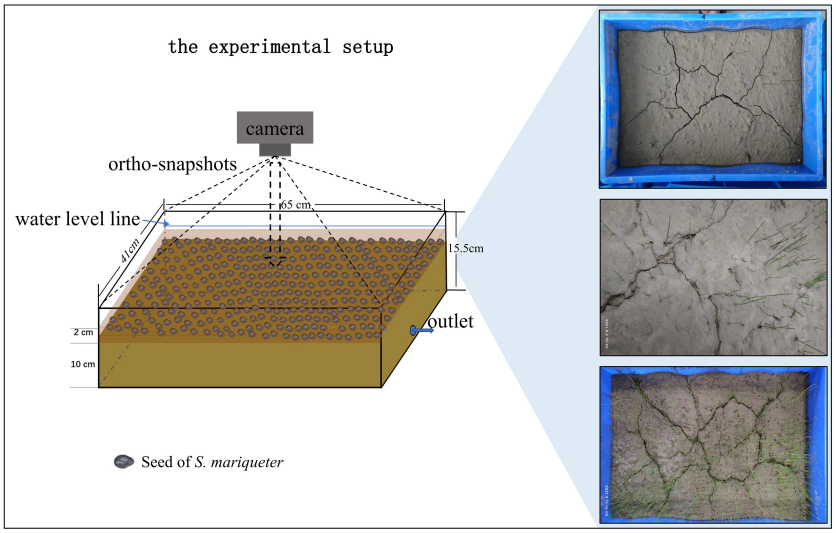

FIGURE 2
Manipulative control experiment and schematic representation of the experimental setup.

2.3.2 Dynamic monitoring of mud cracks and plant growth

Mud cracking and seedling growth were dynamically monitored using a camera throughout the experimental period. The camera was kept at a fixed height for orthophotography at each monitored time (Figure 2). The number of CDOE, which is the probability of mud cracks occurring at a given elevation (Fiot and Gratiot, 2006), was recorded daily until no new cracks appeared. The number of mud cracks was computed based on new mud crack pixels appearing between two successive images. The crack intensity factor (CIF) was introduced as a descriptor of crack surficial dimensions (Miller et al., 1998; Yesiller et al., 2000; Gardel et al., 2009). CIF is defined as the ratio of crack area (Ac) to the total surface area (At) of a dry soil mass. In this study, CIF was used to quantify the number of mud cracks at the study site. Individual seedlings were also counted after germinating.

2.4 Data analysis

All statistical analyses were performed using IBM SPSS Statistics 23.0 (IBM Corporation, Armonk, NY, USA) and OriginPro 2021 (OriginLab Corporation, Northampton, MA, USA). A one-way ANOVA was used to test for significant differences in seedling densities between mud cracks and patches. The level of statistical significance was set at $p < 0.05$.

Additionally, we monitored and recorded the evolution of mud cracks and seedling germination and growth during the experimental period using a camera. Parameters such as the lengths and areas of mud cracks and individual seedlings were analyzed using ArcGIS 10.7.1 (ESRI Inc., Redlands, CA, USA).

TABLE 1 Properties of mud used in the study.

Property	Mean ± SD.
bulk density (g/m^3)	1.34 ± 0.10
pH	8.40 ± 0.10
salinity (ppt)	0.89 ± 0.18
conductivity (mS/m^2)	1790 ± 469
median particle diameter (μm)	26.61 ± 5.76
TN (g/kg)	0.39 ± 0.11
TC (g/kg)	11.55 ± 0.81

3 Results

3.1 Variations in tidal regimes

Tidal regimes influenced the alternating wetting–drying cycles on the mud surfaces, which potentially affected the distribution of mud cracks and the colonization of tidal flats by saltmarsh plants. The variations in tidal heights between April and August 2021 at Chongming Dongtan wetland were not significant, and the average tidal heights in April and August 2021 were 2.2 ± 0.9 m and 2.47 ± 0.9 m (0.54–3.99 m and 0.59–4.5 m), respectively (Figure 3A). The average interval of daily high tide was 11 h and low tide was 5.2 h. In addition, tidal water levels were computed according to tidal regimes at the Chongming Dongtan wetland from January to August 2021 (Figure 3B). The results showed that the waterline ranged from the seaward edge of the low-lying saltmarsh to the bare mudflats. Furthermore, the tidal occurrence zones, that is, from spring tide (high tide) to neap tide (low tide), coincided with the mud cracking zones in the low-lying saltmarsh, which were considered potential mud cracking zones as well as an ecological zone for plant dispersal and colonization (Figure 3B). The potential mud cracking zone was a dynamic area determined by the tidal flat elevation and tidal regime.

3.2 Plant distribution between mud cracks and patches in the study site

According to our findings from the field survey, the mud cracks were irregularly distributed in polygons or lines on the tidal flats, and individual plants disproportionately colonized the mud cracks and patches. The results showed that most individual seedlings in the patches were established near mud cracks (Figure 4A). In addition, the number of seedlings in the mud cracks was significantly higher than that in the patches (p <0.01), and the mean seedling densities in the mud cracks and patches were 291 ± 13.91 individuals/m^2 and 196 ± 7.92 individuals/m^2, respectively (Figure 4B).

3.3 Mud crack formation and colonization by plants under laboratory conditions

3.3.1 Mud crack formation

Figure 5 illustrates the evolution of mud cracks during the experimental period, derived from mud crack images captured by the camera. The results showed that mud crack formation progressed gradually on the mud surface at the beginning of the first wetting–drying cycle and then developed rapidly after three days (Figure 5). Two mud cracks appeared on the mud surface on the second CDOE (Figure 5A), and a new crack appeared on the third CDOE (Figure 5B). The mud cracks were linearly distributed in the containers before new cracks appeared. The number of new mud cracks increased significantly, and the mud cracks gradually transformed into regular polygonal shapes on the fifth CDOE (Figure 5C). The mud cracks completely exhibited polygonal shapes (i.e., quadrilateral) on the seventh CDOE and formed a basic network of mud cracks (Figure 5D). No new mud cracks appeared after the seventh CDOE. Generally, all mud cracks in each container were formed within a period of 5–7 days (CDOE), and their formation decreased after the fifth CDOE, with no significant differences observed in subsequent wetting–drying cycles.

3.3.2 Plant colonization between mud cracks and patches

3.3.2.1 Plant colonization process

According to our results, seedlings emerged from the mud cracks into the patches (Figure 6), which is consistent with field observations. Seedlings colonized the mud cracks after the seventh CDOE (Figure 6B). Moreover, seedlings in the mud cracks germinated earlier than those in the patches (Figures 6A, B). “Seedling circles” based on the morphology of the mud cracks were left on the mud surface at the end of the experimental period, with the seedlings densely distributed in the mud cracks and sparsely distributed in the patches (Figures 6C, D). The number of individual seedlings in the mud cracks (453 seedlings) was higher than that in the patches (311 seedlings) and accounted for 59.3% of the total seedlings in each container.

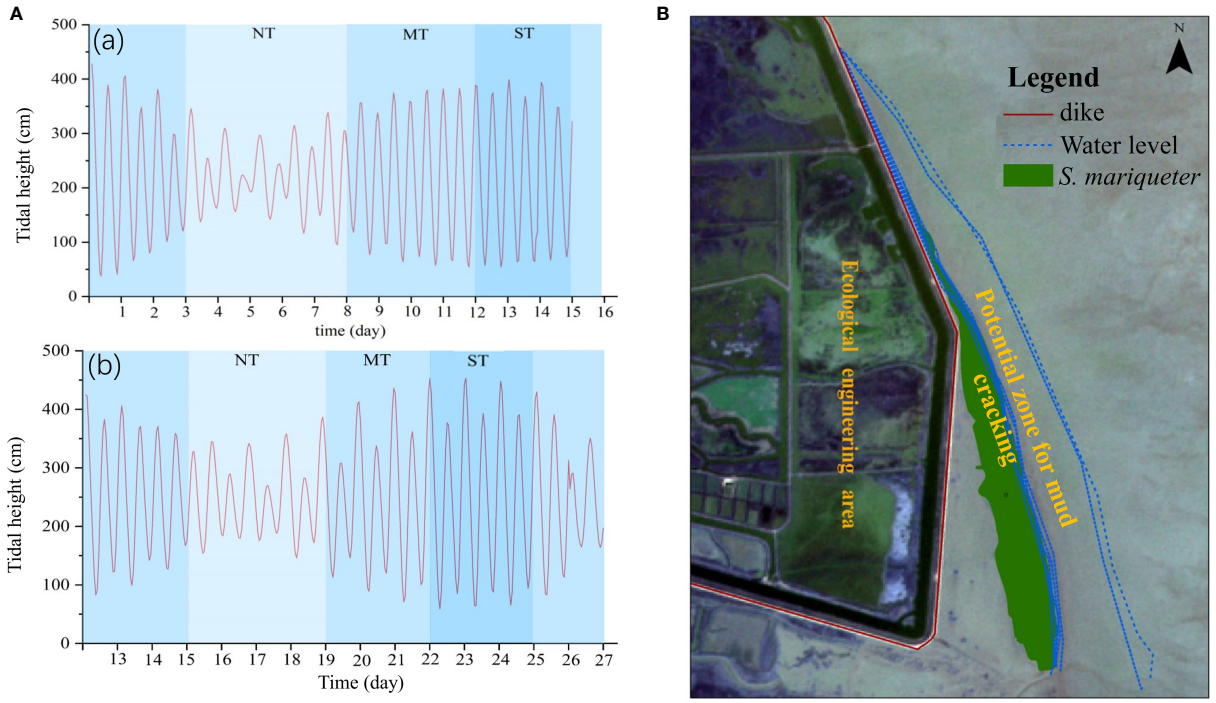

FIGURE 3
Tidal heights and tidal regimes in the Chongming Dongtan wetland. **(A)** Variations in tidal heights in April 2021 (a) and August 2021 (b); NT, MT, and ST are neap tide, middle tide, and spring tide, respectively. **(B)** Variations in tidal regimes from January to August 2021. The zone between water levels is defined as the potential mud cracking zone and a potential ecological restoration zone for plant dispersal and colonization.

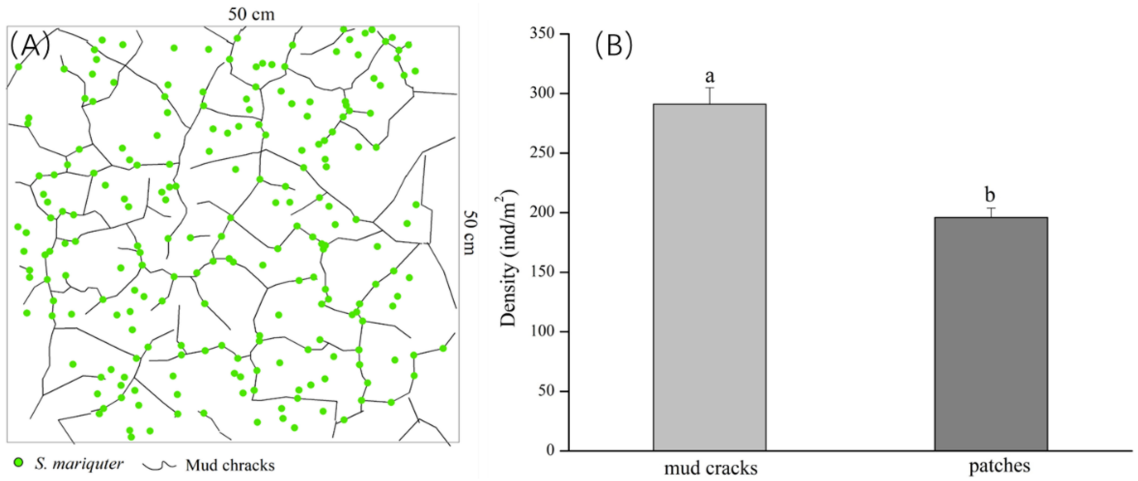

FIGURE 4
Distribution of *S. mariqueter* in mud cracks and patches in the study site. **(A)** An illustration of the distribution patterns of individual plants, and mud cracks: green dots are plants and black lines are mud cracks. **(B)** Bar graphs showing plant densities in the mud cracks and patches.

3.3.2.2 Variations in plant densities between mud cracks and patches

The one-month-long experimental results revealed that the average germination rate of *S. mariqueter* was approximately 23%. Detailed information on seedling properties, such as seedling heights, is presented in Table 2. Mud cracks evolved into irregular polygonal or linear cracks. The average length and width of mud cracks were 2.84 ± 0.31 m and 0.5 ± 0.37 cm, respectively. Generally, 15 ± 3 patches were developed in each container (Figure 7 and Table 2).

3.3.2.3 Variations in seedling density per unit area of mud cracks and patches

Individual seedlings in mud cracks and patches were compared per unit area (cm^2) to assess the effects of mud cracks on saltmarsh colonization (Figure 8). Our results revealed that the total area of mud cracks was significantly smaller than that of patches; however, the mud cracks had more seedlings per unit area than the patches, which contributed to the successful colonization by the seedlings. For example, the length and area of mud cracks in sample 3 were 276.2 cm and 137.0 cm^2, respectively, and the CIF value at the end

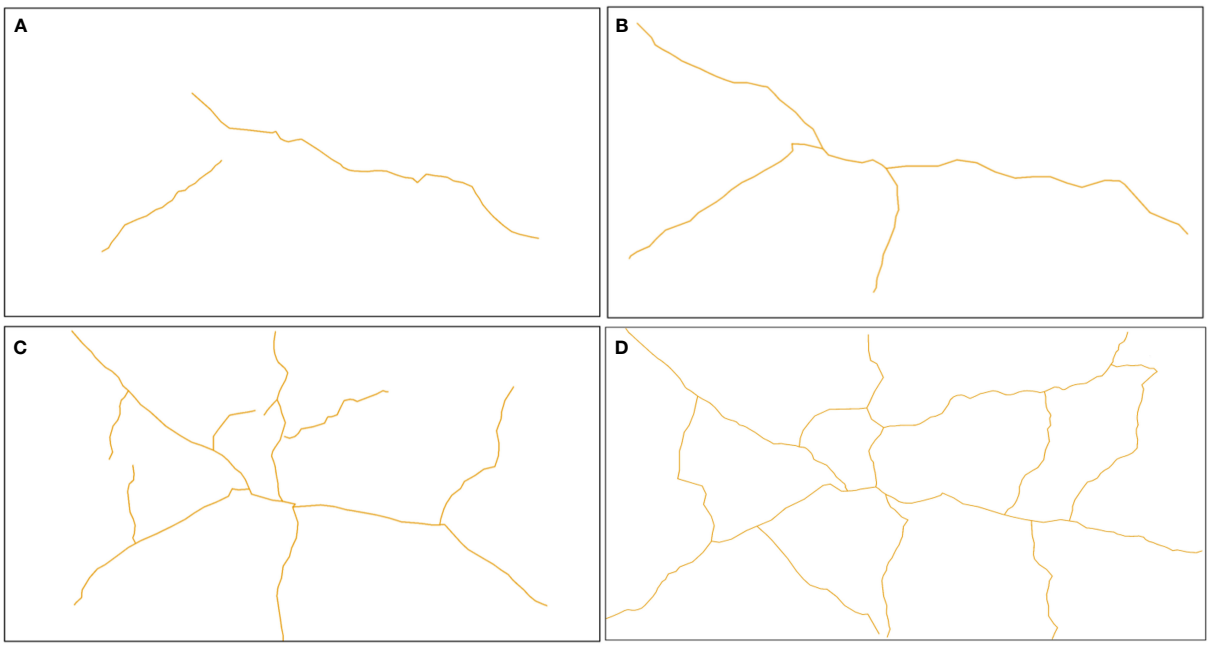

FIGURE 5
Evolution of mud cracks during the experimental period. **(A)** Mud cracks at the end of the second CDOE, **(B)** at the end of the third CDOE, **(C)** at the end of the fifth CDOE, **(D)** and at the end of the seventh CDOE. CDOE is consecutive days of emersion.

of the experiment was 5.1%. Similarly, the seedling density in the mud cracks was 3.31 individuals/cm^2 and 0.12 individuals/cm^2 in the patches. The number of seedlings in the mud cracks accounted for 59.3% of the total seedling count in 5.1% of the area in sample 3 (Figure 8).

Specific details regarding variations in seedling densities between mud cracks and patches are presented in Table 3. Generally, the number of individual seedlings in mud cracks (3.4 individuals/cm^2) was higher than that in patches (0.2 individuals/cm^2). The CIF data are presented in Table 3. Although the mean CIF value was 5.3%, it accounted for 48% of the total number of individual seedlings, indicating that mud cracks promote seedling colonization.

4 Discussion

4.1 Mud crack formation

The present study contributed to the work of Fiot and Gratiot (2006), which investigated the probabilities of mud cracking and confirmed the vital role of mud cracks in promoting *S. mariqueter* propagule establishment. According to our results, the mud cracking zones, which are determined by water levels, were mainly located at low-lying saltmarsh edges. Below such zones, the mud remained soft because frequent inundations prevented extensive dewatering. The establishment of propagules in the zones is difficult because they are easily resuspended by tidal currents (Figure 3). Some studies have investigated mud crack occurrence on mudflats, such as at an elevation of 2.67 m above hydrographic zero (Clarke and Myerscough, 1993; Fiot and Gratiot, 2006; Proisy et al., 2009); however, the ecological functions of mud cracks have not been investigated. Therefore, future field restoration efforts should focus on critical zones under elevation–tidal interrelationships to determine the precise areas for mud cracking, such as the mean water level, mean high water level, and mean neap tide high water level on coastal wetlands, to precisely delineate the potential zones for plant colonization.

In the controlled experiment, the mud cracks were well-formed within a short period; mud cracks emerged on the second CDOE and became stable on the seventh CDOE (CDOE was approximately 7 d). This observation was consistent with the results of a previous laboratory experiment on different soils showing a short and intensive mud crack formation episode during drying after a wetting event (Yesiller et al., 2000). Moreover, our finding was consistent with the results of a field experiment conducted during the 2008 equinoctial spring tide in French Guiana, where mud cracks formed within 1.5 days (Gardel et al., 2009). However, the present study only considered the mud

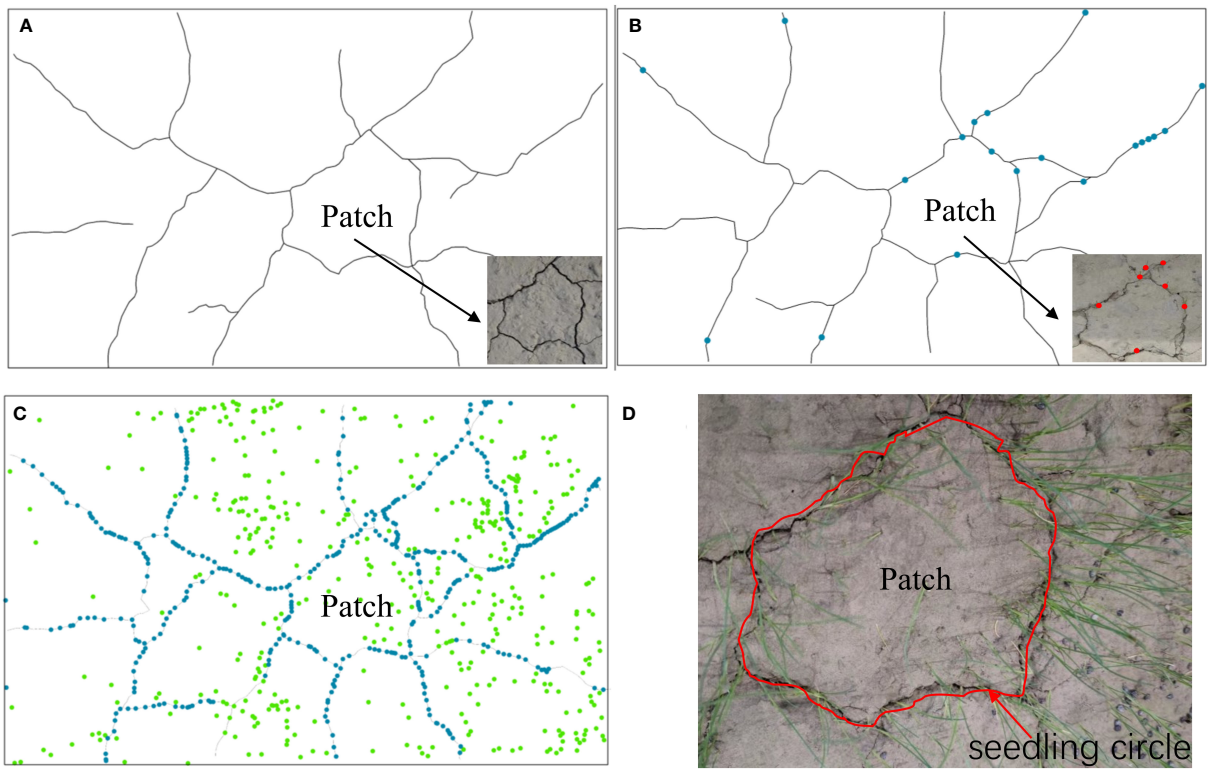

FIGURE 6
An illustration of the seedling colonization process. **(A)** Formation of mud cracks and patches. **(B)** Gradual colonization of mudflats along the mud cracks by individual seedlings. **(C)** Individual seedlings in mud cracks and patches. Green dots represent seedlings in the patches, and blue dots represent seedlings in the mud cracks. **(D)** A "seedling circle" formed at the end of the experimental period.

TABLE 2 Properties of plants and mud cracks.

Parameter	Mean ± SD
height (cm)	9.34 ± 0.80
root length (cm)	2.23 ± 0.21
stem diameter (cm)	0.92 ± 0.06
root number	5.57 ± 0.79
cracks width (cm)	0.50 ± 0.37

cracking process based on CDOE and mud crack morphology, such as crack length and width. We did not consider their depth, as it cannot be estimated from photographs.

Factors influencing tidal flats, such as abiotic and biotic processes, enhance mud cracking. Previous studies have shown that wetting–drying cycles enhance mud crack formation (Yesiller et al., 2000; Gardel et al., 2009). The first drying episode causes shrinkage, which structurally rearranges soil particles and potentially breaks soil particle bonds, thereby weakening the soil (Young, 2012). The subsequent wetting cycle is believed to further weaken and soften the soil and reduce cohesion through water supply. Therefore, a new drying cycle substantially activates the mud cracking process at the weakest part of the soil, where cohesion

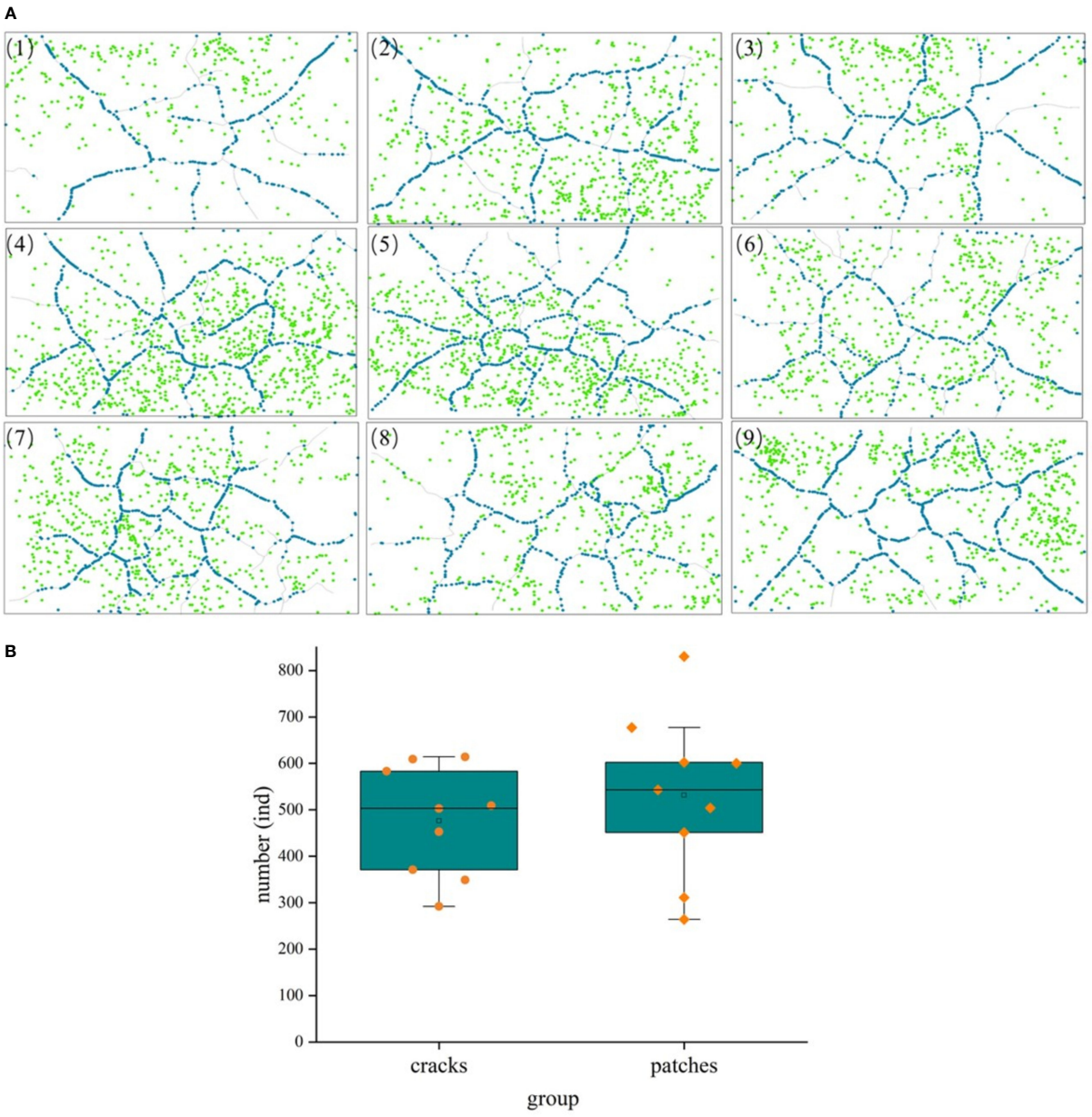

FIGURE 7
A comparison of seedling distribution in mud cracks and patches during the experimental period. **(A)** Distribution of mud cracks and seedlings in nine parallel samples (1 - 9), blue dots represent individual seedlings in mud cracks, whereas green dots represent seedlings in patches. **(B)** A comparison of seedling number in mud cracks and patches.

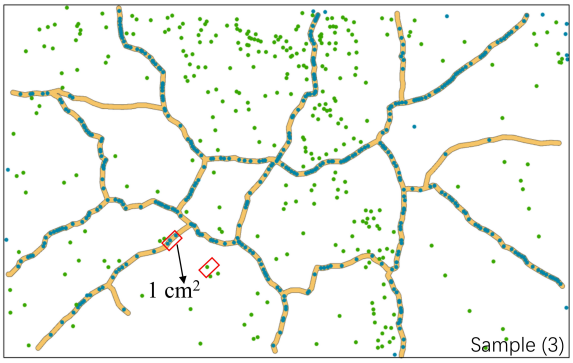

FIGURE 8
Variations in seedling densities between mud cracks and patches. The area marked in red represents one square unit (1 cm^2). The image is from parallel sample 3.

is low (Gardel et al., 2009). In addition, biological activities (bioturbation by burrowing and root penetration) increase the drainage capacity of soils, and they considerably enhance desiccation and mud crack formation (Gardel et al., 2009). Other processes, such as desiccation and shrinkage, freezing and thawing, and syneresis, also influence the development of mud cracks (Yesiller et al., 2000).

Further studies involving the technical measurement of mud cracks are required. Our study was restricted to small areas and could not be repeated at the same site due to difficulties in accessing such soft, muddy, and flooded environments (Proisy et al., 2009). According to Lefebvre et al. (2004), elevation profiles of several hectometers are the most that can be feasibly achieved during a ground survey. Rosso et al. (2006) and Anthony et al. (2008) demonstrated that emerging remote sensing techniques based on lidar (light detection and ranging) may be beneficial for studying intertidal muddy habitats. Moreover, future studies should focus on enhancing our understanding of the relationship between seasonality and the mud cracking process, as well as the role of neap and spring tides in field consolidation processes. The present study recommends interdisciplinary gap-bridging involving sedimentology, geomorphology, hydrology, saltmarsh ecology, and remote sensing.

4.2 Influence of mud cracking zones on saltmarsh colonization

Our results revealed that mud cracking varied with water level and was often accompanied by the establishment of saltmarsh plants. A previous study has shown that a specific functional range for the growth of the genus *Avicennia* in French Guiana is between mean water level and mean high water level (Proisy et al., 2009), which is like the intertidal range for *Avicennia marina* in southeastern Australia (Clarke and Myerscough, 1993). Notably, the extensive mud cracks observed in this study occurred in such intertidal areas. The present study has demonstrated that the outline of mud cracking zones, located at intertidal zones, can act as an indicator for. Therefore, such coastal wetland zones require restoration and more precise and long-term monitoring, considering their key ecological functions. In addition, owing to the disturbances associated with hydrodynamics caused by waves and currents, it is imperative to

TABLE 3 Variations in seedling densities between mud cracks and patches in the nine experimental containers.

	CIF %	crack ind/cm^2	patch ind/cm^2	ratio of individuals in cracks (crack/total)%
1	4.2	2.62	0.10	52.52
2	5.0	3.75	0.24	45.52
3	5.1	3.31	0.12	59.29
4	5.3	4.12	0.33	41.26
5	6.2	3.72	0.27	47.56
6	5.4	2.42	0.20	40.91
7	5.9	3.26	0.22	48.38
8	5.2	2.97	0.17	49.52
9	5.1	4.51	0.24	50.37
mean ± SD	5.3 ± 0.56	3.41 ± 0.68	0.21 ± 0.07	48.37 ± 5.67

understand the influence of sediment dynamics on the formation and stabilization of mud cracks and on saltmarsh plant establishment. Quantifying the total area covered by mud cracks in saltmarshes is essential for determining the role of mud cracks in saltmarsh plant establishment.

4.3 Ecological functions of mud cracks in saltmarshes

Saltmarsh colonization and dispersal cannot increase rapidly on a large scale without the influence of a typical and visible event that strongly enhances seed trapping. We speculate that it is not a single biological event but rather a physical event associated with the mud surface, such as extensive mud cracking. The main ecological functions of mud cracks in saltmarsh colonization are as follows:

(1) Mud cracks act as "seed traps." The number of seeds, floating rate, and germination rate are crucial for saltmarsh plant establishment and dispersal. *S. mariqueter* establishment and dispersal are fast in summer, with high seed density (8,400 seeds/m^2), a high floating rate (up to 80%), and a low germination rate (28%), being observed (Jiang et al., 2022). The high number of seeds produced ensures survival in each reproductive period (Delgado et al., 2001). Furthermore, the open mud cracks acted as cages for floating saltmarsh plant seeds, especially under weak hydrodynamic conditions. The soaked *S. mariqueter* seeds were washed away in August 2021, transported by tides, and then randomly trapped in mud cracks. Notably, the high germination rate of *S. mariqueter* seeds (seven days) and two days for anchorage in summer considerably favor seedling establishment (Jiang et al., 2022). This confirmed the rapid and transient process between seed germination and mud cracking (approximately 7 d). Finally, a large amount of suspended sediment carried by weak tides gradually settled and was retained in mud cracks on tidal flats due to the interaction between sediment viscosity and burial, thereby making it more difficult for seeds trapped in mud cracks to be washed away or easily resuspended. The mud cracks filled with fine sediment particles exhibited multiple linear crack scars on the tidal flat surfaces (Figure 1B). The Chongming Dongtan saltmarsh exhibited continuous sedimentation from April to October, and the accumulated accretion exceeded 20 cm (Li and Yang, 2007). Therefore, the geomorphology of tidal flats changed gradually, which facilitated seed burial.

Our study showed that seedling densities in the mud cracks were significantly higher than those in the patches in field observations, which was consistent with laboratory results. The results obtained in the laboratory could be because the seeds were fixed without hydrodynamic transportation and sediment burial. In addition, mud cracks lost their function as seed traps.

(2) Mud cracks acted as "seedling growth promoters." The network formed by mud cracks influenced water content and water circulation in the tidal sediment. Mud cracks functioned like well-developed miniature tidal creeks on tidal surfaces: at high tide, mud cracks became a channel of seawater and were rapidly filled with seawater, whereas at ebb tide, seawater on tidal flats flowed into the mud cracks and was gradually drained. The phenomenon was vital for saltmarsh plant growth as it provided sufficient water during the early growth stage, especially for young root development. In addition, it alleviated stress caused by waterlogging due to the morphology of low tidal zones, such as pits. For example, the sprouted young seedlings can die due to the exposure of roots to hypoxic conditions caused by prolonged flooding. Therefore, mud cracks can create pathways for seawater transportation on tidal flats and substantially increase the hydraulic conductivity of sediments (Yesiller et al., 2000), which promotes water uptake by plants during the early growth stages. Furthermore, local sediment properties, such as mud compaction and pore water, vary considerably with mud cracking (Fiot and Gratiot, 2006). Mud cracks alter the oxygen content of sediment, increase aeration, and in turn enhanced respiration in saltmarsh plants. Saltmarsh plants consume oxygen and release carbon dioxide during respiration, resulting in a low oxygen content in sediment. Numerous mud cracks in tidal flats allow oxygen to penetrate the sediment from the atmosphere and allow continuous release of carbon dioxide from the sediment into the atmosphere, which in turn enhances the total respiration of saltmarsh plants. The traits of *S. mariqueter* (plant height, root length, and root diameter) in mud cracks and patches were significantly different (Table 2). Mud cracks increase nutrient availability in tidal flat sediments. Both organic and mineral nutrients in sediments must be decomposed by soil microorganisms before they are absorbed and used by plants. Insufficient oxygen in sediments, or anaerobic status, reduces microbial activity, especially for aerobic microorganisms, and inhibits complete organic matter decomposition and the release of soil nutrients (Marschner, 2021). The occurrence of mud cracks improved the oxygen status of the saltmarsh, thereby increasing microbial activity due to sufficient oxygen, which in turn, decomposed organic matter and released large quantities of soil nutrients, as well as improving the content and utilization of nutrients required for plant growth.

The seedling density in the mud cracks at the study site was significantly higher than that in patches, which was consistent with the results of manipulative experiments (CIF = 5.3%). Mud cracks accounted for approximately 48.37% of the total seed germination in 5.3% of the study area (Figure 8 and Table 3). The high density of seedlings that colonized the mud cracks formed a "seedling circle" or "seedling lines" (Figures 6D, 7), which may protect seedlings in the patches in the field from hydrodynamic disturbances, dislodgement, or uprooting.

A strong correlation has been observed between seedling recruitment and mud cracking (Gardel et al., 2009; Proisy et al., 2009). A previous field study revealed that the trapping of *Avicennia germinans* propagules in ephemeral mud cracks accounted for 95% of the sprouting on the coastal fringe. Desiccation was identified as a major mechanism of colonization by the species (Fiot and Gratiot, 2006). According to Proisy et al. (2009), nearly instantaneous mangrove germination over tens of hectares was observed in repeated testing at the same sites. Mud cracks may be sighted across colonized areas whenever seedlings emerge. Similarly, patches of *S. mariqueter* were established simultaneously at the saltmarsh edges within a short period (Jiang et al., 2022), where mud cracking occurred. Nevertheless, the mechanisms associated with the ecological role of mud cracks in saltmarsh colonization

remain unclear. Therefore, future studies should focus on aspects such as seed arrival, seed availability, and seed retention rates. In addition, they should focus variation on propagule dispersal between flooding and dewatering periods.

4.4 Implications for saltmarsh restoration

It is likely that a future pioneer saltmarsh restoration could benefit from the undetermined role of mud cracks highlighted in our study. Suitable restoration measures should be adopted based on the different tidal zones or elevations of saltmarshes. For example, by marking patches ready to be colonized in low-lying saltmarshes, mud cracks can be directly targeted as restoration zones, where the chances of successful replanting are the highest. An efficient approach is sowing large quantities of seeds in mud crack zones during the ebb (neap) tide to promote seed germination. Mud cracks in high-lying saltmarshes may not be conducive to high-water-demanding plants due to desiccation induced by high elevation. Therefore, plants with considerable water-tolerance capacities, such as *Phragmites australis*, could be suitable for such areas.

5 Conclusion

Mud cracks are often considered stressors for plant growth, which may be different in saltmarsh ecosystems. This study demonstrated that mud cracks facilitated colonization by saltmarsh plants. Our key findings were as follows: (1) Mud cracks were easily formed in the narrow zone from the seaward edge of the saltmarsh to the bare mudflats owing to tide-induced wetting–drying cycles, and young seedlings colonized thereafter. (2) The seedling density in the mud cracks was higher than that in the patches; mud cracks were formed within seven days (CDOE: approximately 7 d), and no significant changes were observed in subsequent wetting–drying cycles; seedlings in the mud cracks sprouted earlier than those in the patches. (3) The mud cracks acted as "seed traps" and "seedling growth promoters" for saltmarsh colonization. The results suggest that mud cracks in coastal wetlands can considerably enhance colonization by saltmarsh plants. Our results could facilitate the development of appropriate saltmarsh rehabilitation strategies and enhance our understanding of the interaction between topography and vegetation from the perspective of mud cracks in saltmarshes.

Data availability statement

The original contributions presented in the study are included in the article/supplementary material. Further inquiries can be directed to the corresponding author.

Author contributions

CJ designed the study, analyzed data, and wrote the manuscript. CJ and XL revised the manuscript together. WZ, LX, and LS contributed significantly to data collection and manuscript preparation. All authors contributed to the article and approved the submitted version.

Funding

This work was financially supported by the National Natural Science Foundation of China (Grant Nos. 42176164 and 42141016).

Acknowledgments

The authors would like to thank Bin Yang and Shiwei Lin for helping with experimental setup.

Conflict of interest

The authors declare that the research was conducted in the absence of any commercial or financial relationships that could be construed as a potential conflict of interest.

Publisher's note

References

Anthony, E. J., Dolique, F., Gardel, A., Gratiot, N., Proisy, C., and Polidori, L. (2008). Nearshore intertidal topography and topographic-forcing mechanisms of an Amazon-derived mud bank in French Guiana. *Continental Shelf Res.* 28 (6), 813–822. doi: 10.1016/j.csr.2008.01.003

Bouma, T. J., De Vries, M. B., and Herman, P. M. J. (2010). Comparing ecosystem engineering efficiency of two plant species with contrasting growth strategies. *Ecology* 91 (9), 2696–2704. doi: 10.1890/09-0690.1

Bouma, T. J., van Belzen, J., Balke, T., Zhu, Z. C., Airoldi, L., Blight, A. J., et al. (2014). Identifying knowledge gaps hampering application of intertidal habitats in coastal protection: opportunities & steps to take. *Coast. Eng.* 87, 147–157. doi: 10.1016/j.coastaleng.2013.11.014

Bouma, T. J., Van Belzen, J., Balke, T., Van Dalen, J., Klaassen, P., Hartog, A. M., et al. (2016). Short-term mudflat dynamics drive long-term cyclic salt marsh dynamics. *Limnology Oceanography.* 61 (6), 2261–2275. doi: 10.1002/lno.10374

Clarke, P. J., and Myerscough, P. J. (1993). The intertidal distribution of the grey mangrove (*Avicennia marina*) in southeastern Australia: the effects of physical conditions, interspecific competition, and predation on propagule establishment and survival. *Aust. J. Ecol.* 18 (3), 307–315. doi: 10.1111/j.1442-9993.1993.tb00458.x

Costanza, R., d'Arge, R., De Groot, R., Farber, S., Grasso, M., Hannon, B., et al. (1997). The value of the world's ecosystem services and natural capital. *Nature* 387 (6630), 253–260. doi: 10.1038/387253a0

Costanza, R., de Groot, R., Sutton, P., Van der Ploeg, S., Anderson, S. J., Kubiszewski, L., et al. (2014). Changes in the global value of ecosystem services. *Global Environ. Change* 26, 152–158. doi: 10.1016/j.gloenvcha.2014.04.002

Deegan, L. A., Johnson, D. S., Warren, R. S., Peterson, B. J., Fleeger, J. W., Fagherazzi, S., et al. (2012). Coastal eutrophication as a driver of salt marsh loss. *Nature* 490 (7420), 388–392. doi: 10.1038/nature11533

Delgado, P., Hensel, P. F., Jime´nez, J. A., and Day, J. W. (2001). The importance of propagule establishment and physical factors in mangrove distributional patterns in a Costa Rican estuary. *Aquat. Bot.* 71 (3), 157–178. doi: 10.1016/S0304-3770(01)00188-7

Duarte, C. M., Losada, I. J., Hendriks, I. E., Mazarrasa, I., and Marbà, N. (2013). The role of coastal plant communities for climate change mitigation and adaptation. *Nat. Climate Change* 3 (11), 961–968. doi: 10.1038/nclimate1970

Fan, Y. S., Chen, S. L., Zhao, B., Pan, S. Q., Jiang, C., and Ji, H. Y. (2018). Shoreline dynamics of the active yellow river delta since the implementation of water-sediment regulation scheme: a remote-sensing and statistics-based approach. *Estuarine Coast. Shelf Sci.* 200, 406–419. doi: 10.1016/j.ecss.2017.11.035

Fiot, J., and Gratiot, N. (2006). Structural effects of tidal exposures on mudflats along the French Guiana coast. *Mar. Geology* 228 (1-4), 25–37. doi: 10.1016/j.margeo.2005.12.009

Fredlund, D. G., and Rahardjo, H. (1993). *Soil mechanics for unsaturated soils* (New York: Wiley).

Gardel, A., Proisy, C., Lesourd, S., Philippe, S., Caillaud, J., Gontharet, S., et al. (2009). A better understanding of mud cracking processes gained from *in situ* measurements on an intertidal mudflat in French Guiana. *J. Coast. Res.* 56, 424–428. doi: 10.2307/25737611

Ge, Z. M., Cao, H. B., Cui, L. F., Zhao, B., and Zhang, L. Q. (2015a). Future vegetation patterns and primary production in the coastal wetlands of East China under sea level rise, sediment reduction, and saltwater intrusion. *J. Geophysical Research: Biogeosciences* 120 (10), 1923–1940. doi: 10.1002/2015JG003014

Ge, Z. M., Wang, T. H., Wang, K. Y., and Wang, X. M. (2008). *Characteristics of coastal wetland ecosystem of the Yangtze estuary and conservation for key communities* (Beijing, China: Science Press), 189.

Han, G. X. (2017). Effect of tidal action and drying-wetting cycles on carbon exchange in a salt marsh: progress and prospects. *Acta Ecol. Sin.* 37 (24), 8170–8178. doi: 10.5846/stxb201611182347

Jiang, C., Li, X. Z., Xue, L. M., Yan, Z. Z., Liang, X., and Chen, X. C. (2022). Pioneer salt marsh species *Scirpus mariqueter* disperses quicker in summer with seed contribution from current and last year. *Estuarine Coast. Shelf Sci.* 264, 107682. doi: 10.1016/j.ecss.2021.107682

Kelleway, J. J., Cavanaugh, K., Rogers, K., Feller, L. C., Ens, E., Doughty, C., et al. (2017). Review of the ecosystem service implications of mangrove encroachment into salt marshes. *Global Change Biol.* 23 (10), 3967–3983. doi: 10.1111/gcb.13727

Lefebvre, J. P., Dolique, F., and Gratiot, N. (2004). Geomorphic evolution of a coastal mudflat under oceanic influences: an example from the dynamic shoreline of French Guiana. *Mar. Geology* 208 (2-4), 191–205. doi: 10.1016/j.margeo.2004.04.008

Leonardi, N., and Fagherazzi, S. (2014). How waves shape salt marshes. *Geology* 42 (10), 887–890. doi: 10.1130/G35751.1

Leonardi, N., Ganju, N. K., and Fagherazzi, S. (2016). A linear relationship between wave power and erosion determines saltmarsh resilience to violent storms and hurricanes. *Proc. Natl. Acad. Sci.* 113 (1), 64–68. doi: 10.1073/pnas.1510095112

Li, X. Z., Ren, L. J., Liu, Y., Craft, C., Mander, Ü., and Yang, S. L. (2014). The impact of the change in vegetation structure on the ecological functions of salt marshes: the example of the Yangtze estuary. *Regional Environ. Change* 14 (2), 623–632. doi: 10.1007/s10113-013-0520-9

Li, H., and Yang, S. L. (2007). A review of influence of saltmarsh vegetation on physical processes in intertidal wetland. *Advance Earth Sci.* 22 (16), 583–591.

Ma, Z., Ysebaert, T., Wal, D. V. D., Jong, D. J. D., Li, X. Z., and Herman, P. M. J. (2014). Long-term salt marsh vertical accretion in a tidal bay with reduced sediment supply. *Estuarine Coast. Shelf Science.* 146, 14–23. doi: 10.1016/j.ecss.2014.05.001

Marschner, P. (2021). Processes in submerged soils–linking redox potential, soil organic matter turnover and plants to nutrient cycling. *Plant Soil* 464 (1-2), 1–12. doi: 10.1007/s11104-021-05040-6

McKee, K. L., Mendelssohn, I. A. D., and Materne, M. (2004). Acute salt marsh dieback in the Mississippi river deltaic plain: a drought-induced phenomenon? *Global Ecol. Biogeography* 13 (1), 65–73. doi: 10.1111/j.1466-882X.2004.00075.x

Miller, C. J., Mi, H., and Yesiller, N. (1998). Experimental analysis of desiccation crack propagation in clay liners. *J. Am. Water Resour. Association AWRA* 34 (3), 677–686. doi: 10.1111/j.1752-1688.1998.tb00964.x

Mitchell, J. K. (1993). *Fundamentals of soil behavior* (New York: Wiley).

Möller, I., Kudella, M., Rupprecht, F., Spencer, T., Paul, M., Wesenbeeck, B. K. V., et al. (2014). Wave attenuation over coastal salt marshes under storm surge conditions. *Nat. Geosci.* 7 (10), 727–731. doi: 10.1038/ngeo2251

Morris, P. H., Graham, J., and Williams, D. J. (1992). Cracking in drying soils. *Can. Geotechnical J.* 29 (2), 263–277. doi: 10.1139/t92-030

Proisy, C., Gratiot, N., Anthony, E. J., Gardel, A., Fromard, F., and Heuret, P. (2009). Mud bank colonization by opportunistic mangroves: a case study from French Guiana using lidar data. *Continental Shelf Res.* 29 (3), 632–641. doi: 10.1016/j.csr.2008.09.017

Rosso, P. H., Ustin, S. L., and Hastings, A. (2006). Use of lidar to study changes associated with spartina invasion in San Francisco bay marshes. *Remote Sens. Environ.* 100 (3), 295–306. doi: 10.1016/j.rse.2005.10.012

Silliman, B. R., van de Koppel, J., McCoy, M. W., Diller, J., Kasozi, G. N., Earl, K., et al. (2012). Degradation and resilience in Louisiana salt marshes after the BP-*Deepwater horizon* oil spill. *Proc. Natl. Acad. Sci.* 109 (28), 11234–11239. doi: 10.1073/pnas.1204922109

Temmerman, S., Meire, P., Bouma, T. J., Herman, P. M. J., Ysebaert, T., and Vriend, H. J. D. (2013). Ecosystem-based coastal defence in the face of global change. *Nature* 504 (7478), 79–83. doi: 10.1038/nature12859

Wang, H., van der Wal, D., Li, X. Y., van Belzen, J., Herman, P. M. J., Hu, Z., et al. (2017). Zooming in and out: scale dependence of extrinsic and intrinsic factors affecting salt marsh erosion. *J. Geophysical Research: Earth Surface* 122 (7), 1455–1470. doi: 10.1002/2016JF004193

Xiao, D. R., Zhang, C., Zhang, L. Q., Zhu, Z. C., Tian, K., and Gao, W. (2016). Seed dispersal capacity and post-dispersal fate of the invasive Spartina alterniflora in saltmarshes of the Yangtze Estuary. *Estuar Coast Shelf Sci.* 169, 158–163. doi: 10.1016/j.ecss.2015.11.032

Xie, T., Cui, B., Li, S., and Bai, J. (2019). Topography regulates edaphic suitability for seedling establishment associated with tidal elevation in coastal salt marshes. *Geoderma* 337, 1258–1266. doi: 10.1016/j.geoderma.2018.07.053

Yang, S. L., Belkin, I. M., Belkina, A. I., Zhao, Q. Y., Zhu, J., and Ding, P. X. (2003). Delta response to decline in sediment supply from the Yangtze river: evidence of the recent four decades and expectations for the next half-century. *Estuarine Coast. Shelf Sci.* 57 (4), 689–699. doi: 10.1016/S0272-7714(02)00409-2

Yang, S. L., Luo, X. X., Temmerman, S., Kirwan, M., Bouma, T. J., Xu, K. H., et al. (2020). Role of delta-front erosion in sustaining salt marshes under sea-level rise and fluvial sediment decline. *Limnology Oceanography* 65 (9), 1990–2009. doi: 10.1002/lno.11432

Yesiller, N., Miller, C. J., Inci, G., and Yaldo, K. (2000). Desiccation and cracking behavior of three compacted landfill liner soils. *Eng. Geology* 57 (1-2), 105–121. doi: 10.1016/S0013-7952(00)00022-3

Young, R. N. (2012). *Soil properties and behaviour* (Amsterdam: Elsevier Scientific Publishing Company).

Zhao, L. X., Xu, C., Ge, Z. M., van de Koppel, J., and Liu, Q. X. (2019). The shaping role of self-organization: linking vegetation patterning, plant traits and ecosystem functioning. *Proceeding R. Soc. B: Biol. Sci.* 286 (1900), 20182859. doi: 10.1098/rspb.2018.2859

Zhu, Z. C., van Belzen, J., Zhu, Q., van de Koppel, J., and Bouma, T. J. (2020). Vegetation recovery on neighboring tidal flats forms an achilles' heel of saltmarsh resilience to sea level rise. *Limnology Oceanography* 65 (1), 51–62. doi: 10.1002/lno.11249

frontiers | Frontiers in Marine Science

TYPE Original Research
PUBLISHED 27 April 2023
DOI 10.3389/fmars.2023.1086135

OPEN ACCESS

EDITED BY
Serena Moseman-Valtierra, University of Rhode Island, United States

REVIEWED BY
Stuart James Kininmonth, The University of Queensland, Australia
Peter M. J. Herman, Delft University of Technology, Netherlands

*CORRESPONDENCE
Ana I. Lillebø
lillebo@ua.pt

†These authors have contributed equally to this work and share first authorship

RECEIVED 01 November 2022
ACCEPTED 06 April 2023
PUBLISHED 27 April 2023

CITATION
Genua-Olmedo A, Verutes GM, Teixeira H, Sousa AI and Lillebø AI (2023) A spatial explicit vulnerability assessment for a coastal socio-ecological Natura 2000 site. *Front. Mar. Sci.* 10:1086135. doi: 10.3389/fmars.2023.1086135

A spatial explicit vulnerability assessment for a coastal socio-ecological Natura 2000 site

Ana Genua-Olmedo[1†], Gregory M. Verutes[1,2†], Heliana Teixeira[1], Ana I. Sousa[1] and Ana I. Lillebø[1*]

[1]CESAM – Centre for Environmental and Marine Studies, Department of Biology, University of Aveiro, Aveiro, Portugal, [2]Centro Interdisciplinar de Investigación en Tecnoloxías Ambientais (CRETUS)-Department of Applied Economics, University of Santiago de Compostela, Santiago de Compostela, Spain

In line with the global trend, the Ria de Aveiro coastal lagoon is subjected to multiple co-occurring pressures threatening vital benefits flowing from nature to people. The main objective of this research was to assess the status of habitats important for ecosystem services in the Ria de Aveiro by identifying vulnerable areas to anthropogenic threats. The pressures from seven relevant human activities (recreation, services, aquaculture, agriculture, commercial development, unintended impacts from management, and invasive alien species) were analysed based on their spatiotemporal distribution (exposure) and impact over the EUNIS habitats (EUNIS codes A2.2, A2.22 – sand flats and beaches; A2.3 – mud flats; A2.61 – seagrasses; A2.5, A2.53C, A2.535, A2.545, A2.554 – salt marshes; and, X10 – 'Bocage,' a landscape of small-hedged fields) in seven distinct landscape units. A prospective scenario, co-developed for the year 2030, was evaluated using a map-based risk assessment tool and brought forward the near-term vulnerability of the seagrass biotope. The highest risks posed to intertidal habitats (mud flats and salt marshes) were driven mainly by environmental management activities that support critical socio-economic sectors. Our methodology evaluated plausible threats to habitats in the near term, established baseline knowledge for the adaptive management process in Ria de Aveiro Natura 2000 site, and showcased how future assessments can inform the operationalization of ecosystem-based management as new information becomes available.

KEYWORDS

natural capital, habitat risk assessment, InVEST, ecosystem-based management, coastal planning

1 Introduction

Human-driven global changes threaten the integrity of coastal areas and the provision of ecosystem services (ES). Coastal socio-ecological systems worldwide evidence vulnerability to climate change, namely through mean sea level rise, flooding and storms extreme events, coastal erosion, salinization, and wetland loss and fragmentation (e.g.,

Cazenave and Cozannet, 2014). Due to their natural capital richness, these shoreline areas have been desirable for many sectoral activities for centuries (e.g., tourism, recreation, fishing, aquaculture, agriculture, shipping and transportation, industrial activities) being currently densely populated and under multiple pressures (Neumann et al., 2015). One of the major challenges nowadays is to increase resilience to climate change by promoting sustainable development, targeting social, environmental, and economic objectives, and mitigating the risks that affect the supply of ES. Ecosystem-based management (EBM) combines science-based knowledge from different fields of research with local knowledge (Röckmann et al., 2015) and integrate the concept of adaptive management (Webb et al., 2017). Several definitions of EBM are available in the literature, many conceptual (e.g., Long et al., 2015). Our study will follow the operational description by Delacámara et al. (2020): "EBM can be understood as any management or policy option intended to restore, enhance and/or protect the resilience of the ecosystem". Some relevant examples of the operationalization of the concept are found in Australia's Great Barrier Reef, often given as a reference for a comprehensive EBM (McCook et al., 2010); the Yellow Sea Large Marine Ecosystems, as an example of a global effort to implement EBM from economically developing countries (Sherman, 2014); large marine ecosystems in Alaska, to provide indicators to inform about the management of marine resources (Zador et al., 2017); the Western Mediterranean, to explore participatory research methods (Gómez and Maynou, 2021).

The operationalization of management options, is often supported by modelling tools, such as the InVEST (Integrated Valuation of Ecosystem Services and Trade-offs; https://naturalcapitalproject.stanford.edu/software/invest), an open-source software for analysing how changes in ecosystems are likely to affect the flow of benefits to people. The InVEST model calculates the cumulative risk posed to habitats by human activities in two dimensions: exposure (degree to which a habitat experiences a pressure produced by human activities, given the effectiveness of management practices), and consequence (sensitivity of the habitat to the effects of the pressure). InVEST also explores consequences for the delivery of ES and is designed to inform decisions about natural resources management. Relevant studies have applied InVEST to estimate the cumulative risk to habitats combined with vulnerability indexes at different coastal areas, such as the United States of America (Wyatt et al., 2017), South Korea (Chung et al., 2015), Belize (Arkema et al., 2014), or France (Cabral et al., 2015). In Portugal, Willaert et al. (2019) applied InVEST in a coastal region north of Lisbon, and Caro et al. (2020) in the Mondego estuary.

Ria de Aveiro coastal lagoon (Western Atlantic coast of Portugal) is a Long-Term Socio-Ecological Research (LTsER) platform that gathered a high-resolution and robust data set at the local scale during the last decade, supported by national and EU projects involving natural and social scientists, and the active participation of stakeholders (e.g., LAGOONS (FP7), AQUACROSS (H2020), BioPradaRia (MAR2020/EMFF). This data set is paramount to operationalizing the EBM concept. Ria de Aveiro is classified under Natura 2000 and lays between marine and terrestrial domain, where anthropogenic pressures and natural areas overlap in space and time, being a complex area in terms of environmental management (e.g., Lillebø et al., 2015; O'Higgins et al., 2019; Lillebø et al., 2020).

The primary objective of this work is to identify opportunities for EBM by showing how the InVEST tool can be applied to improve adaptive management. Specifically, how future scenarios for the year 2030, co-developed with stakeholders, could be validated with the InVEST tool, combining the Habitat Risk Assessment model (hereafter InVEST HRA tool) with the spatial explicit supply of ES. The previous projects that enabled the socio-ecologic data set addressed the integrated management of water resources from catchment to coast in the context of climate change (Lillebø et al., 2015), the management of seagrass biotope and restoration actions to mitigate the bioturbation pressure by non-indigenous species (Costa et al., 2022) and the EBM for aquatic biodiversity and ES across EU policies (Lago et al., 2019) complemented with ecological data gathered as part of the LTsER platform monitoring. The year 2030 was chosen because it corresponds to different EU policy and strategy revision cycles, as well as the target year for the United Nations Sustainable Development Goals to which the European Green Deal contributes; and 2021-2030 is the United Nations Decade for Ecosystems Restoration aiming at preventing, halting, and reversing the degradation of ecosystems worldwide.

To address the main objective and showcase Ria de Aveiro Natura 2000, three stepwise research questions were identified: i) Which landscape units and respective habitats are most at risk and where? ii) Which human activities pose the greatest risk in the near term (2030)? iii) What management options might minimise the risk? And iv) How might future delivery of ES in a Natura 2000 site be compromised? Our methodology evaluated plausible threats to habitats in the near-term, established baseline knowledge for the adaptive management process in Ria de Aveiro Natura 2000 site, and showcased how future assessments can inform the operationalization of ecosystem-based management as new information becomes available.

2 Materials and methods

2.1 Study area

Ria de Aveiro is a shallow coastal lagoon that comprises the estuary of the Vouga River (3500 km^2 of catchment area), having a single artificial connection to the Atlantic Ocean (1.3 km length, 350 m wide, and 20 m depth). The lagoon has semi-diurnal tides with a tidal range from 0.6 m (neap tides) to 3.2 m (spring tides); tidal circulation and wind are the main hydrological forcing functions. The tidal phase lag is in the order of 6 hours in the upper reaches of the channels; whilst the water residence time in the lagoon varies from less than 2 days near the ocean boundary, to more than 1 week in the upstream channels (Dias et al., 2000). Under the EU Water Framework Directive (WFD), Ria de Aveiro includes five transitional water bodies (WB): WB1 (Mira), WB2 (São Jacinto-Espinheiro), WB3 (Ílhavo), WB4 (Murtosa), WB5 (Ovar). Except for WB2, which is heavily modified, the others are natural water bodies. In addition, there are three coastal water bodies (CWB) (CWB-II-1B; CWB-I-2; CWB-II-2) here grouped as WB7. These,

together with the 'Bocage' landscape that is characterised by small agriculture fields surrounded by living hedges and a network of water channels, are defined as the seven landscape units in this study (Figure 1). The management boundaries of the Ria de Aveiro Natura 2000 were set within 500 m from the margin, as specified for the river basin and estuary management plans under the EU Water Framework Directive. Both Plans aim to establish priorities, rules, and measures for the integrated management of water resources and associated ES (Lillebø et al., 2015; Lillebø et al., 2020).

The Ria de Aveiro comprises a variety of biotopes, including natural to highly modified habitats, such as large areas of intertidal sand and mud flats, seagrass meadows, salt marshes, open fields, forests, freshwater lakes, and urban areas. It also comprises the 'Bocage' landscape, a human-shaped habitat with water channels and treelined riparian corridors divided by living hedges for agriculture and livestock production. 'Bocage' landscape is located at the Baixo Vouga Lagunar (3000 **ha**), where the Vouga River meets the lagoon water body. The selected Ria de Aveiro Natura 2000 coastal area is classified as a Special Protection Area of ca. 515 km^2 from which ca. 40% are considered marine areas and is classified as a Site of Community Importance. This recognises its importance to the conservation status of the natural habitats of the Mediterranean and, to a minor extent, Atlantic biogeographical regions to which Ria de Aveiro belongs. This coastal area offers a set of ES with significant associated socio-economic activities of high economic value. Relevant examples are agriculture and livestock,

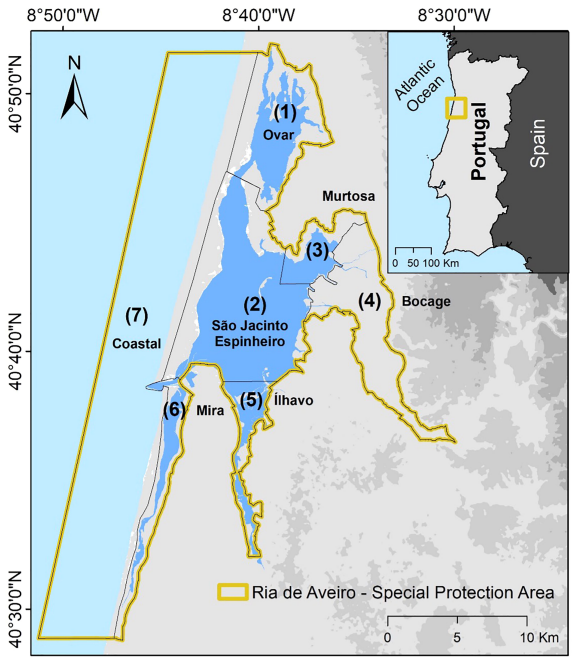

FIGURE 1
Ria de Aveiro and its location in northwest Portugal. The map shows the water bodies (WB) from the EU Water Framework Directive as five transitional WB and one group of coastal WBs. These six together with the terrestrial 'Bocage' landscape are defined as landscape units in this study. They are shown in clockwise order: (1) Ovar - WB5, (2) São Jacinto-Espinheiro - WB2, (3) Murtosa - WB4, (4) Bocage - terrestrial, (5) Ílhavo - WB3, (6) Mira - WB1, (7) Coastal - WB7.

industry, traditional activities (e.g., salt production and bait digging), tourism and recreation (e.g., sailing and surf), maritime port activity, aquaculture, and commercial fishing, where the Aveiro region plays an important role in the Portuguese fisheries market (Lillebø et al., 2015; O'Higgins et al., 2019).

2.2 Data collection

2.2.1 Habitats

Five habitats were identified following the European Nature Information System (EUNIS) from the European Environmental Agency (Table 1 and Figure 2). These habitats were mapped in ArcGIS v10.5 using database from the Long-Term Socio-Ecological Research (LTsER) Ria de Aveiro platform and Sousa et al., 2017; Sousa et al., 2019a; Sousa et al., 2019b. They correspond to five Ria de Aveiro biotopes: (1) sand flats and beaches, (2) mud flats, (3) seagrasses, (4) salt marshes, and (5) 'Bocage' landscape, including the associated network of water channels.

Sand flats and beaches included littoral shores comprising sandy and muddy sand with a relatively high degree of wave action. The mud flats layer focused on littoral mud formed adjacent to salt marshes and seagrasses. Seagrasses included intertidal *Zostera noltei* meadows on littoral sediments adjacent to mud and sand flats (Sousa et al., 2019a; Sousa et al., 2019b). The saltmarshes layer covered saltmarshes and saline reedbeds with additional layers differentiating the low *Spartina maritima* (Curtis) Fernald, synonym of *Sporobolus maritimus* (Curtis) P.M. Peterson & Saarela, and mid-high (e.g., *Halimione portulacoides* (L.) Aellen, synonym of *Atriplex portulacoides* L., *Juncus maritimus* Lam.) zonation. The list of the dominant species considered as salt marshes layer is provided in Table 1. 'Bocage' landscape, including the associated network of water channels, was placed in the agricultural land of the Ria de Aveiro. Detailed description of the habitats is provided in Table 1.

2.2.2 Human activities

Seven types of human activity and the pressures these activities introduce to habitats were identified and mapped by combining different sources of information (Supplementary Table 1). The activity type and pressures were obtained from Borgwardt et al. (2019). They identified activities from seven case studies, including Ria de Aveiro. Ria de Aveiro experts/scientific community identified activities from previous classifications from the European Habitats Directive, WFD, and Marine Strategy Framework. The activities were structured under primary activity types according to the European Commission (EC, 2006). In this study, the selected seven types of human activity were: (1) tourism and recreation, (2) services, (3) aquaculture, (4) agriculture and forestry, (5) commercial development and residential, (6) unintended impacts from environmental management, and (7) multiple activities linked. The spatial extent of consequences of these human activities is provided in Figure 3. Description of the activities and pressures is provided in Supplementary Table 1.

The activity called unintended impacts from environmental management refers to the hydrological measures related with socio-economic and agriculture activities. These were dredging actions to

maintain the navigability of the lagoon water bodies, considering both capital and maintenance dredging, extraction, and disposal of the substrate; and a flood control infrastructure to disable saltwater intrusion and sea level rise inundation into 'Bocage' agricultural areas, including a flood bank, sea walls, and tidal sluices. The flood bank is an embankment built in the 1990's and its extension is expected by 2030. It was designed to prevent surface saltwater intrusion from Ria de Aveiro into agriculture fields. Supplementary Figure 1 showed where the environmental management activities take place, including dredging and flood control.

To add to the above-identified endogenous pressures, two well-documented invasive alien species affecting the aquatic transitional waters ecosystem and the 'Bocage' landscape were included as exogenous pressures. The first corresponds to two lugworm species (benthic macrofauna) grouped by the genus *Arenicola* (*Arenicola marina* and *Arenicola defodiens*) and one species of flora, the pampas grass (*Cortaderia selloana*). Once an alien species is established, the way it spreads may be facilitated by other activities, different from those responsible for the species' introduction.

2.3 Habitat risk assessment

2.3.1 Terminology

The InVEST HRA tool utilizes an exposure-consequence framework to assess cumulative risk posed to habitats by the pressures produced by human activities. For clarity, in this assessment: 'Risk' was measured as 'exposure' (probability of an event happening, i.e., a habitat experiencing pressure from human activity) concerning its potential 'consequences' (or impact, i.e., the habitat-specific response to pressures), if the event was to occur. Habitats at greatest risk were those that were less able to cope with exposure to pressures produced by human activities.

2.3.2 Cumulative risk calculation

The habitat risk assessment InVEST HRA tool was applied to calculate habitat risk as a function of the likelihood of the exposure of each habitat to each pressure, and its consequence, which depended on the impact of a pressure for each habitat (Arkema et al., 2014; Sharp et al., 2018). To assess the risk, two geospatial layers were combined: EUNIS habitat distribution maps (Figure 1) and human activity and pressures produced by human activities (Figures 2, 3). Pressures were used as a proxy of stressors due to the lack of stressors' data. Together with exposure (E) and consequence (C) scores for each habitat-pressure combination, these produced a cumulative risk map at 50 m spatial resolution using the InVEST version 3.8.0. 50 meters was determined through sensitivity testing to be the most appropriate spatial resolution based on the data quality and availability for Ria de Aveiro. The model computes the scores through a weighted average of exposure and consequence for each habitat-pressure interaction (Equation 1). Weighting is obtained by scoring the data quality and the importance given to each criterion. The formulas are given by:

$$E = \frac{\sum_{i=1}^{n} \frac{e_i}{d_i \cdot w_i}}{\sum_{i=1}^{n} \frac{1}{d_i \cdot w_i}} \qquad C = \frac{\sum_{i=1}^{n} \frac{c_i}{d_i \cdot w_i}}{\sum_{i=1}^{n} \frac{1}{d_i \cdot w_i}} \qquad \text{(Eq. 1)}$$

where e_i and c_i are the scores for the respective exposure or consequence criterion i, d_i represents the data quality rating for criterion i, w_i the importance weighting for the criterion, and n the

TABLE 1 Description of the habitats evaluated by this study, with respective occupied areas, in square kilometres, at Ria de Aveiro (Portugal).

Habitats and EUNIS code	EUNIS description
Sand flats and Beaches* (15.31 km^2) A2.2, A2.22	Littoral shores, muddy sand, and sand flats with a relatively high degree of wave action. Barren or amphipod-dominated mobile sand shores
Mud flats* (29.80 km^2) A2.3	Littoral and compacted mud formed adjacent to salt marshes and seagrasses, subject to freshwater and brackish/saline water influence. Associated to polychaetes, bivalves and oligochaetes
Seagrasses*# (2.26 km^2) A2.61	Seagrass beds of *Zostera noltei* (Hornemann, 1832) on littoral sediments adjacent to mud and sand flats.
Salt marshes* (60.38 km^2) A2.5, A2.53C, A2.535, A2.554, A2.545	Coastal salt marshes and saline reedbeds Separated in: Low salt marshes: *Spartina maritima* (Curtis) Fernald, synonym of *Sporobolus maritimus* (Curtis, P. M. Peterson & Saarela) Mid-high salt marshes: e.g., *Juncus maritimus* Lam., A2.545 - *Halimione portulacoides* (L.) Aellen, synonym of *Atriplex portulacoides* L., *Bolboschoenus maritimus* (L.) Palla, *Phragmites australis* (Cav.) Trin, *Sarcocornia perennis* (Mill.) A.J. Scott, synonym of *Salicornia perennis* Mill.
'Bocage' and ditches* (18.02 km^2) X10	Mosaic landscapes bounded by living hedges including the associated network of water channels. The agrarian plots included the production of maize, hay, and rice. Associated with the biodiversity of the agricultural land of the Ria de Aveiro as it is a suitable habitat for birds of prey, reptiles, amphibians, fishes, and mammals

* LTsER platform database; # Sousa et al., 2019a, Sousa et al., 2019b.
Habitats correspondence (code) is available from the EUNIS portal (https://eunis.eea.europa.eu/).
A2.5 - Coastal saltmarshes and saline reedbeds.
A2.554 - *Spartina*.
A2.535 - *Juncus maritimus* mid-upper saltmarshes.
A2.53C - Marine saline beds of *Phragmites australis*.

number of exposure or consequence criteria valued for the habitat-pressure interaction. As the weights are used to divide the effects, this means that a factor with large importance should receive a small value for the weight and vice versa.

For quantifying exposure, we scored four criteria: (1) spatial and (2) temporal overlap between habitats and pressures, (3) intensity of pressure, and (4) management strategy effectiveness for reducing exposure. The model estimates the risk when there is a spatial overlap between habitats and pressures. Otherwise, the model assumes there is no risk, hence $E = 0$ and $C = 0$. For quantifying consequence, we included seven criteria. Three were sensitivity attributes: (1) change in area, (2) change in structure, and (3) frequency of disturbance; and four were resilience attributes: (1) natural mortality, (2) recovery time, (3) recruitment, and (4) connectivity. The resilience attributes are habitat (biotic) specific. The description and applied score of these eleven criteria for exposure and consequence habitat-pressureinteractions, are shown in Table 2. The maximum criteria score was of 3, hence all parameters ranged from 1 (lowest risk) to 3 (greatest risk). The scoring was done following

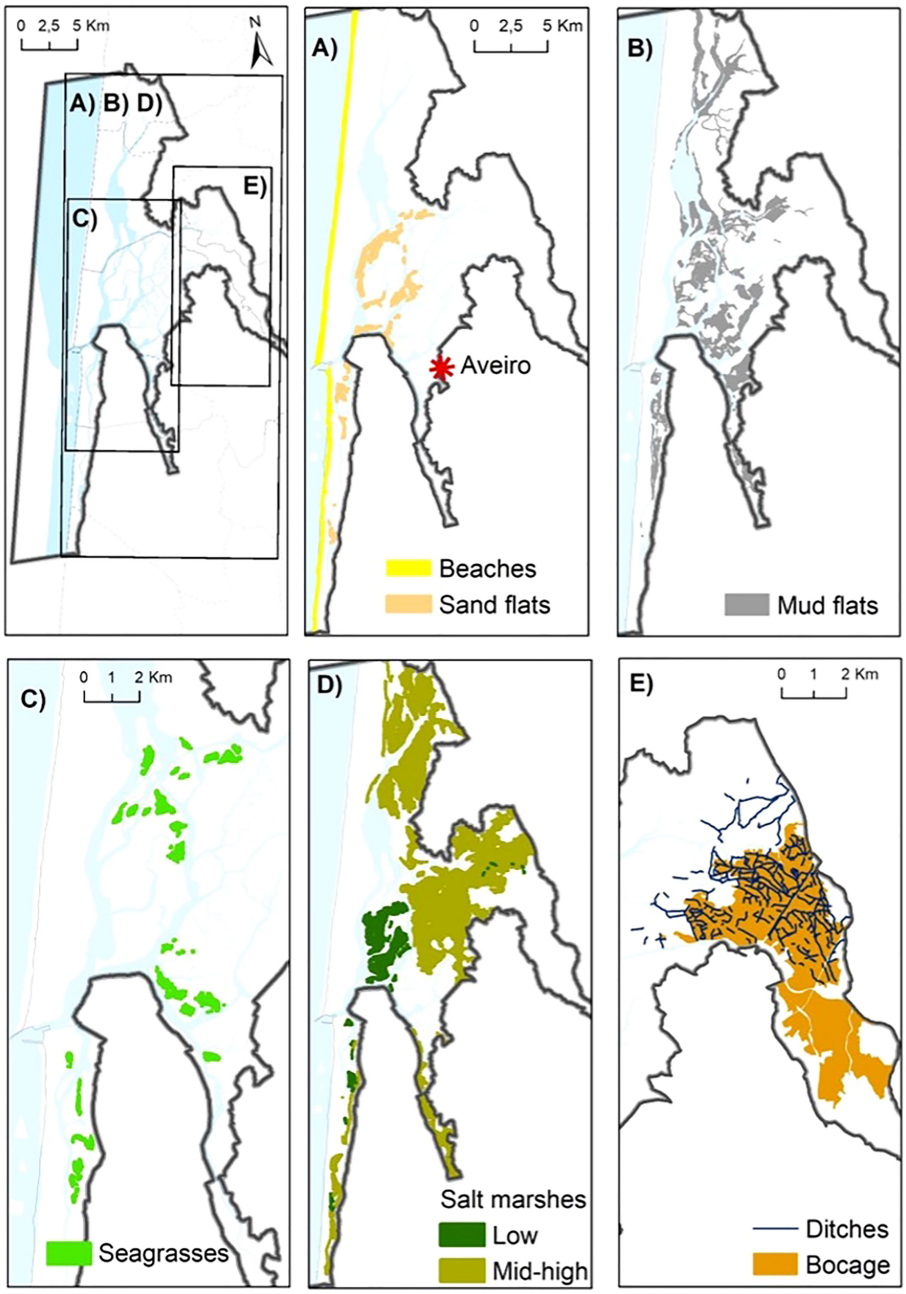

FIGURE 2
Selected habitats identified in the Ria de Aveiro: **(A)** beaches and sand flats, **(B)** mud flats, **(C)** seagrasses, **(D)** salt marshes (low and mid-high height) and **(E)** 'Bocage' with associated ditches. The Aveiro city (red asterisk), counties (dashed line) and the Special Protection Area (black line) are also shown.

data sources including field observations, literature review and expert opinion.

The model also allows assigning weights to score according to data quality and importance of each criterion (Table 3). In this study, we used the same criteria weights (moderately important, 2) with some exceptions when we had data to validate it. For instance, for seagrass habitat, intensity and management effectiveness criteria of the pressure related to environmental trade-offs, seen as unintended impacts from dredging, was scored as 1 because it was cited as important criteria by stakeholders (Lillebø et al., 2019). The individual exposure and consequence criteria, along with scoring for the interaction ratings, data quality and attribute weights by field site are shown in Table 4. These scoring were done through expert judgement with working knowledge of the Ria de Aveiro and marine ecology to rate all possible interactions. The expert elicitation process was conducted in two stages, followed by a final round for revision and consistency check. The methodology followed a process based on iteration and feedback, in which specific doubts were addressed at all stages by the experts (see Teixeira et al., 2019 for more information about the expert elicitation procedure).

As an alternative to assigning a single rating to a criterion that is then applied to the whole study area, we used the spatially explicit criteria feature of the InVEST HRA tool. It allows to indicate spatial variation in the habitat-pressure scores as Geographic Information System layers when there is information on spatial variation in a human activity which could influence the intensity rating of this pressure. These spatially explicit criteria are vector or raster layers, where each vector or raster value may contain a separate rating for a particular area. For any criteria listed in the criteria scores, instead of entering a single number for the rating, a path to a Geographic Information System file may be entered instead, allowing the rating for that criterion to vary across space. This information of the pressures categories was produced by previous studies (see Lillebø et al., 2019 and Borgwardt et al., 2019) and served to characterize the spatial extent of different pressures such as physical change, chemical change, and biological disturbance. In this study, the direct effects of each human activity were translated into spatially explicit criteria layers of exposure (*i.e.*, intensity, management effectiveness) and consequence attributes (*i.e.*, change in structure, recruitment) to characterize the direct effects of these pressures and the impact on habitat. For example, the dredging activities to keep the navigability in the lagoon causes unintended impacts such as increased water velocity due to changes in the system bathymetry. These changes have a different spatial explicit impact in the interior and the fringe of the seagrass patches; therefore, the intensity rate may be higher in the fringe and lower in the interior.

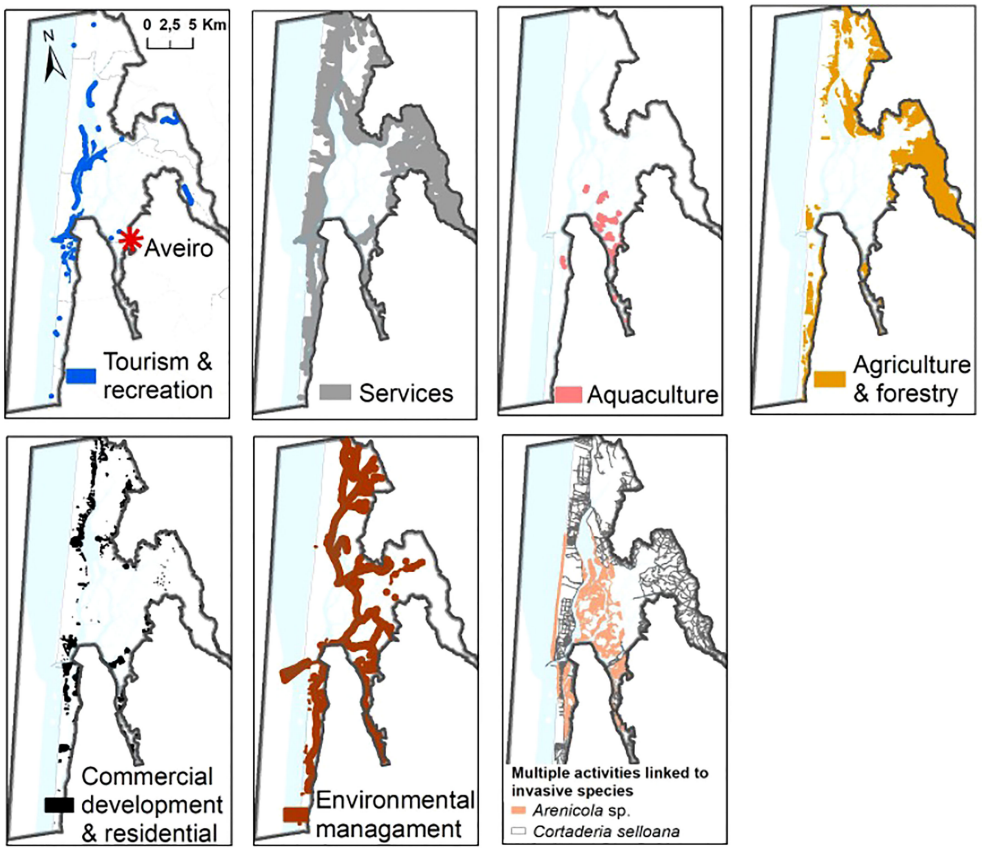

FIGURE 3
The spatial extent of consequences of the select human activities (from left to right): tourism and recreation, services, aquaculture, agriculture and forestry, commercial development and residential, environmental management. Multiple activities linked to invasive species, and affecting selected habitats are mapped.

10.3389/fmars.2023.1086135

TABLE 2 Scoring and definitions for the exposure and consequence criteria.

Criteria	Low risk (1)	Medium risk (2)	High risk (3)	Description
Exposure				
Spatial overlap	<10% of habitat overlaps with pressure	10-30% of habitat overlaps with pressure	>30% of habitat overlaps with pressure	The percentage of each habitat that overlaps with each pressure. The overlap by grid cells is calculated by geospatial tools in InVEST.
Temporal overlap	Co-occur 0-4 months per year	4-8 months per year	8-12 months per year	The duration of time that the habitat and pressure overlap in space.
Intensity	Low	Medium	High	Exposure is also related to the intensity of a pressure. Example: an increase in dredging intensity will increase the likelihood of biological and/or physical disturbance pressures to seagrasses.
Management	Very effective	Somewhat effective	Not effective	Effective management can limit the probability of negative impacts of pressures on habitats, thus reducing exposure even where and when the pressures interact with habitats.
Consequence - sensitivity				
Change in area	Low loss in area (<20%)	Medium loss in area (20-50%)	High loss in area (50-100%)	The percent change in extent of a habitat when exposed to a given pressure. *Example*: the construction of a flood bank will determine the loss of salt marshes due to the lack of migration capacity.
Change in structure	Low loss in structure (<20%)	Medium loss in structure (20–50%)	High loss in structure (50-100%)	The percentage change in structural density of the habitat when exposed to a given pressure. *Example*: the flood bank will impact the salt marshes community composition due to different tolerances of the species to salinity and immersion.
Frequency of natural disturbance	Frequent (daily to weekly)	Intermediate frequency (several times per year)	Rare (annually or less often)	If a habitat is naturally perturbed in a way similar to the pressure, it may be more resistant to additional stress.
Consequence - resilience (habitat specific)				
Natural mortality	>80% mortality	20-50% mortality	0-20% mortality	Habitats with high natural mortality rates are generally more productive and, therefore, more capable of recovery.
Recovery time	<1 year	1-10 years	>10 year	Habitats that reach maturity earlier may be able to recover more quickly from disturbance. Here, we are referring to maturity of the habitat as a whole. Example: the seagrass species in Ria de Aveiro are mostly in a vegetative state, therefore it will need more time to recover than a more mature community.
Recruitment	Every< 1 year	Every 1-2 years	Every 2+ years	Frequent recruitment increases the chance that incoming propagules can re-establish a population in a disturbed area. Example: in Ria de Aveiro, mid-high salt marshes are more established than low salt marshes and will recruit incoming propagules more often.
Connectivity	High dispersion (>100km)	Medium dispersion (10-100km)	Low dispersion (<10km)	Connectivity is relative to the distance a propagule can travel. Example: the vegetative state can be easily dispersed when close spacing of seagrasses patches occur, increasing the recovery potential by increasing the chance that incoming recruits can re-establish a population in a disturbed area.

TABLE 3 Data quality and criteria weight scores. The data quality scores varied based on the source of information.

Data quality		
High quality data (1)	Adequate data (2)	Limited data (3)
Data validated in the field (*e.g.*, data set from the LTsER Ria de Aveiro platform georeferenced from scientific literature, data from the infrastructure Global Biodiversity Information Facility - GBIF)	Data generated through modelling (*e.g.*, Copernicus data set)	Data not scientifically validated, and therefore potentially biased (*e.g.*, qualitative data, citizen science, expert judgement)
	Weight of criteria	
Most important (1)	Moderately important (2)	Less important (3)

TABLE 4A Rating of consequence criteria (resilience attributes).

	Seagrasses			Salt marshes			Mud flats			Beaches			'Bocage'		
Resilience attributes	Rating	DQ	Weight	Rating	DQ	Weight	Rating	DQ	Weight	Rating	DQ	Weight	Rating	DQ	Weight
recruitment	2	2	2	SEC	2	2	0	2	2	0	2	2	0	2	2
natural mortality	2	2	2	2	2	2	0	2	2	0	2	2	0	2	2
connectivity	2	2	2	2	2	2	1	2	2	1	2	2	0	2	2
recovery time	2	2	2	3	2	2	1	2	2	1	2	2	0	2	2

DQ- Data Quality; SEC- Spatially Explicit Criteria.
Parameters ranged from 1 (lowest risk) to 3 (greatest risk).

TABLE 4B Rating of exposure and consequence (sensitivity) criteria for the cumulative risk calculation given each habitat and human activity.

		Recreation			Services			Aquaculture			Agricultural runoff			Development			Environmental management			Invasive species		
	Buffer (m)	250			250			250			0			250			0			0		
	Criteria	Rating	DQ	Weight	Rating	DQ	Weight	Rating	DQ	Weight	Rating	DQ	Weight	Rating	DQ	Weight	Rating	DQ	Weight	Rating	DQ	Weight
Seagrass	freq. of disturbance	2	2	2	0	2	2	2	2	2	3	2	2	0	2	2	3	2	2	2	3	2
	change in area	2	2	2	0	2	2	1	2	2	3	2	2	0	2	2	2	2	2	3	3	2
	change in structure	SEC	2	2	0	2	2	1	2	2	3	2	2	0	2	2	SEC	2	2	SEC	3	2
	temporal overlap	2	2	2	0	2	2	1	2	2	1	2	2	0	2	2	SEC	2	2	3	3	2
	manag. effectiveness	2	2	2	0	2	2	1	2	2	3	2	2	0	2	2	3	2	1	3	3	2
	intensity	2	2	2	0	2	2	1	2	2	SEC	2	1	0	2	2	3	2	1	2	3	2
Salt marshes	freq. of disturbance	1	2	2	0	2	2	2	2	2	3	2	2	0	2	2	3	2	2	3	2	2
	change in area	1	2	2	0	2	2	1	2	2	2	2	2	0	2	2	2	2	2	1	2	2
	change in structure	1	2	2	0	2	2	1	2	2	2	2	2	0	2	2	2	2	2	1	2	2

(Continued)

10.3389/fmars.2023.1086135

TABLE 4B Continued

		Recreation			Services			Aquaculture			Agricultural runoff			Development			Environmental management			Invasive species		
	Buffer (m)	250			250			250			0			250			0			0		
	Criteria	Rating	DQ	Weight	Rating	DQ	Weight	Rating	DQ	Weight	Rating	DQ	Weight	Rating	DQ	Weight	Rating	DQ	Weight	Rating	DQ	Weight
	temporal overlap	1	2	2	0	2	2	1	2	2	1	2	2	0	2	2	SEC	2	3	3	2	2
	manag. effectiveness	1	2	2	0	2	2	1	2	2	3	2	2	0	2	2	3	2	2	3	2	2
	intensity	1	2	2	0	2	2	1	2	2	SEC	2	3	0	2	2	3	2	2	0	3	2
Mud flats	freq. of disturbance	3	2	2	2	2	2	1	2	2	2	2	2	3	2	2	3	2	2	2	3	2
	change in area	3	2	2	1	2	2	1	2	2	1	2	2	2	2	2	3	2	2	2	3	2
	change in structure	3	2	2	1	2	2	2	2	2	1	2	2	2	2	2	3	2	2	SEC	3	2
	temporal overlap	3	2	2	2	2	2	3	2	2	1	2	2	1	2	2	3	2	2	3	3	2
	manag.effectiveness	3	2	2	3	2	2	3	2	2	3	2	2	2	2	2	3	2	2	3	3	2
	intensity	3	2	2	1	2	2	1	2	2	2	2	3	0	2	2	3	2	2	3	3	2
Beaches	freq. of disturbance	3	2	2	2	2	2	1	2	2	0	2	2	3	2	2	3	2	2	0	2	2
	change in area	3	2	2	1	2	2	2	2	2	0	2	2	2	2	2	3	2	2	0	2	2
	change in structure	3	2	2	1	2	2	2	2	2	0	2	2	2	2	2	3	2	2	SEC	2	3
	temporal overlap	2	2	2	2	2	2	3	2	2	0	2	2	1	2	2	1	2	2	0	2	2
	manag. effectiveness	SEC	2	2	3	2	2	3	2	2	0	2	2	2	2	2	3	2	2	0	2	2
	intensity	3	3	2	1	2	2	1	2	2	0	2	2	0	2	2	3	2	2	0	2	2
'Bocage'	freq. of disturbance	1	2	2	1	2	2	0	2	2	1	2	2	1	2	2	0	2	2	2	3	2
	change in area	1	2	2	1	2	2	0	2	2	1	2	2	1	2	2	0	2	2	1	3	2
	change in structure	1	2	2	1	2	2	0	2	2	1	2	2	1	2	2	0	2	2	1	3	2
	temporal overlap	1	2	2	1	2	2	0	2	2	2	2	2	1	2	2	0	2	2	2	3	2
	manag. effectiveness	2	2	2	0	2	2	0	2	2	1	2	2	1	2	2	0	2	2	3	3	2
	intensity	1	2	2	1	2	2	0	2	2	SEC	2	3	1	2	2	0	2	2	2	3	2

DQ- Data Quality; SEC- Spatially Explicit Criteria; frequency of disturbance and management effectiveness criteria appear with their abbreviation, freq and manag, respectively.
Parameters ranged from 1 (lowest risk) to 3 (highest risk).
Buffer distances by activity are shown.

10.3389/fmars.2023.1086135

Two common methods for measuring environmental risk based on expert judgement are Euclidean distance and multiplicative functions. Cumulative impact mapping studies tend to use a multiplicative approach (Halpern et al., 2008; Selkoe et al., 2009; Ban et al., 2010), whereas ecosystem risk assessments typically estimate risk as the Euclidean distance for each habitat-pressure combination in risk plots (Patrick et al., 2010; Hobday et al., 2011; Samhouri and Levin, 2012), which leads to a more precautionary scoring and higher risk (Sharp et al., 2018). Therefore, we selected Euclidean (straight-line) distance from the origin (minimum score) to the average of criteria scores for exposure and consequence, to estimate habitat risk (as in Arkema et al., 2014; Equation 2):

$$R_{ij} = \begin{cases} \sqrt{(E-1)^2 + (C-1)^2}, & E > 0 \ \ and \ \ C > 0 \\ 0, & E = 0 \ \ or \ \ C = 0 \end{cases} \quad \text{(Eq. 2)}$$

where R_{ij} is the individual risk to habitat i caused by pressure j and E and C are the respective exposure and consequence scores. Regardless of the risk function selected, if a habitat and a pressure did not overlap, the tool assumed that $E = 0$, $C = 0$, and therefore $R = 0$ for the grid cell being evaluated. This is calculated per grid cell by summing all risk scores for each habitat.

Finally, the InVEST HRA tool incorporates a buffer approach that spatially estimates of zones of influence, namely, the distance over which the effects of the pressure spread beyond its actual footprint in the input pressure map. Thus, the model allows for the specification of a decay equation, which is how the zone of influence of a pressure will be applied to risk (it is applied before it enters the risk equation, Equation 2). For example, roads and their impact beyond a road's physical location is represented as a buffer and then the decay function to account for different levels of exposure for this buffer. In this study, we applied a linear decay function because the spatial overlap of each pressure was assumed to be reduced linearly (degraded habitats over a larger distance) and not exponentially (degraded to nearby habitats) from the footprint of the pressure to the furthest extent of its zone of influence (Sharp et al., 2018).

2.4 Ecosystem-service potential: the supply side

The InVEST HRA tool, apart from assessing the cumulative risk posed to habitats by human activities, enabled the exploration of where these pressures might compromise biodiversity and ES. To obtain data on ES availability, we used the values reported by Lillebø et al. (2019). Coastal-marine services included the biotic and abiotic outputs from ecosystems following the Common International Classification of Ecosystem Services (CICES V5.1 in Haines-Young and Potschin, 2017) and were aggregated as a list of 10 ES types for stakeholders' elicitation purposes. ES were prioritized by stakeholders' elicitation. First, a questionnaire was prepared as an online Google form to be filled in by each participant anonymously to make pairwise comparisons of the ES to derive a ranking of criteria for the different stakeholder groups. The scaling method for ranking ES preferences was based on a Likert-type scale, using a five levels bidirectional ordinal scale, with an equivalent number of negative and positive statements: much less important (1/4); less important (1/2); equally important (1); more important (2); and much more important (4). Each participant should qualitatively rank the importance of each ES against the others (details on the stakeholders' elicitation process in Martínez-López et al., 2019). ES values by stakeholders were published for the provisioning, regulation and maintenance, and cultural ES divisions (Supplementary Table 2).

2.5 Habitat-ES vulnerability

The vulnerability score for each cell in the grid is obtained by multiplying cumulative risk by availability for each cell in the grid:

$$V = R * A \quad \text{(Equation 3)}$$

where V is the vulnerability, R is the cumulative risk score measured by the HRA model (see Equation 2), and A the expert judgement score on availability. The vulnerability score implied that the highest vulnerability was obtained when a habitat with a high potential to deliver ES was subject to higher levels of risk. Thus, the higher the vulnerability score for a given grid cell, the greater the potential loss of ES in that area (Willaert et al., 2019). We calculated cumulative vulnerability and individual ($V1$ – $V11$) for each of the 10 ES groupings.

3 Results

3.1 Cumulative risk maps

The risk assessment classified the 50 m^2 results for each habitat as either low, medium, or high based on the cumulative risk level (Figure 4). Habitat areas at the highest risk level (relative to their total area) were seagrasses (25.4%) and beaches and sand flats (25%), followed by mud flats (23%), 'Bocage' (17%) and salt marshes (7%). Four of the five habitats showed between 50-60% of their area at medium risk, whereas beaches and sand flats were only 32%. The habitats with the highest proportion of area in the lowest risk classification were salt marshes and beaches (both 43%). Regarding the seven landscape units, São Jacinto-Espinheiro WB2, Mira WB1, and the coastal WB7 experienced the highest habitat risk levels per unit area (Figures 4A–C). The exposure-consequence risk plots revealed a significant driver of risk to mud flats, seagrasses, and salt marshes (Figures 5B–D) from the environmental management pressures (S4), either existing or to be implemented by the year 2030. Interventions to maintain critical economic activities such as shipping and transport are likely to have unintended impacts to these habitats following dredging activities (increase in water velocity and in tidal prism in submerged periods that may experience further coastal squeeze, Martínez-López et al., 2019). Recreation activities were found to pose higher threats to beaches and sand flats and mudflats (Figures 5A, B) due to high intensity of use for water sports, engines of tourist boats, and

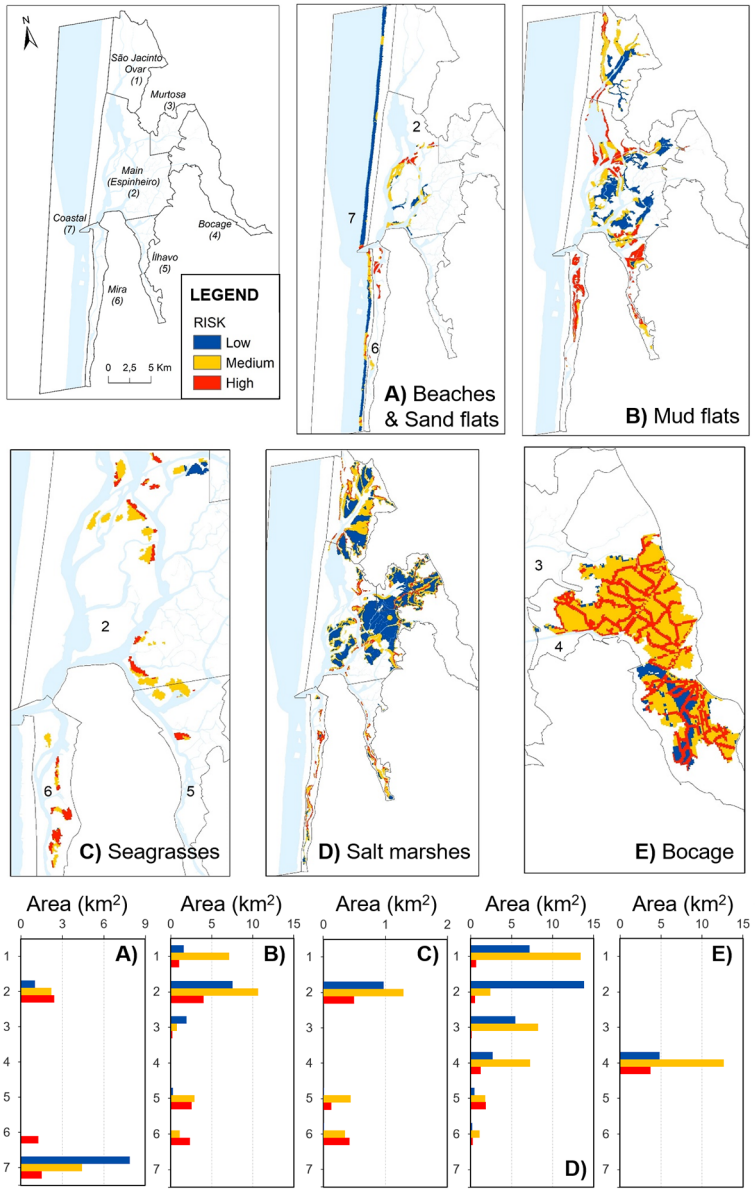

FIGURE 4
Spatially explicit habitat risk assessment outputs, classified as high, medium and low risk. Bar charts show total area (km^2) of habitat in each risk category per landscape units. The habitats are **(A)** beaches and sand flats, **(B)** mud flats, **(C)** seagrasses, **D)** salt marshes, **(E)** 'Bocage'. The landscape units are the Y axis and their total area are (1) Ovar - WB5: 48.60 km^2, (2) São Jacinto-Espinheiro - WB2: 95.98 km^2, (3) Murtosa - WB4: 15.89 km^2, (4) 'Bocage' - terrestrial: 45.14 km^2, (5) Ílhavo - WB3: 17.06 km^2, (6) Mira - WB1: 21.46 km^2 and (7) Coastal - WB7: 235.97 km^2.

fishing. The highest risk posed by the three invasive (alien) species was identified for seagrasses and mud flats, driven by high habitat suitability for the invasive (alien) lugworm *Arenicola* spp. With one exception, most of the pressures evaluated showed limited to no risk to the 'Bocage' habitat. The invasive plant species, *Cortaderia selloana*, showed higher level of exposure driven in part by the high overlap since it is in this habitat where this species is most present (Figure 5E and Table 4). Similarly, pressures from the services sector (i.e., related to ballast water discharge, runoff from roads and emissions) were found to be of concern in beach and mud flat habitats due to poor management of marine shipping and transportation activities (Figure 5A, B; Table 4). Agriculture pressures posed a substantial risk in salt marshes and seagrasses because of nutrient runoff in certain channels of the lagoon.

3.2 Vulnerability of ES supply

Provisioning, regulation and maintenance, and cultural services are depicted as maps in Figure 6. Results showed the highest potential for the regulation and maintenance category, while the supply of provisioning services was lower throughout the Ria. 'Bocage' was cited by stakeholders to supply fewer provisioning services but was highly valued for regulation and maintenance

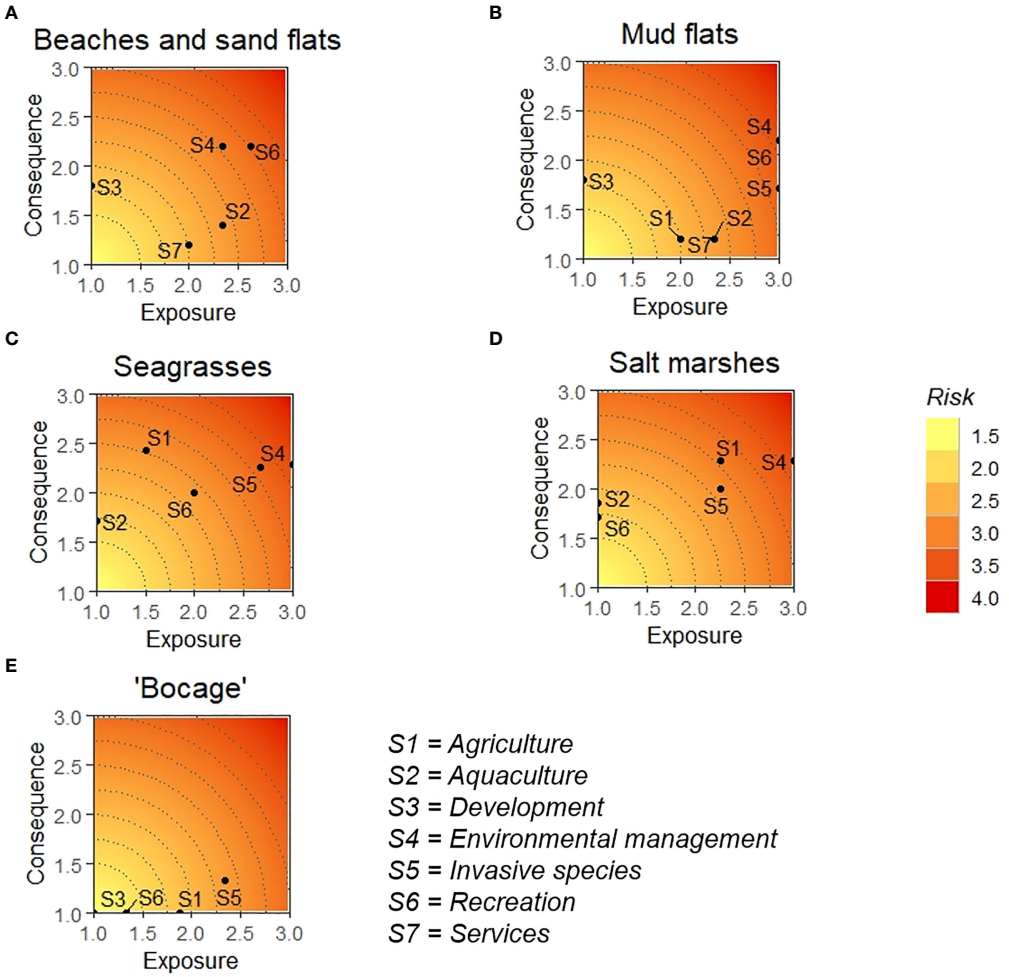

FIGURE 5
Risk plots showing maximum consequence and exposure scores by habitats (**A** beaches and sand flats, **B** mud flats, **C** seagrasses, **D** salt marshes, **E** 'Bocage') with coordinates representing pressures (S1: agriculture, S2: aquaculture, S3: development, S4: environmental management, S5: invasive species, S6: recreation, S7: services).

services. This high potential was also attributed to salt marsh and seagrass habitats. Beaches were also highly valued, especially for cultural services. Mudflats were the least valued habitat in terms of the full suite of potential ES in Ria de Aveiro.

The vulnerability maps for the provisioning, regulation and maintenance, and cultural ES indicated where the stocks of these potential services are at greatest risk now and into the future. ES vulnerability hotspots across the three ES divisions were identified in the northern sections of the landscape (units 2, 5, and 6, corresponding to the São Jacinto-Espinheiro WB2, Ílhavo WB3, and Mira WB1 subareas; Figure 7). The supply of cultural ES was found to be most vulnerable in beach areas located south of the lagoon inlet. This was driven by risk from recreational activities (*e.g.*, tourism boats, water sports) that, paradoxically, both threaten and support the diverse cultural values that beaches offer. These beach-going activities relate to physical and mental health benefits and aesthetic enjoyment. The 'Bocage' showed intermediate vulnerability for cultural services despite being a highly valued habitat in terms of ES availability. Its vulnerability was higher for regulating and cultural services than for provisioning. Mudflats were also found to be at the intermediate vulnerability level for the provisioning services, which are important for the regional food supply through harvesting activities such as bait digging and shellfish collecting. Regulation and maintenance services showed higher vulnerability scores in seagrass habitats than salt marshes, despite high potential in the latter for this service category.

4 Discussion

This research aimed to produce baseline information for EBM by evaluating a future development scenario in 2030. The approach combines a classical risk assessment framework with expert judgement about the relative availability of ES in a Natura 2000 monitoring site. To this end, habitats, human activities, pressures, and ES information provided by the stakeholders, government reports and existing research were combined to evaluate cumulative impacts spatiotemporally. This multi-step approach represents a novel application of the InVEST tool, as previous

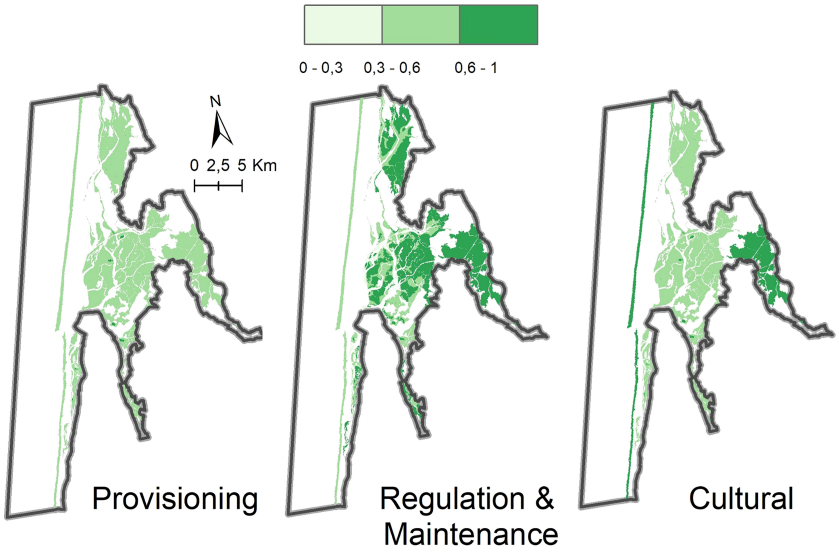

FIGURE 6
Ecosystem-service supply maps for the Ria de Aveiro. Values are the cumulative sum of the availability scores obtained from expert valuation on the identified habitats' ecosystem services availability in three categories: provisioning, regulation and maintenance, and cultural. Scores were normalized from 0 to 1. See Supplementary Table 2 for further detail.

assessments were mainly framed around a single management cycle or policy objective.

4.1 Extensions of the InVEST HRA

Previous applications of the InVEST HRA leveraged diverse data sources and even used the tool in combination with other methodologies, *e.g.*, ES and coastal zone management in Belize coast (Arkema et al., 2014); marine spatial planning in the Northeast and Mid-Atlantic Ocean regions in the United States (Wyatt et al., 2017); statistical analysis of ecology and conservation policies interactions in South Korea coastal area (Chung et al., 2015); InVEST HRA and coastal vulnerability models in Brazil (Elliff and Kikuchi, 2017); Marxan habitat prioritization software in California coastal area (Studwell et al., 2021); spatially explicit criteria based on marine biodiversity habitat suitability maps (Verutes et al., 2020) or habitat connectivity metrics in Iran inland (Ghehi et al., 2020). All these approaches confirm the diversity of options when applying the InVEST HRA tool. In this study, the InVEST HRA tool was applied to assess the risk that habitats involving coastal and terrestrial are due to the pressures

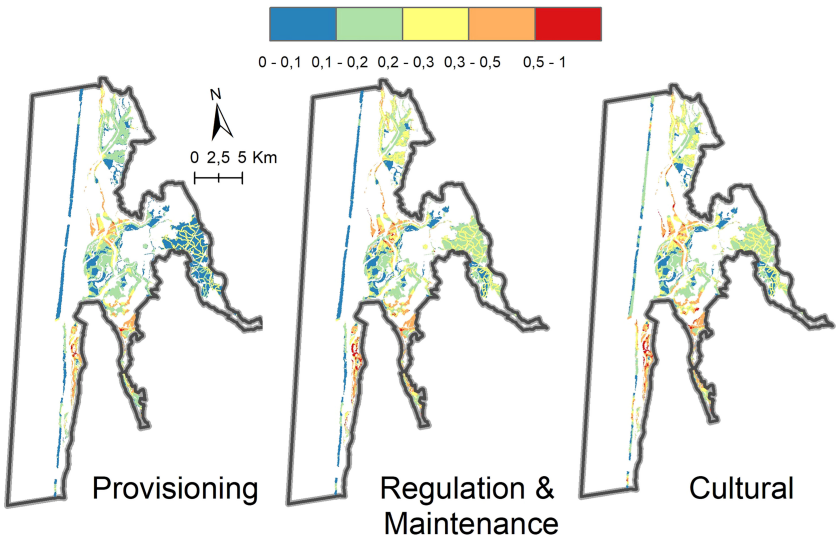

FIGURE 7
Ecosystem-service vulnerability in the Ria de Aveiro. Maps show the vulnerability scores obtained by multiplying cumulative risk by ecosystem services availability (normalized from 0 to 1). Each panel shows one of three ES categories.

produced by human activities, and to identify opportunities for EBM that can be applied to improve adaptative management. Yet, there are known limitations regarding the direct comparison of results because the risk outputs are relative ranks and use a unitless scoring system. This confirms the to'l's baseline characterization, monitoring, and evaluation utility.

In Europe, Willaert et al. (2019) considered the EBM perspective and, like Cabral et al. (2015), by assessing the vulnerability of marine benthic habitats (EUNIS) and their potential ES to physical, chemical, and biological pressures identified by the Marine Strategy Framework Directive. Both studies translated these data into indices that characterize the vulnerability of these habitats when supplying ES in France and Portugal, respectively. Further, Caro et al. (2020) analysed the InVEST HRA and ES abundance data as a resilience descriptor in a Portuguese estuary. Our approach extended these European studies by applying the model at the local scale (the Ria de Aveiro Natura 2000 coastal zone comprises 330 km^2) and producing high-resolution data (outputs at 50 m^2 grid cell size) to inform EBM management cycles with a spatiotemporally explicit decision-support tool.

4.2 Setting the stage for EBM

Building on the initial ES vulnerability assessment in Ria de Aveiro, the methodology is meant to be replicated as new information becomes available. To showcase an approach to EBM in the region that can be guided by an open-source, spatially explicit risk assessment tool, we followed a stepwise approach to address the following questions: (1) Which human activities pose the greatest risk to habitats in the near term (2030)? (2) How might these pressures compromise the future delivery of ES in a Natura 2000 site? (3) What management options might minimise risks? Below we summarise the most salient findings during the three steps of our analytical approach.

Step 1. The human activities that pose significant pressures to the habitats of Ria de Aveiro by 2030 are primarily driven by environmental management objectives. These measures are in place to support economically essential activities such as the dredging of navigation channels and flood control infrastructure extension, as detailed in Lillebø et al. (2019) and Martínez-López et al. (2019). Despite these activities, they all comply with existing environmental policies and regulations, including monitoring program requirements for flora, fauna, and water quality. Agriculture activities also act as pressure due to nutrient runoff to the lagoon contributing to the nitrogen load, which is usually the limiting nutrient in brackish/marine aquatic environments This pressure is most notably in the upper reaches of the lagoon system. This finding aligns with Lopes et al. (2017), where low freshwater input into the lagoon and certain oceanic conditions can lead to exposure from non-point nitrogen sources with current land use and water management. On a unit-area basis, seagrass habitats were estimated to have some of the highest risk levels in the study area (Figure 4C). Caro et al. (2020) also identified seagrasses as habitat at high risk in the Mondego estuary anticipated impacts on ES, located ca. 50 km south of Ria de Aveiro. Both results align with the downward trend in seagrasses distribution globally (Turschwell et al., 2021). The highest cumulative habitat risks were revealed for three landscape units: the coastal one, the São Jacinto-Espinheiro, and Mira (bar charts in Figure 4C). In addition to direct human pressures, beaches and sand flats of the coastal zone are exposed to storm-induced erosion and, consequently, are at risk of collapse r'due to overtopping induced by storm waves (Duck and da Silva, 2012). The São Jacinto-Espinheiro water body is primarily exposed to ecohydrological effects of dredging the inlet that increase the tidal prism in the entire system, aggravated by the backwaters (Picado et al., 2010; Azevedo et al., 2013). In these conditions, the flood bank will inhibit the saltmarshes' adaptation to changes in the hydrological regime, because they cannot shift landward, endangering them due to increasing submergence times (Martínez-López et al., 2019). Mira Channel is described as a subsystem: narrow and shallow as an estuary, where bait-digging activities and oyster production occur (Cunha et al., 2005). Invasive-alien species of lugworm (*Arenicola marina*) was first recorded in Ria de Aveiro in 2009 (Pires et al., 2015) and have driven seagrass fragmentation, degradation, and loss. The lugworm distribution (in our study, two lugworm species are grouped by the genus *Arenicola*) at Ria de Aveiro has been increasing since then and, therefore, restoration actions have been implemented to decrease the pressure due to bioturbation activity of *Arenicola* spp and restore fragmented seagrass meadows (Costa et al., 2022).

Step 2. The second step estimates where and to what extent the future delivery of ES in a Natura 2000 site may be compromised. The coastal-marine habitats that deliver ES in Ria de Aveiro should be in a good environmental status to continue supporting the flows of life- and livelihood-giving services. The EU recognizes the natural capital stocks of this region through a designation of Sites of Community Importance, which highlight the need to maintain and enhance ES in the area. According to our results, regulation and maintenance services were the most vulnerable service values, while provisioning services were the least vulnerable. This approach is based on quantifying ES to represent vulnerability, and recently, Peng et al. (2023) proposed an indicator-based framework to face the imbalance in the representation of social and ecological systems. Spatial planning tools, such as the HRA tool employed in Ria de Aveiro, can guide habitat protection and restoration efforts to areas that will safeguard the most vulnerable services. The cumulative risk maps show spatially the area of the habitats with the highest risk, which are informative to guide where protection is urgent. This form of EBM aligns with EU and UN policy targets that aim to prevent, halt, and reverse the degradation of ecosystems worldwide.

Step 3. The third step identifies management options that are likely to reduce risk. Initially, we searched for overlap between areas of high ES availability and the greatest threat to habitats that supply these services (vulnerability assessment, step 2). Then, we confirmed which activities drive risk to those habitats and locations (HRA, step 1). Based on our findings, efforts could be prioritized to mitigate the unintended impacts of ongoing environmental management. Unfortunately, many of these impacts result from indirect effects, meaning they are not localized to the activity footprint. For example, the flood bank

extension by 2030 is expected to increase coastal squeeze. This flood control measure does not violate Portuguese or EU environmental regulations despite the unintended consequences.

Alternatively, other environmental management activities, such as the direct effects of dredging, present substantial risk to proximate seagrass beds (near maximum exposure score in some areas; Figure 5C, Table 4). Management of dredging has improved significantly through improved ability to predict the spatial extent, however, the susceptibility to environmental changes caused by dredging to seagrasses is not well understood (Erftemeijer and Lewis, 2006). Given the seagrass biotype's importance to ES (regulating and cultural values; Supplementary Table 2), management interventions should aim to reduce seagrass risks from dredging and other human pressures. Ultimately, the unintended impacts from environmental management can be further monitored and analysed to confirm their status and update the findings of this vulnerability assessment over the near term.

4.3 Limitations and assumptions

All models have advantages and disadvantages. When applying the InVEST HRA tool, the following limitations should be considered. Caro et al. (2020) highlighted that the HRA misses detecting the potential increase in vulnerability that comes from impacts to ES that are highly demanded by beneficiaries and decreases in susceptibility of those habitats that safeguard more abundant supplies of natural capital. This is likely due to how the HRA assumes *a priori* additive effects of human pressures (Arkema et al., 2014). Therefore, a future option to consider synergistic or antagonistic interactions based on multiple pressures could improve ecosystem risk assessment (Studwell et al., 2021). Samhouri and Levin (2012) applied a classic risk-assessment framework to regional populations of indicator marine species. They found it helpful to validate the risk scores with alternative sources, such as extinction thresholds or measures of irreversible harm. Another potential HRA model limitation relates to data availability, quality, and uncertainty. Wyatt et al. (2017) raised concerns that the HRA outputs are conditioned on the choice of habitats, pressures, and the area of interest and that the approach is built upon a subjective system (*i.e.*, derived from expert elicitation) for scoring the exposure and consequence criteria.

Our study overcame many of these limitations by leveraging the best available information and detailing all sources of information (see Supplementary Table 1). Similar to the challenges experience by Cabral et al. (2015), it was difficult to harmonize certain pressure data sets (*e.g.*, sightings of invasive species) due to disparate information sources collected at different spatial and temporal scales. Chung et al. (2015) recommends the use of *in-situ* field data to improve the accuracy and reliability of spatial assessments and establish accurate statistical models. When time and resource constraints make this impossible, the HRA tool enables scoring of data quality (d_i) based on the source of information and the confidence in the data accuracy. Knowledge gaps can also be addressed through variable weights (w_i) that impact the importance placed on a criterion through a weighted average. Our approach in Portugal leveraged diverse research methods to assemble spatially explicit information at the local scale and an interdisciplinary team with intimate socio-ecological knowledge of the region to characterize and account for data uncertainty.

While we did not analyse alternative management options in this study, habitat risk and ES vulnerability outputs provide a future roadmap for monitoring and evaluation as additional data are collected about the future 2030 scenario and beyond. With a solid foundation of expert knowledge and InVEST HRA inputs, this approach in Ria de Aveiro can be revisited over time to respond to changes in habitat-pressure interactions that reflect new knowledge and insights (Wyatt et al., 2017), as is typical with EBM management cycles. This framework offers a transparent and generalizable approach that can be applied in most places where human activities threaten biodiversity and ES.

5 Conclusions

We applied a spatially explicit risk assessment for coastal habitats due to pressures produced by human activities. It was combined with expert judgement on the importance of the habitats delivering ES to establish baseline knowledge for future risk management to vulnerable ES. The highest levels of risk were found in seagrasses, salt marshes and mudflat habitats due to the unintended consequences of existing and proposed environmental management measures (flood control and dredging) that pose high risk to the diverse ES they provide. Regulation and maintenance services were the most vulnerable services, while provisioning services were the least vulnerable. Over time, and as new information becomes available, this research sets the stage for additional assessments that identify changes in the risk estimates based on alternative scenarios for managing human activities and their direct effects on critical coastal-marine biotypes. The co-development of spatial explicit scenarios to characterize human pressures as drivers of change enables more accurate estimates of ES vulnerability that can be iteratively refined with robust data and socio-ecological knowledge. To this end, our demonstration in a Natura 2000 monitoring site is meant to guide future evaluation and transparency in support of EBM and its management cycles in Ria de Aveiro.

Data availability statement

The original contributions presented in the study are included in the article/Supplementary Material. Further inquiries can be directed to the corresponding author.

Author contributions

AG-O: Methodology, Software, Writing-Original draft preparation, Investigation, Visualization. GV: Methodology, Software, Writing-Original draft preparation, Formal analysis,

Visualization. HT: Investigation, Writing- Reviewing and Editing, Resources. AS: Investigation, Writing- Reviewing and Editing, Resources. AL: Conceptualization, Methodology, Writing-Reviewing and Editing, Resources, Supervision, Funding acquisition. All authors contributed to the article and approved the submitted version.

Funding

AG-O was funded by the PORBIOTA project (POCI-01-0145-FEDER-022127) financed by the "Programa Operacional de Competitividade e Internacionalização'' and "Programa Operacional Regional de Lisboa, FEDER", and by the "Fundação para a Ciência e a Tecnologia, I.P. (FCT)" through national funds (PIDAC); A.I. Sousa was funded by national funds through the FCT-Foundation for Science and Technology,I.P., under the project CEECIND/00962/2017; and GV was partially funded by the SmartBioR project (Centro-01-0145-FEDER-000018) funded through national funds. Thanks are due to the BioPradaRia project (MAR-01.04.02-FEAMP-0020) funded by "Programa Operacional MAR2020", EMFF – European Maritime and Fisheries Fund, European Union and Portugal 2020; and to the BESIDE project (Horizon 2020 Coordination and support actions (CSA); Grant agreement ID: 951389) funded by the European Commission. We acknowledge also financial support to CESAM by FCT/MCTES (UIDP/50017/2020+UIDB/50017/2020+ LA/P/0094/2020), through national funds.

Conflict of interest

The authors declare that the research was conducted in the absence of any commercial or financial relationships that could be construed as a potential conflict of interest.

Publisher's note

Supplementary material

The Supplementary Material for this article can be found online at: https://www.frontiersin.org/articles/10.3389/fmars.2023.1086135/full#supplementary-material

References

Arkema, K. K., Verutes, G. M., Bernhardt, J. R., Clarke, C., Rosado, S., Canto, M., et al. (2014). Assessing habitat risk from human activities to inform coastal and marine spatial planning: a demonstration in Belize. *Environ. Res. Lett.* 9 (11), 114016. doi: 10.1088/1748-9326/9/11/114016

Azevedo, A., Sousa, A. I., Lencart e Silva, J. D., Dias, J. M., and Lillebø, A. I. (2013). Application of the generic DPSIR framework to seagrass communities of ria de aveiro: a better understanding of this coastal lagoon. *J. Coast. Res.* 65 (10065), 19–24. doi: 10.2112/SI65-004.1

Ban, N. C., Alidina, H. M., and Ardron, J. A. (2010). Cumulative impact mapping: advances, relevance and limitations to marine management and conservation, using canada's pacific waters as a case study. *Mar. Policy* 34, 876–886. doi: 10.1016/j.marpol.2010.01.010

Borgwardt, F., Robinson, L., Trauner, D., Teixeira, H., Nogueira, A. J. A., Lillebø, A. I., et al. (2019). Exploring variability in environmental impact risk from human activities across aquatic ecosystems. *Sci. Total Environ.* 652, 1396–1408. doi: 10.1016/j.scitotenv.2018.10.339

Cabral, P., Levrel, H., Schoenn, J., Thiebaut, E., Le Mao, P., Mongruel, R., et al. (2015). Marine habitats ecosystem service potential: a vulnerability approach in the normand-Breton (Saint malo) gulf, France. *Ecosystem Serv.* 16, 306–318. doi: 10.1016/j.ecoser.2014.09.007

Caro, C., Marques, J. C., Cunha, P. P., and Teixeira, Z. (2020). Ecosystem services as a resilience descriptor in habitat risk assessment using the InVEST model. *Ecol. Indic.* 115, 106426. doi: 10.1016/j.ecolind.2020.106426

Cazenave, A., and Cozannet, G. L. (2014). Sea Level rise and its coastal impacts. *Earth's Future* 2 (2), 15–34. doi: 10.1002/2013EF000188

Chung, M. G., Kang, H., and Choi, S. U. (2015). Assessment of coastal ecosystem services for conservation strategies in south Korea. *PloS One* 10 (7). doi: 10.1371/journal.pone.0133856

Costa, V., Flindt, M. R., Lopes, M., Coelho, J. P., Costa, A. F., Lillebø, A. I., et al. (2022). Enhancing the resilience of *Zostera* noltei seagrass meadows against *Arenicola* spp. bio-invasion: a decision-making approach. *J. Environ. Manage.* 302, 113969. doi: 10.1016/j.jenvman.2021.113969

Cunha, T., Hall, A., and Queiroga, H. (2005). Estimation of the *Diopatra neapolitana* annual harvest resulting from digging activity in canal de Mira, ria de aveiro. *Fish. Res.* 76, 55–66. doi: 10.1016/j.fishres.2005.05.008

Delacámara, G., O'Higgins, T. G., Lago, M., and Langhans, S. (2020). "Ecosystem-based management: moving from concept to practice," in *Ecosystem-based management, ecosystem services and aquatic biodiversity*. Eds. T. O'Higgins, M. Lago and T. DeWitt (Berlin, Germany: Springer, Cham).

Dias, J. M., Lopes, J. F., and Dekeyser, I. (2000). Tidal propagation in ria de aveiro lagoon, Portugal. *Phys. Chem. Earth (B)* 25, 369–374. doi: 10.1016/S1464-1909(00)00028-9h

Duck, R. W., and da Silva, J. F. (2012). Coastal lagoons and their evolution: a hydromorphological perspective. *Estuarine Coast. Shelf Sci.* 110, 2–14. doi: 10.1016/j.ecss.2012.03.007

EC (2006). Regulation (EC) n° 1893/2006 of the European parliament and of the council of 20 December 2006 establishing the statistical classification of economic activities NACE revision 2 and amending council regulation (EEC) no 3037/90 as well as certain EC regulations on specific statistical domains. *Off. J. Eur. Union* 49, L393/1. doi: 10.15468/ucf7eb

Elliff, C. I., and Kikuchi, R. K. P. (2017). Ecosystem services provided by coral reefs in a southwestern Atlantic archipelago. *Ocean Coast. Manage.* 136 (Supplement C), 49–55. doi: 10.1016/j.ocecoaman.2016.11.021

Erftemeijer, P. L., and Lewis, R. (2006). Environmental impacts of dredging on seagrasses: a review. *Mar. pollut. Bull.* 52 (12), 1553–1572. doi: 10.1016/j.marpolbul.2006.09.006

Ghehi, N. K., MalekMohammadi, B., and Jafari, H. (2020). Integrating habitat risk assessment and connectivity analysis in ranking habitat patches for conservation in protected areas. *J. Nat. Conserv.* 56, 125867. doi: 10.1016/j.jnc.2020.125867

Gómez, S., and Maynou, F. (2021). Balancing ecology, economy and culture in fisheries policy: participatory research in the Western Mediterranean demersal fisheries management plan. *J. Environ. Manage.* 291, 112728. doi: 10.1016/j.jenvman.2021.112728

Haines-Young, R., and Potschin, M. B. (2017) *Common international classification of ecosystem services (CICES) V5.1 and guidance on the application of the revised structure. ([online] URL)*. Available at: www.cices.eu.

Halpern, B. S., McLeod, K. L., Rosenberg, A. A., and Crowder, L. B. (2008). Managing for cumulative impacts in ecosystem-based management through ocean zoning. *Ocean Coast. Manage.* 51 (3), 203–211. doi: 10.1016/j.ocecoaman.2007.08.002

Hobday, A. J., Smith, A. D. M., Stobutzki, I. C., Bulman, C., Daley, R., Dambacher, J. M., et al. (2011). Ecological risk assessment for the effects of fishing. *Fish. Res.* 108, 372–384. doi: 10.1016/j.fishres.2011.01.013

Lago, M., Boteler, B., Rouillard, J., Abhold, K., Jähnig, S. C., Iglesias-Campos, A., et al. (2019). Introducing the H2020 AQUACROSS project: knowledge, assessment, and management for AQUAtic biodiversity and ecosystem services aCROSS EU policies. *Sci. Total Environ.* 652, 320–329. doi: 10.1016/j.scitotenv.2018.10.076

Lillebø, A. I., Stålnacke, P., and Gooch, G. D. (2015). *Coastal lagoons in Europe: integrated water resource strategies*. Eds. A. I. Lillebø, P. Stålnacke and G. D. Gooch (United Kingdom: IWA publishing; International Water Association (IWA), 254.

Lillebø, A. I., Teixeira, H., Martínez-López, J., Genua-Olmedo, A., Marhubi, A., Delacámara, G., et al. (2020). "Mitigating negative unintended impacts on biodiversity in the natura 2000 vouga estuary (Ria de aveiro, Portugal)," in *Ecosystem-based management, ecosystem services and aquatic biodiversity*. Eds. T. O'Higgins, M. Lago and T. DeWitt (Cham: Springer).

Lillebø, A. I., Teixeira, H., Morgado, M., Martínez-López, J., Marhubi, A., Delacámara, G., et al. (2019). Ecosystem-based management planning across aquatic realms at the ria de aveiro natura 2000 territory. *Sci. Total Environ.* 650, 1898–1912. doi: 10.1016/j.scitotenv.2018.09.317

Long, R. D., Charles, A., and Stephenson, R. L. (2015). Key principles of marine ecosystem-based management. *Mar. Policy* 57, 53–60. doi: 10.1016/j.marpol.2015.01.013

Lopes, M. L., Marques, B., Dias, J. M., Soares, A. M. V. M., and Lillebø, A. I. (2017). Challenges for the WFD second management cycle after the implementation of a regional multi-municipality sanitation system in a coastal lagoon (Ria de aveiro, Portugal). *Sci. Total Environ.* 586, 215–225. doi: 10.1016/j.scitotenv.2017.01.205

Martínez-López, J., Teixeira, H., Morgado, M., Almagro, M., Sousa, A. I., Villa, F., et al. (2019). Participatory coastal management through elicitation of ecosystem service preferences and modelling driven by "coastal squeeze". *Sci. Total Environ.* 652, 1113–1128. doi: 10.1016/j.scitotenv.2018.10.309

McCook, L. J., Ayling, T., Cappo, M., Choat, J. H., Evans, R. D., De Freitas, D. M., et al. (2010). Adaptive management of the great barrier reef: a globally significant demonstration of the benefits of networks of marine reserves. *Proc. Natl. Acad. Sci.* 107 (43), 18278–18285. doi: 10.1073/pnas.0909335107

Neumann, B., Vafeidis, A. T., Zimmermann, J., and Nicholls, R. J. (2015). Future coastal population growth and exposure to sea-level rise and coastal flooding-a global assessment. *PloS One* 10 (3), e0118571. doi: 10.1371/journal.pone.0118571

O'Higgins, T., Nogueira, A. J. A., and Lillebø, A. I. (2019). A simple spatial typology for assessment of complex coastal ecosystem services across multiple scales. *Sci. Total Environ.* 649, 1452–1466. doi: 10.1016/j.scitotenv.2018.08.420

Patrick, W. S., Spencer, P., Link, J., Cope, J., Field, J., Kobayashi, D., et al. (2010). Using productivity and susceptibility indices to assess the vulnerability of united states fish stocks to overfishing. *Fish. Bull.* 108 (3), 305–322.

Peng, Y., Welden, N., and Renaud, F. G. (2023). A framework for integrating ecosystem services indicators into vulnerability and risk assessments of deltaic social-ecological systems. *J. Environ. Manage.* 326, 116682. doi: 10.1016/j.jenvman.2022.116682

Picado, A., Dias, J. M., and Fortunato, A. B. (2010). Tidal changes in estuarine systems induced by local geomorphologic modifications. *Continental Shelf Res.* 30 (17), 1854–1864. doi: 10.1016/j.csr.2010.08.012

Pires, A., Martins, R., Magalhães, L., Soares, A. M. V. M., Figueira, E., Quintino, V., et al. (2015). Expansion of lugworms towards southern European habitats and their identification using combined ecological, morphological and genetic approaches. *Mar. Ecol. Prog. Ser.* 533, 177–190. doi: 10.3354/meps11315

Röckmann, C., van Leeuwen, J., Goldsborough, D., Kraan, M., and Piet, G. (2015). The interaction triangle as a tool for understanding stakeholder interactions in marine ecosystem based management. *Mar. Policy* 52, 155–162. doi: 10.1016/j.marpol.2014.10.019

Samhouri, J. F., and Levin, P. S. (2012). Linking land-and sea-based activities to risk in coastal ecosystems. *Biol. Conserv.* 145, 118–129. doi: 10.1016/j.biocon.2011.10.021

Selkoe, K. A., Halpern, B. S., Ebert, C. M., Franklin, E. C., Selig, E. R., Casey, K. S., et al. (2009). A map of human impacts to a 'pristine' coral reef ecosystem, the papahānaumokuākea marine national monument. *Coral Reefs* 28 (3), 635–650. doi: 10.1007/s00338-009-0490-z

Sharp, R., Tallis, H. T., Ricketts, T., Guerry, A. D., Wood, S. A., Chaplin-Kramer, R., et al. (2018). InVEST 3.7.0.post17+hbeb7e1912b14 user's guide. the natural capital project, Stanford university, university of Minnesota, the nature conservancy and world wildlife fund.

Sherman, K. (2014). Adaptive management institutions at the regional level: the case of large marine ecosystems. *Ocean Coast. Manage.* 90, 38–49. doi: 10.1016/j.ocecoaman.2013.06.008

Sousa, A. I., da Silva, J. F., Azevedo, A., and Lillebø, A. I. (2019a). Blue carbon stock in zostera noltei meadows at ria de aveiro coastal lagoon (Portugal) over a decade. *Sci. Rep.* 9, 14387. doi: 10.1038/s41598-019-50425-4

Sousa, A. I., Figueiredo da Silva, J., and Lillebø, A. I. (2019b). *Zostera noltei* Seagrass meadows spatial distribution at LTER site ria de aveiro lagoon in 2014. version 1.2. universidade de aveiro, departamento de biologia e centro de estudos do ambiente e do mar (CESAM). occurrence data set accessed *via* GBIF.

Sousa, A. I., Santos, D. B., Silva, E. F. D., Sousa, L. P., Cleary, D. F., Soares, A. M., et al. (2017). 'Blue carbon' and nutrient stocks of salt marshes at a temperate coastal lagoon (Ria de aveiro, Portugal). *Sci. Rep.* 7 (1), 1–11. doi: 10.1038/srep41225

Studwell, A., Hines, E., Nur, N., and Jahncke, J. (2021). Using habitat risk assessment to assess disturbance from maritime activities to inform seabird conservation in a coastal marine ecosystem. *Ocean Coast. Manage.* 199, 105431. doi: 10.1016/j.ocecoaman.2020.105431

Teixeira, H., Lillebø, A. I., Culhane, F., Robinson, L., Trauner, D., Borgwardt, F., et al. (2019). Linking biodiversity to ecosystem services supply: patterns across aquatic ecosystems. *Sci. Total Environ.* 657, 517–534. doi: 10.1016/J.SCITOTENV.2018.11.440

Turschwell, M. P., Connolly, R. M., Dunic, J. C., Sievers, M., Buelow, C. A., Pearson, R. M., et al. (2021). Anthropogenic pressures and life history predict trajectories of seagrass meadow extent at a global scale. *Proc. Natl. Acad. Sci.* 118 (45). doi: 10.1073/pnas.2110802118

UNEP (2011) *Taking steps toward marine and coastal ecosystem-based management - an introductory guide. UNEP regional seas reports and studies no. 189*. Available at: https://osf.io/preprints/marxiv/akh93/download.

Verutes, G. M., Johnson, A. F., Caillat, M., Ponnampalam, L. S., Peter, C., Vu, L., et al. (2020). Using GIS and stakeholder involvement to innovate marine mammal bycatch risk assessment in data-limited fisheries. *PloS One* 15 (8), e0237835. doi: 10.1371/journal.pone.0237835

Webb, J. A., Watts, R. J., Allan, C., and Warner, A. T. (2017). Principles for monitoring, evaluation, and adaptive management of environmental water regimes. *Water Environ.* pp, 599–623). doi: 10.1016/B978-0-12-803907-6.00025-5

Willaert, T., Garcia-Alegre, A. G., Queiroga, H., Cunha e Sá, M. A., and Lillebø, A. I. (2019). Measuring vulnerability of marine and coastal habitats' potential to deliver ecosystem services. *Front. Mar. Sci.* 6. doi: 10.3389/fmars.2019.00199

Wyatt, K. H., Griffin, R., Guerry, A. D., Ruckelshaus, M., Fogarty, M., and Arkema, K. K. (2017). Habitat risk assessment for regional ocean planning in the US northeast and mid-Atlantic. *PloS One* 12 (12). doi: 10.1371/journal.pone.0188776

Zador, S. G., Holsman, K. K., Aydin, K. Y., and Gaichas, S. K. (2017). Ecosystem considerations in Alaska: the value of qualitative assessments. *ICES J. Mar. Sci.* 74 (1), 421–430. doi: 10.1093/icesjms/fsw144

frontiers | Frontiers in Marine Science

TYPE Original Research
PUBLISHED 22 June 2023
DOI 10.3389/fmars.2023.1147106

OPEN ACCESS

EDITED BY
Guanqiong Ye,
Zhejiang University, China

REVIEWED BY
Abhra Chanda,
Jadavpur University, India
Zezheng Liu,
Beijing Normal University, China

*CORRESPONDENCE
Ping Zuo
zuoping@nju.edu.cn

RECEIVED 18 January 2023
ACCEPTED 22 May 2023
PUBLISHED 22 June 2023

CITATION
Liang J, Tian J, Zuo P, Dai Z, Jiang W, Jin J and Yan Y (2023) Wise use of coastal wetlands: 10-year reclamation vs. 3-year eco-governance in the Tiaozini Wetland, Jiangsu, China. *Front. Mar. Sci.* 10:1147106. doi: 10.3389/fmars.2023.1147106

Wise use of coastal wetlands: 10-year reclamation vs. 3-year eco-governance in the Tiaozini Wetland, Jiangsu, China

Jiahui Liang[1,2], Jiahui Tian[1,2], Ping Zuo[1,2,3]*, Ziyi Dai[1,2], Wenkui Jiang[4], Juan Jin[4] and Yuru Yan[3]

[1]Key Laboratory of Coast and Island Development of the Ministry of Education, Nanjing University, Nanjing, Jiangsu, China, [2]School of Geography and Ocean Science, Nanjing University, Nanjing, Jiangsu, China, [3]Key Laboratory of Coastal Salt Marsh Ecosystems and Resources, Ministry of Natural Resources, Nanjing, Jiangsu, China, [4]Tourism Management Department, Dongtai Coastal Wetland Tourism Resort Economic Zone Management Committee, Dongtai, Jiangsu, China

Coastal wetlands provide extensive ecological services for life on Earth but are facing rapid global disappearance influenced by human activities and climate change. From 1984 to 2018, approximately 28% of the natural coastal wetlands in China were lost due to seawater intrusion, reduced sediment acquisition, urbanization, and reclamation. Tiaozini wetland used to be reclaimed during 2010-2019, and quickly shifted for conservation with less than 3 years. We analyzed 3 years of top-down eco-governance and bottom-up activities in Tiaozini, one of the typical wetlands with wise use instead of reclamation. Collaboration of stakeholders, such as the management company, local residents, tourists, scientific committees, NGOs, and media, facilitated the wise use of Tiaozini wetland as a successvie way towards eco-governance, including public participation and environmental education. Adaptive management, ecosystem-based management, and natural-based solutions play very important roles in eco-governance from both bottom-up and top-down approaches. Results showed that 3-year eco-governance induced great achievements in both biodiversity conservation and ecotourism development, which outweighs the 10-year reclamation for coastal wetlands exploitation.

KEYWORDS

coastal wetlands reclamation, wise use, wetlands restoration, biodiversity conservation, eco-governance, ecotourism, the Tiaozini Wetland

1 Introduction

Coastal wetlands are distributed across all continents, except Antarctica, in low-energy tidal environments (Campbell et al., 2022) and provide immense ecosystem services for humanity. However, the long-term and continuing losses of natural wetlands have been confirmed by previous studies (Davidson, 2014; Davidson and Finlayson, 2018; Wang et al., 2020, Wang et al., 2021a; Murray et al., 2022), with drivers of drainage (Zuo et al., 2013;

Watson et al., 2017), eutrophication (Deegan et al., 2012), sediment availability (Kirwan et al., 2011), sea level rise (Kirwan and Megonigal, 2013; Spencer et al., 2016) and anthropogenic pressure (Murray et al., 2022) being the main responsible factors. China's total coastal wetlands decreased by approximately 28% from 1984 to 2018, comprising tidal flats (non-vegetated), salt marshes, and mangrove forests (Wang et al., 2021a), and the policy on Reclamation of More Lands from the Sea in China caused 7% of natural coastal wetlands loss from the 1970s to 2007 (Zuo et al., 2013). Nevertheless, the Blue Bay Remediation Action, which was issued in May 2016, shifted the coastal development policy to restoration approaches at the national level. As a result, the exploitation of coastal wetlands has been halted since then, with a new focus on rehabilitation and conservation.

The Ramsar Convention on Wetlands was signed by national governments in Ramsar, Iran, in 1971 as a global measure to stem the declining state of the world's wetlands and the implications of this for resident and migratory wetland species (Gell et al., 2016). The Ramsar Convention already put forward the fundamental baseline of the wise use and sustainable development of wetlands based on ecosystem-based approaches (Finlayson et al., 2011). What kind of wetland use is wise use? Tiaozini wetland used to be an experimental zone of Yancheng Biosphere Reserve, which is also a Ramsar Site and one of the wintering grounds of Red-crowned cranes in China. The Tiaozini wetland is one of the typical wetlands undergoing sharp conversion from exploitation to conservation, receiving real benefits in many prospects, such as being approved at the 43rd World Heritage Conference as the core area of China's Yellow Sea Migratory Birds Habitat (Phase I) on July 5, 2019. As the first intertidal wetland heritage site in China, the Tiaozini Wetland plays one of the key roles in presenting the current restoration and protection policy, which reinforces its biodiversity conservation in contrast to the former reclamation. With comprehensive eco-governance and the development pathway of ecotourism, it provides us with a typical example of wise and sustainable use of wetlands during the shift from wetland reclamation to conservation.

Till December 2022, there were 1,154 World Heritage sites globally, with 56 World Heritage sites in China, including 38 cultural heritages, 14 natural heritages, and 4 natural and cultural heritages (https://whc.unesco.org/en/list/). Thus, since 2019, Tiaozini has faced a sharp transition from reclamation to ecological conservation as a World Heritage site. With rapid economic development, population growth, and land demand in this century, this wetland has long been considered a potential area for reclamation. Fortunately, the Tiaozini Wetland, with its outstanding universal value for biodiversity conservation, survived the reclamation stage and was transformed into a protected area (Ye and Sun, 2021; Hu et al., 2022).

Based on the published literature, field interviews, and remote sensing technique, we analyzed the land use changes that happened due to top-down governance (those established by the government, including policies both on reclamation and eco-tourism in general) and bottom-up activities (those established by Tiaozini Scenic Spot Management Company, market-oriented, mainly about the planning and implementation of specific objects) in the Tiaozini Wetland since 2010. Ecotourism benefits were analyzed with yearly data in 2021. We aim to report the successful restoration and development path within three years of ecotourism after 10 years of reclamation, a shift that can be copied and recommended for sustainable development in other protected wetlands.

2 Study area and data analysis

2.1 Study area

The Tiaozini Wetland is located on the coast of Yancheng City, Jiangsu Province (Wang et al., 2022). It is located in the subtropical monsoon zone, with an average annual temperature of 14 ~15°C and precipitation of 1,060 mm (Zhan et al., 2021). The wetland covers contiguous non-vegetated mudflats and salt marshes covered with *Suaeda salsa*, *Spartina alterniflora*, *Phragmites australis*, etc. The study area includes the vast mudflats, salt marshes, and the Tiaozini reclamation area (Figure 1), with a total area of 591.41 km^2. The Tiaozini reclamation area starts from the Liangduo River in the north and ends at the Fangtang River in the south.

Both the Yangtze River and the Yellow River (1128-1855) used to join the Yellow China Sea. Huge amounts of sediments fed into the Yellow Sea, contributing extensive silty and muddy tidal flats along the Yancheng coast and huge radial sand ridges filed to the South Yellow Sea. The wetland lies just behind the core of radial sand ridges with active sediment exchange and noticeable siltation. Tiaozini once produced an extensive land for reclamation that, due to sand acquisition, benefited annually from a 100 m width increase of the intertidal area (Ding et al., 2011; Figure 2). Now, due to its unique geographical location and food supply with large amounts of macrobenthos, the Tiaozini Wetland has become an important stopover, wintering, and breeding ground for millions of migrating waterbirds on the East Asian–Australasian Flyway (EAAF; Chen et al., 2015; Wen et al., 2020; Wang et al., 2021b). It has attracted some globally critically endangered species, such as the *Calidris pygmaea*, which uses the area for more than 2 to 3 months as a moulting ground (Peng et al., 2017; Cao et al., 2019; Gao et al., 2021; Hu et al., 2022).

2.2 Data source and data processing

We collected four satellite images of the Tiaozini Wetland, covering the periods of 2010, 2014, 2018, and 2022 (data source: EarthExplorer, https://earthexplorer.usgs.gov/). All satellite images were selected to coincide with the growing season of wetland vegetation (*Suaeda salsa*, *Phragmites australis*, and *Spartina alterniflora*) from May to October, at low tide and with less haze, representing the best available data for the purpose of this study. However, most of the images from May to October 2018 do not match the requirements (both low tide and low haze). We selected the satellite image acquired on 24 December 2018 with a clearer image. Data details are shown in Table 1.

Satellite images were corrected using on-site positioning as a reference. According to the distribution of 20 control points on each

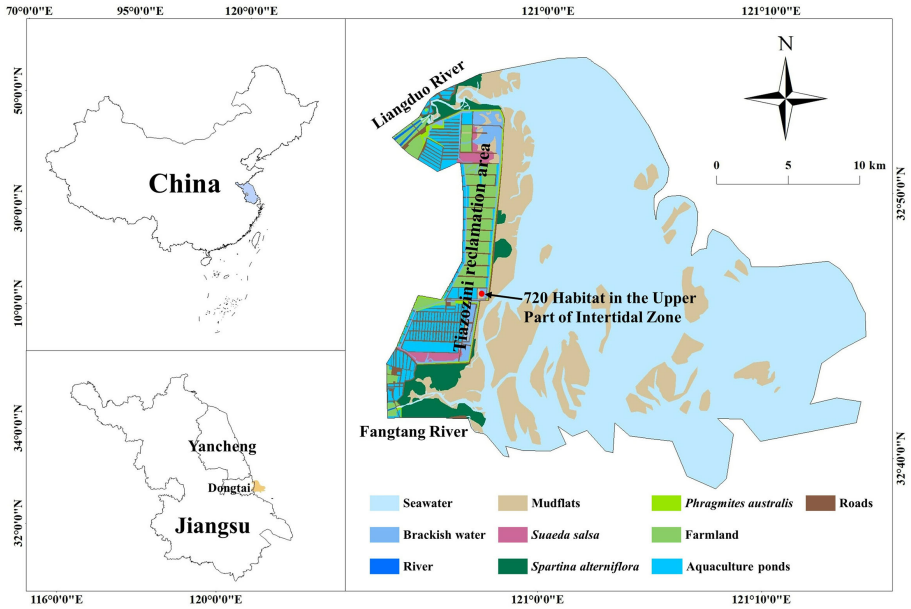

FIGURE 1
Map of the location and land use types of the study area, showing the 720 Habitat in the Upper Part of the Intertidal Zone (720 HUPIZ, red dot). 720 means 720 *mu* (0.48 km^2, 1 km^2 = 1 500 *mu*, *mu* is the area unit used in China).

image, quadratic polynomials were applied to the correction equations. All images were then resampled to a resolution of 30 m×30 m with a root mean square error of <1 pixel. In-situ verification was conducted in the study area with 95% accuracy. Based on the interpretation of these four images, landscape-type data were obtained by supervised classification in ENVI 5.3 software. Overlay analysis was performed in ArcGIS 10.8 software.

In order to learn about the development history and status of the Tiaozini Wetland, we performed a systematic review of the literature through CNKI (China National Knowledge Infrastructure, a Chinese journal full-text database), Web of Science, Elsevier ScienceDirect, SpringerLink, etc., and carried out field investigations in December 2021, March 2022, and August 2022. We also conducted oral interviews with over 20 stakeholders of the Tiaozini Wetland, including management committee officials, ecological photographers, NGO staff, tourists, and fishermen. The tourism data were obtained from the Tiaozini Scenic Spot Management Company and analyzed by Excel.

3 Results

3.1 Background: land use analysis

In general, the Tiaozini reclamation area was mainly used as farmland and aquaculture ponds according to its former planning. The morphology of the intertidal zone changes annually with the strong influence of storm surges. However, the native vegetation is distributed from the land to the sea with a gradient effect. For instance, *Suaeda salsa* grows mostly in the upper part of the intertidal zone and only distributes in the northern and southern parts of the reclamation area after artificial transformation. *Phragmites australis* distributes along the man-made seawall road inside the reclamation area with fresh water supply, while *Spartina alterniflora* forms a single dominant vegetation in the middle and lower parts of the intertidal zone, outside of the road adajacent to the sea directly. We divided the study area into 10 types based on land use, including seawater (SW), brackish water (BW), river

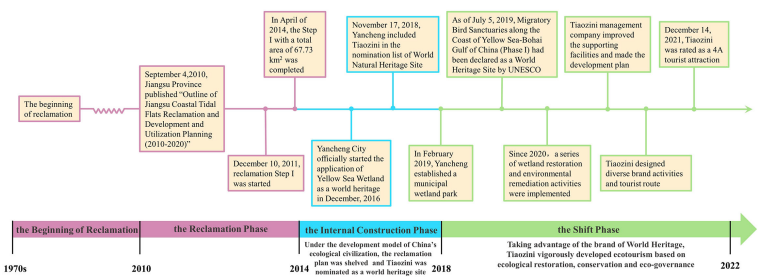

FIGURE 2
The milestones, processes, and political context of the Tiaozini development, including four main phases: the Beginning of Reclamation (1970s-2010), the Reclamation Phase (2010-2014), the Internal Construction Phase (2014-2018), and the Shift Phase (2018-2022).

TABLE 1 Basic information of chosen remote sensing images.

Acquisition date	Path	Row	Data source	Resolution (m)
2010-10-31	119	037	Landsat 5 TM	30
2014-10-26	119	037	Landsat 8 OLI	30
2018-12-24	119	037	Landsat 8 OLI	30
2022-09-06	119	037	Landsat 9 OLI-2	30

(RIV), mudflats (MF), *Suaeda salsa* (SS), *Spartina alterniflora* (SA), *Phragmites australis* (PA), farmland (FL), aquaculture ponds (AP), and roads (RD).

Figure 3 shows the land use changes in temporal and spatial scales during 2010-2022. The landscape of Tiaozini has changed significantly from 2010 to 2022 on the temporal scale (Table 2). Mudflats, as the dominant natural wetlands, declined from 249.80 km^2 to 94.67 km^2 with a 62.11% loss from 2010 to 2022. The land cover of brackish water, *Suaeda salsa*, *Phragmites australis*, and roads increased significantly during 2010-2014, which is called the reclamation phase (Figure 2). In 2014, a dike or seawall with a length of 27.78 km could be clearly identified. The terrestrial part inside of the seawall was converted to artificial wetlands for aquaculture and agriculture. During the period spanning from 2014 to 2018, we referred to it as the internal construction phase (Figure 2). This phase witnessed various companies renting individual aquaculture ponds. The area of farmland increased by 14.03 km^2, aquaculture ponds increased by 16.82 km^2, and roads increased by 7.00 km^2 in 2018 compared to 2014. *Suaeda salsa* covered an area of 4.32 km^2, with a reduction of 56.45% since 2014. *Phragmites australis* habitat increased to 3.46 km^2 due to the construction of ditches within the reclaimed area. From 2018 to 2022, adaptive management for ecotourism and biodiversity conservation resulted in less landscape change in the reclamation area and almost no increase in artificial landscapes. We named this period the shift phase (Figure 2). *Spartina alterniflora* expanded to 17.58 km^2 outside the reclamation area in 2022. Besides, *Suaeda salsa* decreased by 8.80% and *Phragmites australis* increased by 3.20% compared to 2018. The most significant shift in the area was the purchase by the Coastal Development Corporation of use rights related to 720 habitats in the upper part of the intertidal zone (Figure 1). Dongtai Coastal Wetland Tourism Resort Economic Zone Management Committee, which organizes the scenic spot for ecotourism and conservation, purchased the use rights of the 720 *mu* artificial wetland for shorebird conservation from the Coastal Development Corporation in 2020. The event made an outstanding mark between use rights and ownership of biodiversity conservation among Tiaozini wetland-owned stakeholders.

Significant changes could be observed in the last 12 years (Figure 4). In the reclamation phase of 2010-2014, 4.70%, 2.49%, 1.62%, 0.02%, and 1.51% of mudflats were converted to brackish water, *Suaeda salsa*, *Spartina alterniflora*, aquaculture ponds, and

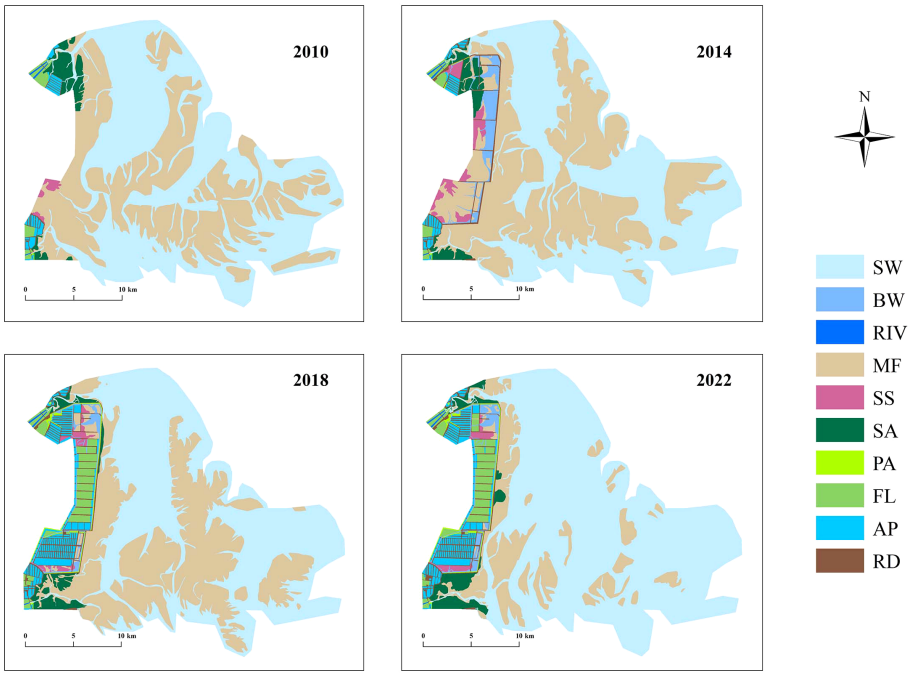

FIGURE 3
Land use changes in Tiaozini from 2010 to 2022.

TABLE 2 Statistics of land use changes from 2010 to 2022.

Year Landscape area	2010		2014		2018		2022	
	Area (km^2)	Proportion (%)	Area (km^2)	Proportion (%)	Area (km^2)	Proportion (%)	Area (km^2)	Proportion (%)
SW	311.52	52.67	268.47	45.40	283.92	48.01	402.72	68.09
BW	0.00	0.00	14.68	2.48	7.82	1.32	9.86	1.67
RIV	0.64	0.11	0.64	0.11	0.64	0.11	0.64	0.11
MF	249.80	42.24	264.57	44.74	221.56	37.46	94.67	16.01
SS	2.45	0.41	9.92	1.68	4.32	0.73	3.94	0.67
SA	14.34	2.42	14.02	2.37	13.00	2.20	17.58	2.97
PA	0.09	0.01	0.26	0.04	3.46	0.59	3.57	0.60
FL	4.61	0.78	4.39	0.74	18.42	3.11	20.41	3.45
AP	5.74	0.97	5.72	0.97	22.54	3.81	22.15	3.75
RD	2.24	0.38	8.74	1.48	15.74	2.66	15.88	2.69

roads, respectively. Other landscape types changed less. During the internal construction phase from 2014 to 2018, the area of brackish water and mudflats decreased due to internal construction in the Tiaozini reclamation area. The area of *Suaeda salsa* marsh changed with 6.89%, 1.41%, 10.94%, 24.84%, 33.50%, and 12.80% of the area being transferred to brackish water, mudflats, *Phragmites australis*, farmland, aquaculture ponds, and roads, respectively. The area of *Spartina alterniflora* marsh was less changed. However, the *Spartina alterniflora* community had been moved out of the reclamation area, which had spread widely on the mudflats adajacent to the sea dike. Moreover, farmland, aquaculture ponds, and roads gained more land from brackish water and mudflats in the reclamation area. The great shift phase of 2018-2022 experienced a sharp conversion for wetlands use and management. Therefore, the landscape tended to be much more stable in the reclamation area. The majority of mudflats turned to seawater, which was impacted by the rising tides. During the 2018-2022 major shift phase, there was a sharp change in wetland use and management. Therefore, the landscape in the reclamation area tended to be much more stable. Most of the tidal flats were transformed into seawater, which was affected by the rising tides. *Spartina alterniflora* spread to 5.81 km^2 along the intertidal zone. In particular, the 720 HUPIZ was first designated as permanent habitat for shorebirds, especially migratory birds in the East Asian–Australasian Flyway, with artificial water level mitigation and food supply.

It was observed that mudflats transferred to other land use types in general. After 2014, when phase I of reclamation was completed,

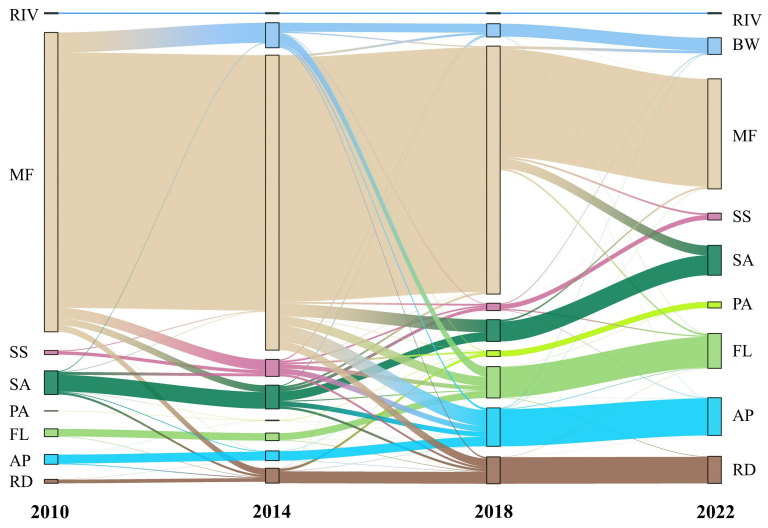

FIGURE 4
Land use transition in Tiaozini from 2010 to 2022, drawn according to Table 2. Bolder lines indicate a bigger transfer.

mudflats outside the seawall were in a state of natural change, almost free from artificial interference. Therefore, the year 2014 was the time when the sea dyke was finished. More intertidal mudflats were converted to *Spartina alterniflora* marsh with natural expansion, while other parts inside the reclamation area were shifted to farmlands, aquaculture ponds, and roads due to intensive infrastructure construction by the Coastal Development Corporation. For salt marshes, which include *Suaeda salsa*, *Spartina alterniflora*, and *Phragmites australis*, the total area increased by 20.74% in 2022 compared to 2018. When the Tiaozini Wetland was nominated as a World Heritage site in 2018, the large, contiguous mudflats and high carbon-storage salt marshes of the Tiaozini Wetland finally survived potential reclamation. Hence, its unique charm has the opportunity to attract more tourists and also provide rich ecosystem services for local organisms and biodiversity.

3.2 Top-down eco-governance: rapid transformation and adaptive management

The reclamation of Tiaozini began in the 1970s with the national policy of *More Land from the Sea* (Ding et al., 2011; Wang et al., 2012; Li et al., 2016). At the beginning of this century, land resources in Jiangsu Province became scarce. Reclamation of coastal wetlands turned to land reserve resources for ports, industrial parks, or aquaculture ponds with urbanization and industrial development. In June 2009, *Jiangsu Coastal Area Development Plan* was approved by the State Council of the People's Republic of China. Therefore, land acquisition from the sea had accelerated since the Provincial Bureau issued *the Outline of Jiangsu Coastal Tidal Flats Reclamation and Development and Utilization Planning (2010-2020)* in 2010 (Zhang et al., 2013; Li et al., 2015; Xu et al., 2017; He et al., 2021). The outline clearly stated three stages for Jiangsu coastal tidal flats reclamation, with the objective of acquiring 1800 km^2 of land in the radial sand ridges. The Tiaozini Wetland was primarily listed in the first development stage for 230.67 km^2 of land reclamation with three steps. As Figure 3 shows, the project finished Step I of 67.73 km^2 of lands from the intertidal zone in 2014, mainly for the usage of aquaculture and agriculture, covering the interconnecting beach between Liangduo Estuary and the north side of Fangtang River sluice (Wang et al., 2012; Li et al., 2016; Sha and Wang, 2021; Yu et al., 2022).

During the internal construction phase, the national coastal development strategy shifted from exploitation to conservation and restoration. The 18th National Congress of the Communist Party of China incorporated ecological civilization construction into the five-sphere Integrated Plan for building socialism with Chinese characteristics, setting the goal of building a beautiful China. The congress also made it clear that China should "enhance its capacity to utilize marine resources, develop marine economy, protect the marine ecological environment, resolutely safeguard China's maritime rights and interests, and build itself into a maritime power", marking the construction of marine ecological civilization being elevated to the height of national strategy (Xu et al., 2016; Ma et al., 2021; Huo et al., 2022; Lei et al., 2022; Li et al., 2022; Zhang et al., 2022). Since then, China had made a series of important plans for ecological civilization construction at the national level, such as the *Implementation Plan for Marine Ecological Civilization Construction*, *Suggestions for Establishing the Marine Ecological Red Line System*, the *Wetland Protection and Restoration Scheme*, and the *Blue Bay Initiative*. As a result, the development model of the marine economy was shifted as the earlier wetland reclamation planning was delayed or canceled. China's coastal restoration has entered a rapid development stage in recent years with the policy of ecological civilization construction. There are various projects focusing on different types of coastal ecosystems, including tidal flats, mangroves, and sandy beaches in the coastal zone. More than 125 restoration projects are being carried out along the Chinese coast. (Liu et al., 2016; Chen et al., 2019; Li et al., 2022). Thus, Tiaozini's Step II reclamation plan was not approved for further construction, nor was Step III.

In December 2016, Yancheng City proposed the application procedure for the Yellow Sea Wetland as a World Heritage site. Tiaozini was included in the nomination list for World Natural Heritage Site through the joint efforts of the local government, NGOs, scientific committee, and environmentalists. From then on, the original reclamation plan was delayed. The local departments quickly shifted the early former policy to restoration and implemented adaptive management to tidal wetlands conservation. The municipal government announced the establishment of Tiaozini Municipal Wetland Park in February 2019. As of 5 July 2019, Migratory Bird Sanctuaries along the Coast of Yellow Sea-Bohai Gulf of China (Phase I) was declared as a World Heritage site by the United Nations Educational, Scientific and Cultural Organization (UNESCO), and was also listed as China's first coastal wetland natural heritage site. As an important part of the Natural Heritage Site, the Tiaozini Wetland completely abandoned the previous reclamation plan and implemented a series of bottom-up activities to realize top-down eco-governance concepts instead, such as converting 11.33 km^2 of fish ponds into wetlands, creating the 720 HUPIZ, and establishing breeding grounds for *Larus saundersi*.

3.3 Bottom-up activities: comprehensive conservation and management

Conservation measures and adaptive management strategies were decided, such as the nature-based planning of landscape and infrastructure, exhibitions focused on biodiversity conservation, environmental education, and media dissemination. Ecotourism in the Tiaozini Wetland developed at the very beginning of the shift phase in 2019, and in less than four years multiple ecotourism products were developed to attract tourists. Besides, a comprehensive recreation center focusing on residents, visitors, and businesses, a sanatorium and space for conferences are being built so as to provide up-market service for whoever needs it, with the aim to promote ecotourism in Tiaozini.

3.3.1 Supervision and management of the ecological environment

The Tiaozini management company converted 0.48 km^2 of fishponds to wetlands and used it as the 720 HUPIZ to provide a

habitat for waterbirds by restoring micro-topography, strictly controlling weed height, and maintaining water quality and water level. To the north of the wetland restoration area, 1.87 km^2 of breeding grounds for *Larus saundersi* were designated with full-time guards patrolling 24 hours a day during the breeding season. Moreover, the company applied a timely intelligent management system for surveillance, with 317 network cameras for bird watching, science popularization, research and education.

3.3.2 Nature-based planning of landscape and infrastructure

Tiaozini successively carried out the project of paving, widening, landscaping, and installing guardrails on the 45 km-long coastal road, with the opening of a visitor center, four break areas, and several parking lots. Tourist attractions such as "Watching the Sea and Listening to the Tide", "Habitat at High Tide Level", and "Breeding ground of *Larus saundersi*" were launched along the seawall. In all, 28 internet-famous sites such as "Two Halves of Water", "One-line Tide", "Wetland Chinese Red", "Mirror of the Sky", and "Tidal Forest" were designed based on the natural landscapes. And the company set up 26 high-power telescopes to enhance the visiting experience. At the same time, in Jianggang, the town near Tiaozini, infrastructure, such as Magnotel, James Joyce Coffetel, Yucun bar, and Tiaozini seafood restaurant, was built to provide tourists with accommodation and catering.

3.3.3 Creation of the multi-platform propaganda position

As the saying goes, "Deeply buried gold cannot shine." Although Tiaozini has made some achievements in ecological restoration, conservation, and infrastructure improvement, laying a good foundation for ecotourism, there is still a need to attract more visitors. In addition to promoting the fascinating wetland scenery and ecological restoration achievements through TV programs, newspapers, and magazines, the management company also relies on new media to carry out online live broadcasting and offline market promotion meetings to promote Tiaozini on multiple platforms.

3.3.4 Development of diverse ecotourism products based on natural heritage

Taking advantage of its World Heritage site status, Tiaozini developed several kinds of nature-based products that both met visitors' expectations and enhanced their experience. More than 40 cultural and creative products such as journals, bookmarks, key rings, jigsaw puzzles, and umbrellas, with coastal wetland elements, such as Spoon-billed Sandpiper, Saunders' Gull, mudskipper, and tide, have been developed. It has become an internet-famous site for WeChat influencers to take selfies with tourist routes, e.g., "Be Close to the World Heritage", "Bird Paradise · Ecological Dongtai", and "Coastal Wetland · World Heritage Tour". Tiaozini organizes thematic activities such as "Beach Fun", "Bird Week", bird scenery photography contests, wetland triathlons, etc., guiding tourists to go into the wetland, enjoy the wetland and participate in protection. Folk performance comes from local fishermen who dress in traditional costumes to help visitors learn about the local fishing culture, such as "Fishing Trumpet", "Picking Shellfish", "Weaving and Mending Nets", and "Casting nets". They earn their living by performing, which also preserves local culture as a kind of alternative livelihood.

3.3.5 Promoting the construction of a recreation center

Tiaozini Wetland has two outstanding advantages of "coastal wetland" and "migratory birds paradise", which is a perfect place for recreation and leisure, science popularization, and as a sanatorium. Focusing on the target audience in the Yangtze River Delta, Tiaozini plans to build a healthy and livable coastal town in Jianggang, which would promote the ecotourism industry and help people live a high-quality green life.

3.4 An example from ecotourism design: response from annual tourists

3.4.1 Annual tourist arrivals

The Tiaozini Wetland received 266,000 tourists in 2021 (data source: Tiaozini Scenic Spot Management Company, 2021, unpublished), with the exception of early August through mid-September due to closure for facility maintenance. Figure 5 shows the 2021 daily tourist arrival data. It can be seen that visitation displayed a perfect peak-forest structure corresponding to national holidays, such as Tomb Sweeping Day, International Labor Day, the Dragon Boat Festival, summer vacation, the Mid-Autumn Festival, and the National Day of October 1st. The regular change of visiting time in Tiaozini Wetland agreed with most of the famous tourist sites in China (Sun and Zhou, 2011; Zhang and Sun, 2014; Rong et al., 2020; Ma et al., 2021), indicating that Tiaozini has become, within 3 years, a healthy scenic spot.

The Tiaozini Wetland is located on the middle east coast of China with approximately 200 km direct distance to the northeast of the Yangtze River estuary. This area shows distinct four-season changes of spring, summer, fall, and winter with the northern subtropical monsoon climate. Therefore, in the cold season, from January to March, fewer tourists come to Tianzini, except naturalists and bird watchers. More tourists come here with daily rising temperatures. When the weather warms up, the number of tourists begins to increase and fluctuate. The annual peak season is from the beginning of May to the end of October, corresponding to the holiday and warm seasons. As the temperature gradually drops in early November, tourism shifts from the peak season to the off-season. In addition, the zigzag peaks could also be clearly described as weekly peaks due to weekend visitors. Apart from the climate, the data show that tourism in Tiaozini is connected to people's working schedules and holiday systems, with most visitors preferring to travel on weekends and holidays.

It should be mentioned that COVID-19 also posed some negative impacts on tourist arrivals. However, tourism in Tiaozini still showed an overall rising trend in 2021, which to some extent reflected the great achievements based on advisable eco-governance, development strategies, and remarkable eco-tourism design.

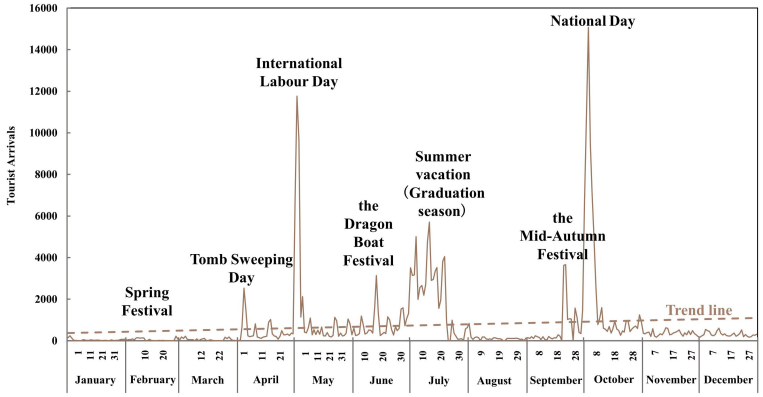

FIGURE 5
The annual tourist arrivals in 2021. Main peaks are noted in the figure, including Spring Festival (February 12th), Tomb Sweeping Day (April 4th), International Labor Day (May 1st), the Dragon Boat Festival (June 14th), summer vacation or graduation season (July to August), the Mid-Autumn Festival (September 21st), and National Day (October 1st).

3.4.2 Monthly tourist arrivals

We took a deep dive into the monthly variation of Tiaozini ecotourism. The number of tourists in January, April, July, and November were selected based on the peak-forest structure and off/peak seasons, as seen in Figure 5. As shown in Figure 6, the number of visitors in January was generally low, peaking in the first few days of the month with fewer than 250 visitors over the New Year's holiday. Tomb Sweeping Day (Qingming Festival, in Chinese) is a traditional holiday dedicated to the memory of deceased relatives, and most people choose to make a short trip after the memorial ceremonies. Therefore, Tiaozini received 2,527 tourists on April 4th as the first peak of the year. The average tourist number was approximately 400 per day in April. Tourism peak season came in July and August corresponding to the summer vacation and graduation season. The number of tourists increased greatly and there were approximately 2,110 tourist arrivals every day. Besides, the number of tourists reached the lowest at the end of July due to the closure of the scenic spot. In November, the off-season of Tiaozini tourism began, and the overall number of tourists showed a downward trend with fluctuation at a low level, approximately 400 per day.

International Labor Day in May and National Day on October 1st are called golden weeks for tourism with 7 days off work in mild and comfortable seasons in China. Both holidays revealed peaks in the tourist numbers, with average daily visitors of 6,261 and 8,121, respectively, of which the highest was over 10,000 per day Figure 7. After the holidays, the daily amount stabilized at around 500 and 700, respectively, after the golden weeks. These two holiday dates showed similar characteristics of peak forest structure. It is worth mentioning that the peak of tourist numbers occurred on May 2nd and October 3rd during the Chinese Golden Weeks. It is inferred that there was a lag effect of 2-3 days in tourist arrivals during the holidays as travelers had to spend one or two days to reach their destinations at the beginning or end of the holidays.

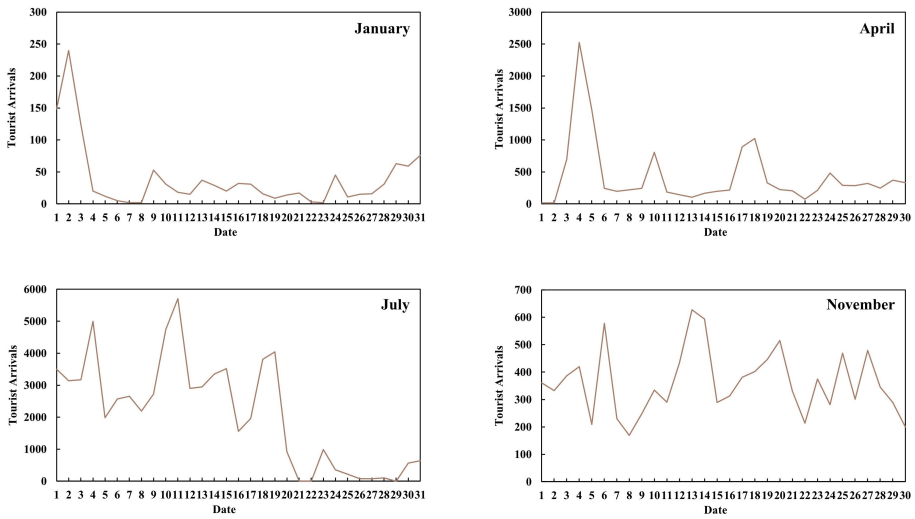

FIGURE 6
The variation of tourist arrivals in typical months (January, April, July, and November).

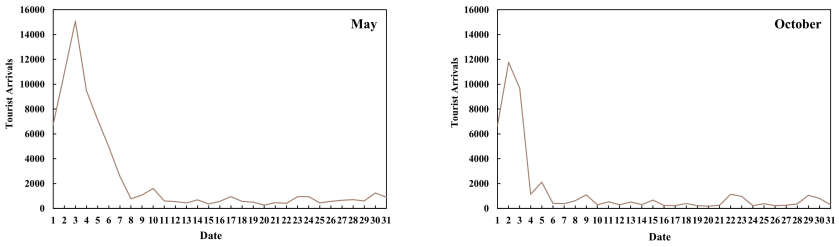

FIGURE 7
The variation of tourist arrivals in May and October.

3.4.3 Tourist arrivals on each weekday in 2021

The number of tourists within 7 weekdays indicated when and how long they would stay in the Tiaozini Wetland. There was a significant difference between weekdays and weekends according to the number of weekly tourists. We found that the number of visitors to Tiaozini on Saturdays and Sundays was much higher than that on weekdays, accounting for nearly 50% of the tourists in 2021 (Figure 8). Tourist arrivals on Fridays accounted for 10%, whereas tourists arriving on Mondays accounted for 17%, which was higher than that of the other four weekdays.

3.5 Stakeholders collaboration, public participation, and environmental education

Six stakeholders were identified: Tiaozini management company, local residents, tourists, the scientific committee, NGOs, and the media. Figure 9 illustrates the relationship between the six stakeholders. Tiaozini management company is the primary stakeholder with the use rights of Tiaozini Wetland. It also fulfills its obligations to maintain infrastructure and manage and develop ecotourism activities.

3.5.1 Local residents

The local coastal residents have the birthright to fish in the sea and use coastal wetlands for survival and livelihood. Local stakeholders are involved in a trade-off between the benefits they receive from tourism and the loss of their historical rights to wetland usage. If they perceive the costs of ecotourism to outweigh the benefits, they will withdraw their support. Therefore, it is incumbent on a tourism-responsible person to try to optimize the well-being of local residents whilst minimizing the costs of tourism development (Sharpley, 2013; Bu et al., 2021). Accordingly, it is also indispensable to provide alternative livelihoods and vocational training for the local residents to increase job opportunities.

In Tiaozini, fishermen are still allowed to engage in productive activities in the coastal area. However, the Tiaozini management company also provides more employment opportunities for local residents. Folk performances related to fishing, clam digging, and other mudflat production activities are scripted into live shows that are performed for tourists at festivals or organized tour groups. All performers come from local communities and used to be fishermen. Well-paid salaries and respect encourage them to actively participate in their new jobs and in wetland protection. Alternative livelihoods, such as folk performers, landscapers, lifeguards, drivers, and tour guides, provide local people with various employment opportunities instead of fishing or other production activities in mudflats. Local people also act as trainees, regularly receiving the knowledge of public awareness of environmental protection and biodiversity conservation offered by

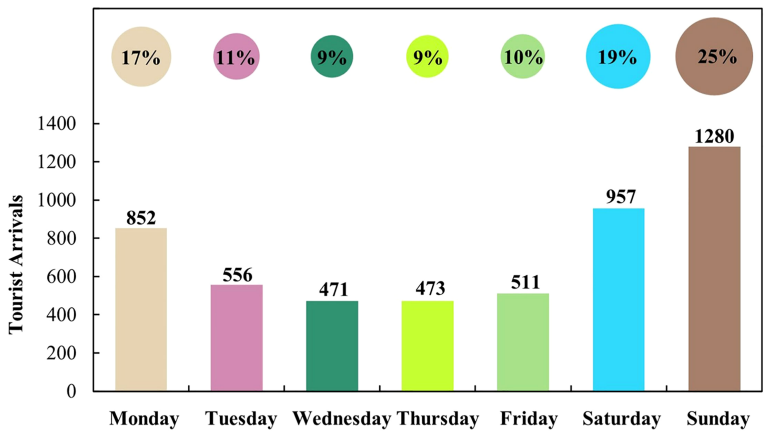

FIGURE 8
Tourists arrival numbers per each weekday. The bar represents the amount of tourists and the filled circle represents the proportion.

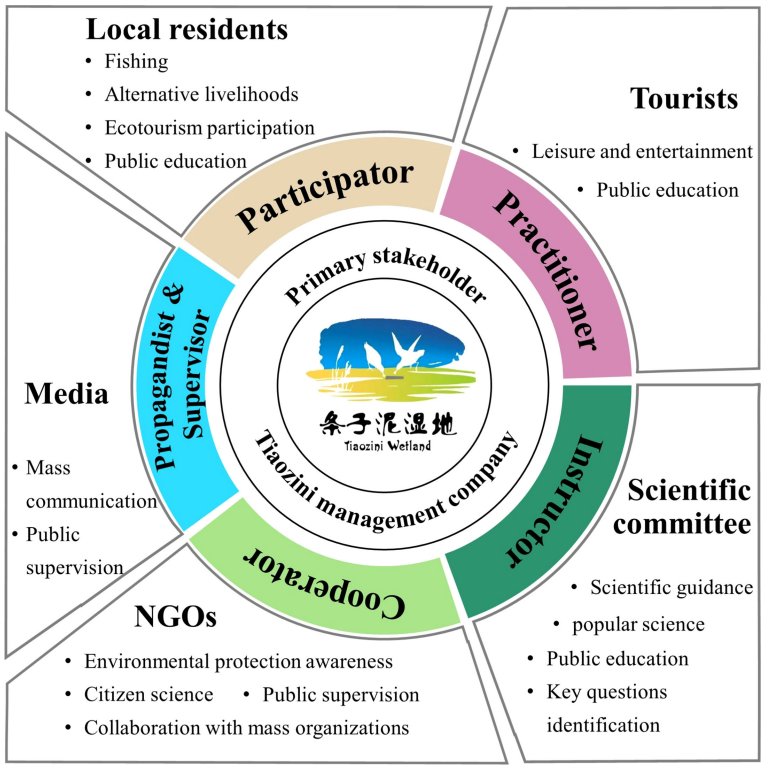

FIGURE 9
Stakeholders' collaboration in Tiaozini eco-governance, showing functions of each role.

the Tiaozini management company. The perceived win-win benefits from ecotourism managers and local stakeholders brought positive effects in terms of economic development, wetland protection, and biodiversity conservation.

3.5.2 Scientific committee

The scientific committee plays a very important role in the wise use of the Tiaozini Wetland, top-down eco-governance, NGO collaboration, and bottom-up adaptive management related to ecotourism development and biodiversity conservation. The Tiaozini Wetland Center offers a laboratory of over 5000 m^2 for professors and students from universities and other academic institutions to carry out research on coastal wetlands. Their original findings related to the Tiaozini Wetlands mostly provide enlightening and concrete visions to local officials, which helps them in eco-governance decision-making. The theoretical guidance that focuses on the identification of key issues used to serve as an important part of ecotourism management, popular science, and public education. In turn, the ecotourism and eco-governance practice in the Tiaozini Wetland has become a realistic laboratory for coastal wetlands management in China.

3.5.3 Tourists

In general, ecotourism is the business of providing vacations and related services that do not harm the environment of the visited area. Economic activities that are environmentally friendly to nature are part of the low-level demands of ecotourism. In addition, it is the responsibility of destinations to provide ecological education for tourists on natural habitats (Powell and Ham, 2008; Lee, 2021). Ecotourism in Tiaozini meets the basic requirements for both environmental protection and economic development. However, the Tiaozini management company tries to promote the nature experience for tourists by being deeply involved in mudflats activities, such as *Meretrix meretrix* L. digging, finding macrobenthos, and bird watching. In addition, the Tiaozini Wetland Committee also tries to educate tourists about both environmental protection and science propagation. Many ecotourism products are developed to enhance tourists' experience of wetland culture, such as clock sites, cultural and creative products, performances in festivals, commemoration days, or anniversaries of important events.

3.5.4 NGOs

The Tiaozini Wetland Center develops good collaboration with many NGOs, such as Shenzhen Mangrove Conservation Foundation (MCF), Spoon-billed Sandpiper Conservation Alliance, Friends of Nature (FON), and so on. One of the missions of NGOs in Tiaozini is to raise public awareness about biodiversity conservation, especially of some flagship species such as *Eurynorhynchus pygmeus*, *Platalea minor*, *Grus japonensis*, *Calidris tenuirostris*, and *Elaphurus davidianus*. The NGOs played a very important role in establishing communication channels through various talks, meetings, workshops, and conferences, either on formal or informal occasions. They are actively involved in ecotourism development plans and provide crucial technical,

financial, educational, and construction support for Tiaozini tourism. NGOs also bridged partnerships to undertake specific conservation projects, helping to organize and empower local communities and provide financial support (Romero-Brito et al., 2016; Wondirad et al., 2019).

3.5.5 Media

The media refers to television, radio, newspapers, and magazines, as well as platforms such as WeChat, Tiktok, and other social media services. The media plays an irreplaceable role in promoting tourism sites and in spreading ecotourism knowledge propagation and environmental education. The Tiaozini management company uses all the abovementioned media for both biodiversity conservation and ecotourism development. Its official account on WeChat provides daily information on the weather, tides, transportation, and available activities, providing convenience for tourists. On the other hand, both tourism activities and infrastructure construction in Tiaozini are under public supervision by the media. The Tiaozini management company has established good communication with many traditional media, such as The People's Daily, China News, and Guangming Daily. It also launches many programs on China Central Television, Jiangsu Television, and so on. New media represented by WeChat, TikTok, Xiaohongshu, and search engines also play an increasingly important role in publicizing the ecological conservation and tourism development of Tiaozini. These media also provide ecological education and popular science to the public, which is not limited to tourists in Tiaozini, drawing their eyes to this new wetland attraction site.

4 Discussion

4.1 Wise use of the Tiaozini Wetland

National policy, such as the Five-Year Plan, dominates land use changes. The land use analysis and top-down eco-governance studied in the present research were consistent with the national policy. Before 2019, the Tiaozini Wetland was on the list for reclamation, and less attention was paid to maintaining its "ecological character" and biodiversity conservation. However, the successful approval of the Tiaozini Wetland as a World Heritage site stopped the reclamation and converted measures into conservation in July 2019. Then, ecological restoration and environmental protection were vigorously promoted by wetland managers with a top-down eco-governance policy.

To achieve sustainability and the wise use of a natural heritage site, it is essential to recognize that support and resources from multiple stakeholders are the most dominant power. The management company cooperated with scientific committees, NGOs, the media, and other stakeholders to develop a new sustainable field for the Tiaozini Wetland, facing the dilemma of sharp conversion from exploitation to conservation with bottom-up activities for better accommodating nature-based solutions (Figure 10).

As the primary stakeholder, the Tiaozini management company adopted diverse approaches to developing ecotourism, including environment monitoring, nature-based planning of landscape, infrastructure construction, multi-platform publicity, diverse cultural and creative production, and recreation center promotion.

Governments often choose ecotourism as a strategy for local economic growth (Lee, 2021), and this was the case with the Tiaozini Wetland. Ecotourism has, in some circumstances, made a significant contribution to sustainable development, but this requires careful governance, compromise, and effective stakeholder collaboration and partnerships (Wall, 1997; Song, 2005; Kuang, 2010; Todd et al., 2016; Wondirad et al., 2020; Salman et al., 2021; Salman et al., 2022). Fortunately, the Tiaozini Scenic Spot Management Company effectively involved multiple stakeholders in ecotourism. Tiaozini tourism income reached 26.60 million *yuan* (approximately US$ 3.85 million with an exchange rate of 6.91, 11 May 2023) in 2021 even with the negative impacts of COVID-19. Tiaozini also plays a far-reaching role in science popularization and education while protecting coastal wetlands,

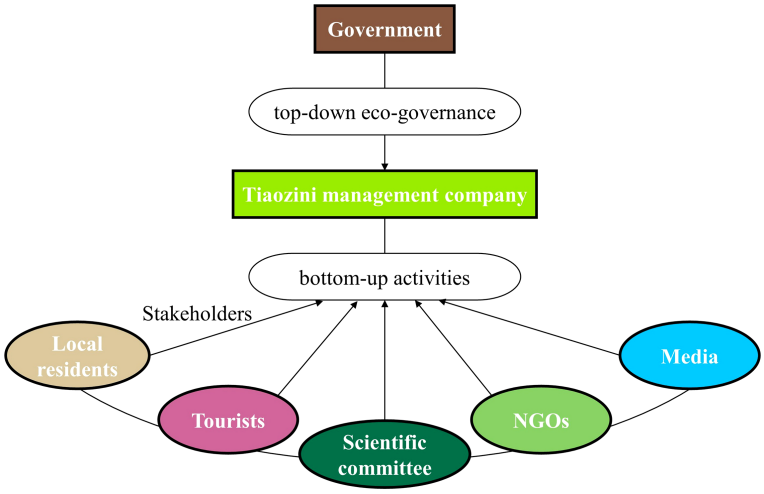

FIGURE 10
Conceptual framework of the wise use of the Tiaozini Wetland.

providing more job opportunities, and improving income for the local community.

The Convention for Wetlands was signed in 1971 as part of a global effort to mitigate the loss and degradation of the world's wetlands (Gell et al., 2016). The Convention is an international treaty for the conservation and wise use of wetlands. All joining Parties of the Ramsar Convention commit themselves to work towards the "three pillars" of the Convention: ① Ensuring the conservation and wise use of wetlands it has designated as Wetlands of International Importance; ② Including as far as possible the wise use of all wetlands in national environmental planning, and ③ Consulting with other Parties about the implementation of the Convention, especially in regard to transboundary wetlands, shared water systems, and shared species (Ramsar Convention Secretariat, 2002). The Convention defines wise use of wetlands as "their sustainable utilization for the benefit of humankind in a way compatible with the maintenance of the natural properties of the ecosystem" and sustainable utilization as "human use of a wetland so that it may yield the greatest continuous benefit to present generations while maintaining its potential to meet the needs and aspirations of future generations". The Tiaozini Wetland provides the best example of not only the wise use of wetlands but also the sustainable utilization of coastal wetlands development and protection, which could be shared and replicated in other places.

4.2 Biodiversity conservation

The Yancheng government spent a huge amount of money on tidal flats reclamation. The original economic input was to keep the Arable Land Dynamic Balance Policy by acquiring more "agricultural land" from the sea and compensating for its loss due to economic development. The local government lost the opportunity for further industrial development after the sharp shift in Tiaozini's management from exploitation to conservation in 2019. However, the ecological benefits are clearly visible to marine biodiversity, especially migratory birds in the East Asian Australian Flyway (EAAF).

In early October 2021, more than 130,000 birds were observed in the Tiaozini Wetland. The number of bird species reached 410 in 2021, among which 21 species were listed in the first-class, and 71 species in the second-class of national protected animals. For local shorebirds and migrating birds, the Tiaozini Wetland is located in the heart of the EAAF and provides a significant amount of macrobenthos for them as breeding grounds, brooding grounds, moulting grounds, and stopovers. The EAAF is considered one of the most important and critically threatened flyways among the nine flyways. Migratory birds dependent on the Yellow Sea ecosystem have attracted more international attention than birds in their regional habitats. As an important part of the Yellow Sea ecosystem, the Tiaozini Wetland plays a significant role in biodiversity conservation and large marine ecosystem protection.

The Tiaozini Wetland was rated as a National AAAA (4A) Class Scenic Spot by the end of 2021. According to China's standard, scenic spots are graded from A (1A) to AAAAA (5A), corresponding with gradually higher attraction and better travel experience. Tiaozini's eco-governance achievements were also nominated as China's sample of sustainable development of natural heritage protection. Therefore, Tiaozini was selected as the Beautiful Bay Excellent Case in 2021 by the Ministry of Ecology and Environment of China.

4.3 Further development of ecotourism

Tourist arrivals in Tiaozini showed obvious seasonal characteristics reaching the peak season from May to October. During the holidays, the number of tourists increased significantly, especially during the May Day and the Chinese National Day holidays, with an obvious peak in the middle of the holidays. In addition, tourists to the Tiaozini Wetland were mostly composed of group tours, packaged-student tours, and family tours, mainly from surrounding areas. The Tiaozini Wetland should continue to promote coastal ecological restoration, strengthen biodiversity conservation, and maintain ecotourism development. Given the seasonal effects, it is essential to develop more ecotourism products to attract more tourists with various demands in the off-season.

It is worth noting that ecotourism products refer to the combination of resources, facilities, and services provided to satisfy tourists' demands, including physical products, activities, and services, and incongruous ecotourism products can result in the failure of the ecotourism industry (Ghorbani et al., 2015; Arsic et al., 2017; Ab Azis et al., 2018). The UNESCO World Heritage is a recognized tourism branding tool to promote destinations (Ryan and Silvanto, 2011), and is used in the case of Tiaozini Wetlands. The rich biodiversity and amazing natural seascape of the Tiaozini heritage site were attractive to children and adolescents, with parents being willing to provide their children with popular science education through ecotourism in Tiaozini. Thus, the ecotourism products of Tiaozini, such as visit routes, activities, and cultural and creative products should be more oriented to teenagers and have more connection with their knowledge system.

5 Conclusion

The research paper systematically revealed the sharp conversion from wetlands drainage/reclamation for agriculture, aquaculture, and industry usage to sustainable utilization, and ecotourism, towards a wiser use of the Tiaozini Wetland. Under the top-level design of eco-governance, adaptative management, and bottom-up activities, Tiaozini management company showed quick action for ecological issues and cooperated with many stakeholders, realizing the rapid transformation from tidal flats reclamation to the sustainable development of ecological environmental protection and economy. The wise use of the Tiaozini Wetland has further demonstrated the immense value of marine biodiversity conservation, especially for those birds migrating through the EAAF. The Tiaozini management company will insist on the wise

use of the wetland as a good example to be shared and replicated in other places around the world.

Data availability statement

The original contributions presented in the study are included in the article/supplementary material. Further inquiries can be directed to the corresponding author.

Ethics statement

Ethical review and approval was not required for the study on human participants in accordance with the local legislation and institutional requirements. Written informed consent from the participants was not required to participate in this study in accordance with the national legislation and the institutional requirements.

Author contributions

JL: investigation, data collection and analyses, and writing the original draft. JT: investigation and data collection. PZ: instruction, writing, reviewing, and editing. ZD: data collection. WJ: investigation. JJ: investigation. YY: instruction, writing, and reviewing. All authors contributed to the article and approved the submitted version.

Funding

This work was supported by the National Key Research and Development Program of China under Grant No. 2017YFC0506506 and the Marine Science & Technology Innovation Project of Jiangsu Department of Natural Resources with Grant No. Of JSZRHYKJ202213.

Acknowledgments

We thank Mr. Weiguo Wang from Dongtai Coastal Economic Zone Management Committee for his help with data collection.

Conflict of interest

The authors declare that the research was conducted in the absence of any commercial or financial relationships that could be construed as a potential conflict of interest.

Publisher's note

All claims expressed in this article are solely those of the authors and do not necessarily represent those of their affiliated organizations, or those of the publisher, the editors and the reviewers. Any product that may be evaluated in this article, or claim that may be made by its manufacturer, is not guaranteed or endorsed by the publisher.

References

Ab Azis, S. S., Sipan, I., Sapri, M., and Zafirah, A. (2018). Creating an innocuous mangrove ecosystem: understanding the influence of ecotourism products from Malaysian and international perspectives. *OCMA* 165, 416–427. doi: 10.1016/j.ocecoaman.2018.09.014

Arsic, S., Nikolic, D., and Zivkovic, Z. (2017). Hybrid SWOT-ANP-FANP model for prioritization strategies of sustainable development of ecotourism in national park djerdap, Serbia. *For. Pol. Econ.* 80, 11–26. doi: 10.1016/j.forpol.2017.02.003

Bu, Y., Wang, E., and Yu, Y. (2021). Analysis on asymptotic stabilization of eco-compensation program for forest ecotourism stakeholders. *Environ. Sci. pollut. Res.* 28, 29304–29320. doi: 10.1007/s11356-021-12703-5

Campbell, A. D., Fatoyinbo, L., Goldberg, L., and Lagomasino, D. (2022). Global hotspots of salt marsh change and carbon emissions. *Nature* 612 (7941), 701–706. doi: 10.1038/s41586-022-05355-z

Cao, M. C., Liu, W., Liu, B., and Sun, X. P. (2019). Yancheng costal wetland and waterfowls' habitat protection. *Environ. Ecol.* 1 (1), 74–79.

Chen, K. L., Yang, X. Z., and Lu, Y. (2015). Vital stopover of shorebirds migration on the EastAsian-Australasian flyway: wetlands of yellow Sea and bohai Sea. *Wetl. Sci.* 13 (1), 1–6. doi: 10.13248/j.cnki.wetlandsci.2015.01.001

Chen, B., Yu, W. W., Chen, G. C., Zheng, X. Q., Huang, H. P., Hu, W. J., et al. (2019). Coastal wetland restoration: an overview. *J. Appl. Oceanogr.* 38 (4), 464–473. doi: 10.3969/J.ISSN.2095-4972.2019.04.002

Davidson, N. C. (2014). How much wetland has the world lost? long-term and recent trends in global wetland area. *Mar. Freshw. Res.* 65 (10), 934–941. doi: 10.1071/MF14173

Davidson, N. C., and Finlayson, C. M. (2018). Extent, regional distribution and changes in area of different classes of wetland. *Mar. Freshw. Res.* 69 (10), 1525–1533. doi: 10.1071/MF17377

Deegan, L. A., Johnson, D. S., Warren, R. S., Peterson, B. J., Fleeger, J. W., Fagherazzi, S., et al. (2012). Coastal eutrophication as a driver of salt marsh loss. *Nature* 490 (7420), 388–392. doi: 10.1038/nature11533

Ding, X. R., Kang, Y. Y., Ge, X. P., Li, Q., and Zhang, T. T. (2011). Tidal flat evolution analysis using remote sensing on tiaozini flat of the radial sand ridges. *J. Hohai Univ. (Nat. Sci. Ed.).* 39 (2), 231–236. doi: 10.3876/j.issn.1000-1980.2011.02.021

Finlayson, C. M., Davidson, N., Pritchard, D., Milton, G. R., and MacKay, H. (2011). The ramsar convention and ecosystem-based approaches to the wise use and sustainable development of wetlands. *J. Int. Wildl. Law Policy.* 14 (3–4), 176–198. doi: 10.1080/13880292.2011.626704

Gao, S., Liu, W., Zhang, S., Yi, J. F., and Wang, Z. (2021). Diversity of wintering waterbirds in Tiaozini Wetland of Dongtai and Rudong Wetland, Jiangsu Province. *J. Ecol. Rural Environ.* 37 (9), 1776–1182. doi: 10.19741/j.issn.1673-4831.2020.0862

Gell, P. A., Finlayson, C. M., and Davidson, N. C. (2016). Understanding change in the ecological character of ramsar wetlands: perspectives from a deeper time – synthesis. *Mar. Freshw. Res.* 67 (6), 869–879. doi: 10.1071/MF16075

Ghorbani, A., Raufirad, V., Rafiaani, P., and Azadi, H. (2015). Ecotourism sustainable development strategies using SWOT and QSPM model: a case study of kaji namakzar wetland, south khorasan province, Iran. *Tour. Manage. Perspect.* 16, 290–297. doi: 10.1016/j.tmp.2015.09.005

He, L., Li, G. S., Cui, L. L., Li, L. J., Chen, Y. H., and Tu, X. S. (2021). Coupling relationship between reclamation and social economics development in north jiangsu coastal area. *Acta Ecol. Sin.* 41 (23), 9228–9238. doi: 10.5846/stxb202007161869

Hu, W., Chen, T. Y., Xu, Z. P., Wu, D. W., and Lu, C. H. (2022). Occurrence dataset of waterbirds in the tiaozini wetland, a world nature heritage, China. *Biodiver. Data J.* 10, e90724. doi: 10.3897/BDJ.10.e90724

Huo, C. L., Ni, G., You, J. J., Shao, X. J., and Liu, P. X. (2022). Promoting marine ecological civilization *via* ecological environment supervision practice of watershed and marine under coordinated land and marine development. *Environ. Sustain. Dev.* 47 (3), 12–15. doi: 10.19758/j.cnki.issn1673-288x.202203012

Kirwan, M. L., and Megonigal, ,. J. P. (2013). Tidal wetland stability in the face of human impacts and sea-level rise. *Nature* 504 (7478), 53–60. doi: 10.1038/nature12856

Kirwan, M. L., Murray, A. B., Donnelly, J. P., and Corbett, D. R. (2011). Rapid wetland expansion during European settlement and its implication for marsh survival under modern sediment delivery rates. *Geology* 39 (5), 507–510. doi: 10.1130/G31789.1

Kuang, X. J. (2010). Location analysis on stakeholders and theirs role orientation in development of ecological tourism. *J. Cent. South Univ. For. Technol.* 20 (9), 81–84. doi: 10.14067/j.cnki.1673-923x.2010.09.040

Lee, J. H. (2021). Using q methodology to analyze stakeholders' interests in the establishment of ecotourism facilities: the case of seocheon, korea. J. *Ecotour* 20 (3), 282–300. doi: 10.1080/14724049.2021.1883626

Lei, G. Y., Liu, X. R., and Chen, M. R. (2022). Present situation of Chinese marine ecological civilization and its fostering methodology. *Trans. Oceanol. Limnol.* 44 (5), 153–161. doi: 10.13984/j.cnki.cn37-1141.2022.05.022

Li, J. G., Pu, L. J., Xu, C. Y., Chen, X. J., Zhang, Y. F., and Cai, F. F. (2015). The changes and dynamics of coastal wetlands and reclamation areas in central jiangsu from 1977 to 2014. *Acta Geogr. Sin.* 70 (1), 17–28. doi: 10.11821/dlxb201501002

Li, J. L., Shen, M. H., Ma, R. F., Yang, H. S., Chen, Y. N., Sun, C. Z., et al. (2022). Marine resource economy and strategy under the background of marine ecological civilization construction. *J. Nat. Resour.* 37 (4), 829–849. doi: 10.31497/zrzyxb.20220401

Li, M. L., Yang, L., Gong, X. L., Xue, W. Y., Yang, Y., Shi, Y., et al. (2016). The geomorphologic response of accreting intertidal flat to reclamation: a case from jianggang, jiangsu. *Mar. Sci. Bull.* 35 (6), 683–693. doi: 10.11840/j.issn.1001-6392.2016.06.011

Liu, Z. Z., Cui, B. S., and He, Q. (2016). Shifting paradigms in coastal restoration: six decades' lessons from China. *Sci. Total Environ.* 566-567, 205–214. doi: 10.1016/j.scitotenv.2016.05.049

Ma, B. B., Chen, X. P., and Chen, F. T. (2021). Multi-scale temporal and spatial differentiation characteristics of dunhuang tourism flow based on social big data. *Econ. Geogr.* 41 (3), 202–212. doi: 10.15957/j.cnki.jjdl.2021.03.021

Murray, N. J., Worthington, T. A., Bunting, P., Duce, S., Hagger, V., Lovelock, C. E., et al. (2022). High-resolution mapping of losses and gains of earth's tidal wetlands. *Science* 376, 744–749. doi: 10.1126/science.abm9583

Peng, H. B., Cai, Z. Y., Zhang, L., Gan, X. J., Liu, W. L., Li, J., et al. (2017). Distribution and conservation status of the spoon-billed sandpiper in China. *Chin. J. Zool.* 52 (1), 158–166. doi: 10.13859/j.cjz.201701021

Powell, R. B., and Ham, S. H. (2008). Can ecotourism interpretation really lead to pro-conservation knowledge, attitudes and behaviour? evidence from the Galapagos islands. *J. Sustain. Tour.* 16 (4), 467–489. doi: 10.2167/jost797.0

Ramsar Convention Secretariat (2002). *The ramsar strategic plan 2003-2008*. Available at: https://www.ramsar.org/sites/default/files/documents/pdf/key_strat_plan_2003_e.pdf (Accessed January 8, 2023).

Romero-Brito, T. P., Buckley, R. C., and Byrne, J. (2016). NGO Partnerships in using ecotourism for conservation: systematic review and meta-analysis. *PloS One* 11 (11), e0166919. doi: 10.1371/journal.pone.0166919

Rong, H. F., Tao, Z. M., Li, T., Lu, S. Y., and Pu, R. (2020). Spatial-temporal evolution and influencing factors of rural tourist market in southern jiangsu based on network data. *Geogr. Geo-Inf. Sci.* 36 (6), 71–77. doi: 10.3969/j.issn.1672-0504.2020.06.011

Ryan, J., and Silvanto, S. (2011). A brand for all the nations: the development of the World Heritage Brand in emerging markets. *Mark. Intell. Plan.* 29 (3), 305–318. doi: 10.1108/02634501111129266

Salman, A., Jaafar, M., and Mohamad, D. (2021). Understanding the importance of stakeholder management in achieving sustainable ecotourism. *Pertanika J. Soc Sci. Hum.* 29 (1), 731–753. doi: 10.47836/pjssh.29.1.40

Salman, A., Jaafar, M., Mohamad, D., and Khoshkam, M. (2022). Understanding multi-stakeholder complexity & developing a causal recipe (fsqca) for achieving sustainable ecotourism. *Environ. Dev. Sustain.* doi: 10.1007/s10668-022-02488-z

Sha, J. M., and Wang, Y. Y. (2021). The success of application from "find treasure from intertidal zone" to the yellow Sea wetland. *Hundred Year Tide.* 1), 44–53. doi: 10.16624/j.cnki.11-3844/d.2021.01.007

Sharpley, R. (2013). Host perceptions of tourism: a review of the research. *Tourism Manage.* 42, 37–49. doi: 10.1016/j.tourman.2013.10.007

Song, R. (2005). On stakeholders of ecotourism: with China as an example. *China Popul. Resour. Environ.* 15 (1), 36–41. doi: 10.3969/j.issn.1002-2104.2005.01.010

Spencer, T., Schuerch, M., Nicholls, R. J., Hinkel, J., Lincke, D., Vafeidis, A. T., et al. (2016). Global coastal wetland change under sea-level rise and related stresses: the DIVA wetland change model. *Glob. Planet. Change.* 139, 15–30. doi: 10.1016/j.gloplacha.2015.12.018

Sun, G. N., and Zhou, R. N. (2011). Research on the tourists' "peak-forest" structure and its causes of lishan scenic spots. *Hum. Geogr.* 26 (3), 128–134. doi: 10.13959/j.issn.1003-2398.2011.03.022

Todd, L., Leask, A., and Ensor, J. (2016). Understanding primary stakeholders' multiple roles in hallmark event tourism management. *Tourism Manage.* 59, 494–509. doi: 10.1016/j.tourman.2016.09.010

Wall, G. (1997). Is ecotourism sustainable? *Environ. Manage.* 21, 483–491. doi: 10.1007/s002679900044

Wang, Y. G., Chen, C., and Huang, H. M. (2012). Beach reclamation related issues of tiaozini in jiangsu. *Zhejiang Hydrotech.* 1, 4–8. doi: 10.13641/j.cnki.33-1162/tv.2012.01.001

Wang, C., Wang, G., Dai, L. J., Liu, H. Y., Li, Y. F., and Qiu, C. Q. (2021b). Study on the effect of habitat function change on waterbird diversity and guilds in yancheng coastal wetlands based on structure–function coupling. *Ecol. Indic.* 122, 107223. doi: 10.1016/j.ecolind.2020.107223

Wang, X. X., Xiao, X. M., Xu, X., Zou, Z. H., Chen, B. Q., Qin, Y. W., et al. (2021a). Rebound in china's coastal wetlands following conservation and restoration. *Nat. Sustain.* 4, 1076–1083. doi: 10.1038/s41893-021-00793-5

Wang, X. X., Xiao, X. M., Zou, Z. H., Chen, B. Q., Ma, J., Dong, J. W., et al. (2020). Tracking annual changes of coastal tidal flats in China during 1986-2016 through analyses of landsat images with Google earth engine. *Remote Sens. Environ.* 238, 110987. doi: 10.1016/j.rse.2018.11.030

Wang, C., Zhou, Y., Zhang, H. B., Li, Y. F., Liu, H. Y., and Dong, B. (2022). Study on the rare waterbird habitat networks of a new UNESCO world natural heritage site based on scenario simulation. *Sci. Total Environ.* 843, 157058. doi: 10.1016/j.scitotenv.2022.157058

Watson, E. B., Wigand, C., Davey, E. W., Andrews, H. M., Bishop, J., and Raposa, K. B. (2017). Wetland loss patterns and inundation-productivity relationships prognosticate widespread salt marsh loss for southern new England. *Estuaries Coasts.* 40 (3), 662–681. doi: 10.1007/s12237-016-0069-1

Wen, C., Gu, Y., and Huang, Y. (2020). The global comparative analysis on the outstanding universal values of the serial nominated properties of migratory bird sanctuaries along the coast of yellow Sea and bohai Sea in China. *Stud. Nat. Cult. Herit.* 5 (4), 1–12. doi: 10.19490/j.cnki.issn2096-698X.2020.04.001-012

Wondirad, A., Tolkach, D., and King, B. (2019). NGOs in ecotourism: patrons of sustainability or neo-colonial agents? evidence from Africa. *Tour. Recreat. Res.* 45 (2), 144–160. doi: 10.1080/02508281.2019.1675269

Wondirad, A., Tolkach, D., and King, B. (2020). Stakeholder collaboration as a major factor for sustainable ecotourism development in developing countries. *Tourism Manage.* 78, 104024. doi: 10.1016/j.tourman.2019.104024

Xu, Y., Liang, B., Lan, D. D., Bao, C. G., Yu, C. Y., Ma, M. H., et al. (2016). Major issues on marine ecological civilization construction in our country. *Ocean Dev. Manage.* 33 (8), 26–30. doi: 10.3969/j.issn.1005-9857.2016.08.005

Xu, Y., Pu, L. J., Zhang, R. S., Zhu, M., Li, X. Y., Shen, H. Y., et al. (2017). Cropland quality evolution following coastal reclamation at the prograding tidal flats of jiangsu province, China. *Acta Geogr. Sin.* 72 (11), 2032–2046. doi: 10.11821/dlxb201711009

Ye, C. L., and Sun, F. H. (2021). Development of a social value evaluation model for coastal wetlands. *Ecol. Inform.* 65, 101417. doi: 10.1016/j.ecoinf.2021.101417

Yu, X. Z., Ji, Y. B., Wang, L., and Xu, M. (2022). Research on landscape pattern change and driving mechanism in tiaozi mud reclamation area in jiangsu. *J. Nanjing Norm. Univ. (Nat. Sci. Ed.).* 45 (1), 55–63. doi: 10.3969/j.issn.1001-4616.2022.01.009

Zhan, L. C., Ma, F. Y., Chen, J. S., and Xin, P. (2021). Relationship between water salinity and vegetation distribution in the tiaozini reclamation area. *Adv. Water Sci.* 32 (1), 127–138. doi: 10.14042/j.cnki.32.1309.2021.01.013

Zhang, Z. F., He, R., Wu, D. Q., and Qi, Y. (2022). Progress,situation and suggestions of marine ecological civilization construction and ecological environment protection in China. *Environ. Sustain. Dev.* 47 (3), 3–6. doi: 10.19758/j.cnki.issn1673-288x.202203003

Zhang, T. S., and Sun, G. N. (2014). Analysis on the tourist volume "Peak-forest" structure and causes of tourism destinations: a comparison between inbound and domestic tourism of fenghuang, hunan. *Tour. Sci.* 28 (1), 44–53 + 75. doi: 10.16323/j.cnki.lykx.2014.01.008

Zhang, X. X., Yan, C. Q., Xu, P., Dai, Y. X., Yan, W. B., Ding, X. R., et al. (2013). Historical evolution of tidal flat reclamation in the jiangsu coastal areas. *Acta Geogr. Sin.* 68 (11), 1549–1558. doi: 10.11821/dlxb201311010

Zuo, P., Li, Y., Liu, C. A., Zhao, S. H., and Guan, D. M. (2013). Coastal wetlands of China: changes from the 1970s to 2007 based on a new wetland classification system. *Estuaries Coasts.* 36 (2), 390–400. doi: 10.1007/s12237-012-9575-y

frontiers | Frontiers in Marine Science

TYPE Original Research
PUBLISHED 12 July 2023
DOI 10.3389/fmars.2023.1201533

OPEN ACCESS

EDITED BY
Xiuzhen Li,
East China Normal University, China

REVIEWED BY
Feng Liu,
Sun Yat-sen University, China
Qinghua Ye,
Deltares, Netherlands

*CORRESPONDENCE
Jinhai Zheng
jhzheng@hhu.edu.cn
Mingjin Zhang
zhangmingjin@tiwte.ac.cn

RECEIVED 06 April 2023
ACCEPTED 21 June 2023
PUBLISHED 12 July 2023

CITATION
Yang Y, Zheng J, Zhang M and Zhu L (2023) Sediment sink-source transitions in the middle and lower reaches of the Yangtze River estuary.
Front. Mar. Sci. 10:1201533.
doi: 10.3389/fmars.2023.1201533

Sediment sink-source transitions in the middle and lower reaches of the Yangtze River estuary

Yunping Yang[1,2], Jinhai Zheng[2]*, Mingjin Zhang[1]* and Lingling Zhu[3]

[1]Tianjin Research Institute for Water Transport Engineering, Ministry of Transport, Tianjin, China, [2]Yangtze Institute for Conservation and Development, Hohai University, Nanjing, China, [3]Bureau of Hydrology Changjiang Water Resources Commission, Wuhan, China

Human activities have severely altered the Yangtze River (Changjiang) Estuary's pattern, beach-trough shape, and delta in recent decades. Existing research has studied the sediment "source–sink" relationship between the Yangtze River mainstream and estuary using gauged suspended sediment data. This method overestimated the decline in the suspended sediment concentration in the estuary, as riverbed scouring or deposition have not filtered out amounts related to sand mining or waterway dredging. This study took the Yangtze River Basin as the research subject and used spot observed runoff, sediment, and riverbed topography data gathered between 1980 and 2020 to analyze the sediment trapping effect of the Three Gorges Reservoir (TGR) and study the "source-sink" relationship of suspended sediment transport in the middle-lower reaches of the Yangtze River. The Yangtze Estuary Delta is dominated by scouring, which shows an increasing trend. During the operation of the TGR (2003–2020), the suspended sediment load entering the Yangtze Estuary from the Yangtze River mainstream decreased by 68% compared to the amount prior to operation commencing (1960–2002). However, studies have found that there are still large amounts of bottom sand with riverbed load movement characteristics after the operation of the Three Gorges Project and that riverbed souring of the downstream dam has increased the degree of deposition recharge. The amount of sediment in the Yangtze Estuary decreased between 2003 and 2018 compared with the period 1981 to 2002, with an annual decrease of 16.9%. The cumulative deposition of the Yichang–Datong and Datong–Xuliujing reaches from 1981–2002 was 3.13×10^8 m^3 and 1.60×10^8 m^3, respectively, and cumulative scouring from 2002–2018 was 28.52×10^8 m^3 and 16.01×10^8 m^3. This study concluded that even if the suspended sediment load entering the estuary decreased significantly after the operation of the TGR, the riverbed in the middle-lower reaches of the Yangtze River has gradually transformed from the "sink" of sediment deposition to the "source" of sediment supply.

KEYWORDS

source-sink effect, sediment transport, riverbed adjustment, estuary delta, Yangtze estuary

1 Introduction

Estuary deltas act as a "sink", holding sediment from upstream river basins before they flow into the sea. In recent years many estuary deltas around the world have been shrinking, affected by a sharp decrease in the amount of sediment supplied by river basins (Manh et al., 2014) as a result of the construction of upstream reservoirs and dams, and the implementation of river control projects (Yang et al., 2011; Manh et al., 2014). Meanwhile, ground subsidence and rising sea levels have increased the degree of delta submergence and increased scouring power (Dai et al., 2018; Nienhuis et al., 2020; Paszkowski et al., 2021; Schmitt et al., 2021). Statistics on the connectivity of $1{,}200\times10^4$ km rivers globally found that only 37% of them flow freely, and 23% flow into the sea without being uninterrupted, with interruptions mainly due to waterway dredging and dam construction (Grill et al., 2019).

In recent decades, climate change and human activities have had a profound impact on the sediment loads and channel morphology of the Yangtze River in China (Li et al., 2018; Li et al., 2019; Guo et al., 2019; Zhou et al., 2020; Zhou et al., 2021). Waterway engineering construction and waterway dredging excavation have changed the shape of the natural shoal and troughs in the estuary delta (Pan et al., 2012; Dai et al., 2013; Wei et al., 2017; Zhao et al., 2018; Zhu et al., 2019). For example, the deep-water waterway project in the North Passage of the Yangtze Estuary prompted the front edge of the estuary to extend to the sea (Wang et al., 2017). Sediment contains life-nourishing resources for an estuary delta because it establishes a stable platform for vegetation growth (Nittrouer and Viparelli, 2014) and acts as a material source for urban land resource expansion (Zhang et al., 2018).

The construction of reservoirs and dams in the river basin blocks the continuous process of material transport from the river basin to the estuary (Wang et al., 2016), and affects material exchange and estuary resource sustainability (Liu et al., 2023). Some dams on small- and medium- sized rivers have been demolished (East et al., 2015; Warrick et al., 2015; Collins et al., 2017) to increase the material continuity of the rivers and alleviate the impact of sediment decrease in the river basin on estuary deltas. Even though there have been disputes regarding the construction of dams on rivers with abundant water resources, (Latrubesse et al., 2017), hydropower is perceived to be a clean energy source, and the operation of hydropower stations has had a positive effect on reducing global carbon emissions (Almeida et al., 2019; Bertassoli et al., 2021). The "source-sink" relationship of sediment traveling from the river basin to the estuary has always been a focus of research (Yang et al., 2015a; Gao et al., 2018; Gao et al., 2019). Existing studies have focused on the "source-sink" relationship of suspended sediment concentrations (Yang et al., 2014; Yang et al., 2015b; Yang et al., 2015c; Guo et al., 2019). River hydrographic stations have measured suspended sediment concentration, but have failed to observe the adjustment of riverbed shape and the sediments on the surface of river channels with load transfer characteristics. From the perspective of the "source-sink" relationship of suspended sediment concentration from the river basin to the estuary, the effect of bottom sand has not often been considered, and this has led to an overestimation of the reduction of suspended sediment concentration in the estuary (Li et al., 2012; Zou et al., 2012; Jing et al., 2013; Yang et al., 2014; Yang et al., 2020), promoting the belief that the scouring of the Yangtze Estuary will continue or worsen (Luan et al., 2016; Yang et al., 2017; Dai et al., 2018; Luan et al., 2021; Cheng et al., 2022; Tang et al., 2022; Xu et al., 2022). After the operation of the TGR, the middle-lower reaches of the Yangtze River (Xia et al., 2016; Zhou et al., 2018; Yang et al., 2019; Yang et al., 2021a), the tidal reach (Mei et al., 2021; Xie et al., 2021), and its South Branch (Wang et al., 2013; Luan et al., 2016; Zhao et al., 2018; Zhu et al., 2019; Guo et al., 2021a) as well as other areas were all scoured. Some of the fine particles from the riverbed replenished the suspended sediment and entered the estuary with the water flow, making estuarine suspended sediment concentration drops much lower than that in the river basin (Yang et al., 2014; Yang et al., 2015b). Other coarse sediment particles entered the estuary in the form of riverbed bottom sand and spread, causing partial estuary deposition (Guo et al., 2021b). In the calculation of riverbed scouring, full consideration should be given to sand mining (Brunier et al., 2014; Anthony et al., 2015; Bendixen et al., 2019; Xu et al., 2021; Yang et al., 2021a) and waterway dredging (Mossa and Chen, 2021; Yang et al., 2021a; Yang et al., 2021b) otherwise the riverbed scouring intensity is overestimated. Therefore, to scientifically assess the "source-sink" relationship of sediment from the Yangtze River Basin and the estuary, the impact of waterway dredging and land reclamation on riverbed scouring as well as suspended sediment and sand mining needs to be considered.

This study took the Yangtze River Basin as the research subject and used spot observed runoff, sediment, and riverbed topography data gathered between 1980 and 2020 to analyze the sediment trapping effect of the TGR and study the "source-sink" relationship of suspended sediment transport in the middle-lower reaches of the Yangtze River. Factors including riverbed scouring or deposition, sand mining, waterway dredging, and shoal reclamation are considered in this analysis of the impact of the bottom sand "source-sink" relationship on the estuary and future evolution trends of the Yangtze Estuary Delta are discussed.

2 Research area

The total length of the Yangtze River is approximately 6,397 km and its basin size is about 180×10^4 km^2 (Figure 1A). The upper reaches (4,504 km) stretch above Yichang hydrographic station, the middle reaches (955 km) run from Yichang hydrographic station to Hukou hydrographic station, and the lower reaches (938 km) run below Hukou hydrographic station. The TGR was filled and opened in June 2003, and its impoundment level reached 175 m from 2009–2020, the total storage capacity is 39.3 billion cubic meters. The operation of the TGR does not change the total amount of runoff, but the regulation and storage effect reduce the peak flow and increase the minimum flow (Zheng, 2016). On the south bank of the downstream channel of the Three Gorges Dam, Dongting Lake, Poyang Lake, and the Yangtze River form a complex river-lake system. The Hanjiang River on the north bank merges into the

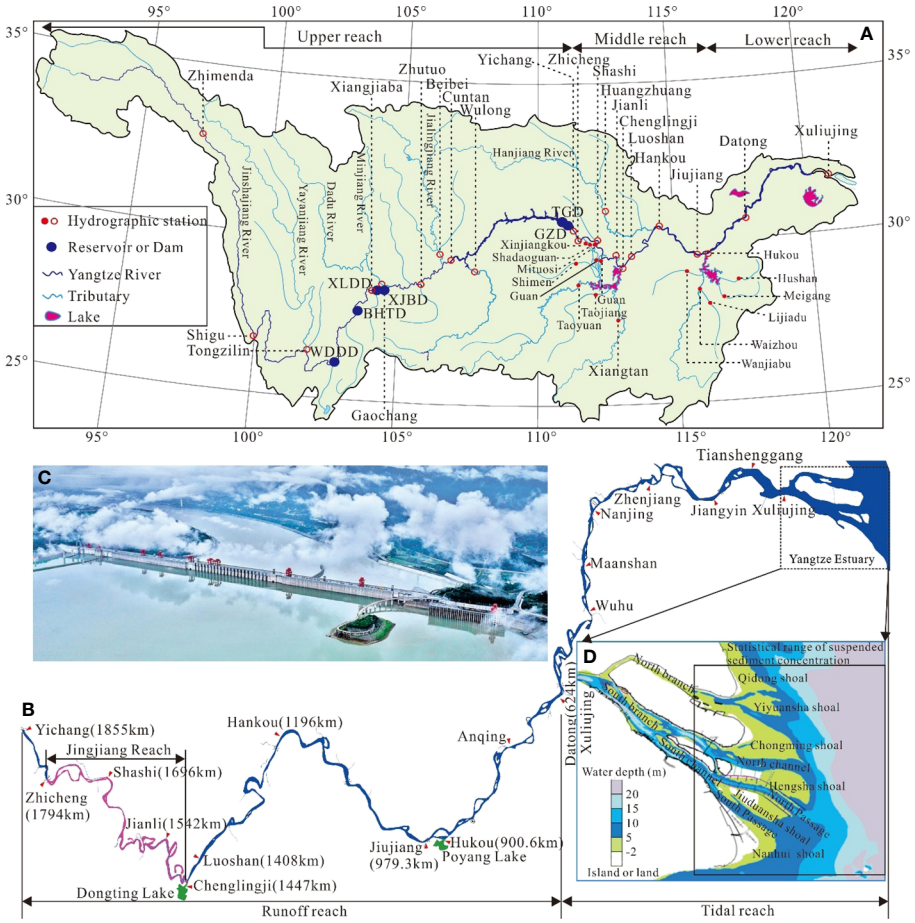

FIGURE 1
Basic information relating to the Yangtze River Basin; **(A)** Yangtze River Basin; **(B)** Three Gorges Dam to estuary; **(C)** Three Gorges Dam; **(D)** Yangtze Estuary. XLDD represents Xiluodu Dam, BHTD represents Baihetan Dam, WDDD represents Wudongde Dam, XJBD represents Xiangjiaba Dam, and GZBD represents Gezhouba Dam.

Yangtze River from Wuhan City (Figures 1A, B). This study takes the section from the TGD to the Yangtze Estuary, the total length of the river's channel is about 1,855 km (Figures 1B, C). Among them, the Yangtze Estuary has a "three-level branching and four outlets" river regime pattern, with Qidong shoal, Yiyuansha shoal, Hengsha shoal, Jiuduansha shoal, Jiangyanansha shoal, Nanhui shoal, and Deltas (Figure 1D).

3 Data collection, and analytical methods

3.1 Data collection

The runoff and sediment load data of the Yangtze River mainstream and tributaries covering the period from 1980–2020 were collected, and the temporal and spatial characteristics of runoff and sediment load changes were analyzed. The riverbed topography data from Yichang hydrographic station to Yangtze Estuary in 1981, 2002, 2011, and 2018 were collected, with a measurement scale of 1:10,000, the vertical measurement error is less than 1.0 cm, and the riverbed scouring volume and intensity were analyzed; the waterway dredging volume, sand mining volume, and land reclamation data from 1984–2020 were collected to analyze the impact of human activities on the intensity of riverbed scouring and bottom sand discharge. The data on the amount of waterway dredging is formed from statistics of the amount of sediment in waterway dredging ships year by year from Changjiang Waterway Bureau. As there is a mixture of water and sediment in the ship, the ratio between the volume of the ship and the amount of excavation on the riverbed is 3:1, following the method from Yang et al. (2021b). The amount of sand mining is the planned amount (Changjiang Water Resources Commission (CWRC); 2004–2022). Due to the uncertainty of illegal sand mining, the planned amount of sand mining is used to analyze the influence

on the riverbed scouring or deposition amount. Research data are shown in Table 1.

3.2 Analytical methods

3.2.1 Sediment exchange and "source-sink" relationship

Treating the discharge of the TGR, riverbed souring, tributaries, and lake exchange as the "source" of sediment and the Yangtze Estuary as the "sink" of sediment. The processes through which sediments travel from "source" to "sink" were analyzed, and the impact of the sediment "source-sink" relationship change on the estuary was studied.

Starting from Yichang hydrographic station ($S_{Yichang}$), we considered the influence of Dongting Lake ($S_{Dongting\ Lake}$), Poyang Lake ($S_{Poyang\ Lake}$), Hanjiang River ($S_{Hanjiang\ River}$), and the inward import relationship of the interval on the sediment amount and the amount of sediment scouring or deposition of the riverbed (S) recharge from Yichang to Datong reaches (Figure 2). Datong hydrographic station (S_{Datong}) is the last hydrographic station of the Yangtze River mainstream. The calculation formula of riverbed recharge suspended sediment from Yichang to Datong reaches is as follows:

$$S = S_{Datong} - S_{Poyang\ Lake} - S_{Hanjing\ River} - S_{Dongting\ Lake} - S_{Yichang} \quad (1)$$

The sediment quantity of Dongting Lake ($S_{Dongting\ Lake}$), into the Yangtze River mainstream is the difference between Chenglingji hydrographic station ($S_{Chenglingji}$) and Three Outlets ($S_{Three\ Outlets}$). The calculation formula is as follows:

$$S_{Dongting\ Lake} = S_{Chenglingji} - S_{Three\ outlets} \quad (2)$$

The Three Outlets at which Dongting Lake diverts sediment from the Yangtze River are Songzikou ($S_{Songzikou}$), Taipingkou ($S_{Taipingkou}$), and Ouchikou ($S_{Ouchikou}$). That is, the formula for calculating the amount of sediment at the three mouths of Dongting Lake is as follows:

$$S_{Three\ outlets} = S_{Songzikou} + S_{Taipingkou} + S_{Ouchikou} \quad (3)$$

The hydrographic station where Poyang Lake merges into the Yangtze River is the Hukou station (S_{Hukou}). Namely:

$$S_{Poyang\ Lake} = S_{Hukou} \quad (4)$$

The hydrographic station where the Hanjiang River merges into the Yangtze River is the Huangzhuang station ($S_{Huangzhuang}$). Namely:

$$S_{Hanjiang\ River} = S_{Huangzhuang} \quad (5)$$

There is no sediment monitoring station in Datong–Xuliujing reaches. A topographic method should be used to calculate the suspended sediment recharge in this section. The river sediment test

TABLE 1 Research data types and sources.

Data type	Period	Data characteristics	Data source
Runoff and sediment	1980–2020	Mainstream and tributaries of the Yangtze River, Dongting Lake, and Poyang Lake	Changjiang Waterway Bureau, Hydrology Bureau of Changjiang Water Resources Committee, Changjiang Hydrographic Survey Center
Riverbed topography	1981–2018	Scale is 1:10,000	
Sand mining	1984–2020	Planning sand production	
Waterway dredging	1980–2020	Amount of channel dredged	

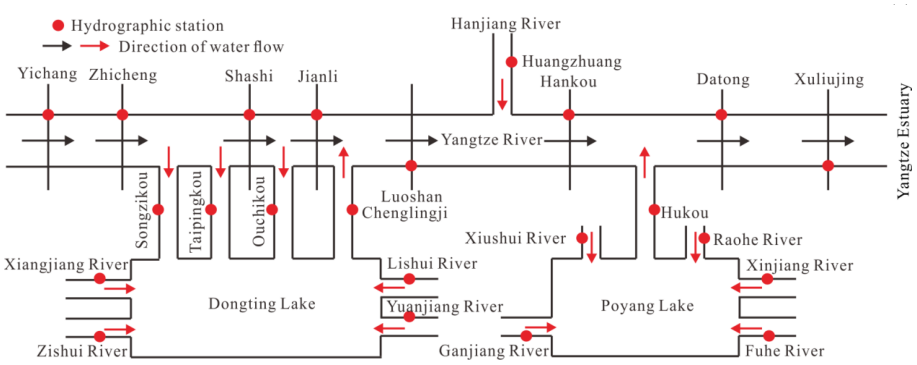

FIGURE 2
Key hydrographic stations and reaches for the calculation of suspended sediment load budget.

primarily aimed to analyze the suspended sediments, and there was an unmeasured area at a certain thickness at the bottom. This part of the sediment has traction load movement characteristics, part of which exchanges with the riverbed sand in the suspended sediment, and most of which is transported downstream along the riverbed surface (Wang et al., 2020; Yang et al., 2021b). The bottom sand exchange was measured by the bottom-supported system at the Yangtze Estuary and was concentrated in the deep-water waterway of the North Passage (Liu et al., 2011). Meanwhile, according to the estimate using the Rousse formula, the sediment content of the unmeasured area at the bottom is significantly higher than the suspended sediment concentration (Wang et al., 2020). At the same time, there is a large amount of waterway dredging (V_{wd}), sand mining (V_{sm}), and land reclamation (V_{lr}) in the river channels, as well as riverbed scouring or deposition. The suspended sediment transport balance and the amount of sediment entering the representative section can be estimated using the following calculation formula:

$$V_{riverbed-sand} = V_{Total} - V_{sm} - V_{lr} - V_{wd} \quad (6)$$

Where $V_{riverbed\text{-}sand}$ is the amount of sediment replenished riverbed scouring; V_{Total} is the total amount of riverbed scouring.

3.2.2 Calculation method of riverbed scouring or deposition

The cross-sectional areas are calculated from the topographic cross-sections along the river (Figure 3A), and the watercourses upstream and downstream of the river channels, according to Eq. (7):

$$A_{i,j} = \frac{(h_{i,j} + h_{i+1,j} + \sqrt{h_{i,j}h_{i+1,j}}) \times b_i}{3} \ (i = 0, 1, 2, 3 \ldots m; j = 0, 1, 2, 3 \ldots n) \quad (7)$$

Where i is the number of points at which the elevation of a transverse of the river is measured; j is the number of rivers profiles; A_i is the cross-sectional area (m^2); h_{i+1} h_i and h_{i+1} are the water depths at two consecutive points of a section (m); and b_i is the width at two consecutive points (m).

The volume of the rivers channel V_j (Figure 3B) between the up and downstream sections at the corresponding water level is calculated according to Eq. (8). Subsequently, the total river channel volume is obtained via Eq. (8):

$$V_j = \frac{(A_{i,j} + A_{i,j+1} + \sqrt{A_{i,j}A_{i,j+1}}) \times L_j}{3} (i = 0, 1, 2, 3 \ldots m; j = 0, 1, 2, 3 \ldots n) \quad (8)$$

$$V = \sum V_j \quad (9)$$

Where V_j is the volume of the channel between adjacent sections (m^3), $A_{i,j}$ and $A_{i,j+1}$ are the areas of adjacent sections (m^2), and L_j is the distance between adjacent sections (m).

Sand mining in the Yangtze River, which increases riverbed scouring, is mainly used to scour for construction materials. The sediment from waterway dredging of the Yangtze River channel is mainly used for reclamation of shoals or land, and will also increase riverbed scouring after waterway dredging. To facilitate the comparison between the amount of riverbed scouring or deposition, the measurement unit of the suspended sediment load from the river basin, the amount of riverbed scouring or deposition, the amount of sand mining, and the amount of waterway dredging are all converted to t/y (tons/year).

4 Results and discussion

4.1 The impact of the TGR's sediment interception on the "source-sink" of sediments

In the period between 2003 and 2020, both the sediment inflow from the Jinshajiang, Minjiang, Yalongjiang, Wujiang, and Jialingjiang Rivers in the upper reaches of the Yangtze River to the TGR area and the sediment outflow from the TGR decreased, from 4.25×10^8 t/y in 1980–2002 to 1.45×10^8 t/y, a decrease of 65.9% (Figure 4A). From 2003 to 2020 sediment inflow to the TGR from the Jinshajiang, Minjiang, Yalongjiang, Wujiang, and Jialingjiang Rivers in the upper reaches of the Yangtze River was 26.15×10^8 t, the sediment outflow from the reservoir was 6.26×10^8 t, and the accumulated sediment in the reservoirs area was 19.89×10^8 t (Figure 4B). In other words, the TGR and upstream cascade reservoir, soil and water conservation, climate change, and sand mining intercepted 76% of the incoming sediment from the upper reaches of the Yangtze River Basin (Figure 4C).

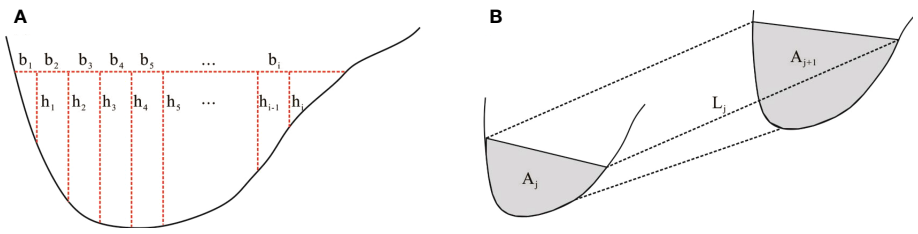

FIGURE 3
An anabraching river channel according to **(A)** areas of the cross-sectional, and **(B)** river channel capacity calculation models.

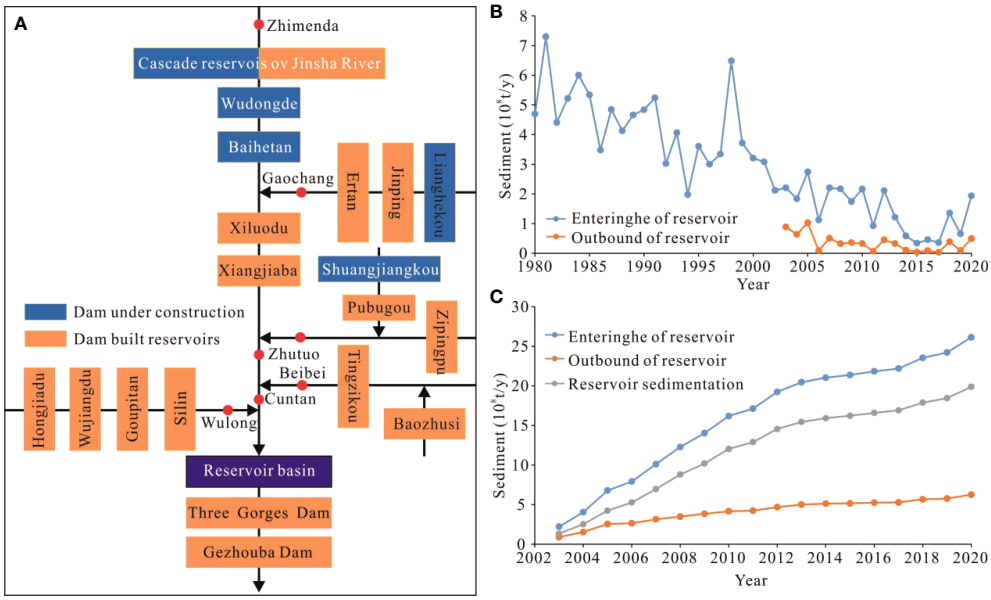

FIGURE 4
Relationship between sediment inflow and outflow of the TGR; **(A)** Distributions of the TGR and the upstream cascade reservoirs; **(B)** Chronological variations of sediment inflow and outflow from the TGR; **(C)** Cumulative variation of sediment inflow and outflow from the TGR.

4.2 The source–sink relationship sediment in the runoff control section of the middle–lower reaches Yangtze River

4.2.1 Composition of the runoff and sediments in the middle-lower reaches of the Yangtze River

According to the operation time of Gezhouba Dam, Three Gorges Dam, and cascade reservoirs in the upper reaches of the Yangtze River, the study period is divided into 1980–2002, 2003–2011, and 2012–2020.

Due to the diversion of Dongting Lake, the runoff at Yichang, Zhicheng, Shashi, and Jianli hydrographic stations decreased, and the rate of decrease slowed down from upstream to downstream. Affected by the inflow of Dongting Lake, Hanjiang River, and Poyang Lake, the runoff at Luoshan, Hankou, and Datong hydrographic stations increased. In general, the operation of the TGR and changes in the relationship between rivers and lakes in the lower reaches of the Yangtze River mainstream has not changed the characteristics of the runoff and had little impact on the total amount of runoff. Around 47% of the runoff entering the Yangtze Estuary from 1980–2020 came from the area above Yichang hydrographic stations (Figure 5A; Table 2). From 1980–2002, the amount of sediment at each hydrographic station first decreased and then increased, and from 2003–2020, it increased along the way (Figure 5B; Table 2). From 1980 until 2002, 2003–2011, and 2012–2020, the runoff and sediment of the three mouths of Dongting Lake all decreased, and the decrease of the sediment was significantly higher than that of the runoff (Figures 5C; D, Table 3). Both the runoff and sediments of the Dongting Lake discharged into the Yangtze River decreased first before increasing, and the amount was smaller after the TGR went into operation. The runoff of Poyang Lake discharged into the Yangtze River first decreased and then increased, the amount of sediment first increased and then decreased. Conversely, the amount of runoff and sediment from the Hanjiang River discharged into the Yangtze River decreased throughout this time.

In the periods of 1980–2002, 2003–2011, and 2012–2020, the runoff at the Datong hydrographic station came from Yichang hydrographic station, Dongting Lake, Hanjiang River, and Poyang Lake; the confluence proportion was 47–48%, 21–24%, 3–5%, 16–18%, and 7–10% respectively, indicating that the composition of the runoff into the Yangtze Estuary before and after the operation of the TGR was stable (Figure 6A). From 1980–2002, the sediment amount at Yichang hydrographic station was higher than that at Datong hydrographic station; the riverbed at Dongting Lake and from Yichang–Datong reaches were all deposition, only 4% of the sediments at Datong hydrographic station came from Poyang Lake and Hanjiang River. From 2002–2011, the sediments at Datong hydrographic station came from Yichang, Dongting Lake, Hanjiang River, and Poyang Lake, with proportions of 34%, 4%, 12%, 8%, and 42%, respectively. These proportions changed in the period from 2012–2020 to 17%, 10%, 4%, 7%, and 62%. From 2012–2020 compared with 2003–2011, the proportion of suspended sediment in Datong hydrographic station in Yichang hydrographic station decreased by 17%, and the proportion of deposition recharge by riverbed scouring in Datong hydrographic station increased by 20% (Figure 6B).

4.2.2 Exchange characteristics between suspended sediment and riverbed sand in the middle-lower reaches of the Yangtze River

The reach from Yichang–Dabujie (120 km) has a sandy pebble riverbed, transitioning to a purely sandy riverbed below Dabujie, with a great riverbed anti-scouring ability. Under the background of

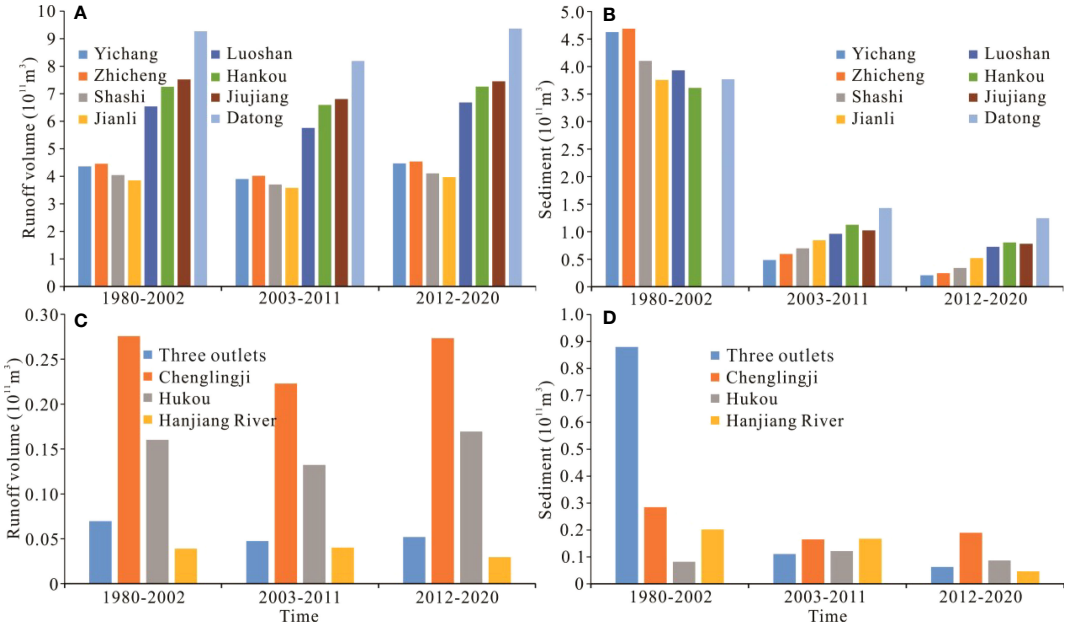

FIGURE 5
Runoff and sediment fluxes downstream of the TGR; **(A)** Runoff of the Yangtze River mainstream; **(B)** Sediment of the Yangtze River mainstream; **(C)** Runoff of the tributaries and lakes; **(D)** Sediment of the tributaries and lakes.

TABLE 2 Variation of runoff and sediment at the hydrographic station of the Yangtze River mainstream.

Type	Hydrographic station	Yichang	Zhicheng	Shashi	Jianli	Luoshan	Hankou	Jiujiang	Datong
Runoff (10^8 m^3/y)	1980-2002	4364	4460	4049	3855	6539	7254	7522	9273
	2003-2011	3903	4023	3706	3585	5763	6596	6811	8194
	2012-2020	4472	4542	4109	3974	6682	7263	7449	9370
	2003-2020	4188	4283	3907	3779	6222	6929	7130	8782
	Amplitude variation (%)	-4.05	-3.98	-3.51	-1.96	-4.84	-4.48	-5.21	-5.30
Sediment (10^4 t/y)	1980-2002	46278	46877	41026	37565	39326	36143	NA	37696
	2003-2011	4884	5956	7012	8461	9630	11273	10263	14329
	2012-2020	2104	2474	3421	5216	7258	8061	7828	12468
	2003-2020	3494	4215	5217	6838	8444	9667	9046	13398
	Amplitude variation (%)	-92.45	-91.01	-87.28	-81.80	-78.53	-73.25	NA	-64.46

reduced sediment discharge from the TGR, the sediment scouring of the alluvial riverbed shows good exchange and sorting characteristics. The main characteristic is that the fine sediment in the riverbed first compensates for the suspended sediment and thus causes the riverbed to be in a scouring state, while the relatively coarse sediment will remain in the riverbed and only start to transport in a flood period. In the scouring process of the sandy riverbed in the middle-lower reaches of the Yangtze River, the fine sediment ($d \leq 0.125$ mm) washed by the riverbed surface fed the suspended sediment, causing an increase in the amount of fine sediment in the suspended sediment (Figure 7A). Coarse sediment ($d>0.125$ mm) was recharged from the reaches between Yichang–Jianli reaches. The coarse sediment showed an increasing trend along the rivers from 2003–2021 (Figure 7B), which is also the area with the greatest scouring intensity in the riverbed downstream of the TGR (Yang et al., 2022a; Yang et al., 2023a; Yang et al., 2023b; Yang et al., 2023c). In the reach of the sandy and cobble-riverbed, due to the small thickness of the sandy overburden of the riverbed, the scouring of fine sediment in the riverbed is complete at present (Figure 7C), and the anti-scouring of the riverbed is in a quasi-equilibrium state due to the significant coarsening of the riverbed. The median particle size of suspended sediment at the Yichang hydrographic station during 1987–2002, 2003–2012, and 2013–2021 was 0.022 mm, 0.005 mm, and 0.009 mm, respectively, and that at Hankou hydrographic station was 0.018 mm, 0.014 mm, and 0.015mm. At Datong hydrographic station, the values are 0.017 mm, 0.010 mm, and 0.015 mm. The median particle size of suspended sediment decreases first and then increases (Figure 7D),

TABLE 3 Variation of runoff and sediment at the hydrographic station in the tributaries and lakes of the Yangtze River.

Type	Time	Three outlets	Chenglingji	Hukou	Hanjiang River
Runoff (10^8 m^3/y)	1980-2002	696	2758	1602	392
	2003-2011	475	2229	1324	403
	2012-2020	520	2735	1696	298
	2003-2020	498	2482	1510	350
	Amplitude variation (%)	-28.49	-9.99	-5.77	-10.58
Sediment (10^4 t/y)	1980-2002	8804	2851	821	2020
	2003-2011	1113	1656	1220	1680
	2012-2020	633	1899	871	465
	2003-2020	873	1778	1046	1072
	Amplitude variation (%)	-90.09	-37.65	27.35	-46.92

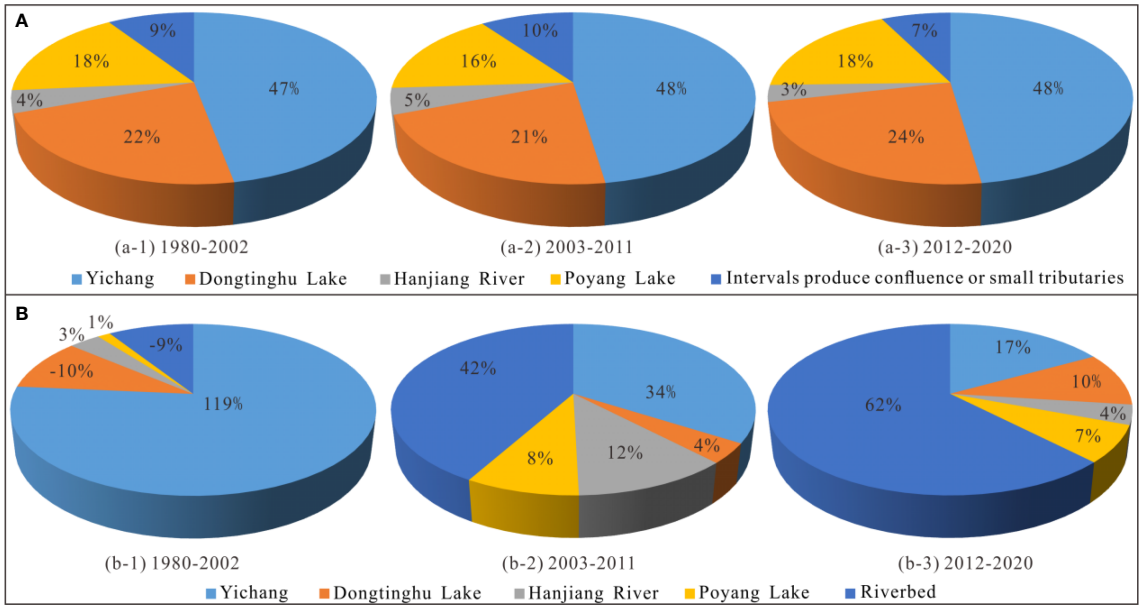

FIGURE 6
Composition of runoff and sediment at the Datong hydrographic station of the Yangtze River. **(A)** Composition of runoff; **(B)** Composition of sediment.

that is, the coarse sediment scoured by the riverbed gradually recharges the suspended sediment. Therefore, under the background of riverbed scouring, the sediment on the riverbed surface near the dam section is significantly coarsened, while the sediment coarsening phenomenon is not significant when it enters the sandy riverbed.

4.2.3 Calculation of sediment source–sink relationships of the Yichang–Datong reaches

After the operation of the TGR, the riverbeds between Yichang–Zhicheng, Jingjiang (Zhicheng–Chenglingji), Chenglingji–Hankou, Hankou–Hukou, Hukou–Datong reaches all experienced cumulative scouring. Since 2012, this scouring intensity has increased (Figure 8A). The cumulative deposition of the Yichang–Datong reaches from 1981–2002 was 3.13×10^8 m^3, respectively (Figure 8B). The cumulative scouring of the Yichang–Datong reaches from 2002–2018 was 28.52×10^8 m^3. In the periods of 1981–2002, 2003–2011, and 2012–2018, the amounts of sediments passing through the Datong section of the Yangtze River Basin decreased. Based on the topographic difference calculation, the amount of riverbed scouring increased (switching from deposition to scouring). The amount of scouring after sand mining and waterway dredging deducted also increased, indicating a switch from deposition to scouring (Figure 8C). In the 1981–2002,

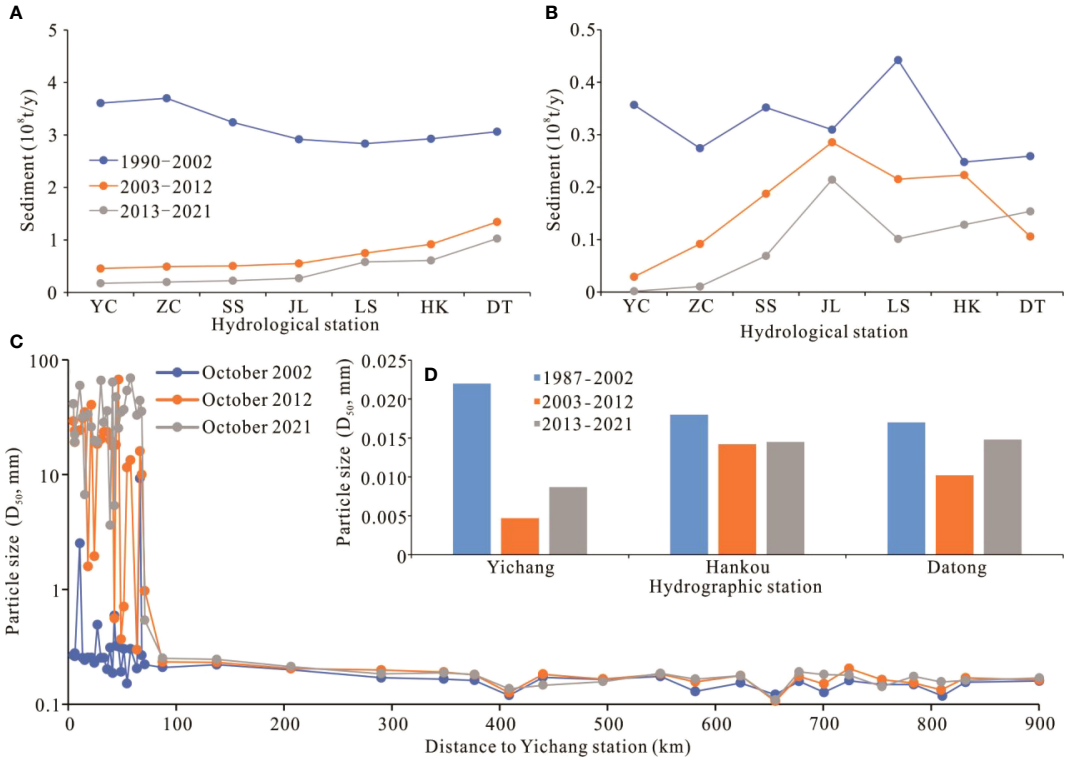

FIGURE 7
Condition of transport of particle size and grouped sediment in the middle–lower reaches of the Yangtze River. **(A)** Amount of suspended sediment d ≤ 0.125 mm; **(B)** Amount of suspended sediment d > 0.125 mm; **(C)** Median sediment particle size of the riverbed surface; **(D)** Median particle size of suspended sediment at the main hydrographic stations.

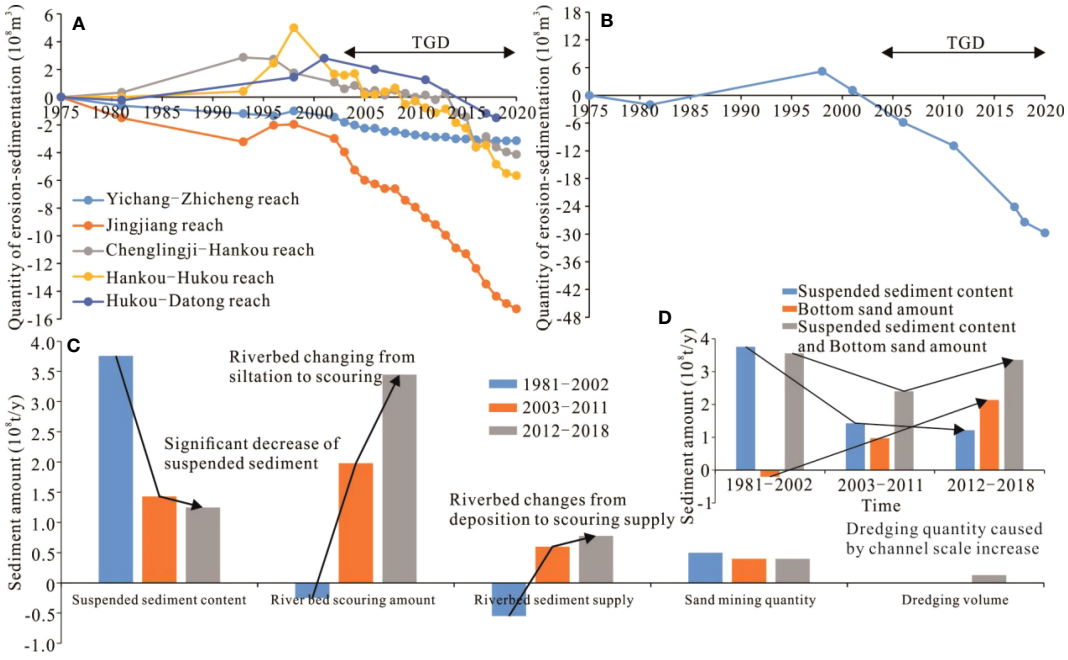

FIGURE 8
Changes in riverbed scouring or deposition along the Yichang–Datong reaches of the Yangtze River; **(A)** Cumulative scouring or deposition of riverbed sections based on river channel topography data; **(B)** Total amount of riverbed scouring or deposition; **(C)** Sediment source-sink relationship in the Yichang–Datong reaches.

2003–2011, and 2012–2018 periods, the amount of suspended sediment passing through the Datong section were 3.73×10^8 t/y, 1.43×10^8 t/y, and 1.22×10^8 t/y, respectively. From 1981–2002, 2003–2011 and 2012–2018, the riverbed scouring or deposition of the Yichang–Datong reaches were -0.25×10^8 t/y, 1.98×10^8 t/y, and 3.45×10^8 t/y, the amount of sand mining was 0.50×10^8 t/y, 0.40×10^8 t/y and 0.40×10^8 t/y, the waterway dredging amount was 0, 40×10^4 t/y and 0.13×10^8 t/y, respectively. The amount that entered the bottom sediment of the tidal reach of the Yangtze River through the Datong section was -0.20×10^8 t/y, (suspended sediments deposition in the riverbed and no bottom sand migrated downstream) 0.98×10^8 t/y, and 2.14×10^8 t/y, respectively (Figure 8D). The total amount of suspended and bottom sand that entered the Datong section was 3.56×10^8 t/y, 2.41×10^8 t/y, and 3.36×10^8 t/y, respectively, which first decreased and then increased, in the periods 1981–2002, 2003–2011, and 2012–2018, respectively (Figure 8D).

4.3 Effect of riverbed scouring in tidal reach on estuary "source-sink"

4.3.1 Relationship of suspended sediment concentration in the tidal reach of the Yangtze River

Whether the suspended sediment concentration in the Yangtze Estuary will decrease or not is still under debate (Yang et al., 2014; Yang et al., 2015b). Most studies believe that the estuarine suspended sediment concentration will decrease (Li et al., 2012; Zou et al., 2012; Jing et al., 2013; Yang et al., 2014; Yang et al., 2015b), and some even overestimated the reduction in suspended sediment (Yao et al., 2015), as it provides direct evidence of delta scouring (Luan et al., 2016; Zhu et al., 2016; Yang et al., 2017; Dai et al., 2018; Luan et al., 2021);, front tidal flat scouring (Wei et al., 2015) and riverbed scouring (Pan et al., 2012; Dai et al., 2013; Wei et al., 2017). The suspended sediment concentrations at Xuliujing, Sheshan, and Hengsha stations did not reduce between 1998 and 2001, which can be attributed to the resuspension effect (Jin et al., 2006). The suspended sediment concentration in the flood and dry seasons of 2003 and 2004 did not decrease when compared with their corresponding annual averages (between 1950 and 2002 at the Datong hydrographic station) (Zhai, 2006). From 1980–2020, the runoff at the Xuliujing hydrographic section was equal to that at Datong hydrographic station (Figure 9A) and was related to the quasi-balanced runoff at the interval branch (Zhang et al., 2011). The sediment concentration in the Yangtze Estuary from 1980–2020 was similar to the value of the Datong hydrographic station, with a consistent decreasing trend (Figure 9B). In 2002–2011 and 2012–2018, the amount of sediment deposition on the inner edge was equivalent to the amount of sediment compensation in the riverbed along the way, indicating in a quasi-balanced state. Due to the decrease in the amount of sediment from the Yangtze River mainstream, the degree of unsaturation in the stream flow in the Datong–Xuliujing reaches increased, increasing the transport intensity of bottom sediments. Therefore, the sediment entering the Yangtze Estuary through the Xuliujing section was composed of suspended sediment in the drainage basin and bottom sand scouring from the riverbed in the hydrographic section between Datong and Xuliujing. Comparing 2003–2020 with 1980–2002, the vertical suspended sediment concentration from outside the Yangtze Estuary decreased by 21.4% (Figure 9C), which is consistent with existing research findings (Jing et al., 2013; Yang

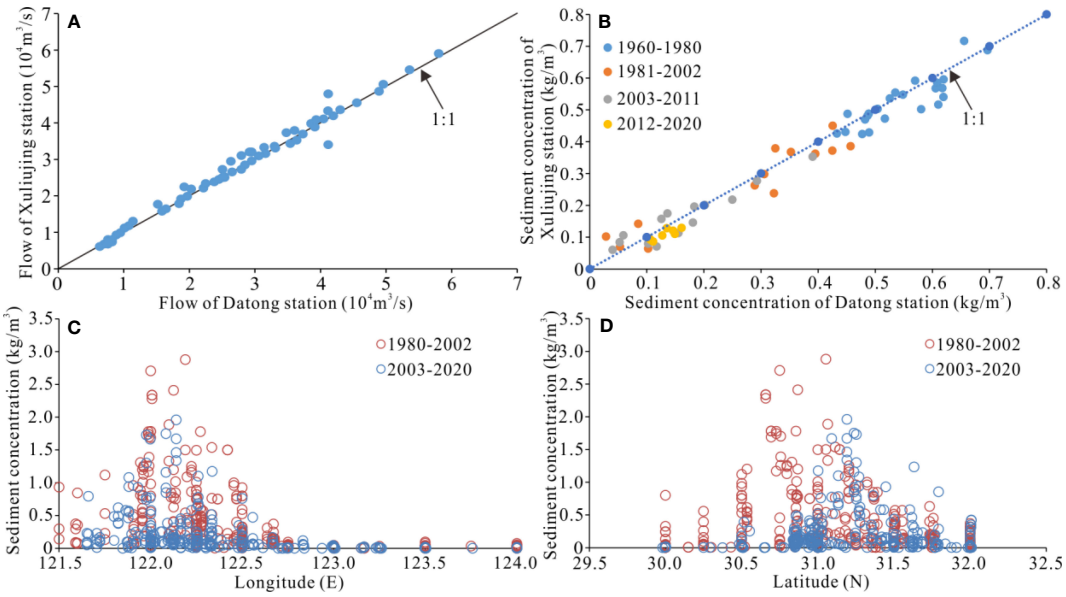

FIGURE 9
Changes in water and sediment conditions in the Yangtze Estuary; **(A)** Relationship between runoff at Xuliujing and Datong hydrographic stations of 1998–2020; **(B)** Relationship between sediment concentration at Xuliujing and Datong hydrographic stations of 1960–2020; **(C)** Longitudinal variations in the suspended sediment concentration in Yangtze Estuary of 1980–2020; **(D)** Latitude variation of suspended sediment concentration in Yangtze Estuary of 1980–2020.

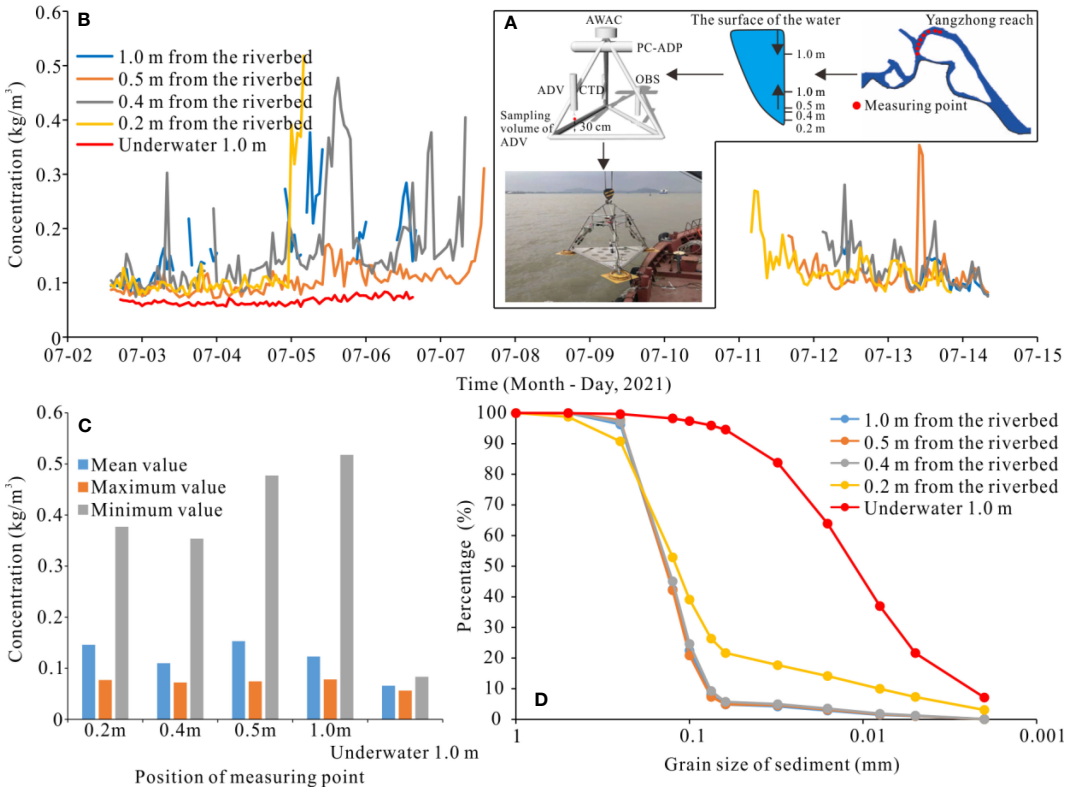

FIGURE 10
Monitoring results of suspended sediment and bottom sand in the tidal reach; **(A)** Placement of field monitoring points; **(B)** Changes in sediment concentrations monitored on site; **(C)** Comparison of monitoring results; **(D)** Variation of sediment particle size.

et al., 2014; Yang et al., 2015b). The peak area of horizontal suspended sediment has been gradually moving to the north and expanding to the deep-water waterway of the North Passage (Figure 9D). This is one of the reasons why the North Passage has required waterway dredging and maintenance in recent years (Dai et al., 2013; Luan et al., 2016; Luan et al., 2018).

4.3.2 Analysis of transport relationship between suspended sediment and riverbed sand in the tidal reach

According to Changjiang Sediment Bulletin (Changjiang Water Resources Commission (CWRC), 2004–2022), few stations test riverbed load sediment in the middle-lower reaches of the Yangtze River, and the amount of riverbed load sediment is much smaller than that of suspended sediment. In the middle–lower reaches of the Yangtze River, only the Yichang–Dabujie reaches have a sandy and cobbly bed with a certain amount of bedload. Below the Dabujie, the riverbed load sediment of the sandy riverbed is small (Yao et al., 2017), but the development of sediment wave is significant (Zheng et al., 2022). In July 2021, suspended sediment and bottom sand were monitored by way of sitting bottom-mounted observation (Figure 10A), in the straight reach of the Yangtze River tidal reach. The sediment concentration above the 1.0 m of the riverbed surface was significantly higher than that below the 1.0 m of the riverbed surface (Figure 10B), with an average ratio of 2.21 (Figure 10C).

Under the influence of hydrodynamic environments such as runoff, tidal currents, water waves, and salt water in the Yangtze Estuary, the sediment deposited by saltwater action flocculation in the mouth bar area is fine particles. In the other areas, the surface sediment of the riverbed is the same as that in the tidal reach (Yan et al., 2009; Yan et al., 2011; Luo et al., 2012; Chen et al., 2021), and there is a good relationship between sediment particle changes and riverbed scouring or deposition (Chen et al., 2021). Therefore, the sediment from the Yangtze River Basin into the estuarine includes two parts, fine grained sediment in the river water body and bottom sand in the riverbed surface. The composition of deposition sediment in the estuary is different due to the differences in the hydrodynamic environment.

The high sand-bearing water (bottom sand) in the above 1.0 m of the riverbed surface links the areas of the suspended sediment and the areas of riverbed scouring or deposition, with the exchange of bed sediment between the riverbed and the water body. The grain size of the sediment in this area is significantly coarser than the suspended sediment in the water body (Figure 10D). After the operation of the TGR, the suspended sediment particles in the estuary were refined (Yang et al., 2018; Yang et al., 2022b), and the sediment in the riverbed was slightly coarse (Luo et al., 2012). The grain size characteristics of sediments in different areas of the Yangtze Estuary are significantly different. The surface sediment particles in the mouth groin dam area are fine, and the surface

sediment particles in the south branch and South channel are the same as those in the tidal reach (Zhang and Zhao, 2016).

4.3.3 Calculation of sediment source–sink relationships of the Datong–Xuliujing reaches

After the operation of the TGR, the riverbeds between Datong–Jiangyin and Jiangyin–Xuliujing reaches all experienced cumulative scouring. Since 2012, this scouring intensity has increased (Figure 11A). The cumulative deposition of the Datong–Xuliujing reaches from 1981–2002 was 1.60×10^8 m^3, respectively (Figure 10B). The cumulative scouring of the Datong–Xuliujing reaches from 2002–2018 was 16.01×10^8 m^3, respectively (Figure 11B). The total amount of suspended and bottom sand that entered the Datong section were 3.56×10^8 t/y, 2.41×10^8 t/y, and 3.36×10^8 t/y, respectively, which first decreased and then increased. In the periods 1981–2002, 2003–2011, and 2012–2018, the total sediment passing through the Xuliujing section in the upper reaches of the river basin decreased. Based on topographic difference calculation, the amount of riverbed scouring increased (switching from deposition to scouring). The amount of scouring after sand mining and waterway dredging also increased (switching from deposition to scouring) (Figure 11C). Suspended sediment passing through the Xuliujing section in the periods from 1981–2002, 2003–2011, and 2012–2018 were 3.73×10^8 t/y, 1.43×10^8 t/y, and 1.22×10^8 t/y, respectively, showing decreasing trends; the amount of bottom sand entering the Yangtze Estuary through the Xuliujing section were -0.61×10^8 t/y (suspended sediments deposition in the riverbed and no bottom sand migrated downstream), 0.89×10^8 t/y, and 1.51×10^8 t/y (Figure 11D). From 1981–2002, 2003–2011, and 2012–2018, the riverbed scouring or deposition of the Datong–Xuliujing reaches were -0.11×10^8 t/y, 1.11×10^8 t/y and 1.98×10^8 t/y, the amount of sand mining was 0.50×10^8 t/y, 0.22×10^8 t/y, and 0.37×10^8 t/y, and the waterway dredging amount was 0, 20×10^4 t/y and 0.11×10^8 t/y, respectively. The total amount of suspended and bottom sand entering the Yangtze Estuary was 3.12×10^8t/y, 2.32×10^8t/y, and 2.73×10^8t/y, respectively, which first decreased and then increased. This study believes that the total sediment passing through the Datong–Xuliujing reaches from 2003–2020 did not show a continuous decreasing trend due to the reduction in suspended sediment load, while the supply from bottom sand volume exhibited an increasing trend and the "sink" of sediment scouring or deposition turned into the "source" of sediment replenishing.

4.4 Contribution of watershed sediment to the Yangtze Estuary

4.4.1 Distribution of riverbed scouring or deposition and variation in the shoal rear of the Yangtze Estuary

The north branch of the Yangtze Estuary was dominated by deposition between 2002–2018, and the south branch, north channel, and south channel mainly scouring. The high shoal area of the front tidal flat mainly experienced deposition, and the front of the delta mainly experienced scouring (Figures 12A, B). In the Yangtze River Estuary, the continent body is at the condition of sediment deposition, which is caused by the "sink" of the sediment after

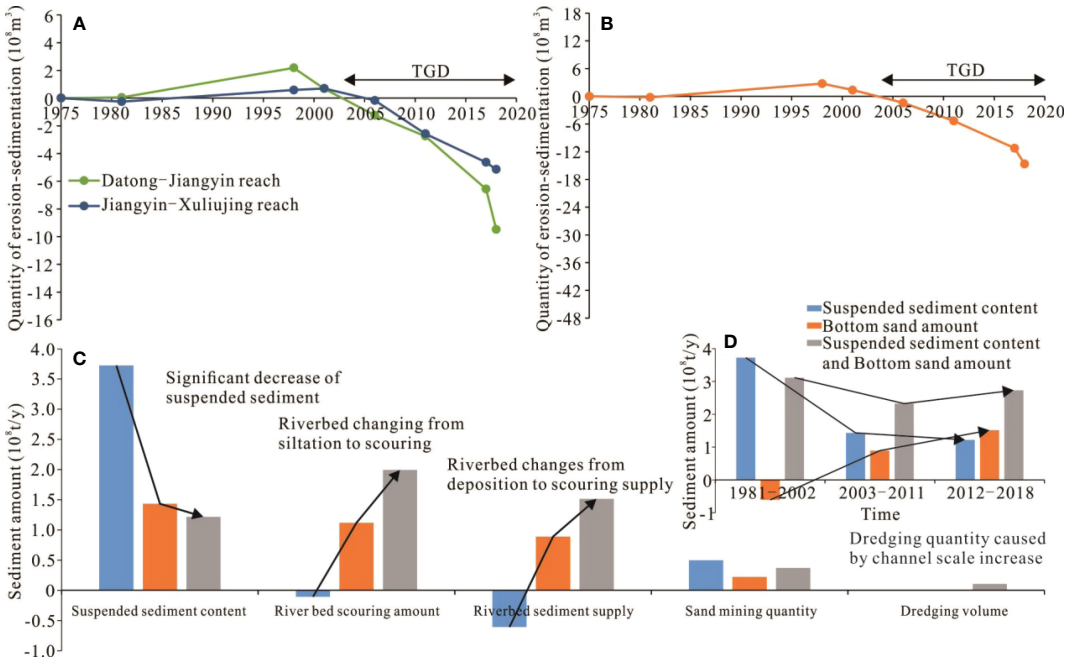

FIGURE 11
Changes in riverbed scouring and deposition along the Datong–Xuliujing reaches of the Yangtze River; **(A)** Cumulative scouring or deposition of riverbed sections based on rivers channel topography data; **(B)** Total amount of riverbed scouring or deposition; **(C)** Sediment source-sink relationship in the Datong–Xuliujing reaches.

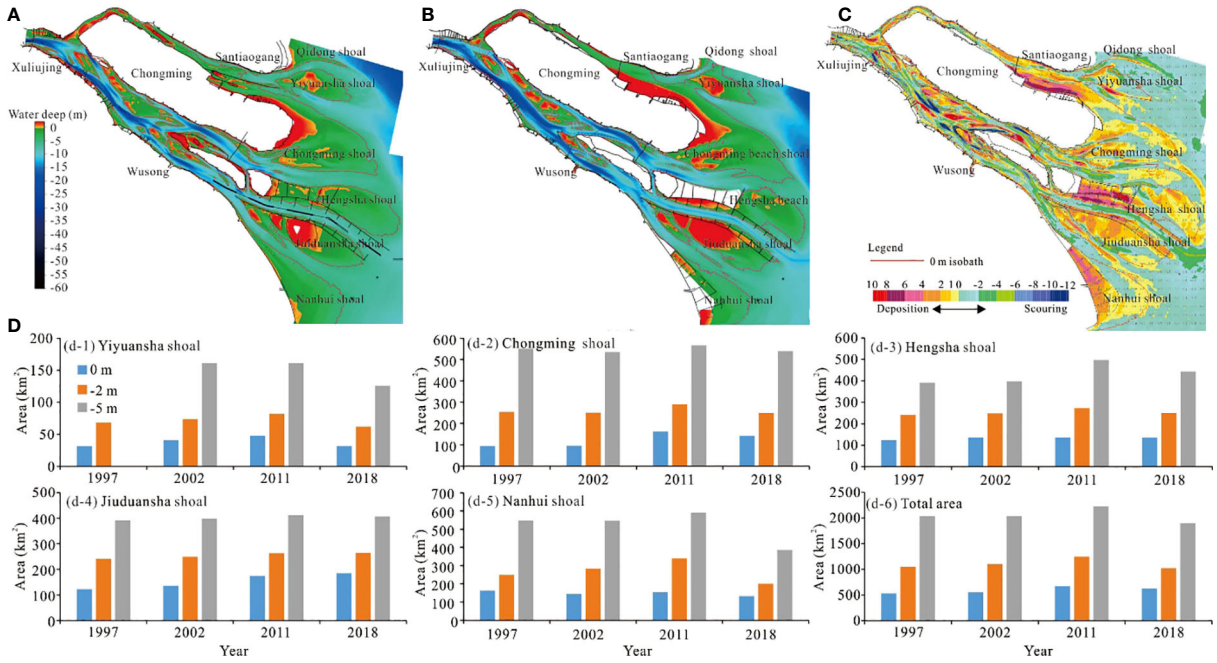

FIGURE 12
Distribution characteristics of riverbed scouring or deposition in the Yangtze Estuary; **(A)** Terrain in 2002, data from Yu and Zhang (2021); **(B)** Terrain in 2018, data from Yu and Zhang (2021); **(C)** Distribution of riverbed scouring or deposition; **(D)** Shoal area.

entering the Yangtze Estuary. The waterway area is scouring due to the regulation of buildings, and the deltas area scouring (Figure 12C). Simultaneously, all the areas of the front tidal flat increased at first and then decreased. During 2002–2011, the areas at the water depths of 0 m, 2 m, and 5 m were 22.12%, 12.67%, and 9.35% respectively, while during 2011–2018 it became –7.13%, –17.58%, and –14.67% respectively (Figure 12D). During 2002–2018, the changes of the areas at the water depths of 0 m were –21.09%, +47.63%, –0.57%, +35.91%, and –7.23% for Yiyuansha shoal, Chongming shoal, Hengsha shoal, Jiuduansha shoal, and Nanhui shoal respectively, with an increased total area of 13.41% (Figure 12D).

4.4.2 Calculation of sediment source–sink relationships in the Yangtze Estuary

From 1982–2018, both the north and south branches experienced cumulative scouring, but the total amount of riverbed sand in the Yangtze Estuary was relatively small, which means that without considering the impact of riverbed scouring or deposition in engineering areas such as land reclamation, waterway dredging, the Yangtze Estuary was in a quasi-balanced state between scouring or deposition (Figure 13A). The cumulative waterway dredging volume of the North Passage of the Yangtze Estuary between 1982 and 2018 was 11.07×10^8 m^3 (ship volume/topographic volume=1.30, sediment wet bulk density/dry bulk density=1.65, converted to a weight of 14.05×10^8 t) (Figure 13B). During this period, the land reclamation area of the Yangtze Estuary was 820.57 km^2, and the amount of deposition caused by the reclamation was 12.31×10^8 m^3 (sediment wet bulk density/dry bulk density=1.65, and the average thickness of waterway dredging filling was calculated as 1.5 m (Figure 13B), and the converted sediment weight was 20.31×10^8 t) (Figures 13C, D). The total amount of suspended and bottom sand entering the estuary area through the Xuliujing section in the 1982–2002, 2003–2011, and 2012–2018 periods was 3.12×10^8 t/y, 2.32×10^8 t/y, and 2.73×10^8 t/y, a decrease of 16.9% in 2003–2018 compared with 1984–2002. In the above periods, after deducting the amount of riverbed scouring or deposition, land reclamation, and waterway dredging, through the Yangtze Estuary, the amount of dispersed sediment was 2.82×10^8 t/y, 1.81×10^8 t/y, and 1.28×10^8 t/y, respectively.

4.5 Sediment supplies from the riverbed as a new source to sustain the Yangtze Estuary Deltas

Calculated by the measured topographic data of 1958–2015 (The years are 1958, 1978, 1997, 2002, 2007, 2010, 2012, and 2015), the critical suspended sediment volume for the balance of scouring or deposition of the front tidal shoals and deltas at the Yangtze Estuary was calculated as 2.18×10^8 t/y (Luan et al., 2021). A large amount of waterway dredging has been carried out in the construction of the north channel of the Yangtze Estuary deep-water waterway, and the waterway regulation structures have interfered with the local geomorphic evolution characteristics, after deducting the impact of the estuary project from 1997–2010, the corresponding critical suspended sediment volume was 2.34×10^8 t/y (Luan et al., 2021). However, the amount of sediment at Datong hydrographic station from 2003–2011 was

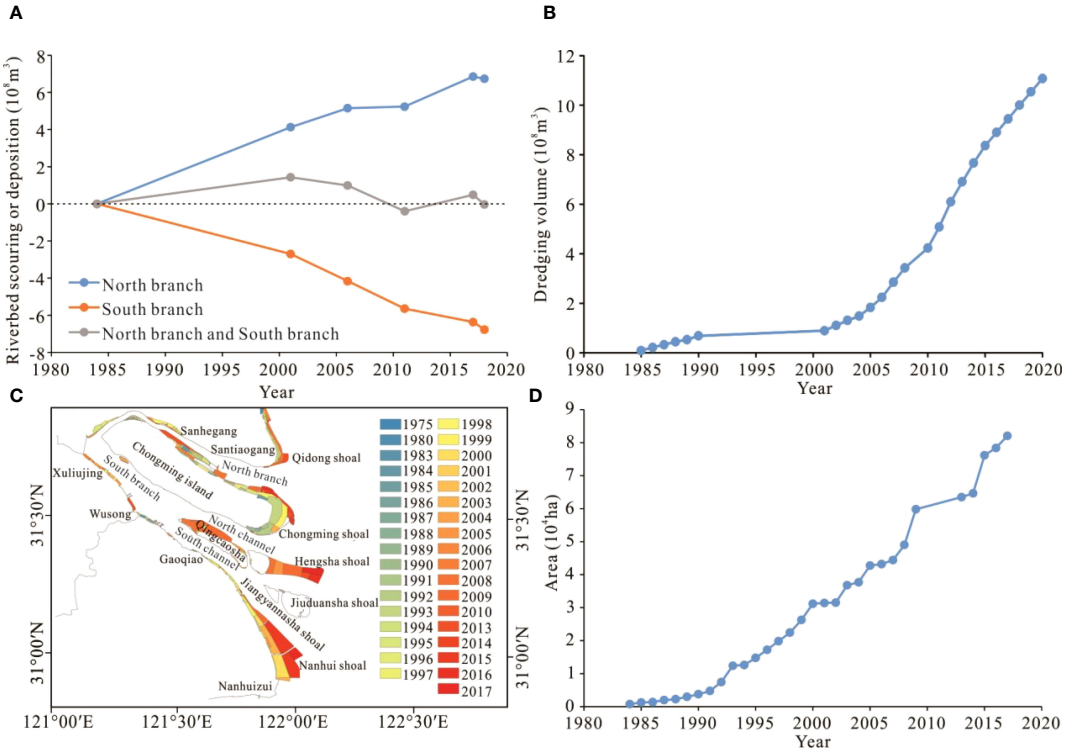

FIGURE 13
Sediment supply relationship in the Yangtze Estuary; **(A)** Cumulative amount of riverbed scouring or deposition; **(B)** Waterway dredging volume; **(C)** Reclamation area, data from Qiu et al. (2019); **(D)** Shoals area.

significantly lower than before the TGR began to operate, with an average value of 1.29×10^8 t/y, which was significantly lower than the critical amount of sediment for scouring or deposition balance. Many studies during this period believed that the deltas were dominated by scouring (Wei et al., 2015; Luan et al., 2016; Zhu et al., 2016; Yang et al., 2017; Dai et al., 2018; Luan et al., 2021). Simultaneously, the construction of dams on the upper reaches of the Yangtze River and lakes may cause the interruption of sediment supply to the lower reaches. It is possible that in the near future, the Yangtze Estuary landform system will experience large-scale scouring (Dai et al., 2018). Regarding the amount of sediment in the Yangtze Estuary, when only considering the balance of suspended sediment exchange, the amount of sediment at Datong hydrographic station in the 1980s and 2000s was calculated to be 4.51×10^8 t/y and 1.51×10^8 t/y, respectively, and the amount of suspended sediment entering the estuary through Xuliujing section were 4.06×10^8 t/y and 1.72×10^8 t/y respectively, and the amount entering the deltas area was 3.70×10^8 t/y and 1.75×10^8 t/y (Yang et al., 2015a; Xie et al., 2017a). This significantly reduced the suspended sediment concentration in the estuary, which will cause the delta area to switch to scouring. Taking human activities into account like sand mining and waterway dredging, through the comprehensive calculation of suspended sediment transport and riverbed scouring or deposition, the total amount of suspended and bottom sand in the Yangtze River Basin that entered the estuary through the Xuliujing section during the 2003–2011 and 2012–2018 periods were calculated as 2.32×10^8 t/y and 2.73×10^8 t/y, respectively. The riverbed scouring intensity of the reach from the Yichang–Xuliujing reaches was increasing, which was beneficial to safeguarding the sediment resources of the Yangtze Estuary. Recent studies have also proven that Jiuduansha shoal deposition is, significantly, in its natural state (Wei et al., 2016; Wei et al., 2017; Zhao et al., 2018; Zhu et al., 2019; Zhang et al., 2021). Meanwhile, in the deposition center of the Yangtze Estuary Delta, the deposition rate remained at 10 cm/y from 1958–2009 (Dai et al., 2014): between 1997–2015, only the net scouring depth from 2011–2013 was 10.76 cm/y, and the net scouring depth was 0.91–3.48 cm/y in other years (Sun, 2018). In 2021, the amount of river sediment outside of the Xinliuhesha and Qingcaosha Reservoirs did not decrease but instead started to increase, representing the first natural increase in recent years (https://view.inews.qq.com/a/20211114V02W9E00). In addition, the decrease in the amount of sediment entering the sea from the Yangtze River has no significant impact on the landform evolution of Hangzhou Bay, mainly due to the buffering effect of existing sediment outside the Yangtze Estuary (Xie et al., 2017b).

Human activities have put tremendous pressure on global rivers (Best, 2019). The overall water connectivity of the Yangtze River Basin is still maintained. However, several studies have proposed that blocking sediment through dams and relative sea level rise will result in the submersion of the estuary delta and front tidal flats. In nearly 1,000 deltas around the world, dam construction has led to a severe reduction of anthropogenic sediment flux (by more than 50%), forcing an annual loss of delta land of about 12 ± 3.5 km^2. Not

all estuary deltas lose land resources due to dams (Nienhuis et al., 2020). For example, the supply of sand from the Mississippi River is stable and sustainable (Edmonds and Slingerland, 2010; Nittrouer and Viparelli, 2014), and these sediments can form deltas through engineering measures capturing sediment from the Mississippi River. The thickness of the sand layer from the Dabujie section to the estuary of the Yangtze River is more than 100 m (Cao et al., 2012; Mei et al., 2021). The ancient river channel has a wide range of lateral swing space, and a large amount of fine-grained sediment remains (Song et al., 2013). In the future, regardless of whether the amount of suspended sediment in the Yangtze River Basin decreases, the riverbed scouring of the Yichang–Xuliujing reaches will have abundant bottom sand to replenish, and this amount will show an increasing trend due to the continuous decrease in the amount of sediment in the river basin, which can guarantee the amount of sediment entering the Yangtze Estuary from the river basin. Comprehensive analysis suggests that the Yichang–Datong and Datong–Xuliujing reaches have gradually transformed from the condition of sediment deposition to the condition of sediment scouring, which provide an important sediment source for the deposition of estuary shoals, and stability of deltas and land resources.

Although the supply of suspended sediments from the Yangtze Estuary has been significantly reduced, the amount of bottom sand in the riverbed is still abundant, with its replenishment capacity and supply increasing. A comprehensive analysis has shown that even if the amount of suspended sediment entering the estuary after the TGR went into operation are significantly reduced, the riverbed will gradually transform from a "sink" of deposition to a "source" of sediment supply, which will still provide a rich scouring of sediments for the Yangtze Estuary. Therefore, the Yangtze Estuary Delta, front tidal flats, and urban land resources are likely to be sustained.

5 Conclusions

Since the TGR began operating, the "source-sink" relationship of sediments from the middle-lower reaches of the Yangtze River has been significantly adjusted, which has directly affected the sustainability of the estuary. Based on the analysis of *in-situ* observed runoff, sediment load, and riverbed topography from 1981 to 2018, the present study examined the influence of the adjustment of the Yangtze River sediment "source-sink" relationship of the Yangtze River Basin on the estuary delta.

The TGR stored 76% of the sediment in the upper reaches of the Yangtze River and caused a decline of 68–97% in sediment load in the middle-lower reaches. These sharp declines in sediment supplies resulted in a decrease of 21.4% in the suspended sediment concentration in the estuary delta. From 2003–2020, cumulative river channel scouring occurred in the Yichang–Xuliujing reaches of the Yangtze River, and the riverbed transformed from being the "sink" of sediment to the "source" of sediment transport into the sea. The river basin to the estuary also experienced an adjustment in the sediment "source-sink" relationship, which released more sediment "sources" for those entering the sea. From 2012 to 2018, the amount of sediment at the Xuliujing section of the upper reaches of the river mouth exhibited an increasing trend. In the periods of 1980–2002, 2003–2011, and 2012–2018, the total amount of suspended and bottom sand entering the delta in the Yangtze River Basin first decreased and then increased. During 2012–2018, the total amount of suspended sediment and riverbed sediment entering the estuary of the Yangtze River Basin was equivalent to the critical sediment amount of the delta from deposition to flushing, but the total sediment entering the estuary of the Yangtze River Basin did not decrease significantly.

Data availability statement

The original contributions presented in the study are included in the article/supplementary material. Further inquiries can be directed to the corresponding authors.

Author contributions

YY and MZ conceived the full text, and wrote and completed the drawing of the graph. JZ provided the revision and discussion of the whole paper. LZ was responsible for the processing of the Yangtze Estuary topography and maintenance data. All authors contributed to the article and approved the submitted version.

Funding

This study was funded by the National Natural Science Foundation (52279066; 51979132), Fundamental Research Funds for Central Welfare Research Institutes (TKS20230105), Jiangsu Water Conservancy Science and Technology Project (2020001) and the Hydrographic Bureau of Yangtze River, and Yangtze River waterway bureau.

Conflict of interest

The authors declare that the research was conducted in the absence of any commercial or financial relationships that could be construed as a potential conflict of interest.

Publisher's note

References

Almeida, R. M., Shi, Q. R., Gomes-Selman, J. M., Wu, X. J., Xue, Y. X., Angarita, H., et al. (2019). Reducing greenhouse gas emissions of Amazon hydropower with strategic dam planning. *Nat. Commun.* 10, 4281. doi: 10.1038/s41467-019-12179-5

Anthony, E., Brunier, G., Besset, M., Goichot, M., Dussouillez, P., and Nguyen, V. L. (2015). Linking rapid erosion of the Mekong river delta to human activities. *Sci. Rep.* 5, 14745. doi: 10.1038/srep14745

Bendixen, M., Best, J. L., Hackney, C., and Iversen, L. L. (2019). Time is running out for sand. *Nature* 571 (7763), 29–31. doi: 10.1038/d41586-019-02042-4

Bertassoli, D. J. J., Sawakuchi, H. O., Araújo, K. R. D., Camargo, M. G. P. D., Alem, V. A. T., Pereira, T. S., et al. (2021). How green can Amazon hydropower be? net carbon emission from the largest hydropower plant in Amazonia. *Sci. Adv.* 7 (26), eabe1470. doi: 10.1126/SCIADV.ABE1470

Best, J. (2019). Anthropogenic stresses on the world's big rivers. *Nat. Geosci.* 12 (1), 7–21. doi: 10.1038/s41561-018-0262-x

Brunier, G., Anthony, E. J., Goichot, M., Provansal, M., and Dussouillez, P. (2014). Recent morphological changes in the Mekong and bassac river channels, Mekong delta: the marked impact of river-bed mining and implications for delta destabilization. *Geomorphology* 224 (1), 177–191. doi: 10.1016/j.geomorph.2014.07.009

Cao, G. J., Cuan, J. B., and Li, Y. Y. (2012). Characteristics of the Yangtze river paleo-valley in jiangsu province in the last glacial maximum. *Scientia Geographica Sin.* 32 (8), 986–992. doi: 10.1007/s11783-011-0280-z

Changjiang Water Resources Commission (CWRC) (2004–2022). *Changjiang sediment bulletin*. 2003–2021. Available at: http://www.cjw.gov.cn/zwzc/bmgb/nsgb/.

Chen, Y. W., Sheng, H., Xu, Q. H., Qu, Y. B., Xing, F., Li, Z. H., et al. (2021). Analysis of sediment grain size change and its response to erosion and deposition pattern within the Yangtze river estuary for the past 40 years. *Hydro-Science Eng.* 189 (5), 8–18.

Cheng, H. Q., Chen, W., Li, J. F., Jiang, Y. H., Hu, X., Zhang, X. L., et al. (2022). Morphodynamic changes in the Yangtze estuary under the impact of the three gorges dam, estuarine engineering interventions and climate-induced sea level rise. *Earth Planetary Sci. Lett.* 580, 117385. doi: 10.1016/j.epsl.2022.117385

Collins, M. J., Snyder, N. P., Boardman, G., Banks, W. S. L., Andrews, M., Baker, M. E., et al. (2017). Channel response to sediment release: insights from a paired analysis of dam removal. *Earth Surface Processes Landforms* 42 (11), 1636–1651. doi: 10.1002/esp.4108

Dai, Z. J., Liu, J. T., Fu, G., and Xie, H. L. (2013). A thirteen-year record of bathymetric changes in the north passage, changjiang (Yangtze) estuary. *Geomorphology* 187, 1010–1107. doi: 10.1016/j.geomorph.2013.01.004

Dai, Z. J., Liu, J. T., Wei, W., and Chen, J. Y. (2014). Detection of the three gorges dam influence on the changjiang (Yangtze river) submerged delta. *Sci. Rep.* 4, 6600. doi: 10.1038/srep06600

Dai, Z. J., Mei, X. F., Darby, S. E., Lou, Y. Y., and Li, W. H. (2018). Fluvial sediment transfer in the changjiang (Yangtze) river-estuary depositional system. *J. Hydrology* 566, 719–734. doi: 10.1016/j.jhydrol.2018.09.019

East, A. E., Pess, G. R., Bountry, J. A., Magirl, C. S., Ritchie, A. C., Logan, J. B., et al. (2015). Large-Scale dam removal on the elwha river, Washington, USA: river channel and floodplain geomorphic change. *Geomorphology* 228, 765–786. doi: 10.1016/j.geomorph.2014.08.028

Edmonds, D. A., and Slingerland, R. L. (2010). Significant effect of sediment cohesion on delta morphology. *Nat. Geosci.* 3 (2), 105–109. doi: 10.1038/ngeo730

Gao, J. H., Jia, J. J., Kettner, A. J., Xing, F., Wang, Y. P., Li, J., et al. (2018). Reservoir-induced changes to fluvial fluxes and their downstream impacts on sedimentary processes: the changjiang (Yangtze) river, China. *Quaternary Int.* 493, 187–197. doi: 10.1016/j.quaint.2015.03.015

Gao, J. H., Shi, Y., Shen, H., Kettner, A. J., Yang, Y., Jia, J., et al. (2019). Rapid response of the changjiang (Yangtze) river and East China Sea source-to-sink conveying system to human induced catchment perturbations. *Mar. Geology* 414, 1–17. doi: 10.1016/j.margeo.2019.05.003

Grill, G., Lehner, B., Thieme, M., Geenen, B., Tickner, D., Antonelli, F., et al. (2019). Mapping the world's free-flowing rivers. *Nature* 569 (7755), 215–221. doi: 10.1038/s41586-019-1111-9

Guo, X. J., Fan, D. D., Zheng, S. W., Wang, H. M., Zhao, B. C., and Qin, C. J. (2021a). Revisited sediment budget with latest bathymetric data in the highly altered Yangtze (Changjiang) estuary. *Geomorphology* 391, 107873. doi: 10.1016/j.geomorph.2021.107873

Guo, L. C., Su, N., Townend, I., Wang, Z. B., Zhu, C. Y., Wang, X. Y., et al. (2019). From the headwater to the delta: a synthesis of the basin-scale sediment load regime in the changjiang river. *Earth-Science Rev.* 197, 102900. doi: 10.1016/j.earscirev.2019.102900

Guo, L. C., Xie, W. M., Xu, F., Wang, X. Y., Zhu, C. Y., Meng, Y., et al. (2021b). A historical review of sediment export–import shift in the north branch of changjiang estuary. *Earth Surface Processes Landforms* 47 (1), 5–16. doi: 10.1002/esp.5084

Jin, M., Yu, Z. Y., and He, Q. (2006). On the relationship between maintenance conditions of Yangtze estuary deep-water channel and water & sediment transport from the valley. *Port Waterway Eng.* 386 (3), 46–51. doi: 10.3969/j.issn.1002-4972.2009.01.014

Jing, X. Z., Lu, B., and He, Y. H. (2013). Response of the turbidity maximum zone to fluctuations in sediment discharge from river to estuary in the changjiang estuary (China). *Estuarine Coast. Shelf Sci.* 131, 24–30. doi: 10.1016/j.ecss.2013.07.003

Latrubesse, E. M., Arima, E. Y., Dunne, T., Park, E., Baker, V. R., d'Horta, F. M., et al. (2017). Damming the rivers of the Amazon basin. *Nature* 546 (7658), 363–369. doi: 10.1038/nature22333

Li, D. F., Lu, X. X., Chen, L., and Wasson, R. J. (2019). Downstream geomorphic impact of the three gorges dam: with special reference to the channel bars in the middle Yangtze river. *Earth Surface Processes Landforms* 44 (13), 2660–2670. doi: 10.1002/esp.4691

Li, D. F., Lu, X. X., Yang, X. K., Chen, L., and Lin, L. (2018). Sediment load responses to climate variation and cascade reservoirs in the Yangtze river: a case study of the jinsha river. *Geomorphology* 322, 41–52. doi: 10.1016/j.geomorph.2018.08.038

Li, P., Yang, S. L., Milliman, J. D., Xu, K. H., Qin, W. H., Wu, C. S., et al. (2012). Spatial, temporal, and human-induced variations in suspended sediment concentration in the surface waters of the Yangtze estuary and adjacent coastal areas. *Estuaries Coasts* 35 (5), 1316–1327. doi: 10.1007/s12237-012-9523-x

Liu, X. B., Chen, J., Yue, W., Wang, Q., Zhan, C., Zeng, L., et al. (2023). Tracing the source-sink process of fluvio-clastic materials: magnetic records of surface sediments in the Yangtze river basin. *Front. Mar. Sci.* 9, 1002335. doi: 10.3389/fmars.2022.1002335

Liu, G. F., Zhu, J. R., Wang, Y. Y., Wu, H., and Wu, J. X. (2011). Tripod measured residual currents and sediment flux: impacts on the silting of the deepwater navigation channel in the changjiang estuary. *Estuar. Coast. Shelf Sci.* 93 (3), 192–201. doi: 10.1016/j.ecss.2010.08.008

Luan, H. L., Ding, P. X., Wang, Z. B., Ge, J. Z., and Yang, S. L. (2016). Decadal morphological evolution of the Yangtze estuary in response to river input changes and estuarine engineering projects. *Geomorphology* 265, 12–23. doi: 10.1016/j.geomorph.2016.04.022

Luan, H. L., Ding, P. X., Wang, Z. B., Yang, S. L., and Lu, J. Y. (2018). Morphodynamic impacts of large-scale engineering projects in the Yangtze river delta. *Coast. Eng.* 141, 1–11. doi: 10.1016/j.coastaleng.2018.08.013

Luan, H. L., Ding, P. X., Yang, S. L., and Wang, Z. B. (2021). Accretion-erosion conversion in the subaqueous Yangtze delta in response to fluvial sediment decline. *Geomorphology* 382, 107680. doi: 10.1016/j.geomorph.2021.107680

Luo, X. X., Yang, S. L., and Zhang, J. (2012). The impact of the three gorges dam on the downstream distribution and texture of sediments along the middle and lower Yangtze river (Changjiang) and its estuary, and subsequent sediment dispersal in the East China Sea. *Geomorphology* 179, 126–140. doi: 10.1016/j.geomorph.2012.05.034

Manh, N. V., Dung, N. V., Hung, N. N., Merz, B., and Apel, H. (2014). Large-Scale suspended sediment transport and sediment deposition in the Mekong delta. *Hydrology Earth System Sci.* 18 (8), 3033–3053. doi: 10.5194/hess-18-3033-2014

Mei, X. F., Dai, Z. J., Darby, S. E., Zhang, M., Cai, H. Y., Wang, J., et al. (2021). Landward shifts of the maximum accretion zone in the tidal reach of the changjiang estuary following construction of the three gorges dam. *J. Hydrology* 592, 125789. doi: 10.1016/j.jhydrol.2020.125789

Mossa, J., and Chen, Y. H. (2021). Geomorphic insights from eroding dredge spoil mounds impacting channel morphology. *Geomorphology* 376, 107571. doi: 10.1016/j.geomorph.2020.107571

Nienhuis, J. H., Ashton, A. D., Edmonds, D. A., Hoitink, A. J. F., Kettner, A. J., Rowland, J. C., et al. (2020). Global-scale human impact on delta morphology has led to net land area gain. *Nature* 577 (7791), 514–518. doi: 10.1038/s41586-019-1905-9

Nittrouer, J. A., and Viparelli, E. (2014). Sand as a stable and sustainable resource for nourishing the Mississippi river delta. *Nat. Geosci.* 7 (5), 350–354. doi: 10.1038/ngeo2142

Pan, L. Z., Ding, P. X., and Ge, J. Z. (2012). Impacts of deep waterway project on morphological changes within the north passage of the changjiang estuary, China. *J. Coast. Res.* 284 (5), 1165–1176. doi: 10.2112/JCOASTRES-D-11-00129.1

Paszkowski, A., Goodbred, S., Borgomeo, E., Khan, M., and Hall, J. W. (2021). Geomorphic change in the Ganges–Brahmaputra–Meghna delta. *Nat. Rev. Earth Environ.* 2 (11), 763–780. doi: 10.1038/s43017-021-00213-4

Qiu, C. Y., Li, X., Liu, S. A., and Chen, D. (2019). Monitoring tidal flats in the Yangtze river delta using landsat images. *J. Geo-information Sci.* 21 (2), 269–278. doi: 10.12082/dqxxkx.2019.180344

Schmitt, R. J. P., Giuliani, M., Bizzi, S., Kondolf, G. M., Daily, G. C., and Castelletti, A. (2021). Strategic basin and delta planning increases the resilience of the Mekong delta under future uncertainty. *Proc. Natl. Acad. Sci.* 118 (36), e2026127118. doi: 10.1073/pnas.2026127118

Song, B., Li, Z., Saito, Y., Okuno, J., Li, Z., Lu, A. Q., et al. (2013). Initiation of the changjiang (Yangtze) delta and its response to the mid-Holocene sea level change. *Palaeogeography Palaeoclimatology Palaeoecol.* 388, 81–97. doi: 10.1016/j.palaeo.2013.07.026

Sun, G. (2018). *Accretion-erosion evolution and its driving mechanisms of Yangtze underwater delta over the past nearly 20 years* (Chengdu: Chengdu University of Technology).

Tang, M., Cheng, H. Q., Xu, Y., Hu, H., Zheng, S. W., Wang, B., et al. (2022). Channel bed adjustment of the lowermost Yangtze river estuary from 1983 to 2018: causes and implications. *Water* 14 (24), 4135. doi: 10.3390/w14244135

Wang, Y. H., Dong, P., Oguchi, T., Chen, S. L., and Shen, H. T. (2013). Long-term, (1842–2006) morphological change and equilibrium state of the changjiang (Yangtze) estuary, China. *Continental Shelf Res.* 56, 71–81. doi: 10.1016/j.csr.2013.02.006

Wang, S., Fu, B. J., Piao, S. L., Lü, Y. H., Ciais, P., Feng, X. M., et al. (2016). Reduced sediment transport in the yellow river due to anthropogenic changes. *Nat. Geosci.* 9 (1), 38–41. doi: 10.1038/ngeo2602

Wang, J. J., Yang, Y. P., Shen, X., Ying, H. H., and Qiao, H. Q. (2020). Study on the deformation of the Point/Channel bar of the variable section of the tidal current limit of Yangtze river and its influence on the scouring and silting of dredged channel. *J. Basic Sci. Eng.* 28 (4), 751–762. doi: 10.16058/j.issn.1005-0930.2020.04.001

Wang, C. L., Zhao, Y. F., Zou, X. Q., Xu, X. W. H., and Ge, C. D. (2017). Recent changing patterns of the changjiang (Yangtze river) estuary caused by human activities. *Acta Oceanologica Sin.* 36 (4), 87–96. doi: 10.1007/s13131-017-1017-z

Warrick, J. A., Bountry, J. A., East, A. E., Magirl, C. S., Randle, T. J., Gelfenbaum, G., et al. (2015). Large-Scale dam removal on the elwha river, Washington, USA: source-to-sink sediment budget and synthesis. *Geomorphology* 246, 729–750. doi: 10.1016/j.geomorph.2015.01.010

Wei, W., Dai, Z. J., Mei, X. F., Liu, J. P., Gao, S., and Li, S. S. (2017). Shoal morphodynamics of the changjiang (Yangtze) estuary: influences from river damming, estuarine hydraulic engineering and reclamation projects. *Mar. Geology* 386, 32–43. doi: 10.1016/j.margeo.2017.02.013

Wei, W., Mei, X. F., Dai, Z. J., and Tang, Z. H. (2016). Recent morphodynamic evolution of the largest uninhibited island in the Yangtze (Changjiang) estuary during 1998–2014: influence of the anthropogenic interference. *Continental Shelf Res.* 124, 83–94. doi: 10.1016/j.csr.2016.05.011

Wei, W., Tang, Z. H., Dai, Z. J., Lin, Y. F., Ge, Z. P., and Gao, J. (2015). Variations in tidal flats of the changjiang (Yangtze) estuary during 1950s–2010s: future crisis and policy implication. *Ocean Coast. Manage.* 108, 89–96. doi: 10.1016/j.ocecoaman.2014.05.018

Xia, J. Q., Deng, S. S., Lu, J. Y., Xu, Q. X., Zong, Q. L., and Tan, G. M. (2016). Dynamic channel adjustments in the jingjiang reach of the middle Yangtze river. *Sci. Rep.* 6, 22802. doi: 10.1038/srep22802

Xie, D. F., Pan, C. H., Wu, X. G., Gao, S., and Wang, Z. B. (2017a). The variations of sediment transport patterns in the outer changjiang estuary and hangzhou bay over the last 30 years. *J. Geophysical Research: Oceans* 122 (4), 2999–3020. doi: 10.1002/2016JC012264

Xie, D. F., Pan, C., Wu, X. G., Gao, S., and Wang, Z. B. (2017b). Local human activities overwhelm decreased sediment supply from the changjiang river: continued rapid accumulation in the hangzhou bay qiantang estuary system. *Mar. Geology* 392, 66–77. doi: 10.1016/j.margeo.2017.08.013

Xie, Q. C., Yang, J., and Lundström, T. S. (2021). Sediment and morphological changes along Yangtze river's 500 km between datong and xuliujing before and after three gorges dam commissioning. *Sci. Rep.* 11, 13662. doi: 10.1038/s41598-021-93004-2

Xu, W., Cheng, H. Q., Zheng, S. W., Jiang, Y. H., Zhou, Q. P., Yang, G. Q., et al. (2022). Riverbed deformation and its response to human intervention on the lower reaches of the Yangtze river. *River Res. Appl.* 38 (2), 222–234. doi: 10.1002/rra.3899

Xu, Q. X., Li, S. X., Yuan, J., and Yang, C. G. (2021). Analysis of equilibrium sediment transport in the middle and lower reaches of the Yangtze river after the impoundment of the three gorges reservoir. *J. Lake Sci.* 33 (3), 806–818. doi: 10.18307/2021.0316

Yan, H., Dai, Z. J., Li, J. F., Zhao, J. C., and Zhang, X. L. (2009). Distribution of surficial tidal flat sediments in the Yangtze estuary. *Acta Geographica Sin.* 64 (5), 629–637. doi: 10.3321/j.issn:0375-5444.2009.05.012

Yan, H., Dai, Z. J., Li, J. F., Zhao, J. C., Zhang, X. L., and Zhao, J. K. (2011). Distributions of sediments of the tidal flats in response to dynamic actions, Yangtze (Changjiang) estuary. *J. Geographical Sci.* 21 (4), 719–732. doi: 10.1007/s11442-011-0875-0

Yang, Y. P., Deng, J. Y., Zhang, M. J., Li, Y. T., and Liu, W. L. (2015b). The synchronicity and difference in the change of suspended sediment concentration in the Yangtze river estuary. *J. Geographical Sci.* 25 (4), 399–416. doi: 10.1007/s11442-015-1176-9

Yang, Y. P., Li, M., Liu, W. L., Chai, Y. F., Zhang, J., and Yu, W. J. (2023b). Relationship between potential waterway depth improvement and evolution of the jingjiang reach of the Yangtze river in China. *J. Geographical Sci.* 33 (3), 547–575. doi: 10.1007/s11442-023-2096-8

Yang, Y. P., Li, Y. T., Sun, Z. H., and Fan, Y. Y. (2014). Suspended sediment load in the turbidity maximum zone at the Yangtze river estuary: the trends and causes. *J. Geographical Sci.* 24 (1), 129–142. doi: 10.1007/s11442-014-1077-3

Yang, H. F., Li, B. C., Zhang, C. Y., Qiao, H. J., Liu, Y. T., Bi, J. F., et al. (2020). Recent spatio-temporal variations of suspended sediment concentrations in the Yangtze estuary. *Water* 12 (3), 818. doi: 10.3390/w12030818

Yang, S. L., Milliman, J. D., Li, P., and Xu, K. H. (2011). 50,000 dams later: erosion of the Yangtze river and its delta. *Global Planetary Change* 75 (1–2), 14–20. doi: 10.1016/j.gloplacha.2010.09.006

Yang, S. L., Xu, K. H., Milliman, J. D., Yang, H. F., and Wu, C. S. (2015c). Decline of Yangtze river water and sediment discharge: impact from natural and anthropogenic changes. *Sci. Rep.* 5, 12581. doi: 10.1038/srep12581

Yang, H. F., Yang, S. L., Xu, K. H., Wu, H., Shi, B. W., Zhu, Q., et al. (2017). Erosion potential of the Yangtze delta under sediment starvation and climate change. *Sci. Rep.* 7, 10535. doi: 10.1038/s41598-017-10958-y

Yang, Y. P., Yin, H., Li, M., Liu, W. L., Li, K. Y., and Yu, W. J. (2023c). Effect of water depth and waterway obstructions on the divergence and confluence areas of dongting lake and the Yangtze river after the operation of the three gorges project. *River* 2 (1), 88–108. doi: 10.1002/rvr2.31

Yang, Y. P., Zhang, M. J., Fan, Y. Y., Li, Y. T., and Liu, W. L. (2018). Variation trend and causes of suspended sediment characteristic in Yangtze estuary. *J. Basic Sci. Eng.* 24 (6), 1203–1218. doi: 10.16058/j.issn.1005-0930.2016.06.012

Yang, Y. P., Zhang, M. J., Li, Y. T., and Zhang, W. (2015a). The variations of suspended sediment concentration in Yangtze river estuary. *J. Hydrodynamics* 27 (6), 845–856. doi: 10.1016/S1001-6058(15)60547-9

Yang, Y. P., Zhang, M. J., Liu, W. L., Wang, J. J., and Li, X. X. (2019). Relationship between waterway depth and low-flow water levels in reaches below the three gorges dam. *J. Waterway Port Coastal Ocean Eng.* 145 (1), 04018032. doi: 10.1061/(ASCE)WW.1943-5460.0000482

Yang, Y. P., Zheng, J. H., Zhang, H. Q., Chai, Y. F., Zhu, Y. D., and Wang, C. Y. (2022a). Impact of the three gorges dam on riverbed scour and siltation of the middle reaches of the Yangtze river. *Earth Surface Processes Landforms* 47 (6), 1514–1531. doi: 10.1002/esp.5332

Yang, Y. P., Zheng, J. H., Zhang, W., Zhu, Y. D., Chai, Y. F., Wang, J. J., et al. (2021b). Quantitative relationship between channels and bars in a tidal reach of the lower Yangtze river: implications for river management. *J. Geographical Sci.* 31 (12), 1837–1851. doi: 10.1007/s11442-021-1925-x

Yang, Y. P., Zheng, J. H., Zhang, M. J., Zhu, L. L., Zhu, Y. D., Wang, J. J., et al. (2021a). Sandy riverbed shoal under anthropogenic activities: the sandy reach of the Yangtze river, China. *J. Hydrology* 603, 126861. doi: 10.1016/j.jhydrol.2021.126861

Yang, Y. P., Zheng, J. H., Zhu, L. L., Zhang, H. Q., and Wang, J. J. (2022b). Influence of the three gorges dam on the transport and sorting of course and fine sediments downstream of the dam. *J. Hydrology* 615, 128654. doi: 10.1016/j.jhydrol.2022.128654

Yang, Y. P., Zhou, L. P., Zhu, L. L., Liu, W. L., and Wang, J. J. (2023a). Impact of upstream reservoirs on geomorphic evolution in the middle and lower reaches of the Yangtze river. *Earth Surface Processes Landforms* 48 (3), 582–595. doi: 10.1002/esp.5504

Yao, J., Shi, Y., and Zhang, G. A. (2015). The change process of water and sediment volume of branching channel in the Yangtze river during 1958–2013. *Acta Geographica Sin.* 70 (5), 828–836. doi: 10.11821/dlxb201505013

Yao, S. M., Wang, H. Y., and Mao, B. P. (2017). Research on bed-load transport formula in the Cheng-han reach of the middle Yangtze river. *Adv. Water Sci.* 28 (3), 329–337. doi: 10.14042/j.cnki.32.1309.2017.03.002

Yu, W. C., and Zhang, Z. L. (2021). Evolution trend of basic channel scour and morphological adjustment in Yangtze river estuary from 2002 to 2018. *J. Yangtze River Sci. Res. Institute* 38(8), 1–8, 13. doi: 10.11988/ckyyb.20201057

Zhai, X. M. (2006). *Elementray discussion of hydrodynamic and suspended sediment distribution characteristic in the Yangtze estuary [D]* (Shanghai: East China Normal University).

Zhang, E. F., Savenije, H. G., Chen, S. L., and Chen, J. Y. (2011). Water abstraction along the lower Yangtze river, China, and its impact on water discharge into the estuary. *Phys. Chem. Earth* 47–48, 76–85. doi: 10.1016/j.pce.2011.05.002

Zhang, X. D., Xie, R., Fan, D. D., Yang, Z. S., Wang, H. M., Wu, C., et al. (2021). Sustained growth of the largest uninhabited alluvial island in the changjiang estuary under the drastic reduction of river discharged sediment. *Sci. China Earth Sci.* 64 (10), 1687–4697. doi: 10.1007/s11430-020-9746-3

Zhang, X. B., Zhang, Y. X., Zhu, L. H., Chi, W. Q., Yang, Z. S., Wang, B. Y., et al. (2018). Spatial-temporal evolution of the eastern nanhui mudflat in the changjiang (Yangtze river) estuary under intensified human activities. *Geomorphology* 309, 38–50. doi: 10.1016/j.geomorph.2018.02.023

Zhang, J. Y., and Zhao, D. Z. (2016). Analysis of temporal and spatial distribution characteristics of bedload in south chanel and north passage, Yangtze estuary. *Resour. Environ. Yangtze Basin* 25 (10), 1520–1527. doi: 10.11870/cjlyzyyhj20161006

Zhao, J., Guo, L. C., He, Q., Wang, Z. B., van Maren, D. S., and Wang, X. Y. (2018). An analysis on half century morphological changes in the changjiang estuary: spatial variability under natural processes and human intervention. *J. Mar. Syst.* 181, 25–36. doi: 10.1016/j.jmarsys.2018.01.007

Zheng, S. R. (2016). Reflections on the three gorges project since its operation. *Engineering* 2 (4), 389–397. doi: 10.1016/J.ENG.2016.04.002

Zheng, S. W., Hu, H., Xu, S. J., Cheng, H. Q., Li, Z. J., and Liu, E. F. (2022). Spatial distribution and response of dunes to anthropogenic factors in the lower Yangtze river. *Catena* 212, 106045. doi: 10.1016/j.catena.2022.106045

Zhou, Y. J., Li, D. F., Lu, J. Y., Yao, S. M., Yan, X., Jin, Z. W., et al. (2020). Distinguishing the multiple controls on the decreased sediment flux in the jialing river basin of the Yangtze river, southwestern China. *Catena* 193, 104593. doi: 10.1016/j.catena.2020.104593

Zhou, L., Shi, Y., Zhao, Y. Q., Yang, Y., Jia, J. J., Gao, J. H., et al. (2021). Extreme floods of the changjiang river over the past two millennia: contributions of climate change and human activity. *Mar. Geology* 433, 106418. doi: 10.1016/j.margeo.2020.106418

Zhou, M. R., Xia, J. Q., Deng, S. S., and Lin, F. F. (2018). Channel adjustments in a gravel-sand bed reach owing to upstream damming. *Global Planetary Change* 170, 213–220. doi: 10.1016/j.gloplacha.2018.08.014

Zhu, C. Y., Guo, L. C., van Maren, D. S., Tian, B., Wang, X. Y., He, Q., et al. (2019). Decadal morphological evolution of the mouth zone of the Yangtze estuary in response to human interventions. *Earth Surface Processes Landforms* 44 (12), 2319–2332. doi: 10.1002/esp.4647

Zhu, L., He, Q., Shen, J., and Wang, Y. (2016). The influence of human activities on morphodynamics and alteration of sediment source and sink in the changjiang estuary. *Geomorphology* 273, 52–62. doi: 10.1016/j.geomorph.2016.07.025

Zou, S. H., Zhang, N. C., Li, B., and Chen, S. L. (2012). A study of suspended sediment concentration in yangshan deep-water port in shanghai, China. *Int. J. Sediment Res.* 27 (1), 50–60. doi: 10.1016/S1001-6279(12)60015-8

Frontiers in Marine Science

Explores ocean-based solutions for emerging global challenges

The third most-cited marine and freshwater biology journal, advancing our understanding of marine systems and addressing global challenges including overfishing, pollution, and climate change.

Discover the latest Research Topics

See more →

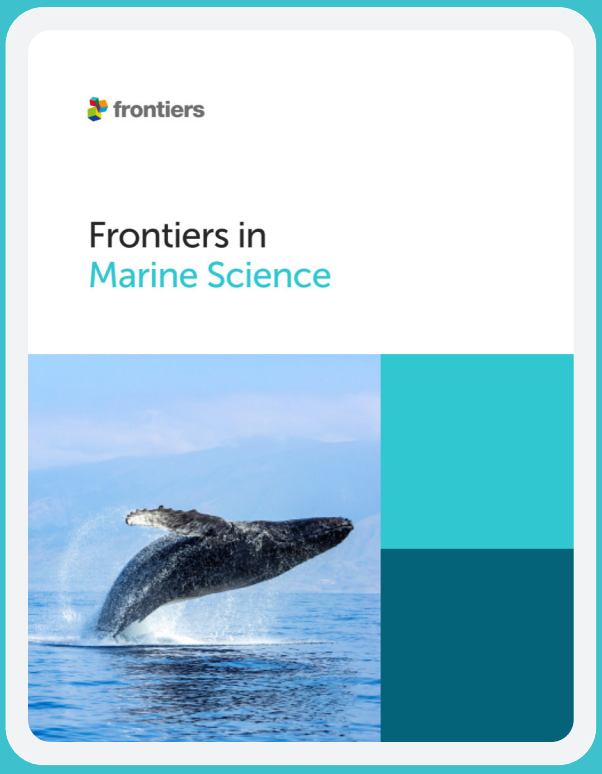

Frontiers

Avenue du Tribunal-Fédéral 34
1005 Lausanne, Switzerland
frontiersin.org

Contact us

+41 (0)21 510 17 00
frontiersin.org/about/contact